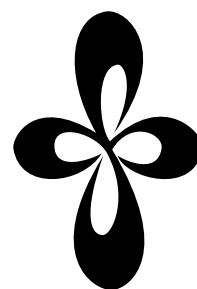


ANNUAL REVIEW

***INSTITUTE
FOR
MOLECULAR
SCIENCE***



1999

Published by

Institute for Molecular Science
Okazaki National Research Institutes
Myodaiji, Okazaki 444-8585, Japan
Phone: +81-564-55-7418 (Secretary Room)
Facsimile: +81-564-54-2254 (Secretary Room)
URL: <http://www.ims.ac.jp/>

Editorial Committee 1999

Chairperson	INOUE, Katsuya	
Vice-Chairperson	SUZUKI, Toshiyasu	
	SUGITA, Yuji	MIZUTANI, Yasuhisa
	INOKUCHI, Yoshiya	OGATA, Hironori
	MIZUTANI, Masakazu	MIZUKAWA, Tetsunori
	TAKAMI, Toshiya	WATANABE, Kazuo
	YAMAMOTO, Hisayo	SATO, Atzko

IMS 1999

Since the Institute for Molecular Science was founded in 1975, almost a quarter of a century has past and we will celebrate 21st century in two years. Over the past 25 years, IMS has played an important role for the development of fundamental research in the field of molecular science and has given appreciable influence upon the research fields related to molecular science. As is clearly understood from the Annual Review for 1999, IMS maintains high activity and quality of research.

In this annual review, recent development of researches in 6 departments and six research facilities of IMS will be introduced. At the end of the booklet, result of the joint study programs which is one of the important functions of IMS, will be reported. This review also clarifies that IMS nowadays is covering wide range of molecular systems from simple atom systems to complex bio-molecule systems. Regarding time and energy domains, IMS now covers wide range of time scale down to femto-second and wide range of energy from soft x-ray to far infrared region. For the further development of molecular science in IMS, we need intimate interactions with surrounding sciences such as solid state physics, environmental science, and life science.

This year, new research project for bio-environmental science has started by the collaboration of three research institutes at Okazaki.

It is one of the most important tasks for IMS to develop new feature of molecular science by the interactions with the groups of different scientific field.

September, 1999



A handwritten signature in black ink, consisting of stylized characters that appear to be 'Kaya' followed by 'Koji'.

KAYA, Koji
Director General

CONTENTS

IMS 1999	KAYA, Koji iii
CONTENTS	v
ORGANIZATION AND STAFF	1
COUNCIL	13
BUILDINGS AND CAMPUS	15
RESEARCH ACTIVITIES I	17

Department of Theoretical Studies

I-A Development of New Theoretical and Numerical Techniques in the Study of Molecular Structure

I-A-1 Multireference Linear Response Theory Utilizing the State Universal Coupled Cluster Formalism	17
I-A-2 Size-extensive Calculations of Static Structure Factors from the Coupled Cluster Singles and Doubles Model	17
I-A-3 Local Resolution of Identity for Scalable Molecular Orbital Calculations	17
I-A-4 On Connection Between The Reference Interaction Site Model Integral Equation Theory and The Partial Wave Expansion of The Molecular Ornstein-Zernike Equation	17
I-A-5 Non-Adiabatic Relaxation Through a Conical Intersection	17

I-B Water Clusters and Their Complexes with Atomic Ions

I-B-1 Theoretical Studies of Structures and Ionization Threshold Energies of Water Cluster Complexes with a Group 1 Metal, $M(H_2O)_n$ ($M = Li$ and Na)	18
I-B-2 The Electron-Hydrogen Bonds and the Harmonic Frequency Shifts in Water Cluster Complexes with a Group 1 Metal Atom, $M(H_2O)_n$ ($M = Li$ and Na)	18
I-B-3 The Energies, the Structures and the Harmonic Frequencies of the Small Water Cluster Anions, $(H_2O)_n^-$ ($n = 3, 4$ and 6)	18
I-B-4 Theoretical Study of Vibrational Spectra for $Cl^-(H_2O)$: Temperature Dependence and the Influence of Ar_n ($n = 1-3$)	19

I-C Computational Chemistry of Atomic and Molecular Processes in Atmospheric Environment

I-C-1 Accurate Potential Energy and Transition Dipole Moment Curves of Several Electronic States of CO^+	19
I-C-2 Accurate Potential Energy Curves of Several Electronic States of N_2^+ and O_2^+	19
I-C-3 Absorption and Emission Spectra Among the Rovibrational Levels of the Electronic Ground State of $CO X^1\Sigma^+$	20
I-C-4 Theoretical Study of the Reactions of OH Radical with Hydrocarbons	20
I-C-5 <i>Ab Initio</i> Study of the Low-Lying Excited States of $ClOCl$	20
I-C-6 <i>Ab Initio</i> Study of the Excited States of $HOBr$	20
I-C-7 Theoretical Study of the Molecular Structure of the $NO_3^-(HNO)_m$ and $NO_3^-(HNO)_m \cdot H_2O$ Anions	20
I-C-8 Investigation of the Potential Energy Surfaces for the Ground \tilde{X}^1A_1 and Excited \tilde{C}^1B_2 Electronic states of SO_2	20

I-D Application of Ab Initio Molecular Orbital Methods to Experimentally Relevant Systems

I-D-1 Theoretical Study on Spectroscopic Properties of Positive, Neutral, and Negative Species of BCl_2 and $AlCl_2$: The Stability of the Negative Species	21
I-D-2 The Structures of the Ground and Excited States of (H_3NHNH_3) Radical	21
I-D-3 The Heat of Formation of the SiF_2^{++} Dication: A Theoretical Prediction	21
I-D-4 Electronic Isomers in $[(CO_2)_nROH]^-$ Cluster Anions. II. <i>Ab initio</i> Calculations	21
I-D-5 Theoretical Studies of $[Si_4NO]^-$ Clusters with <i>Ab Initio</i> MO and DFT Methods	22
I-D-6 Theoretical Studies of Core-Excitation and Auger-Decay Processes in Site- or State-Specific Bond Dissociation Reaction with <i>Ab Initio</i> MO Methods	22

I-E Prediction of Protein Tertiary Structures from the First Principles

I-E-1 Classification of Low-Energy Conformations of Met-Enkephalin in the Gas Phase and in a Model Solvent Based on the Extended Scaled Particle Theory	23
I-E-2 Temperature Dependence of Distributions of Conformations of a Small Peptide	23
I-E-3 α -Helix Propensities of Homo-Oligomers in Aqueous Solution Studied by Multicanonical Algorithm	23
I-E-4 Replica-Exchange Molecular Dynamics Method for Protein Folding	23

I-F Theoretical Studies of Chemical Reaction Dynamics

I-F-1 Quantum Reaction Dynamics of Heavy-Light-Heavy Systems: Reduction of the Number of Potential Curves and Transitions at Avoided Crossings	24
I-F-2 Quantum Reaction Dynamics of $\text{Cl} + \text{HCl} \rightarrow \text{HCl} + \text{Cl}$: Vibrationally Nonadiabatic Reactions	24
I-F-3 Quantum Reaction Dynamics of an Asymmetric Exoergic Heavy-Light-Heavy System: $\text{Cl} + \text{HBr} \rightarrow \text{HCl} + \text{Br}$	24
I-F-4 On the <i>J</i> -Shift Approximation in Quantum Reaction Dynamics	24
I-F-5 Electronically Adiabatic Chemical Reactions Analyzed by the Semiclassical Theory of Nonadiabatic Transition	25
I-G Theory of Nonadiabatic Transition	
I-G-1 Patterns of Time Propagation on the Grid of Potential Curves	25
I-G-2 Analytic Solution of Two-State Time-Independent Coupled Schrödinger Equations in an Exponential Model	25
I-G-3 Semiclassical Theory of Nonadiabatic Transitions in a Two-State Exponential Model	25
I-H New Way of Controlling Molecular Processes	
I-H-1 New Way of Controlling Molecular Processes by Time-Dependent External Fields	25
I-H-2 Control of Molecular Photodissociation with Use of the Complete Reflection Phenomenon	26
I-I Molecular Switching with Use of the Complete Reflection Phenomenon	
I-I-1 Molecular Switching in a Two-Dimensional Constriction	26
I-J Theoretical Study of Dissociative Recombination	
I-J-1 Analytical Treatment of Singular Equations in Dissociative Recombination	26
I-K Theoretical Studies of Ultrafast Nonlinear Optical Spectroscopy of Molecules in Condensed Phases	
I-K-1 The Fifth- and Seventh-Order Two-Dimensional Raman Spectroscopy for Harmonic System with Nonlinear System-Bath Interactions: Gaussian-White Case	27
I-K-2 The Fifth and Seventh Order 2D Raman Spectroscopy for Harmonic System with Nonlinear System-Bath Interactions: Gaussian-Markovian Case	27
I-K-3 Structural Information from Two-Dimensional Fifth-Order Raman Spectroscopy	27
I-K-4 Two-Dimensional Line Shape Analysis of Photon Echo Signal	27
I-K-5 Cage Dynamics in the Third-Order Off-Resonant Response of Liquid Molecules: A Theoretical Realization	28
I-K-6 Dynamical Stokes Shift Observed by Two-Dimensional Raman Spectroscopy	28
I-K-7 A Thermal Bath Induced New Resonance in Linear and Nonlinear Spectra of Two-Level Systems	28
I-L Ab Initio Molecular Orbital Studies of Organic Conductors	
I-L-1 Structures and Electronic Phases of the Bis(Ethylenedithio)Tetrathiafulvalene (BEDT-TTF) Clusters and κ -(BEDT-TTF) Salts: A Theoretical Study Based on Ab Initio Molecular Orbital Methods	28
I-L-2 Ab Initio MO Studies on Electronic States of DCNQI Molecules	28
I-L-3 Theoretical Study on Electron Correlation of 1-D (DCNQI) ₂ M (M = Li, Ag)	29
I-M Electron, Positron and Heavy Particle Scattering Dynamics	
I-M-1 Strong Mode Dependence of 3.8-eV Resonance in CO ₂ Vibrational Excitation by Electron Impact	30
I-M-2 Strong Suppression of Positronium Formation in Fluorinated Hydrocarbons in Positron Scattering: A Possibility of Bound States	30
I-M-3 Electron Capture in Collisions of Protons with CO Molecules in the keV Region: The Steric Effect	30
I-M-4 The Isomer Effect on Charge Transfer: Collisions of Ground State C ⁺ Ions with Allene and Propyne (C ₃ H ₄)	30
I-M-5 Electron Capture and Excitation in Collisions of Si ²⁺ Ions with He Atoms at Intermediate Energies	31
I-N Electronic Structure of a Molecule in Solution	
I-N-1 The Syn-/Anti- Conformational Equilibrium of Acetic Acid in Water Studied by the RISM-SCF/MCSCF Method	32
I-N-2 RISM-SCF Study for the Free Energy Profile of Menshutkin Type Reaction $\text{NH}_3 + \text{CH}_3\text{Cl} \rightarrow \text{NH}_3\text{CH}_3^+ + \text{Cl}^-$ in Aqueous Solution	32
I-N-3 Thermodynamic Analysis of the Solvent Effect on Tautomerization of Acetylacetone: An Ab Initio Approach	33
I-N-4 Solvation Dynamics of Benzonitrile Excited State in Polar Solvents: A Time-Dependent Reference Interaction Site Model Self-Consistent Field Approach	33
I-N-5 Revisiting the Acid-Base Equilibrium in Aqueous Solutions of Hydrogen Halides: Study by the <i>ab Initio</i> Electronic Structure Theory Combined with the Statistical Mechanics of Molecular Liquids	33

I-N-6	Ab Initio Study on Molecular and Thermodynamic Properties of Water: A Theoretical Prediction of pK_w over a Wide Range of Temperature and Density	33
I-O	Solvation Thermodynamics of Protein and Related Molecules	
I-O-1	Calculation of Solvation Free Energy for Peptide in Salt Solution Using the RISM Theory	34
I-O-2	Singular Behavior of the RISM Theory Observed for Peptide in Salt Solution	34
I-O-3	Analysis on Conformational Stability of C-Peptide of Ribonuclease A in Water Using the Reference Interaction Site Model Theory and Monte Carlo Simulated Annealing	35
I-P	Collective Density Fluctuations in Polar Liquids and Their Response to Ion Dynamics	
I-P-1	Effect of Molecular Symmetry on Electrical Potential Fluctuations of Solvent around Solute in Polar Liquid	35
I-P-2	Mode-Coupling Theory for Molecular Liquids Based on the Interaction-Site Model	36
I-P-3	Time-Correlation Functions in Molecular Liquids Studied by the Mode-Coupling Theory Based on the Interaction-Site Model	36
I-P-4	Dynamics of Ions in Liquid Water: An Interaction-Site-Model Description	36
I-P-5	Interaction-Site-Model Description of Collective Excitations in Liquid Water. I: Theoretical Study	36
I-P-6	Interaction-Site-Model Description of Collective Excitations in Liquid Water. II: Comparison with Simulation Results	36
I-P-7	Solvation Dynamics of a Quadrupolar Solute in Dipolar Liquids	37
I-P-8	Density Matrix for an Excess Electron in a Classical Fluid: Results for a One-Dimensional System	37
I-P-9	Polaron Density Matrix and Effective Mass at Finite Temperature	37
I-Q	Liquid-Solid Interface	
I-Q-1	Acceleration of Liquid Structure Calculations by Modified Direct Inversion in the Iterative Subspace	38
I-Q-2	Extended States of a Shallow Donor Located Near a Semiconductor-Insulator Interface	38
I-Q-3	Free Energy Profiles of Electron Transfer at Water-Electrode Interface Studied by the Reference Interaction Site Model Theory	38
I-Q-4	Self-Consistent Description of a Metal-Water Interface by the Kohn-Sham Density Functional Theory and the Three-Dimensional Reference Interaction Site Model	38
I-Q-5	Effective Interaction between Hard Sphere Colloidal Particles in a Polymerizing Yukawa Solvent	39
I-Q-6	Potential of Mean Force between Two Molecular Ions in a Polar Molecular Solvent: A Study by the Three-Dimensional Reference Interaction Site Model	39
I-Q-7	Self-Consistent, Kohn-Sham DFT and Three-Dimensional RISM Description of a Metal-Molecular Liquid Interface	39
I-R	Dimensional Crossovers and Randomness Effects in Quasi-One-Dimensional Organic Conductors	
I-R-1	Spin-Density-Wave Phase Transitions in Quasi-One-Dimensional Dimerized Quarter-Filled Organic Conductors	40
I-R-2	Phase Transitions from Incoherent and from Coherent Metal Phases in Quasi-One-Dimensional Organic Conductors	40
I-R-3	Quantum Phase Transition and Collapse of Mott Gap in $d = 1 + \epsilon$ Dimensional Half-Filled Hubbard Systems	40
I-R-4	Charge Gap and Interchain Correlation in Quasi-One-Dimensional Dimerized Organic Conductors	40
I-R-5	Magnetic and Pairing Correlation Functions and Interchain Coherence in Quasi-One-Dimensional Dimerized Organic Conductors	41
I-R-6	Effects of Dimerization on Spin, Charge and Hopping Correlation Functions in Quasi-One-Dimensional Organic Conductors	41
I-R-7	Interplay of Correlation, Randomness and Dimensionality Effects in Weakly-Coupled Half-Filled Random Hubbard Chains	41
I-R-8	Dimensionality Effects in Half-Filled Random Hubbard Chains	41
I-S	Competition among Different Charge and Lattice Ordering States in One-Dimensional Metal Complexes	
I-S-1	Numerical Studies of Ground State Phase Diagrams for the MMX Chains	42
I-S-2	Magnetic Property of MMX Chains as Dimerized Quarter-Filled Systems	42
I-S-3	Structural and Magnetic Transitions in Quasi-One-Dimensional Halogen-Bridged Binuclear Metal Complexes	42
I-S-4	Electric-Field Response of Exciton in Electroluminescent Polymer	42
I-T	Transport and Magnetic Properties of Two-Dimensional Metal-Complex, Organic and Oxide Conductors	
I-T-1	Possible Magnetic Orders and Cation Dependence of $(Et_nMe_{4-n}Z)[Pd(dmit)_2]_2$	43
I-T-2	Role of Dimensionality in Dimerized Two-Band Systems	43
I-T-3	Quasi-One-Dimensional Natures in $(Et_nMe_{4-n}Z)[Pd(dmit)_2]_2$	43

I-T-4 Possible Ground State Phases of Pd(dmit) ₂ Salts	43
I-T-5 Collective Excitations around Charge Ordering States and Coexistent States with Different Orders	43
I-T-6 Ab Initio Molecular Orbital, Hartree-Fock, and Exact Diagonalization Studies of Structures and Electronic Phases of (BEDT-TTF) Clusters and κ -(BEDT-TTF) Salts	44
I-T-7 Two-Loop Renormalization-Group Analysis of Two-Dimensional Electron Systems	44

RESEARCH ACTIVITIES II -----45

Department of Molecular Structure

II-A Laboratory and Astronomical Spectroscopy of Transient Molecules	
II-A-1 The detection of the Free Radical FO ($X^2\Pi_{3/2}$) by Microwave Spectroscopy	45
II-A-2 Microwave Spectroscopic Detection of Transition Metal Hydroxide: CuOH and AgOH	45
II-A-3 Microwave Spectrum of the Inversion-Rotation Transition of the D ₃ O ⁺ Ion: $\Delta k = \pm 3n$ Interaction and Equilibrium Structure	46
II-B Laser Cooling and Trapping of Neutral Atoms	
II-B-1 Quantum Statistical Effects in Ultracold Ionizing Collisions between Spin-Unpolarized Metastable He($2s^3S_1$) Atoms	47
II-C Spectroscopy of Atoms and Ions in Liquid Helium	
II-C-1 Spectroscopic Study of Alkali-Earth Atoms in Liquid ³ He	47
II-D Endohedral Metallofullerenes: New Fullerene Molecules with Novel Properties	
II-D-1 Endohedrally Metal-Doped Heterofullerenes: La@C ₈₁ N and La ₂ @C ₇₉ N	49
II-D-2 Isolation and Characterization of a Pr@C ₈₂ Isomer	49
II-E Structure and Function of Respiratory Terminal Oxidases	
II-E-1 Fourier-Transform Infrared Studies on Azide Binding to the Binuclear Center of the <i>Escherichia coli</i> <i>bo</i> -Type Ubiquinol Oxidase	50
II-E-2 Fluoride-Binding to the oxidized <i>Escherichia coli</i> <i>bd</i> -Type Ubiquinol Oxidase Studied by Visible Absorption and EPR Spectroscopies	50
II-E-3 Azide- and Cyanide-Bindings to the <i>Escherichia coli</i> <i>bd</i> -Type Ubiquinol Oxidase Studied by Visible Absorption, EPR and FTIR Spectroscopies	50
II-F Structure and Function of Transmembrane Electron Transfer System in Neuroendocrine Secretory Vesicles	
II-F-1 Diethylpyrocarbonate-Modification Abolishes Fast Electron Accepting Ability of Cytochrome <i>b</i> ₅₆₁ from AsA ⁻ but Does Not Influence on Electron Donation to MDA Radical: Identification of the Modification Sites by Mass Spectrometric Analyses	51
II-G Biomolecular Science	
II-G-1 Time-Resolved UV Resonance Raman Detection of a Transient Open Form of the Ligand Pathway in Tyr64(E7) Myoglobin	52
II-G-2 UV Resonance Raman Studies of α -Nitrosyl Hemoglobin Derivatives: Relation between the $\alpha 1$ - $\beta 2$ Subunit Interface Interactions and the Fe-Histidine Bonding of α Heme	52
II-G-3 Observation of Cu-N ₃ ⁻ Stretching and N ₃ ⁻ Asymmetric Stretching Bands for <i>mono</i> -Azide Adduct of <i>Rhus vernicifera</i> Laccase	53
II-G-4 Studies of Bovine Enterovirus Structure by Ultraviolet Resonance Raman Spectroscopy	53
II-G-5 Spectroscopic Characterization and Kinetic Studies of a Novel Plastocyanin from the Green Alga <i>Ulva pertusa</i>	53
II-G-6 Aliphatic Hydroxylation by a Bis(μ -Oxo)Dinickel(III) Complex	53
II-G-7 The Structure and Unusual pH Dependence of Plastocyanin from the Fern <i>Dryopteris</i> <i>Crassirhizoma</i> : The Protonation of an Active Site Histidine is Hindered by π - π Interactions	54
II-G-8 Model Complexes of the Active Form of Galactose Oxidase. Physicochemical Properties and Reactivity of Cu(II)- and Zn(II)- Phenoxyl Radical Complexes of the Novel Organic Cofactor	54
II-G-9 A Bis(μ -Oxo)Dicopper(III) Complex with Sterically Hindered Aromatic Nitrogen Donors: Structural Characterization and Reversible Conversion between Copper(I) and Bis(μ -Oxo)Dicopper(III) Species	55
II-H Fast Dynamics of Photoproducts in Solution Phases	
II-H-1 Intramolecular Vibrational Energy Redistribution and Intermolecular Energy Transfer in the (<i>d,d</i>) Excited State of Nickel Octaethylporphyrin	55
II-H-2 Time-Resolved Resonance Raman Study of Intermediates Generated after Photodissociation of Wild-type and Mutant CO-Myoglobins	56
II-H-3 Characterization of Stimulated Raman Scattering of Hydrogen and Methane Gases as a Light Source of Picosecond Time-Resolved Raman Spectroscopy	56
II-H-4 Nanosecond Temperature Jump and Time-Resolved Raman Study of Thermal Unfolding of Ribonuclease A	56

II-H-5 Evidence for π - π Interactions in the S_1 State of Zn Porphyrin Dimers Revealed by Picosecond Time Resolved Resonance Raman Spectroscopy -----	57
II-I Molecular and Electronic Structures of Metallofullerenes and the Fullerene Radical Anions	
II-I-1 Spin Chemistry of Metallofullerenes -----	58
II-J Site Selective Spectroscopy in Solid Crystals	
II-J-1 NQR by Coherent Raman Scattering of a Triplet Exciton in a Molecular Crystal -----	58
II-K State Correlated Raman Spectroscopy	
II-K-1 An Analysis of Polarized Raman Scattering Measurements for the Orientational Ordering of Ferro- and Antiferroelectric Liquid Crystal -----	59
RESEARCH ACTIVITIES III -----	61
Department of Electronic Structure	
III-A States of Molecular Associates in Solutions	
III-A-1 Raman Spectroscopic Study on Acetic Acid Clusters in Aqueous Solutions: Dominance of Acetic-Acid Association Producing Micro-Phases -----	61
III-A-2 Structures and Energies of Acetic Acid Aggregates in Aqueous Solution Studied by the RISM-SCF Method -----	62
III-A-3 Rayleigh Wing Spectra and Microphase Formation -----	62
III-A-4 Structures of Clusters in Methanol-Water Binary Solutions Studied by Mass Spectrometry and X-ray Diffraction -----	63
III-A-5 Structure and Dynamics of 1,4-Dioxane-Water Binary Solutions Studied by X-ray diffraction, Mass Spectrometry, and NMR Relaxation -----	63
III-B Ultrafast Dynamics of Photoexcited Molecules	
Studied by Transient Absorption and Transient Raman Spectroscopy Methods	
III-B-1 Construction of a Tunable and Synchronized Picosecond-Femtosecond Double Laser System for the Study of Photodissociation Dynamics of Molecular Clusters in Solution -----	64
III-C Spectroscopic and Dynamical Studies on Charge Delocalization and Charge Transfer in Aromatic Molecular Cluster Ions	
III-C-1 Photodissociation Spectroscopy of Benzene-Acetic acid Mixed Cluster Ions -----	65
III-C-2 Structural Isomers of Benzene-Phenol Mixed Dimer Cation -----	66
III-D Spectroscopy and Dynamics of Vibrationally Excited Molecules and Clusters	
III-D-1 Overtone Spectroscopy of Jet-Cooled Phenol Studied by Nonresonant Ionization Detected IR Spectroscopy -----	67
III-C-2 Structure of 1-Naphthol-Water Clusters Studied by IR Dip Spectroscopy and Ab Initio Molecular Orbital Calculation -----	67
III-E Femtosecond Time-Resolved Photoelectron Imaging	
III-E-1 Femtosecond Time-Resolved Photoelectron Imaging on Ultrafast Electronic Dephasing in an Isolated Molecule -----	68
III-F Dynamical Stereochemistry	
III-F-1 Vector Correlation in Molecular Photodissociation -----	68
III-G Photochemistry on Well-Defined Surfaces	
III-G-1 Photo-stimulated Desorption of Rare Gas Atoms Induced by UV-NIR Photons at a Semiconductor Surface -----	69
III-G-2 Photochemistry of Methane on Cu(111) -----	69
III-G-3 Coadsorption Effect of Cs on Photochemistry of Methane on Pt(111) -----	69
III-H Multiphoton Photoelectron Spectroscopy of Electronic States at Metal Surfaces	
III-H-1 Visible and VUV Two-Photon Photoelectron Spectroscopy of the Surface State of a Clean Pt(111) Surface -----	70
III-I Ultrafast Reaction Dynamics of Photochromism and Related Phenomena	
III-I-1 Time-Resolved Study on Unconventional Fluorescence of an Azobenzene Liquid Crystal and Its Phase Transition -----	71
III-I-2 Solvation Dynamics of Excited p-Methoxy-p'-cyanodiphenylacetylene in n-Butanol: Simultaneous Analysis of Time-Resolved Fluorescence Anisotropy and Stokes Shift -----	71
III-I-3 A Combined Experimental and Theoretical Study on the Photochromism of Aromatic Anils	71
III-I-4 Photochromism in 2-(2',4'-Dinitrobenzyl)pyridine Studied by Ultrafast Laser Spectroscopy	71
III-J Photophysics and Photochemistry in Interface Layers and Mesoscopic Systems	
III-J-1 Time-Resolved and Near-Field Scanning Optical Microscopy Study on Porphyrin J-Aggregate -----	72
III-J-2 Excitation Energy Transfer in Langmuir-Blodgett Films of 5-(4-N-Octadecylpyridyl)-10,15,20-tri-p-tolylporphyrin on Gold-Evaporated Glass Substrates Studied by Time-resolved Fluorescence Spectroscopy ----	72
III-J-3 Carrier Dynamics on Titanium Dioxide Single Crystals by Femtosecond Transient Grating Spectroscopy -----	72

RESEARCH ACTIVITIES IV -----75

Department of Molecular Assemblies

IV-A Solid State Properties of Phthalocyanine Salts and Related Compounds

- IV-A-1 ESR Properties of Oriented Single Crystals of $\text{Co}_x\text{Ni}_{1-x}\text{Pc}(\text{AsF}_6)_{0.5}$ -----75
 IV-A-2 Pressure-Temperature Phase Diagram of $\text{NiPc}(\text{AsF}_6)_{0.5}$ -----75
 IV-A-3 New Raman Bands Found in the Mixed Crystals of $\text{Ni}_{1-x}\text{Co}_x\text{Pc}(\text{AsF}_6)_{0.5}$ -----76

IV-B Structure and Properties of Organic Conductors

- IV-B-1 Spectroscopic Study of Isostructural Charge-Transfer Salts:
 Non-Metallic DMTTA- BF_4 and Metallic DMTSA- BF_4 -----76
 IV-B-2 Suppression of the Metal-Insulator Transition
 under High Pressure in 1:1 Metallic DMTSA- BF_4 -----77
 IV-B-3 Band Structure of Organic Metals $(\text{BDT-TTP})_2\text{X}$ ($\text{X} = \text{ClO}_4, \text{ReO}_4$), $(\text{ST-TTP})_2\text{AsF}_6$,
 and $(\text{BDS-TTP})_2\text{AsF}_6$ Studied by Reflection Spectroscopy -----77
 IV-B-4 Insulator-Insulator Phase Transition of θ -(BDT-TTP) $_2\text{Cu}(\text{NCS})_2$:
 Strongly Correlated Two-Dimensional System -----77
 IV-B-5 Phase Transition in Narrow-band Organic Metals $(\text{BEDT-ATD})_2\text{X}(\text{solvent})$
 ($\text{X} = \text{PF}_6, \text{AsF}_6, \text{BF}_4$; solvent = THF, DHF, DO) -----78
 IV-B-6 Experimental and Theoretical Estimation of the Site-Energy Difference
 in $\text{Et}_4\text{N}(\text{DMTCNQ})_2$ -----78
 IV-B-7 κ' -(ET) $_2\text{Cu}_2(\text{CN})_3$ —Superconductor with Mixed $\text{Cu}_2(\text{CN})_3$ and $\text{N}(\text{CN})_2$ Ligands
 in the Anion Layer Studied by Polarized Reflection Spectroscopy -----79
 IV-B-8 Raman-active C=C Vibrations of κ -(BEDT-TTF) $_2\text{Cu}[\text{N}(\text{CN})_2]\text{Br}$
 and Its Deuterated Analogues -----79
 IV-B-9 Determination of the Charge on BEDO-TTF in Its Complexes by Raman Spectroscopy ----79
 IV-B-10 Re-examination of Bromide, Chloride and Iodide Salts
 of Bis(ethylenedioxy)tetrathiafulvalene (BEDO-TTF) by Spectroscopic Methods -----79
 IV-B-11 First Observation of the Plasmon Absorption by Reflection Spectroscopy
 in the Single Crystal of Two-dimensional Organic Metal -----80

IV-C Microscopic Investigation of Molecular-Based Conductors

- IV-C-1 Low-Temperature Electronic States in θ -(BEDT-TTF) $_2\text{RbZn}(\text{SCN})_4$:
 Competition of Different Ground States -----81
 IV-C-2 Magnetic Properties of a New Two-Chain Organic Conductor: (CPDT-STF)-TCNQ -----81
 IV-C-3 ESR and NMR Investigation of β' - $\text{R}_4\text{Z}[\text{Pd}(\text{dmit})_2]_2$ -----82
 IV-C-4 New Type Charge Localization in θ -(BEDT-TTF) $_2\text{CsZn}(\text{SCN})_4$ -----82

IV-D Thermodynamic Study of Organic Conductors

- IV-D-1 Electronic Ground States of $(\text{BEDT-TTF})_2\text{X}$ System
 Studied by Specific Heat Measurements -----83
 IV-D-2 Thermodynamic Investigation of the Electronic States
 of Deuterated κ -(BEDT-TTF) $_2\text{Cu}[\text{N}(\text{CN})_2]\text{Br}$ -----83
 IV-D-3 Electronic Specific Heat at the Boundary Region of Mott Transition
 in Two-Dimensional Electronic System of κ -(BEDT-TTF) $_2\text{Cu}[\text{N}(\text{CN})_2]\text{Br}$ -----84

IV-E Photoelectron Spectroscopy of Organic Solids in Vacuum Ultraviolet Region

- IV-E-1 Angle-Resolved Photoemission Spectra of ω -(*n*-pyrrolyl) Alkanethiol Self-Assembled
 Monolayers: Possible Assemblies of Substituent Pyrrole -----85
 IV-E-2 Structure of Copper- and H_2 -Phthalocyanine Thin Films on MoS_2
 Studied by Angle-Resolved Ultraviolet Photoelectron Spectroscopy
 and Low Energy Electron Diffraction -----85
 IV-E-3 Electronic Structure of Poly (1,10-Phenanthroline-3,8-diyl) and Its K-doped State
 Studied by Photoelectron Spectroscopy -----86
 IV-E-4 Electronic Structures of $\text{Alq}_3/\text{LiF}/\text{Al}$ Interfaces Studied by UV Photoemission -----86

IV-F Electrical Conduction and its Related Properties of Organic Solid

- IV-F-1 Three Component Organic Superconductors: Intercalation of KH into C_{60} -----86
 IV-F-2 Hydrogen Intercalation in Potassium- C_{60} -----86

IV-G Magnetism and Superconductivity of BETS Conductors

- IV-G-1 Chemical Control of Electrical Properties and Phase Diagram
 of a Series of λ -Type BETS Superconductors, λ - $\text{BETS}_2\text{GaBr}_x\text{Cl}_{4-x}$ -----87
 IV-G-2 Evidence for the First Order Transition between High-temperature Superconducting
 and Low-temperature Insulating Phases in λ - $\text{BETS}_2\text{Fe}_x\text{Ga}_{1-x}\text{Cl}_4$ ($x \approx 0.45$) -----87
 IV-G-3 Coexistence of Antiferromagnetically Ordered Fe^{3+} Spins and Metal π -Electrons
 in λ - $\text{BETS}_2\text{FeCl}_4$ -----88
 IV-G-4 Pressure-Induced Superconducting Transition of λ -(BETS) $_2\text{FeCl}_4$
 with π -d Coupled Antiferromagnetic Insulating Ground State at Ambient Pressure -----88

IV-G-5 Electric and Magnetic Properties of BETS Conductor with Modified λ -type Structure, λ' -BETS ₂ GaBr ₄ -----	89
IV-G-6 Antiferromagnetic Organic Metal Exhibiting Superconducting Transition, κ -(BETS) ₂ FeBr ₄ -----	89
IV-G-7 A New κ -Type Organic Superconductor Based on BETS Molecules, κ -(BETS) ₂ GaBr ₄ ----	90
IV-H Structural and Electrical Properties of Molecular Crystals at Low Temperature and/or High Pressure	
IV-H-1 Low Temperature Structure Analysis of Unannealed TDAE* <i>C</i> ₆₀ Single Crystal -----	90
IV-H-2 X-Ray Diffraction Study of a TDAE* <i>C</i> ₆₀ Single Crystal -----	91
IV-H-3 Structure Transformation of a <i>C</i> ₆₀ *Na _x (THF) _y below 70 K -----	91
IV-H-4 High Pressure Structure of [(C ₂ H ₅) ₂ (CH ₃) ₂ N][Pd(dmit) ₂] ₂ -----	92
IV-H-5 High-Pressure Four-Probe Resistivity Measurements of the Soft Organic Single Crystals up to 100 kbar -----	92
IV-H-6 Resistivity Behavior of Organic Conductor, β' -(BEDT-TTF) ₂ ICl ₂ up to 100 kbar -----	92
IV-I Development of New Molecular Conductors	
IV-I-1 New Stable Metallic Salt Based on a Donor Molecule Containing <i>peri</i> -Ditellurium Bridges, TMTTeN(SCN) _{0.88} -----	93
IV-I-2 Synthesis, Structures and Properties of New Organic Conductors Based on Tellurocycle-Fused TTF Donor Molecules -----	93
IV-I-3 New π -Extended Organic Donor Containing a Sable TEMPO Radical as a Candidate for Conducting-Magnetic Multifunctional Materials -----	94
IV-I-4 Synthesis and Properties of New Organic Donor Containing Two Sable TEMPO Radical Parts -----	94
IV-I-5 Origin of the High Electrical Conductivity of Neutral [Ni(ptdt) ₂] —A Route to Neutral Molecular Metal -----	95
IV-I-6 Structural, Electrical and Magnetic Properties of Low-dimensional Conductors Based on Unsymmetrical π Donor EDT-TTF and Analogous Selenium-substituted Molecules -----	95
IV-J Development of Pulsed Field Gradient NMR Spectroscopy	
IV-J-1 Self-diffusion Coefficients of a Reentrant Liquid Crystal CBOBP -----	96
IV-J-2 Self-diffusion Coefficients of OBBC and OBBF -----	96
IV-J-3 Self-Diffusion Coefficients of an Anti-Ferroelectric Liquid Crystal MHPOBC -----	97
IV-J-4 Self-diffusion Coefficients of a Hexatic Liquid Crystal PHOAB -----	97
IV-J-5 Calculation of Dipole Moments by MOPAC7 -----	97
IV-J-6 Measurement of Anisotropic Self-Diffusion Coefficient Tensors by PGSE-NMR -----	97
IV-K Phase Transitions and Dynamical Ordering in Liquid Crystals	
IV-K-1 A Bent and Asymmetrically Hindered Chiral Alkyl Chain of an Antiferroelectric Liquid Crystal as Observed by ² H NMR -----	97
IV-K-2 Experimental Spectroscopy of Liquid Crystals, No. 4-6. NMR Spectroscopy, Pt. 1-3 -----	98
IV-L Electronic Properties of Alkali-Hydrogen-Carbon Systems	
IV-L-1 NMR Study of Stage-6 Sodium-Hydrogen-Graphite Intercalation Compound -----	98
IV-L-2 <i>In-situ</i> NMR Study of the Reaction Process in Alkali-Hydrogen-Fullerene Systems -----	99
IV-L-3 Synthesis and NMR study of Alkali-Hydrogen-Single-Walled Carbon Nanotubes -----	100
IV-M Structural and Electronic Properties of New Carbon Materials	
IV-M-1 ¹³ C NMR Study of Single-Walled Carbon Nanotubes -----	100
IV-M-2 Dynamics of Water Molecules Confined in Activated Carbon Fiber -----	101
IV-N Structural and Electronic Properties of Fullerene-Based Compounds	
IV-N-1 Electronic Properties of Alkali-THF- <i>C</i> ₆₀ Single Crystals -----	102
IV-N-2 NMR Study of Sodium-THF- <i>C</i> ₆₀ Single Crystals -----	102
IV-N-3 Magnetic Behaviors of High-Temperature Reaction Products of Cerium Metal and <i>C</i> ₆₀ Solid -----	103
IV-N-4 Structure and Raman Scatterings of Cs ₃ <i>C</i> ₆₀ under High Pressure -----	104
IV-O Magnetic Local Structure and Magnetic Interactions in Molecule Based and Organic-Inorganic Hybrid Magnets	
IV-O-1 Solid State High Resolution Deuterium NMR Study of Electron Spin Density Distribution of Hydrogen-bonded Organic Ferromagnetic Compound 4-Hydroxyimino-TEMPO -----	105
IV-O-2 Magic Angle Spinning ¹ H-NMR Study of the Spin Density Distribution of Pyridyl Nitronyl Nitroxides in the Crystalline Phase -----	105
IV-O-3 Local Magnetic Structure of Layered Compounds Cu ₂ (OD) ₃ X with Exchangeable Acid Anion X Studied by Solid State High Resolution Deuterium NMR ----	106
IV-O-4 Solid State High Resolution NMR Studies of Electron Spin Densities in Charge-Transfer Complex-Based Organic Ferromagnets -----	106
IV-O-5 Variable Magnetism of Layer-Structured Compounds Cu ₂ (OD) ₃ X with Exchangeable Anion X: Magnetic Local Structure and Magnetic Interactions Determined by Solid-State High-Resolution Deuterium NMR -----	106

IV-P Proton Transfer Tunneling in Interacting Hydrogen Bonds in the Solid State	
IV-P-1 Proton Dynamics in Interacting Hydrogen Bonds in the Solid State: Proton Tunneling in the NHO Hydrogen Bonds of N,N'-Di(2-Hydroxy-1-Naphthylmethylene)-p-Phenylenediamine	107
IV-Q Systematic Study of Organic Conductors	
IV-Q-1 Structural Genealogy of BEDT-TTF-Based Organic Conductors I. Parallel Molecules: β and β'' Phases	108
IV-Q-2 Structural Genealogy of BEDT-TTF-Based Organic Conductors II. Inclined Molecules: θ , α , and κ Phases	108
IV-Q-3 $2k_F$ CDW Transition in β -(BEDT-TTF) $_2$ PF $_6$ Family Salts	109
IV-Q-4 Transport Properties of α'' -Phase Organic Conductors, (BEDT-TTF) $_2$ CsHg(SCN) $_4$ and (BEDT-TTF) $_2$ K $_{1.4}$ Co(SCN) $_4$	109
RESEARCH ACTIVITIES V	111
Department of Applied Molecular Science	
V-A Molecular Mechanisms of Oxygen Activation by Heme Enzymes	
V-A-1 Formation and Catalytic Roles of Compound I in the Hydrogen Peroxide-Dependent Oxidation by His64 Myoglobin Mutants	111
V-A-2 The Mechanisms of <i>N</i> -Demethylation Catalyzed by Heme Enzymes: Mechanisms of Sulfoxidation Catalyzed by High-Valent Intermediates of Heme Enzymes: Electron Transfer vs Oxygen Transfer Mechanism	111
V-A-3 Effects of the Arrangement of a Distal Catalytic Residue on Regioselectivity and Reactivity in the Coupled Oxidation of Sperm Whale Myoglobin Mutants	112
V-B Model Studies of Non-Heme Proteins	
V-B-1 A Model for Peroxo Intermediates in Reactions Catalyzed by Non-Heme Iron Enzymes	112
V-B-2 An Unusual Conversion of a Ni(III) $_2(\mu\text{-O})_2$ Core into a Ni(II) $_2(\mu\text{-OO})_2$ Core by H $_2$ O $_2$ and Oxygenation of Ligand	112
V-B-3 Structural and Functional Model Complexes for the Catechol-Bound Intermediate of Intradiol-Cleaving Catechol Dioxygenases	113
V-C Transition Metal Oxide Clusters	
V-C-1 Direct Observation by Electrospray Ionization Mass Spectrometry of a Key Intermediate in the Formation of a Double Bookshelf-Type Oxide Cluster	114
V-D Aqueous Organometallic Chemistry	
V-D-1 A Unique pH-Dependent Transfer Hydrogenation of Water-Soluble Carbonyl Compounds with an Organometallic Aqua Complex as a Catalyst Precursor in Water	114
V-E Synthesis of New High-spin Molecule	
V-E-1 Structure and Magnetic Property of the Organic Triradical with Triazine Skeleton; 1,3,5-Tris{ <i>p</i> -(<i>N</i> -oxy- <i>N</i> - <i>tert</i> -butylamino)-phenyl}triazine	115
V-F Construction of New Molecule-Based Magnets	
V-F-1 One-Dimensional Ferro- and Ferrimagnetic Chains Made up of an Alternating Array of 1,3-Bis(<i>N</i> - <i>tert</i> -Butyl- <i>N</i> -oxy-amino)-benzene Derivatives and Mn(II)(hfac) $_2$	115
V-F-2 Influence of the Thermal Excitations of the Ferrimagnetic ($1/2, 5/2, 1/2$) Linear Trimer on the Paramagnetic Behavior of the Layered Metal-Radical Complex {Mn(hfac) $_2$ } $_3$ (R $_N$) $_2$ $\cdot n$ -C $_7$ H $_{16}$	116
V-G Mn(II)-Induced Formation of a [3+3] Benzene Dimer Derivatives	
V-G-1 Mn(II)-Induced Formation and Structural Elucidation of a [3+3] Benzene Dimer Derivative from <i>m</i> -Phenylenebis(<i>N</i> - <i>tert</i> -butylaminoxyl)	117
V-H Synthesis of Chiral Molecule-Based Magnets	
V-H-1 A Chiral Molecule-based Metamagnet Made by a Chiral Triplet Organic Radical and Manganese Ion	117
V-H-2 Synthesis and Characterization of a Novel Chiral Molecular-based Ferrimagnet Prepared from a Chiral Nitronyl Nitroxide Radical and Manganese(II) Ion	118
V-I Synthesis and Characterization of Quantum-Spin Systems	
V-I-1 Magnetic Properties of Low Dimensional Quantum Spin Systems Made of Stable Organic Biradicals PNNNO, F $_2$ PNNNO and PIMNO	119
V-I-2 Construction of a Quantum-Spin System of $S = 1/2$ Antiferromagnetic Chain with the Next-Nearest-Neighbor Interactions	119
V-J Pressure Effects on Magnetic Materials	
V-J-1 Pressure-Induced Crossover from Alternating to Uniform Interaction in an $S = 1/2$ One-Dimensional Heisenberg Antiferromagnet	120
V-J-2 Pressure Effects on Organic Radicals with Ferromagnetic and Antiferromagnetic Interactions	120
V-J-3 Pressure Effect on Mn Complexes of Bisaminoxyl Radicals	120

V-J-4 The Magnetic Phase Diagram and Pressure Effect on the Magnetic Properties of the $Y_{1-x}Gd_xMn_2$ Intermetallic Compounds	121
V-J-5 Concentration and Pressure Dependence of the Magnetic Ordering in the $Y(Mn_{1-x}Me_x)_2$ Compounds with Me = Al, Fe and Ni	122
V-K Desorption Induced by Electronic Transitions at the Surface of van der Waals Condensates	
V-K-1 Absolute Measurement of Total Photo Desorption Yield of Solid Ne in Vacuum Ultraviolet Range	123
V-K-2 Desorption of an Excimer from the Surface of Solid Ne by Low Energy Electron or Photon Impact	123
V-L Synthesis and Physical Properties of Novel Molecular Metals	
V-L-1 (CPDT-STF)(TCNQ): A New Charge-Transfer Complex Metallic Down to Low Temperature	124
V-L-2 Structures and Electrical Properties of $(EO-TTP)_2AsF_6$	124
V-L-3 A Quasi Three-Dimensional Organic Conductor Based on a TTP Analogue Containing Thiopyran-4-ylidene	125
V-L-4 Structures and Properties of Organic Metals Based on Dimethyl Substituted TTP Analogue	125
V-L-5 Synthesis and Properties of Methylthio Substituted ST-TTP Derivatives	125
V-M Development of Model Core Potentials and Post Hartree-Fock Calculations to Atoms and Molecules	
V-M-1 Theoretical Study of Low-Lying Electronic States of TiCl and ZrCl	127
V-M-2 Benchmarking of Model Core Potentials: Application to the Group 4 Metal Halogen Complexes (MX_4 : M = Ti, Zr, Hf and X = F, Cl, Br, I)	127
V-M-3 Configuration Interaction Study of Differential Correlation Energies in Ca^+ , Ca and Ca^-	127
V-N Theoretical Study of the Electronic Structures of Weakly Bound Molecules	
V-N-1 <i>Ab initio</i> Study of the van der Waals Molecule ArHF	128
V-N-2 <i>Ab initio</i> Molecular Orbital Study of $Fe(CO)_n$ ($n = 1, 2$ and 3)	128
V-N-3 <i>Ab initio</i> Study on the Ground State of the C_3O_2 Molecule	128
V-N-4 On the Calculation of Binding Energy of the $(C_6H_6)^{3+}$ Ion	128
V-O Molecular Dynamics Study Using Potentials by <i>ab initio</i> Molecular Orbital Calculations	
V-O-1 Molecular Dynamics Study of Liquid Mercury in the Density Region between Metal and Nonmetal	129
V-O-2 The Liquid-Vapor Coexistence Curves of Fluid Mercury	129
V-P Millimeter-Wave Spectroscopy Combined with Pulsed-Jet Expansion Technique for the Detection of the Novel Unstable Species and the van der Waals Mode Transitions of Molecular Clusters	
V-P-1 Millimeter-Wave Spectroscopy of the van der Waals Bending Band of the ArDCN Cluster	131
V-P-2 Direct Observation of the van der Waals Bending Hot Bands of the Ar-HCN Cluster by Millimeter-Wave Spectroscopy	131
V-P-3 Submillimeter-Wave Spectroscopy of the van der Waals Bending Band of Ar-HBr	132
V-P-4 Millimeter-Wave Spectroscopy of the van der Waals Bending Band of OCO-HF with a Supersonic Jet Expansion Technique	133
V-Q Ion-Molecule Reactions in the Troposphere	
V-Q-1 Measurements of Mobility and Mass Spectra of Tropospheric Ions	134
RESEARCH ACTIVITIES VI	135

Department of Vacuum UV Photoscience

VI-A Electronic Structure and Decay Mechanism of Inner-Shell Excited Molecules	
VI-A-1 Partial Electron Yield Spectrum of N_2 : Doubly Excited States at the K-Shell Threshold	135
VI-A-2 Inner-Shell Excitation of PF_3 , PCl_3 , PCl_2CF_3 , OPF_3 and SPF_3	135
VI-A-3 The Sulphur 2p Photoabsorption Spectrum of NSF_3	135
VI-A-4 Jahn-Teller Effect and Rydberg-Valence Mixing in the $C1s \rightarrow 3p_{t2}$ and $3d_{t2}$ Rydberg Excited States of CH_4	135
VI-A-5 Renner-Teller Splitting in the $1s \rightarrow 1\pi_g^*$ Excited States of C_2H_2	136
VI-A-6 Enhancement of the $O1s \rightarrow ns\sigma_g$ Rydberg Series of CO_2 through the $5\sigma_g$ -Valence Mixing	136
VI-A-7 Vibronic Coupling and Valence Mixing in the $1s \rightarrow$ Rydberg Excited States of C_2H_2 in Comparison with N_2 and CO	136
VI-B Soft X-Ray Photoelectron-Photoabsorption Spectroscopy and Electronic Structure of Transition Metal Compounds	
VI-B-1 Ni 2p-3d Photoabsorption and Strong Charge Transfer Satellites in Divalent Ni Complexes with Molecular Ligands. Evaluation of π -Back Donation Based on the DFT Approach	137

VI-B-2 Ni-Ni Chemical Bond in $[\text{Ni}_2(\text{npy})_4\text{Br}_2][\text{B}(\text{C}_6\text{H}_5)_4]$ Studied by Linearly Polarized Ni 2p Photoabsorption	137
VI-B-3 Valence Band Excitation Observed in Resonant Soft X-Ray Emission Spectra of $\text{K}_2\text{Ni}(\text{CN})_4 \cdot \text{H}_2\text{O}$ at the Ni 2p Edge	137
VI-B-4 Resonant X-Ray Emission Spectra of $\text{K}_2\text{Ni}(\text{CN})_4 \cdot \text{H}_2\text{O}$ at the Ni 1s Edge	138
VI-C Generation of Ultrashort Optical Pulse for Time-Resolved Spectroscopy	
VI-C-1 Development of UV-Excited Transient Absorption Spectrometer Based on 10-fs Pulses	139
VI-C-2 Generation of Ultra-Short Pulses Using a Krypton Gas-Filled Hollow Fiber	139
VI-D Studies of Primary Photochemical/Physical Processes Using Femtosecond Fluorescence and Absorption Spectroscopy	
VI-D-1 Vibronic Relaxation of Polyatomic Molecule in Non-polar Solvent: Femtosecond Anisotropy/Intensity Measurements of the S_n and S_1 Fluorescence of Tetracene	140
VI-D-2 Determination of the Excited-State Transition-Moment Directions of 7-Azaindole Dimer by Femtosecond Fluorescence Anisotropy Measurements	142
VI-D-3 Investigation of Excited State Intramolecular Proton Transfer in Anthralin by Femtosecond Time-Resolved Fluorescence Spectroscopy	142
VI-D-4 Relaxation Kinetics of the S_n and S_1 States of Biphenyl Probed by Femtosecond Fluorescence Anisotropy	143
VI-D-5 Lifetime Measurements of S_2 Emission from Zinc(II) Porphyrins by the Femtosecond Up-Conversion Method	143
VI-D-6 Femtosecond Absorption Study on Ultrafast Decay Dynamics of Photoexcited $\text{Cu}(\text{II})(\text{TMpy-P4})$ in Water Solvent	144
VI-E Studies of Photochemical Reactions Using Picosecond Time-Resolved Vibrational Spectroscopy	
VI-E-1 Picosecond Time-Resolved Raman Study of Trans-Azobenzene	145
VI-E-2 Molecular Structure of S_1 Azobenzene: Vibrational Frequency of the NN Stretch Mode in the S_1 and S_0 State	146
VI-E-3 Observation of Resonance Hyper-Raman Scattering of <i>all-trans</i> Retinal	146
VI-F Synchrotron Radiation Stimulated Surface Reactions	
VI-F-1 Vibration Analysis of SiH_n Bending Modes on Hydrogenated Si(100) Surface Using Infrared Reflection Absorption Spectroscopy	148
VI-F-2 Scanning Tunneling Microscopy for the Study of the Synchrotron-Radiation Stimulated Processes; Synchrotron-Radiation Stimulated Desorption of SiO_2 Films on Si(111) Surface	148
VI-F-3 Synchrotron-Radiation Stimulated Desorption of SiO_2 Thin Films on Si(111) Surfaces Observed by Scanning Tunneling Microscopy	148
VI-F-4 Direct Observation of Synchrotron Radiation Stimulated Desorption of Thin SiO_2 Films on Si (111) by Scanning Tunneling Microscopy	149
VI-F-5 Scanning Tunneling Microscopy Study of Surface Morphology of Si(111) after Synchrotron Radiation Illumination	149
VI-F-6 Construction of the Multilayered-mirror Monochromator Beam Line for the Study of Synchrotron Radiation Stimulated Process	149
VI-F-7 Excitation Energy Dependence on Composition of an Al Deposited-thin Film Stimulated by Monochromatized SR	150
VI-F-8 SR-stimulated Etching and OMVPE Growth for Semiconductor Nano-structure Fabrication	150
VI-G Ion Desorption Induced by Core-Electron Transitions Studied by Electron Ion Coincidence Spectroscopy Combined with Synchrotron Radiation	
VI-G-1 Study of Ion Desorption Induced by a Resonant Core-Electron Transition of Condensed H_2O by Using Auger Electron Photoion Coincidence (AEPICO) Spectroscopy Combined with Synchrotron Radiation	151
VI-H Photoionization Dynamics Studied by Electron Spectroscopy Combined with a Continuous Synchrotron Radiation Source	
VI-H-1 Autoionization of a Dipole-Forbidden Superexcited State of CS_2	152
VI-I Laser Photoionization of Polarized Atoms Produced by Excitation with Synchrotron Radiation	
VI-I-1 Laser Photoionization Electron Spectroscopy of Polarized Rare Gas Atoms Excited with Synchrotron Radiation	153
VI-I-2 Theoretical Angular Distribution of Photoelectrons from Polarized Ar Atoms	153
VI-J Vacuum UV Spectroscopy Making Use of a Combination of Synchrotron Radiation and a Mode-Locked or Pulsed UV Laser	
VI-J-1 Improvement in the Energy Resolution of Laser Induced Fluorescence Excitation Spectroscopy of Ionic Species Produced by SR Photoexcitation	154
VI-J-2 Rotational State Distribution of N_2^+ Produced from N_2O	154
VI-K Monochromator Newly Developed on the Beam Line BL2B2 in UVSOR	
VI-K-1 First Performance Test of the 18 m-Spherical Grating Monochromator	155
VI-L Ultraviolet Photoelectron Spectroscopy on Organic Thin Films Using Synchrotron Radiation	

VI-L-1	Origin of Photoemission Intensity Oscillation of C_{60} -----	156
VI-L-2	Penning Ionization Electron Spectroscopy on Self-Assembled Monolayer of 1-Mercapto-8-Bromooctane on Au(111) -----	156
VI-L-3	Thickness-Dependent Orientation of the Pendant Phenyl Group at the Surface of Polystyrene Thin Films -----	156
VI-L-4	Structure of Copper- and H_2 -phthalocyanine Thin Films on MoS_2 Studied by Angle Resolved Ultraviolet Photoelectron Spectroscopy and Low Energy Electron Diffraction -----	156
VI-L-5	Electronic Structure of Poly(1,10-phenanthroline-3,8-diyl) and Its K-doped State Studied by Photoelectron Spectroscopy -----	157
VI-L-6	A Differential Thermal Analysis and Ultraviolet Photoemission Study on Surface Freezing of n-Alkanes -----	157
VI-L-7	Angle-Resolved UPS Studies of Organic Thin Films -----	157
VI-M	Thin Film Preparation of SiO_2 by Photo-Chemical Vapor Deposition Using Vacuum Ultraviolet Radiation	
VI-M-1	SiO_2 Thin Film Preparation Using Dielectric Barrier Discharge-Driven Excimer Lamps -	158
VI-M-2	SiO_2 Film Coatings with VUV Excimer Lamp CVD -----	158
VI-M-3	Thin Film Preparation Using Vacuum Ultraviolet Rare Gas Excimer Lamps -----	158
VI-M-4	Photo-Dissociation Process of Tetraethoxyorthosilicate (TEOS) Induced by Synchrotron Radiation -----	158
VI-N	Vacuum Ultraviolet Lasers and Their Applications to Surface Modification of Silica Glass	
VI-N-1	The State of the Art of Rare Gas Excimer Lasers and Lamps as a Light Source for Giga-Bit Lithography -----	159
VI-N-2	Radiation Effects of Vacuum Ultraviolet Lasers on Silica Glasses -----	159
VI-N-3	X-Ray Emission Spectroscopic Studies of Silicon Precipitation in Surface Layer of SiO_2 Induced by Argon Excimer Laser Irradiation -----	159
VI-N-4	Polycrystalline Silicon Precipitation on SiO_2 Using an Argon Excimer Laser -----	160
VI-O	Photo-Stimulated Luminescence as Data Storage in UV to Vacuum UV Regions	
VI-O-1	Response Characteristics of Imaging Plate in UV Region -----	160
VI-P	Nano-Structure Fabrication Using Synchrotron Radiation Stimulated Processing	
VI-P-1	Design and Construction of BL-4A2 Beam Line for Nano-Structure Processing -----	160
VI-Q	Desorption Induced by Electronic Transitions from Cryogenic Surfaces	
VI-Q-1	Desorption of Excimers from the Surface of Solid Ne by Low Energy Electron or Photon Impact -----	162
VI-Q-2	Photon Stimulated Ion Desorption from Solid Rare Gases in the Core Excitation Region -	162
VI-R	Structure and Vibrational Spectra of Molecules Physisorbed on Metal Surfaces	
VI-R-1	Upgraded Infrared Beamline BL6A1 at UVSOR -----	162
VI-R-2	Development of High Sensitivity EELS -----	163
VI-S	Structure and Vibrational Spectra of Molecules on Metal Surfaces	
VI-S-1	Adsorption Structures of NO on Pt(111) Investigated by Scanning Tunneling Microscopy	163
VI-S-2	Dynamical LEED Analyses of the Pt(111)-p(2 \times 2)-NO Structures -----	163
VI-T	Ultraviolet, Visible and Infrared Spectroscopy of Solids	
VI-T-1	Reconstruction of BL7B for UV, VIS and IR Spectroscopy with a 3 m Normal-Incidence Monochromator -----	164
VI-T-2	Absorption and Luminescence Spectra of Amorphous CdI_2 Thin Films -----	164
VI-T-3	Optical Study of the Metal-Nonmetal Transition in $Ni_{1-\delta}S$ -----	164
VI-U	Electronic Structure and Optical Properties of III-V Nitrides	
VI-U-1	Soft X-ray Absorption Study of III-V Nitrides -----	164
VI-V	Site-Specific Fragmentation Following Core-Level Photoexcitation	
VI-V-1	Site-Specific Phenomena in Si:2p Core-Level Photoionization of $X_3Si(CH_2)_nSi(CH_3)_3$ (X = F or Cl, n = 0–2) Condensed on a Si(111) Surface -----	166
VI-V-2	Ion Desorption Induced by Core-Electron Transitions Studied with Electron-Ion Coincidence Spectroscopy -----	166
VI-V-3	Development of Electron-Ion Coincidence Spectroscopy for Study of Surface and Vapor-Phase Dynamics -----	166
VI-W	Study on RF-Photocathode for Compact X-Ray Sources	
VI-W-1	Measurement of Quantum Efficiency of Cesium Telluride as a Photocathode -----	167
RESEARCH ACTIVITIES VII -----		169
Coordination Chemistry Laboratories		
VII-A	New Insight into Mechanism of Oxygen Activation in Biological Oxygenases	
VII-A-1	Important Role of Substrate in Activation of Dioxygen in Biological Oxygenases -----	169
VII-A-2	Structural Variety of Copper(II)-Peroxide Adducts and its Relevance to DNA Cleavage	170

VII-A-3 Mechanism of DNA Cleavage due to Green Cobalt(III)-Bleomycin Hydroperoxide Irradiated by Visible Light	170
VII-A-4 Selective Dioxygenation of Cyclohexane Catalyzed by Hydrogen Peroxide and Dinuclear Iron(III) Complexes with μ -Alkoxo Bridge	170
VII-A-5 Interaction between the Peroxide Ion and Acetate Moiety of the Ligand System in a Cobalt(II) Complex with a Binucleating Ligand	171
VII-A-6 Electrospray Mass Spectrometry of Peroxide Adduct of Monomeric Fe(III) Complex Containing Phenol Group	171
VII-A-7 High Activity of Binuclear Cobalt(II) Complex for Ethylene Evolution from 1-Aminocyclopropane-1-carboxylic Acid in the presence of Hydrogen Peroxide	172
VII-A-8 Oxygenation of Nucleosides by Peroxide Adduct of Binuclear Iron(III) Complex with a μ -Oxo Bridge	172
VII-B Electronic Structure and Reactivity of Metal Cluster Complexes	
VII-B-1 Synthesis, Structure and Redox Behavior of Tricobalt Cluster with Capping Benzyldiyne and Bridging halogen $[\text{Co}_3\text{Cp}_3(\mu_3\text{-CPh})_2(\mu\text{-X})]^+$ (X = Cl, Br, I)	173
VII-B-2 Bis- μ_3 -Benzyldiyne Tri(cyclopentadienylcobalt) Cluster with Edge-bridging Silver(I): Synthesis, Structure and Solution Properties of $[\text{Co}_3\text{Cp}_3(\mu_3\text{-CPh})_2\{\mu\text{-Ag(X)}\}]$ (X = CF_3CO_2 , NO_3) and $[\text{Co}_3\text{Cp}_3(\mu_3\text{-CPh})_2\{\mu\text{-Ag}(\text{NCCH}_3)\}]\text{PF}_6$	173
VII-C Bio-Inspired Molecular Architecture	
VII-C-1 Synthesis of a Novel Nucleoside for Alternative DNA Base Pairing through Metal Complexation	175
VII-C-2 An Approach to Metal-Assisted DNA Base Pairing: Novel β -C-Nucleosides with a 2-Aminophenol or a Catechol as the Nucleobase	175
VII-C-3 Cyclic Metallopeptides, <i>cyclo</i> [-Gly-L-Cys(terpyPt ^{II})] _n Cl _n	176
VII-C-4 Construction of a Unique Alternating-Chain Array with Copper(II) and a New Diazamesocycle Bearing One Functional Pendant	176
VII-C-5 Spontaneously Resolved Chiral Molecular Box: A Cyclic Tetranuclear Zn(II) Complex with DPTZ (DPTZ = 3,6-Di-2-Pyridyl-1,2,4,5-Tetrazine)	176
VII-D Research on the Relationship between Structure of Vanadyl Complex and Insulin-Mimetic Activity	
VII-D-1 Syntheses, Structure, and Insulin-like Activities of Oxovanadium (IV) Complexes with Tetra- and Penta-Dentate Histidine Derivatives	177
VII-D-2 Insulin-Mimetic Vanadyl-Dithiocarbamate Complexes	177
VII-D-3 A New Insulin-mimetic Vanadyl Complex, (<i>N</i> -Pyridylmethylaspartate) Oxovanadium (IV) with VO(N_2O_2) Coordination Mode, and Evaluation of its Effect on Uptake of <i>D</i> -Glucose by Ehrlich Ascites Tumor Cells	177
VII-E Syntheses of Transition Metal-Sulfur Clusters and Development of Their Catalysis	
VII-E-1 Syntheses and Structures of Mixed-Metal Sulfido Clusters Containing Incomplete Cubane-Type $\text{M}_2\text{M}'\text{S}_4$ and Cubane-Type $\text{M}_2\text{M}'_2\text{S}_4$ Cores (M = Mo, W; M' = Rh, Ir)	178
VII-E-2 Synthesis and Reactivities of Ir ₂ Ru Heterobimetallic Sulfido Clusters Derived from a Hydrogensulfido-Bridged Diiridium Complex	178
VII-E-3 Formation of Linear Tetradentate Phosphine Ligand <i>o</i> -C ₆ H ₄ (PPhCH ₂ CH ₂ PPh ₂) ₂ by Coupling of Two Diphosphine Ligands Bound to Low-Valent Mo or W Center. Synthesis and Structure of $[\text{M}\{o\text{-C}_6\text{H}_4(\text{PPhCH}_2\text{CH}_2\text{PPh}_2)_2\}(\text{Ph}_2\text{PCH}_2\text{CH}_2\text{PPh}_2)]$ (M = Mo, W)	178
VII-F Activation of Carbon Dioxide and Creation of Reactive Hydroxy- and Oxo-metal Complexes through Activation of Water Molecules on Metals	
VII-F-1 Stabilization of $[\text{Ru}(\text{bpy})_2(\text{CO})(\eta^1\text{-CO}_2)]$ and Unprecedented Reversible Oxide Transfer Reactions from CO_3^{2-} to $[\text{Ru}(\text{bpy})_2(\text{CO})_2]^{2+}$ and from $[\text{Ru}(\text{bpy})_2(\text{CO})(\eta^1\text{-CO}_2)]$ to CO_2	179
VII-F-2 First Artificial Energy Conversion from Proton Gradient to Electricity	179
VII-F-3 Two-Electron Reduction of $[\{(\text{bpy})_2\text{Ru}(\text{dmbbbpy})\}_3\text{Ru}]^{8+}$ from (BNA) ₂ via Photoinduced Electron Transfer [dmbbbpy = 2,2'-Bis(<i>N</i> -Methylbenzimidazole-2-yl)-4,4'-bipyridine]	180
VII-F-4 Selective Production of Acetone in Electrochemical Reduction of CO_2 Catalyzed by Ru-naphthyridine Complex	180
VII-F-5 Basicity of $\mu_3\text{-X}$ and $\eta^1\text{-Y}$ Ligands (X, Y = S, Se) of Reduced, Oxidized and Super-Oxidized Forms of $[\text{Fe}_4\text{X}_4(\text{YAd})_4]^{2-}$ (Ad = 1-Adamantane) in Aqueous Solutions	180
VII-F-6 Double Addition of CO_2 and CH_3OH to Ruthenium Carbonyl Complex with Novel Mono-Dentate Dithiolene	181
VII-G Molecular Self-assembly Through Coordination	
VII-G-1 Encapsulation of Large, Neutral Molecules in a Self-Assembled Nanocage Incorporating Six Palladium(II) Ions	182
VII-G-2 "Ship-in-a-Bottle" Formation of Stable Hydrophobic Dimers of <i>cis</i> -Azobenzene and -Stilbene Derivatives in a Self-assembled Coordination Nanocage	182
VII-G-3 A Nonometer-Sized Hexahedral Coordination Capsule Assembled from 24 Components	182

VII-G-4 Spontaneous Assembly of Ten Components into a Two Interlocked, Identical Coordination Cages -----	182
VII-G-5 Quantitative Formation of Coordination Nanotubes Templated by Rod-like Guests -----	183
VII-G-6 Guest-Selected Formation of Pd(II)-Linked Cages from a Prototypical Dynamic Library	183
VII-G-7 Quantitative and Spontaneous Formation of a Doubly Interlocking [2]Catenane using Copper(I) and Palladium(II) as Templating and Assembling Centers -----	184
VII-G-8 Flexible Coordination Networks with Fluorinated Backbones. Remarkable Ability for Made-to-Order Enclathration of Organic Molecules -----	184
VII-G-9 Kinetic and Thermodynamic Aspects in the Substrate-Induced Assembly of Optimal Receptors from a Dynamic Library -----	184
VII-G-10 Dynamic Behavior of Rod-like Guest Accommodated in Coordination Nanotubes -----	184
VII-G-11 Wacker Oxidation in an Aqueous Phase Through the Reversed Phase-Transfer Catalysis of a Self-Assembled Nanocage -----	185
VII-G-12 Hydrophobic Assembling of a Coordination Nanobowl into a Dimeric Capsule Which can Accommodate upto Six Large Organic Molecules -----	185
VII-G-13 Porous Coordination Polytubes -----	185
VII-G-14 X-Ray And NMR Observation of Encapsulated Molecules in a Self-Assembled Coordination Nanocage -----	186
VII-H Synthesis and Reactivity of Complexes Containing Peculiar Bonds between Transition Elements and Main Group Elements	
VII-H-1 Fluxional Behavior of Alkoxy-Bridged Bis(silylene)ruthenium Complexes Cp*(Me ₃ P)Ru{SiMe ₂ ...O(R)...SiMe ₂ } (R = Me, 'Bu) Caused by Rotation of the Silylene Ligands -----	187
VII-H-2 Preparation of Silanediyl-Bridged Fe-Fe and Fe-W Dinuclear Complexes. X-Ray Structures of [Cp*Fe(CO)(μ-CO){μ-Si(H)CHPh ₂ }(CO) _n MCp] (Cp* = C ₅ Me ₅ , Cp = C ₅ H ₅ , M = Fe, n = 1; M = W, n = 2) -----	187
VII-H-3 Extremely Facile Arene Exchange on a Ruthenium(II) Complex Having a Novel Bis(silyl) Chelate Ligand (9,9-Dimethylxanthene-4,5-diyl)bis(dimethylsilyl) (Xantsil) -----	188
VII-H-4 Synthesis and Structures of Heterometallic Trinuclear Clusters [CpFe(CO) ₂] ₂ (μ ₃ -S ₂)W(CO) ₅ and Cp ₂ Fe ₂ (CO) ₂ (μ-CO)(μ ₃ -S)W(CO) ₅ and Kinetic Study of Migration of the W(CO) ₅ Moiety in the Disulfido Complex -----	188
RESEARCH ACTIVITIES VIII -----	189
Computer Center	
VIII-A Theoretical Studies on Electronic Structure and Dynamics of Electronically Excited States in Polyatomic Molecules	
VIII-A-1 Theoretical Study on the Spectroscopy and Dynamics of Electronically Excited States of HCP Molecule -----	189
VIII-A-2 Development of <i>Ab Initio</i> MD Method Based on the Direct Evaluation of CAS-SCF Energy Derivatives -----	189
VIII-A-3 Theoretical Study on the Unimolecular Reaction Dynamics of Acetyl Radical CH ₃ CO → CH ₃ + CO -----	189
VIII-A-4 <i>Ab Initio</i> Molecular Orbital Studies of Isomerization Reaction from c-OSiH ₂ O to t-OSiHOH -----	189
VIII-A-5 <i>Ab Initio</i> Study of PH ₂ + O ₂ Reaction Relevant to the PH ₃ Combustion -----	190
VIII-A-6 Semiclassical Study of Nonintegrable Systems -----	190
VIII-A-7 A Theoretical Study on Structures and Vibrational Spectra of C ₈₄ Fullerene Isomers ----	190
Laser Research Center for Molecular Science	
VIII-B Developments of Advanced Lasers for Chemical Reaction Controls and ZEKE Photoelectron Spectroscopy	
VIII-B-1 Developments of Liquid Crystal Spatial Light Modulator -----	191
VIII-B-2 ZEKE Electron Spectroscopy of Azulene and Azulene-Argon -----	191
VIII-C Developments and Researches of New Laser Materials	
VIII-C-1 Intense THz Radiation from Femtosecond Laser Pulses Irradiated InAs in a Strong Magnetic Field -----	192
VIII-C-2 High-Repetition-Rate, High-Average-Power Mode-Locked Ti:sapphire Laser with an Intracavity cw-Amplification Scheme -----	192
VIII-C-3 Compact THz-radiation Source Consisting of a Bulk Semiconductor, a Mode-Locked Fiber Laser, and a 2-T Permanent Magnet -----	192
VIII-C-4 Spectrum Control of THz Radiation from InAs in a Magnetic Field by Duration and Frequency Chirp of the Excitation Pulses -----	193

VIII-C-5 LiCAF Crystal as a New Vacuum Ultraviolet Optical Material with Transmission down to 112 nm	193
VIII-D Development and Research of Advanced Tunable Solid State Lasers	
VIII-D-1 Frequency-Doubled Tunable Yb:YAG Microchip Laser for Holographic Volume Memories	195
VIII-D-2 Design Criteria for Optimization of Fiber-Coupled Diode Longitudinally-Pumped Laser Using Pump-beam M_2 Factor	195
VIII-D-3 Highly Nd^{3+} -Doped YAG Ceramic for Microchip Lasers	196
VIII-D-4 Nondestructive Characterization of Quasi-Phase-Matched Wavelength Converter	196

Research Center for Molecular Materials

VIII-E Development of Novel Heterocyclic Compounds and their Molecular Assemblies for Advanced Materials	
VIII-E-1 Cation Radical Salts of TTF Vinylogues with $\text{Au}(\text{CN})_2$ Anion	197
VIII-E-2 Control of Packing Mode in Crystals of Cation Radical Salts of TTF Vinylogues	197
VIII-E-3 Non-Planar BEDT-TTF Derivatives Fused with Tetrahydrofuran Rings Affording Cation Radical Salts with Unusual Structures	198
VIII-E-4 Bithiophene-TCNQ Analogue with Fused 1,2,5-Thiadiazole Rings	198
VIII-E-5 First Stable Tetracyanodiphenoquinodimethane with a Completely Planar Geometry: Preparation, X-Ray Structure, and Highly Conductive Complexes of Bis[1,2,5]thiadiazolo-TCNDQ	199
VIII-E-6 Novel Supramolecular Synthon in Crystal Engineering: Ionic Complexes of 4,4'-Bipyridine and 1,2-Bis(2-pyridyl)ethylene with 2,5-Dichloro-3,6-dihydroxy-1,4-benzoquinone	199
VIII-E-7 Design and Synthesis of Soluble Linear Macromolecules with Highly Extended π -Conjugated Backbone	200
VIII-F Electronic Structures and Rectivities of Active Sites of Metalloproteins	
VIII-F-1 High-Spin (<i>meso</i> -Tetraalkylporphyrinato)iron(III) Complexes As Studied by X-ray Crystallography, EPR, and Dynamic NMR Spectroscopies	201
VIII-F-2 Insensitivity of Vanadyl-Oxygen Bond Strengths to Radical Type ($^2\text{A}_{1\text{u}}$ vs. $^2\text{A}_{2\text{u}}$) in Vanadyl Porphyrin Cation Radicals	201
VIII-F-3 Electron Configuration of Ferric Ions in Low-Spin (Dicyano)(<i>meso</i> -tetraarylporphyrinato)iron(III) Complexes	201
VIII-F-4 Resonance Raman Spectra of Legitimate Models for the Ubiquitous Compound I Intermediates of Oxidative heme Enzymes	202
VIII-F-5 Newly Designed Iron-Schiff Base Complexes as Models of Mononuclear Non-Heme Iron Active Sites	202
VIII-F-6 ^{17}O -NMR Study of Oxygen Molecules Bound to Copper Ions of Mononuclear and Dinuclear Copper Complexes	202
VIII-G Molecular Mechanism of Heme Degradation and Oxygen Activation by Heme Oxygenase	
VIII-G-1 Molecular Oxygen Oxidizes the Porphyrin Ring of the Ferric α -Hydroxyheme in Heme Oxygenase in the Absence of Reducing Equivalent	203
VIII-H Designing Artificial Photosynthesis at Molecular Dimensions	
VIII-H-1 Synthesis and Characterization of Manganese Complexes	204
VIII-H-2 Synthesis and Photochemical Reaction of Porphyrin/Cobalt-complex Dyad Molecules	204
VIII-I Development of New Metal Complexes as Redox Catalysts	
VIII-I-1 Synthesis of Terpyridine-catechol Linked Ligands and Their Cobalt(III) Complexes	205
VIII-J Organic Molecular Materials with Novel Electronic Properties	
VIII-J-1 Synthesis and Electron-Transporting Properties of Perfluorinated Decaphenylenes	206
VIII-K The Effects of the 2D Spin-Echo NMR Pulse Sequence on Homonuclear Spin Systems	
VIII-K-1 Novel Satellites in a Two-Dimensional Spin-Echo NMR Spectrum for a Homonuclear Spin-1/2 Pair in Rotating Solids	207

Equipment Development Center

VIII-L Development of "IMS Machines"	
VIII-L-1 Surface Profiler of Mirrors for High-Resolution Monochromator	208
VIII-L-2 Preparation and Transfer System for Ice-Embedding Sample	209
VIII-M Development of New Laser Materials	
VIII-M-1 Amplification of Impurity-Associated Auger-Free Luminescence in Mixed Rubidium-Caesium Chloride Crystals under Core-Level Excitation with Undulator Radiation	209

Ultraviolet Synchrotron Orbital Radiation Facility

VIII-N Development of the UVSOR Light Source	
VIII-N-1 Influence of Electron Beam Properties on Spontaneous Radiation from an Optical Klystron	210

VIII-O Researches by the USE of UVSOR

VIII-O-1 Nano-Second Desorption of Alkali Fluorides Excited by Synchrotron Radiation Pulses	210
VIII-O-2 Photo-Induced Change in Semiconductor-Vacuum Interface of p-GaAs(100) Studied by Photoelectron Spectroscopy	210
VIII-O-3 Electronic Structures of Organic Salts DMTSA-BF ₄ Using Photoelectron Spectromicroscopy	210
VIII-O-4 Photoemission Study of Si(111) Clean Surfaces at High Temperature Using Laser Annealing	211
VIII-O-5 Behavior of the "6eV Satellite" in Ni Thin Film Observed by Valence Band Photoemission	211
VIII-O-6 Magnetic Stability of Co-Film Grown on Oxygen-Rich Cu(001) Surface	212
VIII-O-7 Thickness Dependent Oxidization of Co Films and Observation of Different CoO Phases	213
VIII-O-8 Satellite Structure Observed in 2p XPS of Co Thin Film	213
VIII-O-9 Design Study for a Varied-Line-Spacing Plane Grating Monochromator	214
VIII-O-10 Photodissociation of Ozone in the K-Edge Region	214
VIII-O-11 Infrared Magnetic Circular Dichroism of Strongly Correlated 4f Electron Systems with Synchrotron Radiation	215
VIII-O-12 Optical Conductivity of the Kondo Insulator YbB ₁₂ : Gap Formation and Low-Energy Excitations	215

RESEARCH FACILITIES -----217

Computer Center	217
Laser Research Center for Molecular Science	217
Research Center for Molecular Materials	217
Equipment Development Center	217
Ultraviolet Synchrotron Orbital Radiation Facility	218

SPECIAL RESEARCH PROJECTS -----221**(1) Development of Microscopic Environments with Functionality and Quantum Steering for Reactions**

Structures, Reactions and Spectroscopies of Molecules and Clusters	221
Folding Mechanism of Protein Molecules Studied by Generalized-Ensemble Algorithms	221
Studies of Nonadiabatic Transitions, Chemical Reaction Dynamics, and Their Control	221
The 5th- and 7th-order 2D Raman Spectroscopy for Intramolecular Vibrational Modes	222
Constructing Molecular Theory of Chemical Process in Solution	222
(1) Studies on Laser Cooling and Trapping of Neutral Atoms	222
(2) Laser Spectroscopic Studies of Atoms and Ions in Liquid Helium	222
Time-Resolved Resonance Raman Study on Mechanisms of Oxygen Reduction by Cytochrome <i>c</i> Oxidase	222
Laser Raman Beat Detection of Magnetic Resonance	223
Environment Dependent Association of Acetic Acid in Liquid Phase	223
Higher Vibrational States of Molecules and Clusters as Studied by Nonresonant Ionization Detected IR Spectroscopy	223
Imaging of Chemical Dynamics	224
Theoretical Study on the Electronic Structures of Atoms, Molecules, and Clusters	224
Supersonic Jet Submillimeter-Wave Absorption Spectrometer with Backward Wave Oscillator	224
Experimental Study of Ion-Induced Nucleation	225
Time-Resolved Spectroscopic Study of Photochemical Dynamics in Condensed Phase	225
SR-Pump and Laser-Probe Experiments for the Photofragmentation Dynamics of Atoms and Molecules	225
Vibrational Spectroscopy on Cryogenic Surfaces Using Synchrotron Radiation	226
Similarity Transformed Preconditioners for Green Function Evaluation in Cumulative Reaction Probability Calculations	226
Developments of Advanced Lasers for Chemical Reaction Controls	226
Developments and Researches of New Laser Materials	226
Development and Research of Advanced Tunable Solid State Lasers	227
UHV Tribometer	227
Investigation of Dynamics on photo-excited Solids and Surfaces by Using Synchrotron Radiation	227
Non-Linear Phenomena and Related Beam Physics in Storage Ring Free Electron Lasers	227
Photoelectron Spectroscopy Studies of Solids, Surfaces and Interfaces	228

(2) Study of Molecular Solid toward Molecular Electronics

Theory of Electronic Phases in Molecular Conductors and Insulators: Electron Correlations and Dimensional Crossovers	229
---	-----

π -d Interaction in Molecular Metals	229
Search for Negative- <i>U</i> Materials in Molecular Solid	229
Investigation of Novel Electronic Phases in Molecular-Based Conductors	230
Development and Solid State Properties of New Organic Conductors	230
NMR Studies of Liquid Crystals	230
Construction and Characterization of Chiral Molecule-Based Magnets in a Systematic Way	231
Studies on Electronic States of Organic Thin Films by Angle-Resolved UPS	231
New Advanced Organic Materials Based on Novel Heterocyclic Compounds	232
Design and Synthesis of New Tellurium-Containing Donors	232
(3) Material Control in Multi-Reaction Centers	
Asymmetric Oxidation Catalyzed by Myoglobin Mutants	233
Bio-Inspired Molecular Architecture	233
Activation of Carbon Dioxide Directed Toward Carbon-Carbon Bond Formation and Energy Conversion from Proton Gradients to Electricity	233
Self-Assembling Molecular Systems	234
Molecular Mechanism of Oxygen Activation by Metalloenzymes	235
Generation of Reactive Species via Electron Transfer on Metal Complexes, as Basis of Chemical Energy Conversion Systems	235
OKAZAKI CONFERENCES	237
JOINT STUDIES PROGRAMS	241
(1) Special Projects	
(2) Research Symposia	
(3) Cooperative Research	
(4) Use of Facility	
(5) UVSOR	
FOREIGN SCHOLARS	245
AWARDS	249
LIST OF PUBLICATIONS	251
REVIEW ARTICLES AND TEXTBOOKS	269
AUTHOR INDEX	273

Abbreviations

IMS: Institute for Molecular Science
GUAS: The Graduate University for Advanced Studies

ORGANIZATION AND STAFF

Organization

The Institute for Molecular Science comprises twenty three research laboratories — each staffed by a professor, an associate professor, two research associates and several technical associates —, two research laboratories with foreign visiting professors, and five research facilities.

The laboratories are grouped into six departments and one facility for coordination chemistry:

Department of Theoretical Studies	Theoretical Studies I Theoretical Studies II Theoretical Studies III ¹⁾ Theoretical Studies IV
Department of Molecular Structure	Molecular Structure I Molecular Structure II ¹⁾ Molecular Dynamics
Department of Electronic Structure	Excited State Chemistry Excited State Dynamics Electronic Structure ¹⁾ Molecular Energy Conversion ²⁾
Department of Molecular Assemblies	Solid State Chemistry Molecular Assemblies Dynamics Molecular Assemblies ¹⁾
Department of Applied Molecular Science	Applied Molecular Science I Applied Molecular Science II ¹⁾ Molecular Clusters ³⁾
Department of Vacuum UV Photoscience	Photochemistry Chemical Dynamics Interface Molecular Science ³⁾
Coordination Chemistry Laboratories	Synchrotron Radiation Research ²⁾ Synthetic Coordination Chemistry ³⁾ Complex Catalysis Functional Coordination Chemistry Coordination Bond ¹⁾

The research facilities are:

Computer Center	Advanced Lasers for Chemical Reaction Studies
Laser Research Center for Molecular Science	Advanced Lasers for Synchrotron Radiation Applications Advanced UV and IR Tunable Lasers
Research Center for Molecular Materials	Organic Materials Section Hybrid Materials Section Materials Characterization Section Structure Control Section
Equipment Development Center	
UVSOR (Ultraviolet Synchrotron Orbital Radiation) Facility	

1) Professors and associate professors are visiting professors from other universities.

2) Research laboratories with foreign visiting professors.

3) Professors, associate professors, and research associates, along with their positions, are transferred from other universities.

Scientific Staff

KAYA, Koji

Professor, Director-General

Emeritus Professors

NAGAKURA, Saburo

President, The Kanagawa Academy of Science and Technology

HIROTA, Eizi

President, The Graduate University for Advanced Studies

KIMURA, Katsumi

MOROKUMA, Keiji

Professor, Emory University, U.S.A.

INOKUCHI, Hiroo

Distinguished Research Consultant, Institute for Molecular Science

MARUYAMA, Yusei

Professor, Hosei University

YOSHIHARA, Keitaro

Professor, Japan Advanced Institute of Science and Technology

HANAZAKI, Ichiro

Professor, Hiroshima University

IWAMURA, Hiizu

Professor, National Institute for Academic Degrees

Department of Theoretical Studies

Theoretical Studies I

IWATA, Suehiro

Professor

OKAMOTO, Yuko

Associate Professor

IKEGAMI, Tsutomu

Research Associate

SUGITA, Yuji

Research Associate

TSURUSAWA, Takeshi

Technical Associate

KOVALENKO, Andriy F.

Research Associate of Research for the Future Program

NISHIKAWA, Takeshi

Research Associate of Research for the Future Program (October '98–)

ITOH, Masakatsu

Research Associate of Research for the Future Program (April '99–)

CHEN, Feiwu

IMS Fellow (–March '99), Research Fellow (April '99–)

BAECK, Kyong-Koo

Visiting Scientist (from Kang-Nung National University, Korea); MONBUSHO Invited Fellow (December '98–February '99)¹⁾

SUTCLIFFE, Brian T.

Visiting Scientist (from University of York, UK);

MONBUSHO Invited Fellow (March–June '99)²⁾

LEE, Sang Yeon

Visiting Scientist (from Kyungpook National University, Korea); MONBUSHO Invited Fellow (July–August '99)³⁾

SATOH, Katsuhiko

JSPS Post-Doctoral Fellow

HIRATA, So

Graduate Student (–September '98), JSPS Post-Doctoral Fellow (October '98–March '99)⁴⁾

HASHIMOTO, Tomohiro

Research Fellow (April '99–)

BANDYOPADHYAY, Pradipta

Graduate Student (–March '99)⁵⁾

MITSUTAKE, Ayori

Graduate Student

SUZUKI, Tadayoshi

Graduate Student (–March '99)

OHTSUKA, Hiroshi

Graduate Student

OKADA, Kazutoshi

Graduate Student

NELSON, Alistair David

Graduate Student (from University of Edinburgh, UK)* (July–August '99); MONBUSHO Research Fellowship⁶⁾

ENGLAND, James Arthur

Graduate Student (from University of Surrey, UK)* (July–August '99); MONBUSHO Research Fellowship⁷⁾

Theoretical Studies II

NAKAMURA, Hiroki

Professor

TANIMURA, Yoshitaka

Associate Professor

ZHU, Chaoyuan

Research Associate

OKUMURA, Ko

Research Associate

SUZUKI, Yoko

Technical Associate

MIYAZAKI, Kunimasa

IMS Fellow

MARUYAMA, Yutaka

Graduate Student (–September '98), Research Fellow (October '98–December '98), IMS Fellow (January–March '99)⁸⁾

MISHIMA, Kenji
OSHEROV, Vladimir Iosifovich

SHIN, Seokmin

MIL'NIKOV, Gennady V.

USHAKOV, Valdimiv G.

HORACEK, Jiri

IMAMURA, Yutaka

TERANISHI, Yoshiaki
PICHL, Lukas
NAGAYA, Kuninobu
KAMISAKA, Hideyuki
HINO, Osamu

Theoretical Studies III

IKEDA, Kensuke

TANAKA, Hideki
KIMURA, Mineo

HASHIMOTO, Kenro

TEN-NO, Seiichiro
NOBUSADA, Katsuyuki

Theoretical Studies IV

HIRATA, Fumio
TEMBE, Bhalachandra Laxmanrao

YONEMITSU, Kenji
SATO, Hirofumi
KISHINE, Jun-ichiro
ASHOK, Sethia
KUWABARA, Makoto
AKIYAMA, Ryo
OGAWA, Takuhiro
MORI, Michiyasu
IMAI, Takashi
HARANO, Yuichi
YAMAZAKI, Takeshi
MIYASHITA, Naoyuki

Department of Molecular Structure

Molecular Structure I

SAITO, Shuji
MORITA, Norio
MORIWAKI, Yoshiki
FUJIWARA, Hideo
KUMAKURA, Mitsutaka
KOBAYASHI, Kaori
WHITHAM, Christopher, J.

TAMASSIA, Filippo

ARAKI, Mitsunori

Molecular Structure II

TANIMOTO, Mitsutoshi

IMS Fellow (April '99–)
Visiting Scientist (from Russian Academy of Sciences, Russia) (December '98–March '99)⁹⁾
Visiting Scientist (from Seoul National University, Korea);
MONBUSHO Invited Fellow (January–March '99)¹⁰⁾
Visiting Scientist (from Institute of Structural Macrokinetics, Russia); JSPS Post-Doctoral Fellow (March '99–)¹¹⁾
Visiting Scientist (from Russian Academy of Sciences, Russia); (February–March '99)¹²⁾
Visiting Scientist (from Charles University, Czech Rep.) (July '99)¹³⁾
Graduate Student (–March '99), JSPS Post-Doctoral Fellow (April '99–)
Graduate Student (–March '99)¹⁴⁾
Graduate Student
Graduate Student
Graduate Student
Graduate Student

Visiting Professor (from Ritsumeikan University) (–March '99)
Visiting Professor (from Okayama University) (April '99–)
Visiting Associate Professor (from Yamaguchi University) (–March '99)
Visiting Associate Professor (from Tokyo Metropolitan University) (April '99–)
Research Associate (–August '99)¹⁵⁾
Research Associate (–December '98)¹⁶⁾

Professor
Visiting Professor (from I. I. T. Bombay, India) (November '98–March '99)¹⁷⁾
Associate Professor
Research Associate
Research Associate
IMS Fellow
IMS Fellow
JSPS Post-Doctoral Fellow
JSPS Post-Doctoral Fellow (–March '99)
JSPS Post-Doctoral Fellow
Graduate Student
Graduate Student (from Kobe University)*
Graduate Student (April '99–)
Graduate Student (April '99–)

Professor (–March '99)¹⁸⁾
Associate Professor
Research Associate
Research Associate (–April '99)¹⁹⁾
Technical Associate
Technical Associate (–April '99)²⁰⁾
Visiting Scientist (from Physical and Theoretical Chemistry Laboratory, U.K.) (October '98–March '99)²⁰⁾
Visiting Scientist (from Physical and Theoretical Chemistry Laboratory, U.K.) (August–September '99)²¹⁾
Graduate Student (–March '99)²²⁾

Visiting Professor (from Shizuoka University) (–March

AKASAKA, Takeshi
TSUBAKI, Motonari

OZEKI, Hiroyuki

Molecular Dynamics

KITAGAWA, Teizo
KATO, Tatsuhisa
MATSUSHITA, Michio
MIZUTANI, Yasuhisa
HAYASHI, Naoki
NAGATOMO, Shigenori
UESUGI, Yuki
UCHIDA, Takeshi

PRONIEWICZ, Leonard M.

KIM, Younkyoo

NAKUL, Chandra M.

HU, Ying

CHU, Grace C.

IWASE Tadashi

AKI, Michihiko
YAMAMOTO, Kohji
HARUTA, Nami
OKUNO, Daichi
OKUBO, Shingo

Department of Electronic Structure

Excited State Chemistry

NISHI, Nobuyuki
WATANABE, Kazuya
NAKABAYASHI, Takakazu
WATANABE, Kazuo
ANAZAWA, Toshihisa
KOSUGI, Kentaroh
OHTA, Michiharu
KODAMA, Yoichi

Excited State Dynamics

FUJII, Masaaki
MÜLLER-DETHLEFS, Klaus

SUZUKI, Toshinori
CHOI, Jong-Ho

KOHGUCHI, Hiroshi
SAKAI, Makoto
KATAYANAGI, Hideki
SAEKI, Morihisa
MO, Yuxiang
WANG, Li

SHIBATA, Takeshi
ISHIUCHI, Shun-ichi
YOKOYAMA, Hiroshi

'99)²³⁾

Visiting Professor (from Niigata University) (April '99–)
Visiting Associate Professor (from Himeji Institute of
Technology)

Research Associate (–March '99)²⁴⁾

Professor

Associate Professor

Research Associate

Research Associate

Technical Associate

Technical Associate

IMS Fellow (–March '99)²⁵⁾

IMS Fellow (–March '99), JSPS Post-Doctoral Fellow (April
'99–)

Visiting Scientist; MONBUSHO Invited Fellow (from
Jagiellonian University, Poland) (December '98–March
'99)²⁶⁾

Visiting Scientist; MONBUSHO Invited Fellow (from
Hankuk University of Foreign Studies, Korea) (June '99–)

Visiting Scientist; JSPS Post-Doctoral Fellow (from Tata
Institute of Fundamental Research, India)

Visiting Scientist; JSPS Post-Doctoral Fellow (from Fudan
University, China) (December '98–)

Visiting Scientist (from Case Western Reserve University
School of Medicine, U.S.A.) (July–August '99)²⁷⁾

Graduate Student (–March '99), Research Fellow (April
'99–)

Graduate Student

Graduate Student

Graduate Student

Graduate Student (April '99–)

Graduate Student (April '99–)

Professor

Research Associate (–March '99)²⁸⁾

Research Associate

Technical Associate (–November '98)²⁹⁾

JSPS Post-Doctoral Fellow (–February '99)³⁰⁾

Graduate Student

Graduate Student (–March '99)³¹⁾

Graduate Student (from Tsukuba University)* (–March
'99)

Professor

Visiting Professor (from The University of York, U.K.)
(July '99–)

Associate Professor

Visiting Associate Professor (from Korean University,
Korea) (July '99–)

Research Associate

Research Associate (November '98–)

Technical Associate

IMS Fellow (April '99–)

JSPS Post-Doctoral Fellow (–March '99)³²⁾

Visiting Scientist (from Dalian Institute of Chemical
Physics, China)

Graduate Student (–March '99)³³⁾

Graduate Student

Graduate Student (from Waseda University) * (–March

YOSHIDA, Keigo

'99)³⁴⁾Graduate Student (from Waseda University) * (–March '99)³⁵⁾

HOSSAIN, Delwar

Graduate Student (October '98–)

TSUBOUCHI, Masaaki

Graduate Student (April '99–)

Electronic Structure

MATSUMOTO, Yoshiyasu

Visiting Professor (from GUAS)

TAKAYANAGI, Masao

Visiting Associate Professor (from Tokyo University of Agriculture and Technology) (–March '99)³⁶⁾

TAMAI, Naoto

Visiting Associate Professor (from Kwansei Gakuin University) (April '99–)

INOKUCHI, Yoshiya

Research Associate

Molecular Energy Conversion

MARKOSYAN, Ashot Surenovich

Visiting Professor (from M. V. Lomonosov Moscow State University, Russia) (April '99–)

BU, Xian-He

Visiting Associate Professor (from Nankai University, China) (December '98–June '99)⁶⁵⁾

OSHEROV, Vladimir Iosifovich

Visiting Associate Professor (from Institute for Chemical Physics Research Russian Academy of Sciences, Russia) (July '99–)

Department of Molecular Assemblies*Solid State Chemistry*

YAKUSHI, Kyuya

Professor

NAKAMURA, Toshikazu

Associate Professor

NAKAZAWA, Yasuhiro

Research Associate

IMAEDA, Ken-ichi

Research Associate (–August '99)³⁷⁾

YAMAMOTO, Kaoru

Research Associate (April '99–)

URUICHI, Mikio

Technical Associate

MAKSIMUK, Mikhail

IMS Fellow (October '98–)

TSUKADA, Hiroshi

IMS Fellow (April '99–)

NAKANO, Chikako

Research Fellow

YONEHARA, Yukako

Graduate Student (–March '99)

OUYANG, Jianyong

Graduate Student

DING, Yuqin

Graduate Student (October '98–)

SIMONYAN, Mkhitar

Visiting Scientist (–March '99)³⁸⁾*Molecular Assemblies Dynamics*

KOBAYASHI, Hayao

Professor

MIYAJIMA, Seiichi

Associate Professor (–March '99)³⁹⁾

OGATA, Hironori

Research Associate

FUJIWARA, Hideki

Research Associate

OISHI, Osamu

Technical Associate

NARYMBETOV, Bakhyt

Visiting Scientist; JSPS Post-Doctoral Fellow

TANAKA, Hisashi

JSPS Post-Doctoral Fellow (April '99–)

ADACHI, Takafumi

Research Fellow

SATO, Akane

Graduate Student (–March '99)⁴⁰⁾

OJIMA, Emiko

Graduate Student

Molecular Assemblies

NOGAMI, Takashi

Visiting Professor (–March '99)⁴¹⁾

TAKEDA, Sadamu

Visiting Associate Professor (–March '99)⁴²⁾

TOKUMOTO, Madoka

Visiting Professor (from Electrotechnical Laboratory) (April '99–)

MORI, Takehiko

Visiting Associate Professor (from Tokyo Institute of Technology) (April '99–)

HASEGAWA, Shinji

Research Associate

Department of Applied Molecular Science*Applied Molecular Science I*

WATANABE, Yoshihito

Professor

INOUE, Katsuya

Associate Professor

OZAKI, Shin-ichi
HOSOKOSHI, Yuko
KUMAGAI, Hitoshi

HAYAMI, Shinya
MATSUI, Toshitaka
ROACH, Mark
TANAKA, Motoko

KATOH, Keiichi
YAMAHARA, Ryo

GHALSASI, Prasanna S.

GOTO, Yoshio
MAKIHARA, Nobuyuki
IWAHORI, Fumiyasu
KUGA, Takako
YANG, Huijun
SUZUKI, Kentaro
HARA, Isao

Applied Molecular Science II

ARAKAWA, Ichiro
MISAKI, Yoji
OGO, Seiji

Molecular Clusters

MIYOSHI, Eisaku
TANAKA, Keiichi
NAGATO, Kenkichi
HARADA, Kensuke
GHOSH, Tapas K.
MIZOGUCHI, Asao
BAILLEUX, Stephane
SUMI, Tomonari

Department of Vacuum UV Photoscience

Photochemistry

KOSUGI, Nobuhiro
TAHARA, Tahei
TAKATA, Yasutaka
TAKEUCHI, Satoshi
ADACHI, Jun-ichi
MIZUNO, Misao
ÅGREN, Hans Arvid

ARZHANTSEV, Sergei Yur'evich

FUJINO, Tatsuya
PETTERSSON, Lars Gunnar Moody

HATSUI, Takaki
FUJIYOSHI, Satoru

Chemical Dynamics

URISU, Tsuneo
MITSUKE, Koichiro
MASE, Kazuhiko
MIZUTANI, Masakazu
NAGASONO, Mitsuru
HATTORI, Hideo
MIYAMAE, Takayuki

Research Associate (–May '99)⁴³⁾
Research Associate
IMS Fellow (–March '99); JSPS Post-Doctoral Fellow
(April '99–)
IMS Fellow (–March '99)⁴⁴⁾
JSPS Post-Doctoral Fellow
Visiting Scientist; JSPS Post-Doctoral Fellow
Visiting Scientist (from The University of Tokyo) (April
'99–)
Visiting Scientist (from The University of Tokyo)
Visiting Scientist (from Nagoya Institute of Technology)
(March '98–)
Visiting Scientist (from University of Mumbai, India)
(April '99–)
Graduate Student (–March '99)⁴⁵⁾
Graduate Student
Graduate Student
Graduate Student (–March '99)⁴⁶⁾
Graduate Student
Graduate Student
Graduate Student

Visiting Professor (from Gakushuin University)
Visiting Associate Professor (from Kyoto University)
Research Associate

Professor
Associate Professor
Associate Professor
Research Associate
IMS Fellow
IMS Fellow
JSPS Post-Doctoral Fellow (–August '99)⁴⁷⁾
JSPS Post-Doctoral Fellow (April '99–)

Professor
Associate Professor
Research Associate
Research Associate
Technical Associate
Technical Associate (April '99–)
Visiting Scientist; MONBUSHO Invited Fellow (from
Linköping University, Sweden) (November '98–January
'99)⁴⁸⁾
Visiting Scientist; JSPS Post-Doctoral Fellow (November
'98–)
JSPS Post-Doctoral Fellow (April '99–)
Research Fellow (from Stockholm University, Sweden)
(February '99–March '99)⁴⁹⁾
Graduate Student (–March '99)⁵⁰⁾
Graduate Student (April '99–)

Professor
Associate Professor
Research Associate (–July '99)⁵¹⁾
Research Associate
Technical Associate (–March '99)⁵²⁾
Technical Associate (–December '98)⁵³⁾
IMS Fellow (–March '99)⁵⁴⁾

ONO, Masaki
IWASAKI, Kota

MEKARU, Harutaka

HIRANO, Shinya
NIKURA, Hiromichi
NODA, Hideyuki
YOSHIMURA, Daisuke
AZUMA, Yasushi

Interface Molecular Science

UENO, Nobuo
KUROSAWA, Kou
SAKURAI, Makoto
NAGAOKA, Shin-ichi
FUKUI, Kazutoshi
MATSUMOTO, Masuaki
NONOGAKI, Youichi
TAKASHIMA, Yoshifumi
TAKEZOE, Noritaka
YANAGITA, Hideaki
MIURA, Hiroshi
SAKAKIBARA, Tsutomu

Synchrotron Radiation Research

UMAPATHY, Siva

ULANSKI, Jacek Pawel

Pettersson, Lars Gunnar Moody

GAO, Yongli

SEIJO, Luis

Coordination Chemistry Laboratories

TANAKA, Koji

Synthetic Coordination Chemistry

NISHIDA, Yuzo
TSUJI, Yasushi
EBIHARA, Masahiro
OZAWA, Tomohiro
KUMITA, Hideyuki
KOBAYASHI, Teruyuki
OKUTSU, Wataru
TAKAHASHI, Yasuyuki
NISHINO, Satoshi
KUNITA, Mami

Complex Catalysis

SHIONOYA, Mitsuhiro
SAKURAI, Hiromu
MIZOBE, Yuji

TANAKA, Kentaro
TASAKA, Motoyuki
MORISHITA, Hiromasa
SHIGEMORI, Kazuki
HATANO, Akihiko
CAO, Honghua

IMS Fellow (April '99–)
Visiting Scientist (–March '99), JSPS Post-Doctoral Fellow (April '99–)
Graduate Student (–March '99), Research Fellow (April '99–)
Graduate Student (–March '99)⁵⁵⁾
Graduate Student
Graduate Student
Graduate Student (from Nagoya University)*
Graduate Student (from Chiba University)*

Professor (–March '99)⁵⁶⁾
Professor (April '99–)
Associate Professor (–March '99)⁵⁷⁾
Associate Professor (April '99–)
Associate Professor (April '99–)
Research Associate (–March '99)⁵⁸⁾
Research Associate (–March '99)⁵⁹⁾
Research Associate (April '99–)
IMS Fellow (April '99–)
Graduate Student (from Miyazaki University)*
Graduate Student (from Fukui University)*
Graduate Student (from Miyazaki University)*

Visiting Professor (from Indian Institute of Science, India) (September '98–February '99)⁶⁰⁾
Visiting Professor (from Technical University of Lodz, Poland) (March–August '99)⁶¹⁾
Visiting Associate Professor (from Stockholm University, Sweden) (–January '99)⁴⁹⁾
Visiting Associate Professor (from University of Rochester, USA) (February–July '99)⁶²⁾
Visiting Associate Professor (from University Autonoma de Madrid, Spain) (August '99–)⁶³⁾

Director

Professor
Associate Professor (–October '98)⁶⁴⁾
Associate Professor (April '99–)
Research Associate
Graduate Student (from Nagoya Institute of Technology)*
Graduate Student (from Yamagata University)*
Graduate Student (from Yamagata University)*
Graduate Student (from Yamagata University)*
Graduate Student (from Yamagata University)*
Graduate Student (from Yamagata University)*

Professor (–April '99)⁶⁵⁾
Visiting Professor (from Kyoto Pharmaceutical University)
Visiting Associate Professor (from the University of Tokyo)
Research Associate (–May '99)⁶⁵⁾
Graduate Student (–May '99)⁶⁵⁾
Graduate Student (–May '99)⁶⁵⁾
Graduate Student (–May '99)⁶⁵⁾
Graduate Student (–May '99)⁶⁵⁾
Graduate Student (–May '99)⁶⁵⁾

Functional Coordination Chemistry

TANAKA, Koji	Professor
FUJITA, Makoto	Associate Professor (–April '99) ⁶⁶⁾
TSUGE, Kiyoshi	Research Associate
KUSUKAWA, Takahiro	Research Associate (–April '99) ⁶⁶⁾
MIZUKAWA, Tetsunori	Technical Associate
SUGIMOTO, Hideki	IMS Fellow (–March '99) ⁶⁷⁾
SAKAMOTO, Youichi	IMS Fellow (–January '99)
YU, Shu-yan	Visiting Scientist; JSPS Post-Doctoral Fellow (–August '99) ⁶⁶⁾
BIRADHA, Kumar	Visiting Scientist; JSPS Post-Doctoral Fellow (October–August '99) ⁶⁶⁾
AOYAGI, Masaru	Graduate Student (–August '99) ⁶⁶⁾
IBUKURO, Fumiaki	Graduate Student (–August '99) ⁶⁶⁾
ALI, Md. Meser	Graduate Student (from Mie University)* (–April '99) ⁶⁸⁾
WADA, Toru	Graduate Student
ITO, Hirokazu	Graduate Student (–August '99) ⁶⁶⁾
UMEMOTO, Kazuhiko	Graduate Student (–August '99) ⁶⁶⁾
FUJITA, Norifumi	Graduate Student (–August '99) ⁶⁶⁾
HOSSAIN, Delower Md.	Graduate Student (from Mie University)* (–August '99)
TOMON, Takashi	Graduate Student (April '99–)

Coordination Bond

ADACHI, Ginya	Visiting Professor (from Osaka University) (–March '99)
TOBITA, Hiromi	Visiting Associate Professor (from Tohoku University) (–March '99)
AIDA, Takuzo	Visiting Professor (from the University of Tokyo) (April '99–)
HAMACHI, Itaru	Visiting Professor (from Kyusyu University) (April '99–)

Research Facilities*Computer Center*

IWATA, Suehiro	Director
AOYAGI, Mutsumi	Associate Professor
NANBU, Shinkoh	Research Associate
TAKAMI, Toshiya	Research Associate
MINAMINO, Satoshi	Technical Associate
ITO, Masakatsu	IMS Fellow (–March '99) ⁶⁹⁾
HIROTSU, Masakazu	Research Fellow (–October '98), IMS Fellow (October '98–February '99)
GRAY, Stephen K.	Visiting Scientist (from Argonne National Laboratory, U.S.A.) (May–June '99)
CHUNG, Gysung	Visiting Scientist (from Konyang University, Korea) (June–July '99)
NISHIKAWA, Takeshi	Graduate Student (from Keio University) (–October '98) ⁶⁹⁾
KINOSHITA, Tomoko	Graduate Student

Laser Research Center for Molecular Science

SAITO, Shuji	Director (–March '99)
FUJII, Masaaki	Director (April '99–)

Advanced Lasers for Chemical Reaction Studies

SATO, Shin-ichiro	Associate Professor
WATANABE, Kazuo	Research Associate (December '98–)

Advanced Lasers for Synchrotron Radiation Applications

SARUKURA, Nobuhiko	Associate professor
OHTAKE, Hideyuki	Research Associate
IZUMIDA, Shinji	Graduate Student
LIU, Zhenlin	Graduate Student
KAWAHATA, Eiji	Graduate Student (April '99–)
KOZEKI, Toshimasa	Graduate Student (April '99–)
ONO, Shingo	Graduate Student (September '98–)

Advanced UV and IR Tunable Lasers

TAIRA, Takunori
 KURIMURA, Sunao
 SHOJI, Ichiro
 PAVEL, Nicolaie
 SAIKAWA, Jiro
 SATO, Yoichi

Associate Professor
 Research Associate (March '99–)
 IMS Fellow (April '99–)
 Visiting Scientist; JSPS Post-Doctoral Fellow (March '99–)
 Graduate Student
 Graduate Student (April '99–)

Research Center for Molecular Materials

KOBAYASHI, Hayao
 WATANABE, Yoshihito
 KUWAHARA, Daisuke

Director (–March '99)
 Director (April '99–)
 Research Associate

Organic Materials Section

YAMASHITA, Yoshiro
 TANAKA, Shoji
 TOMURA, Masaaki
 ZAMAN, Mohammed Badruz
 SUZUKI, Kazuharu

Associate Professor
 Research Associate
 Technical Associate
 IMS Fellow (November '98–)
 Graduate Student

Hybrid Materials Section

FUJII, Hiroshi
 FUNAHASHI, Yasuhiro
 MIZUTANI, Mamoru

Associate Professor
 Research Associate (March '99–)
 IMS Fellow (April '99–)

Materials Characterization Section

NAGATA, Toshi
 ITO, Hajime
 KIKUZAWA, Yoshihiro

Associate Professor
 Research Associate (March '99–)
 Graduate Student

Structure Control Section

SUZUKI, Toshiyasu
 SAKAMOTO, Youichi
 HEIDENHAIN, Sophie

Associate Professor
 Research Associate (January '99–)
 Visiting Scientist (July '99–)

Equipment Development Center

KITAGAWA, Teizo
 YAKUSHI, Kyuya
 WATANABE, Michio
 ASAKA, Shuji

Director (–March '99)
 Director (April '99–)
 Associate Professor
 Research Associate

Ultraviolet Synchrotron Orbital Radiation Facility

KOSUGI, Nobuhiro
 KAMADA, Masao
 SHIGEMASA, Eiji
 KINOSHITA, Toyohiko
 HAMA, Hiroyuki
 TANAKA, Hitoshi
 KIMURA, Shin-ichi

Director
 Associate Professor
 Associate Professor (May '99–)
 Associate Professor (–November '98)⁷⁰⁾
 Associate Professor (–September '99)⁷¹⁾
 Visiting Associate Professor (–March '99)⁷²⁾
 Visiting Associate Professor (from Kobe University) (April '99–)
 Research Associate
 Research Associate
 Research Associate
 Research Associate
 IMS Fellow (–January '99)⁷³⁾
 Graduate Student (–March '99)⁷⁴⁾

TANAKA Shin-ichiro
 HOSAKA Masahito
 GEJO, Tatsuo
 KOUDA, Shigeru
 HARUYAMA Yuichi
 NATH, Krishna G.

* Carries out graduate research of IMS on Cooperative Education Program of IMS with other graduate schools.

Technical Staff

SAKAI, Kusuo	Technical Division Head
MATSUDO, Osamu	Technical Section Chief
KATO, Kiyonori	Technical Section Chief
NISHIMOTO, Fumio	Technical Section Chief
HORIGOME, Toshio	Technical Section Chief (–September '98) ⁷⁵⁾
YAMANAKA, Takaya	Technical Section Chief
KINOSHITA, Toshio	Electronic Structure (Unit Chief)
MIZUTANI, Fumiyasu	Computer Center (–May '99), Unit Chief (June '99–)
TESHIMA, Fumitsuna	Computer Center
NAITO, Shigeki	Computer Center
NAGATA, Masaaki	Research Center for Molecular Materials (Unit Chief)
YOSHIDA, Hisashi	Research Center for Molecular Materials (Unit Chief)
NOMURA, Sachiyo	Research Center for Molecular Materials
SAKAI, Masahiro	Research Center for Molecular Materials
TAKAYAMA, Takashi	Research Center for Molecular Materials
MIZUTANI, Nobuo	Equipment Development Center (Unit Chief)
SUZUI, Mitsukazu	Equipment Development Center (Unit Chief) (October '98–)
TORII, Tatsuharu	Equipment Development Center (–September '98) ⁷⁵⁾
UCHIYAMA, Kouichi	Equipment Development Center
TOYODA, Tomonori	Equipment Development Center
YANO, Takayuki	Equipment Development Center
KONDOU, Takuhiko	Equipment Development Center
KOBAYASHI, Kazuhiro	Equipment Development Center (October '98–)
HAYASHI, Kenji	UVSOR Facility (–May '99), Equipment Development Center (June '99–)
HASUMOTO, Masami	UVSOR Facility (Unit Chief)
YAMAZAKI, Jun-ichiro	UVSOR Facility
NAKAMURA, Eiken	UVSOR Facility (June '99–)
KONDO, Naonori	UVSOR Facility

List of Present Addresses

- 1) Department of Chemistry, Kang-Nung, University Kang-Nung 210-702, Korea
- 2) Laboratoire de Chimie, Physique Moléculaire, Faculté des Sciences, Université Libre de Bruxelles, 50 av F. D. Roosevelt, 050 Bruxelles, Belgium
- 3) Department of Industrial Chemistry, Kyungpook National University, 1370 Sankyuk-dong, Puk-ku, Taegu, 702-701 S. Korea
- 4) Quantum Theory Project, University of Florida, Gainesville, FL 32611-8435, U.S.A.
- 5) Department of Chemistry, Iowa State University, AMES, IA 50011, U.S.A.
- 6) Department of Chemistry, Univ. of Edinburgh, West Mains Road, Edinburgh, U.K.
- 7) Department of Chemistry, University of Surrey, Guildford, Surrey GU2 5XH, U.K.
- 8) School of informatics and sciences, Nagoya University, Nagoya 464-8601
- 9) Department of Electronic Structure, IMS
- 10) Department of Chemistry, Seoul National University, Seoul, Korea
- 11) Institute of Structural Macrokinetics, Russian Academy of Science, Chernogolovka, Moscow, Russia
- 12) Institute for Chemical Physics Research (ICPR), Russian Academy of Sciences, 142432, Chernogolovka, Moscow region, RUSSIA
- 13) Faculty of Mathematics and Physics, Dept. of Theoretical Physics, Charles University, V Holesovickach 2, 180 00 Praha 8, Czech Republic
- 14) Institute of Physical and Chemical Research (RIKEN), Hirosawa 2-1, Wako, Saitama 351-0198
- 15) School of informatics and sciences, Nagoya University, Nagoya 464-8601
- 16) Division of Chemistry, Graduate School of Science, Hokkaido University, Sapporo 060-0810
- 17) Department of Chemistry, Indian Institute of Technology, Bombay, Powai, Mumbai-400 076, INDIA
- 18) Research Center for Development of Far-infrared Region, Fukui University, 3-9-1 Bunkyo, Fukui 910-8507
- 19) Department of Chemical System Engineering, School of Engineering, University of Tokyo, Hongo 7-3-1, Bunkyo-ku, Tokyo 113-8685
- 20) Department of Chemistry, Brookhaven National Laboratory, Upton, NY 11973-5000, U.S.A.
- 21) Physical and Theoretical Chemistry Laboratory, South Parks Road, Oxford, OX1 3QZ, U.K.

- 22) Astronomical Data Analysis Center, National Astronomical Observatory, Osawa 2-21-1, Mitaka, Tokyo 181-8588
- 23) Department of Chemistry, Faculty of Science, Shizuoka University, 836 Ohya, Shizuoka 422-8529
- 24) Space Utilization Research Program, National Space Development Agency of Japan, Tsukuba Space Center, 2-1-1 Sengen, Tsukuba, Ibaraki, 305-8505.
- 25) The 2nd Group, National Research Institute for Metals, 1-2-1, Sengen, Tsukuba-shi, Ibaraki 305-0047
- 26) Chemistry and Physics Division, Jagiellonian University, Ingardena 3, 30-60 Krakow, Poland
- 27) Department of Physiology and Biophysics, Case Western Reserve University School of Medicine, Cleveland, OH 44106-4970, U.S.A.
- 28) Department of Photoscience, School of Advanced Science, GUAS, 1560-35 Hayama 240-0193
- 29) Laser Research Center for Molecular Science, IMS
- 30) Fujitsu Laboratories Ltd., 10-1 Morinosato-Wakamiya, Atsugi 243-0197
- 31) Department of Photoscience, School of Advanced Science, GUAS, 1560-35 Hayama 240-0193
- 32) Department of Chemistry, Iowa State University, Ames, Iowa 50011, USA
- 33) Toshiba, Kawasaki 210-8520
- 34) Fujifilm, Ashigara 250-0193
- 35) Dai Nippon Printing Co. Ltd., Kashiwa 277-0871
- 36) Graduate School of Bio-Applications and Systems Engineering, Tokyo University of Agriculture and Technology, Koganei 184-8588
- 37) Department of Electrical Electronic Eng., Toyohashi University of Technology, Tempaku-cho, Toyohashi 441-8580
- 38) Institute for Physical Research of Armenian National Academy of Science, IPR, Ashtarak-2, 378410, Armenia
- 39) Miyajima Shoyu Co. Ltd., Funamiya, Karatsu 847-0062
- 40) Microcalorimetry Research Center, Faculty of Science, Osaka University, Toyonaka, Osaka 560-8531
- 41) Department of Applied Physics and Chemistry, The University of Electro-Communications, Chyofu, 182-8585
- 42) Department of Chemistry, Faculty of Engineering, Gunma University, Kiryu, Gunma 376-8515
- 43) Yamagata University, 1-4-12 Koshirakawa, Yamagata 990-8560
- 44) Special Research Laboratory for Optical Science, Kanagawa Academy of Science and Technology
- 45) University of California, Berkeley, CA 94720, U.S.A
- 46) Yoshinagachou 273-10, Nijou Shinmanomachi Nishiiru, Sakyoku, Kyoto
- 47) Universite des Sciences et Technologies de dille, F-59655, Villeneuve D'ASCQ Cedex, France
- 48) Theoretical Chemistry, Teknikringen 30, Royal Institute of Technology, S-10044 Stockholm, Sweden
- 49) Institute of Physics, Stockholm University, Box 6730, S-11385, Sweden
- 50) Department of Chemistry, Faculty of Science, The University of Tokyo, 7-3-1, Hongo, Bunkyo-ku, Tokyo 113-0033
- 51) Photon Factory, Institute of Materials Structure Science, High Energy Accelerator Research Organization, 1-1 Oho, Tsukuba, Ibaraki 305-0801
- 52) Max-lab, Beam Line 1511, Lund University, P. O. Box 118, S-221 00 Lund, Sweden
- 53) Nitto Technical Information Center Co., Ltd., Toyohashi, Aichi 441-3194
- 54) National Institute of Materials and Chemical Research, Agency of Industrial Science and Technology, Ministry of International Trade and Industry, 1-1 Higashi, Tsukuba, Ibaraki 305-8565
- 55) Production Engineering Research Laboratory, Hitachi, Ltd., 292 Yoshida-cho, Totuka-ku, Yokohama, Kanagawa 224-0817
- 56) Department of Materials Science, Faculty of Engineering, Chiba University, 1-33, Yayoi-cho, Inage-ku, Chiba-shi, Chiba, 263-8522
- 57) Department of Physics, Faculty of Science, Kobe University, 1-1 Rokkodaicho, Nada-ku, Kobe 657-8501
- 58) Institute of Industrial Science, The University of Tokyo, 7-22-1, Roppongi, Minato-ku, Tokyo 106-8558
- 59) Graduate School of Engineering, Nagoya University, Furo-cho, Chikusa-ku, Nagoya 464-8603
- 60) Department of Inorganic and Physical Chemistry, India Institute of Science, Bangalore-560012, India
- 61) Institute of Polymers, Technical University of Lodz, Zeromskiego street No. 116; 90-924 Lodz, Poland
- 62) Department of Physics and Astronomy, University of Rochester, Rochester, NY 14627, U.S.A.
- 63) Department of Chemistry, University Automona de Madrid, 28049 Madrid, Spain
- 64) Catalysis Research Center, Hokkaido University, Kita-ku, Sapporo 060
- 65) Graduate School of Science, The University of Tokyo, 7-3-1 Hongo, Bunkyo-ku, Tokyo 113-0033
- 66) Graduate School of Science, Nagoya University, Furo-cho, Chokusa-ku, Nagoya 464-8601
- 67) Graduate School of Science, Osaka City University, 3-3-138 Sugimoto, Sumiyoshi-ku, Osaka
- 68) Department of Chemistry & Biochemistry, P. O. Box 19065, University of Texas, Arlington, Texas 76019, U.S.A.
- 69) Department of Theoretical Studies, IMS
- 70) Synchrotron Radiation Laboratory, Institute of Solid State Physics, Tokyo University, 1-1 Oho, Tsukuba, Ibaraki 305-0801
- 71) Laboratory of Nuclear Science, Tohoku University, 1-2-1 Mikamimine, Taihaku-ku, Sendai, Miyagi 982-0826
- 72) Japan Synchrotron Radiation Research Institute, 1-1-1 Mikazuki, Sayo-gun, Hyogo 679-5198
- 73) Laboratory of Advanced Science and Technology for Industry, Himeji Institute of Technology, 1479-6 Kanaji,

Kamigori, Ako, Hyogo 678-1201

74) Device Physics Laboratory, NTT Basic Research Laboratories, 3-1 Morinosato, Wakamiya, Atsugi, Kanagawa 243-0198

75) Graduate School of Polymathematics, Nagoya University, Furo-cho, Chigusa-ku, Nagoya 464-0814

COUNCIL

KAYA, Koji

Director-General

Councillors

Chairperson
Vice-Chairperson

HOSOYA, Haruo
HIROTA, Noboru
OHTSUKA, Eiko
OGINO, Hiroshi
KIHARA, Motohiro

KYOOGOKU, Yoshimasa

GOTO, Keishi
KONDOW, Tamotsu
SAHARA, Makoto
SHIMIZU, Ryoichi
TAKAHASHI, Riichi

TSUCHIYA, Soji

NAKANISHI, Atsuo

FUKUYAMA, Hidetoshi

HONDA, Kenichi

MATSUO, Minoru
YAMAZAKI, Toshimitsu

YAMAMURA, Shosuke
KIEFER, Wolfgang*
ZARE, Richard N.*

Professor, Ochanomizu University
Professor, Kyoto University
Professor, Hokkaido University
Professor, Tohoku University
Director, Accelerator Laboratory, High Energy Accelerator Research Organization
Director-General, Institute for Protein Research, Osaka University
President, Toyohashi University of Technology
Invited Professor, Toyota Technological Institute
Director-General, National Museum of Japanese History
Director, The Institute of Statistical Mathematics
Vice President, Toyota Central Research & Development Laboratories, Inc.
Professor, Japan Women's University; Professor Emeritus, The University of Tokyo
Executive Director, Chemical Society of Japan; Executive Director, Japan Academic Association for Copyright Clearance
Director, Institute for Solid State Physics, The University of Tokyo
President, Tokyo Institute of Polytechnics; Professor Emeritus, The University of Tokyo
President, Nagoya University
Inspector, Japan Society for the Promotion of Science; Professor Emeritus, The University of Tokyo
Professor, Keio University
Professor, Wuerzburg University
Professor, Stanford University

The Council is the advisory board for the Director-General.

* Two of the councillors are selected among distinguished foreign scientists.

Distinguished Research Consultants

BABA, Hiroaki
INOKUCHI, Hiroo
NAGAKURA, Saburo

TANAKA, Ikuzo

Professor Emeritus, Hokkaido University
Professor Emeritus, Institute for Molecular Science
President, The Kanagawa Academy of Science and Technology
Chancellor, Nezu Scholarship Association, Educational Foundation; Professor Emeritus, Tokyo Institute of Technology

Administration Bureau

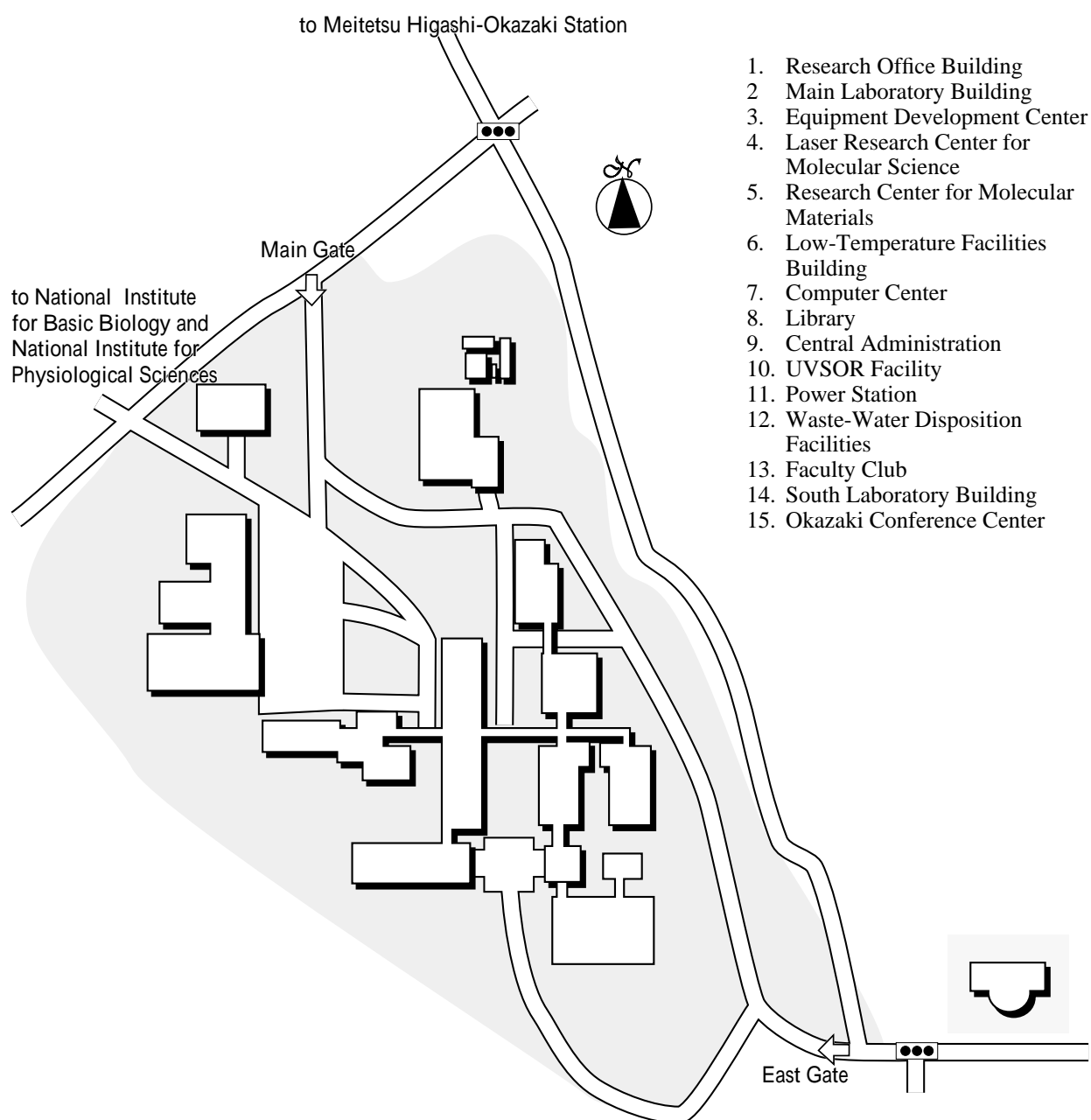
OSAKA, Kouichiro
TERAO, Shigemi
OKADA, Kazuhiko
SAISHO, Chikashi
KAWANO, Masatoshi
NARUSE, Hakaru
IWAI, Youji
INDEN, Toshio
TAIMA, Hitoshi
TAKAHARA, Kouji
ONO, Yukitsugu
IWAKAMI, Nobuyoshi
WATABE, Hidemasa
FUNATO, Hideaki
MOCHIZUKI, Yoshitaka
SATO, Hisashi

Director-General, Administration Bureau (–November '98)
Director-General, Administration Bureau (December '98–)
Director, General Affairs Department
Director, Finance and Facilities Department (–March '99)
Director, Finance and Facilities Department (April '99–)
Head, General Affairs Division
Head, Personnel Division (–April '99)
Head, Personnel Division (April '99–)
Head, Research Cooperation Division
Head, International Affairs Division (–March '99)
Head, International Affairs Division (April '99–)
Head, Budget Division
Head, Accounts Division
Head, Construction Division
Head, Equipment Division (–March '99)
Head, Equipment Division (April '99–)

BUILDINGS AND CAMPUS

The IMS campus covering 62,343 m² is located on a low hill in the middle of Okazaki city. The inequality in the surface of the hill and growing trees are preserved as much as possible, and low-storied buildings are adopted for conservation of the environment. The buildings of IMS are separated according to their functions as shown in the map. The Research Office Building and all Research Facilities except for the Computer Center are linked organically to the Main Laboratory Buildings by corridors. Computer Center, Library and Administration Buildings are situated between IMS and neighboring National Institute for Basic Biology and National Institute for Physiological Sciences, because the latter two facilities are common to these three institutes.

The lodging facility of IMS called Yamate Lodge, located within ten minutes' walk, has sleeping accommodations for 15 guests and two families. Mishima Lodge, located within four minutes' walk east of IMS can accommodate 74 guests and 20 families. Scientists who visit IMS as well as the two other institutes can make use of these facilities. Foreign visiting scientists can also live at these lodgings with their families during their stays. The Okazaki Conference Center was built in April, 1997 in Mishima area, which has four conference rooms capable of between 50 and 250 attendance.





Okazaki (population 330,000) is 260 km west of Tokyo, and can be reached by train in about 3 hours from Tokyo via Shinkansen and Meitetsu Line.
The nearest large city is Nagoya, about 40 km northwest of Okazaki.



RESEARCH ACTIVITIES I

Department of Theoretical Studies

I-A Development of New Theoretical and Numerical Techniques in the Study of Molecular Structure

Theories of the electronic structure of molecules have been extensively developed for last decades. There are, however, plenty of challenging and practically important problems to be solved.

I-A-1 Multireference Linear Response Theory Utilizing the State Universal Coupled Cluster Formalism

TEN-NO, Seiichiro; IWATA, Suehiro; MUKHERJEE, Debashis¹
(¹Indian Inst. Cultivation Sci., Calcutta)

In the multireference linear response theory (MRLRT), energy differences (excitation energies, ionization potentials, and electron affinities) including multielectron processes are calculated accurately in a size-intensive manner. The original formalism follows the generalization of the coupled cluster linear response theory (CCLRT) employing the Adamowicz-type wave operator ansatz for the state specific coupled cluster (SSCC) theory. The effective Hamiltonian is however contaminated by near-degeneracy correlation effects at far from the equilibrium geometry of the specified state. We develop a time-dependent perturbation theory which utilizes the state universal CC formalism. It is shown that the present MRLRT describes our-valence states more naturally such that they are size-intensive to all valence excited states in the complete model space.

I-A-2 Size-extensive Calculations of Static Structure Factors from the Coupled Cluster Singles and Doubles Model

WATANABE, Noboru¹; TEN-NO, Seiichiro; PAL, Sourav²; IWATA, Suehiro; UDAGAWAL, Yasuo¹
(¹Tohoku Univ.; ²Natl. Chem. Lab., India)

[*J. Chem. Phys.* **111**, 827 (1999)]

The X-ray incoherent scattering factor $S(q)$, which is also called the static structure factor, is very sensitive to electron correlation. In this study a method for calculating $S(q)$ based on coupled cluster singles and doubles (CCSD) approach is developed and the computed $S(q)$ of H_2O , CH_3OH , CH_3CN , C_6H_6 , and C_6H_{12} are compared with experimental results. It is shown that the CCSD method improves theoretical $S(q)$ of large molecules significantly compared with those by configuration interaction singles and doubles (CISD) previously employed.

I-A-3 Local Resolution of Identity for Scalable Molecular Orbital Calculations

TEN-NO, Seiichiro; IWATA, Suehiro

The resolution of identity (RI) technique in the calculations of four-center electron repulsion integrals has been used in the density functional, HF, MCSCF, MP2, CCSD and CCSD(T) molecular orbital theories. The use of RI reduces the formal scaling of the integral calculation and storage to be only $O(n^3)$. This does not however mean that any step of the theories reduces the scaling of the calculation. To mitigate this situation, we develop a new decomposition scheme, the local resolution of identity (LRI), employing different expansion sets for different charge distributions of local basis functions. It is shown that LRI provides powerful alternatives with possibly wider applicability for computing large molecular systems.

I-A-4 On Connection Between The Reference Interaction Site Model Integral Equation Theory and The Partial Wave Expansion of The Molecular Ornstein-Zernike Equation

TEN-NO, Seiichiro; IWATA, Suehiro

[*J. Chem. Phys.* **111**, 4865 (1999)]

We develop a systematic integral equation theory based on the partial wave (PW) expansion of the Ornstein-Zernike (OZ) equation for molecular fluids. The obtained partial OZ (POZ) equation indicates that the total correlation function is a chain sum of the direct ones in the PW form joined by the "full" intra-molecular correlation functions, including angular dependency explicitly. On this basis, the site-site OZ (SSOZ) equation in the reference interaction site model (RISM) is identified as an approximation to POZ, truncated at the lowest order in the angular expansion. This fact provides us a rigorous and transparent framework to formulate integral equation theories for multiple site treatments. We also derive proper Helmholtz free energy and closure expressions based on the PW formalism.

I-A-5 Non-Adiabatic Relaxation Through a Conical Intersection

IKEGAMI, Tsutomu; IWATA, Suehiro

The non-adiabatic transition through a conical intersection is studied for a two-dimensional two-level model system. The two adiabatic potential energy surfaces are set up to be flat, except for the conical intersection located at the origin. Around the conical intersection, the upper adiabatic surface is concaved, so

that the classical trajectories running on the upper surface are attracted to the intersection. Since the non-adiabatic coupling between two adiabatic surfaces diverges at the conical intersection, trajectories passing nearer to the intersection have larger probability to relax

to the lower surface. Therefore, the rate of the non-adiabatic relaxation is expected to increase with the decrease of the kinetic energy. The above expectation is confirmed by both the quantum-classical mixed dynamics and the wavepacket (quantum) dynamics.

I-B Water Clusters and Their Complexes with Atomic Ions

While we have been studying water cluster anions $(\text{H}_2\text{O})_n^-$, we have found a unique structural unit in which the OH bonds surround an excess electron. We call it $\text{OH}\{\text{e}\}\text{HO}$ structure. This structure is also found in the water cluster complexes with a group 1 metal atom. The interaction between the electron and HO bonds is very similar to the hydrogen bond; in the structure $\text{OH}\{\text{e}\}\text{HO}$, the bond length of OH is lengthened and the harmonic frequency of OH stretching modes shifts substantially downward. The structure is expected to be ubiquitous, and further both theoretical and experimental studies are required.

I-B-1 Theoretical Studies of Structures and Ionization Threshold Energies of Water Cluster Complexes with a Group 1 Metal, $\text{M}(\text{H}_2\text{O})_n$ ($\text{M} = \text{Li}$ and Na)

TSURUSAWA, Takeshi; IWATA, Suehiro

[*J. Phys. Chem. A* **103**, 6134 (1999)]

Water cluster complexes with a group 1 metal atom, $\text{M}(\text{H}_2\text{O})_n$ ($\text{M} = \text{Li}$ and Na), for $n = 3$ –6 were studied with ab initio MO methods. The singly occupied molecular orbitals (SOMO) are classified into three types; surface, quasi-valence and semi-internal. They are the isomers of structures with semi-internal SOMO that are responsible for the observed convergence of the ionization threshold energy. They are the ion-pair complexes, $\text{M}^+(\text{H}_2\text{O})_m \cdot (\text{H}_2\text{O})_{n-m-l} \cdot (\text{H}_2\text{O})_l^-$, and their vertical ionization energies (VIEs) are determined by the local structure of $(\text{H}_2\text{O})_l^-$ and the electrostatic potential from the cation $\text{M}^+(\text{H}_2\text{O})_m$. The model also explains why the experimental ionization threshold energy converges at $n = 4$.

I-B-2 The Electron-Hydrogen Bonds and the Harmonic Frequency Shifts in Water Cluster Complexes with a Group 1 Metal Atom, $\text{M}(\text{H}_2\text{O})_n$ ($\text{M} = \text{Li}$ and Na)

TSURUSAWA, Takeshi; IWATA, Suehiro

The stable isomers of the water cluster complexes with a group 1 metal atom can be modeled as $\text{M}(\text{H}_2\text{O})_n = \text{M}^+(\text{H}_2\text{O})_m \cdot (\text{H}_2\text{O})_{n-m-l} \cdot (\text{H}_2\text{O})_l^-$, and the similar structural unit was found as in water cluster anions. The unit consists of an localized electron distribution and the surrounding HO bonds, and we can call it the $\text{OH}\{\text{e}\}\text{HO}$ structure. In the $\text{M}(\text{H}_2\text{O})_n$, the electron is stabilized by both the OH bonds of water molecules surrounding the electron and the electrostatic potential from the hydrated metal ion part $\text{M}^+(\text{H}_2\text{O})_m$. The interaction makes the SOMO extent measure (SEM: the volume of the sphere which contains a half of the SOMO electron) shrunken to as small as 50–60 Å³. When the surrounding OH bonds interact with the shrunken SOMO electron in the $\text{M}(\text{H}_2\text{O})_n$, the HO bonds are lengthened and their harmonic frequencies are shifted to low. The changes in

both OH bond lengths and the harmonic frequencies are similar to those in the usual hydrogen bond. As we call the interaction in the clusters $\text{X}^-(\text{H}_2\text{O})_n$, ($\text{X} = \text{F}, \text{Cl}, \text{Br}$ and I) the ionic hydrogen bond, we may call the interaction between an electron and its surrounding OH bonds the electron-hydrogen bond. The electron-hydrogen bond is as strong as the ordinal hydrogen bonds, when the water molecule having the OH bond interacting with electron is a double proton acceptor. The calculations indicate that the spectral patterns in the OH stretching frequencies are well correlated with the geometric structure surrounding the electron $\{\text{e}\}$, and that the vibrational spectra help us to identify the isomers.

I-B-3 The Energies, the Structures and the Harmonic Frequencies of the Small Water Cluster Anions, $(\text{H}_2\text{O})_n^-$ ($n = 3, 4$ and 6)

TSURUSAWA, Takeshi; IWATA, Suehiro

[*Chem. Phys. Lett.* in press]

For the small water cluster anions $(\text{H}_2\text{O})_n^-$ ($n = 3, 4$ and 6), the isomers which have the internally bound electron in the cluster have found by the ab initio MO method. We have added four, three and two diffuse functions on all oxygen atoms for trimer, tetramer and hexamer clusters, respectively. For trimer, the obtained structure contains three fragments (each fragment is a water molecule) surrounding the excess electron and there is no bond between the fragments. For the tetramer, the isomers contain two fragments which surround the excess electron between the fragments. For hexamer anions, the structure of the isomers determined in this calculations have a ring structure. Because the SOMO extent measure (SEM) is large even in the hexamer anions (150–250 Å³), the change of OH bond length and the change of the harmonic frequencies are not large as in the water cluster complexes containing a group 1 metal atom $\text{M}(\text{H}_2\text{O})_n$. The excess electron in the water cluster anions are stabilized by the surrounding OH bonds and the electrostatic potential made by the dipole moment of the fragments of the cluster. Because the electrostatic potential from the dipole moment of the fragment water cluster does not make the SEM shrunken as in the $\text{M}(\text{H}_2\text{O})_n$, the interaction

between the excess electron and surrounding OH bonds are not strong. Due to the large SEM of the excess electron in the hexamer anions, those structures are not exactly the internal structures. For the hexamer, the isomers which have separate fragments surrounding the excess electron might be possible and those might have smaller SEM than the isomers determined in this calculations.

I-B-4 Theoretical Study of Vibrational Spectra for $\text{Cl}^-(\text{H}_2\text{O})$: Temperature Dependence and the Influence of Ar_n ($n = 1-3$)

SATOH, Katsuhiko; IWATA, Suehiro

[Chem. Phys. Lett. in press]

Vibrational spectra for $\text{Cl}^-(\text{H}_2\text{O})$ in the OH stretching region were studied theoretically. The theoretical results are compared with the experimental results from two groups. They are in closer agreement with one of the reported spectra. By adiabatically separating the intermolecular and intramolecular modes, the potential surfaces for the intermolecular modes are drawn with and without the excitation of the OH stretching mode. The contribution from the hot bands are examined by solving the 2-dimensional vibrational nuclear Schrödinger equation. The argon clusters attached to $\text{Cl}^-(\text{H}_2\text{O})$ as a spectator contribute the substantial downward shift of the ionic hydrogen-bonded OH stretching frequency.

I-C Computational Chemistry of Atomic and Molecular Processes in Atmospheric Environment

We have started a new research project, "Computational Chemistry for Atmospheric Environmental Molecule" under Research and Development Applying Advanced Computational Science and Technology administrated by Japan Science and Technology Corporation (ACT-JST). Because almost all of molecules in the atmosphere on the earth are simple molecules, we can perform the state-of-the-art calculations for the atmospheric molecules, and the calculational results are accurate enough to be used as "the experimental data" if they are not available. Physical and chemical phenomena in the atmosphere sometimes involve a sequence of complex processes. To explore the processes, development of new theoretical methods might be required.

I-C-1 Accurate Potential Energy and Transition Dipole Moment Curves of Several Electronic States of CO^+

OKADA, Kazutoshi¹; IWATA, Suehiro
(¹GUAS)

[J. Chem. Phys. in press]

Accurate calculations are performed for several doublet and quartet states of CO^+ with the multi-reference configuration interaction method using augmented quadruple zeta basis set. To calculate the transition probability among the electronic states and to draw well-balanced potential energy curves, a single set of molecular orbitals determined by Iwata's VALVAC

method is used in the multi-reference single-double configuration interaction calculations. Spectroscopic constants and the lifetimes of vibronic states are calculated and compared with the available experimental data. Table 1 shows the lifetimes of the vibronic states of the $B^2\Sigma^+$ state. Experimental and theoretical results by Marian *et al.* are also shown. The calculated lifetimes of the vibronic states are in perfect agreement with the available experimental data within the experimental error. Our calculations confirm the lifetime measurement by Marian *et al.* The accuracy in our calculations is expected to hold for higher vibrational quantum numbers. It should be emphasized that the evaluation of the lifetime of the vibronic states in the B state requires the Einstein's A coefficients to the vibronic levels of both $A^2\Pi$ and $X^2\Sigma^+$ states.

Table 1. The lifetimes (in n sec.) of the vibronic levels of $B^2\Sigma^+$ state

$B^2\Sigma^+$ state v'	$v' = 0$	1	2	3	4	5
Lifetime	56.40	61.48	66.87	72.31	78.32	83.34
Marian <i>et al.</i> (exp.)	57.1 ± 1.0	61.8 ± 1.0	68.9 ± 1.0	72.5 ± 2.7		
Marian <i>et al.</i> (theo.)	50.00	54.9	59.7	64.9		

I-C-2 Accurate Potential Energy Curves of Several Electronic States of N_2^+ and O_2^+

OKADA, Kazutoshi¹; IWATA, Suehiro
(¹GUAS)

Accurate calculations are performed for several

doublet and quartet states of N_2^+ and O_2^+ with the multi-reference configuration interaction method using augmented quadruple zeta basis set. Spectroscopic constants are obtained and are compared with latest PFI-PE experiment. The calculated spectroscopic constants well reproduce the existing experimental data. The high ionic states, which have been detected in the low

resolution photoelectron spectra as shake-up bands, are well characterized.

I-C-3 Absorption and Emission Spectra Among the Rovibrational Levels of the Electronic Ground State of CO $X^1\Sigma^+$

OKADA, Kazutoshi¹; IWATA, Suehiro
(¹GUAS)

Carbon monoxide molecule is one of the important molecules in the atmosphere not only on the earth but also on the other planet. With the spectrometer on a satellite, high resolution infrared absorption spectra of solar atmosphere are reported up to high $J \geq 100$, and the data were used to determine Dunham's coefficients accurately. In this study, rovibrational levels of CO $X^1\Sigma^+$ state are calculated, and the calculated spectroscopic constants well reproduce the experimental Dunham's coefficients. By evaluating Einstein's A and B coefficients, the lifetime of each rovibrational level is estimated, and the rotational resolved IR absorption and emission spectra are simulated for $\Delta v = 2$ and 3 as well as $\Delta v = 1$ transitions.

I-C-4 Theoretical Study of the Reactions of OH Radical with Hydrocarbons

HASHIMOTO, Tomohiro¹; IWATA, Suehiro
(¹JST and Keio Univ.)

OH radical is one of the most reactive chemical species with hydrocarbons. In this study, atmospheric chemical reactions of OH radical with some simple hydrocarbons are investigated using ab initio molecular orbital methods. Molecular geometries are optimized at the MP2/aug-cc-pVDZ level and single point energy calculations are performed at the CCSD(T)/aug-cc-pVDZ level. In the hydrogen abstraction reactions with saturated hydrocarbons such as methane and ethane, weakly-bound reactant complexes are found as the experiment suggests. Calculated binding energies of the reactant complexes are 0.74 kcal/mol for $\text{CH}_4 \cdots \text{OH}$ system and 0.83 kcal/mol for $\text{C}_2\text{H}_6 \cdots \text{OH}$ system. On the other hand, the product complexes have the binding energies of 1.99 kcal/mol and 3.25 kcal/mol, respectively. The reaction barrier heights are computed at 6.48 kcal/mol for $\text{CH}_4 \cdots \text{OH}$ system and 3.70 kcal/mol for $\text{C}_2\text{H}_6 \cdots \text{OH}$ system. Electron correlation effect has a large influence on both molecular structures and relative energies.

I-C-5 Ab Initio Study of the Low-Lying Excited States of ClOCl

NELSON, Alistair¹; IWATA, Suehiro
(¹Univ. Edinburgh)

The photo-dissociation spectrum of ClOCl, from Nickolaissen *et al.* (*J. Chem. Phys.* **104**, 2857 (1996)), was investigated using the Multi-Reference Configuration Interaction (MRCI) method; the aug-cc-pVTZ basis set was used for all the calculations. Twelve low-lying states are examined in all 6 singlet states and 6 triplet

states, which correlated to the $\text{ClO}(^2\Pi) + \text{Cl}(^2\text{P})$. Our calculations, as well as the calculations shown by Nickolaissen *et al.*, strongly suggest that a weak and broad band at 2.3 eV cannot be assigned to OCl_2 , and that the next band at 2.9 eV is assigned to the transition to the triplet state 1^3B_1 . The low lying excited states, both singlet and triplet, are all dissociative to $\text{ClO} + \text{Cl}$.

I-C-6 Ab Initio Study of the Excited States of HOBr

LEE, Sang Yeon¹; HASHIMOTO, Tomohiro²; IWATA, Suehiro
(¹Kyungpook Natl. Univ.; ²IMS, JST and Keio Univ.)

To analyse the recently reported absorption spectrum of HOBr by Ingham *et al.* (*J. Phys. Chem. A* **102**, 3293 (1998)), CASSCF and multi-reference CI calculations were carried out with aug-cc-pVDZ basis set augmented by a set of Rydberg orbitals. The first weak band at 2.71 eV, previously not reported, is assigned to the transition to the lowest triplet state $^3\text{A}''$. Two UV bands at 3.53 and 4.37 eV are the transitions to $1^1\text{A}''$ and $2^1\text{A}'$ states, respectively. Because the triplet states are closely lying near these states, to study the photodissociation processes after the UV irradiation, the spin-orbit coupling should be taken into account. There are several valence and Rydberg excited states between 6.5 and 8.0 eV, which contribute the absorption spectra near 200 nm.

I-C-7 Theoretical Study of the Molecular Structure of the $\text{NO}_3^-(\text{HNO})_m$ and $\text{NO}_3^-(\text{HNO})_m\text{-H}_2\text{O}$ Anions

ENGLAND, James¹; IWATA, Suehiro
(¹Univ. Surrey)

The molecular structure of the atmospheric $\text{NO}_3^-(\text{HNO})_m$ and $\text{NO}_3^-(\text{HNO})_m\text{-H}_2\text{O}$ anions were studied at both the MP2 and DFT (using the B3LYP functional) levels of theory with the Gaussian 98 program. Using a 6-31++G* basis set, the geometry of the anions were optimized. The symmetric structure $[\text{O}_2\text{NO-H-ONO}_2]^-$ is not at the local minimum on the potential energy surface, and the NO_3^- plane is almost perpendicular to the plane of HONO_2 . The calculated binding energy at the MP2 level for $\text{NO}_3^-(\text{HNO})$ was found to be 123.37 kJ/mol, and 120.58 kJ/mol at the DFT. Work is currently underway to study the effect of water hydrogen bonding to the anion, as well as increasing m to two and eventually three.

I-C-8 Investigation of the Potential Energy Surfaces for the Ground $X^1\text{A}_1$ and Excited $C^1\text{B}_2$ Electronic states of SO_2

NACHTIGAL, Petr¹; HRUŠÁK, Jan¹; BLUDSKÝ, Ota¹; IWATA, Suehiro
(¹J. Heyrovsky Inst. Phys. Chem.)

[*Chem. Phys. Lett.* **303**, 441 (1999)]

The stationary points along the dissociation path are investigated by means of high-level ab initio MO

methods and the reliability of different methods is discussed. The multi-reference AQCC method using the ANO-type basis set is shown to give geometrical parameters and relative energies in very good agreement

with experiment. At this level of theory, the $\tilde{C}^1B_2(^1A')$ state has an asymmetrical equilibrium geometry and double-minimum potential with a barrier of 170 cm^{-1} , in good agreement with experimental data.

I-D Application of Ab Initio Molecular Orbital Methods to Experimentally Relevant Systems

The quantum chemical calculations now are indispensable tools for analyzing the experimental data and for planning new experiments. We have been collaborating with many experimental groups. Some of them have attained enough experience and started their own calculations. The close collaborative works are, yet, continuing.

I-D-1 Theoretical Study on Spectroscopic Properties of Positive, Neutral, and Negative Species of BCl_2 and AlCl_2 : The Stability of the Negative Species

BAECK, Kyoung K.¹; CHOI, Heechol¹; IWATA, Suehiro
(¹Hang-Nung Univ.)

[*J. Phys. Chem. A* in press]

Accurate and predictive values of the bond lengths and angles, dipole moments, and vibrational frequencies of $\text{BCl}_2^+(\text{X}^1\Sigma_g^+)$, $\text{BCl}_2(\tilde{\text{X}}^2\text{A}_1)$, and $\text{BCl}_2^-(\tilde{\text{X}}^1\text{A}_1, \tilde{\text{a}}^3\text{B}_1)$ and the corresponding aluminum analogs are calculated by Becke's three parameter density-functional-theory (B3LYP) method with the augmented correlation consistent triple- and quadruple-zeta (aug-cc-pVTZ and aug-cc-pVQZ, respectively) basis sets. The coupled-cluster singles, doubles, and noniterative triples (CCSD(T)) method with aug-cc-pVTZ is also used to augment the B3LYP results. The ionization energies and electron affinities are also calculated by the B3LYP/aug-cc-pV5Z method at the B3LYP/aug-cc-pVQZ geometry and the CCSD(T)/aug-cc-pVQZ method at the CCSD(T)/aug-cc-pVTZ geometry, as well as by the G1, G2, CBS-4, and CBS-Q methods. It is shown that the negatively charged species, which have never been studied experimentally, are stable both in singlet and triplet spin states with electron affinities of $1.40\text{ eV}/0.25\text{ eV}$ and $2.37\text{ eV}/0.46\text{ eV}$ for singlet/triplet states of BCl_2^- and AlCl_2^- , respectively. The photoelectron spectra for the electron detachment of the anions are simulated by calculating the Franck-Condon factors. The photoelectron spectra for the singlet and triplet states of BCl_2^- turn out to be very similar to AlCl_2^- analogs. While the photoelectron spectra for $\tilde{\text{X}}^2\text{A}_1(\text{MCl}_2) \leftarrow \tilde{\text{X}}^1\text{A}_1(\text{MCl}_2^-)$, $\text{M} = \text{B}$ and Al , have complicated combination bands, those for $\tilde{\text{X}}^2\text{A}_1(\text{MCl}_2) \leftarrow \tilde{\text{a}}^3\text{B}_1(\text{MCl}_2)$, $\text{M} = \text{B}$ and Al , have only one vibrational progression of the symmetric stretch mode.

I-D-2 The Structures of the Ground and Excited States of $(\text{H}_3\text{NHNH}_3)$ Radical

CHEN, Feiwu¹; OKADA, Kazutoshi²; IWATA, Suehiro
(¹JST; ²GUAS)

The potential energy surface of the cation

$(\text{H}_3\text{NHNH}_3)^+$ ground state was calculated by MP2 with aug-cc-pVTZ basis set, and the surface was fitted to an analytical function by Levenberg-Marquardt method. The potential energy curves of the neutral $(\text{H}_3\text{NHNH}_3)$ ground state and first three excited states were calculated with UHF-CIS with the same basis set as for the cation. It can be seen from those curves that the barrier for proton transfer becomes lower and the tunneling effect, especially for the first excited state, becomes significant when the distance between two nitrogen nuclei is smaller. The bond length of the cation calculated by MP2 is 2.697 \AA , which is in excellent agreement with the experiment data $2.69(5)\text{ \AA}$, while the bond length calculated by HF is a little larger, 2.822 \AA . These data show the importance of the correlation effect in the computation. The frequencies for the cation and the neutral's first excited state are also calculated to attempt analyzing the recently reported absorption spectrum of $(\text{H}_3\text{NHNH}_3)$ radical.

I-D-3 The Heat of Formation of the SiF_2^{++} Dication: A Theoretical Prediction

HRUŠÁK, Jan¹; HERMAN, Zdenek; IWATA, Suehiro
(¹J. Heyrovsky Inst. Phys. Chem.)

[*Int. J. Mass Spectrom.* in press]

The energetics of the SiF_2^{++} dication and of its related fragments were calculated using different ab initio MO method, including the semiempirically corrected G2, the complete basis set (CBS) method, and the coupled cluster method up to the CCSD(T)/aug-cc-pVQZ level. The individual values of bond energies and ionization potentials were carefully compared to the available experimental data in order to get an insight into the accuracy of these approaches. In addition, reaction enthalpies for the possible fragmentation reactions were calculated. All these calculations allow a reliable prediction of the heat of formation of the SiF_2^{++} dication of $546 \pm 2\text{ kcal/mol}$.

I-D-4 Electronic Isomers in $[(\text{CO}_2)_n\text{ROH}]^-$ Cluster Anions. II. *Ab initio* Calculations

SAEKI, Morihisa¹; TSUKUDA, Tatsuya¹; IWATA, Suehiro; NAGATA, Takashi¹
(¹Univ. Tokyo)

[J. Chem. Phys. in press]

Ab initio MO calculations have been performed for the $[(\text{CO}_2)_n\text{ROH}]^-$ ($\text{R} = \text{H}$ and CH_3) anions with $n = 1$ and 2. Three stable structures are found for $[(\text{CO}_2)\text{H}_2\text{O}]^-$, and two structures for $[(\text{CO}_2)\text{CH}_3\text{OH}]^-$. All the $[(\text{CO}_2)\text{ROH}]^-$ structures are characterized by the charge localization on the CO_2 moiety, which interacts with ROH through an $\text{O}-\text{H}\cdots\text{O}$ linkage. It is also revealed that the addition of ROH to CO_2^- leads to the formation of a potential barrier against autodetachment higher than that of a bare CO_2^- , which results in the increasing stability of $[(\text{CO}_2)\text{ROH}]^-$ species. For $n = 2$ the calculations predict the existence of two types of isomers having different degrees of the excess electron localization: $\text{CO}_2^--\text{CO}_2(\text{ROH})$ and $\text{C}_2\text{O}_4^--\text{ROH}$ isomers. These “electronic isomers” are calculated to be close in energy, while their calculated vertical detachment energies (VDEs) differ by more than 1 eV. The *ab initio* results are discussed in comparison with recent experimental ones derived from photoelectron spectra of $[(\text{CO}_2)_n\text{ROH}]^-$.

I-D-5 Theoretical Studies of $[\text{Si}_4\text{NO}]^-$ Clusters with *Ab Initio* MO and DFT Methods

WANG, Wen-Ning¹; TANG, Hai-Rong¹; FAN, Kang-Nian¹; IWATA, Suehiro
(¹Fudan Univ.)

[Chem. Phys. Lett. **310**, 313 (1999)]

Various isomers of $[\text{Si}_4\text{NO}]^-$ cluster have been studied at both UHF/6-31G* and UB3LYP/6-31G* levels. The optimized structures and harmonic vibrational frequencies were calculated at both levels of approximations. Two obviously different groups of isomers have been found as in the case of $[\text{Si}_4\text{NO}]^+$, and the Si_4^- cluster shows higher reactivity toward NO molecule than Si_4^+ . The differences between anionic and cationic Si_4NO clusters and the comparison with the experimental results were discussed.

I-D-6 Theoretical Studies of Core-Excitation and Auger-Decay Processes in Site- or State-Specific Bond Dissociation Reaction with *Ab Initio* MO Methods

MITANI, Masaki¹; TAKAHASHI, Osamu¹; SAITO, Ko¹; IWATA, Suehiro
(¹Hiroshima Univ.)

In several recent experiments using soft X-ray light source, molecules having CO and CN groups separated by a CH_2 chain, such as $\text{CH}_3\text{OCOCH}_2\text{CN}$ and $\text{CH}_3\text{CO}(\text{CH}_2)_3\text{CN}$, indicate the site- or state-specific bond dissociation after photo-excitation of core electron. These reactions suggest the possibility of controlling chemical reaction by inner shell excitation by selectively breaking a chemical bond at a desired atomic site. Thus, to predict the selective chemical processes, it is important to theoretically explore the reaction mechanisms of core-excitation, Auger-decay and bond-dissociation processes.

Photo-absorption spectrum is calculated by the static exchange (STEX) approximation as follows: (i) electronic structure calculations of ground and core-holed states, (ii) construction of STEX Hamiltonian and (iii) imaging of spectrum. STEX procedure is applied to $\text{CH}_3\text{OCO}(\text{CH}_2)_n\text{CN}$ ($n = 0-3$) using DZP+Rydberg and TZP+Rydberg basis sets with 20s20p20d functions on the core-holed atom. The comparison between theoretical and experimental results for $\text{CH}_3\text{OCOCH}_2\text{CN}$ indicates that the former basis set is too small for quantitative estimation of peak positions in both N- and O-edge spectra. Two peaks assigned to $\text{N}(1s) \rightarrow \pi^*(\text{CN})$ and $\text{N}(1s) \rightarrow \pi^*(\text{CO})$, respectively, have been observed by N-edge experiment around 400 eV. If N and CO are separated by a CH_2 unit, however, the direct excitation $\text{N}(1s) \rightarrow \pi^*(\text{CO})$ has no transition moment. Therefore, only one peak, which corresponds to the $\text{N}(1s) \rightarrow \pi^*(\text{CN})$ excitation, is found in the STEX calculations. On the other hand, in the experimental spectra there are two peaks found. The theoretical $\text{N}(1s) \rightarrow \pi^*(\text{CN})$ peak for the enol-isomer of this molecule is shifted by about 0.4 eV from that of the keto-isomer. It is most probable that one of experimental peaks is the band of the enol structure.

Auger transition rates from core-holed molecules are estimated by means of Mulliken population analysis. Because the exact calculation of Auger intensity is difficult for molecular systems, approximated procedures may be desired. Transition probability in Auger decay process is expressed by the integrals including unknown Auger electron orbital, and such calculations have been performed only for diatomic molecules. As for polyatomic molecules, the estimation is carried out frequently by employing the integrals for isolated atoms. If the contribution of Auger electron is omitted, Auger intensity correlates with the orbital overlap between initial core-holed and final valence-holed orbitals. Since core molecular orbital (MO) is localized on specific atom, it is expected that the intensity may be approximated by Mulliken populations of valence-holed MOs at core-holed site. Auger final state is two-hole state, and we examine three-types of approximation as sum, product and square of two valence MO populations. These methods are applied to simple molecules of H_2O , CO, H_2CO , C_2H_2 , C_2H_6 , CH_3CN , CF_3CN with cc-pVDZ basis functions. MO populations are calculated from Hartree-Fock MO for neutral molecules. These approximations seems to be able to use for qualitative analysis of experimental normal Auger spectrum. Further refinement with the CI wave function for two-hole final states are now in progress.

I-E Prediction of Protein Tertiary Structures from the First Principles

Prediction of the three-dimensional structures of protein molecules by computer simulations is a very challenging problem in theoretical molecular science. The difficulty of the problem lies in two facts: (1) the inclusion of accurate solvent effects is non-trivial and time-consuming (2) there exist huge number of local minima in the energy function, forcing conventional simulations to get trapped in states of energy local minima. We have been exploring the strategies that allow us to overcome these difficulties.

I-E-1 Classification of Low-Energy Conformations of Met-Enkephalin in the Gas Phase and in a Model Solvent Based on the Extended Scaled Particle Theory

MITSUTAKE, Ayori¹; IRISA, Masayuki²; OKAMOTO, Yuko; HIRATA, Fumio
(¹GUAS; ²Kyushu Inst. Tech.)

[*Bull. Chem. Soc. Jpn.* **72**, 1717 (1999)]

We employed Monte Carlo simulated annealing method to classify the low-energy conformations of Met-enkephalin in the gas phase and in aqueous solution. In order to include the free energy of cavity formation in aqueous solution, we used the method of extended scaled particle theory. This was the first attempt to combine the Monte Carlo simulated annealing method and the extended scaled particle theory. We conducted 20 Monte Carlo simulated annealing runs of 10000 Monte Carlo sweeps both in the gas phase and in aqueous solution. It was found that the obtained conformations (20 each) can be classified into 3 groups of similar structure both in the gas phase and in aqueous solution. We studied in detail the structural characteristics of the classified conformations. It was found that the cavity-formation effects of aqueous solution do not drastically change the backbone structures obtained in the gas phase. The relation between the solvent-accessible surface area and the cavity-formation free energy was studied in detail. The results show unambiguously that the cavity-formation free energy is not necessarily proportional to the accessible surface area, at least for a small peptide.

I-E-2 Temperature Dependence of Distributions of Conformations of a Small Peptide

MITSUTAKE, Ayori¹; HANSMANN, Ulrich H. E.²; OKAMOTO, Yuko
(¹GUAS; ²Michigan Tech. Univ.)

[*J. Mol. Graphics Modell.* **16** (1999) in press]

We have performed a multicanonical Monte Carlo simulation of Met-enkephalin in order to study its low-energy conformations in detail. The obtained conformations are classified into six groups of similar structures by the pattern of intrachain hydrogen bonds. We have identified six such groups. Several thermodynamic quantities such as the distributions of hydrogen bonds and those of backbone dihedral angles are obtained as a function of temperature. From these results, it was concluded that at least four of the six

groups are well-defined local-minimum-energy states.

I-E-3 α -Helix Propensities of Homo-Oligomers in Aqueous Solution Studied by Multicanonical Algorithm

MITSUTAKE, Ayori¹; OKAMOTO, Yuko
(¹GUAS)

[*Chem. Phys. Lett.* **309**, 95 (1999)]

Helix-coil transitions of homo-oligomers in aqueous solution are studied by multicanonical Monte Carlo simulations. The solvation effects are represented by the term that is proportional to the solvent-accessible surface area of the peptides. Homo-oligomers of length 10 are considered for two characteristic amino acids, alanine and glycine, which are helix former and helix breaker, respectively. It is shown that the helix-coil transition temperature for homo-alanine in water is considerably lower than in gas phase. The helix propagation parameter s and nucleation parameter σ for both alanine and glycine are calculated and shown to be in remarkable agreement with experimental results.

I-E-4 Replica-Exchange Molecular Dynamics Method for Protein Folding

SUGITA, Yuji; OKAMOTO, Yuko

[*Chem. Phys. Lett.* in press]

We have developed a formulation for molecular dynamics algorithm for the replica-exchange method. The effectiveness of the method for protein folding problem is tested with a penta peptide, Met-enkephalin. The method can overcome the multiple-minima problem by exchanging non-interacting replicas of the system at several temperatures. From only one simulation run, one can obtain probability distributions in canonical ensemble for a wide temperature range by the multiple-histogram reweighting techniques, which allows the calculation of any thermodynamic quantity as a function of temperature in that range.

I-F Theoretical Studies of Chemical Reaction Dynamics

I-F-1 Quantum Reaction Dynamics of Heavy-Light-Heavy Systems: Reduction of the Number of Potential Curves and Transitions at Avoided Crossings

NOBUSADA, Katsuyuki¹; TOLSTIKHIN, Oleg I.²; NAKAMURA, Hiroki
(¹Hokkaido Univ.; ²IMS and Lebedev Phys. Inst.)

[*J. Phys. Chem. A* **102**, 9445 (1998)]

Two decoupling procedures are proposed within the framework of the hyperspherical coordinate approach in order to reduce the number of states in the close-coupling calculations and to clarify the reaction mechanisms. Sharply avoided adiabatic states are diabatically connected and relabeled without any diabatic coupling there. This is named diabatic decoupling and is useful for decoupling two manifolds of states belonging to different categories. Furthermore, the number of states is reduced in such a way that only a limited number of adjacent adiabatic states are taken into account in the close-coupling calculations for each relevant state. This is called adiabatic decoupling scheme. These reductions of the number of states enable us to analyze reactions in terms of nonadiabatic transitions at avoided crossings among the small number of adiabatic potential curves. The method is applied to $O(^3P) + HCl \rightarrow OH + Cl$ and $Cl + HCl \rightarrow HCl + Cl$. The idea of vibrationally nonadiabatic transitions at avoided crossings together with the concept of potential ridge introduced in our previous paper can untangle the congested potential curves and clarify reaction mechanisms.

I-F-2 Quantum Reaction Dynamics of $Cl + HCl \rightarrow HCl + Cl$: Vibrationally Nonadiabatic Reactions

NOBUSADA, Katsuyuki¹; TOLSTIKHIN, Oleg I.²; NAKAMURA, Hiroki
(¹Hokkaido Univ.; ²IMS and Lebedev Phys. Inst.)

[*J. Mol. Struct. (THEOCHEM)* **461-462**, 137 (1999)]

Quantum reaction dynamics of $Cl + HCl \rightarrow HCl + Cl$ for J (total angular momentum) = 0 is studied with use of the hyperspherical *elliptic* coordinate approach recently proposed by the authors. Thanks to the numerical efficiency of this approach, the reactions involving vibrational quantum jumps up to three are calculated accurately. Actually, all transitions among the states up to $v = 3$ and $j = 15$, in other words up to the total energy $E = 1.3$ eV, are covered, where v and J represent vibrational and rotational quantum numbers, respectively. Because of the symmetry of the system, the vibrationally adiabatic reactions are generally more probable than the nonadiabatic ones. However, some specific vibrationally nonadiabatic reactions even with two or three vibrational quantum jumps are found to occur efficiently. The concepts of potential ridge and non-adiabatic transitions at avoided crossings near the

ridge lines enable us to comprehend the reaction mechanisms nicely.

I-F-3 Quantum Reaction Dynamics of an Asymmetric Exoergic Heavy-Light-Heavy System: $Cl + HBr \rightarrow HCl + Br$

MIL'NIKOV, Gennady V.¹; TOLSTIKHIN, Oleg I.²; NOBUSADA, Katsuyuki³; NAKAMURA, Hiroki
(¹IMS and Inst. Struct. Macrokinetics, Russia; ²IMS and Lebedev Phys. Inst.; ³Hokkaido Univ)

[*Phys. Chem. Chem. Phys.* **1**, 1159 (1999)]

Quantum dynamics calculations for $HBr + Cl \rightarrow Br + HCl$ are carried out using the hyperspherical elliptic coordinates. The concepts of potential ridge and nonadiabatic transitions at avoided crossings introduced previously for isoergic and symmetric three-dimensional heavy-light-heavy reactions are confirmed to be useful to clarify the mechanisms of vibrationally non-adiabatic reactions in this exo-(or endo-)ergic system. The role of important avoided crossings which dominate the reaction dynamics is illustrated.

I-F-4 On the J -Shift Approximation in Quantum Reaction Dynamics

NOBUSADA, Katsuyuki¹; NAKAMURA, Hiroki
(¹Hokkaido Univ.)

[*J. Phys. Chem. A* **103**, 6715 (1999)]

The validity of the J -shift or the energy-shift approximation is investigated numerically by taking the reaction $O(^3P) + HCl \rightarrow OH + Cl$ as an example. The approximation based only on the results of J (total angular momentum quantum number) = 0, which is the ordinary J -shift approximation, cannot reproduce the exact reaction dynamics well, especially when the initial rotational quantum number is high. The reaction rate constants for specified initial rovibrational states are over- or underestimated depending on the initial state and temperature. The good agreement with the accurate result of the thermal rate constant seems to be rather accidental because of the cancellations of these over- and underestimates. An extended J -shift approximation is proposed, in which accurate calculations should be carried out up to $J = j_i$ with $|\Omega| \leq \Omega_{\max}$ when $j_i \leq \Omega_{\max}$, or up to $J = \Omega_{\max}$ when $j_i > \Omega_{\max}$, where Ω_{\max} is the maximum of the absolute values of the body-fixed projection quantum number Ω that give noticeable contributions to the reaction dynamics. When the maximum J required to have a well converged cross-section and rate constant is much larger than j_i it is recommended to carry out accurate calculations at some representative J values and to use these values to estimate probabilities at other J values by an appropriate interpolation or extrapolation procedure.

I-F-5 Electronically Adiabatic Chemical Reactions Analyzed by the Semiclassical Theory of Nonadiabatic Transition

ZHU, Chaoyuan; NAKAMURA, Hiroki; NOBUSADA, Katsuyuki¹

(¹Hokkaido Univ.)

The previously proposed qualitative conceptualization of heavy-light-heavy (HLH) chemical reactions on single potential energy surface (PES) as vibrationally nonadiabatic transitions at avoided crossings along the potential ridge lines is confirmed and further extended. An analytical as well as quantitative analysis of three-dimensional HLH reactions is carried out by applying the new semiclassical theory of nonadiabatic transition established by Zhu and Nakamura. About one thousand of avoided crossings which appear in the sea of adiabatic potential curves obtained in the hyperspherical

coordinate approach are classified into relevant and irrelevant ones for reactive transitions by introducing a diabatic decoupling procedure based on the dimensionless parameter of the new semiclassical theory. Thus about one hundred of three kinds of avoided crossings relevant for reactive transitions are specified and treated analytically. The cumulative reaction probabilities can be quite nicely reproduced quantitatively. This indicates that the clarification and conceptualization of reaction mechanisms can be done even analytically. State-to-state reaction processes can be qualitatively nicely comprehended as before, but cannot be quantitatively well reproduced, simply because inelastic transitions are not necessarily localized and cannot be well comprehended in terms of nonadiabatic transitions. An interesting series of avoided crossings responsible for rotationally inelastic transitions are found at energies lower than the threshold of reaction in the case of exo-(or endo-)ergic reaction.

I-G Theory of Nonadiabatic Transition

I-G-1 Patterns of Time Propagation on the Grid of Potential Curves

[*Phys. Rev. A* **59**, 2486 (1999)]

OSTROVSKY, Valentin N.¹; NAKAMURA, Hiroki

(¹Inst. Phys., Univ. St. Petersburg, Russia)

[*Phys. Rev. A* **58**, 4293 (1998)]

Time-propagation patterns are studied for a network formed by two bands of equidistant rectilinear parallel diabatic potential curves that cross each other. In the case of weak coupling between the bands the propagation proceeds mostly via a diabatic path. In the case of strong coupling a different regime of anti-diabatic propagation is revealed. For the intermediate case of coupling strength the propagation is basically described by an overlay of diabatic and anti-diabatic patterns; interestingly, the adiabatic propagation is never operative. The present dynamic quantum model is compared with those models that assume a reduction of the problem to a succession of pairwise transitions between the states.

I-G-2 Analytic Solution of Two-State Time-Independent Coupled Schrödinger Equations in an Exponential Model

OSHEROV, Vladimir I.¹; NAKAMURA, Hiroki

(¹IMS and Inst. Chem. Phys., Russia)

Quantum mechanically exact analytical solutions are obtained for a two-state exponential model, in which the exponent of diabatic coupling is one-half of that of the diabatic potential curve. A very simple and accurate semiclassical formula is found for the nonadiabatic transition probability. This gives a direct generalization of the Landau-Zener and Rosen-Zener formulas.

I-G-3 Semiclassical Theory of Nonadiabatic Transitions in a Two-State Exponential Model

PICHL, Lukas¹; OSHEROV, Vladimir I.²; NAKAMURA, Hiroki

(¹GUAS; ²IMS and Inst. Chem. Phys., Russia)

The two-state exponential model (repulsive potential case) is investigated and the two channel scattering problem is solved by means of semiclassical theory and high energy approximation. The analytical expression for the nonadiabatic transition matrix agrees with the previous attractive case. The only variables in this formula are the model-independent adiabatic momenta contour integrals. Oscillations of the overall transition probability when the energy is below the crossing of diabatic potentials can be observed in the case of large coupling. Unified theory of nonadiabatic transitions, covering the Landau-Zener-Stueckelberg and Rosen-Zener-Demkov models, is the aim of the present study.

I-H New Way of Controlling Molecular Processes

I-H-1 New Way of Controlling Molecular Processes by Time-Dependent External Fields

[*J. Chem. Phys.* **111**, 1415 (1998)]

TERANISHI, Yoshiaki¹; NAKAMURA, Hiroki

(¹GUAS)

A new idea of controlling molecular processes by time-dependent external fields is proposed. Molecular processes in external fields are considered to be

composed of a sequence of time-dependent nonadiabatic transitions in which the external fields play a role of adiabatic parameters. Unit final transition probability can be achieved with the use of the interference effects among various paths created by nonadiabatic transitions. The basic idea is to sweep the external field periodically at each avoided crossing and to control the transition there completely as we desire. This idea is quite general, and can hold whatever the external field is. Various control schemes can be proposed corresponding to the various types of time-dependent nonadiabatic transitions. The methods of π -pulse and chirped laser pulse with the adiabatic rapid passage may be considered as special cases of the present idea. As an example, a one-dimensional model of the laser-induced ring-puckering isomerization of trimethylenimine is considered, and comparative studies on the effectiveness and the stability of the various control schemes proposed in this paper are made together with presentation of numerical examples.

I-H-2 Control of Molecular Photodissociation with Use of the Complete Reflection Phenomenon

NAGAYA, Kuninobu¹; TERANISHI, Yoshiaki²; NAKAMURA, Hiroki
(¹GUAS; ²Inst. Phys. Chem. Res.)

In the one-dimensional nonadiabatic tunneling type curve crossing, there always occurs the intriguing phenomenon of complete reflection at certain discrete energies. We may think of controlling molecular processes with use of this phenomenon by applying a strong static laser field. By dressing up the electronic ground state of a molecule and adjusting the laser frequency appropriately, we can create the nonadiabatic tunneling potential surface crossing and the complete reflection condition to stop the dissociation into a certain direction. Although the complete reflection cannot be "complete" in a multi-dimensional space, we can control molecular photodissociation to some extent. Even in the case that a molecule cannot dissociate into a certain direction because of a high potential barrier in the excited state, we can dissociate that molecule into such a channel with use of the present method in principle. Two-dimensional model systems mimicking HOD and CH₃SH molecules are numerically studied.

I-I Molecular Switching with Use of the Complete Reflection Phenomenon

I-I-1 Molecular Switching in a Two-Dimensional Constriction

NAKAMURA, Hiroki

[*J. Chem. Phys.* **110**, 10253 (1999)]

The new idea of molecular switching discussed previously for the one-dimensional system [Nanbu, Nakamura and Goodman; *J. Chem. Phys.* **107**, 5445

(1997)] is extended to a two-dimensional constriction model. Analytical formulation is provided with use of the Mathieu functions and the semiclassical theory of nonadiabatic transition. Numerical demonstrations are also carried out. Both reflection and transmission, and thus the switching cannot be complete like in the one-dimensional case, but the switching is demonstrated to be quite effective. Although this is a purely theoretical model at this stage, some practical implications are discussed.

I-J Theoretical Study of Dissociative Recombination

I-J-1 Analytical Treatment of Singular Equations in Dissociative Recombination

PICHL, Lukas¹; NAKAMURA, Hiroki; HORACEK, Jiri²

(¹GUAS; ²IMS and Charles Univ., Czech Rep.)

[*Comput. Phys. Commun.* in press]

The Lippmann-Schwinger type singular integral equation, which arises in the multi-channel quantum defect theory of dissociative recombination process, is investigated. The singularity of its kernel is treated analytically by introducing an energy dependent quadrature. In many cases of physical interest the energy-dependent coupling potential, which gives the integral kernel of the equation, is quasi-separable in a way that allows to write down an analytical solution. The analytical treatment as well as the new solution are

illustrated by taking the H₂⁺ as an example. Our method is demonstrated to be much better than the conventional ones, such as the first order perturbation theory and the grid method.

I-K Theoretical Studies of Ultrafast Nonlinear Optical Spectroscopy of Molecules in Condensed Phases

I-K-1 The Fifth- and Seventh-Order Two-Dimensional Raman Spectroscopy for Harmonic System with Nonlinear System-Bath Interactions: Gaussian-White Case

STEFFEN, Thomas¹; TANIMURA, Yoshitaka
(¹Univ. Groningen)

The quantum Fokker-Planck equation is derived for a system that is nonlinearly coupled to a harmonic heat bath. The interaction between the two subsystems is assumed to be linear in the bath coordinate but quadratic in the system coordinate. The relaxation-induced dynamics of the system are investigated by simulating the third-, fifth-, and seventh-order Raman response of a harmonic mode. The Wigner phase space representation of the wave packet dynamics provides useful insight in the nonlinear character of the system-bath coupling. For weak system-bath coupling the third-order Raman response can be explained by the perturbation theory of Okumura and Tanimura, which predicts a line width linear proportional to temperature. When the two subsystems interact strongly, the first-order perturbation theory breaks down. The impulsive fifth-order Raman response shows that in addition to the frequency fluctuations induced by the bath higher-order energy transfer between system and bath has to be considered. The nonlinearity of the system-bath interaction yields also an interesting feature in the impulsive seventh-order Raman echo response: The calculations predict a finite signal for the case of a harmonic potential and a linear coordinate dependence of the polarizability while for linear system-bath coupling this response vanishes completely due to destructive interference of different Liouville space pathways.

I-K-2 The Fifth and Seventh Order 2D Raman Spectroscopy for Harmonic System with Nonlinear System-Bath Interactions: Gaussian-Markovian Case

TANIMURA, Yoshitaka; STEFFEN, Thomas¹
(¹Univ. Groningen)

A potential system nonlinearly coupled to a Gaussian-Markovian heat bath is considered. The interaction between the two subsystems is assumed to be linear in the bath coordinate but quadratic in the system coordinate. This model delivers the frequency modulation of the potential and can be regarded as a half-breed of a Brownian oscillator model and stochastic two-level model. We deduce the quantum Fokker-Planck equation for a Gaussian-Markovian noise bath for this nonlinear system-bath interaction in the hierarchy form. An inhomogeneous broadening of molecules, which was traditionally modeled by the overdamped limit of a stochastic two-level system, is studied for a harmonic potential system by numerically integrating the equation of motion. The third-, fifth- and seventh-order off-resonant Raman signal, which are expressed by the two-,

three-, and four-time correlation function of polarizability, respectively, are calculated as the subject of two-dimensional Raman spectroscopy. These signals are very different from the result of a Brownian oscillator case. Raman echo peaks, which were predicted from the stochastic two-level theory, are observed in the two-dimensional seventh-order signal. It was shown that the seventh-order two-dimensional Raman spectroscopy is useful to measure the inhomogeneity of liquids, in the case where the fifth-order 2D signals were very weak.

I-K-3 Structural Information from Two-Dimensional Fifth-Order Raman Spectroscopy

OKUMURA, Ko; TANIMURA, Yoshitaka; TOKMAKOFF, Andrei¹
(¹MIT)

[*J. Chem. Phys.* **111**, 492 (1999)]

Two-dimensional (2-D) fifth-order Raman spectroscopy is a coherent spectroscopy that can be used as a structural tool, in a manner analogous to 2-D nuclear magnetic resonance (NMR) but with much faster time scale. By including the effect of dipole-induced dipole interactions in the molecular polarizability, it is shown that 2-D Raman experiments can be used to extract distances between coupled dipoles, and thus elucidate structural information on a molecular level. The amplitude of cross peaks in the 2-D Raman spectrum arising from dipole-induced dipole interactions is related to the distance between the two dipoles (r) and the relative orientation of the dipoles. In an isotropic sample with randomly distributed dipole orientations, such as a liquid, the cross peak amplitude scales as r^6 . In an anisotropic sample such as a solid, where the orientational averaging effects do not nullify the leading order contribution, the amplitude scales as r^3 . These scaling relationships have analogy to the dipole coupling relationships that are observed in solid state and liquid 2-D NMR measurements.

I-K-4 Two-Dimensional Line Shape Analysis of Photon Echo Signal

OKUMURA, Ko; TOKMAKOFF, Andrei¹; TANIMURA, Yoshitaka
(¹MIT)

[*Chem. Phys. Lett.* in press]

We analyze the two-dimensional (2D) line shape obtained by 2D Fourier transforming the time-domain response of a photon echo signal as a function of the two coherence periods, t_1 and t_3 . The line shape obtained for a two level system with homogeneous and inhomogeneous broadening is shown to be sensitive to the magnitude of both of these line-broadening mechanisms. It is shown that the ellipticity of the 2D

line shape can be related to the ratio of homogeneous to inhomogeneous broadening.

I-K-5 Cage Dynamics in the Third-Order Off-Resonant Response of Liquid Molecules: A Theoretical Realization

OKUMURA, Ko; BAGCHI, Biman¹; TANIMURA, Yoshitaka
(¹*Indian Inst. Sci.*)

It is generally believed that the ultrafast initial spectroscopic response from the molecules in the condensed phase originates from small amplitude inertial motions within the cage formed by the nearest-neighbor solvent molecules surrounding the probe, or the cage effect. However, no quantitative estimate of this dynamics has been available for the currently popular experiments which measure the third-order off-resonant response. In this work, we fill this gap by a microscopic approach and demonstrate that the cage dynamics alone can produce the initial rise in the subpicosecond (≈ 200 fs) range in the third-order response. A simple analytical expression for the initial Gaussian time constant relevant to various kinds of the third-order off-resonant experiments is presented, which is found to be rather strongly dependent on the temperature. Connection with the non-polar solvation dynamics is also discussed.

I-K-6 Dynamical Stokes Shift Observed by Two-Dimensional Raman Spectroscopy

SUZUKI, Yoko; TANIMURA, Yoshitaka

We analyze the effect of relaxation process of wavepackets created in the electronic excited state on off-resonant two-dimensional Raman spectroscopy, employing the Brownian motion model with a non-equilibrium initial condition described by a displaced Gaussian wavepacket. We calculate three-time correlation functions of the excited state polarizability, which correspond to the fifth-order Raman signal in the excited state by using the Feynman's path integral formalism. It is found that the fifth-order signal is sensitive to the initial position of the Gaussian wavepacket not only for the underdamped case but also for the overdamped case.

I-K-7 A Thermal Bath Induced New Resonance in Linear and Nonlinear Spectra of Two-Level Systems

GANGOPADHAYAY, Gautam¹; GHOSHAL, Sharmistha¹; TANIMURA, Yoshitaka
(¹*S. N. Bose Natl. Cent. Basic Sci.*)

[*Chem. Phys.* **242**, 367 (1999)]

Within the scope of generalized master equation we have shown the effect of bath with finite bandwidth on the linear absorption and on the resonance fluorescence and absorption spectra of a driven two-state system. It is found that depending on the bandwidth and temperature of the bath a reversible dynamics may set in even in the case of linear absorption induced by weak field. At higher temperature the bath induces new resonance on the spectral profiles.

I-L Ab Initio Molecular Orbital Studies of Organic Conductors

I-L-1 Structures and Electronic Phases of the Bis(Ethylenedithio)Tetrathiafulvalene (BEDT-TTF) Clusters and κ -(BEDT-TTF) Salts: A Theoretical Study Based on Ab Initio Molecular Orbital Methods

IMAMURA, Yutaka¹; TEN-NO, Seiichiro; YONEMITSU, Kenji; TANIMURA, Yoshitaka
(¹*GUAS*)

[*J. Chem. Phys.* **111**, 5986 (1999)]

Electronic and geometrical structures of bis-(ethylenedithio)tetrathiafulvalene (BEDT-TTF) molecules are studied using ab initio molecular orbital methods. The optimized structure of a BEDT-TTF monomer is close to the experimental one within errors of 0.02 Å and 0.5 degree in bond length and angle, respectively, except the ethylene group. Ab initio parameters such as transfer integrals and Coulomb interactions are determined from the BEDT-TTF dimer and tetramer calculations. Using model Hamiltonians with the ab initio parameters, we investigate the electronic states based on the exact diagonalization

method. The results show that the ground state has antiferromagnetic correlation which is consistent with experimental results. We study the effects of long-range Coulomb interactions employing the 2-D extended Hubbard model with the Hartree-Fock approximation. It is found that the ground state shows various phases; antiferromagnetic, charge ordering, and paramagnetic ones, controlled by the long-range interactions.

I-L-2 Ab Initio MO Studies on Electronic States of DCNQI Molecules

IMAMURA, Yutaka¹; TEN-NO, Seiichiro; TANIMURA, Yoshitaka
(¹*GUAS*)

[*J. Phys. Chem. B* **103**, 266 (1999)]

Electronic and geometrical structures of DR-DCNQI molecules (R = H, Cl, Br, I, Me and OMe) were studied by performing ab initio MO calculations at the HF/DZP level. We carried out DCNQI monomer calculations and found that the optimized structures are close to experimental ones within errors of 0.04 Å in a six-

membered ring. We then discussed the basis set dependence of geometrical parameters and concluded that the polarization functions improve the description for double and triple bond states. Ab initio parameters such as transfer integrals were calculated for DCNQI dimers and trimers and compared with formerly calculated parameters. We found that the transfer integrals correlate well with lattice parameters of the *c* axis.

I-L-3 Theoretical Study on Electron Correlation of 1-D (DCNQI)₂M (M = Li, Ag)

IMAMURA, Yutaka¹; TEN-NO, Seiichiro;
YONEMITSU, Kenji; TANIMURA, Yoshitaka
(¹GUAS)

[*Chem. Phys. Lett.* **298**, 15 (1998)]

We study electronic states of the (DCNQI)₂M (M = Li and Ag) salts based on the full configuration interaction (FCI) method using effective Hamiltonians derived from the ab initio molecular orbital theory. FCI results of the DCNQI tetramer and octamer models indicate that the ground state has the antiferromagnetic and charge ordering correlations. It corresponds to the 2 kF spin density wave and 4 kF charge density wave states (SDW and CDW). In the octamer model, it is also found that some low-lying excited states have similar spin-flipped CDW correlations and the antiferromagnetic correlation is weakened. Electronic and geometrical structures of DR-DCNQI molecules (R = H, Cl, Br, I, Me and OMe) were studied by performing ab initio MO calculations at the HF/DZP level. We carried out DCNQI monomer calculations and found that the optimized structures are close to experimental ones within errors of 0.04 Å in a six-membered ring. We then discussed the basis set dependence of geometrical parameters and concluded that the polarization functions improve the description for double and triple bond states. Ab initio parameters such as transfer integrals were calculated for DCNQI dimers and trimers and compared with formerly calculated parameters. We found that the transfer integrals correlate well with lattice parameters of the *c* axis.

I-M Electron, Positron and Heavy Particle Scattering Dynamics

We are concerned with theoretical aspects on scattering dynamics resulting from electron, positron, and ion and atom collisions with polyatomic molecules. A few subjects we put emphasize are: (i) a comparative study of electron and positron scattering from polyatomic molecules, (ii) dissociative positron attachment, (iii) resonances in electron, positron and ion impacts on molecules, and (iv) atomic collisions at ultra-low temperature.

I-M-1 Strong Mode Dependence of 3.8-eV Resonance in CO₂ Vibrational Excitation by Electron Impact

KIMURA, Mineo¹; TANAKA, Hiroshi²; KITAJIMA, Masashi²; TAKEKAWA, Michiya³; ITIKAWA, Yukikazu³

(¹Yamaguchi Univ. and IMS; ²Sophia Univ.; ³Inst. Space Astro. Sci.)

Vibrational excitation modes are significantly enhanced by the presence of the shape resonance at 3.8 eV in a CO₂ molecule, but these modes are found to show quite different energy-dependence in the resonance peak. This feature arises from the different interaction scheme for excitation to each mode, *i.e.*, the weak polarization interaction for excitation to the symmetric stretching mode, weak dipole interaction for excitation to the bending mode, and strong dipole interaction for excitation to the asymmetric stretching mode. The asymmetric stretching shows sharp increase in differential cross sections (DCSs) toward small angle scattering due to the strong dipole interaction which washes out resonance features appeared at intermediate angles. DCSs for the symmetric and bending modes clearly show conspicuous isotropic features around 3.8 eV, thus emerging a sharp resonance.

I-M-2 Strong Suppression of Positronium Formation in Fluorinated Hydrocarbons in Positron Scattering: A Possibility of Bound States

SUEOKA, Osamu¹; KIMURA, Mineo^{1,2}

(¹Yamaguchi Univ.; ²IMS)

Strong suppression in positronium (Ps) formation is observed, for the first time, in fluorinated hydrocarbons. The reduction in Ps-formation cross sections is significantly pronounced, and the Ps-formation cross sections for fluorinated hydrocarbons (CF₄, C₂F₆, C₃F₈) are smaller by a factor of four-to-five than those for hydrocarbon counterparts (CH₄, C₂H₆, C₃H₈). This finding is a strong indication for the existence of bound states in fluorinated hydrocarbons because the high electronegativity of F atoms form F⁻ ions, and this in turn attracts positrons and forms a bound state near the edge of the charge distribution, thus reducing Ps formation.

I-M-3 Electron Capture in Collisions of Protons with CO Molecules in the keV Region: The Steric Effect

KIMURA, Mineo¹; GU, Jian-ping²; HIRSCH,

Gerhard²; BUENKER, Robert J.²; STANCIL, P. C.³
(¹Yamaguchi Univ. and IMS; ²Bergische Univ.; ³Oak Ridge Natl. Lab.)

Electron capture resulting from collisions of H⁺ ions with CO molecules has been investigated based on the molecular representation within the fully quantum mechanical formalism below 10 keV/u. Three different molecular configurations have been considered for collision dynamics, *i.e.*, (i) the proton approaches the center of mass of the CO molecule in the perpendicular configuration, (ii) the proton approaches the C atom in the collinear configuration, and (iii) the proton approaches the O atom in the collinear configuration. Electron capture dynamics and corresponding capture cross sections depend very sensitively on the molecular configuration, thus revealing a strong steric effect. The capture cross section from the CO electronic ground state is about 1.3×10^{-15} cm² at 10 keV/u, which is in good agreement with experimental findings. Differential cross sections (DCS's) for three molecular orientations have been examined both for elastic and electron capture processes, and the DCS averaged over all the configurations was found to agree well with a measurement from 0.02° to 1° at 1.5 keV/u.

I-M-4 The Isomer Effect on Charge Transfer: Collisions of Ground State C⁺ Ions with Allene and Propyne (C₃H₄)

KIMURA, Mineo¹; KUSAKABE, Toshio²; IMOU, Kazumichi²; SATOH, Shinichi²; NAKANISHI, Hiroshi²; TOMITA, Noriaki²; TAWARA, Hiroyuki³; NAKAI, Yohta²

(¹Yamaguchi Univ. and IMS; ²Kinki Univ.; ³Natl. Inst. Fusion Sci.)

The isomer effect on charge transfer in collisions of C⁺ ions with allene and propyne (C₃H₄) molecules has been observed for the first time experimentally in the collision energy from 0.15 keV to 4.5 keV. In the present experiment, the ground state C⁺ (²P) ion projectiles have been produced by carefully energy-controlled electron impact to minimize the influence of the metastable-state ions. The observed cross sections are found that charge transfer cross sections for allene are slightly larger than those of propyne below 1 keV, although the difference becomes smaller as the collision energy increases. Both cross sections gradually decrease from around 1×10^{-14} cm² to 3×10^{-15} cm² as the collision energy increases from 0.2 keV to 4 keV. Since the molecular size of both molecules is similar, the size effect does not influence strongly on the cross section, but electronic structure is expected to be responsible to this difference. The dipole moment of propyne is larger

by a factor of four than that of allene, which should cause the more pronounced effect on the dynamics at much lower collision energies.

I-M-5 Electron Capture and Excitation in Collisions of Si^{2+} Ions with He Atoms at Intermediate Energies

KIMURA, Mineo¹; SUZUKI, Satoshi²; SHIMAKURA, Noriyuki²; GU, Jian-ping³; HIRSCH, Gerhart³; BUENKER, Robert J.³; STANCIL, P. C.⁴

(¹*Yamaguchi Univ. and IMS*; ²*Niigata Univ.*; ³*Bergische Univ.*; ⁴*Oak Ridge Natl. Lab.*)

We have investigated electron capture and excitation in collisions of Si^{2+} ions with He atoms in the collision energy range from 0.02 keV/u to 6 keV/u based on a molecular representation. Molecular states are determined by using the multireference single- and double excitation configuration interaction method. We have considered electron capture and excitation both by the ground singlet and metastable triplet Si^{2+} ions. The capture cross section by the ground singlet Si^{2+} ion increases with increasing collision energy, and reaches a value of $\sim 1.3 \times 10^{-16} \text{ cm}^2$, while that by the metastable triplet ion is found to be large with a magnitude of $4 \times 10^{-16} \text{ cm}^2$ at the highest energy studied. Weak, but conspicuous, oscillatory structures are found for both cases, which are due to multichannel interference. The present rate coefficient for the ground singlet Si^{2+} ion impact is found to be much smaller than those of the $[\text{Si}^{4+} + \text{He}]$ system earlier studied

I-N Electronic Structure of a Molecule in Solution

Chemical reaction is undoubtedly the most important issue in the theoretical chemistry, and the electronic structure is a key to solve the problem. As long as molecules in the gas phase are concerned, the theory for the electronic structure has been enjoying its great success. However, when it comes to molecules in solution, the stage of theory is still an infant. We have recently proposed a new method referred to as RISM-SCF based on the integral equation theory of molecular liquids (RISM) and the *ab initio* electronic structure theory (SCF).¹⁾ The integral equation approach replaces the reaction field in the continuum models by a microscopic expression in terms of the site-site radial distribution functions between solute and solvent.

$$V_{\lambda} = \sum_j \int 4\pi r^2 \frac{q_j}{r} g_{j\lambda}(r) dr$$

where j and λ specify solvent and solute sites, respectively, and r denotes the solvent density. The site-site radial distribution functions $g_{j\lambda}(r)$ can be calculated from the extended RISM equation. Using V_{λ} the solvated Fock operator is defined as,

$$F^s = F^g - \sum_{\lambda} V_{\lambda} b_{\lambda}$$

where b_{λ} is a population operator of solute atoms. The statistical solvent distribution around solute is determined by the electronic structure or the partial charges of solute, while the electronic structure of solute is influenced by the solvent distribution. Therefore, the Hartree-Fock equation and the RISM equation should be solved in a self-consistent manner. It is this self-consistent determination of the solute electronic structure and the solvent distribution around the solute that features the RISM-SCF procedure.

The same Fock operator can be derived from a variation principle.²⁾ Defining the Helmholtz free energy A as following;

$$A = E_{\text{solute}} + \Delta\mu$$

where E_{solute} is the energy of solute under solvent influence, and $\Delta\mu$ is the solvation free energy represented in terms of the Singer-Chandler formula. The Fock operator for a solute molecule in solvent as well as the RISM-HNC equations can be obtained as the first order variations with respect to the wave functions and the pair correlation functions under the constraint of the orthonormality to the molecular orbitals. The latest development along this line are reported below.

References

- 1) S. Ten-no, F. Hirata and S. Kato, *Chem. Phys. Lett.* **214**, 391 (1993); *J. Chem. Phys.* **100**, 7443 (1994)
- 2) H. Sato, F. Hirata and S. Kato, *J. Chem. Phys.* **105**, 1546 (1996).

I-N-1 The Syn-/Anti- Conformational Equilibrium of Acetic Acid in Water Studied by the RISM-SCF/MCSCF Method

SATO, Hirofumi; HIRATA, Fumio

[*J. Mol. Struct. (THEOCHEM)* **461**, 113 (1999)]

The syn-/anti- conformational equilibrium of acetic acid in water is studied by the RISM-SCF/MCSCF method, a hybridized method of the *ab initio* quantum chemistry and the statistical mechanics of molecular liquids. The solvent effect on the two conformers is examined in terms of the solvation free energy. Significant stabilization due to solvation was observed on the anti-conformer, while only slight decrease in the free energy is resulted in the syn-conformer. Due to the greater stabilization in the anti-conformer, the energy gap between the two conformers is dramatically reduced in solution; 1.7 kcal/mol in solution compared with 6.9 kcal/mol in gas phase. The change in the electron density of acetic acid upon transferring the solute from gas phase into aqueous solution is visualized to understand the polarization effects due to solvent.

I-N-2 RISM-SCF Study for the Free Energy Profile of Menshutkin Type Reaction $\text{NH}_3 + \text{CH}_3\text{Cl} \rightarrow \text{NH}_3\text{CH}_3^+ + \text{Cl}^-$ in Aqueous Solution

NAKA, Kazunari¹; SATO, Hirofumi; MORITA, Akihiro¹; HIRATA, Fumio; KATO, Shigeki¹
(¹Kyoto Univ.)

[*Theor. Chem. Acc.* **102**, 165 (1999)]

The free energy profile for the Menshutkin type reaction $\text{NH}_3 + \text{CH}_3\text{Cl} \rightarrow \text{NH}_3\text{CH}_3^+ + \text{Cl}^-$ in aqueous solution is studied using the RISM-SCF method. The effect of electron correlation on the free energy profile is estimated by the RISM-MP2 method at the HF optimized geometries along the reaction coordinate. The vibrational frequencies at the reactant, transition state and product are found to undergo a large influence by the solvation and these are utilized to calculate the zero-point energy correction of the free energy profile. The computed barrier height and reaction exothermicity are in reasonably agreement with those of the experiment and the previous calculations. The change of solvation structure along the reaction path are represented by the

radial distribution functions between the solute-solvent atomic sites. The mechanisms of the reaction are discussed from the view points of solute electronic and solvation structures.

I-N-3 Thermodynamic Analysis of the Solvent Effect on Tautomerization of Acetylacetone: An *Ab Initio* Approach

ISHIDA, Tateki¹; HIRATA, Fumio; KATO, Shigeki¹
(¹Kyoto Univ.)

[*J. Chem. Phys.* **110**, 3938 (1999)]

The keto-enol tautomerism of acetylacetone in solution is studied with the reference interaction site model self-consistent-field (RISM-SCF) method. We choose three solvents, H₂O, dimethyl sulfoxide (DMSO), and carbon tetrachloride (CCl₄), representing, respectively, protic polar, aprotic polar and nonpolar solvents. The analysis is made taking account of the solute electronic as well as geometrical change of the tautomers due to solvent effect. In addition, the electronic correlation energy of solute molecule and solute vibrational energies are considered. The free energy differences are analyzed by decomposing them into the enthalpy and entropy terms. The theory reproduces the total free energy determined by the experiment fairly well. We also find that, as solvent polarities increase, the keto tautomer shows the drastic geometric change in order to make its dipole moment larger and that the geometric change of the keto tautomer is enthalpically driven in H₂O and entropically in DMSO. It is made clear that these depend on the solvent property protic or aprotic.

I-N-4 Solvation Dynamics of Benzonitrile Excited State in Polar Solvents: A Time-Dependent Reference Interaction Site Model Self-Consistent Field Approach

ISHIDA, Tateki¹; HIRATA, Fumio; KATO, Shigeki¹
(¹Kyoto Univ.)

[*J. Chem. Phys.* **110**, 11423 (1999)]

The solvation dynamics of benzonitrile (C₆H₅CN) after the 2¹A₁ ← 1¹A₁ vertical transition in water (H₂O), methanol (CH₃OH), and acetonitrile (CH₃CN) solvents is studied with the reference interaction site model self-consistent field (RISM-SCF) method. The evolution of solute electronic states associated with the solvent relaxation is described by a time-dependent RISM-SCF method, incorporating the time-dependent solute-solvent site-site radial distribution functions, which are derived from the surrogate linear response theory. *Ab initio* electronic structure calculations reveal that the 2¹A₁ state is of ionic nature whose dipole moment is larger by 2.41 D than that of the ground state. It is found that the excited state dipole moment is enhanced in the solutions, which provides the red shift of ~6000 cm⁻¹ in the vertical excitation energy. The solvent relaxation further increases the charge polarization in solute, indicating the electronic state of excited

C₆H₅CN is sensitive to the electrostatic field coming from the solvent. The dynamic Stokes shift is characterized by the solvation time correlation function (STCF). The calculated STCFs show that the solvent relaxation exhibits a nonexponential behavior and almost completes within 5 ps in H₂O and CH₃CN while a long-time tail is observed up to 20 ps in CH₃OH. The slow component of the decay rate is consistent with other simulation calculations though the fast one is smaller. In order to analyze the solute charge polarization during the solvent relaxation, the solute charge time correlation function (CTCF) is calculated and the resultant CTCFs are discussed in terms of the solvent charge polarization in the vicinity of solute molecule.

I-N-5 Revisiting the Acid-Base Equilibrium in Aqueous Solutions of Hydrogen Halides: Study by the *ab Initio* Electronic Structure Theory Combined with the Statistical Mechanics of Molecular Liquids

SATO, Hirofumi; HIRATA, Fumio

[*J. Am. Chem. Soc.* **121**, 2460 (1999)]

The classical problem of acid strength of the hydrogen halides in aqueous solution is revisited by means of the RISM-SCF/MCSCF theory, an *ab initio* electronic structure theory combined with the statistical mechanics of molecular liquids. Free energy changes associated with the chemical equilibrium $\text{HX} + \text{H}_2\text{O} \rightarrow \text{X}^- + \text{H}_3\text{O}^+$ are studied for a series of hydrogen halides (X: F, Cl, Br, I). The free energy differences between hydrogen halides and the dissociated anions are mainly governed by the subtle balance of the two energetic components—formation energies of hydrogen halides and solvation energies of the anions. It is shown that hydration structure around hydrogen fluoride is qualitatively different from the other three hydrogen halides. The well-known specificity of the hydrogen fluoride with respect to the acidity in aqueous solution is explained in terms of the characteristic hydration structure. Molecular geometries and electronic structures of the solute molecule as well as the solvation structure and free energy components are also discussed in detail. The old concept of electronegativity proposed by Pauling is reexamined on the basis of the modern theoretical approach.

I-N-6 *Ab Initio* Study on Molecular and Thermodynamic Properties of Water: A Theoretical Prediction of pK_w over a Wide Range of Temperature and Density

SATO, Hirofumi; HIRATA, Fumio

[*J. Phys. Chem. B* **103**, 6596 (1999)]

The ionic product of water (pK_w) has been calculated in a wide range of temperature (0–600 °C) and density (0.6–1.4 g/cm³) by means of *ab initio* electronic structure theory combined with the extended reference interaction site model in statistical mechanics for molecular liquids (RISM-SCF/MCSCF). We

consider the autoionization process ($\text{H}_2\text{O} + \text{H}_2\text{O} \rightarrow \text{H}_3\text{O}^+ + \text{OH}^-$) by regarding H_2O , H_3O^+ and OH^- as “solute” molecules in an aqueous solution and evaluate molecular geometries, electronic structure, solvation structure, and free energy components of these species as functions of thermodynamical conditions. The results for $\text{p}K_w$ obtained from the theory have shown a monotonical decrease with increasing density at all the temperatures investigated, in good accord with the experimental observation. The behavior is determined essentially by

the difference in solvation free energies, $\Delta\mu(\text{H}_3\text{O}^+) + \Delta\mu(\text{OH}^-) - 2\Delta\mu(\text{H}_2\text{O})$, associated with the reaction. The $\Delta\mu(\text{OH}^-)$ shows the density dependence, which is entirely different from that of the other species and which gives rise to the observed behavior for $\Delta\log K_w$. It is shown through analyses of the electronic structure of the “solutes” that the distinct density dependence of $\Delta\mu(\text{OH}^-)$ has the origin in its rather “soft” electronic cloud interacting with solvent polarization.

I-O Solvation Thermodynamics of Protein and Related Molecules

Concerning biomolecules such as protein, it is a final goal for the biochemistry and biophysics to explore the relation between conformations and biological functions. The first important step toward the goal would be to explain the conformational stability of biomolecules in terms of the microscopic structure of the molecules in solvent. It is an extremely difficult problem by any means due to the overwhelmingly large degrees of freedom to be handled, including protein and solvent. As long as the small and/or short-time fluctuations of protein around the native structure is concerned, a variety of molecular simulation techniques provides a quite powerful tool to explore the microscopic structure of protein and solvent. However, the techniques are not so effective to characterize stability of the macromolecules in solution, to which the thermodynamic limit ($V \rightarrow \infty$, $N \rightarrow \infty$, with $V/N = \text{const.}$) is concerned. In such a case, methods based on the statistical mechanics of liquids should be natural choice for sampling configurations of solvent interacting biomolecules. The extended RISM theory is the most promising candidate of such methods, which provides not only solvation thermodynamics but also microscopic description at the level of the pair correlation functions.¹⁾ Obvious technical difficulties which one may face in applying the theory to such a large system are not only the computation time but also the stability of the numerical solution.²⁾

Here, we present our recent effort to tackle the problem using the two theoretical tools based on the statistical mechanics of liquids: the extended RISM and the scaled particle theories (SPT).³⁾ The studies for the solvation thermodynamics of small molecules such as ions are also included because it is regarded as elementary processes for the solvation of biomolecules, and because it is prerequisite for studying the more complicated molecules.

References

- 1) M. Kinoshita, Y. Okamoto and F. Hirata, *J. Am. Chem. Soc.* **120**, 1855 (1998).
- 2) A. Kitao, F. Hirata and N. Go, *J. Phys. Chem.* **97**, 10231 (1993).
- 3) M. Irida, K. Nagayama and F. Hirata, *Chem. Phys. Lett.* **207**, 430 (1993).

I-O-1 Calculation of Solvation Free Energy for Peptide in Salt Solution Using the RISM Theory

**KINOSHITA, Masahiro¹; OKAMOTO, Yuko;
HIRATA, Fumio**
(¹Kyoto Univ.)

[*J. Comput. Chem.* **19**, 1724 (1998)]

We have developed a robust, highly efficient algorithm for solving the full reference interaction site model (RISM) equations for salt solutions near a solute molecule with many atomic sites. It is obtained as an extension of our previously reported algorithm for pure water near the solute molecule. The algorithm is a judicious hybrid of the Newton-Raphson and Picard methods. The most striking advantage is that the Jacobian matrix is just part of the input data and need not be recalculated at all. To illustrate the algorithm, we have solved the full RISM equations for a dipeptide ($\text{NH}_2\text{-CHCH}_3\text{-CONH-CHCH}_3\text{-COOH}$) in a 1M-NaCl solution. The extended simple point charge (SPC/E) model is employed for water molecules. Two different conformations of the dipeptide are considered. It is assumed for each conformation that the dipeptide is

present either as an unionized form or as a zwitterion. The structure of the salt solution near the dipeptide and salt effects on the solvation free energy have also been discussed.

I-O-2 Singular Behavior of the RISM Theory Observed for Peptide in Salt Solution

**KINOSHITA, Masahiro¹; OKAMOTO, Yuko;
HIRATA, Fumio**
(¹Kyoto Univ.)

[*Chem. Phys. Lett.* **297**, 433 (1998)]

We examine the reference interaction site model theory applied to a peptide-salt solution system, with the assumption that a zwitterionic dipeptide (Ala-Ala) is present in NaCl solution at the infinite-dilution limit. For some sets of the parameters in the peptide-cation and peptide-anion potentials, the theory exhibits singular behavior: as the salt concentration decreases, the ionic concentration around the peptide increases and the theory eventually loses its solution. The singularity is interpreted as a signal of the ion condensation. A trend of aggregation of peptide molecules is also found.

For other sets of the potential parameters, however, no such singularity occurs. As far as the salt effects are concerned, the qualitative aspects of the conclusions are somewhat sensitive to the potential parameters employed.

I-O-3 Analysis on Conformational Stability of C-Peptide of Ribonuclease A in Water Using the Reference Interaction Site Model Theory and Monte Carlo Simulated Annealing

KINOSHITA, Masahiro¹; OKAMOTO, Yuko; HIRATA, Fumio
(¹Kyoto Univ.)

[*J. Chem. Phys.* **110**, 4090 (1999)]

Solvation structure and conformational stability of the C-peptide fragment of ribonuclease A in pure water, have been analyzed using the full reference interaction site model (RISM) theory. The charged groups in the side chains of Lys-1⁺, Glu-2⁻, Lys-7⁺, Arg-10⁺, and His-12⁺ (in particular, the four like-charged groups) play substantial roles in stabilizing the conformations. The solvation free energy and the conformational energy are governed by the contribution from the

electrostatic interaction with water and the intramolecular Coulombic energy, respectively, and the conformational stability is determined by competition of these two factors. The contribution from the hydrophobic hydration and the van der Waals and torsion terms in the conformational energy are less important, which is in contrast with the result for Met-enkephalin. The Monte Carlo simulated annealing combined with the RISM theory has been applied to the C-peptide using an almost fully extended conformation as the initial one. The conformation first changes in the direction that the charged groups in the side chains are more exposed to water, and in particular, the positively charged groups are closer together. Thus, the solvation free energy decreases greatly in the initial stage. Although this leads to significant increase in the intramolecular Coulombic repulsion energy, the decrease in the solvation free energy dominates. In the later stage, however, further decrease in the solvation free energy gives rise to even larger increase in the intramolecular Coulombic repulsion energy, and the conformational change is greatly decelerated. The conformations thus stabilized in four different runs of the combined program are quite similar. The peptide conformation in water is stabilized far more rapidly than in gas phase.

I-P Collective Density Fluctuations in Polar Liquids and Their Response to Ion Dynamics

As to the model for molecular diffusion in polar liquids, there are two quite different points of view. One is the conventional rot-translation model, and the other the interaction-site description which sees the diffusion of a molecule as a correlated motion of each atom (site).¹⁾ It is clearly advantageous to use the interaction-site description compared to the rot-translation model to account for chemical characteristics of solvent as well as solute dynamics. However, the interaction-site description has its own disadvantage in interpreting physical meaning of the results, since it does not give an explicit picture for the rotational relaxation of molecules, which can be directly probed by many experimental means including the dielectric and NMR relaxation. We have solved the problem by extracting collective modes of the density fluctuation from the site-site density correlation functions. In our recent study for dynamics of molecular liquids based on the interaction-site model, we have succeeded to abstract the collective excitations in liquids, which can be identified as optical and acoustic modes, by diagonalizing the collective frequency matrix appearing in the generalized Langevin equation. The two modes arise essentially from the rotational and translational motions of molecules.²⁾ We applied the method to the ion dynamics in a dipolar liquid, and could have explained successfully the peculiar size dependence of friction of alkali and halide ions in terms of response of the collective excitations in solvent to the solute displacement.³⁾

In the past year, we have elaborated the memory kernel in our generalized Langevin equation base on the mode coupling theory. We have also extended our treatment to dynamics of water and hydrated ions. Those studies as well as other related topics are reviewed below.

References

- 1) F. Hirata, *J. Chem. Phys.* **96**, 4619 (1992).
- 2) S. Chong and F. Hirata, *Phys. Rev. E* **57**, 1691 (1998).
- 3) S. Chong and F. Hirata, *J. Chem. Phys.* **108**, 7339 (1998).

I-P-1 Effect of Molecular Symmetry on Electrical Potential Fluctuations of Solvent around Solute in Polar Liquid

CHONG, Song-Ho¹; HIRATA, Fumio
(¹Kyoto Univ.)

[*Chem. Phys. Lett.* **293**, 119 (1998)]

The electrical potential fluctuations of solvent around solute in polar liquid are studied using the recently developed method based on an integral equation theory of molecular liquids. We focus on how the molecular symmetry of solvent and solute affects the free energy profile governing electrical potential fluctuations of solvent around solute and characteristic parameters relevant to electron transfer reactions in solutions.

I-P-2 Mode-Coupling Theory for Molecular Liquids Based on the Interaction-Site Model

CHONG, Song-Ho¹; HIRATA, Fumio
(¹Kyoto Univ.)

[*Phys. Rev. E* **58**, 6188 (1998)]

We develop a microscopic theory for dynamics of molecular liquids which is based on the interaction-site model for polyatomic fluids, the projection-operator formalism of Zwanzig and Mori, and the mode-coupling theory. Closed nonlinear equations are derived for a self-consistent treatment of density propagation in a classical polyatomic liquid, which enable one to calculate dynamic structure factors provided the equilibrium structure functions of liquids are known.

I-P-3 Time-Correlation Functions in Molecular Liquids Studied by the Mode-Coupling Theory Based on the Interaction-Site Model

CHONG, Song-Ho¹; HIRATA, Fumio
(¹Kyoto Univ.)

[*Phys. Rev. E* **58**, 7296 (1998)]

Numerical results for longitudinal current spectra, velocity autocorrelation functions and diffusion coefficients of a model diatomic liquid are presented using the recently developed theory for dynamics of classical polyatomic fluids. The theory is based on the interaction-site model for molecular liquids, the projection-operator formalism of Zwanzig and Mori, and the mode-coupling theory. The effect of the inclusion of the slow contribution in memory kernels, represented by the mode-coupling expression, on the aforementioned dynamical quantities is discussed. The molecular dynamics simulation of the same system is also performed to test the accuracy of our theory, and the theoretical results are found to be in fair agreement with those obtained from the simulation.

I-P-4 Dynamics of Ions in Liquid Water: An Interaction-Site-Model Description

CHONG, Song-Ho¹; HIRATA, Fumio
(¹Kyoto Univ.)

[*J. Chem. Phys.* **111**, 3654 (1999)]

We present a molecular theory for investigating the dynamics of ions in polar liquids. The theory is based on the interaction-site model for molecular liquids and on the generalized Langevin equation combined with the mode-coupling theory. The velocity autocorrelation function, diffusion and friction coefficients of ions in water at 25 °C and at infinite dilution are studied. The theoretical results for the velocity autocorrelation functions exhibit a gradual change from oscillatory to monotonic decay as the ion size increases. The diffusion (friction) coefficients of ions in aqueous solutions pass through a maximum (minimum) as a function of the ion size, with distinct curves and maxima (minima) for

positive and negative ions. These trends are in complete accord with those of the molecular dynamics simulation results performed on the same system by Rasaiah and co-workers [*J. Phys. Chem. B* **102**, 4193 (1998)]. It is worthwhile to mention that this is the first molecular theory that is capable of describing the difference in the dynamics of positive and negative ions in aqueous solutions. A further analysis of the friction coefficients of ions in water is presented in which the friction is decomposed into the “Stokes,” dielectric and their cross terms. The Stokes and dielectric terms arise from the coupling of the ion dynamics to essentially the acoustic dynamics of the solvent via the short-range interaction, and from the coupling to the optical mode of the solvent via the long-range interaction. The most striking feature of our results is that the Stokes friction so defined does not increase monotonically with increasing ion size, but decreases when ions are very small, implying a formation of a molecular “complex” comprising the ion and its nearest neighbor solvent molecules. Interesting observations concerning the cross term are: (1) its magnitude is rather large for small ions and cannot be neglected at all, and (2) the cross term for small ions seems to cancel out the Stokes part, and consequently the total friction for small ions seems to be to a large extent determined by its dielectric component.

I-P-5 Interaction-Site-Model Description of Collective Excitations in Liquid Water. I: Theoretical Study

CHONG, Song-Ho¹; HIRATA, Fumio
(¹Kyoto Univ.)

[*J. Chem. Phys.* **111**, 3083 (1999)]

Collective excitations in liquid water are investigated using the recently developed theory for dynamics of molecular liquids which is based on the interaction-site model for polyatomic fluids, the projection-operator formalism of Zwanzig and Mori, and the simple approximation scheme for memory functions. It is shown that all the essential features of collective excitations in water, reported previously by neutron-scattering experiments, molecular dynamics simulations and dielectric theories, are well reproduced by the present theory.

I-P-6 Interaction-Site-Model Description of Collective Excitations in Liquid Water. II: Comparison with Simulation Results

CHONG, Song-Ho¹; HIRATA, Fumio
(¹Kyoto Univ.)

[*J. Chem. Phys.* **111**, 3095 (1999)]

Theoretical results for dynamical correlation functions characterizing collective excitations in liquid water reported in a previous paper are compared with molecular dynamics simulation results performed on the same system. We also examine the validity and accuracy of the approximation scheme for memory functions employed in our theory by investigating

whether the assumed form for memory functions and resulting expressions for dynamical correlation functions can be used as faithful models to reproduce the "experimental" data determined from the simulation.

I-P-7 Solvation Dynamics of a Quadrupolar Solute in Dipolar Liquids

SETHIA, Ashok; BAGCHI, Biman¹
(¹Indian Inst. Sci.)

[*J. Phys. Soc. Jpn.* **68**, 303 (1999)]

A microscopic calculation of solvation dynamics of dipolar and quadrupolar solutes in liquid water and acetonitrile is presented. The solvation is found to be biphasic. The calculated solvation time correlation function of ionic quadrupolar solute (K^+) in water is in good agreement with recent computer simulation results. Present study reveals some interesting aspects of quadrupolar solvation dynamics which differ significantly from that of ionic and dipolar solvation.

I-P-8 Density Matrix for an Excess Electron in a Classical Fluid: Results for a One-Dimensional System

SETHIA, Ashok; HIRATA, Fumio; SINGH, Yashwant¹
(¹Banaras Hindu Univ.)

[*J. Chem. Phys.* **110**, 10086 (1999)]

We extend the theory of Chandler, Singh, and Richardson [*J. Chem. Phys.* **81**, 1975 (1984)] to calculate the density matrix for an excess electron in a classical liquid like bath. For a one-dimensional fluid of hard rods and for two model potentials representing the

electron fluid atom interaction (one representing the excluded volume effect and the other attractive interaction), we calculate the density matrix using the values of solvent induced potential surfaces for the electron found from our earlier calculations [*Phys. Rev. B* **42**, 6090 (1990)]. The resulting density matrix is diagonalized and values of energies and wave-functions of the electron including the effective mass and root mean square (RMS) displacement R_β in imaginary time $\beta\hbar/2\pi$. The transition of the electron to a state of self-trapping is visualized through a sudden change in the value of R_β or the effective mass m^* at a value of β or solvent density ρ^* . For a potential model of hard rods, we find that the RMS displacement R_β for a given solvent density varies as $(\beta\hbar/2\pi)^\nu$. Values of ν are evaluated for several solvent densities.

I-P-9 Polaron Density Matrix and Effective Mass at Finite Temperature

SETHIA, Ashok; HIRATA, Fumio; TANIMURA, Yoshitaka; SINGH, Yashwant¹
(¹Banaras Hindu Univ.)

[*Phys. Rev. B* **60**, 7245 (1999)]

We calculate the density matrix elements of the polaron using the Feynman's variational method. The density matrix is diagonalized and the eigenvalues and eigenfunctions are derived. These results and the calculated density matrix are used to evaluate the root mean square (RMS) displacements R_β and the effective mass (EM) m^* for various values of coupling strengths between electron and medium and the temperature. We find that EM is related to the RMS displacement. The temperature dependence of EM is in qualitative agreement with experiment.

I-Q Liquid-Solid Interface

Due to recent progress in experimental techniques in the in situ measurements, the electrochemistry seems making a new epoch in understanding the chemical processes at electrode-solution interfaces. For examples, the scanning tunneling microscope (STM) applied to the interface has been revealing detailed atomic structure of the interface.¹⁾ The surface enhanced infrared absorption spectroscopy has provided detailed picture regarding the orientation of water molecules at the surface.²⁾ The information in atomic level have been combined with the traditional techniques in the electrochemistry such as the cyclic voltammogram to provide more complete picture of electrode-solution interfaces. Obviously, the traditional descriptions using electric double layer models, which are based on the continuum models of solvent, mismatch the level of detailness attained by the recent experimental techniques.

Theoretical understanding of the interface has also made great progress in the last two decades, especially, in terms of solvent configuration near electrode surfaces.³⁾ The progress has been mainly driven by two theoretical methods in the statistical mechanics of liquids: the molecular simulation and the integral equation methods. The two methods have reached consistent molecular pictures regarding reorganization of the water structure in the vicinity of the flat electrode surface. Latest topics in those approaches concern the electronic structure of electrode. The method features a self-consistent treatment of the liquid state and the electronic structure of the metal surface. Significance of such treatments will become more and more clear as the methods are extended to chemical reactions at the interface, which are primary motivation for the electrochemistry.

Although the integral equation methods have great advantage in the overall description of the electrode-solution interface both at phenomenological and molecular levels, the models which have been employed for the metal surface seems oversimplified considering the resolution attained by latest development in the experimental techniques stated above. Here, we propose a new approach for the electrode-solution interface based on the reference interaction site method (RISM) of liquids, which can handle both the structured metal surface and water in atomic level.

References

- 1) K. Itaya and E. Tomita, *J. Surf. Sci.* **201**, L507 (1988).
- 2) K. Ataka, T. Yotsuyanagi and M. Osawa, *J. Phys. Chem.* **100**, 10664 (1996).
- 3) L. Blum, *Adv. Chem. Phys.* **78**, 171 (1990).

I-Q-1 Acceleration of Liquid Structure Calculations by Modified Direct Inversion in the Iterative Subspace

KOVALENKO, Andriy F.; TEN-NO, Seiichiro; HIRATA, Fumio

[*J. Comput. Chem.* **20**, 928 (1998)]

We proposed a modified procedure of the direct inversion in the iterative subspace (DIIS) method to accelerate convergence in the integral equation theory of liquids. We update the DIIS basis vectors at each iterative step by using the approximate residual obtained in the DIIS extrapolation. The procedure is tested by solving the three-dimensional (3D) generalization of the reference interaction site model (RISM) equation together with the hypernetted chain (HNC) closure as well as their one-dimensional version. We calculated the 3D site distribution of water, represented by the simple point charge (SPC) model, around one water molecule considered as a central particle.

I-Q-2 Extended States of a Shallow Donor Located Near a Semiconductor-Insulator Interface

KOVALENKO, Andriy F.

[*Int. J. Quantum Chem.* **66**, 435 (1998)]

Scattering of a conduction electron by a charged shallow donor located near a semiconductor-insulator interface in the semiconductor or by a charged center embedded in the insulator is considered within the model of a hydrogen-like atom in a semi-infinite space. The interface influence is allowed for by spatial confinement of the electron envelope wavefunction. The impurity electrostatic image at the interface is taken into account. The problem is separable in prolate spheroidal coordinates and thus is solvable exactly. A rapidly convergent expansion is proposed for the angular eigenfunctions. The radial eigenfunctions are calculated directly by numerical integration of the radial boundary value problem. Expansions of the scattering wavefunction and the scattering amplitude in terms of the eigenfunctions of the problem are obtained. Using the extended and localized state wavefunctions, the photoionization cross-section of a shallow donor near a semiconductor-insulator interface is calculated. It is presented as a superposition of the oscillator strengths of transitions to the partial extended eigenstates that constitute the scattering wavefunction. Near the interface, the cross-section is enhanced significantly and redistributed over the direction of photoionized electron escape. The photoionization threshold follows the localized state energy varying with the donor - interface distance.

I-Q-3 Free Energy Profiles of Electron Transfer at Water-Electrode Interface Studied by the Reference Interaction Site Model Theory

AKIYAMA, Ryo; KINOSHITA, Masahiro¹; HIRATA, Fumio

(¹Kyoto Univ.)

[*Chem. Phys. Lett.* **305**, 251 (1999)]

Free energy profiles governing electron transfer from a reactant to an electrode surface in water are investigated, based on the reference interaction site model (RISM) theory. Three models of a redox pair for charge separation reactions are examined: a pair of atomic solutes, and systems consisting of an atom and a surface with a localized or a delocalized electron. The profile becomes highly asymmetrical, when an electron in the electrode is delocalized. The behaviors are essentially due to the asymmetrical response of water polarization to positive and negative charges of solute. The results are related to models of ion-hydration.

I-Q-4 Self-Consistent Description of a Metal-Water Interface by the Kohn-Sham Density Functional Theory and the Three-Dimensional Reference Interaction Site Model

KOVALENKO, Andriy F.; HIRATA, Fumio

[*J. Chem. Phys.* **110**, 10095 (1999)]

We have developed a self-consistent description of an interface between a metal and a molecular liquid by combination of the density functional theory in the Kohn-Sham formulation (KS DFT) for the electronic structure, and the three-dimensional generalization of the reference interaction site model (3D RISM) for the classical site distribution profiles of liquid. The electron and classical subsystems are coupled in the mean field approximation. The procedure takes account of many-body effects of dense fluid on the metal-liquid interactions by averaging the pseudopotentials of liquid molecules over the classical distributions of the liquid. The proposed approach is substantially less time-consuming as compared to a Car-Parrinello-type simulation since it replaces molecular dynamics with the integral equation theory of molecular liquids. The calculation has been performed for pure water at normal conditions in contact with the (100) face cubic centered (fcc) surface of a metal roughly modeled after copper. The results are in good agreement with the Car-Parrinello simulation for the same metal model. The shift of the Fermi level due to the presence of water conforms with experiment. The electron distribution near an adsorbed water molecule is affected by dense water, and so the metal-water attraction follows the shapes of the metal effective electrostatic potential. For the metal model employed, it is strongest at the hollow

site adsorption positions, and water molecules are adsorbed mainly at the hollow and bridge site positions rather than over metal atoms. Layering of water molecules near the metal surface is found. In the first hydration layer, adsorbed water molecules are oriented in parallel to the surface or tilted with hydrogens mainly outwards the metal. This orientation at the potential of zero charge agrees with experiment.

I-Q-5 Effective Interaction between Hard Sphere Colloidal Particles in a Polymerizing Yukawa Solvent

GEE, Richard H.¹; HENDERSON, Douglas²; KOVALENKO, Andriy F.

(¹Snow College; ²Brigham Young Univ.)

[*J. Chem. Phys.* **110**, 8189 (1999)]

The effective interaction between colloidal hard sphere particles in a Yukawa solvent that can polymerize with the formation of chains and rings is studied and compared with the corresponding results for colloidal hard sphere particles in a solvent of polymerizing hard spheres. The attractive nature of the polymerizing Yukawa solvent particles induces significant changes in the effective interactions between the colloid particles as compared to a polymerizing solvent of hard spheres that was investigated in previous studies. The results for the colloid-solvent mixture are obtained using the associative Percus-Yevick approximation for Wertheim's Ornstein-Zernike integral equation; the colloidal species are taken at a non-vanishing but very small concentration throughout this article. We present the effects of the size ratio of colloid spheres to solvent spheres, the degree of polymerization, and the solvent density on the effective interactions between colloid and solvent particles. The intercolloidal potential of mean force (PMF) is found to be highly dependent on these parameters for Wertheim's model. It is found that the correlations between colloid particles obtained using the Yukawa solvent model are longer ranged and more attractive than those found using the hard sphere solvent model. A greater depletion of the solvent density around the colloidal particles is also observed for the Yukawa solvent model as compared to the hard sphere model; an increased polymer chain length also enhances the depletion of the solvent density. The PMF is found to be oscillatory in structure. The oscillatory structure also depends upon the average polymer chain length, specifically, the oscillatory structure in the PMF is strongly diminished as the average polymer chain length increases. Additionally, as the average polymer length increases, the attraction at the colloid-colloid contact distance decreases.

I-Q-6 Potential of Mean Force between Two Molecular Ions in a Polar Molecular Solvent: A Study by the Three-Dimensional Reference Interaction Site Model

KOVALENKO, Andriy F.; HIRATA, Fumio

[*J. Phys. Chem. B* **103**, 7942 (1999)]

The orientationally dependent potential of mean force (PMF) between two charged polyatomic solutes immersed in a polar molecular solvent is obtained by using the three-dimensional reference interaction site model (3D RISM) of the integral equation theory. We propose the partially linearized hypernetted chain (PLHNC) closure. The method is applied to the *N,N*-dimethylaniline cation (DMA⁺) and the anthracene anion (AN⁻) in acetonitrile solvent (CH₃CN). We solve the 3D RISM integral equations by employing the modified direct inversion in the iterative subspace (MDIIS) method. The 3D site distributions of solvent around each solute are obtained and discussed. The PMF between the solutes is calculated as a 3D profile dependent on the relative position of the solutes at six characteristic relative orientations. The PMF obtained is in qualitative agreement with the results of molecular dynamics simulations. In solvent, the AN⁻ solute effectively attracts the DMA⁺ dimethylamino group and repels its phenyl ring. We found that the most stable relative arrangement of the DMA⁺ and AN⁻ molecules in acetonitrile solvent is different from that in gas phase.

I-Q-7 Self-Consistent, Kohn-Sham DFT and Three-Dimensional RISM Description of a Metal-Molecular Liquid Interface

KOVALENKO, Andriy F.; HIRATA, Fumio

[*J. Mol. Liq.* submitted]

We have developed a self-consistent description of a metal-molecular liquid interface by combination of the Kohn-Sham density functional theory (KS DFT) for the electronic density, and the three-dimensional reference interaction site model (3D RISM) integral equation theory for the classical site distribution profiles of molecular liquid. The electron and classical subsystems are coupled in the mean field approximation. The classical potentials of the metal acting on species of the liquid are taken in the linear response regime. Many-body effects of dense liquid on metal valence electrons are allowed for by averaging pseudopotentials of liquid molecules over the site distributions of liquid. The coupled KS DFT and 3D RISM equations are solved simultaneously by using the procedure of dynamic relaxation. The proposed approach is substantially less time-consuming as compared to a Car-Parrinello type simulation. A partial linearization of the hypernetted chain (PLHNC) closure to the RISM equation is proposed. The calculation is performed in the supercell technique for water at normal conditions in contact with the (100) FCC slab of a metal roughly modeled after copper. The results are in good agreement with the Car-Parrinello simulation for the same model. Further applications of the method proposed are discussed.

I-R Dimensional Crossovers and Randomness Effects in Quasi-One-Dimensional Organic Conductors

Electronic states in pure one dimension and those in two or three dimensions are very different from each other. In many organic conductors and copper oxides, applying external or chemical pressure controls dimensionality. The induced dimensional crossovers are classified by what kind of transverse coherence is restored by increasing dimensionality, i.e., one-particle coherence or two-particle coherence. Which coherence is restored depends on the asymptotic property of the corresponding one-dimensional system. The Tomonaga-Luttinger liquid is known to be unstable against interchain hopping since the transverse one-particle coherence is easily restored. In other one-dimensional phases, however, the transverse one-particle process is strongly suppressed by electron correlation, and then the transverse two-particle coherence is relatively easily restored. In the quasi-one-dimensional organic conductor, (TMTTF)₂X, the charge gap suppresses the transverse one-particle coherence and the two-particle crossover is accompanied by the antiferromagnetic transition. The details are investigated by the perturbative renormalization-group method from high to low temperatures and by the density-matrix renormalization-group method for the ground states. We also study the effects of random potential scattering on the competition among the Mott insulator, the Anderson localization, and the Fermi liquid phases, all of which are realized in (DI-DCNQI)₂Ag_{1-x}Cu_x and (DMe-DCNQI)₂Li_{1-x}Cu_x.

I-R-1 Spin-Density-Wave Phase Transitions in Quasi-One-Dimensional Dimerized Quarter-Filled Organic Conductors

KISHINE, Jun-ichiro; YONEMITSU, Kenji

[*J. Phys. Soc. Jpn.* **68**, 2790 (1999)]

We have studied spin density wave (SDW) phase transitions in dimerized quarter-filled Hubbard chains weakly coupled via interchain one-particle hopping, t_{b0} . It is shown that there exists a critical value of t_{b0} , t_{b0}^* , between the incoherent metal regime ($t_{b0} < t_{b0}^*$) and the Fermi liquid regime ($t_{b0} > t_{b0}^*$) in the metallic phase above the SDW transition temperature. By using the 2-loop perturbative renormalization-group approach together with the random-phase-approximation, we propose a SDW phase diagram covering both of the regimes. The SDW phase transition from the incoherent metal phase for $t_{b0} < t_{b0}^*$ is caused by growth of the intrachain electron-electron umklapp scattering toward low temperatures, which is regarded as pre-formation of the Mott gap. We discuss relevance of the present result to the SDW phase transitions in the quasi-one-dimensional dimerized quarter-filled organic conductors, (TMTTF)₂X and (TMTSF)₂X.

I-R-2 Phase Transitions from Incoherent and from Coherent Metal Phases in Quasi-One-Dimensional Organic Conductors

KISHINE, Jun-ichiro; YONEMITSU, Kenji

[*J. Low Temp. Phys.* in press]

We study effects of a preformed Mott gap and dimensionality on interchain one-particle coherence and spin-density-wave phase transitions in weakly coupled, dimerized quarter-filled Hubbard chains. A phase diagram is given, based on the two-loop perturbative renormalization-group (RG) approach together with the random phase approximation. Feedback effects of interchain processes on the umklapp process are examined by the $1 + \epsilon$ expansion. We discuss relevance of the present result to the SDW phase transitions in the quasi-

one-dimensional dimerized quarter-filled organic conductors, (TMTTF)₂X and (TMTSF)₂X.

I-R-3 Quantum Phase Transition and Collapse of Mott Gap in $d = 1 + \epsilon$ Dimensional Half-Filled Hubbard Systems

KISHINE, Jun-ichiro

[*Recent Prog. Many-Body Theories* **3** submitted]

A correlation-induced charge gap (Mott gap) plays the key role on physical properties of low-dimensional strongly correlated electron systems such as organic conductors or high- T_c cuprate superconductors. In this paper, we study dimensionality effects on the gap in $d = 1 + \epsilon$ continuous dimension, where $0 < \epsilon \ll 1$. By solving the one-loop renormalization-group equations, we found a quantum phase transition at a critical dimension, d_c , which depends on the strength of the Hubbard repulsion, U . For $d < d_c$, the Mott gap opens at the fixed point, $g_{3,\infty} = -G_\infty = \infty$, while for $d > d_c$, the Mott gap collapses at the fixed point, $g_{3,\infty} = \text{const.}$, $G_\infty = 0$. This result indicates that the Mott gap decreases with raising dimensionality.

I-R-4 Charge Gap and Interchain Correlation in Quasi-One-Dimensional Dimerized Organic Conductors

YONEMITSU, Kenji

[*Mol. Cryst. Liq. Cryst.* in press]

We study the relation between the charge gap and the interchain one-body correlation function in quasi-one-dimensional dimerized organic conductors at quarter filling, by applying the density matrix renormalization group method to a three-chain extended Hubbard model. The charge gap increases with the degree of dimerization in the intrachain hopping integrals. When the charge gap is larger than the interchain hopping integral, the interchain hopping correlation is strongly suppressed, as observed in the (TMTTF)₂X salts.

I-R-5 Magnetic and Pairing Correlation Functions and Interchain Coherence in Quasi-One-Dimensional Dimerized Organic Conductors

YONEMITSU, Kenji

[*J. Low Temp. Phys.* in press]

We study how magnetic and pairing correlation evolves with an increasing interchain hopping integral and decreasing dimerization of intrachain hopping integrals, by applying the density matrix renormalization group (DMRG) method to a three-chain extended Hubbard model at quarter filling for quasi-one-dimensional organic conductors, $(\text{TMTTF})_2\text{X}$ and $(\text{TMTSF})_2\text{X}$. Magnetic correlation changes from weakly coupled chains of large-amplitude spin density waves to an interchain-coherence-developed spin density wave. Pairing correlation increases, though it still decays exponentially owing to a charge gap for parameters considered here.

I-R-6 Effects of Dimerization on Spin, Charge and Hopping Correlation Functions in Quasi-One-Dimensional Organic Conductors

YONEMITSU, Kenji

[*Physica B* in press]

In order to see the effects of dimerization, interchain hopping, and nearest-neighbor repulsion on various one- and two-body correlation functions in quasi-one-dimensional organic conductors, $(\text{TMTTF})_2\text{X}$ and $(\text{TMTSF})_2\text{X}$, we apply the density matrix renormalization group method to a three-chain extended Hubbard model at quarter filling. The hopping correlation function shows that the interchain one-particle coherence is strongly suppressed when a charge gap due to the dimerization is larger than the interchain hopping integral. Meanwhile, the spin-spin and charge-charge correlation functions show that the interchain particle-hole coherence is rather insensitive. The charge-charge correlation function is more sensitive to the nearest-neighbor repulsion than the charge gap.

I-R-7 Interplay of Correlation, Randomness and Dimensionality Effects in Weakly-Coupled Half-Filled Random Hubbard Chains

KISHINE, Jun-ichiro; YONEMITSU, Kenji

[*Mol. Cryst. Liq. Cryst.* in press]

We study interplay of electronic correlation, randomness and dimensionality effects in half-filled random Hubbard chains weakly coupled via an interchain one-particle hopping. Based on the two-loop renormalization-group approach, phase diagrams are given in terms of temperature vs. strengths of the intra-chain electron-electron umklapp scattering, the random scattering and the interchain one-particle hopping. For strong umklapp scattering and weak interchain hopping, the antiferromagnetic phase is replaced by the Anderson localization phase with increasing random scattering. For weak umklapp scattering and strong random scattering, the Anderson localization phase is replaced by the Fermi liquid phase with increasing interchain hopping. For strong umklapp scattering and weak random scattering, the antiferromagnetic phase is replaced by the Fermi liquid phase with increasing interchain hopping.

I-R-8 Dimensionality Effects in Half-Filled Random Hubbard Chains

KISHINE, Jun-ichiro; YONEMITSU, Kenji

[*Physica B* in press]

We discuss interplay of randomness, electron correlation and dimensionality effects in half-filled random Hubbard chains. Low-temperature phases are given based on the two-loop renormalization group (RG) analysis. Feedback effects of interchain processes on the umklapp process are examined by the $1 + \epsilon$ expansion. We comment on relevance of the present result to a phase diagram of a doped organic compound, $(\text{DI-DCNQI})_2\text{Ag}_{1-x}\text{Cu}_x$.

I-S Competition among Different Charge and Lattice Ordering States in One-Dimensional Metal Complexes

The quasi-one-dimensional halogen-bridged binuclear metal complexes (MMX chains) have strong electron-lattice coupling and electron-electron interaction. They have various electronic phases. Recently, a metallic phase has been found for the ligand dta. Meanwhile, for the ligand pop, a new insulator phase is experimentally suggested in addition to the charge density wave phase. Generally considered, possible electronic phases are i) an averaged-valence (AV) state, ii) a charge-density-wave (CDW) state, iii) a charge-polarization (CP) state, iv) an alternate-charge-polarization (ACP) state, and v) a bond-charge-density-wave state. To understand the competition among these electronic states, we need to include the on-site, two kinds of nearest-neighbor, and next-nearest-neighbor repulsion strengths between electrons in M d orbitals, as well as two types of electron-lattice couplings. To reproduce both of the electronic phases for the ligand dta and those for the ligand pop, we need two types of elastic couplings among M and X ions. Thus we have several parameters to control the electronic phases. So far, changing these parameters qualitatively reproduces general tendency for the dependence of the electronic state on the interdimer distance. However, the low-temperature phase of $\text{Pt}_2(\text{dta})_4\text{I}$ has the crystal structure of the ACP phase and considerably large spin susceptibility, which remain mysterious and need further investigations.

I-S-1 Numerical Studies of Ground State Phase Diagrams for the MMX Chains

KUWABARA, Makoto; YONEMITSU, Kenji

[*Mol. Cryst. Liq. Cryst.* in press]

We study ground state phase diagrams for the MMX chains, using a one-dimensional dimerized 3/4-filled extended Hubbard-Peierls model with site diagonal and off-diagonal electron-lattice interactions. The ground states are obtained mainly in the Hartree-Fock approximation, and their accuracy is checked by the exact diagonalization of small clusters. We find a new phase in addition to frequently considered phases and compare our results with experimental results. Without electron-electron interactions, the charge-density-wave, alternate-charge-polarization (ACP), and bond-charge-density-wave (BCDW) phases are realized depending on the electron-lattice interactions. As the site off-diagonal electron-lattice interaction increases, the ACP phase becomes stable. As the site diagonal electron-lattice interaction increases, the BCDW phase becomes stable. The on-site repulsion stabilizes the averaged-valence and charge-polarization phases, while the nearest-neighbor and next-nearest-neighbor repulsion destabilizes them.

I-S-2 Magnetic Property of MMX Chains as Dimerized Quarter-Filled Systems

KUWABARA, Makoto; YONEMITSU, Kenji

[*Physica B* in press]

We study ground state phase diagrams for the MMX chains, using a one-dimensional dimerized 3/4-filled extended Hubbard-Peierls model with site diagonal and off-diagonal electron-lattice interactions. The ground states are obtained both in the Hartree-Fock approximation and by the exact diagonalization. It has been experimentally shown that the electronic structure of $\text{Pt}_2(\text{CH}_3\text{CS}_2)_4\text{I}$ is the alternate-charge-polarization (ACP) phase below 80K and has large magnetic susceptibility at low temperatures. Our results show the ACP phase is stable, if the site off-diagonal electron-lattice interaction, α , is strong enough, for any set of electron-electron interaction strengths. This phase is analogous to the spin-Peierls state. The spin gap is reduced as α becomes small because the lattice distortion becomes weak and the alternation of exchange interactions decreases. A possibility for the large magnetic susceptibility is that

the ACP state is realized in the vicinity of the averaged-valence (AV) or charge-polarization (CP) phase. The boundary between the ACP phase and the AV or CP phase is sensitive to the interdimer-nearest-neighbor repulsion.

I-S-3 Structural and Magnetic Transitions in Quasi-One-Dimensional Halogen-Bridged Binuclear Metal Complexes

KUWABARA, Makoto; YONEMITSU, Kenji

[*Mol. Cryst. Liq. Cryst.* submitted]

We investigate ground state phase diagrams for the MMX chains, using a one-dimensional dimerized 3/4-filled extended Hubbard-Peierls model with site diagonal (α) and off-diagonal (β) electron-lattice interactions. Possible electronic states include an averaged-valence (AV) state, a charge-density-wave (CDW) state, a charge-polarization (CP) state, and an alternate-charge-polarization (ACP) state. The ground state can be controlled by choosing the metal (M), bridging halogen (X), ligand, and counter ion. The variation of X affects the model parameters, α , β , the interdimer transfer through X (t_{MXM}), the elastic constant between M and X (K_{MX}) and the interdimer repulsion strengths. As to the competition between the CDW and CP states, the boundary between them shifts upward as K_{MX} increases, and is almost independent of t_{MXM} . These results suggest the possibility of the phase control by changing the halogen ion. The CP state is characterized by coexistence of lattice distortion and gapless spin excitations. Therefore the structural transition between CDW and CP states is accompanied with a magnetic transition.

I-S-4 Electric-Field Response of Exciton in Electroluminescent Polymer

LI, Lei¹; FU, Rouli²; SUN, Xin¹; YONEMITSU, Kenji
(¹Fudan Univ.; ²Natl. Lab. Infrared Phys.)

[*Phys. Status Solidi B* **214**, 337 (1999)]

In electroluminescent polymers, the exciton is polarized by a weak electric field E and dissociated by strong E . These effects can quantitatively elucidate the observed dependence of the luminous intensity of the luminescent polymer on the electric field and the field-induced charge generation in conjugated polymers.

I-T Transport and Magnetic Properties of Two-Dimensional Metal-Complex, Organic and Oxide Conductors

Antiferromagnetism and superconductivity are realized in two-dimensional, strongly correlated, organic materials. In $\kappa\text{-(BEDT-TTF)}_2\text{X}$ with the quarter-filled HOMO band and strong dimerization, the electronic phases are controlled by the ratio of the effective on-site repulsion strength to the bandwidth. The metal-assembled complexes, $\text{Et}_n\text{Me}_{4-n}\text{Z}[\text{Pd}(\text{dmit})_2]_2$, has also strong dimerization. In contrast to the former organic materials, they have a rather one-dimensional LUMO band and a two-dimensional HOMO band, both of which are largely split due to the dimerization. The phase diagram is richer than that of $\kappa\text{-(BEDT-TTF)}_2\text{X}$ in that applied pressure induces a

metal or superconductor phase depending on the cation $\text{Et}_n\text{Me}_{4-n}\text{Z}$. By using a strong-coupling expansion and mapping to an effective model, we find that the electronic phases are controlled by dimensionality and frustration due to the much more complex molecular configuration than that of $\kappa\text{-(BEDT-TTF)}_2\text{X}$. For example, for the cation $\text{Et}_2\text{Me}_2\text{Sb}$, a metallic phase appears under pressure and the antiferromagnetic order is absent because the transfer integral between next-nearest-neighbor dimers are comparable to that between nearest-neighbor ones. In addition to the materials above, many other organic conductors with various degrees of dimerization have been synthesized and the mechanisms of their insulator phases are being studied. To clarify the importance of the long-range electron-electron interactions, we are going to study optical spectra as well. The importance of the long-range electron-electron interactions is clarified also in *ab initio* molecular orbital, Hartree-Fock, and exact diagonalization studies of (BEDT-TTF) clusters and $\kappa\text{-(BEDT-TTF)}_2\text{X}$. Furthermore, the important effect of umklapp scattering processes on the quasiparticle weight is studied in the two-loop renormalization-group analysis.

I-T-1 Possible Magnetic Orders and Cation Dependence of $(\text{Et}_n\text{Me}_{4-n}\text{Z})[\text{Pd(dmit)}_2]_2$

MORI, Michiyasu; YONEMITSU, Kenji; KINO, Hiori¹
(¹JRCAT)

[*J. Phys. Soc. Jpn.* submitted]

We study the cation dependence of the insulating phase of Pd(dmit)_2 salts, based on the dimerized two-band Hubbard model. By using a strong coupling expansion, we obtain an effective Heisenberg model on an anisotropic triangular lattice. Two different magnetic orders are found possible depending on interaction strengths and the energy difference between the two bands. The variation of the cation leads to the variation of the ratio of a transfer integral in one direction to one in another direction, resulting in the variation of the ratios among the magnetic interaction strengths and that of the magnetic frustration. We calculate a sublattice magnetization at zero temperature within the linear spin wave theory and find that the antiferromagnetic order is stable except for the cation $\text{Et}_2\text{Me}_2\text{Sb}$, where the magnetic frustration is important. Our results are consistent with the ESR measurement.

I-T-2 Role of Dimensionality in Dimerized Two-Band Systems

MORI, Michiyasu; YONEMITSU, Kenji; KINO, Hiori¹
(¹JRCAT)

[*Mol. Cryst. Liq. Cryst.* in press]

We have studied the ground state properties of Pd(dmit)_2 salts using an effective dimer model. This model describes low-energy excitations of the two-band Hubbard model and is derived by a strong coupling expansion. Substituting the cation simultaneously controls dimensionality of the Fermi surface, density-of-states singularity, and magnetic frustration in the dimer model. For the cation Me_4P , the effective Fermi surface has much better nesting property and the effective Fermi level is located in the vicinity of the van Hove singularity. For the cation $\text{Et}_2\text{Me}_2\text{Sb}$, the effective Fermi surface is rather isotropic and the effective Fermi level is far from the singularity. Such cation dependence implies that the salt with Me_4P ($\text{Et}_2\text{Me}_2\text{Sb}$) prefers an insulating (metallic) phase, which is consistent with the experiments.

I-T-3 Quasi-One-Dimensional Natures in $(\text{Et}_n\text{Me}_{4-n}\text{Z})[\text{Pd(dmit)}_2]_2$

MORI, Michiyasu; YONEMITSU, Kenji; KINO, Hiori¹
(¹JRCAT)

[*J. Low Temp. Phys.* in press]

We studied one of possible ground states for Pd(dmit)_2 salts in a dimerized two-band Hubbard model. By using a strong-coupling expansion, we obtained an effective dimer model, which has a quasi-one-dimensional Fermi surface. In the insulating phase, it leads to the Heisenberg model on an anisotropic triangular lattice. We calculated effective exchange coupling strengths within the second order perturbation theory and found that both ferromagnetic and antiferromagnetic couplings are possible. Similarities to and differences from Ni(dmit)_2 salts are discussed.

I-T-4 Possible Ground State Phases of Pd(dmit)_2 Salts

MORI, Michiyasu; YONEMITSU, Kenji; KINO, Hiori¹
(¹JRCAT)

[*Physica B* in press]

We have studied possible ground state phases of Pd(dmit)_2 salts using the two-band Hubbard model. From a strong coupling expansion, an effective model is derived and used to describe low-energy excitations. It is found that mutual interactions and dimensionality of effective bands cooperatively determine the transport and magnetic properties.

I-T-5 Collective Excitations around Charge Ordering States and Coexistent States with Different Orders

MORI, Michiyasu; YONEMITSU, Kenji

[*Mol. Cryst. Liq. Cryst.* submitted]

Novel ground states have recently been studied in molecular conductors. One is the coexistence of a spin density wave (SDW) and a charge density wave (CDW) in $(\text{TMTSF})_2\text{PF}_6$, which has a quasi-one-dimensional electronic state and is the quarter-filled system with dimerization. The Hartree calculation for the one-

dimensional extended Hubbard model found the coexistence of SDW and CDW. It is known that not only the on-site but also the nearest-neighbor and the next-nearest-neighbor repulsive interactions are significant. Another is the charge ordering state in θ -(BEDT-TTF)₂MM'(SCN)₄, which has a rather-two-dimensional electronic state and is the quarter-filled system with dimerization. The Hartree calculation for a two-dimensional extended Hubbard model found various charge ordering states depending on the anisotropy of the transfer integrals and that of the intersite Coulomb interaction strength. In this paper, we study collective excitations around such novel ground states and clarify effects of the dimensionality, the dimerization and the intersite Coulomb interaction on the excitation spectra. First, the ground states of one- and two-dimensional extended Hubbard models are calculated in the fully unrestricted Hartree-Fock (UHF) level to confirm the former results. Next, response functions are calculated in the random phase approximation on the basis of the UHF states to obtain the qualitative features of optical and magnetic excitations. Owing to the intersite Coulomb interaction, excitons appear in the optical spectra. These peaks are sensitive to the dimensionality of the electronic state. The dimerization, the anisotropy of transfer integrals and the intersite Coulomb interaction affect overall feature of collective excitation spectra.

I-T-6 Ab Initio Molecular Orbital, Hartree-Fock, and Exact Diagonalization Studies of Structures and Electronic Phases of (BEDT-TTF) Clusters and κ -(BEDT-TTF) Salts

IMAMURA, Yutaka¹; TEN-NO, Seiichiro;
YONEMITSU, Kenji; TANIMURA, Yoshitaka
(¹GUAS)

[*J. Chem. Phys.* **111**, 5986 (1999)]

Electronic and geometrical structures of bis-(ethylenedithio)tetrathiafulvalene (BEDT-TTF) molecules are studied using ab initio molecular orbital methods. The optimized structure of a BEDT-TTF monomer is close to the experimental one within errors of 0.02 Å and 0.5 degree in bond length and angle, respectively, except the ethylene group. Ab initio parameters such as transfer integrals and Coulomb interactions are determined from the BEDT-TTF dimer and tetramer calculations. Using model Hamiltonians with the ab initio parameters, we investigate the electronic states based on the exact diagonalization method. The results show that the ground state has antiferromagnetic correlation, which is consistent with experimental results. We study the effects of long-range Coulomb interactions employing the 2-D extended Hubbard model with the Hartree-Fock approximation. It is found that the ground state shows various phases; antiferromagnetic, charge ordering, and paramagnetic ones, controlled by the long-range interactions.

I-T-7 Two-Loop Renormalization-Group Analysis of Two-Dimensional Electron Systems

KISHINE, Jun-ichiro; FURUKAWA, Nobuo¹;
YONEMITSU, Kenji
(¹Aoyama Gakuin Univ.)

[Recent Prog. Many-Body Theories **3** submitted]

Recently there has been renewal of interest in understanding two-dimensional (2D) electron systems based on the renormalization-group (RG) framework. In these attempts, possible instabilities occurring in the system have been discussed based on the *one-loop* RG analysis and little attention has been given to the RG flow of the quasiparticle weight that is treated in the *two-loop* level. In this paper, we consider the two-dimensional electron systems where the two-loop RG analysis works well. We take up the following two examples. As the first example, we consider a 2D Fermi surface that consists of flat regions and round-arc regions. We found that the RG flow of the quasiparticle weight depends on the location of the electron wave number, \mathbf{k} , on the Fermi surface due to the kinematical restriction to the logarithmically divergent processes in the flat regions of the Fermi surface. As the second example, we consider a 2D Fermi surface which touches the Umklapp surface at the 4 points ($\pm\pi/2, \pm\pi/2$). In this case, growth of the umklapp processes between ($\pm\pi/2, \pm\pi/2$) points cause the vanishing quasiparticle weight at these points.

RESEARCH ACTIVITIES II

Department of Molecular Structure

II-A Laboratory and Astronomical Spectroscopy of Transient Molecules

Vast, cold, and low-density space environment is a unique laboratory, whose physical and chemical conditions are rarely attained in the laboratory on Earth. The unique space laboratory is favorable to the existence of transient molecules such as molecular ions, free radicals, and unstable molecules, most of which are very exotic and nonterrestrial. These exotic transient molecules are generally difficult and challenging problems for laboratory spectroscopy. Laboratory spectroscopy may be enriched by astronomical studies on non-terrestrial transient species which represent new developments in high-resolution molecular spectroscopy. On the other hand, detailed knowledge about new transient molecules obtained by laboratory spectroscopy is essential to a deeper understanding of physical and chemical processes in space. We developed a high-sensitivity submillimeter-wave and far-infrared spectrometers suitable for high-resolution spectroscopy of transient molecules of astronomical interest. We expect that our laboratory spectroscopy may accelerate the mutually beneficial aspect between laboratory spectroscopy, and astrochemistry and astrophysics.

II-A-1 The detection of the Free Radical FO ($X^2\Pi_{3/2}$) by Microwave Spectroscopy

TAMASSIA, Filippo¹; BROWN, John M.²; SAITO, Shuji
(¹Oxford Univ. and IMS; ²Oxford Univ.)

The FO radical is the most fundamental halogen oxide free radical and has been studied since 1979 by high-resolution infrared spectroscopy, CO₂-LMR spectroscopy,¹⁾ diode laser spectroscopy²⁾ and Fourier transform IR spectroscopy.³⁾ A full spectroscopic characterization has been recently achieved with the detection of the fine-structure transition $^2\Pi_{1/2}-^2\Pi_{3/2}$ by FIR-LMR.⁴⁾ No pure rotational spectra have been reported in literature to date. McKellar,⁵⁾ in a Stark spectroscopy experiment, demonstrated that the electric dipole moment is exceptionally small, *i.e.* 0.0043(4) D for the $v = 0$ level and 0.0267(9) D for $v = 1$.

We detected for the first time the pure rotational spectrum of the free radical FO ($X^2\Pi_{3/2}$) by microwave spectroscopy, using a reaction of ozone with atomic fluorine. Four rotational transitions $J = 7/2-5/2$ to $13/2-11/2$ have been measured in the frequency region 219–408 GHz. All the observed transitions are magnetic dipole in character. No electric dipole transitions have been observed in this experiment. Each rotational transition is split into four components by fluorine magnetic hyperfine interaction ($I_F = 1/2$) and by Λ -type doubling. The analysis of the observed data allowed a considerable improvement of some spectroscopic parameters: $B_0 = 31539.33542(32)$ MHz.

References

- 1) A. R. W. McKellar, *Can. J. Phys.* **57**, 2106 (1979).
- 2) A. R. W. McKellar, C. Yamada and E. Hirota, *J. Mol. Spectrosc.* **97**, 425 (1983).
- 3) J. B. Burkholder, P. D. Hammer, C. J. Howard and A. R. W. McKellar, *J. Mol. Spectrosc.* **118**, 471 (1986).
- 4) F. Tamassia, J. M. Brown and K. M. Evenson, *J. Chem. Phys.* **110**, 7273 (1999).
- 5) A. R. W. McKellar, *J. Mol. Spectrosc.* **101**, 186 (1983).

II-A-2 Microwave Spectroscopic Detection of Transition Metal Hydroxide: CuOH and AgOH

WHITHAM, Christopher J.¹; OZEKI, Hiroyuki; SAITO, Shuji
(¹Oxford Univ. and IMS)

[*J. Chem. Phys.* **110**, 11109 (1999) and *ibid.* in press]

A number of microwave spectroscopic studies on metal hydroxide molecules have been reported: alkali metal hydroxides NaOH to CsOH, alkali earth metal hydroxides MgOH to BaOH, and recently, AlOH and InOH. Linearity or nonlinearity of the metal hydroxides depend on a balance between ionic and covalent structures.¹⁾ In contrast, there has been no previous microwave spectroscopy of transition metal hydroxides, where a contribution of d orbital in transition metal influences the balance between both structures. There is a need for microwave spectroscopy of such molecules, which can supply substantial information on this problem through their structural determination.

We detected rotational spectra of CuOH and AgOH for the first time by millimeter- and submillimeter-wave spectroscopy (see Figure 1). Both molecules were directly produced in the hollow cathode discharge cell by sputtering metal from the hollow cathode made of the corresponding metal, and showed asymmetric-top a-type R-branch transitions. The deuterated species CuOD and AgOD were also observed by using D₂O adsorption on the electrode in advance of measurements. From the observed molecular constants for isotopic species of both molecules their harmonic force field and zero-point averaged (r_z) structures were derived and discussed in terms of the balance between competing ionic and covalent interactions.

References

- 1) C. W. Bauschlicher, S. R. Langhoff and H. Partridge, *J. Chem. Phys.* **84**, 901 (1986).

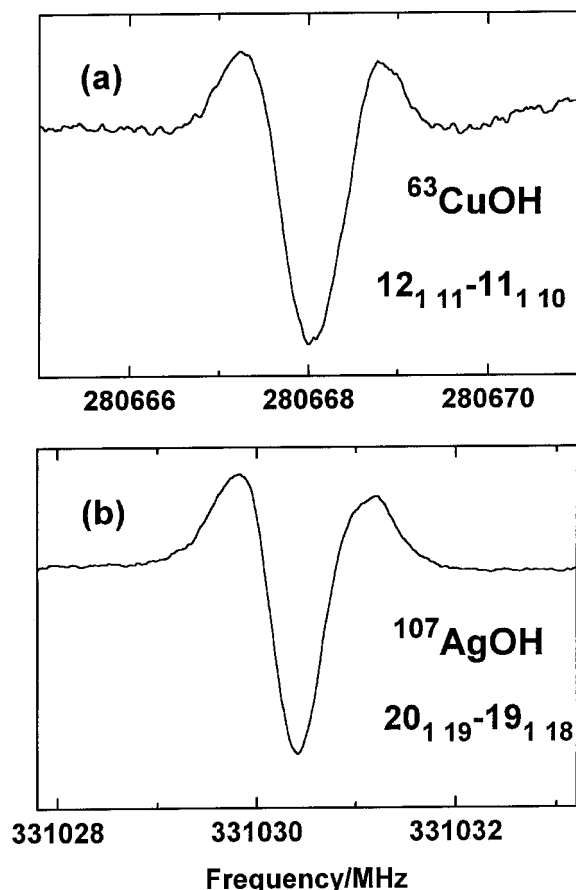


Figure 1. (a) The $12_{1,11}-11_{1,10}$ transition of $^{63}\text{CuOH}$ observed in a discharge cell, with a copper hollow cathode. (b) The $20_{1,19}-19_{1,18}$ transition of $^{107}\text{AgOH}$ observed with silver sheets inserted inside a stainless steel hollow cathode.

II-A-3 Microwave Spectrum of the Inversion-Rotation Transition of the D_3O^+ Ion: $\Delta k = \pm 3n$ Interaction and Equilibrium Structure

ARAKI, Mitsunori¹; OZEKI, Hiroyuki; SAITO, Shuji
(¹GUAS)

[*Mol. Phys.* **97**, 177 (1999)]

In the last Annual Review we reported the experimental determination of the ground-state inversion splitting in D_3O^+ by microwave spectroscopy.¹⁾ We further measured 28 Q-branch lines including $J = K + 5$ in the 399–458 GHz region and analyzed them with previously measured R-branch and Q-branch lines, 53 lines in total. We found that inclusion of $\Delta k = \pm 3n$ interactions in the Hamiltonian was essential for a full explanation of the observed lines, with measurement uncertainty of 20 to 60 kHz. The molecular constants, including C for the 0^+ and 0^- levels, as well as the $\Delta k = \pm 3n$ interaction parameters, were derived from the fit of all data. The inversion splitting was determined to be $15.35550338(107) \text{ cm}^{-1}$, where the number in parentheses denote one standard deviation of the fit. Zero-point corrections to the rotational constants of H_3O^+ and D_3O^+ were calculated from a harmonic potential of H_3O^+ and the r_z structures were derived from the zero-

point corrected rotational constants:

$\text{D}_3\text{O}^+(0^+)$: $r_z = 0.9818(23) \text{ \AA}$, $\theta_z = 112.68(100)^\circ$,

$\text{D}_3\text{O}^+(0^-)$: $r_z = 0.9830(23) \text{ \AA}$, $\theta_z = 112.02(100)^\circ$.

From the shift between the r_z structures of H_3O^+ and D_3O^+ the equilibrium structural parameters of H_3O^+ was estimated to be $r_e = 0.9702(89) \text{ \AA}$, $\theta_e = 109.4(38)^\circ$.

References

- 1) M. Araki, H. Ozeki and S. Saito, *J. Chem. Phys.* **109**, 5707 (1998) and *Annu. Rev. II-A-5* (1998).

II-B Laser Cooling and Trapping of Neutral Atoms

When atoms absorb or emit photons, the atoms are accelerated or decelerated because photons have momenta. On the other hand, a strong radiation field modifies the internal energy of an atom, so that an atom in an inhomogeneous radiation field receives a force from the field. The former mechanism allows us to decrease the translational temperature of neutral atoms down to an extremely low temperature by means of laser radiation, and the latter enables the spatial control of neutral atoms with lasers. As the translational temperature goes down to the nano kelvin region, the atomic de Broglie wavelength becomes a macroscopic size and some macroscopic quantum-mechanical collective motion of atoms can then be expected to occur. Such a long de Broglie wavelength also enables us to realize the atomic interferometry. On the other hand, easy control of the atomic spatial position and velocity with lasers is expected to open the possibility of various applications. For these reasons, we have been studying the laser cooling and trapping of neutral atoms.

II-B-1 Quantum Statistical Effects in Ultracold Ionizing Collisions between Spin-Unpolarized Metastable $\text{He}(2s^3S_1)$ Atoms

KUMAKURA, Mitsutaka; MORITA, Norio

[*Phys. Rev. Lett.* **82**, 2848 (1999)]

We have carried out a precise theoretical investigation on the cause of the isotopic difference in collisional ionization rate coefficients between cold $^4\text{He}(2s^3S_1) + ^4\text{He}(2s^3S_1)$ and $^3\text{He}(2s^3S_1) + ^3\text{He}(2s^3S_1)$ collisions at 0.5 mK, which is observed in our previous magneto-optical trap experiments on He atoms. The rate coefficients experimentally obtained for ^4He - ^4He and ^3He - ^3He collisions are $(3.8 \pm 1.1) \times 10^{-10} \text{ cm}^3/\text{s}$ and $(1.1 \pm 0.4) \times 10^{-9} \text{ cm}^3/\text{s}$, respectively, and there is a large isotopic difference of a factor of 3 between them. Through our theoretical calculation, we have found that this difference is an explicit manifestation of the differing quantum statistics of those isotopes: at such a low temperature, the ionization process is mainly caused by only a single scattering partial wave (*s*-wave). Therefore, the electronic states that can contribute to the ionization explicitly differ between ^4He - ^4He and ^3He - ^3He collisions because of the differing quantum statistical symmetries of the isotopes. This is the main reason why there is a large isotopic difference in the ionization rate coefficients. Our calculation, which is based on this consideration and takes into account not only the spin

conservation rule in the ionization process but also a small contribution of the *p*-wave tunneling through its centrifugal barrier, has given the rate coefficients of $2.2 \times 10^{-10} \text{ cm}^3/\text{s}$ and $1.0 \times 10^{-9} \text{ cm}^3/\text{s}$ for ^4He - ^4He and ^3He - ^3He collisions, respectively. These values agree well with the experimental results. It is interesting that the rate coefficient for the fermionic isotope (^3He) is larger than for the bosonic one (^4He), which is just contrary to the results of similar experiments on cold ionizing collisions of spin-polarized $\text{Kr}^{1)}$ and $\text{Xe}^{2)}$ atoms. From our calculation, we have found that this is because the spin conservation rule holds good in He atoms while in heavier rare gas atoms it breaks down. An optical enhancement of the collisional ionization is also observed in our previous experiment on the cold atomic collision irradiated with trap laser beams. Our theoretical values are in good agreement with the experimental results, and this enhancement has been attributed to the fact that in the presence of the laser irradiation many partial waves up to the 6-th order can contribute to the ionization. We have also found that this fact results in the smaller isotopic difference in the enhanced ionization rates.

References

- 1) H. Katori, H. Kunugita and T. Ido, *Phys. Rev. A* **52**, R4324 (1995).
- 2) C. Orzel, M. Walhout, U. Sterr, P. S. Julienne and S. L. Rolston, *Phys. Rev. A* **59**, 1926 (1999).

II-C Spectroscopy of Atoms and Ions in Liquid Helium

Ions and atoms in liquid helium are known to reside in bubble-like cavities due to the Pauli repulsive force between electrons. Physical properties in these exotic surroundings are determined by the potential energy of the impurity- He_n system, the surface tension energy of the liquid helium, and the pressure-volume energy. Spectroscopic studies of ions in liquid helium are expected not only to give information on the structure and dynamics of the bubbles, but also to contribute to the study on the property of superfluid liquid helium. Moreover, if we can study ions distributed just below the liquid helium, it will be a new method for the experimental research on the low dimension plasma physics.

II-C-1 Spectroscopic Study of Alkali-Earth Atoms in Liquid ^3He

MORIWAKI, Yoshiki; MORITA, Norio

The comparison between spectra of atoms in liquid ^3He and ^4He can allow us to find interesting phenomena

arising from differing quantum features of each liquid helium, such as the quantum statistics and fluidity (normal and super). From this viewpoint, we have measured some spectra of Mg and Ca in liquid ^3He . As a result, it has been found that (a) excitation spectra of both atoms in liquid ^3He are much narrower and their blue shifts are significantly smaller than the ones in

liquid ^4He , and that (b) there is a large isotope shift in the emission spectrum of Mg while such a shift is not observed for Ca. The smaller width and shift in each excitation spectrum can be explained by the difference in the number density and surface tension between liquid ^3He and ^4He : because of the smaller mass of ^3He , its wavefunction has a size larger than ^4He , so that the number density of ^3He should be smaller. Moreover, because of the difference in the quantum statistical symmetry, the surface tension of liquid ^3He is about one third of that of liquid ^4He at 1.4 K. These facts make the size of an atomic bubble much larger in liquid ^3He than in liquid ^4He (soft cage effect), so that perturbations by surrounding ^3He atoms is much weaker. This effect results in the smaller peak shift and spectral width in the excitation spectra for liquid ^3He . In the case of Mg, while its excitation spectrum for liquid ^3He is narrower than for liquid ^4He , the width of its emission spectrum is almost the same as the one in liquid ^4He . These facts result in that the emission and excitation spectra for liquid ^3He have almost the same widths, although such a situation is quite unusual and hardly seen in ordinary bubble spectra. This fact can be understood with a model of exciplex formation in the excited state, which is similar to the one previously introduced to explain the emission spectrum of Mg in liquid ^4He . This model also consistently explains the red shift of the peak position in the emission spectrum, since it just agrees with an isotope shift estimated from the molecular vibrations.

II-D Endohedral Metallofullerenes: New Fullerene Molecules with Novel Properties

Endohedral metallofullerenes (fullerenes containing metal atoms inside hollow carbon cage) have long attracted special interest as new spherical molecules with novel properties. Recent important progress has been marked by successful isolation and purification in macroscopic quantities. With the availability of such purified samples, it has been possible to investigate the electronic properties and chemical reactivities.

II-D-1 Endohedrally Metal-Doped Heterofullerenes: $\text{La@C}_{81}\text{N}$ and $\text{La}_2\text{@C}_{79}\text{N}$

AKASAKA, Takeshi¹; OKUBO, Shingo²; WAKAHARA, Takatsugu²; YAMAMOTO, Kazunori³; KOBAYASHI, Kaoru⁴; NAGASE, Shigeru⁴; KATO, Tatsuhisa; KAKO, Masahiro⁵; NAKADAIRA, Yasuhiro⁵; KITAYAMA, Yoshie²; MATSUURA, Kenji⁶
(¹IMS and Niigata Univ.; ²Niigata Univ.; ³PRN; ⁴Tokyo Metropolitan Univ.; ⁵Univ. Electro-Commun.; ⁶JEOL)

[*Chem. Lett.* 945 (1999)]

The first evidence of the gas-phase formation of endohedrally La-doped azafullerene ions $\text{La@C}_{81}\text{N}$ and $\text{La}_2\text{@C}_{79}\text{N}$ was obtained by the fast atom bombardment mass fragmentation of the adducts, $\text{La@C}_{82}(\text{NCH}_2\text{Ph})$ and $\text{La}_2\text{@C}_{80}(\text{NCH}_2\text{Ph})$.

II-D-2 Isolation and Characterization of a Pr@C_{82} Isomer

AKASAKA, Takeshi¹; OKUBO, Shingo²; WAKAHARA, Takatsugu²; YAMAMOTO, Kazunori³; KATO, Tatsuhisa; SUZUKI, Toshiyasu; NAGASE, Shigeru⁴; KOBAYASHI, Kaoru⁴
(¹IMS and Niigata Univ.; ²Niigata Univ.; ³PRN; ⁴Tokyo Metropolitan Univ.)

A minor isomer of Pr@C_{82} ($\text{Pr@C}_{82}\text{-II}$) has been isolated with an efficient two-step HPLC method, accompanied with a major isomer ($\text{Pr@C}_{82}\text{-I}$). The isolated $\text{Pr@C}_{82}\text{-II}$ was well identified as a stable endohedral metallofullerene molecule. Mass spectra of both isomers confirmed that they were Pr@C_{82} . Visible and near-IR absorption spectra, and cyclic and differential pulse voltammograms for $\text{Pr@C}_{82}\text{-II}$ showed characteristic features different from those for $\text{Pr@C}_{82}\text{-I}$. Chemical derivatization of both isomers were also accomplished. These data reveal that $\text{Pr@C}_{82}\text{-II}$ is a carbon-cage isomer of $\text{Pr@C}_{82}\text{-I}$.

II-E Structure and Function of Respiratory Terminal Oxidases

In the aerobic respiratory chain of *Escherichia coli*, there are structurally unrelated two terminal oxidases. A heme-copper oxidase, cytochrome *bo* is predominantly expressed under highly aerated growth conditions while an alternative oxidase, a putative heme-heme oxidase, cytochrome *bd*, is predominant under microaerobic conditions. Both oxidases catalyze the two-electron reduction of ubiquinol-8 and the four-electron reduction of dioxygen, whereas only cytochrome *bo* exhibits vectorial proton transport. However, only a little structural information has been given for these ubiquinol oxidases. To clarify the molecular mechanism of electron transfer, chemical reaction of dioxygen, and proton pumping in the two respiratory terminal oxidases, we utilize various molecular spectroscopic techniques (*e.g.*, resonance Raman, EPR, FTIR) in conjunction with methods of molecular biology and biochemistry.

II-E-1 Fourier-Transform Infrared Studies on Azide Binding to the Binuclear Center of the *Escherichia coli bo*-Type Ubiquinol Oxidase

[*J. Biochem.* **126**, 98 (1999)]

TSUBAKI, Motonari¹; MOGI, Tatsushi²; HORI, Hiroshi³
(¹IMS and Himeji Inst. Tech.; ²Univ. Tokyo; ³Osaka Univ.)

[*FEBS Lett.* **449**, 191 (1999)]

Azide-binding to the heme-copper binuclear center of *bo*-type ubiquinol oxidase from *Escherichia coli* was investigated with Fourier-transform infrared spectroscopy. Deconvolution analyses of infrared spectra of the azide (¹⁴N₃)-inhibited air-oxidized form showed a major infrared azide antisymmetric stretching band at 2041 cm⁻¹. An additional band developed at 2062.5 cm⁻¹ during a longer incubation. Isotope substitutions with terminally ¹⁵N-labeled azides did not show a splitting of the major band, indicating that the geometry of the bound azide is mainly in a bridging configuration between high-spin heme *o* and Cu_B.^{1,2} The band at 2062.5 cm⁻¹ showed clear splittings upon substitution with the terminally ¹⁵N-labeled azides, indicating the Cu_B²⁺-N=N=N structure. Partial reduction of the oxidase with β-NADH in the presence of azide (¹⁴N₃) caused an appearance of new infrared bands at 2038.5 (major) and 2009 (minor) cm⁻¹. The former band also showed clear splittings in the presence of the terminally ¹⁵N-labeled azides, indicating that reduction of low-spin heme *b* alters the structure of the binuclear center leading to the Fe_o³⁺-N=N=N configuration.³

References

- 1) Tsubaki, M., Mogi, T., Anraku, Y. and Hori, H., *Biochemistry* **32**, 6065 (1993).
- 2) Tsubaki, M., Matsushita, K., Adachi, O., Hirota, S., Kitagawa, T. and Hori, H., *Biochemistry* **36**, 13034 (1997).
- 3) Tsubaki, M., *Biochemistry* **32**, 164 (1993).

II-E-2 Fluoride-Binding to the oxidized *Escherichia coli bd*-Type Ubiquinol Oxidase Studied by Visible Absorption and EPR Spectroscopies

TSUBAKI, Motonari¹; MOGI, Tatsushi²; HORI, Hiroshi³
(¹IMS and Himeji Inst. Tech.; ²Univ. Tokyo; ³Osaka Univ.)

Cytochrome *bd*-type ubiquinol oxidase in the aerobic respiratory chain of *Escherichia coli* contains two hemes *b* (*b*₅₅₈ and *b*₅₉₅) and one heme *d* as redox metal centers.¹⁾ To clarify the structure of the reaction center, we analyzed the fully oxidized enzyme by visible and EPR spectroscopies using fluoride ion as a monitoring probe. The visible spectral changes upon fluoride-binding were typical of ferric iron-chlorine species, indicating heme *d* as a primary binding site. The negative peak at 645 nm in the difference spectrum indicates that heme *b*₅₉₅ also provides the low-affinity fluoride-binding site. Fluoride-binding caused a complete disappearance from the EPR spectra of the low-spin signals ascribable to heme *d* and spectral changes in both rhombic and axial high-spin signals. After fluoride-binding, each component of the rhombic high-spin signal showed superhyperfine splitting arising from the interaction of the unpaired spin of the heme *d* iron with the nuclear magnetic moment of ¹⁹F. The axial high-spin species was converted to a new rhombic high-spin species assignable to heme *b*₅₉₅-fluoride. The *g* = 2 component of this new species also gave ¹⁹F-superhyperfine splitting. These results indicate that both heme *d* and heme *b*₅₉₅ can coordinate with a fluoride ion with different affinities in the fully oxidized state.

Reference

- 1) Mogi, T., M. Tsubaki, H. Hori, H. Miyoshi, H. Nakamura and Y. Anraku, *J. Biochem. Mol. Biol. Biophys.* **2**, 79 (1998).

II-E-3 Azide- and Cyanide-Bindings to the *Escherichia coli bd*-Type Ubiquinol Oxidase Studied by Visible Absorption, EPR and FTIR Spectroscopies

TSUBAKI, Motonari¹; MOGI, Tatsushi²; HORI, Hiroshi³
(¹IMS and Himeji Inst. Tech.; ²Univ. Tokyo; ³Osaka Univ.)

[*J. Biochem.* **126**, 510 (1999)]

Cytochrome *bd*-type ubiquinol oxidase contains two hemes *b* (*b*₅₅₈ and *b*₅₉₅) and one heme *d* as the redox metal centers. To clarify the structure of the reaction center, we analyzed *Escherichia coli* cytochrome *bd* by visible absorption, EPR and FTIR spectroscopies using

azide and cyanide as monitoring probes for the exogenous ligand binding site. Azide-binding caused the appearance of a new EPR low-spin signal characteristic of ferric iron-chlorin-azide species and a new visible absorption band at 647 nm. However, the bound azide ($^{14}\text{N}_3$) anti-symmetric stretching infrared band ($2,010.5\text{ cm}^{-1}$) showed anomalies upon ^{15}N -substitutions, indicating interactions with surrounding protein residues or heme b_{595} in close proximity. The spectral changes upon cyanide-binding in the visible region were typical of those observed for ferric iron-chlorin species with diol substituents in macrocycles. However, we found no indication of a low-spin EPR signal corresponding to the ferric iron-chlorin-cyanide complexes. Instead, derivative-shaped signals at $g = 3.19$ and $g =$

7.15 , which could arise from the heme $d(\text{Fe}^{3+})\text{-CN-}$ heme $b_{595}(\text{Fe}^{3+})$ moiety,¹⁾ were observed. After the addition of cyanide, a part of ferric heme d showed the rhombic high-spin signal that coexisted with the $g_z = 2.85$ signal ascribed to the minor heme $b_{595}\text{-CN}$ species. This indicates strong steric hindrance of cyanide-binding to ferric heme d with the bound cyanide at ferric heme b_{595} .

Reference

- 1) M. Tsubaki, H. Hori, Mogi, T. Mogi and Y. Anraku, *J. Biol. Chem.* **270**, 28565 (1995).

II-F Structure and Function of Transmembrane Electron Transfer System in Neuroendocrine Secretory Vesicles

In neuroendocrine secretory vesicles of higher animals, intravesicular ascorbate (AsA^-) functions as the electron donor for copper-containing monooxygenases. Upon these monooxygenase reactions, monodehydroascorbate (MDA) radical is produced by oxidation of AsA^- . The MDA radical is reduced back to AsA^- by membrane-spanning cytochrome b_{561} and subsequently the oxidized cytochrome b_{561} is reduced by cytosolic AsA^- . To clarify the molecular mechanism of the electron transfer, we utilize various biophysical techniques (*e.g.* EPR, resonance Raman, and pulse radiolysis) in conjunction with methods of molecular biology and biochemistry. We found previously that purified cytochrome b_{561} from bovine adrenal medulla contains two hemes B per molecule, each exhibiting an independent EPR signal in oxidized state. The reaction of MDA radical with purified cytochrome b_{561} was investigated by the technique of pulse radiolysis. Radiolytically generated MDA radical oxidized rapidly reduced cytochrome b_{561} to yield the oxidized form. Subsequently, the oxidized form was re-reduced by AsA^- in the medium. At excess MDA radical, only half of the heme was oxidized, indicating that only one of the two heme centers can react with MDA radical.

II-F-1 Diethylpyrocarbonate-Modification Abolishes Fast Electron Accepting Ability of Cytochrome b_{561} from AsA^- but Does Not Influence on Electron Donation to MDA Radical: Identification of the Modification Sites by Mass Spectrometric Analyses

TSUBAKI, Motonari¹; KOBAYASHI, Kazuo²; ICHISE, Tomoko³; TAKEUCHI, Fusako³; TAGAWA, Seiichi²

(¹IMS and Himeji Inst. Tech.; ²Osaka Univ.; ³Himeji Inst. Tech.)

Cytochrome b_{561} in bovine adrenal chromaffin vesicles contains two hemes B¹⁾ and transports electron equivalents across the vesicle membranes to convert intravesicular MDA radical to AsA^- . To elucidate the mechanism of the transmembrane electron transfer, effects of the treatment of purified cytochrome b_{561} with diethylpyrocarbonate, a reagent specific for histidyl residues, were examined. We found that, when AsA^- was added to the oxidized form of diethylpyrocarbonate-treated cytochrome b_{561} , less than half of the heme iron was reduced but with a very slow rate. In contrast, radiolytically-generated MDA radical was oxidized rapidly by the reduced form of diethylpyrocarbonate-modified cytochrome b_{561} , as observed for untreated cytochrome b_{561} .²⁾ These results indicate that the heme center specific for the electron acceptance from AsA^- is perturbed by the modification of amino

acid residues nearby. We identified the major modification sites by mass spectrometry at Lys85, His88, and His161, all of which are fully conserved and located at extravesicular side of cytochrome b_{561} in the membranes. We suggest that specific *N*-carbethoxylation of the histidyl ligands of the heme b at extravesicular side abolish the electron accepting ability from AsA^- .

References

- 1) M. Tsubaki, M. Nakayama, E. Okuyama, Y. Ichikawa and H. Hori, *J. Biol. Chem.* **272**, 23206 (1997).
- 2) K. Kobayashi, M. Tsubaki and S. Tagawa, *J. Biol. Chem.* **273**, 16038 (1998).

II-G Biomolecular Science

Elucidation of a structure-function relationship of metalloproteins is a current subject of this group. The primary technique used for this project is the stationary and time-resolved resonance Raman spectroscopy monitored by near IR to UV lasers. The main themes that we want to explore are (1) mechanism of oxygen activation by enzymes, (2) mechanism of active proton translocation and its coupling with electron transfer, (3) coupling mechanism of proton- and electron transfers by quinones in photosynthetic reaction center, (4) higher order protein structures and their dynamics, and (5) reactions of biological NO. In category (1), we have examined a variety of terminal oxidases, cytochrome P450s, and peroxidases, and also treated their enzymatic reaction intermediates by using the mixed flow transient Raman apparatus and the Raman/absorption simultaneous measurement device. For (2) the third generation UV resonance Raman (UVR) spectrometer was constructed and we are going to use it to the peroxy and ferryl intermediates of cytochrome c oxidase. In (3) we succeeded in observing RR spectra of quinones A and B in bacterial photosynthetic reaction centers for the first time last year, but we focused our attention on tyrosine radical this year. For (4) we developed a novel technique for UV resonance Raman measurements based on the combination of the first/second order dispersions of gratings and applied it successfully to 235-nm excited RR spectra of several proteins including mutant hemoglobins and myoglobins. Nowadays we can carry out time-resolved UVR experiments with nanosecond resolution to discuss protein dynamics. We have succeeded in isolating the spectrum of β 145-Tyr, β 35-Tyr and α 140-Tyr of Hb A separately and their changes upon quaternary structure transition. For (5) we purified soluble guanylate cyclase from bovine lung and observed its RR spectra. To understand the implication, we examined Raman spectra of NO adducts of various mutant Mbs.

II-G-1 Time-Resolved UV Resonance Raman Detection of a Transient Open Form of the Ligand Pathway in Tyr64(E7) Myoglobin

MUKAI, Masahiro¹; NAKASHIMA, Satoru²; OLSON, John S.³; KITAGAWA, Teizo
(¹RIKEN; ²Osaka Univ.; ³Rice Univ.)

[*J. Phys. Chem.* **102**, 3624 (1998)]

X-ray crystallographic analyses of myoglobin (Mb) in the deoxy- and CO-bound states noted the absence of a preformed pathway for ligand movement from the heme iron to the solvent. To explore a mechanism of ligand entry, time-resolved UV resonance Raman experiments have been carried out, using a mutant with tyrosine at the distal histidine position. The results indicate the presence of a transient, open pathway which is generated after photodissociation of CO in the H64Y mutant. The Raman spectra were probed at 235 and 416 nm with a time resolution of 7 ns in the range -100 ns to 10 ms following photolysis at 532 nm. In the 235-nm excited spectra, the tyrosine bands of H64Y Mb at 1618 (Y8a) and 1176 cm⁻¹ (Y9a) are noticeably intensity-enhanced shortly after photolysis but the original intensity is restored by 5 ms. The time range in which the Tyr bands are intensified is prolonged by addition of glycerol to the solvent. This intensity change is not seen with the native Mb which has three naturally occurring Tyr residues. Thus, the intensity increase observed for the mutant Mb is attributed to Tyr64. The corresponding bands of *para*-cresol derivative exhibit greater intensity in polar (H-bond forming) solvents than in nonpolar solvents. This result suggests that the increase in intensity of the Tyr bands in the transient form of the mutant myoglobin compared to that in the equilibrium form is due to exposure of Tyr64 to solvent water. Increased solvation indicates an outward movement of the phenol side chain and formation of an open channel to the distal pocket.

II-G-2 UV Resonance Raman Studies of α -Nitrosyl Hemoglobin Derivatives: Relation between the α 1- β 2 Subunit Interface Interactions and the Fe-Histidine Bonding of α Heme

NAGATOMO, Shigenori; NAGAI, Masako¹; TSUNESHIGE, Antonio²; YONETANI, Takashi²; KITAGAWA, Teizo
(¹Kanazawa Univ.; ²Univ. Pennsylvania)

[*Biochemistry* **38**, 9659 (1999)]

Human α -nitrosyl β -deoxy hemoglobin A, $\alpha^{\text{NO}}\beta^{\text{deoxy}}$, is considered to have a T(tense) structure with the low O₂ affinity extreme and the Fe-histidine(His87) (Fe-His) bond of α heme cleaved. The Fe-His bonding of α heme and the intersubunit interactions at α 1- β 2 contact of α^{NO} -Hbs have been examined under various conditions with EPR and UV resonance Raman (UVR) spectra excited at 235 nm, respectively. NOHb at pH 6.7 gave the UVR spectrum of the R structure, but in the presence of inositol-hexakis-phosphate (IHP) for which the Fe-His bond of the α heme is broken, UVR bands of Trp residues behaved half T-like while Tyr bands remained in the R-like. The half ligated nitrosylHb, $\alpha^{\text{NO}}\beta^{\text{deoxy}}$, in the presence of IHP at pH 5.6, gave T-like UVR spectra for both Tyr and Trp, but binding of CO to its β heme ($\alpha^{\text{NO}}\beta^{\text{CO}}$) changed the UVR spectrum to half T-like. Binding of NO to its β heme (NOHb) changed the UVR spectrum to 70% T-type for Trp but almost R-type for Tyr. When pH was raised to 8.2 in the presence of IHP, the UVR spectrum of NOHb was the same as that of COHb. EPR spectra of these Hbs indicated that the Fe-His bond of α^{NO} heme is partially cleaved. On the other hand, the UVR spectra of $\alpha^{\text{NO}}\beta^{\text{deoxy}}$ in the absence of IHP at pH 8.8 showed the T-like UVR spectrum but EPR spectrum indicated that 40-50% of the Fe-His bond of α hemes was intact. Therefore, it became evident that there is qualitative correlation between the cleavage of the Fe-His bond of α heme and T-like contact of Trp- β 37. We note that the

behaviors of Tyr and Trp residues at the α 1- β 2 interface are not synchronous. It is likely that the behaviors of Tyr residues are controlled by the ligation of β heme through His- β 92(F8) \rightarrow Val- β 98(FG5) \rightarrow Asp- β 99(G1) \rightarrow Tyr- α 42(C7) or Tyr- β 145(HC2).

II-G-3 Observation of Cu-N₃⁻ Stretching and N₃⁻ Asymmetric Stretching Bands for mono-Azide Adduct of *Rhus vernicifera* Laccase

HIROTA, Shun¹; MATSUMOTO, Hiroki¹; HUANG, Hong-Wei; SAKURAI, Takeshi; KITAGAWA, Teizo; YAMAUCHI, Osamu¹
(¹Nagoya Univ.)

[*Biochem. Biophys. Res. Commun.* **243**, 435 (1998)]

Mono-azide adduct of *Rhus vernicifera* laccase, a multicopper oxidase containing one type-1 (blue) copper, one type-2 (non-blue normal) copper, and a pair of type-3 (binuclear and EPR silent) coppers, of which type-2 and type-3 coppers constitute a trinuclear site, was investigated with resonance Raman (RR) and Fourier transform infrared (FT-IR) spectroscopies as a step toward elucidation of the structure and function of the trinuclear site. The Cu-N₃⁻ stretching ($\nu_{\text{Cu-N}_3^-}$) RR band was observed for azide-bound multicopper oxidases for the first time. The $\nu_{\text{Cu-N}_3^-}$ band was located at 400 cm⁻¹ for mono-¹⁴N₃⁻ laccase, which shifted to 396 cm⁻¹ with the ¹⁵N¹⁴N¹⁴N₃⁻ analog. The N₃⁻ asymmetric stretching ($\nu_{(\text{N}_3^-)\text{asym}}$) band was observed by FT-IR spectroscopy at 2035 cm⁻¹ for mono-¹⁴N₃⁻ laccase and at 2025 cm⁻¹ for the ¹⁵N¹⁴N¹⁴N₃⁻ analog. The $\nu_{\text{Cu-N}_3^-}$ and $\nu_{(\text{N}_3^-)\text{asym}}$ frequencies and their ¹⁵N¹⁴N¹⁴N₃⁻ isotope shifts for azido laccase correspond well with those of metazido hemocyanin, indicating that both derivatives should have a similar binding geometry of azide.

II-G-4 Studies of Bovine Enterovirus Structure by Ultraviolet Resonance Raman Spectroscopy

KAMINAKA, Shouji¹; IMAMURA, Yoshihiro¹; SHINGU, Masahisa¹; KITAGAWA, Teizo; TOYODA, Tetsuya¹
(¹Kurume Univ.)

[*J. Virol. Methods* **77**, 117 (1999)]

The structural comparison of bovine enterovirus MZ468 strain before and after the heat treatment was studied by ultraviolet resonance Raman (UVR) spectra excited at both 235 and 251 nm. The difference between full, heated full and purified empty particles, which were expected as an in vitro model of uncoating, were demonstrated. At 235 nm excitation, the Raman bands of the capsid protein dominated in all the UVR spectra. The UVR spectra of the empty particles exhibited non-homogenous broadening for tryptophan W3 band and W7 Fermi doublet bands, which were characteristics of hydrophobic environment, when compared with those of the full particles. The results indicate that some Trp indole rings of the full particles were packaged inside the viral capsids and not strained

by virion assembly. On the other hand, the Raman bands assigned to guanine residues of the single stranded-RNA genome were enhanced strongly in the 251-nm excited UVR spectrum. The spectral differences between the packaged (full particles) and the unpackaged virions (heated full particles) indicates that some guanine residues had strong hydrogen bonds in the full particles.

II-G-5 Spectroscopic Characterization and Kinetic Studies of a Novel Plastocyanin from the Green Alga *Ulva pertusa*

SASAKAWA, Yuki¹; ONODERA, Kazuhiko¹; KARASAWA, Machiko¹; IM, Sang-Choul¹; SUZUKI, Eiji¹; YOSHIZAKI, Fuminori²; SUGIMURA, Yasutomo²; SHIBATA, Naoki³; INOUE, Tsuyoshi³; KAI, Yasushi³; NAGATOMO, Shigenori; KITAGAWA, Teizo; KOHZUMA, Takamitsu¹
(¹Ibaraki Univ.; ²Toho Univ.; ³Osaka Univ.)

[*Inorg. Chim. Acta* **283**, 184 (1998)]

A novel plastocyanin from the green alga *Ulva pertusa* was isolated and characterized. The electronic absorption and the electron paramagnetic resonance spectroscopic properties of *Ulva* plastocyanin showed features characteristic of the usual plastocyanins reported so far. However, the resonance Raman spectrum on excitation at 607 nm indicated the Raman band of Cu-S_{cys} at 413 cm⁻¹; this is at a lower frequency than the corresponding Raman band of higher plant plastocyanins. Electron-transfer reactions were investigated with [Fe(CN)₆]³⁻ and [Co(phen)₃]³⁺ complexes. The electron-transfer rate constant of *Ulva* plastocyanin was determined to be $(1.18 \pm 0.06) \times 10^5 \text{ M}^{-1}\text{s}^{-1}$ for the reaction with [Fe(CN)₆]³⁻ at pH 7.5, and the intramolecular electron-transfer rate constant and equilibrium constant for complex formation for the reaction with [Co(phen)₃]³⁺ were evaluated to be $7.7 \pm 0.6 \text{ s}^{-1}$ and $(4.2 \pm 0.4) \times 10^2 \text{ M}^{-1}$ respectively. The electron-transfer rate constant for the reaction with [Fe(CN)₆]³⁻ at pH 7.5 is two times larger than the values obtained from the other higher plant plastocyanins. The kinetic behavior suggested that the structure is slightly different from those of other plastocyanins. It has been reported that the electron-transfer reaction of plastocyanin is inhibited by the protonation of the active site histidine (His87 in poplar plastocyanin) at acidic pH. The dependence on pH of the rate constant for the reaction with [Fe(CN)₆]³⁻ was investigated. The acid-dissociation constant accompanying the electron-transfer reaction was determined to be pK_H = 5.8. Second-order rate constants for the reduction of plastocyanin by cytochrome c were determined to be $(1.71 \pm 0.04) \times 10^6 \text{ M}^{-1}\text{s}^{-1}$ at *I* = 0.1 M (NaCl), pH 7.0 (20 mM Tris-HCl buffer). The saturation kinetic behavior for the reaction was not observed even at the lower ionic strength (20 mM Tris-HCl).

II-G-6 Aliphatic Hydroxylation by a Bis(μ -Oxo)-Dinickel(III) Complex

ITOH, Shinobu¹; BANDO, Hideki¹; NAGATOMO, Shigenori; KITAGAWA, Teizo; FUKUZUMI, Shunichi¹

(¹Osaka Univ.)

[J. Chem. Soc. in press]

Treatment of $[(L^XNi^{II})_2(\mu-OH)_2]^{2+}$ ($L^X = p$ -substituted *N,N*-bis[2-(2-pyridyl)ethyl]-2-phenylethylamine; X = OMe, Me, H, Cl) with one equivalent of H_2O_2 gave a bis(μ -oxo)dinickel(III) complex, $[(L^XNi^{III})_2(\mu-O)_2]^{2+}$, the formation of which has been confirmed by a characteristic absorption band at 408 nm ($\epsilon = 6000 \text{ M}^{-1}\text{cm}^{-1}$) and a resonance Raman band at 612 cm^{-1} that shifts to 580 cm^{-1} upon ^{18}O -substitution. The bis(μ -oxo)-dinickel(III) complex gradually decomposes to lead to benzylic hydroxylation of the ligand side arm (phenethyl group). Rates of the formation and decay of the bis(μ -oxo)dinickel(III) complex were determined directly by monitoring the absorption change at 408 nm at low temperatures. The kinetic data of the ligand hydroxylation process including kinetic deuterium isotope effect (KIE), *p*-substituent effects (Hammett plot), and activation parameters (ΔH^\ddagger and ΔS^\ddagger) have indicated that the bis(μ -oxo)dinickel(III) complex behaves as an electrophilic radical as in the case of bis(μ -oxo)dicopper(III) complexes.

II-G-7 The Structure and Unusual pH Dependence of Plastocyanin from the Fern *Dryopteris Crassirhizoma*: The Protonation of an Active Site Histidine is Hindered by π - π Interactions

KOHZUMA, Takamitsu¹; INOUE, Tsuyoshi²; YOSHIZAKI, Fuminori³; SASAKAWA, Yuki¹; ONODERA, Kazuhiko¹; NAGATOMO, Shigenori; KITAGAWA, Teizo; UZAWA, Sachiko³; ISOBÉ, Yoshiaki³; SUGIMURA, Yasutomu³; GOTOWDA, Masaharu²; KAI, Yasushi²
(¹Ibaraki Univ.; ²Osaka Univ.; ³Toho Univ.)

[J. Biol. Chem. **274**, 11817 (1999)]

Spectroscopic properties, amino acid sequence, electron transfer kinetics, and crystal structures of the oxidized (at 1.7 Å resolution) and reduced form (at 1.8 Å resolution) of a novel plastocyanin from the fern *Dryopteris crassirhizoma* are presented. Kinetic studies show that the reduced form of *Dryopteris* plastocyanin remains redox-active at low pH under conditions where the oxidation of the reduced form of other plastocyanins is inhibited by the protonation of a solvent-exposed active site residue, His87 (equivalent to His90 in *Dryopteris* plastocyanin). The x-ray crystal structure analysis of *Dryopteris* plastocyanin reveals π - π stacking between Phe12 and His90, suggesting that the active site is uniquely protected against inactivation. Like higher plant plastocyanins, *Dryopteris* plastocyanin has an acidic patch, but this patch is located closer to the solvent-exposed active site His residue, and the total number of acidic residues is smaller. In the reactions of *Dryopteris* plastocyanin with inorganic redox reagents, the acidic patch (the “remote” site) and the hydrophobic patch surrounding His90 (the “adjacent” site) are equally efficient for electron transfer. These results indicate the significance of the lack of protonation at the

active site of *Dryopteris* plastocyanin, the equivalence of the two electron transfer sites in this protein, and a possibility of obtaining a novel insight into the photosynthetic electron transfer system of the first vascular plant fern, including its molecular evolutionary aspects. This is the first report on the characterization of plastocyanin and the first three-dimensional protein structure from fern plant.

II-G-8 Model Complexes of the Active Form of Galactose Oxidase. Physicochemical Properties and Reactivity of Cu(II)- and Zn(II)- Phenoxyl Radical Complexes of the Novel Organic Cofactor

ITOH, Shinobu¹; TAKI, Masayasu¹; KUMEI, Hideyuki¹; TAKAYAMA, Shigehisa¹; NAGATOMO, Shigenori; KITAGAWA, Teizo; SAKURADA, Norio²; ARAKAWA, Ryuichi²; FUKUZUMI, Shunichi¹
(¹Osaka Univ.; ²Kansai Univ.)

[Angew. Chem., Int. Ed. Engl. in press]

Model complexes of the active sites of galactose oxidase (GAO) and glyoxal oxidase (GLO) have been prepared using new cofactor models, 2-methylthio-4-*tert*-butyl-6-[[bis[2-(2-pyridyl)ethyl]amino]methyl]-phenol (**1H**) and 2,4-di-*tert*-butyl-6-[[bis[2-(2-pyridyl)ethyl]amino]methyl]phenol (**2H**). Deprotonated ligand **1⁻** forms dimeric Cu(II)- and Zn(II)-complexes, $[\text{Cu}^{II}_2(\mathbf{1}^-)_2](\text{PF}_6)_2$ and $[\text{Zn}^{II}_2(\mathbf{1}^-)_2](\text{PF}_6)_2$, in the solid state, but those complexes were converted into the monomers, $[\text{Cu}^{II}(\mathbf{1}^-)(\text{AcO}^-)]$ and $[\text{Zn}^{II}(\mathbf{1}^-)(\text{CH}_3\text{CN})]^+$, in solution by the coordination of acetate ion and CH_3CN , respectively. On the other hand, **2⁻** forms monomeric Cu(II)- and Zn(II)-complexes, $[\text{Cu}^{II}(\mathbf{2}^-)(\text{CH}_3\text{CN})]\text{PF}_6$ and $[\text{Zn}^{II}(\mathbf{2}^-)(\text{CH}_3\text{CN})]\text{PF}_6$, both in the solid state and in solution. The structures and the physical properties of the Cu(II)- and the Zn(II)-complexes of the phenolate derivatives (**1⁻** and **2⁻**) have been explored as the models for the resting state of the enzymes. Oxidation of the Cu(II)- and Zn(II)-complexes of **1⁻** and **2⁻** by $(\text{NH}_4)_2[\text{Ce}^{IV}(\text{NO}_3)_6]$ (CAN) affords the corresponding phenoxyl radical complexes, $[\text{M}^{II}(\mathbf{1}^\bullet)(\text{NO}_3^-)]^+$ and $[\text{M}^{II}(\mathbf{2}^\bullet)(\text{NO}_3^-)]^+$ (M = Cu and Zn), the electronic structures and the physicochemical properties of which have been examined by UV-vis, resonance Raman, ESI-MS, and ESR. The radical complexes $[\text{M}^{II}(\mathbf{1}^\bullet)(\text{NO}_3^-)]^+$ are relatively stable at ambient temperature to show very broad absorption bands in the long wavelength region ($\lambda_{\text{max}} = 867$ and 887 nm for Cu(II)- and Zn(II)-complexes, respectively) as observed for the *active form* of the native enzymes. The Cu(II)-phenoxyl radical complexes oxidize benzyl alcohol derivatives to benzaldehydes quantitatively via a formal $2e^-/2H^+$ mechanism, where the Cu(II)-phenoxyl radical complexes are converted into the corresponding Cu(I)-phenol complexes. On the other hand, oxidation of benzyl alcohols by the Zn(II)-phenoxyl radical complexes requires two equivalents of the radical complex per alcohol, indicating that the redox reaction takes place only at the phenoxyl radical site in a dimeric form. Such a difference in the reactivity between the

Cu(II)- and the Zn(II)-complexes clearly demonstrates the importance of the redox cycle between Cu(I) and Cu(II) as well as the interconversion between the phenol and phenoxyl radical forms for the efficient two-electron oxidation of alcohols at the *mononuclear copper site* of GAO. Substituent effects of the thioether group on the reactivity are also discussed in relation with the physicochemical properties of the Cu(II)- and Zn(II)-phenoxyl radical complexes.

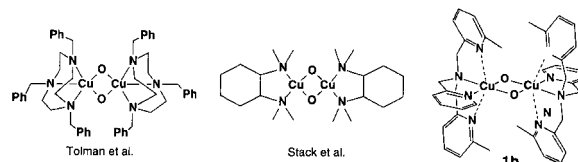
II-G-9 A Bis(μ -Oxo)Dicopper(III) Complex with Sterically Hindered Aromatic Nitrogen Donors: Structural Characterization and Reversible Conversion between Copper(I) and Bis(μ -Oxo)-Dicopper(III) Species

HAYASHI, Hideki¹; FUJINAMI, Shuhei¹; NAGATOMO, Shigenori; OGO, Seiji; SUZUKI, Masatatsu¹; UEHARA, Akira¹; WATANABE, Yoshihito; KITAGAWA, Teizo
(¹Kanazawa Univ.)

[*J. Am. Chem. Soc.* in press]

Recently, Tolman *et al.* and Stack *et al.* have prepared high-valent Cu(III)₂(μ -O)₂ species generated by the O-O bond scission of O₂²⁻ which exhibited monooxygenase activity. Crystallographically characterized bis(μ -oxo)dicopper(III) complexes reported so far consist of tridentate or bidentate aliphatic nitrogen

donors. It is important to explore how the nature of donor atoms and the stereochemistry of ligands influence the structures and properties of bis(μ -oxo)-dicopper(III) complexes. In this context, we have synthesized a bis(μ -oxo)dicopper(III) complex, [Cu₂(O)₂(Me₂-tpa)₂](PF₆)₂·2(CH₃)₂CO (**1b**), having a tetradentate tripodal ligand containing aromatic nitrogen donors. Complex **1b** is the first crystallographically characterized bis(μ -oxo)dicopper(III) complex having



aromatic nitrogen donors.

The most striking feature of **1b** is the reversible conversion with a precursor copper (I) complex [Cu(Me₂-tpa)]⁺ (**1a**) in CH₂Cl₂ at -80 °C by bubbling N₂ gas. Such reversible behavior has not been observed for the bis(μ -oxo)dicopper(III) complexes. Complex **1b** exhibited monooxygenase activity for the Me₂-tpa ligand to produce a N-dealkylated product, (6-methyl-2-pyridylmethyl)(2-pyridylmethyl)amine together with 6-methylpyridine-2-carbaldehyde in which oxygen atom comes from dioxygen. The results indicate that N-dealkylation appears to proceed through oxygen atom transfer from the bridging oxo group to the methylene carbon atom of the 6-methyl-2-pyridylmethyl side arm.

II-H Fast Dynamics of Photoproducts in Solution Phases

Picosecond time-resolved resonance Raman (ps-TR³) spectroscopy is a promising technique to investigate ultrafast structural changes of molecules. However, this technique has not been used as widely as nanosecond TR³ spectroscopy, mainly due to the lack of light source which has suitable repetition rates of pulses and wavelength tunability. In order to obtain qualified TR³ spectra, first we need two independently tunable light sources for pump and probe pulses. Second, the repetition rate should be higher than kilohertz to keep a moderate average laser power without allowing the photon density of probe pulse too high. We succeeded in developing light sources for ps-TR³ spectroscopy having wide tunability and kHz repetition, and applied them to study fast dynamics of photo-excited molecules. For carbonmonoxy myoglobin (MbCO), vibrational relaxation with the time constant of 1.9 ps was observed for CO-photodissociated heme. For Ni-octaethylporphyrin in benzene, differences in rise times of population in vibrationally excited levels among various modes were observed in the anti-Stokes spectra for the first time. For the same molecule in piperidine, coordination of two solvent molecules was observed in the transient (*d,d*) excited state. The ps-TR³ experiments were also applied to Zn-porphyrin dimers, for which some evidence for the π - π interaction in the S₁ state was obtained. The UV ns-TR³ experiments on MbCO demonstrated the presence of a transient open form of the ligand pathway.

II-H-1 Intramolecular Vibrational Energy Redistribution and Intermolecular Energy Transfer in the (*d,d*) Excited State of Nickel Octaethylporphyrin

MIZUTANI, Yasuhisa; UESUGI, Yuki; KITAGAWA, Teizo

[*J. Chem. Phys.* **111**, 8950 (1999)]

The formation of a vibrationally excited photoproduct of nickel octaethylporphyrin (NiOEP) upon (π,π^*) excitation and its subsequent vibrational energy relaxation were monitored by picosecond time-resolved

resonance Raman spectroscopy. Stokes Raman bands due to the photoproduct instantaneously appeared upon the photoexcitation. Their intensities decayed with a time constant of ~300 ps, which indicates electronic relaxation from the (*d,d*) excited state (B_{1g}) to the ground state (A_{1g}), being consistent with the results of transient absorption measurements by Holten and coworkers [D. Kim, C. Kirmaier and D. Holten, *Chem. Phys.* **75**, 305 (1983); J. Rodriguez and D. Holten, *J. Chem. Phys.* **91**, 3525 (1989)]. The Raman frequencies of NiOEP in the (*d,d*) excited state are shifted to lower frequencies compared to those of the ground state species, and it is reasonably interpreted by the core size expansion of the macrocycle by 0.05 Å upon the

electron promotion from the d_{z^2} to the $d_{x^2-y^2}$ orbital. Anti-Stokes ν_4 intensity in vibrationally excited (d,d) state of NiOEP appeared promptly and decayed with time constants of 11 ± 2 and 330 ± 40 ps. The former is ascribed to vibrational relaxation, while the latter corresponds to the electronic relaxation from the (d,d) excited state to the electronic ground state. In contrast, the rise of anti-Stokes ν_7 intensity was not instantaneous, but delayed by 2.6 ± 0.5 ps, which indicates that intramolecular vibrational energy redistribution has not been completed in subpicosecond time regime. The peak position of ν_4 band shifted by nearly 5 cm^{-1} between 0 and 50 ps. The time constant for the shift of the ν_4 band was 9.2 ± 1.3 ps, which was close to that for the fast component of intensity decay of anti-Stokes bands. The ν_4 band became narrower and symmetric as the delay time increases. These can be ascribed to intramolecular anharmonic coupling of the ν_4 mode with the low frequency modes which can exchange energy with solvent molecules. The intra- and intermolecular vibrational energy relaxation in the metal excited state will be discussed.

II-H-2 Time-Resolved Resonance Raman Study of Intermediates Generated after Photodissociation of Wild-type and Mutant CO-Myoglobins

NAKASHIMA, Satoru¹; KITAGAWA, Teizo; OLSON, John S.²
(¹Osaka Univ.; ²Rice Univ.)

[*Chem. Phys.* **228**, 323 (1998)]

Time-resolved resonance Raman (TR³) spectroscopy was applied to elucidate transient structures of myoglobin (Mb) involved in its ligand binding. Pump/probe Raman measurements of the Fe-CO stretching bands ($\nu_{\text{Fe-CO}}$) were carried out for various delay times ($\Delta t = -20 \text{ ns} - 1 \text{ ms}$ with a time resolution of 7 ns) after laser photolysis of native and mutant COMb complexes. His64(E7) and Leu29(B10) were replaced with an aliphatic and aromatic residues. The static $\nu_{\text{Fe-CO}}$ frequencies of the mutants depended strongly on the environments around the bound CO and correlated more with the hydrophathy indices of the replaced residues than with their sizes. The kinetics of bimolecular CO recombination correlate with the static $\nu_{\text{Fe-CO}}$ frequencies; a lower frequency generally results in faster rebinding. Despite these differences, all the proteins exhibited the shift of a porphyrin band from 370 to 379 cm^{-1} upon binding of CO and also a transient Raman band at $\sim 497 \text{ cm}^{-1}$, which occurred before recovery of the original $\nu_{\text{Fe-CO}}$ band. The latter frequency was unaffected by isotopically labeling the ligand with $^{13}\text{C}^{18}\text{O}$. The 497 cm^{-1} band was absent in the spectrum at $\Delta t = 0 \text{ ns}$ for all of the myoglobins examined except for the His64 \rightarrow Leu (H64L) mutant which shows the band immediately after photolysis. The 370 and 497 cm^{-1} bands are associated with the $\text{C}_\beta\text{C}_\alpha\text{C}_\delta$ in-plane bending of the propionic side chains and the out-of-plane γ_{12} containing pyrrole swiveling and propionic bending motions, respectively. The 497 cm^{-1} transient band appears to reflect a deoxyheme

intermediate in which the hydrogen bonding lattice between Arg45(CD3), His64(E7), the heme-6-propionate, and an external distal pocket water molecule is temporarily disrupted. This disruption allows larger movements of the propionate side chain, explaining intensity enhancement of the 497 cm^{-1} band. Recovery of the hydrogen bonding lattice dampens the movements of the propionate $\text{C}_\beta\text{C}_\alpha\text{C}_\delta$ bond system and finally fixes it in the heme plane in the CO-bound form, causing the frequency shift of the bending mode from 370 cm^{-1} back to 379 cm^{-1} . In the Leu64 mutant, the external water molecule is already absent, facilitating rapid movement of the heme-6-propionate after photolysis. Larger scale movements of all three side chains could create an open conformation with a channel from the heme iron to the solvent, allowing ligand escape and/or rebinding.

II-H-3 Characterization of Stimulated Raman Scattering of Hydrogen and Methane Gases as a Light Source of Picosecond Time-Resolved Raman Spectroscopy

UESUGI, Yuki; MIZUTANI, Yasuhisa; KRUGLIK, Sergei G.¹; SHVEDKO, Alexander G.¹; ORLOVICH, Valentin A.¹; KITAGAWA, Teizo
(¹Natl. Acad. Sci. Belarus)

[*J. Raman Spectrosc.* in press]

Stimulated Raman scattering (SRS) in compressed hydrogen and methane gas has been characterized in terms of pulse energy, temporal width, and spectral width in the range of gas pressures of 10–60 atm. to use it as a light source of picosecond time-resolved resonance Raman spectroscopy. SRS was pumped by the second harmonic of a Ti:sapphire oscillator-regenerative amplifier laser system with pulse energy up to 200 μJ , duration of ~ 2.5 ps and repetition rate of 1 kHz. The output spectral region of 421–657 nm was covered by the first and second Stokes SRS components on tuning of the pump wavelength in the range of 375–425 nm. Energy conversion to the first Stokes SRS component was more than 10% with H_2 and more than 20% with CH_4 . The temporal width of SRS-pulse (1.1–2.1 ps) was shorter than that of a pump pulse. Spectral band shape was found to be modulated, since the SRS is generated in a transient regime. When more than 100 pulses were averaged over, the temporal and spectral profiles of SRS-pulses were sufficiently smooth and energy fluctuations were sufficiently small for spectroscopic applications. On the basis of the results obtained, an optimized condition as a Raman shifter was settled. The Raman shifter served as a light source for two-color pump-probe time-resolved resonance Raman (TR³) experiments and to demonstrate its capabilities, picosecond TR³ spectra of nickel tetraphenylporphyrin in toluene solution have been measured.

II-H-4 Nanosecond Temperature Jump and Time-Resolved Raman Study of Thermal Unfolding of Ribonuclease A

YAMAMOTO, Kohji¹; MIZUTANI, Yasuhisa;

KITAGAWA, Teizo
(¹GUAS)

A nanosecond temperature jump (T-jump) apparatus heating at 1.56 μm was constructed and combined with time-resolved Raman measurements to investigate thermal unfolding of a protein for the first time. The 1.56 μm -heat pulse with 9 ns width was obtained through the two-step stimulated Raman scattering in D_2 gas involving seeding and amplification excited by the fundamental (1064 nm) of a Nd:YAG laser. The energy of the heat pulse was 135 mJ at 10 Hz repetition when the power of the 1064 nm-input was 560 mJ, and the pulse-to-pulse fluctuation was less than 10%. To achieve uniform temperature rise in the illuminated part, the counter-propagation geometry was adopted. The magnitude of temperature rise was determined by anti-Stokes to Stokes Raman intensity ratio of the 317 and 897 cm^{-1} bands of MoO_4^{2-} aqueous solution measured at various delay times with the second harmonic (532 nm) of another Nd:YAG laser. The T-jump as large as 9 $^\circ\text{C}$ was attained within the temporal width of the heat pulse. The thermal unfolding of bovine pancreatic ribonuclease A (RNase A) was monitored with time-resolved Raman spectroscopy following T-jump with this apparatus. In the initial 200 ns after T-jump, the C-S stretching Raman band of methionine residues exhibited 10% change of that expected from the steady state spectra and another 10% in 5 ms. The Raman intensity of SO_4^{2-} ions around 980 cm^{-1} increased and was shifted to a lower frequency than the steady state frequency of the elevated temperature at 100 μs delay, presumably due to partial release from the active site. The Raman bands of S-S stretches and tyrosine doublets displayed little change within 5 ms, although appreciable changes were expected from the steady state spectra. Thus, it has been demonstrated for the first time for proteins that the combination of laser T-jump with time-resolved Raman spectroscopy will serve as a powerful tool for studies of thermal unfolding and that the conformation change in the initial step of unfolding is not always concerted.

II-H-5 Evidence for π - π Interactions in the S_1 State of Zn Porphyrin Dimers Revealed by Picosecond Time Resolved Resonance Raman Spectroscopy

**NAKASHIMA, Satoru¹; TANIGUCHI, Seiji¹;
OKADA, Tadashi¹; OSUKA, Atsuhiko²; MIZUTANI,
Yasuhisa; KITAGAWA, Teizo**
(¹Osaka Univ.; ²Kyoto Univ.)

[J. Phys. Chem. A in press]

The S_1 states of Zn(II) porphyrin dimers have been investigated with picosecond time-resolved resonance Raman spectroscopy. The transient absorption and Raman spectra of porphyrin dimers, in which two Zn(II)-porphyrins are covalently linked at the *ortho* or *meta* positions of phenylene spacers, are compared with those of their component monomer unit. Although Q-band of the *ortho* dimer was definitely different from those of the *meta* dimer and reference monomer, the

ground state Raman spectra of the *ortho* and *meta* dimers are nearly the same as that of monomer, suggesting that the porphyrin π - π interactions do appear in the excited state of the *ortho* dimer but little in the ground state. Several characteristic Raman bands were observed for the S_1 excited state at 2 ps after photoexcitation. The monomer in the S_1 state gave the marker bands at slightly lower frequencies (by 3–4 cm^{-1}) than the corresponding ground state molecules and they did not show frequency shifts with time between 2 and 300 ps. On the contrary, in the case of the *ortho* dimer, two characteristic bands (ν_2 , ν_4) appeared at frequencies significantly lower (by 10–13 cm^{-1}) than the corresponding ground state bands, and in addition the frequency of ν_4 band exhibited an upshift around 10–20 ps following photoexcitation. The frequency shift of the *ortho* dimer was appreciably perturbed by steric hindrance between the two porphyrin groups introduced through bulky *tert*-butyl group at *para* position. The behaviors of transient Raman bands of the *meta* dimer appeared intermediate between the monomer and the *ortho* dimer. These observations give the first clear evidence for the presence of π - π interactions in the S_1 excited state of porphyrin dimers with phenylene spacer and the occurrence of relaxation toward the monomer-type structure in several tens picoseconds.

II-I Molecular and Electronic Structures of Metallofullerenes and the Fullerene Radical Anions

The continued interest in radical ions of fullerenes and metallofullerenes has resulted from the discovery of superconductivity in the CT complexes of alkali metals with fullerenes. Spectroscopic information concerning the electronic and spin states of the metallofullerenes has been obtained by EPR and ENDOR measurements.

II-I-1 Spin Chemistry of Metallofullerenes

KATO, Tatsuhisa; OKUBO, Shingo; AKASAKA, Takeshi¹
(¹Niigata Univ.)

The consideration of crystal field effect due to the fullerene cage with the low symmetry was indispensable

for the analysis of the electronic and spin states for the metal ion encapsulated inside the fullerene cage. The ESR spectrum of Gd@C₈₂ could not be reproduced by the simulation without the assumption of the crystal field splitting of the ground electronic state. The ESR spectrum of Pr@C₈₂ exhibited no resolved band, this result could be also explained by the crystal field splitting.

II-J Site Selective Spectroscopy in Solid Crystals

The line broadening due to the variation of the environment over the some sites in the crystal structure prevents from determining small energy splitting between pair of closely spaced levels with high accuracy. However the broadening effects give a nice prove to investigate the intermolecular interaction in the crystal structure. On the other hand some techniques of the site selective spectroscopy to eliminate the disturbance were proposed. We are applying the technique of the heterodyne detection of optical magnetic double-resonance to some systems of crystal.

II-J-1 NQR by Coherent Raman Scattering of a Triplet Exciton in a Molecular Crystal

MATSUSHITA, Michio; KATO, Tatsuhisa

[*Phys. Rev. Lett.* **83**, 2018 (1999)]

Nuclear quadrupole resonance (NQR) of a linear triplet exciton in 1,4-dibromonaphthalene crystals has been observed as coherent Raman scattering. The Br NQR scattering originates from the hyperfine interaction between the electron spin and the Br spins. Since delocalization of the electron spin decreases the interaction, the intensity of the NQR scattering reflects the chain length of the exciton. The exciton is found to be delocalized over about 10 molecules, indicating the coherence length of the exciton is limited by scattering due to ¹³C isomers.

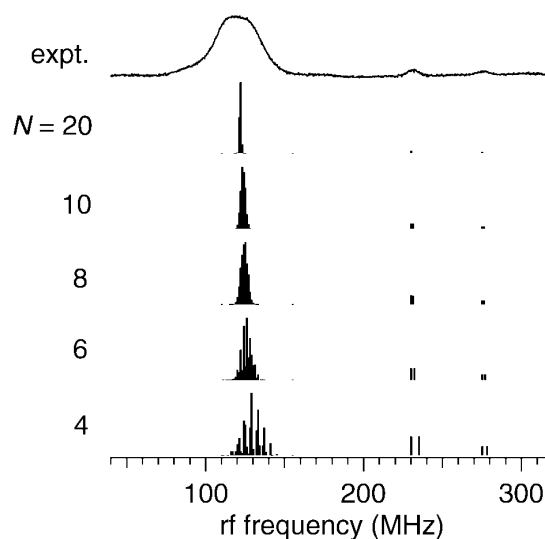


Figure 1. Coherent Raman spectrum calculated for the exciton in 1,4-DBN delocalized over N molecules. The result is shown as histograms of the width of 1 MHz. The observation is shown on the top for the sake of comparison.

II-K State Correlated Raman Spectroscopy

The vibrational Raman polarizability tensor responds to molecular reorientational relaxation process, and the structural environment in condensed media. The measurement of Raman scattering is a powerful technique for the study of molecular motion and of the mechanism of phase transition. We've built up the system of multichannel type detection of Raman scattering combined with the temperature controlled cell.

II-K-1 An Analysis of Polarized Raman Scattering Measurements for the Orientational Ordering of Ferro- and Antiferroelectric Liquid Crystal

HAYASHI, Naoki; KATO, Tatsuhisa

The orientational ordering of the ferro- and antiferroelectric liquid crystal molecule, MHPOBC was investigated in the series of the successive smectic phases by means of the polarized Raman scattering measurement. The improved equation of the polarized Raman intensity was derived as a function of the orientational order parameter and the incident laser polarization. According to the equation the second and the fourth orientational order parameters, $\langle P_2 \rangle$ and $\langle P_4 \rangle$, could be evaluated even in the chiral smectic phases. An unusual change of the orientational order parameter was observed with decreasing of temperature as shown in Figure 1. It was concluded that the irregular variation of the order parameter stemmed from the biaxiality of the molecular orientational distribution. It could be attributed to the difference of the angle between the optical axis and the center axis of the molecular orientational distribution as the increasing of biaxiality.

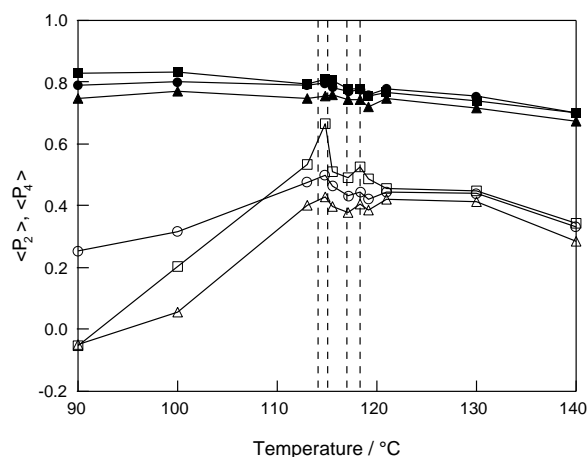


Figure 1. Temperature dependence of the orientational order parameter, $\langle P_2 \rangle$ (solid circle: phenyl, solid square: chiral C=O, solid triangle: core C=O) and $\langle P_4 \rangle$ (open circle: phenyl, open square: chiral C=O, open triangle: core C=O). The broken lines show the phase transition points. The phase sequence is as SmA-SmC $_{\alpha}$ *-SmC*-SmC $_{\gamma}$ *-SmC $_{\alpha}$ *.

RESEARCH ACTIVITIES III

Department of Electronic Structure

III-A States of Molecular Associates in Solutions

States of molecular association particularly in aqueous solutions are of great importance in understanding the role of molecules in living organism. Our recent studies of low frequency Raman spectroscopy of binary aqueous solutions of alcohols and carboxylic acids have shown that these amphiphilic molecules form microphases of clusters with the same solute species. This observation is in accord with the results of the ultrasonic absorption measurement of the binary mixtures. Kaatz and his coworkers found that acetic acid/water mixtures shows two relaxation terms attributed to the existence of two microphases, one with high and the other with low water contents. The water rich phase was assumed to fill the space between the acid-rich microphase aggregates. They also reported that the fluctuation correlation lengths in monohydric alcohol/water mixtures were expected to exceed some molecular diameters in contrast to much longer lengths expected for acid-rich phases in carboxylic acid/water mixtures. Low frequency Raman spectroscopy provides information on local structure of solutions coupled with hindered translational and librational motions. The Raman signals originating from dipole-induced dipole interaction are dominated with the interaction between the neighboring molecules. Theoretical prediction of intermolecular vibrational frequencies and Raman intensities is also applied for the assignment of observed Raman bands. These results are discussed not only with the mass spectrometric measurement of the clusters isolated from the liquid droplets through adiabatic expansion in vacuum, but also with the X-ray diffraction studies.

III-A-1 Raman Spectroscopic Study on Acetic Acid Clusters in Aqueous Solutions: Dominance of Acetic-Acid Association Producing Micro-Phases

NISHI, Nobuyuki; NAKABAYASHI, Takakazu;
KOSUGI, Kentaroh¹
(¹GUAS)

[*J. Phys. Chem. A* in press]

With the addition of water into liquid acetic acid, the C=O stretching vibration band of acetic acid shows high frequency shift from 1665 cm⁻¹ to 1715 cm⁻¹. This means that the hydrogen-bond of the C=O group of acetic acid is not so strong as those seen in liquid acetic acid or in CCl₄ solution (in which the band appears at 1668 cm⁻¹). A bent type hydrogen-bond is accountable for this observation. On the other hand, the increase of acetic acid in water drastically decreases the intensity of the hydrogen-bonded O-H stretching Raman band of water at 3200 cm⁻¹. This suggests that acetic acid breaks the hydrogen-bond networks of water. Low frequency $R(\bar{\nu})$ spectra of acetic acid/water binary solutions are reexamined with new experimental data and ab initio molecular orbital analysis of intermolecular vibrational modes. The $R(\bar{\nu})$ spectrum of the aqueous mixture at $x_A = 0.5$ bears a very close resemblance to that of the acetic acid/methanol mixture with $x_A = 0.5$, indicating that the molecular complexes responsible to the Raman spectra are acetic acid clusters. The calculated low-frequency Raman feature of a side-on type dimer with bent-type hydrogen-bonds based on ab initio molecular orbital theory reproduces the observed Raman pattern nicely. Any evidence of the formation of stable acid-water pairs is not found in the low frequency Raman spectra. Furthermore, an isosbestic point is seen in the region of $0.1 \leq x_A$ (mole fraction of acetic acid) ≤ 0.5 , and another one is also observed in $0.5 \leq x_A \leq 1.0$. The observed spectra in the region of $0 < x_A < 0.5$ are reproduced simply by linear

combinations of the pure water spectrum and the spectrum at $x_A = 0.5$. Figure 1 shows some examples of the spectral analyses. These results strongly suggest the presence of the two microphases with homogeneously associated molecules: a water cluster phase and an acetic acid cluster phase. The spectral change in $0.5 < x_A < 1.0$ is attributed to the coexistence of the acetic acid cluster phase in aqueous environment and the acid associated phase characteristic of liquid acetic acid.

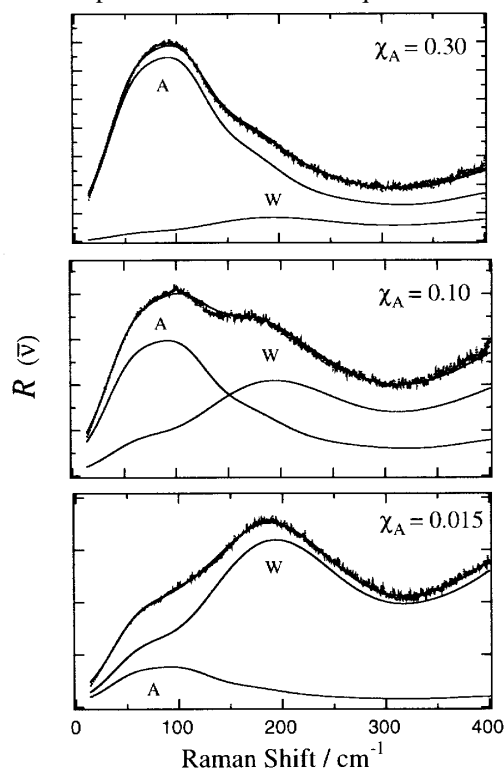


Figure 1. Decomposition of the observed $R(\bar{\nu})$ spectra of the binary solutions with $x_A = 0.015$, 0.10 and 0.30 into linear combination of the $R(\bar{\nu})$ spectra of pure water and the mixture with $x_A = 0.5$. The sum spectra calculated by a least square fitting are shown with solid lines.

III-A-2 Structures and Energies of Acetic Acid Aggregates in Aqueous Solution Studied by the RISM-SCF Method

NAKABAYASHI, Takakazu; SATO, Hirofumi; NISHI, Nobuyuki; HIRATA, Fumio

Acetic acid has been thought to form a cyclic dimer having a planar ring structure of C_{2h} symmetry in aqueous solution. From an analysis of Raman spectra of acetic acid/water binary solutions, however, we have suggested that a side-on dimer, not the cyclic dimer, is most likely for acetic acid in aqueous solution (structures of both the dimers are depicted in Figure 1). This means that the side-on dimer is more stable than the cyclic dimer in aqueous solution, although the cyclic structure is quite stable in the gas phase. In the present study, we calculate the hydrogen-bonding energies and structures of the cyclic dimer and the side-on dimer in aqueous solution by the RISM-SCF method. The advantage of the RISM-SCF method is to maintain the molecular aspects of solvents and thus to appropriately describe local interactions such as hydrogen bonds. The total energies and their energy components calculated for the monomer and the dimer species are collected in Table 1. The total energy (E_{tot}) in the RISM-SCF theory is defined as the sum of the following three energy components: (1) the electronic energy of solute molecule in the gas phase (E_{iso}), (2) the reorganization energy arising from the relaxation of the electronic

structure and the molecular geometry upon transferring solute from gas to aqueous solution (E_{reorg}), and (3) the excess chemical potential coming from solute-solvent interaction ($\Delta\mu$). The RISM-SCF calculations predict that the excess chemical potential of the side-on dimer is lower by 7.0 kcal/mol than that of the cyclic dimer. From the decomposition of the excess chemical potential into its constituents, the contribution from one of the carbonyl-oxygen atoms, which is free from the hydrogen bonding interaction with the other acetic acid molecule, is found to be much greater than the other atoms. Owing to such a stabilization in the side-on dimer, the energy difference between the two clusters is calculated to be reduced in solution; 2.0 kcal/mol in solution compared with 8.1 kcal/mol in the gas phase. Since the dipole moment of the side-on dimer is estimated to be 4.0 Debye in contrast to the null dipole moment of the cyclic dimer, the dipole-dipole interaction between the side-on dimers is expected to be sufficiently large. It is thus conceivable that the interaction energy between the side-on dimers exceeds over that between the cyclic dimers and contributes the stability of the side-on dimers in aqueous solution.

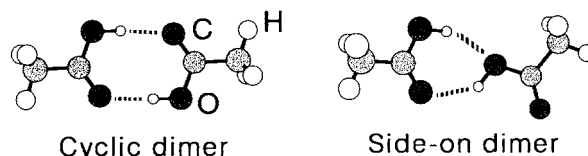


Figure 1. Structures of acetic acid dimers.

Table 1. Total energies and their energy components of acetic acid monomer and dimers in aqueous solution at the HF/DZP level.

	E_{total} (hartress)	E_{gas} (hartless)	E_{reorg} (kcal/mol)	$\Delta\mu$ (kcal/mol)
<i>cis</i> -Monomer	-227.8648503	-227.8721748	3.94	0.66
Cyclic dimer	-455.7318117	-455.7672506	4.05	18.19
Side-on dimer	-455.7270251	-455.7543088	5.96	11.16

III-A-3 Rayleigh Wing Spectra and Microphase Formation

NISHI, Nobuyuki; NAKABAYASHI, Takakazu; KOSUGI, Kentaroh¹
(¹GUAS)

Motion of molecular clusters causing dipole-dipole or dipole-induced dipole interaction between the clusters can be observed in a very low frequency Raman spectrum of a solution. Rousset *et al.*¹⁾ assumed that the low frequency temperature-dependent Raman scattering comes from oscillations of transient water aggregates with a somewhat ordered structure on the basis of the Raman studies of nuclei in glasses and silica particles in aerogels. Orientational relaxation coupled with long range dipole-dipole interaction can be also responsible to the Raman spectrum at the low frequency of 1–20 cm^{-1} . Figure 1 shows Bose-Einstein (BE) corrected very low frequency Raman spectra of water (spectrum A), aqueous mixtures with $x_A = 0.0075$ (spectrum B) and

0.07 (spectrum C). As reported by Rousset *et al.*,¹⁾ the water spectrum at 298 K exhibits a hump at 10 cm^{-1} . This signal is temperature dependent in intensity and the position. The frequency increases with increasing temperature and falls to zero at -30°C . Addition of a small amount of acetic acid in water enhances the wing intensity drastically, particularly in the region from 4 to 8 cm^{-1} . The 10 cm^{-1} component in the water spectrum in the figure must be related to this orientational relaxation of large water clusters. Rousset *et al.* estimated the average size of the clusters at room temperature to be 11 Å. In the aqueous mixture of acetic acid, orientational relaxation of the clusters is expected to take much longer time than that of water because of their longer sizes and larger dipole moments of the side-on type acetic acid dimer and higher clusters with this dimer unit. The clusterization of acetic acid molecules with large dipole-dipole interaction thus provides us a reasonable elucidation for the enhanced activity of the very low frequency Raman component as compared with that of water. The microphase model is in accord

with the present observation of the enhancement in the very low frequency component of the Raman spectra of the mixtures. As expected from the crystal structure of acetic acid, dipole-dipole interaction could be dominated in the acetic acid clusters elongating the lifetimes of the clusters in aqueous solutions.

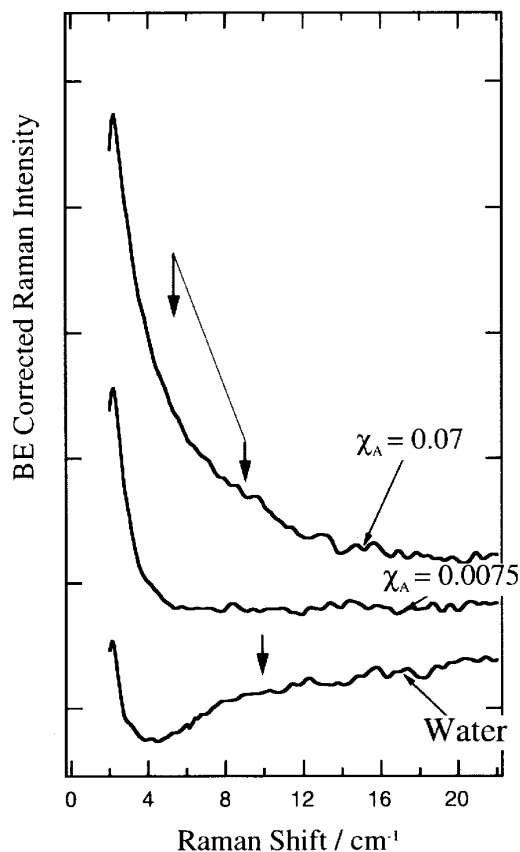


Figure 1. Mixing ratio dependence of the $R(\bar{\nu})$ spectra in acetic acid-water binary system.

III-A-4 Structures of Clusters in Methanol-Water Binary Solutions Studied by Mass Spectrometry and X-ray Diffraction

TAKAMUKU, Toshiyuki¹; YAMAGUCHI, Toshio²; ASATO, Masaki³; MATSUMOTO, Masaki³; NISHI, Nobuyuki
(¹Saga Univ.; ²Fukuoka Univ.; ³Kyushu Univ.)

[J. Phys. Chem. B submitted]

The structure of clusters in methanol-water binary solutions has been investigated as a function of methanol mole fraction, x_M , by mass spectrometry on clusters isolated from submicron droplets by adiabatic expansion in vacuum and by X-ray diffraction on the bulk binary solutions. The mass spectra have shown that the average hydration number, $\langle n_m \rangle$, for m -mer methanol clusters, $M_m W_n$ (M = methanol, and W = water), decreases with increasing mole fraction of methanol, accompanied with two inflection points approximately at $x_M = 0.3$ and 0.7 . Figure 1 shows the plots of average hydration numbers, $\langle n_m \rangle$, for methanol m -mer hydrates with $m = 6, 8, 10$ and 12 . The X-ray diffraction data have also revealed a similar change in

the number of hydrogen bonds per water and/or methanol oxygen atom at 2.8 \AA to that found from mass spectrometry. On the basis of the results from the two methods, the most likely models of clusters formed in the binary solutions have been proposed; at $0 \leq x_M \leq 0.3$ the tetrahedral-like water clusters are the main species, at $0.3 \leq x_M \leq 0.7$ chain clusters of methanol molecules are gradually evolved with increasing methanol content, and at $x_M \geq 0.7$ chain clusters of methanol molecules become predominant. A comparison of the present results on the methanol-water mixtures with those of ethanol-water ones has shown that the tetrahedral-like water structure is broken down at a lower mole fraction of 0.2 and more sharply in the ethanol-water mixtures than in the methanol-water ones due to the large hydrophobic effect of ethanol. The behavior of the heat of mixing with varying alcohol concentration in the methanol-water mixtures is consistent with that of the average clusters formed in the mixtures, and thus anomalies in the physico-chemical data of alcohol-water probably originate from clusters formed in the mixtures.

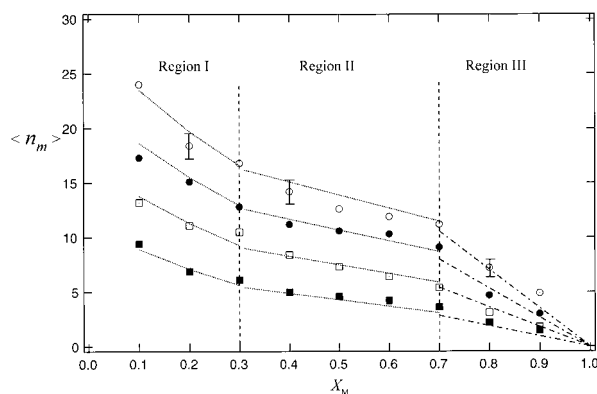


Figure 1. Plots of average hydration numbers, $\langle n_m \rangle$, for methanol m -mer hydrates with $m = 6$ (■), 8 (□), 10 (●) and 12 (○) as functions of methanol mole fractions (x_M). Dotted lines were obtained from the equations: $\langle n_m \rangle = 3(m - 0.5)(x_M - 0.3)^2 + 0.45(m - 3.8)$ for $0 \leq x_M \leq 0.3$, $\langle n_m \rangle = m(x_M - 0.3)^2 + 1.4(m - 3.8)$ for $0.3 \leq x_M \leq 0.7$, and $\langle n_m \rangle = 4.3(m - 3.8)x_M$ for $x_M \geq 0.7$.

III-A-5 Structure and Dynamics of 1,4-Dioxane-Water Binary Solutions Studied by X-ray diffraction, Mass Spectrometry, and NMR Relaxation

TAKAMUKU, Toshiyuki¹; YAMAGUCHI, Atsushi¹; TABATA, Masaaki¹; NISHI, Nobuyuki; YOSHIDA, Koji²; WAKITA, Hisanobu²; YAMAGUCHI, Toshio²
(¹Saga Univ.; ²Fukuoka Univ.)

[J. Mol. Liq. in press]

The structure of clusters formed in 1,4-dioxane-water binary solutions has been investigated at ambient temperature as a function of 1,4-dioxane concentration by X-ray diffraction for the corresponding solutions and by mass spectrometry for liquid droplets formed in vacuum from the liquid mixtures by an adiabatic expansion method. The ^2H spin-lattice relaxation times of D_2O and 1,4-dioxane- d_8 molecules in 1,4-dioxane-water binary solutions have also been measured at 30°C

over a whole range of 1,4-dioxane mole fraction. It has been found from the analysis of X-ray radial distribution functions that the number of hydrogen-bonds per water and 1,4-dioxane oxygen atom decreases with increasing 1,4-dioxane mole fraction X_{dio} , accompanied by two inflection points at approximately $X_{\text{dio}} = 0.1$ and 0.3 : at $X_{\text{dio}} \geq 0.3$ the inherent structure of 1,4-dioxane is mostly observed, water molecules probably involved in the structure by hydrogen bonding, and at $0.15 \leq X_{\text{dio}} \leq 0.2$ both structures of water and 1,4-dioxane are ruptured to form small binary clusters of one or two dioxane and several water molecules. The mass spectra have revealed that at $X_{\text{dio}} = 0.01$ water clusters W_n ($W =$

water) are mostly formed, but with increasing X_{dio} to 0.4 the water cluster reduced with evolving 1,4-dioxane clusters $D_m W_n$ ($D = 1,4\text{-dioxane}$). The ^2H spin-lattice relaxation data of D_2O molecules in the mixtures showed that the rotation of water molecules is gradually retarded with increasing X_{dio} to 0.3 , where the rotation is the slowest, and is then gradually accelerated with further increase in X_{dio} . The corresponding data of 1,4-dioxane- d_8 molecules showed a similar tendency, but the slowest motion observed at $X_{\text{dio}} = 0.2$. The present microscopic cluster structure and dynamic properties of the mixtures are discussed in connection with the heat of mixing, viscosity, and hydrophobic hydration.

III-B Ultrafast Dynamics of Photoexcited Molecules Studied by Transient Absorption and Transient Raman Spectroscopy Methods

Ultrafast transient absorption spectroscopy and transient Raman spectroscopy is now an universal and popular method for the study of reaction pathways induced by electronic or vibrational excitation of organic or metal complex molecules. We have constructed a new femto-pico synchronized multi-laser beam system. This unique system is open for collaborations in the field of molecular science.

III-B-1 Construction of a Tunable and Synchronized Picosecond-Femtosecond Double Laser System for the Study of Photodissociation Dynamics of Molecular Clusters in Solution

NAKABAYASHI, Takakazu; SATO, Shin-ichiro; INOKUCHI, Yoshiya; WATANABE, Kazuo; SAKAI, Makoto; FUJII, Masaaki; NISHI, Nobuyuki

Many time-resolved spectroscopic techniques require two broadly and independently tunable, synchronized light pulses with sufficient pulse energies. Since femtosecond time resolution simultaneously implies the loss of frequency resolution, a complementary use of picosecond and femtosecond pulse lasers is attractive for studying molecular dynamics. In order to meet these requirements, we have first constructed a tunable and synchronized picosecond-femtosecond double laser system, which is schematically shown in Figure 1. Two independently tunable OPAs are pumped by the output from a picosecond regenerative amplifier operating at 1 kHz repetition rate, 3 mJ pulse energy with 4 ps pulse duration and at 790 nm. By using sum- and difference frequency mixings, we have obtained the continuous tuning of light between 189 and 11200 nm with keeping microjoule pulse energy. Another OPA is excited by the output from a femtosecond regenerative amplifier (1 kHz, 2 mJ, 200 fs, 800 nm) to generate femtosecond pulses over a 300-10000 nm spectral

range. A portion of the output from the femtosecond regenerative amplifier is separated and used for harmonic generations. The pulse energy obtained is about 120 μJ for the third harmonic and about 10 μJ for the fourth harmonic, when amplified pulses with 1 mJ pulse energy are used. Two femtosecond mode-locked Ti:sapphire lasers are used to seed the picosecond and femtosecond regenerative amplifiers, respectively. The phase-detection method is adopted to lock the timing of the femtosecond lasers. A typical cross correlation function of pulses from the femtosecond lasers is shown in Figure 2a. The FWHM of the cross-correlation is observed to be 2.5 ps, which corresponds to the timing jitter between pulses from the femtosecond lasers. The two regenerative amplifiers are excited by the output from Q-switched cw Nd:YLF lasers, which are triggered externally by the output from one of the femtosecond laser. Figure 2b shows the cross correlation function of pulses from the regenerative amplifiers. The FWHM of the cross-correlation is found to be about 8 ps, indicating that the regenerative amplifiers are synchronized with the timing jitter of several picoseconds. The femtosecond regenerative amplifier has also been modified to be further excited by a Q-switched pulsed Nd:YAG laser to generate amplified pulses with 10 mJ pulse energy at 10 Hz repetition rate. We have observed time-resolved absorption and Raman spectra of some polyatomic molecules by using this laser system.

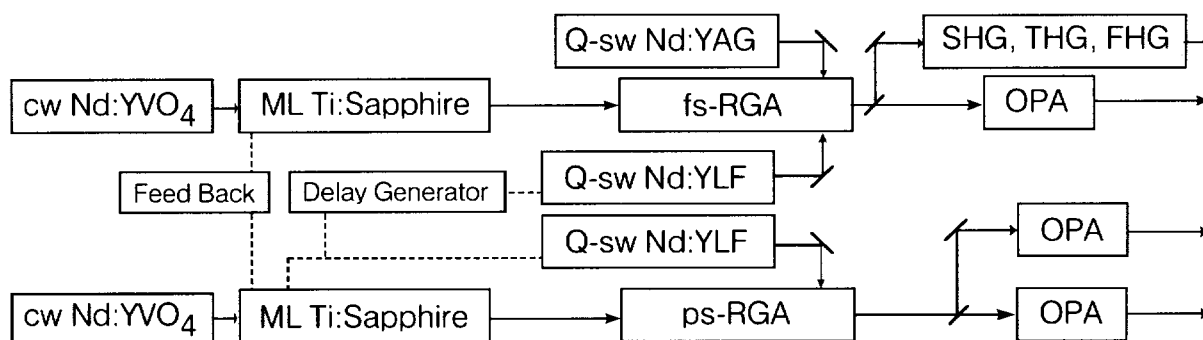


Figure 1. Block diagram of the picosecond-femtosecond double laser system.

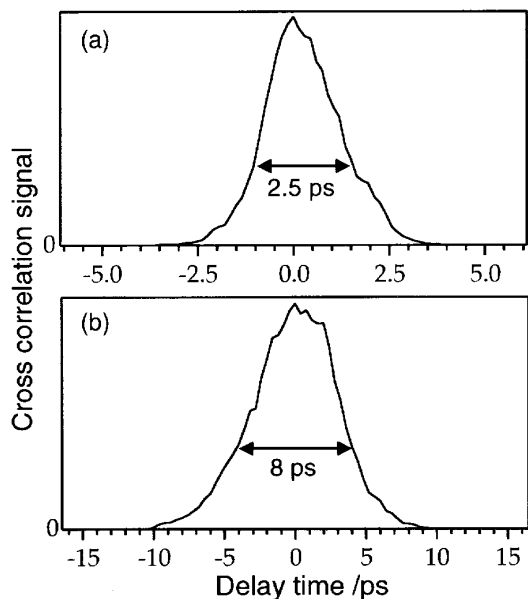


Figure 2. Cross correlation functions observed for pulses from (a) the femtosecond mode-locked lasers and (b) the picosecond and femtosecond regenerative amplifiers.

III-C Spectroscopic and Dynamical Studies on Charge Delocalization and Charge Transfer in Aromatic Molecular Cluster Ions

Charge transfer processes resulting in dynamical charge delocalization such as consecutive proton or electron hopping in molecular clusters and even in pure liquids are highly interesting in relation to the charge transportation in insulating materials. Not only in aromatic molecular liquids but also in pure water itself electric conductivity is very low when they do not contain impurities of ionic atoms or molecules. It is possible to control charge hopping with near infrared photons in such aromatic liquids. Here we investigate the role of impurity or neighboring molecules in changing the electronic properties of benzene cluster cations.

III-C-1 Photodissociation Spectroscopy of Benzene-Acetic acid Mixed Cluster Ions

KOSUGI, Kentaroh; INOKUCHI, Yoshiya; NISHI, Nobuyuki

It is now well known that the charge resonance interactions between the π -electron systems dominate the structures of the benzene cluster ions. On the other hand, the π electrons of the carboxyl group of acetic acid is expected to show strong interaction with the π -electron systems of the aromatic cations. In this study, we measure the photodissociation spectra of benzene-acetic acid mixed cluster ions for investigating the positive charge localization and the structure of the

binary complexes.

The experiment is done by using a tandem mass spectrometer coupled with infrared (IR), near IR, and visible lasers. Figure 1(a) displays the photodissociation spectra of $[(C_6H_6)_2(CH_3COOH)_n]^+$ with $n = 1-4$ in the near IR region. All the spectra show very broad bands with a maximum at 920 nm. Since the spectral features well resemble that of benzene dimer cation, we ascribe the bands to the charge resonance bands of benzene dimer ion cores in $[(C_6H_6)_2(CH_3COOH)_n]^+$. In the mixed cluster ions, the positive charge is localized in the benzene dimer site. The photodissociation spectrum in the IR region is thought to be a much better probe of the cluster structure. Figure 1(b) shows the photodissociation spectrum of $[(C_6H_6)_2(CH_3COOH)_1]^+$ in the

IR region. Three bands emerge at 3084, 3585, and 3627 cm^{-1} . According to the spectrum of $[(\text{C}_6\text{H}_6)_2(\text{CD}_3\text{-COOH})_1]^+$, the band at 3084 cm^{-1} is assigned to the CH stretching vibration of the benzene dimer ion core, and the bands at 3585 and 3627 cm^{-1} are to the OH stretching vibrations of acetic acid. The two OH stretching vibrations imply the existence of two isomers. Possible isomers are *cis*- and *trans*-acetic acid molecules in $[(\text{C}_6\text{H}_6)_2(\text{CH}_3\text{COOH})_1]^+$. In the gas phase, the free OH stretching vibration of a *cis*-acetic acid monomer emerges at 3583 cm^{-1} . Theoretical investigation of the acetic acid monomer by Turi et al. implied that the OH stretching vibration of *trans*-acetic acid has higher frequency than that of the *cis*-acetic acid. According to the facts, we can assign the band at 3585 cm^{-1} to the OH stretching vibration of $[(\text{C}_6\text{H}_6)_2(\text{cis-CH}_3\text{COOH})_1]^+$, and the band at 3627 cm^{-1} to that of $[(\text{C}_6\text{H}_6)_2(\text{trans-CH}_3\text{COOH})_1]^+$. In these ions, the acetic acid points the lone pair electrons on the oxygen of the carbonyl group to the benzene dimer ion core, and the OH group of the acetic acid is free from any binding. The benzene dimer ion core makes the *trans*-acetic acid comparatively stable with the *cis*-acetic acid, and the OH vibrations of both *cis*- and *trans*-acetic acid molecules in $[(\text{C}_6\text{H}_6)_2(\text{CH}_3\text{COOH})_1]^+$ are observed in the IR spectrum.

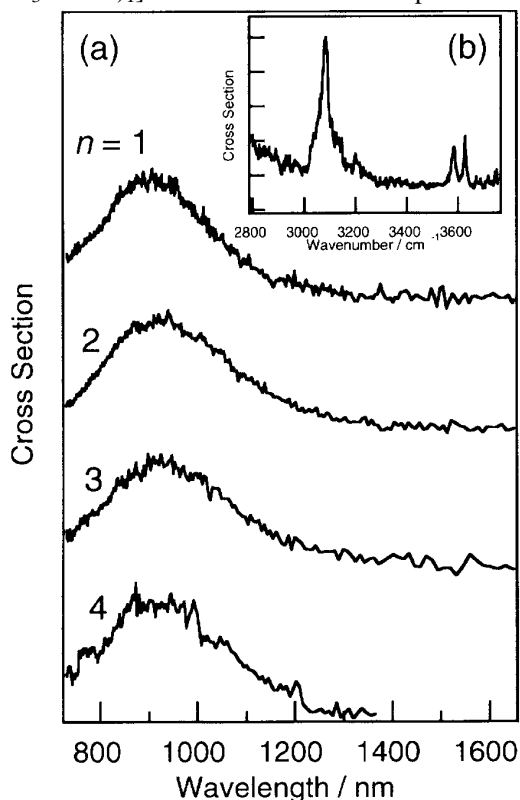


Figure 1. (a) Photodissociation spectra of $[(\text{C}_6\text{H}_6)_2(\text{CH}_3\text{COOH})_n]^+$ with $n = 1-4$ in the near IR region. (b) Photodissociation spectrum of $[(\text{C}_6\text{H}_6)_2(\text{CH}_3\text{COOH})_1]^+$ in the IR region.

III-C-2 Structural Isomers of Benzene-Phenol Mixed Dimer Cation

INOKUCHI, Yoshiya; NISHI, Nobuyuki

The benzene dimer cation with a parallel sandwich

structure has a broad and strong absorption band at 920 nm. This band is assigned to the charge resonance (CR) band. The existence of the CR band implies that the positive charge is delocalized in the parallel dimer. On the other hand, the benzene-phenol mixed dimer cation does not show any strong band in the near infrared (IR) region. Therefore, the structure of the mixed dimer cation is thought to be dominated with the hydrogen bonding of the OH group to the π electrons of the benzene. We measure the photodissociation spectra of ordinary and deuterated benzene-phenol mixed dimer cations in the IR region in order to get information on their structures with the help of theoretical calculation.

Figure 1 displays the photodissociation spectra of the benzene-phenol mixed dimer cations. The spectrum at the top is similar to that measured by Mikami *et al.* There are two maxima at 3200 and 3060 cm^{-1} . These bands could be assigned to the OH stretching vibration and CH stretching vibrations of the mixed dimer cation. We also measure the spectrum of the deuterated mixed dimer cation, $[(\text{C}_6\text{D}_6)(\text{C}_6\text{D}_5\text{OH})]^+$, showed in the bottom of Figure 1. The spectral feature of the deuterated cation is almost the same as that of the non-deuterated one. Thus, we can confirm that both bands are ascribed to the OH stretching vibrations. Appearance of the two OH stretching vibrations suggests that there are two structural isomers. The frequency of 3060 cm^{-1} is very low as a normal OH stretching frequency, even for a hydrogen-bonded dimer. One possibility is a proton transferred ion complex, $[(\text{C}_6\text{H}_6\text{-H}^+)\cdots(\text{OC}_6\text{H}_5)] \longleftrightarrow [(\text{C}_6\text{H}_6)\cdots(\text{H}^+\text{-OC}_6\text{H}_5)]$. *Cis*- and *trans*-type orientation of the two aromatic rings must be responsible for the presence of the two peaks in the IR spectra. A theoretical calculation with various basis sets is now going on for checking the validity of the assignment.

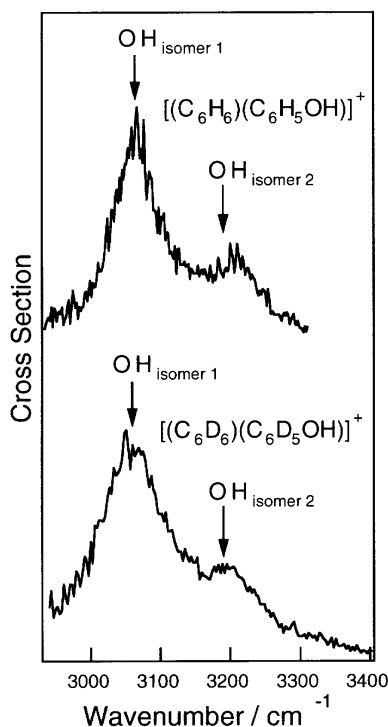


Figure 1. Photodissociation spectra of $[(\text{C}_6\text{H}_6)(\text{C}_6\text{H}_5\text{OH})]^+$ (top) and $[(\text{C}_6\text{D}_6)(\text{C}_6\text{D}_5\text{OH})]^+$ (bottom) in the IR region.

III-D Spectroscopy and Dynamics of Vibrationally Excited Molecules and Clusters

This research group, which started in April 1997, is planning to study spectroscopy and dynamics of molecules and clusters in higher vibrational state by two-color double resonance spectroscopy. New spectroscopic methods will also be developed to observe the higher vibrational state under collision-free condition.

III-D-1 Overtone Spectroscopy of Jet-Cooled Phenol Studied by Nonresonant Ionization Detected IR Spectroscopy

ISHIUCHI, Shun-ichi¹; FUJII, Masaaki
(¹GUAS)

[Proc. 9th Int. Symp. Reson. Ionization Spectrosc. Appl. (1998)]

Vibrational transitions of jet-cooled phenol have been detected by nonresonant two-photon ionization due to UV laser from 3400 cm⁻¹ to 14000 cm⁻¹. The UV frequency dependence of IR-UV double resonance signals is used for discussion on the mechanism of ionization. The spectrum shows a well-resolved structure due to the first to the fourth quantum of OH stretching vibrations, CH overtones and various combination vibrations. The vibrational frequency, anharmonicity and the dissociation energy of the OH stretching mode has been measured. The bandwidth of the OH overtone is found to decrease with increase in the vibrational quantum number.

III-C-2 Structure of 1-Naphthol-Water Clusters Studied by IR Dip Spectroscopy and Ab Initio Molecular Orbital Calculation

YOSHINO, Ruriko¹; HASHIMOTO, Kenro²; OMI, Takuichiro¹; ISHIUCHI, Shun-ichi³; FUJII, Masaaki
(¹Waseda Univ.; ²Tokyo Metropolitan Univ.; ³GUAS)

[*J. Phys. Chem. A* **102**, 6227 (1998)]

IR spectrum of *cis*-1-naphthol, *trans*-1-naphthol, and 1-naphthol·(H₂O)_{*n*} (*n* = 1–3) clusters has been measured by the IR dip spectroscopy in a supersonic jet. The spectra show clear vibrational structures of the monomers and the clusters in the energy region from 3000 cm⁻¹ to 3800 cm⁻¹. Observed vibrational transitions are assigned to the OH stretching vibrations of 1-naphthol and waters in the clusters. The size dependence of the IR bands and the cluster geometries are analyzed by using the ab initio MO method at MP2/6-31G level. From the comparison between the observed and calculated IR spectra, we have concluded that the 1-naphthol acts as the proton donor and a cyclic hydrogen-bond network is formed in the *n* = 2 and 3 clusters.

III-E Femtosecond Time-Resolved Photoelectron Imaging

Photodissociation dynamics has been studied extensively by measuring quantum state and scattering distributions of products. However, the most unambiguous experimental elucidation of reaction mechanism is by real-time observation of the reaction. Photoelectron spectroscopy is useful for this purpose, since it projects the wavepacket dynamics in the excited state to an accurately-known cation potential. Other advantages of photoelectron spectroscopy are (1) capability of detecting both singlet and triplet states, enabling direct observation of intersystem crossing and internal conversion processes, (2) high sensitivity due to efficient collection of electrons by electromagnetic fields, and (3) applicability of ultrafast laser with fixed wavelength. The analysis of photoelectron scattering distribution has been performed most often by the time-of-flight (TOF) method. However, a standard TOF method has a poor collection efficiency of electrons. The magnetic bottle spectrometer significantly improved the efficiency, but angular resolution is sacrificed. Photoelectron imaging (PEI) achieves the highest collection efficiency of electrons while providing routine measurements of speed and angular distributions. This work presents PEI coupled with femtosecond pump-probe technique, for the first time.

III-E-1 Femtosecond Time-Resolved Photoelectron Imaging on Ultrafast Electronic Dephasing in an Isolated Molecule

SUZUKI, Toshinori; WANG, Li; KOHGUCHI, Hiroshi

[*J. Chem. Phys.* **111**, 4859 (1999)]
[*Faraday Discuss. Chem. Soc.* in press]

The femtosecond time-resolved photoelectron imaging is reported for the first time. The method was applied to ultrafast dephasing in an intermediate case molecule Pyrazine. Figure 1 shows the snapshot of photoelectron scattering distribution measured as a function of pump-probe time delay. The decay of the optically-prepared S_1 character (the outer ring) and the build-up of dark triplet character (the inner ring) are clearly seen. The result also suggests the possibility that intersystem crossing is mediated by $T_2(\pi, \pi^*)$ state. This work is the first direct observation of the dynamics in the triplet manifold of this benchmark system.

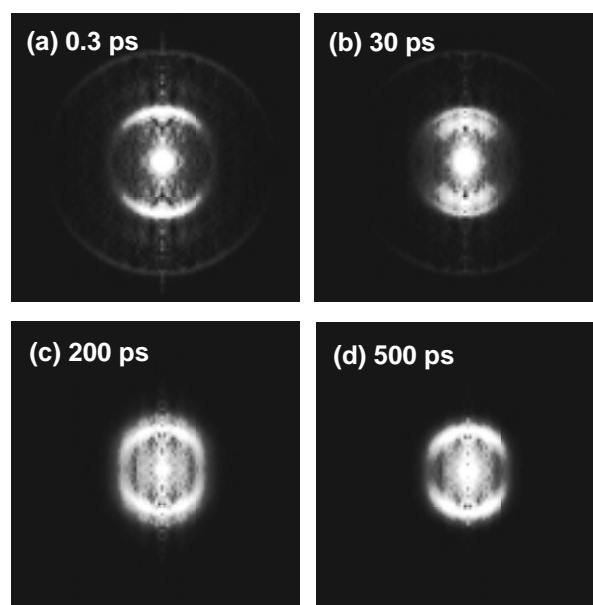


Figure 1. Inverse Abel transforms (512×512 pixels) of photoelectron images of $[1+2']$ REMPI of Pyrazine via the $S_1[{}^1B_{3u}(n, \pi^*)]$ 0^0 level at the time delays of (a) 0.3, (b) 30, (c) 200, and (d) 500 ps. The original images were integrated for 36 000 laser shots.

III-F Dynamical Stereochemistry

Stereodynamics in molecular photodissociation is investigated experimentally and theoretically. Efforts are made to determine multipole moments (density matrix) of a photofragment completely and interpret them quantum-mechanically.

III-F-1 Vector Correlation in Molecular Photodissociation

MO, Yuxiang; SUZUKI, Toshinori

[*J. Chem. Phys.* in press]

The quantum mechanical expression for the angle-dependent photofragment multiple moments is rigorously derived with only the dipole approximation. The angular momentum coupling between the two fragments is taken into account for the first time. The result is also compared with the *formal expansion*

method assuming fixed $\mu\text{-}\nu\text{-}\mathbf{J}$ vector correlation for all scattering angles [Y. Mo and T. Suzuki, *J. Chem. Phys.* **108**, 6780 (1998)]. The condition that reduces the rigorous formula to the approximate formula is examined.

III-G Photochemistry on Well-Defined Surfaces

Upon the irradiation of light in the wavelength range from visible to ultraviolet, a number of adsorbed molecules on metal surfaces reveal variety of photochemical processes, including photo-stimulated desorption, rearrangement of adsorbed states, photodissociation, and photo-initiated reactions with coadsorbates. A central and fundamental question in the surface photochemistry is to clarify how adsorbate-substrate systems are excited by photon irradiation. In addition, since photo-initiated reactions can be induced without any thermal activation of reactants, they may provide good opportunities for studying a new class of surface reactions which may not be induced thermally. We have studied photochemistry of various adsorption systems on well-defined metal and semiconductor surfaces mainly by temperature-programmed desorption (TPD), x-ray photoelectron spectroscopy (XPS), work function measurements, near edge x-ray absorption fine structure (NEXAFS) and angular-resolved time-of-flight (TOF) spectroscopy of photodesorbed species associated with pulsed laser irradiation. We have shown that methane weakly adsorbed on Pt(111) and Pd(111) is dissociated or desorbed by irradiation of 6.4-eV photons, which is far below the excitation energy for the first optically allowed transition of methane in the gas phase. This work has been extended to Cu(111), where photo-induced C-C coupling takes place. In addition, more thorough investigations have been done on the photodesorption of rare gas atoms from clean and modified Si(100) surfaces.

III-G-1 Photo-stimulated Desorption of Rare Gas Atoms Induced by UV-NIR Photons at a Semiconductor Surface

[*Surf. Sci.* in press]

WATANABE, Kazuya; MATSUMOTO, Yoshiyasu

[*Surf. Sci. Lett.* submitted]

Desorption induced by electronic transitions (DIET) of rare gases provides a good opportunity for understanding fundamental questions in electron- and photon-induced surface processes because no internal nuclear motions are involved compared with other DIET of polyatomic adsorbates. The DIET of rare gas atoms has been observed in the past by using electrons or photons whose energy exceeds 7 eV, since it requires high energy to ionize or excite valence- and core-electrons of rare gas atoms. However, we show that heavy rare gas atoms (Kr and Xe) are desorbed from clean and modified Si(100) surfaces by irradiating photons with energy as low as 1.16 eV.

Rare gas atoms are adsorbed on the surfaces at 50 K. UV and visible photons are irradiated onto the surfaces. Post-irradiation TPD is observed as a function of irradiated photon numbers. The area of TPD peaks decreases with increase of the number of photons, indicating the coverage of Xe is reduced by the photon irradiation. On the clean Si(100) surface, the kinetic energy distributions of the rare gas atoms are well represented by the Maxwell-Boltzmann distribution, but the obtained temperature is quite higher than that expected by surface heating with employed laser fluence. Furthermore, they do not depend on the excitation photon energy from 1.16 eV to 6.43 eV nor on the laser fluence. Thus, these features cannot be explained by conventional laser-induced thermal desorption. The most plausible mechanism for the desorption is that hot surface phonons created by recombination of photo-generated electron-hole pairs at a semiconductor surface directly couple to the desorption channel before they decay into bulk phonons.

III-G-2 Photochemistry of Methane on Cu(111)

WATANABE, Kazuo; MATSUMOTO, Yoshiyasu

Conversion of methane into useful chemical reagents has been extensively studied for several decades owing to the increasing industrial and environmental importance. However, methane is the most stable hydrocarbon and the previous efforts to break the methane C-H bond *thermally* have not necessary been successful regarding the efficiency and costs even with sophisticated catalysts.

In this work photochemistry of methane physisorbed on Cu(111) at 35 K have been investigated by temperature-programmed desorption (TPD). Methane is photodissociated into hydrogen, methylene, and methyl by 6.4-eV photon irradiation as in the case of Pt(111) and Pd(111). However, there are unique features on Cu(111). Post-irradiation TPD showed new desorption peaks of ethylene at 115 K and 380 K, in addition to the 430 K peak reported before. They are attributed to molecular desorption of ethylene formed by methane photodissociation at 35 K, associative recombination of two methylene groups, and concerted reactions of four methyl groups, respectively. The photoreaction cross section is estimated $2.0 \times 10^{-20} \text{ cm}^2$. Thus, photochemical C-C coupling in the photochemistry of methane is observed for the first time.

III-G-3 Coadsorption Effect of Cs on Photochemistry of Methane on Pt(111)

ANAZAWA, Toshihisa; WATANABE, Kazuo; MATSUMOTO, Yoshiyasu

We have reported that methane on Pt(111) is dissociated by irradiating uv photons.¹⁾ The excitation is understood as a transition from the ground state localized at methane to the excited state of the methane-substrate atoms complex where the excited Rydberg-like state of methane significantly mixed with the substrate empty states. Another way to understand the excitation mechanism is in the following. When the complete charge transfer to the substrate is assumed in the excited state of methane, the image force stabilizes the excited state by 1.9 eV. The ionization potential of physisorbed methane should then be reduced by 1.9 eV + the work function of the metal. Taking a work

function of 5.6 eV and the gas phase ionization potential of 12.6 eV, the excitation energy for the complete charge transferred state is calculated to be 5.1 eV, which is accessible with a 6.4-eV photon. When Cs is adsorbed, the work function is significantly reduced. By using this feature, we measured how the photochemical cross section is affected by the coadsorption of Cs to examine further the excitation mechanism. The

measurements show that the cross section is significantly reduced by the Cs coadsorption, in agreement with the expectation of the complete charge transfer model.

Reference

- 1) Y. Matsumoto, Y. A. Gruzdkov, K. Watanabe and K. Sawabe, *J. Chem. Phys.* **105**, 4775 (1996).

III-H Multiphoton Photoelectron Spectroscopy of Electronic States at Metal Surfaces

A central and fundamental question in surface photochemistry is to clarify how adsorbate-substrate systems are excited with photon irradiation. Thus, direct information on the excited states at surfaces is needed. One of the best methods, and most relevant to surface photochemical measurements, is multiphoton photoelectron spectroscopy. We have extended this method by using two-color (visible and VUV) beams for pump-and-probe experiments. In this year, the method is applied to surface states of clean and Xe-covered Pt(111) surfaces.

III-H-1 Visible and VUV Two-Photon Photoelectron Spectroscopy of the Surface State of a Clean Pt(111) Surface

KINOSHITA, Ikuo¹; WATANABE, Kazuya; INO, Daisuke²; MATSUMOTO, Yoshiyasu
(¹Yokohama City Univ.; ²GUAS)

The sp-derived surface state of a clean Pt(111) surface has been experimentally confirmed by visible two-photon photoelectron spectroscopy.¹⁾ We have extended this measurement by using visible and VUV photons. This method allows us to detect empty states near the Fermi level. The VUV photons are generated by tripling the frequency-doubled Ti:sapphire output in a Xe cell. Photoelectrons are detected and analyzed by a time-of-flight electron energy analyzer. The surface state is located at 0.2 eV below the Fermi level when detected along the surface normal. Since this state has a free-electron like parabolic dispersion curve, the state is expected to be unoccupied at large parallel momenta. In fact, we found that the photoelectron peak originating in the empty surface state appears at large detection angles from the surface normal. This gives a more complete picture of the dispersion curve of the surface state.

Reference

- 1) I. Kinoshita, T. Anazawa and Y. Matsumoto, *Chem. Phys. Lett.* **229**, 445 (1996).

III-I Ultrafast Reaction Dynamics of Photochromism and Related Phenomena

Photochromic reactions of some organic molecules are of considerable interest because of their wide applications including optical information processing, data storage, and nonlinear optics. The photochromism defined as a reversible transformation in chemical species between two forms is based on simple photochemical reactions such as bond cleavage, pericyclic, proton transfer, and isomerization reactions. As a result of different molecular structures between these two forms, the two isomers differ from one another in various properties such as absorption spectra, dipole moments, refractive indices, and so on. To understand the primary processes and functional properties of photochromic systems, we have examined several photochromic compounds by femtosecond and picosecond laser spectroscopic techniques.

III-I-1 Time-Resolved Study on Unconventional Fluorescence of an Azobenzene Liquid Crystal and Its Phase Transition

AZUMA, Jun¹; TAMAI, Naoto^{1,2}; SHISHIDO, Atsushi³; IKEDA, Tomiki³
(¹Kwansei Gakuin Univ.; ²IMS; ³Tokyo Inst. Tech.)

[*Mol. Cryst. Liq. Cryst.* **314**, 83 (1998)]

As far as the luminescence of azobenzene derivatives is concerned, it is well known that azobenzene do not show appreciable emission because of the trans-cis isomerization and the $n\pi^*$ character of the first-excited singlet state. Fluorescence properties of azobenzene liquid crystal, 4,4'-dioctyloxy-azobenzene (8AB8), were examined by steady-state and picosecond single-photon timing spectroscopy. It was found that the fluorescence from azobenzene aggregate with a peak at ~ 630 nm was observed in the solid phase in addition to the very weak S_2 fluorescence of azobenzene monomer centered at 420 nm. The structure of aggregate was estimated to be J-like structure. The fluorescence lifetimes of both J-aggregate and monomer S_2 state were estimated to be approximately 150 ps and shorter than 2 ps. The fluorescence lifetime of J-aggregate and relative fluorescence intensity of aggregate/monomer were found to be strongly dependent on temperature and liquid crystalline phases. Microscopic aggregate structure of 8AB8 in various liquid crystalline phases was discussed on the basis of these results.

III-I-2 Solvation Dynamics of Excited p-Methoxy-p'-cyanodiphenylacetylene in n-Butanol: Simultaneous Analysis of Time-Resolved Fluorescence Anisotropy and Stokes Shift

TAMAI, Naoto^{1,2}; NOMOTO, Takeo³, TANAKA, Fumio⁴; MATAGA, Noboru⁵
(¹Kwansei Gakuin Univ.; ²IMS; ³Mie Univ.; ⁴Mie Pref. College of Nursing; ⁵Inst. Laser Tech.)

[*Mol. Cryst. Liq. Cryst.* **314**, 131 (1998)]

Solvation dynamics of p-methoxy-p'-cyano-diphenylacetylene in n-butanol was investigated by observing time-resolved fluorescence anisotropy and dynamic Stokes shift in picosecond time domain. Fluorescence spectra of p-methoxy-p'-cyanodiphenylacetylene exhibited a large Stokes shift, depending on

the solvent polarity. The observed time-resolved anisotropy and Stokes shift were simultaneously analyzed with the theory based on the continuum model, in which dielectric friction in polar solvent was introduced through rotational motion of solute molecules with non-Markov process according to the framework of Nee and Zwanzig. The both experimental decays satisfactory fit with the theory. The dipole moments in the excited state and the ground state were estimated to be ~ 14 Debye and negligibly small.

III-I-3 A Combined Experimental and Theoretical Study on the Photochromism of Aromatic Anils

MITRA, Sivaprasad¹; TAMAI, Naoto^{1,2}
(¹Kwansei Gakuin Univ.; ²IMS)

[*Chem. Phys.* **246**, 463 (1999)]

Dynamics of photochromism have been studied in anil compounds using femtosecond transient absorption and picosecond fluorescence spectroscopies. The experimental observations were compared with the theoretical results obtained from AM1-SCF calculations. Excited-state intramolecular proton transfer (ESIPT) and photochromic reactions were found to occur from the S_1 state whereas normal fluorescence appears from the second excited singlet state. The photochromic processes are seen to be very fast which occur within few hundred of femtoseconds. The lifetime of the S_2 state was observed to be relatively long. This slower decay from higher excited singlet state was explained on the basis of the mixed nature of electronic transition comprising this state and relatively weak $S_2 \leftarrow S_1$ internal conversion. Theoretical results predict the ESIPT state to be zwitterionic in character, however, the final product may be a mixture of zwitterionic and nonionic in nature.

III-I-4 Photochromism in 2-(2',4'-Dinitrobenzyl)-pyridine Studied by Ultrafast Laser Spectroscopy

MITRA, Sivaprasad¹; ITO, Hirotugu¹; TAMAI, Naoto^{1,2}
(¹Kwansei Gakuin Univ.; ²IMS)

[*Chem. Phys. Lett.* submitted]

Ultrafast transient behavior of photochromic 2-(2',4'-dinitrobenzyl)pyridine have been studied using femtosecond transient absorption spectroscopy. Three

different transient signals could be found in the experiment at different time delays. The dynamics of the transient behavior in the short time scale reveal that very fast relaxation (within $\sim 400 \pm 100$ fs) from the initial excited state leads to the formation of a relatively stable intermediate which is the precursor of excited

state proton transfer. This intermediate decays to the ground state of proton transferred aci-nitro structure in nanosecond time scale. Solvent hydrogen bonding in ethanol plays an important role in the deactivation of the excited state giving different photophysical behavior.

III-J Photophysics and Photochemistry in Interface Layers and Mesoscopic Systems

Photochemical and photophysical processes in thin films, liquid/electrode interface layers, and some confined systems are considerable interest because of their characteristic properties different from those in the bulk. For analyzing the dynamics in these systems, we have applied various ultrafast spectroscopic techniques such as femtosecond transient grating spectroscopy, picosecond single-photon timing spectroscopy, and scanning probe microscopy (SPM). The development of time-resolved scanning near-field optical microscopy (SNOM) and STM are indispensable for these studies. The mesoscopic structures and dynamics of molecular aggregates on solid surfaces have been examined by time-resolved SPM. The photoelectrochemistry is an another important subject to analyze the role of interface layers. The characteristic properties of carrier and electron transfer dynamics in liquid/electrode interface layers have been also examined by femtosecond laser spectroscopy.

III-J-1 Time-Resolved and Near-Field Scanning Optical Microscopy Study on Porphyrin J-Aggregate

MIURA, Atsushi¹; MATSUMURA, Kazuo¹; SU, Xingguang¹; TAMAI, Naoto^{1,2}
(¹Kwansei Gakuin Univ.; ²IMS)

[*Acta Phys. Pol.* **94**, 835 (1998)]

Water-soluble porphyrin, 5,10,15,20-tetraphenyl-21H,23H-porphinetetrasulfonic acid (TPPS), forms J-aggregate in aqueous solution depending on experimental conditions such as pH, dye concentration, and/or ionic strength. The steady-state fluorescence and picosecond single-photon timing spectroscopy were applied for protonated monomer and J-aggregate in aqueous solution and in thin films to reveal the dynamics in the S_2 and S_1 states. The S_2 fluorescence spectra from the protonated monomer and J-aggregate were observed in addition to the normal S_1 fluorescence. The lifetime of the S_2 state was estimated to be shorter than a few ps for J-aggregate. The mesoscopic structures of J-aggregate in thin film with and without polymer on the glass surface were examined by scanning near-field optical microscopy (SNOM). With the surface topography and SNOM transmission images, TPPS J-aggregate was found to form a long and narrow tube-like structure which has a few μm length, 0.2–0.5 μm width, and 5–30 nm height. An unidirectional orientation of the structure was also found, which may be originated from the spin-coating process.

III-J-2 Excitation Energy Transfer in Langmuir-Blodgett Films of 5-(4-N-Octadecylpyridyl)-10,15,20-tri-p-tolylporphyrin on Gold-Evaporated Glass Substrates Studied by Time-resolved Fluorescence Spectroscopy

ZHANG, Zhijun¹; VERMA, Atul¹; TAMAI, Naoto^{1,2}; NAKASHIMA, Kenichi³; YONEYAMA,

Michio⁴; IRIYAMA, Keiji⁵; OZAKI, Yukihiro¹
(¹Kwansei Gakuin Univ.; ²IMS; ³Saga Univ.; ⁴Mitsubishi Chem. Co.; ⁵Jikei Univ.)

[*Thin Solid Films* **333**, 1 (1998)]

The fluorescence decays in mono- and multilayer Langmuir-Blodgett (LB) films of 3-(4-N-octadecylpyridyl)-10,15,20-tri-p-tolylporphyrin (porphyrin338a) deposited on gold evaporated glass substrates were measured to explore various channels for excitation energy transfer processes. The decays in the 1-layer LB films of porphyrin 338a separated from gold surface by LB film of arachidic acid were also measured as a function of the thickness of spacer, *i.e.* the thickness of the LB films of arachidic acid. Consistent with our previous steady-state fluorescence study, the expectation values of the lifetime obtained by fitting the decay curves indicate that at the short separation distance, the energy transfer from the porphyrin molecules to the gold surface overshadows other processes, including intra- and interlayer energy transfers. The deviation of energy transfer rate from Chance *et al.* (CPS) prediction of inverse distance cubed in our case may be interpreted by assuming the presence of additional excitation energy decay pathways in the LB films of porphyrin 338a on the gold evaporated glass substrates.

III-J-3 Carrier Dynamics on Titanium Dioxide Single Crystals by Femtosecond Transient Grating Spectroscopy

YANG, Xiujuan¹; TAMAI, Naoto^{1,2}; NAKATO, Yoshihiro³
(¹Kwansei Gakuin Univ.; ²IMS; ³Osaka Univ.)

The photogenerated carrier dynamics in bare titanium dioxide (TiO_2) single crystals with (100), (110), and (001) faces was examined by femtosecond transient grating spectroscopy. The dynamics of transient grating signal at low excitation intensity was

found to be very similar to that of the luminescence observed at ~ 430 nm, suggesting that the same species were probed by both time-resolved spectroscopies existing in the surface layer of TiO_2 single crystals. The decay curves of transient grating were strongly dependent on the excitation intensity but independent on the types of crystal faces. The rate of the formation of Γ -state or electron trapping in TiO_2 single crystal was found to be faster than 50 fs. The subsequent intensity-dependent relaxation was analyzed in terms of electron-hole recombination kinetics, and the recombination rate constants in single crystals were compared with that of TiO_2 nanoparticles.

RESEARCH ACTIVITIES IV

Department of Molecular Assemblies

IV-A Solid State Properties of Phthalocyanine Salts and Related Compounds

Some phthalocyanine molecules contain unpaired d-electrons in the conjugated π -electron system. Due to this special nature, the itinerant π -electrons and localized unpaired d-electrons coexist in solid phthalocyanine salts, in which a one-dimensional double-chain system (metal and ligand chain) is formed. Furthermore these chains make up wide (π -band) and narrow (d-band) one-dimensional bands, the energy of the narrow band being close to the Fermi energy of the wide band. The phthalocyanine conductor is thus a two-chain and two-band system. The exchange interaction of itinerant π -electrons with localized magnetic moments is a new aspect in the field of organic metals. For the sake of basic understanding of these materials, where a magnetic interaction takes an important role, we prepare and characterize the solid phthalocyanine salts and related compounds.

IV-A-1 ESR Properties of Oriented Single Crystals of $\text{Co}_x\text{Ni}_{1-x}\text{Pc}(\text{AsF}_6)_{0.5}$

SIMONYAN, Mkhitar; YONEHARA, Yukako¹;
DING, Yuqin¹; YAKUSHI, Kyuya
(¹GUAS)

Phthalocyanine conductor $\text{CoPc}(\text{AsF}_6)_{0.5}$ has two magnetic subsystems: the localized 3d-electron of Co and itinerant π -electron of Pc. However, this compound is ESR silent, since the spin-orbit interaction in Co and dipole-dipole interaction between molecules are strong. The magnetically diluted system $\text{Co}_x\text{Ni}_{1-x}\text{Pc}(\text{AsF}_6)_{0.5}$ is formed by mixing $\text{CoPc}(\text{AsF}_6)_{0.5}$ in non-magnetic nearly isostructural $\text{NiPc}(\text{AsF}_6)_{0.5}$. When $x = 0.01$, we found an anisotropic hyperfine structure at 3.2 K. From the angular dependence of the hyperfine structure, the hyperfine constants and principal g -values are determined as $A = 0.017 \text{ cm}^{-1}$, $B = 0.032 \text{ cm}^{-1}$, $g_{\parallel} = 2.056$, and $g_{\perp} = 3.045$ at 3.2 K. The hyperfine constants A and B are very close to those of insulating mixed crystal $\text{Co}_{0.001}\text{Ni}_{0.999}\text{Pc}$ but the g -values are very different between them, which means the different electronic state in Co 3d-orbital. In contrast to $\text{Co}_{0.001}\text{Ni}_{0.999}\text{Pc}$, the ESR signal of $\text{Co}_{0.01}\text{Ni}_{0.99}\text{Pc}(\text{AsF}_6)_{0.5}$ shows strong temperature dependence. As shown in Figure 1, the hyperfine structure collapse into a single Lorentzian line above 40 K, the metal-insulator transition temperature. This is direct evidence that the conduction electrons in ligand (Pc) site are interacting with the local magnetic moment of Co site. This exchange interaction is strongly reflected on the temperature dependence of g_{\perp} as well.

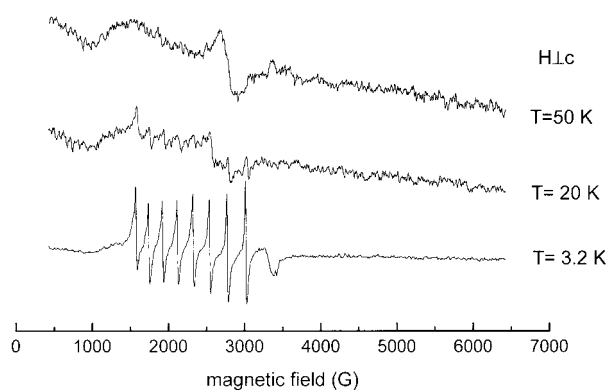


Figure 1. Hyperfine structure of the ESR signal of $\text{Co}_{0.01}\text{Ni}_{0.99}\text{Pc}(\text{AsF}_6)_{0.5}$ at 3.2 K. Above 40 K, in a metallic phase, this hyperfine structure collapse into a single Lorentzian through the exchange coupling with itinerant π -electrons.

IV-A-2 Pressure-Temperature Phase Diagram of $\text{NiPc}(\text{AsF}_6)_{0.5}$

SIMONYAN, Mkhitar; YAKUSHI, Kyuya

We have shown before that $\text{NiPc}(\text{AsF}_6)_{0.5}$ shows a continuous charge transfer from the metal 3d-band to the ligand π -band and this charge transfer begins at 1 GPa.^{1,2} From the analysis of the plasmon absorption band, we predicted that a metal-insulator (MI) transition accompanied this continuous charge transfer phenomenon. It is therefore expected that the MI transition occurs at the same pressure, *ca.* 1 GPa, at room temperature. On the other hand this compound undergoes a MI transition around 40 K at ambient pressure. This observation suggests that the temperature of this MI transition will increase from 40 K to room temperature when the high-pressure is applied to this compound. Figure 1 actually realizes our expectation: the resistance minimum monotonously increases up to 283 K at 0.95 GPa. The insulator phase of $\text{NiPc}(\text{AsF}_6)_{0.5}$ brought about by the 3d- π charge transfer is likely to be a state of Anderson localization. The mechanism of this MI transition is unique among the organic conductors.

References

- 1) T. Hiejima and K. Yakushi, *J. Chem. Phys.* **103**, 3950 (1995).
- 2) Y. Yonehara and K. Yakushi, *Synth. Met.* **94**, 149 (1998).

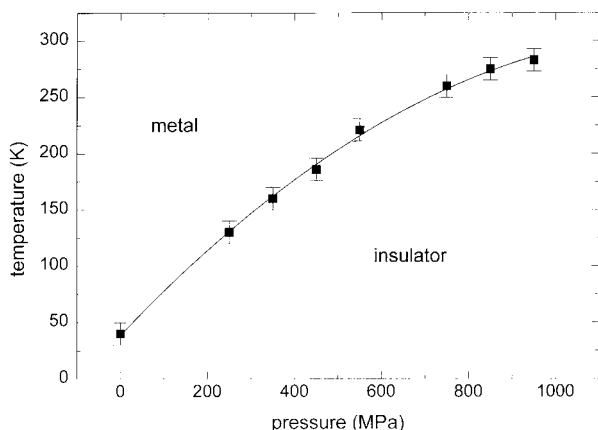


Figure 1. P-T Phase diagram of $\text{NiPc}(\text{AsF}_6)_{0.5}$: The squares represent the resistivity-minimum temperature against the pressure. Note that the insulator phase expands according to the pressure, which is associated with the continuous charge-transfer phenomenon.

IV-A-3 New Raman Bands Found in the Mixed Crystals of $\text{Ni}_{1-x}\text{Co}_x\text{Pc}(\text{AsF}_6)_{0.5}$

YONEHARA, Yukako¹; DING, Yuqin¹; SIMONYAN, Mkhitar; YAKUSHI, Kyuya (¹GUAS)

We show by X-ray diffraction and EPMA that the nearly isostructural $\text{NiPc}(\text{AsF}_6)_{0.5}$ and $\text{CoPc}(\text{AsF}_6)_{0.5}$ make mixed crystals $\text{Ni}_{1-x}\text{Co}_x\text{Pc}(\text{AsF}_6)_{0.5}$ in a wide range of x ($1 \geq x \geq 0$). We find new Raman bands at 370 cm^{-1} and 740 cm^{-1} that appear only in the mixed crystals, when the He-Ne laser (632.8 nm) is polarized parallel to the c -axis (conducting axis). The symmetry of these Raman modes is a_{1g} , since they appear in the configuration of $b(c,c)-b$ or $a(c,c,-a)$. When we change the excitation light to Ar^+ laser (514.5 nm), these new Raman bands are remarkably weakened or disappear. This suggests the resonance effect for the appearance of the new bands, thereby new excited state is formed around $15 \times 10^3\text{ cm}^{-1}$ in the mixed crystals and the transition moment to this excited state is parallel to the c -axis. This excited state is proposed to be a charge-transfer state from the filled $3d_{z^2}$ -orbital of NiPc to the partly vacant $3d_{z^2}$ -orbital of CoPc . The 370 cm^{-1} and its overtone mode 740 cm^{-1} are associated with the deformation mode of isoindole ring.

IV-B Structure and Properties of Organic Conductors

The study of organic metals rapidly developed when the dimensionality of an intermolecular charge-transfer interaction is expanded. This expansion of dimensionality has been brought about by the discovery of new molecules such as BEDT-TTF or C_{60} . The most basic physical parameters are the transfer integrals that represent the dimensionality and itinerancy of the electron, and the on-site Coulomb energy and coupling constants with molecular vibration, which represent the localized character of the electron. We systematically determine these parameters by polarized reflection spectroscopy assembling a microscope, multi-channel detection system, FT-IR, and liquid helium cryostat.

Another ongoing program is to look for negative- U organic charge-transfer compounds, the strategy of which is described in the special research project of this issue. In this research program, the most important parameter is the charge or valence of the molecule in a mixed-valent state. The examination of the electronic and vibrational spectra at low temperature or high pressure is most efficient to characterize the valence. Molecular metals consisting of large or long molecules are examined by reflection and Raman spectroscopy at low temperature.

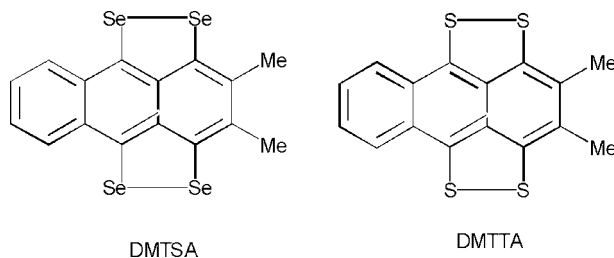
IV-B-1 Spectroscopic Study of Isostructural Charge-Transfer Salts: Non-Metallic DMTA- BF_4 and Metallic DMTSA- BF_4

OUYANG, Jianyong¹; DONG, Jian¹; YAKUSHI, Kyuya; TAKIMIYA, Kazuo²; OTSUBO, Tetsuo² (¹GUAS; ²Hiroshima Univ.)

[*J. Phys. Soc. Jpn.* in press]

We present the polarized reflection spectra of non-metallic DMTA- BF_4 and the isostructural metallic DMTSA- BF_4 . From these spectra, both compounds were regarded as quasi-one-dimensional conductors. From the analysis of these spectra we show that DMTA- BF_4 is a Mott insulator with $U/4t \sim 0.8\text{--}1.2$ and DMTSA- BF_4 is a weakly correlated metal with structural fluctuation near the room temperature. Resistivity, thermopower, and ESR are consistent with the above picture, and demonstrate the phase transitions at *ca.* 100 K for DMTA- BF_4 and at *ca.* 150 K for DMTSA- BF_4 . The low-temperature reflection spectra of

both compounds strongly suggest the breaking of screw-axis symmetry along the conducting axis. These phase transitions are regarded as the spin Peierls transition (DMTTA- BF_4) and Peierls (DMTSA- BF_4) transition. Assuming a dimerized stack, we estimate the transfer integrals t_1 and t_2 as 0.25 and 0.21 eV from the 10 K spectrum of DMTSA- BF_4 . The coupling constants of molecular vibration of DMTSA with the inter-molecular charge-transfer excitation are obtained analyzing the polarized reflection spectrum of DMTSA- ClO_4 having a dimerized structure.



IV-B-2 Suppression of the Metal-Insulator Transition under High Pressure in 1:1 Metallic DMTSA-BF₄

SIMONYAN, Mkhitar; YAKUSHI, Kyuya; TAKIMIYA, Kazuo¹; OTSUBO, Tetsuo¹
(¹Hiroshima Univ.)

DMTSA-BF₄ undergoes a metal-insulator transition of a Peierls type.¹⁾ This phase transition is suppressed by applying 400 MPa as shown in the figure. Probably the inter-chain transfer integral t_{ab} is enhanced by the high pressure. Taking t_{ab} into account, we have examined the band structure of this compound. However, this transfer integral provides no change in one-dimensional Fermi surface, if the band is half-filled. The high-pressure experiment requires the further examination of the band-filling factor or inter-chain coupling through the counter anion BF₄.

We have measured the resistance of 500 MPa down to 0.23 K using the ³He cryostat equipped in the Molecular Materials Center. However, superconductivity was not found in this compound at this pressure. All organic compound which shows superconductivity has TTF skeleton. This might suggest that the high-frequency phonon structure is associated with the mechanism of the superconductivity in organic superconductor.

Reference

- 1) J. Dong, K. Yakushi, K. Takimiya and T. Otsubo, *J. Phys. Soc. Jpn.* **67**, 971 (1998).

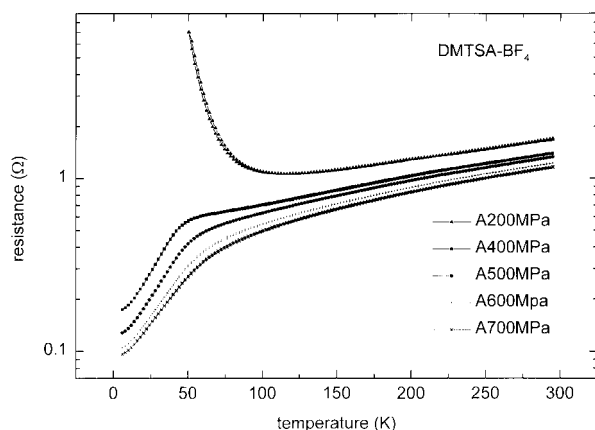


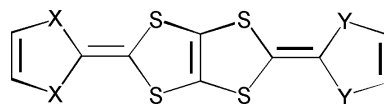
Figure 1. Temperature dependence of the resistance of DMTSA-BF₄. The metallic state is maintained at least down to 2 K above 400 MPa.

IV-B-3 Band Structure of Organic Metals (BDT-TTP)₂X (X = ClO₄, ReO₄), (ST-TTP)₂AsF₆, and (BDS-TTP)₂AsF₆ Studied by Reflection Spectroscopy

OUYANG, Jianyong¹; YAKUSHI, Kyuya; MISAKI, Yohji²; TANAKA, Kazuyoshi²
(¹GUAS; ²Kyoto Univ.)

The charge-transfer salts of BDT-TTP with β -type molecular arrangement have quasi-one-dimensional metallic band. We have experimentally determined the

intra (t_a)- and inter-chain (t_p) transfer integrals of (BDT-TTP)₂X (X = AsF₆, SbF₆)_{0.5}. We apply the same spectroscopic method to the title compounds. (ST-TTP)₂AsF₆ and (BDS-TTP)₂AsF₆ are isostructural to (BDT-TTP)₂SbF₆ with P1 space group. The transfer integrals are $t_a = -0.24$ eV, $t_p = -0.042$ eV for (ST-TTP)₂AsF₆ and $t_a = -0.26$ eV, $t_p = -0.044$ eV for (BDS-TTP)₂AsF₆. These values are not significantly enhanced compared with (BDT-TTP)₂X (X = AsF₆, SbF₆), although selenium atoms are introduced at the outer sulfur position. Probably the increase of the overlap between selenium-sulfur orbitals is compensated by the decrease of the sulfur-sulfur overlap. This system became more anisotropic at low temperatures as well as (BDT-TTP)₂X (X = AsF₆, SbF₆). (BDT-TTP)₂X (X = ClO₄, ReO₄) are isostructural to each other with the space group of C2/c. The intra-chain (t_b) and inter-chain (t_p) transfer integrals are estimated as $t_b = 0.26$ eV, $t_p = -0.048$ eV for ClO₄ salt and $t_b = 0.25$ eV, $t_p = -0.047$ eV for ReO₄ salt. From the spectral data we corrected the chemical ratio of ReO₄ salt as 2:1, although it was reported as (BDT-TTP)₂(ReO₄)_{0.72}. We analyze the reflectivity curve $R(\omega)$ using generalized Drude model and find $R(\omega)$ along the inter-chain direction deviates significantly from the simple Drude model.



X = Y = S: BDT-TTP
X = S, Y = Se: ST-TTP
X = Y = Se: BDS-TTP

IV-B-4 Insulator-Insulator Phase Transition of θ -(BDT-TTP)₂Cu(NCS)₂: Strongly Correlated Two-Dimensional System

OUYANG, Jianyong¹; YAKUSHI, Kyuya; MISAKI, Yohji²; TANAKA, Kazuyoshi²
(¹GUAS; ²Kyoto Univ.)

Contrary to the metallic properties of β -type (BDT-TTP)₂X, θ -type (BDT-TTP)₂Cu(NCS)₂ is an insulator, although a simple tight-binding calculation leads to a two-dimensional metallic band. A phase transition is found at 250 K in the electrical resistance measurement, the activation energy being changed from 30-40 meV (HT phase) to 100 meV (LT phase). The spin susceptibility changes the temperature dependence at 250 K, below which it conforms to a Curie-Weiss law with $C = 0.143$ and $\theta = 19$ K. Although this magnetic property is not well understood, it is safely concluded that the charge on BDT-TTP is rather localized in the LT phase. The reflectivity exhibits the so-called charge-transfer (CT) band in two polarization directions, which means the inter-molecular interaction is two-dimensional. This CT band dramatically changes at the phase transition temperature, increasing the gap energy below the phase transition temperature. This behavior strongly suggests the structural change through the phase transition, although the LT phase structure is not known. As shown in the figure, the Raman spectrum of the C=C stretching mode has an asymmetric broad lineshape in HT phase.

It shows a complicated splitting accompanied by the appearance of new peaks below the phase transition temperature. This splitting may be associated with the charge disproportionation.

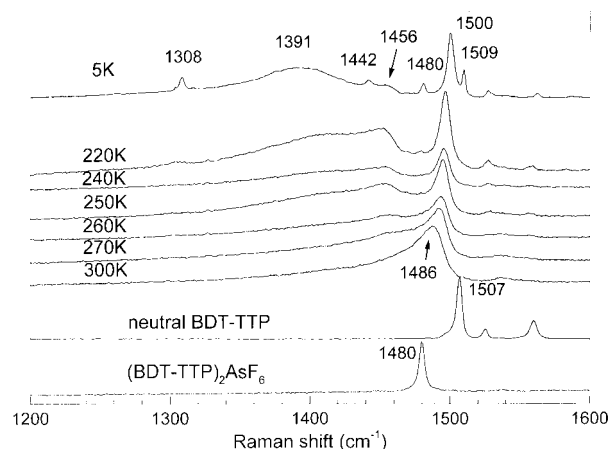


Figure 1. Temperature dependence of the Raman spectrum of C=C stretching mode in θ -(BDT-TTP) $_2$ Cu(NCS) $_2$ along with the room-temperature spectrum of BDT-TTP and (BDT-TTP) $_2$ AsF $_6$ crystals. This charge-sensitive mode continuously changes during the phase transition.

IV-B-5 Phase Transition in Narrow-band Organic Metals (BEDT-ATD) $_2$ X(solvent) (X = PF $_6$, AsF $_6$, BF $_4$; solvent = THF, DHF, DO)

YAKUSHI, Kyuya; URUICHI, Mikio; YAMASHITA, Yoshiro

[*Synth. Met.* in press]

We present the metal-insulator (MI) transition of the title compounds examined by reflection spectroscopy, X-ray diffraction, and magnetic susceptibility. Below the MI transition temperature, the space group changes from $P2_1/a$ to Pa with $4k_F$ lattice modulation in (BEDT-ATD) $_2$ PF $_6$ (DHF) and (BEDT-ATD) $_2$ BF $_4$ (THF) which undergo MI transitions at 150 K and 200 K, respectively. On the other hand, the symmetry change is not observed at about 80 K in (BEDT-ATD) $_2$ PF $_6$ (DO) (T_{MI} = 100 K), (BEDT-ATD) $_2$ PF $_6$ (THF) (T_{MI} < 50 K), and (BEDT-ATD) $_2$ AsF $_6$ (THF) (T_{MI} < 50 K). The $4k_F$ lattice modulation is supported by the magnetic susceptibility experiment as well. The precursor phenomenon of this structural change is observed already at room temperature in (BEDT-ATD) $_2$ PF $_6$ (DO). All of these data suggest the view that (BEDT-ATD) $_2$ X(solvent) is a strongly correlated 1D metal.

The breaking of the center of symmetry in several solvent-containing crystals requires that asymmetric solvents are aligned ferroelectrically below the MI transition temperature as shown in the figure. This suggests the possibility of the ferroelectric state just below the phase transition temperature. The experiment to examine this unusual possibility is now in progress.

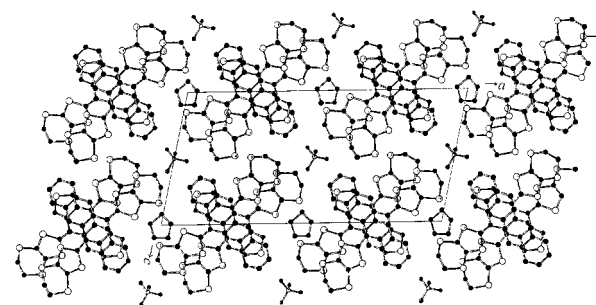
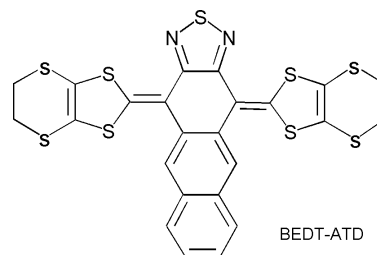


Figure 1. Low-temperature crystal structure of (BEDT-ATD) $_2$ BF $_4$ (THF).

IV-B-6 Experimental and Theoretical Estimation of the Site-Energy Difference in Et $_4$ N(DMTCNQ) $_2$

NAKANO, Chikako; YAKUSHI, Kyuya; UEDA, Kazushi¹; SUGIMOTO, Toyoshige¹
(¹Osaka Pref. Univ.)

[*Chem. Phys. Lett.* in preparation]

DMTCNQ forms a dimerized stack in (Et $_4$ N)-(DMTCNQ) $_2$ with two crystallographically independent sites. Although the average charge of DMTCNQ is -0.5 , the charge in different site has a different value such as $-0.5 + \delta$ and $-0.5 - \delta$. We have estimated this δ as 0.1 by the Raman spectroscopy. The different charge on the non-equivalent site comes from the site-energy difference in the unit cell. This kind of charge disproportionation is sometimes accompanied by the phase transition in organic conductors such as (DI-DCNQI) $_2$ -Ag and α' -(BEDT-TTF) $_2$ IBr $_2$ and is attracting an attention as a new ground state. The pattern of the charge distribution is not only determined by the repulsive force between the adjacent localized charges but also by the electrostatic force with counter anion/cation. Following the last year's experimental work, we conducted the numerical calculation of the Madelung energy, which brings about the site-energy difference. We first calculate the charge distribution in DMTCNQ 0 , DMTCNQ $^-$, and Et $_4$ N $^+$ using the PM3 semi-empirical method in the HyperChem-R5.1 program system. The infinite sum of the electrostatic energy between these point charges is calculated using the Ewald method. The site-energy difference is calculated as 0.14 eV. On the other hand, this site energy difference is estimated based on the ion-neutral dimer model analyzing the reflection and Raman spectra. It is experimentally estimated as 0.082 eV. The agreement with numerical estimation is satisfactory.

IV-B-7 κ' -(ET)₂Cu₂(CN)₃—Superconductor with Mixed Cu₂(CN)₃ and N(CN)₂ Ligands in the Anion Layer Studied by Polarized Reflection Spectroscopy

DROZDOVA, Olga¹; YAKUSHI, Kyuya; SAITO, Gunzi¹; OOKUBO, Kenji¹; YAMACHI, Hideki¹; KONDO, Tetsuo; URUICHI, Mikio; OUAHAB, Lahcène²

(¹Kyoto Univ.; ²Univ. Rennes)

Since the first discovery of (ET)₂Cu₂(CN)₃ with κ -type donor packing, controversial results were reported concerning its conducting properties. “ κ ” Abbreviation was introduced to distinguish an ambient pressure superconductor with $T_c = 3.8$ K from the semiconductor “ κ' ” with $E_a = 0.04$ – 0.05 eV. The same preparation conditions give the 11.2 K superconductor κ -(ET)₂Cu(CN)[N(CN)₂]. Polarized reflection spectra were measured on the conductive (*bc*) plane of κ -(ET)₂Cu₂(CN)₃, κ' -(ET)₂Cu₂(CN)₃ and κ -(ET)₂Cu(CN)-[N(CN)₂]. Despite the overall similarity of the spectra at 293 K, clear difference in the 2100–2300 cm⁻¹ range was observed. Namely, κ' -(ET)₂Cu₂(CN)₃ exhibits CN stretching peaks characteristic for both κ -(ET)₂Cu₂(CN)₃ and κ -(ET)₂Cu(CN)[N(CN)₂]. Thus anion layer of κ' is regarded as mixture of Cu₂(CN)₃ and Cu(CN)-[N(CN)₂] anions. The mixing ratio was estimated as 2:1 in most samples. Angle dependence suggested that the orientation of the original features conserved within the anion layer of κ' . Homogeneity of the mixing was supported by Raman spectroscopy. Temperature evolution of the reflection spectra followed conducting properties. The chemical formula of κ' -(ET)₂Cu₂(CN)₃ was modified to κ -(ET)₂Cu^{+(2-x-y)}Cu^{2+x}(CN)_(3-2y)-[N(CN)₂]_y, where $x < 0.01$ and $0.1 \leq y \leq 0.8$.

IV-B-8 Raman-active C=C Vibrations of κ -(BEDT-TTF)₂Cu[N(CN)₂]Br and Its Deuterated Analogues

MAKSIMUK, Mikhail; YAKUSHI, Kyuya; KAWAMOTO, Atsushi¹; TANIGUCHI, Hiromi²; KANODA, Kazushi²

(¹Hokkaido Univ.; ²Tokyo Univ.)

The set of progressively deuterated isotopic analogues of κ -(BEDT-TTF)₂Cu[N(CN)₂]Br lies on the border between metals and insulators. Below 80 K, a crystal volume is divided into a metallic phase and an insulating one. The amount of the latter increases with deuteration and depends on the cooling rate near 80 K. These crystals have several anomalies in temperature dependencies of their various physical properties. We studied d[0,0], d[2,2], d[3,3] and d[4,4] single crystals, the numbers being the numbers of deuterium atoms in every end of a BEDT-TTF molecule. The C=C stretching modes in resonance Raman spectra (laser wavelength 514.5 nm) have been measured at temperatures between 4.2 and 300 K. In d[2,2], d[3,3] and d[4,4], four modes have been observed: well-known totally symmetric ν_2 , ν_3 ; vibronically coupled $\nu_{27}^-(B_{1u})$ and a mode near 1463 cm⁻¹ (at 5 K) which we assign to $\nu_{27}^+(B_{1u})$. In d[0,0] below 200 K, in addition to that, it

has been possible to resolve dimer-dimer splitting of ν_2 and ν_3 . ν_2 and ν_3 have different temperature dependence of this splitting. In d[2,2] all ν_{27}^- parameters and the width of ν_2 depend on the cooling rate near 80 K as well as they are sample-dependent. In both cases it can be explained as the influence of the electronic system: for ν_{27}^- by electron-molecular vibration coupling and for ν_2 width by a change of the dimer-dimer splitting.

IV-B-9 Determination of the Charge on BEDO-TTF in Its Complexes by Raman Spectroscopy

DROZDOVA, Olga¹; YAMACHI, Hideki¹; YAKUSHI, Kyuya; URUICHI, Mikio; HORIUCHI, Sachio; SAITO, Gunzi¹

(¹Kyoto Univ.)

[J. Am. Chem. Soc. submitted]

Raman spectroscopy was employed as a fast and exact method to determine the charge on BEDO-TTF (BO) in its complexes. Linear dependencies between two totally symmetric C=C stretching modes (ν_2 : ring C=C and ν_3 : central C=C) and charge on BO were found and used to evaluate the charge transfer (CT) degree. The CT degree was evaluated by the following equation.

$$\rho = (1524.9 - \nu_{3,\text{obs}} (\text{cm}^{-1}))/109.0$$

$$\rho = (1660.8 - \nu_{2,\text{obs}} (\text{cm}^{-1}))/74.1$$

Using the above equation, 19 complexes, including single crystals, powders and films were examined for the first time. The border between neutral (insulating) and partially CT (conducting) complex based on BO was estimated as 0.3.

IV-B-10 Re-examination of Bromide, Chloride and Iodide Salts of Bis(ethylenedioxy)tetra-thiafulvalene (BEDO-TTF) by Spectroscopic Methods

ULANSKI, Jacek; YAKUSHI, Kyuya; URUICHI, Mikio; DROZDOVA, Olga¹; YAMACHI, Hideki¹; SAITO, Gunzi¹

(¹Kyoto Univ.)

[J. Phys. B: Condens. Matter in preparation]

Recent results of polarized reflectivity, absorption and Raman spectroscopic studies of (BEDO-TTF)₂Br·(H₂O)₃, (BEDO-TTF)₂I₃, and (BEDO-TTF)₂Cl·(H₂O)₃ salts are summarized and analyzed. The experimentally obtained plasma frequencies and transfer integrals are considerably smaller than the theoretical values calculated including 3d orbitals; the theoretical calculations neglecting the sulfur 3d orbitals yield more realistic band structure. The polarized reflectance and optical conductivity spectra of the investigated BEDO-TTF salts in the direction perpendicular to the conducting plane reveal some unique features: very strong vibrational bands which originate from vibrations of BEDO-TTF molecules, and in some cases new bands around 5000 cm⁻¹ due to directional dispersion. Detailed analysis of the bands in the range 3200–3500 cm⁻¹ shows that the compositions of the chloride and of

the bromide salts are still not clear in respect to possible presence of the hydroxonium ions and to the role of water molecules. The BEDO-TTF salts containing water molecules are not stable in vacuum, losing both water and anion molecules, what should be taken into account in further investigations of these materials. The absorption spectra for thin, semitransparent single crystal of BEDO-TTF bromide salt, taken at different angles of incident light, demonstrate that the high transparency is due to specific orientation of the BEDO-TTF molecules.

IV-B-11 First Observation of the Plasmon Absorption by Reflection Spectroscopy in the Single Crystal of Two-dimensional Organic Metal

YAKUSHI, Kyuya; ULANSKI, Jacek; YAMACHI, Hideki¹; SAITO, Gunzi¹
(¹Kyoto Univ.)

Plasmon cannot be detected by the optical absorption method, since it is a longitudinal excitation. However, it becomes detectable in an anisotropic material, if the wave vector of light is not parallel to the principal axis of the anisotropic material. We present the observation and simulation of the plasmon by the method of normal incidence reflection spectroscopy in two-dimensional organic metals $\text{BO}_2\text{Cl}(\text{H}_2\text{O})_3$ and $\text{BO}_{2.4}\text{I}_3$. The plasmon was observed in the specular reflection normal to (111) and (11 $\bar{1}$) crystal faces, which respectively make angles of 71.0° and 78.7° with conducting sheet in $\text{BO}_2\text{Cl}(\text{H}_2\text{O})_3$, and that to the (101) crystal face, which makes an angle of 67.0° with the conducting sheet in $\text{BO}_{2.4}\text{I}_3$. The plasmon spectrum is theoretically reproduced solving the Fresnel equation with the principal dielectric function for a two-dimensional metal. We have given the analytical solution of the two-dimensional case. In both cases, the theoretical prediction agrees very well with the observation of the reflectivity at each crystal face. This is the first observation of the plasmon in organic metals. Incidentally, this is physically the same phenomenon as the directional dispersion in an exciton absorption of organic dye.

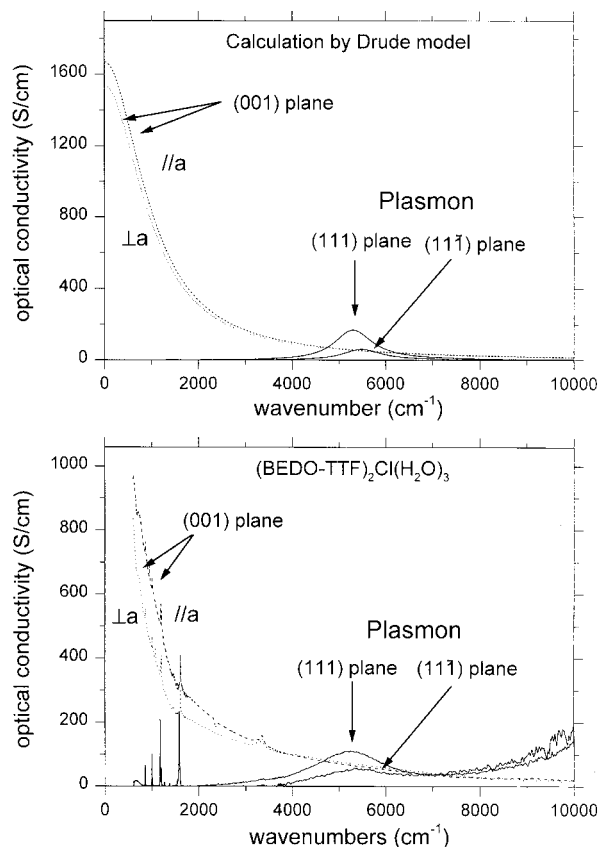


Figure 1. Observed and calculated conductivity spectra in the principal directions //a and ⊥a on the (001) conducting plane and non-principal directions on (111) and (11 $\bar{1}$) plane in the crystal of $\text{BO}_2\text{Cl}(\text{H}_2\text{O})_3$. Plasmon peak appears at 5000–6000 cm^{-1} in the spectra on the (111) and (11 $\bar{1}$) planes.

IV-C Microscopic Investigation of Molecular-Based Conductors

One of the most remarkable features of molecular-based conductors is taking various electronic phases. Especially, the competition of the ground states is one of the crucial problems of them. Although detailed electronic structure of them are not clear so far, these curious behaviors are believed to be originated from their characteristic natures; highly electronic correlation.

To clarify the low temperature electronic states, we performed the static susceptibility, EPR, ^1H - and ^{13}C -NMR measurements for molecular based conductors.

IV-C-1 Low-Temperature Electronic States in θ -(BEDT-TTF) $_2\text{RbZn}(\text{SCN})_4$: Competition of Different Ground States

NAKAMURA, Toshikazu; MINAGAWA, Waka¹; KINAMI, Ryoji¹; KONISHI, Yukihiro¹; TAKAHASHI, Toshihiro¹
(¹Gakushuin Univ.)

[*Synth. Met.* **103**, 1898 (1999)]

Magnetic properties of θ -(BEDT-TTF) $_2\text{RbZn}(\text{SCN})_4$ were studied. The compounds of this family are expected to be 2D-metals with a quarter-filled band. However the title salt undergoes a M-I transition around 190 K. The mechanism of the M-I transition and the low-temperature electronic states of the θ -type are not known. To clarify the electronic states of the low-temperature non-metallic phase and the mechanism of the M-I transition, we performed SQUID, EPR, ^1H - and ^{13}C -NMR measurements.

The low temperature behavior of the spin susceptibility, χ_{spin} , was found to depend on the cooling speed around 190 K. The EPR linewidth, ΔH_{pp} , analyses show that a phase transition exists around 190 K, and that the electronic state realized by the rapid-cooling is a metastable state. In the case of slow-cooling, the electron spin concentration exponentially decreases through the formation of spin-gap, and only residual spins concern the NMR relaxation. In the case of rapid-cooling, a large enhancement of the $\text{NMR-}T_1^{-1}$ was observed below 90 K where the χ_{spin} shows an abrupt increase. These facts suggest that the NMR relaxation is caused by dilute local magnetic moments. The quenched state may be understood as a new-type charge localization. A small amount of chemical doping caused pronounced influence on the electronic states. The sensitivity to impurities suggests that this spin-singlet state may be a low-dimensional phenomenon. The EPR relaxation rate measurements show a spin-gap even in the doped system.

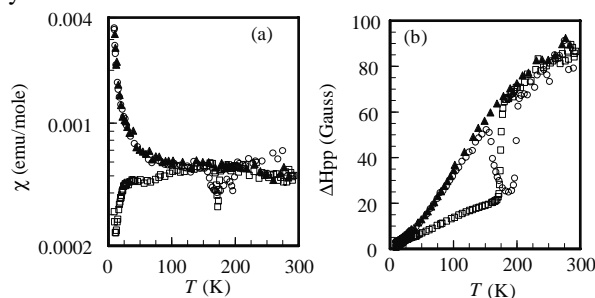


Figure 1. Temperature dependence of the (a) χ_{spin} , and (b) ΔH_{pp} along the a -axis (slow-cooling (open square), rapid-cooling (open circle) and the MT 5% doped salt (solid triangle)).

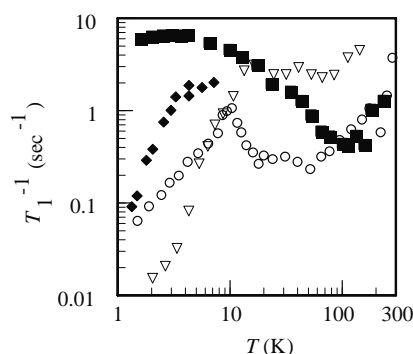


Figure 2. Temperature dependence of the $\text{NMR-}T_1^{-1}$ under slow-cooling ($^1\text{H-}T_1^{-1}$ (circle), $^{13}\text{C-}T_1^{-1}$ (triangle)) and rapid-cooling ($^1\text{H-}T_1^{-1}$ (square), $^{13}\text{C-}T_1^{-1}$ (diamond)).

IV-C-2 Magnetic Properties of a New Two-Chain Organic Conductor: (CPDT-STF)-TCNQ

NAKAMURA, Toshikazu; TAKAHASHI, Toshihiro¹; TANIGUCHI, Masateru²; MISAKI, Yohji²; TANAKA, Kazuyoshi²
(¹Gakushuin Univ.; ²Kyoto Univ.)

[*Synth. Met.* **103**, 1900 (1999)]

(CPDT-STF)-TCNQ is a new organic conductor based on TCNQ and CPDT-STF where CPDT-STF is one of selenium-containing analogs of DT-TTF. Although the resistivity shows a metallic behavior down to 0.5 K, the spin susceptibility, χ_{spin} , is Curie-like at low temperatures. The purpose of the present study is to clarify the origin of the paramagnetic moments from microscopic points of view. Between 50 K and 300 K, the g -values gradually change with temperature. This indicates that the relative contributions to χ_{spin} of the CPDT-STF and TCNQ stacks are significantly temperature dependent. The decomposition of the χ_{spin} of (CPDT-STF)-TCNQ into the contributions of CPDT-STF, χ_{D} , and TCNQ, χ_{A} , was performed. The χ_{A} shows Curie-like behavior up to at least 200 K, indicating the existence of local moments on the TCNQ stacks. The spin concentration determined from the Curie constant is about 0.17 per formula unit assuming $S = 1/2$. On the other hand, the χ_{D} is almost temperature independent, suggesting a Pauli paramagnetism on the CPDT-TTF layers. It is quite natural that the metallic conduction is attributed to the itinerant electron on the CPDT-STF.

The nature of the local moments on TCNQ is now an open question. The spin concentration is different from the case of (BEDT-TTF)-TCNQ, where one spin per TCNQ dimer is localized. Experiments to address this problem are in progress.

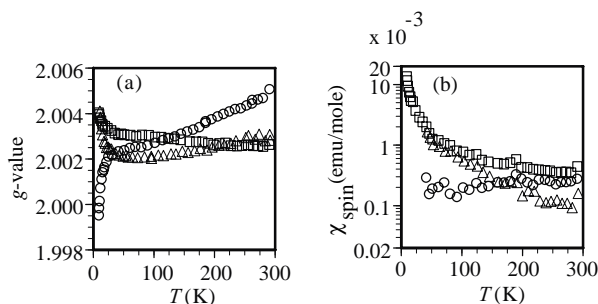


Figure 1. (a) Temperature dependence of the g -values ($//a^*$ (square), $//b^*$ (circle), $//c^*$ (triangle)). (b) Temperature dependence of the total χ_{spin} (square), and separate contributions of CPDT-STF (circle), TCNQ (triangle).

IV-C-3 ESR and NMR Investigation of β' - R_4Z [Pd(dmit)₂]₂

NAKAMURA, Toshikazu; TAKAHASHI, Toshihiro¹; AONUMA, Shuji²; KATO, Reizo²
(¹Gakushuin Univ.; ²ISSP, Tokyo Univ.)

[Synth. Met. **103**, 2142 (1999)]

β -type Pd(dmit)₂ salts and related salts show non-metallic behavior at ambient pressure. They undergo an antiferromagnetic transition, and that the paramagnetic states at ambient pressure should be considered as a Mott-Hubbard insulator. However, several problems remain unsolved; ¹H-NMR investigations showed the antiferromagnetic states possesses a small local magnetization. The local magnetizations and transition temperatures, T_N , are different between the Pd(dmit)₂ and the selenium-containing analogs Pd(dmise)₂ based salts. The main aim of this study is to clarify the antiferromagnetic states by systematic investigations of Pd(dmit)₂ salts. Figure 1 shows the temperature dependence of the EPR parameters of the Et₂Me₂P salts. The abrupt decrease of the χ_{spin} and the divergence of the ΔH_{pp} around 18 K obviously show the existence of the magnetic order. The observed g -tensor cannot be explained by that of single Pd(dmit)₂ molecule. We believe that this is due to the strong dimer structure of the Pd(dmit)₂ based organic conductors. The T_N and the amplitude of antiferromagnetic local moments determined by ¹H-NMR shows a close correlation with the cation size. The T_N seems to decrease as the inter-dimer interaction within stacks decreases. The Et₂Me₂-Sb salt, of which the inter-dimer interactions within stacks is comparable to those between stacks, shows no antiferromagnetic order down to 7 K. The detailed analysis is now going on.

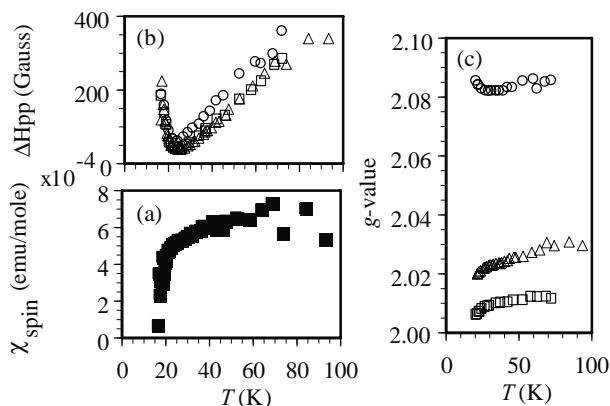


Figure 1. Temperature dependence of (a) the spin susceptibility, χ_{spin} , determined by EPR intensity, (b) the EPR linewidth, ΔH_{pp} , and (c) the g values ($//a^*$ (square), $//b^*$ (circle), $//c^*$ (triangle)).

IV-C-4 New Type Charge Localization in θ -(BEDT-TTF)₂CsZn(SCN)₄

NAKAMURA, Toshikazu; MINAGAWA, Waka¹; KINAMI, Ryoji¹; TAKAHASHI, Toshihiro¹
(¹Gakushuin Univ.)

[J. Phys. Soc. Jpn. submitted]

¹H-NMR, EPR and static magnetic susceptibility measurements have been performed on an organic conductor, θ -(BEDT-TTF)₂CsZn(SCN)₄. The ¹H-NMR- T_1^{-1} and the spin susceptibility exhibit anomalous enhancements at low temperatures. Around 20 K, where the spin susceptibility shows a minimum, the principal axes of the EPR g -tensor changed their directions, keeping the principal values constant. It indicates a possible change of the electronic nature. The low-temperature electronic state is discussed.

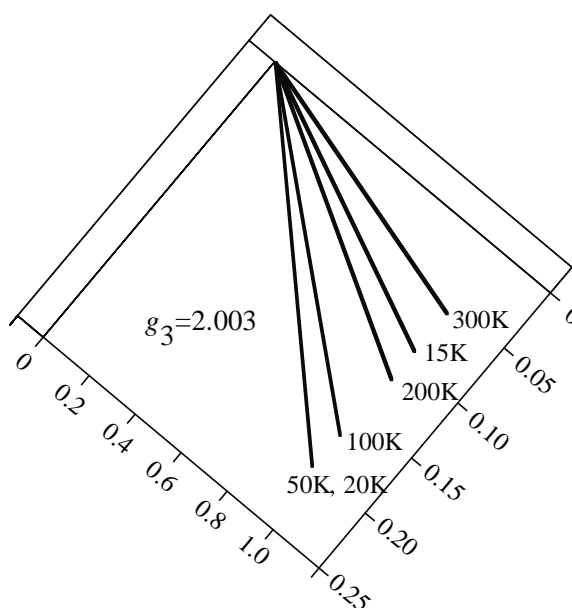


Figure 1. Temperature dependence of the direction of the principal axes of the g -tensor; magnified the scale for g_3 (top of view) at typical temperatures.

IV-D Thermodynamic Study of Organic Conductors

In order to get reliable information on the electron density of states and entropy distribution around various types of phase transitions, specific heat studies are inevitable. In this project, we aim at constructing several types of calorimeters available at low-temperatures and under magnetic fields and performing systematic investigation on organic materials from a thermodynamic viewpoint.

IV-D-1 Electronic Ground States of (BEDT-TTF)₂X System Studied by Specific Heat Measurements

NAKAZAWA, Yasuhiro; KANODA, Kazushi¹
(¹Univ. Tokyo)

[Synrh. Met. **103**, 1903 (1999)]

The 2:1 organic salts, (BEDT-TTF)₂X, give a variety of electronic phases such as metallic, superconductive, spin/charge density wave and antiferromagnetic insulating phases, etc. due to the variation of the molecular arrangement in the donor layers. The efforts to inquire into the origin and the peculiar features of the electronic structure of these phases have been widely made in these days, since they provide numerous interesting information of the condensed matter physics related to low-dimensional, low carriers and strongly correlated systems. Systematic studies to get an overall picture on the relationship between donor arrangement and the electronic ground states produced by π -electrons is now being performed from both experimental and theoretical viewpoints. In this study, we compare the low-temperature specific heat behavior of several 2:1 salts consist of BEDT-TTF molecules in order to get a systematic understanding of these π -electron systems from the thermodynamic viewpoint. Figures 1 and 2 show typical specific heat curves of metallic salts and Mott insulating salts, respectively. Although one can find finite γ term in the metallic samples, the Mott insulating salts does not have any electronic contribution in C_p/T vs T^2 curves at low-temperatures due to formation of charge-gap by the electron correlation effect.

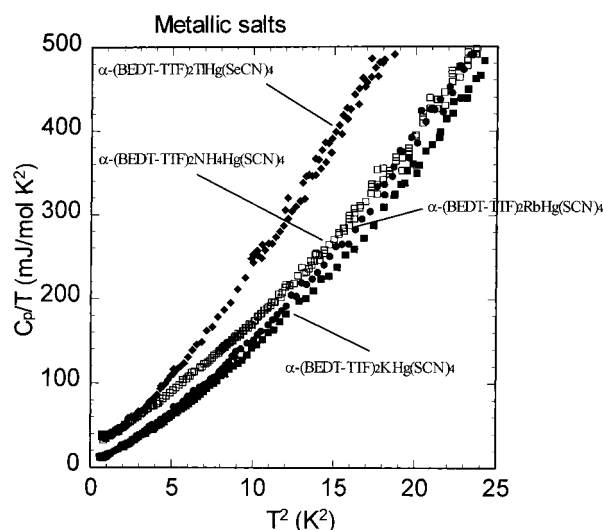


Figure 1. C_p/T vs T^2 plot of several metallic salts of (BEDT-TTF)₂X.

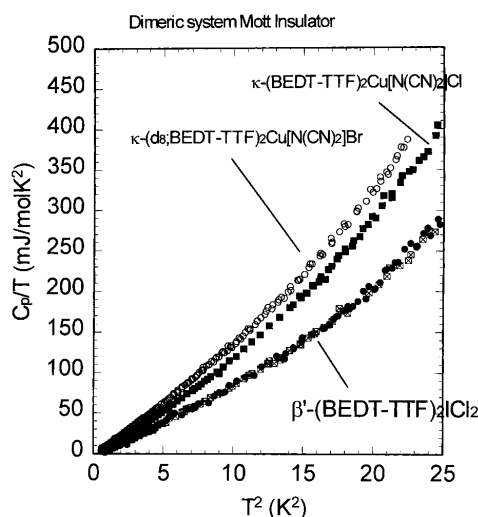


Figure 2. C_p/T vs T^2 plot of Mott insulating salts of (BEDT-TTF)₂X.

IV-D-2 Thermodynamic Investigation of the Electronic States of Deuterated κ -(BEDT-TTF)₂-Cu[N(CN)₂]Br

NAKAZAWA, Yasuhiro; KANODA, Kazushi¹
(¹Univ. Tokyo)

[Phys. Rev. B **60**, 4263 (1999)]

The low-temperature specific heat of the deuterated κ -(BEDT-TTF)₂Cu[N(CN)₂]Br situated in the critical region of the Mott transition in the κ -(BEDT-TTF)₂X systems was measured after different cooling processes, which are known to affect the superconducting volume fraction from the resistivity and the magnetic susceptibility measurements. Temperature and magnetic field dependences of the electronic specific heat do not show distinct variation by changing cooling rate from 0.07 K/min to 50 K/min and under magnetic field up to 6 T. We show in Figure 1 the low-temperature data obtained by a dilution refrigerator cooled down with the rates of 0.07 K/min, 0.8 K/min and 1.7 K/min from room temperature down to 4.2 K. The electronic specific heat coefficient, γ is found to be 0–1 mJ/molK² in all three curves and this values are much smaller than those of bulk superconducting materials of hydrogenated X = Cu[N(CN)₂]Br and Cu(NCS)₂.

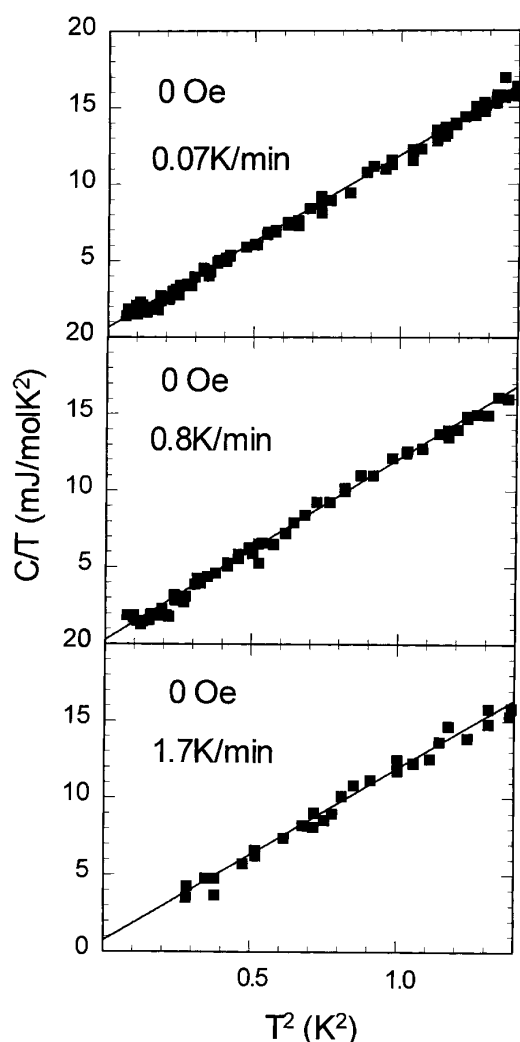


Figure 1. Low-temperature specific heat curves of κ -(d₈;BEDT-TTF)₂Cu[N(CN)₂]Br cooled down at different rates of 0.07, 0.8, and 1.7 K/min.

IV-D-3 Electronic Specific Heat at the Boundary Region of Mott Transition in Two-Dimensional Electronic System of κ -(BEDT-TTF)₂Cu[N(CN)₂]Br

NAKAZAWA, Yasuhiro; TANIGUCHI, Hiromi¹;
KAWAMOTO, Atsushi²; KANODA, Kazushi¹
(¹Univ. Tokyo; ²Hokkaido Univ.)

The electronic specific heat studies of partially deuterated single crystals of organic conductors κ -(BEDT-TTF)₂Cu[N(CN)₂]Br which are situated across the critical boundary of band-width control type of Mott transition in two dimension are performed at low-temperatures below 3 K and under magnetic fields up to 10 T. In order to see the variation of normal-state electronic density of states near the transition, we had gradually access to the M-I boundary with the progressive dueteration of BEDT-TTF molecules and found that the electron density of states or effective mass in the metallic states diminishes towards the Mott boundary. This is in fine contrast to the case of V₂O₃, where the Brinkmann and Rice's prediction of electron mass enhancement occurs in the critical region. This

result is marked a basis for the future study of electronic feature related to the unconventional superconductivity and also on the universality and variation of the Mott transition in two dimensional systems.

IV-E Photoelectron Spectroscopy of Organic Solids in Vacuum Ultraviolet Region

The works of ultraviolet photoelectron spectroscopy (UPS) with synchrotron radiation light source (UVSOR-UPS) of advanced organic materials have been proceeded to find their quantitative electronic structures and also to analyze their structures of assemblies.

IV-E-1 Angle-Resolved Photoemission Spectra of ω -(*n*-pyrrolyl) Alkanethiol Self-Assembled Monolayers: Possible Assemblies of Substituent Pyrrole

HASEGAWA, Shinji; YAKUSHI, Kyuya; INOKUCHI, Hiroo; OKUDAIRA, Koji K.¹; UENO, Nobuo¹; SEKI, Kazuhiko²; WILLICUT, J. Robert³; MACCARLEY, L. Robin³; MORIKAWA, Eizi⁴; SPRUNGER, T. Phillip⁴; SAILE, Volker⁴
(¹Chiba Univ.; ²Nagoya Univ.; ³Louisiana State Univ.; ⁴Louisiana State Univ. CAMD)

Angle resolved ultraviolet photoelectron spectra (ARUPS) on pyrrolyl-SAMs on polycrystalline Ag were measured by using synchrotron radiation. We found the π bands originated from the substituent pyrrole which are distinguishably observed from the bands of alkyl backbone. Since the π bands are available for the clue to probe the surface structures of pyrrole, we calculated the photoelectron angular distributions of them for the model structures obtained by molecular dynamics (MD) calculations. We revealed that two surface structures of pyrrole, face-stacked and herringbone structures, are possible for pyrrolyl-SAMs on Ag(111) and the herringbone structure is energetically favored.

The calculated photoelectron angular distributions can clearly distinguish between the face-stacked and herringbone structures of surface pyrrole, and give information on the orientation of pyrrole, the direction of pyrrolyl facing axis, and symmetry of the surrounding molecules. The ARUPS measurement for pyrrolyl-SAMs is promising for quantitative determinations of surface structures and now in progress.

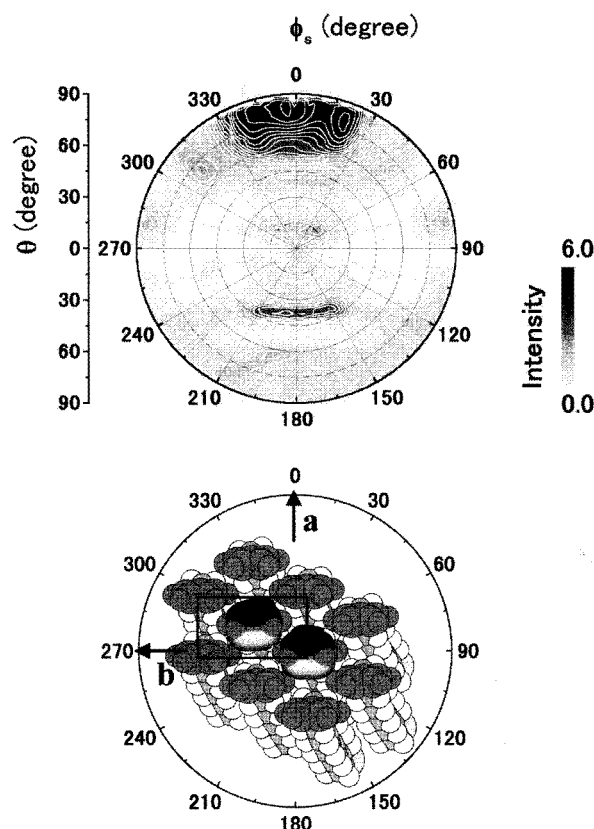


Figure 1. Calculated photoelectron angular distribution of π state within the single-scattering approximation. The photoelectron intensity is displayed by shading by the two-dimensional mapping with θ and ϕ_s . The illustration shows the face-stacked structure of pyrrolyl-SAMs obtained by MD calculation.

IV-E-2 Structure of Copper- and H₂-Phthalocyanine Thin Films on MoS₂ Studied by Angle-Resolved Ultraviolet Photoelectron Spectroscopy and Low Energy Electron Diffraction

OKUDAIRA, Koji K.¹; HASEGAWA, Shinji; ISHII, Hisao²; SEKI, Kazuhiko²; HARADA, Yoshiya¹; UENO, Nobuo
(¹Chiba Univ.; ²Nagoya Univ.)

[*J. Appl. Phys.* **85**, 6453 (1999)]

Angle-resolved ultraviolet photoelectron spectra (ARUPS) of copper phthalocyanine (CuPc) and metal-free phthalocyanine (H₂Pc) films (thickness from monolayer to 50–80 Å) on cleaved MoS₂ substrates were measured using monochromatic synchrotron radiation. Observed take-off angle (θ) and azimuthal angle (ϕ) dependencies of the top π band intensity were

analyzed quantitatively by the single-scattering approximation theory combined with molecular orbital calculations. The analysis indicated that the molecules lie flat on the MoS₂ surface in monolayer films of CuPc and H₂Pc. The azimuthal orientation of the molecules (angle between molecular axis and surface crystal axis of MoS₂), was found to be about -7° , -37° , or -67° for both monolayer films of CuPc and H₂Pc. In the azimuthal orientation, the analyses indicated that there are only molecules with counterclockwise rotation, although both clockwise and counterclockwise rotations are expected. From the low energy electron diffraction, the two-dimensional lattice structure of the monolayer film was obtained. On the basis of these two kinds of experimental results, the full structure of the monolayer film, the two-dimensional lattice and the molecular orientation at the lattice points, was determined. Furthermore, for the thick films it is found from the analyses of ARUPS that CuPc and H₂Pc molecules tilt about 10° from the surface plane.

IV-E-3 Electronic Structure of Poly (1,10-Phenanthroline-3,8-diyl) and Its K-doped State Studied by Photoelectron Spectroscopy

MIYAMAE, Takayuki; UENO, Nobuo; HASEGAWA, Shinji; SAITO, Yutaka¹; YAMAMOTO, Takakazu¹; SEKI, Kazuhiko²

(¹Tokyo Inst. Tech.; ²Nagoya Univ.)

[*J. Chem. Phys.* **110**, 2552 (1999)]

Ultraviolet photoelectron spectra were measured using synchrotron radiation for thin films of poly(1,10-

phenanthroline-3,8-diyl) (PPhen) and its potassium-doped state. Upon potassium doping of PPhen, two new states, which could be assigned to bipolaron bands, appear in the originally empty energy gap. The electronic structure of the neutral and potassium-doped states was theoretically analyzed using single-scattering approximation combined with semiempirical molecular orbital calculations.

IV-E-4 Electronic Structures of Alq₃/LiF/Al Interfaces Studied by UV Photoemission

YOSHIMURA, Daisuke; YOKOYAMA, Takahiro¹; ITO, Eisuke¹; ISHII, Hisao¹; OUCHI, Yukio¹; HASEGAWA, Shinji; SEKI, Kazuhiko¹

(¹Nagoya Univ.)

[*Synth. Met.* **102**, 1145 (1999)]

The electronic structure of tris (8-hydroxyquinolino) aluminum (Alq₃)/LiF/Al system was studied in relation to the enhancement of electron-injection efficiency by the insertion of LiF insulating layer at Alq₃/Al contact, using UV photoemission spectroscopy (UPS), X-ray photoelectron spectroscopy (XPS), and metastable atom electron spectroscopy (MAES). The observed energy separation between the HOMO of Alq₃ and the Fermi level of Al substrate increased from 2.7 eV to 3.0 eV by inserting 0.5 nm thick LiF layer. This result indicates that the LiF layer induces the decrease of the electron injection barrier. We also found extra states probably caused by the interaction at the Alq₃/Al interface. The spectral intensity of this extra state decreased with increasing LiF thickness, and vanished at 0.5 nm.

IV-F Electrical Conduction and its Related Properties of Organic Solid

To expand the research field of molecular conductors, we always consider to find a new category. One of them is three components organic semiconductors, conductors and superconductors. In this section, we present the works of three components organic superconductors based on C₆₀.

IV-F-1 Three Component Organic Superconductors: Intercalation of KH into C₆₀

IMAEDA, Kenichi; TIAN, Fuli; INOKUCHI, Hiroo; ICHIMURA, Kenji¹

(¹Kumamoto Univ.)

[*J. Solid State Chem.* **145**, 421 (1999)]

We have prepared (KH)₃C₆₀ as an initial composition by direct reaction of potassium hydride (KH) to C₆₀. (KH)₃C₆₀ had higher *T_c* (19.5 K) and larger lattice constant (14.351 Å), compared with K₃C₆₀ prepared by doping of potassium metal. The expanded lattice constant is suggestive of the intercalation of hydrogen. The evidence of the inclusion of hydrogen was given by mass-analyzed thermal desorption experiment. We have also prepared (NaH)_{4-x}(KH)_xC₆₀ to study the substitutional effect of KH to (NaH)₄C₆₀. It was found that the superconducting phase is stabilized by

substitution of only a few percent KH as seen in (NaH)_{3.9}(KH)_{0.1}C₆₀.

IV-F-2 Hydrogen Intercalation in Potassium-C₆₀

IMAEDA, Kenichi; INOKUCHI, Hiroo; ICHIMURA, Kenji¹; INOUE, Shin-ichi²; NAKAKITA, Satoshi²; OKAMOTO, Hiroshi²

(¹Kumamoto Univ.; ²Aichi Inst. Tech.)

[*Proceedings of ISIC10*]

Solid state ¹H NMR of (KH)₃C₆₀ was measured in the temperature range between -80 and 60°C . A doublet spectrum composed of main peak at -7.0 ppm and shoulder peak at ~ 0 ppm was observed at room temperature. The negative chemical shift of the main peak indicates that hydrogen in (KH)₃C₆₀ exists as a hydride-like ion. The 60°C spectrum became singlet at -5.8 ppm due to motional narrowing.

IV-G Magnetism and Superconductivity of BETS Conductors

Since the discovery of one-dimensional organic metals in early 1970s, a large progress has been made in the field of molecular conductors. The first discovery of organic superconductor (TMTSF)₂PF₆ was reported in 1980. We have found two new organic superconductors in 1986-87, one of which was the first κ -type organic superconductor, κ -(BEDT-TTF)₂I₃. The tremendous boom of copper oxide superconductor was started around the same time. Although many organic superconductors (especially κ -type organic superconductors based on BEDT-TTF) have been discovered since then, almost all people do not think that T_c of the hitherto-reported type of organic superconductor will become able to compete with the T_c of oxide superconductor. Therefore, it may be natural that the development of multifunctional conductors such as magneto-conducting systems attracts an increasing attention.

We have examined a series of BETS (= bis(ethylenedithio)tetraselenafulvalene) conductors with tetrahalide anions, MX₄ (M = Ga, Fe; X = Cl, Br). Our main interest is in the development of new types of conducting systems by incorporating Fe³⁺ magnetic ions in organic conductors having stable two-dimensional metal states. Two years ago, we have discovered an unprecedented superconductor-to-insulator transition in λ -type BETS conductors, λ -BETS₂Fe_{1-x}Ga_xCl₄ (0.35 < x < 0.5), where the interaction between localized magnetic moments of Fe³⁺ ions and π conduction electrons play an essential role. We have recently discovered the first antiferromagnetic organic metal exhibiting a superconducting transition.

IV-G-1 Chemical Control of Electrical Properties and Phase Diagram of a Series of λ -Type BETS Superconductors, λ -BETS₂GaBr_xCl_{4-x}

TANAKA, Hisashi¹; KOBAYASHI, Akiko¹; SATO, Akane; AKUTSU, Hiroki; KOBAYASHI, Hayao
(¹Univ. Tokyo)

[J. Am. Chem. Soc. **121**, 760 (1999)]

λ -BETS₂GaBr_xCl_{4-x} (0 < x < 2) is a molecular superconductor with strongly correlated conduction electrons. At ambient pressure, the superconducting transition could be observed for x < 0.75. The pressure and x dependencies of T_c were examined. The M - H curve at 2 K indicated the almost perfect Meissner state of the superconducting phase of λ -(BETS)₂GaCl₄ (M = magnetization; H = magnetic field). The magnetic susceptibility of λ -BETS₂GaBr_xCl_{4-x} increases with decreasing temperature down to about 60 K, below which the susceptibility becomes x -dependent and tends to be suppressed with increasing x . The isotropic decrease of the static susceptibility at lower temperature observed in the insulating system with x > 1.0 indicates the insulating ground state seems not to be antiferromagnetic but probably non-magnetic. The crystal structure determinations of a series of λ -BETS₂GaBr_xCl_{4-x} and the calculations of the intermolecular overlap integrals of the highest occupied molecular orbital of BETS were made to elucidate a key factor of the superconducting transition mechanism. The x dependence of intermolecular overlap integrals seems to suggest that the magnitude of the "spin gap" of the non-magnetic insulating state tends to be diminished with decreasing x .

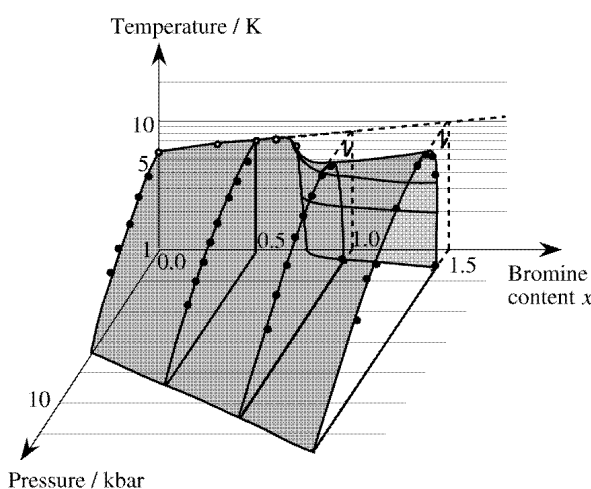


Figure 1. T - P - x phase diagram of λ -BETS₂GaBr_xCl_{4-x}. The region surrounded by shaded plane corresponds to the superconducting region.

IV-G-2 Evidence for the First Order Transition between High-temperature Superconducting and Low-temperature Insulating Phases in λ -BETS₂Fe_xGa_{1-x}Cl₄ ($x \approx 0.45$)

TANAKA, Hisashi; KOBAYASHI, Hayao; KOBAYASHI, Akiko¹
(¹Univ. Tokyo)

We have recently discovered a novel superconductor-to-insulator transition in λ -BETS₂Fe_xGa_{1-x}Cl₄ (0.35 < x < 0.5). A sharp drop of the susceptibility at superconducting transition (T_c) and its recovery at lower temperature (T_{SC-I}) indicated that the crystal once transforms into superconducting state and then returns to the non-superconducting state with decreasing temperature. The large diamagnetic susceptibility at T_{SC-I} < T < T_c observed by SQUID magnetometer showed conclusively the SC-I transition to be a bulk transition. In order to contribute to the better understanding of this unprecedented superconductor-to-insulator transition, we have carefully measured the temperature dependence of the resistivity on the freshly prepared crystal of λ -BETS₂Fe_xGa_{1-x}Cl₄ ($x = 0.45$). As

shown in Figure 1, the crystal showed the SC and SC-I transitions with decreasing temperature. In contrast to the sharp superconducting transition at 4.6 K, the SC-I transition showed a distinct hysteresis, showing the first-order nature of the SC-I transition.

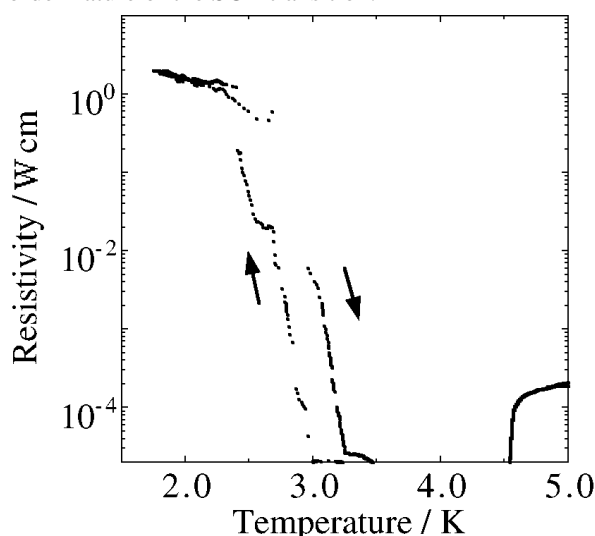


Figure 1. Resistivity behavior of λ -BETS₂Fe_xGa_{1-x}Cl₄ ($x \approx 0.45$).

IV-G-3 Coexistence of Antiferromagnetically Ordered Fe³⁺ Spins and Metal π -Electrons in λ -BETS₂FeCl₄

SATO, Akane; OJIMA, Emiko; KOBAYASHI, Hayao; HOSOKOSHI, Yuko; INOUE, Katsuya; KOBAYASHI, Akiko¹; CASSOUX, Patrick²
(¹Univ. Tokyo; ²CNRS)

[*Adv. Mater.* in press]

Recently we have studied the magnetic properties of λ -BETS₂FeCl₄ at high pressure. Since the 30 mg of the crystals was required for the high-pressure magnetic susceptibility measurements, the electrocrystallization experiments were repeated 25 times. The susceptibility was measured on SQUID magnetometer by using oriented thin needle crystals of λ -BETS₂FeCl₄ sealed in Teflon capsule and the Ti-Cu alloy high-pressure cell. The magnetic field was applied along the needle axes of the crystals ($\parallel c$). At 2 kbar, sharp drop of magnetization suggesting strong π -d coupling was disappeared and only broad maximum was observed at low magnetic field. The broad maximum indicating the separation between π and d electron systems at high pressure became conspicuous with decreasing magnetic field. Only Fe³⁺ spins seems to be antiferromagnetically ordered at low temperature. Similar behavior was also observed at 3, 4 and 5 kbar. The M - H curve measured at 1 bar, 3 kbar and 5 kbar showed the spin flop behavior, consistent with the antiferromagnetic ordering of Fe³⁺ spins with easy axis along c . These facts indicate λ -BETS₂FeCl₄ to be the first organic conductor with the antiferromagnetic metal phase at high pressure.

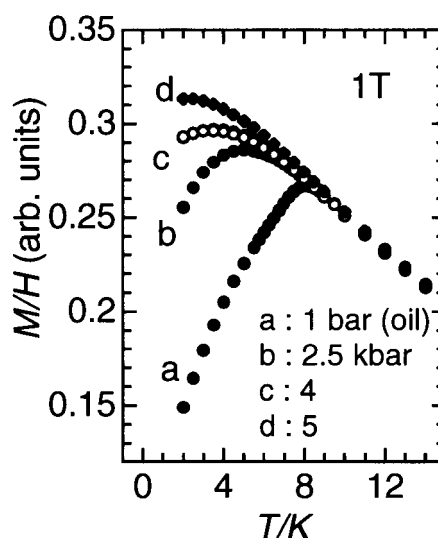


Figure 1. Temperature dependence of the susceptibility of λ -BETS₂FeCl₄ at high pressure.

IV-G-4 Pressure-Induced Superconducting Transition of λ -(BETS)₂FeCl₄ with π -d Coupled Antiferromagnetic Insulating Ground State at Ambient Pressure

TANAKA, Hisashi; ADACHI, Takafumi¹; OJIMA, Emiko; FUJIWARA, Hideki; KOBAYASHI, Hayao; KOBAYASHI, Akiko²; CASSOUX, Patrick³
(¹IMS and Electrotech. Lab.; ²Univ. Tokyo; ³CNRS)

[*J. Am. Chem. Soc.* in press]

The resistivities of λ -(BETS)₂FeCl₄ were measured at high pressure down to 0.5 K. The characteristic π -d coupled antiferromagnetic insulating ground state was destabilized under pressure and the superconducting transition was observed above 3 kbar. Since the Fe³⁺ spins has been reported to be antiferromagnetically ordered at the temperature region above the superconducting phase, the present results suggest that λ -(BETS)₂FeCl₄ undergoes a transition from antiferromagnetic metal phase to superconducting phase at high pressure. T_c was decreased with increasing pressure: the value of dT_c/dP (-0.5 deg/kbar) is almost equal to that of λ -(BETS)₂GaCl₄. The field-restored highly conducting state (FRHCS) was observed at 2.5 kbar. The critical magnetic field of FRHCS (55 kOe) was almost a half of that at ambient pressure (110 kOe). When the magnetic field was applied perpendicular to the ac plane (conduction plane) at 3.5 kbar and 0.55 K, the superconducting state was broken at 5–8 kOe. While, for the field parallel to the ac plane, the resistivity began to appear at 0.5 kOe and increased up to 13 kOe.

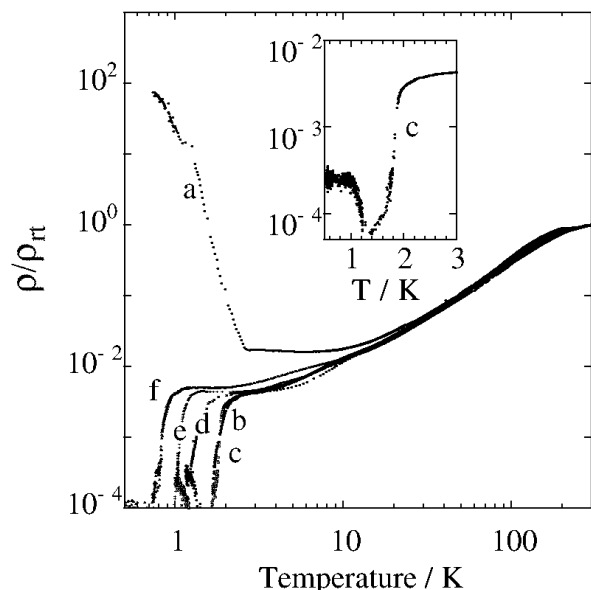


Figure 1. The resistivity of λ -(BETS) $_2$ FeCl $_4$ at 2.5 (a), 3.0 (b), 3.2 (c), 4.0 (d), 4.5 (e) and 5.0 (f) kbar. The inset shows the anomalous resistivity behavior observed at 3.2 kbar.

IV-G-5 Electric and Magnetic Properties of BETS Conductor with Modified λ -type Structure, λ' -BETS $_2$ GaBr $_4$

TANAKA, Hisashi¹; KOBAYASHI, Akiko¹; KOBAYASHI, Hayao
(¹Univ. Tokyo)

[Chem. Lett. 133 (1999)]

We have studied a series of BETS conductors with mixed-halogen gallate anions, GaBr $_x$ Cl $_{4-x}$ ⁻. The anion sites of the λ -type salt cannot accommodate large anions. Then the structure is modified into " λ' -structure" for $x > 2.0$. The physical properties of λ' -(BETS) $_2$ GaBr $_4$ are quite different from those of λ -(BETS) $_2$ GaBr $_x$ Cl $_{4-x}$. The resistivity was almost temperature independent down to 50 K below which it increased gradually. Above *ca.* 3 kbar, the metallic state was stabilized, but the superconducting behavior could not be found down to 2 K. Extended-Hückel tight-binding band calculation and temperature dependencies of resistivity and magnetic susceptibility of λ' -(BETS) $_2$ -GaBr $_4$ suggest the semimetal-to-insulator transition around 50 K. Thus despite of the apparent structural similarity of the λ - and λ' -salts, the electronic state of these two systems are completely different.

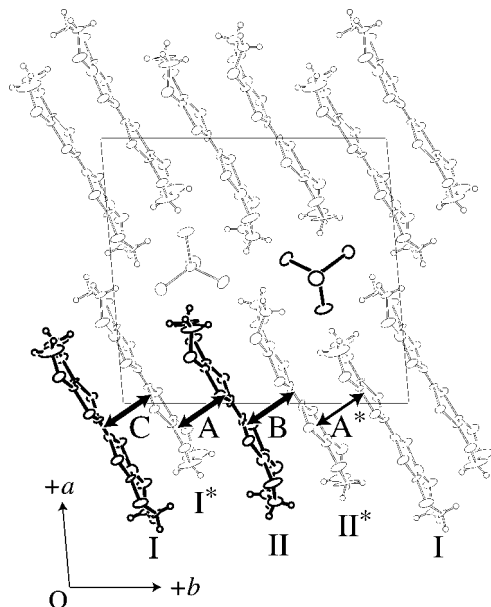


Figure 1. Crystal structure of λ' -BETS $_2$ GaBr $_4$ viewed along the c axis.

IV-G-6 Antiferromagnetic Organic Metal Exhibiting Superconducting Transition, κ -(BETS) $_2$ FeBr $_4$

OJIMA, Emiko; FUJIWARA, Hideki; KATO, Kiyonori; KOBAYASHI, Hayao; TANAKA, Hisashi¹; KOBAYASHI, Akiko¹; TOKUMOTO, Madoka²; CASSOUX, Patrick³
(¹Univ. Tokyo; ²Electrotech. Lab.; ³CNRS)

[J. Am. Chem. Soc. **121**, 5581 (1999)]

The electric and magnetic properties of κ -(BETS) $_2$ -FeBr $_4$ show this system to be the first ambient-pressure antiferromagnetic organic metal ($T_N = 2.5$ K). The characteristic field dependence of the magnetization at 2 K indicates a helical spin structure. When the magnetic field is applied to the conduction plane (\parallel crystal plane), the magnetization increases very rapidly and tends to be saturated above 20 kOe. While the magnetization increases almost linearly up to about 70 kOe for the field perpendicular to the crystal plane. A small resistivity drop observed at T_N gives a clear evidence for the existence of the interaction between π metal electrons and localized magnetic moments. Furthermore, this system undergoes a superconducting transition at 1.0 K.

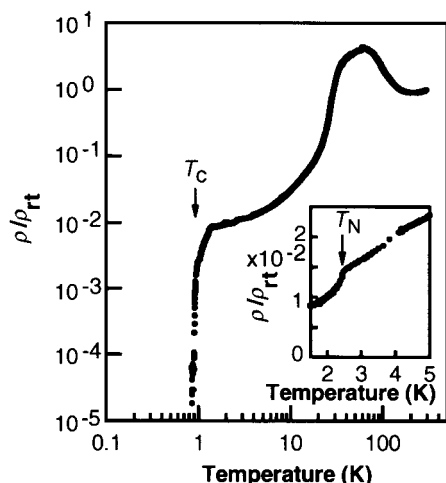


Figure 1. Resistivity of κ -(BETS) $_2$ FeBr $_4$ at 0.5-300 K measured along the *ac* plane.

IV-G-7 A New κ -Type Organic Superconductor Based on BETS Molecules, κ -(BETS) $_2$ GaBr $_4$

TANAKA, Hisashi; OJIMA, Emiko; FUJIWARA, Hideki; NAKAZAWA, Yasuhiro; KOBAYASHI, Hayao; KOBAYASHI, Akiko¹
(¹Univ. Tokyo)

We have recently reported that κ -(BETS) $_2$ FeBr $_4$ undergoes successive phase transitions with lowering temperature from paramagnetic metal state to antiferromagnetic metal state at 2.5 K (T_N) and from antiferromagnetic metal state to superconducting state at 1.0 K (T_c). Furthermore, it is highly possible that κ -(BETS) $_2$ -

FeBr $_4$ is the first antiferromagnetic organic superconductor, which was one of the final targets of the studies on the development of new organic conductors. Since the resistivity behavior of κ -(BETS) $_2$ GaBr $_4$ has been reported to resemble to that of κ -(BETS) $_2$ FeBr $_4$, a superconducting transition will be expected also in κ -(BETS) $_2$ GaBr $_4$. In fact, we have found the superconducting transition of κ -(BETS) $_2$ GaBr $_4$ around 0.5-1.0 K. This finding indicates T_c of κ -(BETS) $_2$ MBr $_4$ (M = Fe, Ga) to be almost independent of the existence of magnetic anions. A way to develop novel organic superconductors with controlled antiferromagnetic interactions is suggested.

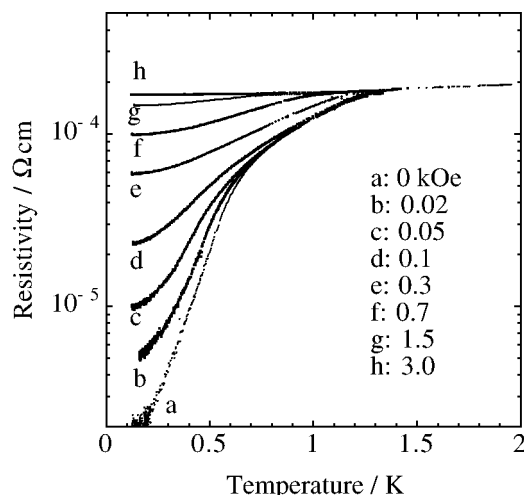


Figure 1. The magnetic field-dependence of the resistivities of κ -(BETS) $_2$ GaBr $_4$ at 0-3.0 kOe.

IV-H Structural and Electrical Properties of Molecular Crystals at Low Temperature and/or High Pressure

Since the molecular crystal is very soft and rich in the structural freedom, various structural phase transitions will be expected at high pressure and/or low temperature. Moreover, the electronic properties of molecular crystal are very sensitive to the structure change. Therefore the precise three-dimensional X-ray structure analyses at high pressure and/or low temperature are important in the studies on solid state properties of molecular crystals. More than several years ago we have developed a simple X-ray imaging plate system equipped with low-temperature refrigerator, which made the low-temperature X-ray study very easy. At present, we are trying the high-pressure (or high-pressure and low-temperature) X-ray experiments by using specially designed diamond anvil cell and X-ray imaging plate system.

Usually, the high-pressure resistivity measurements of molecular conductors have been made by using clamp type pressure cell, which enables us to measure the resistivities up to about 20 kbar. For the studies on the solid state properties of molecular solid at high pressure, it is highly desired to find a way to perform the resistivity measurements by using diamond anvil cell. We have recently succeeded to measure the resistivity of thin needle crystals of organic materials up to 100 kbar.

IV-H-1 Low Temperature Structure Analysis of Unannealed TDAE* C_{60} Single Crystal

NARYMBETOV, Bakhyt¹; KOBAYASHI, Hayao; TOKUMOTO, Madoka²; OMERZU, Ales³; MIHAJLOVIC, Gragan³
(¹IMS and Uzbek Acad. Sci.; ²Electrotech. Lab.; ³Jozef Stefan Inst., Slovenia)

[Chem. Commun. 1511 (1999)]

Since the discovery of the ferromagnetism in TDAE* C_{60} compound (TDAE = tetrakis(di-methyl-amino)ethylene) with the $T_c = 16$ K it has been intensively studied by various experimental methods. However, till now a detailed crystal structure based on single crystal diffraction data has not been determined because in this materials the C_{60} molecules have

orientational disorder at room temperatures. We have carried out an X-ray diffraction study of an unannealed TDAE* C_{60} single crystal at low temperatures down to 7 K which have allowed access to detailed structural characteristics of the compound (freshly grown, unannealed crystal of TDAE* C_{60} doesn't show the ferromagnetic properties but they become ferromagnet after annealing the crystal at 20–100 °C). The structure was solved and refined based on the space group $C2/c$ for the set of data obtained at 7 and 11 K. There are four chemically equivalent C_{60} · $C_2(NC_2H_5)_4$ units per unit cell. The packing of the unit cell shows that C_{60} anions are located at inversion centers and form a chain along the c -axis with the shortest distance between molecular centers equal to 9.915 Å at that temperatures. The obtained configurations of TDAE are in reasonable agreement with predictions, which testifies to a charge state of TDAE of +1.

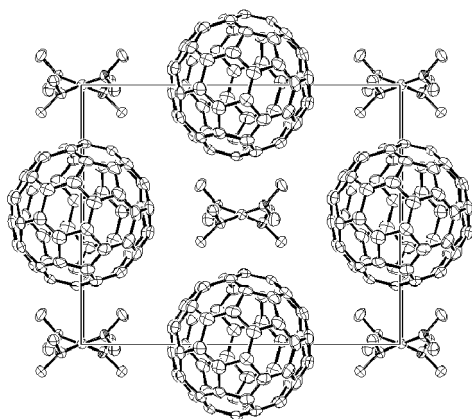


Figure 1. The projections of the C_{60} *TDAE crystal structure along the c -axis.

IV-H-2 X-Ray Diffraction Study of a TDAE* C_{60} Single Crystal

NARYMBETOV, Bakhyt¹; KOBAYASHI, Hayao; TOKUMOTO, Madoka²; OMERZU, Ales³; MIHAJLOVIC, Grgan³
(¹IMS and Uzbek Acad. Sci.; ²Electrotech. Lab; ³Jozef Stefan Inst., Slovenia)

Despite extensive efforts of researchers, there still remain questions about the origin and the nature of low temperature ground state of a TDAE* C_{60} compound. It has been suggested that there is a rotational randomness of C_{60} molecules in TDAE* C_{60} crystals and that the magnetism could strongly depend on the merohedral degree of freedom. The freshly grown single crystals are found to be ordered antiferromagnetically and annealing in temperature range 20–100 °C results in an enhanced ferromagnetic ordering of the samples. We have performed X-ray diffraction studies of TDAE* C_{60} single crystal in temperature range 270–7 K before and after annealing the crystal at 70 °C as well as its structure characterization at temperatures 160, 30, 11 and 7 K for unannealed sample and at low temperatures (below 16 K) for annealed sample. These studies show that for both unannealed and annealed TDAE* C_{60} single crystal at low temperatures there are structure transformations below 50 K. Remarkable changes of X-

ray diffraction patterns occur below 50 K and a characteristic feature of it is an appearance of diffuse lines. Observed appearance of diffuse lines on diffraction patterns below 50 K confirms the presence of ordering process, which proceeds several hours. Low temperature state of unannealed crystal is characterized by disappearing of the diffuse lines after keeping the crystal at temperatures below 50 K for about 3–4 hours. Distinctive feature in the case of annealed TDAE* C_{60} crystal is that below 50 K with the time the diffuse lines are transformed in an additional diffraction spots. X-ray oscillation patterns show that the positions of additional spots coincide with those for a primitive unit cell, which testify to a tendency of the crystal lattice to transformation from C-centered type to primitive one.

IV-H-3 Structure Transformation of a C_{60} * Na_x (THF)_y below 70 K

NARYMBETOV, Bakhyt¹; OJIMA, Emiko; OGATA, Hironori; KOBAYASHI, Hayao; KOBAYASHI, Akiko²; MORIYAMA, Hiroshi³
(¹IMS and Uzbek Acad. Sci.; ²Univ. Tokyo; ³Toho Univ.)

$Na_x(THF)_yC_{60}$ is the first metallic single crystal C_{60} compound grown by an electrocrystallization process. The studies of conductivity and magnetic properties of the crystals have revealed presence of metal-metal transition at 175 K and another phase transition at around 50 K. It has been found that the crystals have a hexagonal unit cell and the presence of phase transition around 170 K has been confirmed by X-ray diffraction experiments earlier. We have carried out low temperature X-Ray diffraction studies of $Na_x(THF)_yC_{60}$ by using the IP system equipped with liquid helium cooling device. The obtained diffraction patterns testify that there is a structure transformation of the crystal below 70 K which is shown as increase of the unit cell volume three times. Observed reflections on the diffraction patterns at low temperatures are indexed in hexagonal unit cell and the lattice parameters at 15 K are: $a = 26.207(12)$, $c = 9.868(3)$ Å, $V = 5869(8)$ Å³. Analysis of the collected intensity array shows that the space group is $P-3c1$ (or $P-3$) with the six molecules of C_{60} per unit cell, one independent position for C_{60} molecule and two positions for $Na_x(THF)_y$ with partial population of the equivalent positions. It seems that even at low temperatures fullerene molecules have a strong orientational disorder as well as a strong disorder of $Na_x(THF)_y$ on the symmetrically equivalent positions.

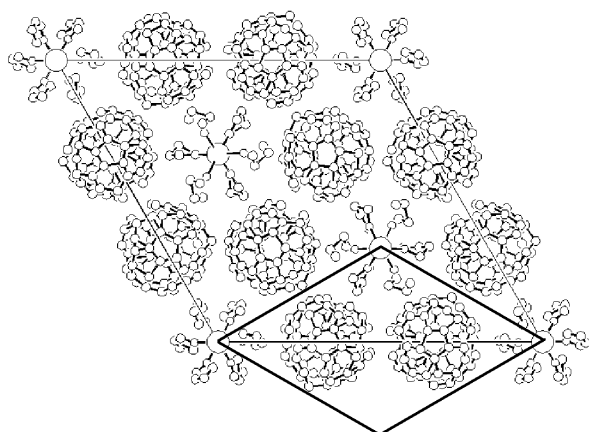


Figure 1. Schematic presentation of $C_{60}Na_x(THF)_y$ unit cell below 50 K. Unit cell at room temperature is shown by bold lines.

IV-H-4 High Pressure Structure of $[(C_2H_5)_2-(CH_3)_2N][Pd(dmit)_2]_2$

ADACHI, Takafumi¹; NARYMBETOV, Bakhyt²; KOBAYASHI, Hayao; KOBAYASHI, Akiko³
(¹IMS and Electrotech. Lab.; ²IMS and Uzbek Acad. Sci.; ³Univ. Tokyo)

With the aim of setting up the high pressure (or high-pressure and low-temperature) single crystal X-ray apparatus by using diamond anvil cell, we are examining the crystal structure of a high-pressure superconductor, $[(CH_3)_2(C_2H_5)_2N][Pd(dmit)_2]_2$ ($T_c = 4$ K at 2.4 kbar). Several years ago, we have proposed a HOMO-LUMO inversion mechanism to explain an anomalous P - T phase diagram of $[(CH_3)_2(C_2H_5)_2N][Pd(dmit)_2]_2$ where the insulating phase appears at higher pressure region above the superconducting phase. We have analyzed the structure up to 10 kbar by using specially designed diamond anvil cell without Be-supporting disks. The diffraction spots were detected by X-ray imaging device. In order to obtain the information on the high-pressure structure at low-temperature, we are trying the high-pressure X-ray experiments by using low-temperature imaging plate system.

IV-H-5 High-Pressure Four-Probe Resistivity Measurements of the Soft Organic Single Crystals up to 100 kbar

ADACHI, Takafumi¹; KOBAYASHI, Hayao; MIYAZAKI, Takafumi²; TOKUMOTO, Madoka³
(¹IMS and Electrotech. Lab.; ²Ehime Univ.; ³Electrotech. Lab.)

Recently, the electric properties of solids at extremely high pressure has attracted much attention. The superconductivity of oxygen discovered around 1 Mbar by using diamond anvil cell may be one of the best examples. On the other hand, the pressure of the usual clamp-type high pressure cell used for the single crystal experiments on the organic compounds cannot exceed *ca.* 25 kbar. In order to obtain the sufficiently accurate resistivity data above 100 kbar, an improvement of diamond anvil technique seems to be

inevitable. Since the report by Mao and Bell who measured the resistivity of string-shaped metal sample by using MgO gasket and pressure medium of soft powder (*e.g.* NaCl), the four-probe high-pressure resistivity measurements were made by diamond anvil cell. In order to apply high-pressure resistivity technique to soft organic crystals, the requirements for good Ohmic contacts and quasi-hydrostatic pressure will be essential. We have recently established an improved method applicable for the single crystal resistivity measurements up to 100 kbar.

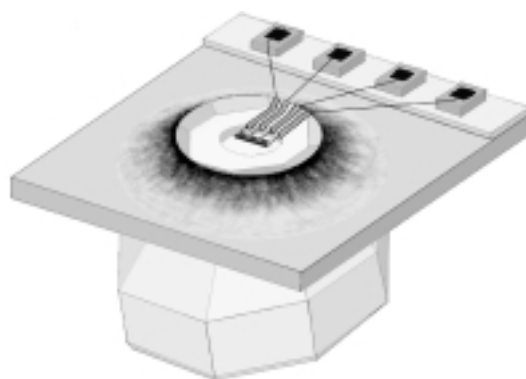


Figure 1. An illustration of the setup of diamond anvil four-probe resistivity cell.

IV-H-6 Resistivity Behavior of Organic Conductor, $\beta'-(BEDT-TTF)_2ICl_2$ up to 100 kbar

ADACHI, Takafumi¹; KOBAYASHI, Hayao; MIYAZAKI, Takafumi²; TOKUMOTO, Madoka³
(¹IMS and Electrotech. Lab.; ²Ehime Univ.; ³Electrotech. Lab.)

$\beta-(BEDT-TTF)_2I_3$ is one of the well-known organic superconductors discovered in 1984. An analogous conductor with smaller anions and modified β -type structure, $\beta'-(BEDT-TTF)_2ICl_2$ has an antiferromagnetic insulating ground state at ambient pressure. We have tried to check the possibility of the superconducting transition at high pressure by adopting the diamond anvil four-probe resistivity technique. The resistivities were successfully measured up to 100 kbar. To our knowledge, this is the first four-probe resistivity measurements on single organic crystal around 100 kbar. The activation energy was decreased with increasing pressure and metallic state appeared around 80 kbar. The room-temperature resistivity was $10^{-2} \Omega$ cm around 80 kbar, which was about three orders of magnitude smaller than that at ambient pressure (20Ω cm). However, the superconducting phase could not be found. Unexpectedly, around 100 kbar, the resistivity was gradually increased with the time, indicating a pressure-induced solid state reaction.

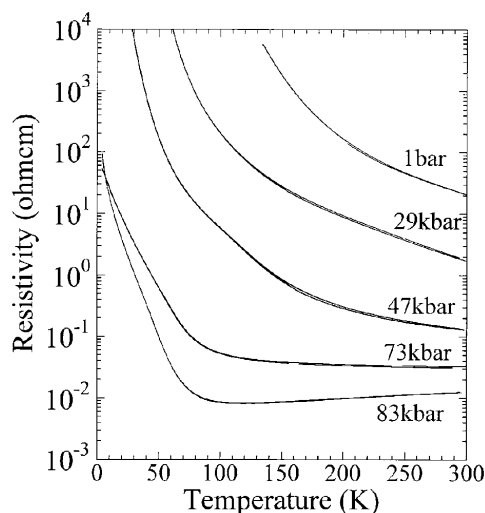


Figure 1. Resistivities of β' -(BEDT-TTF) $_2$ ICl $_2$ up to 80 kbar.

IV-I Development of New Molecular Conductors

The development of new materials is the most important driving force for the field of solid state chemistry. The recent progress in the concept of the molecular design enriched greatly the physics and chemistry of crystalline molecular solids. The appearance of various types of molecular metals, superconductors and molecular ferromagnets have attracted an increasing interest of chemists and physicists. We must grow out of the conventional design of molecular conductors for the future development. In these points of view we have performed the development of several types of new molecular components for organic molecular conductors. In the study of ditellurium bridged polyacene donors and propyleneditelluro substituted TTF, we have determined the whole of the crystal structures and physical properties. We are now examining new guiding principles for designing the organic conductors. Furthermore we have developed the novel organic donor containing a stable organic radical part to investigate the interaction between itinerant electrons of the charge-transfer complexes and localized spins of the organic stable radical parts for the development of novel organic conducting-magnetic hybrid materials.

IV-I-1 New Stable Metallic Salt Based on a Donor Molecule Containing *peri*-Ditellurium Bridges, TMTTeN(SCN) $_{0.88}$

OJIMA, Emiko; NARYMBETOV, Bakhyt; FUJIWARA, Hideki; KOBAYASHI, Hayao; KOBAYASHI, Akiko¹; TAKIMIYA, Kazuo²; OTSUBO, Tetsuo²; OGURA, Fumio³
(¹Univ. Tokyo; ²Hiroshima Univ.; ³Kinki Univ.)

[Chem. Lett. 845 (1999)]

Recently we have discovered the TMTTeN salts with Ag(CN) $_2^-$ and Au(CN) $_2^-$ anions showing metallic behavior down to 50 K. They have tetragonal structures and quasi three-dimensional Fermi surfaces. Recently, we have found a new stable metallic salt, TMTTeN(SCN) $_{0.88}$. The crystal structure is not isostructural to the structures of the Ag(CN) $_2^-$ and Au(CN) $_2^-$ salts. That is, penetration of the SCN $^-$ anion into the TMTTeN lattice leads to a modification of the packing of the TMTTeN molecules along the *c*-axis of the crystals. As shown in Figure 1, there are many intermolecular Te...Te contacts less than the sum of the van der Waals radii (4.2 Å) and three-dimensional network through the tellurium atoms is developed. The salt shows very high room-temperature conductivities (400–600 S cm $^{-1}$) and stable metallic behavior down to low temperature (4.2 K). The paramagnetic susceptibility of TMTTeN(SCN) $_{0.88}$ is almost constant throughout the

temperature range, indicating Pauli paramagnetism of the system [$1.6\text{--}1.9 \times 10^{-4}$ emu mol $^{-1}$]. Thus, the salt is considered to keep stable metallic nature down to liquid helium temperature.

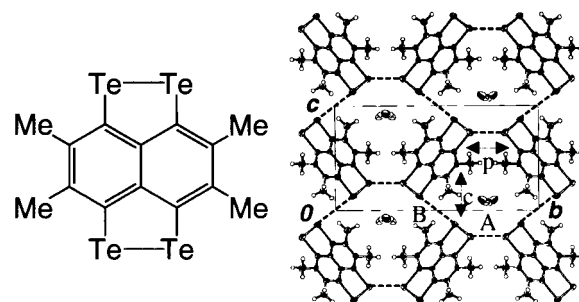


Figure 1. Structure of TMTTeN and crystal structure of TMTTeN(SCN) $_{0.88}$.

IV-I-2 Synthesis, Structures and Properties of New Organic Conductors Based on Tellurocycle-Fused TTF Donor Molecules

OJIMA, Emiko; FUJIWARA, Hideki; KOBAYASHI, Hayao; KOBAYASHI, Akiko¹
(¹Univ. Tokyo)

[Adv. Mater. in press]

In the search for excellent electron donors compos-

ing organic conductors, the concern for the tellurium-containing tetrathiafulvalene (TTF) derivatives has been growing for the last several years because a new metallic system with wide bandwidth and high dimensionality is expected to appear due to the large electron cloud of tellurium atoms. In addition, the conducting salts based on tellurium-containing donor molecules are interesting because the tellurium network is dominant for the construction of whole the crystal structure. Therefore we focused on the tellurocycle-fused TTF donor molecules. In this communication we reported the synthesis, crystal structure and electrochemical property of a new tellurocycle-fused TTF donor, 4,5-dimethyl-4',5'-propyleneditelluro-TTF **1**. We clarified the DA type crystal structure of the TCNQ complex of **1**. Furthermore, we prepared the several cation radical salts by use of the donor **1** and cleared that the unsymmetrical donor **1** are subject to the transformation to the dimerized donor **2** during the electrochemical oxidation. Although the obtained conducting salts are all semiconductors, those tellurium-containing donors have very interesting and unique molecular and crystal structures.

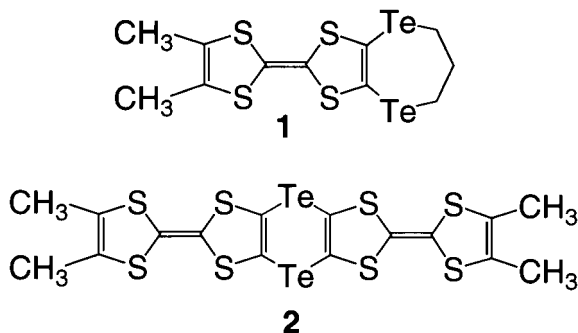


Figure 1. Structures of **1** and **2**.

IV-I-3 New π -Extended Organic Donor Containing a Stable TEMPO Radical as a Candidate for Conducting-Magnetic Multifunctional Materials

FUJIWARA, Hideki; KOBAYASHI, Hayao

[Chem. Commun. in press]

Recent studies on the molecular conductors and superconductors containing magnetic transition metal anions, such as the $(\text{ET})_2[(\text{H}_2\text{O})\text{Fe}(\text{C}_2\text{O}_4)_3] \cdot \text{C}_6\text{H}_5\text{CN}$ salt, a series of λ -(BETS) $_2\text{Fe}_x\text{Ga}_{1-x}\text{Cl}_4$ alloy salts and κ -(BETS) $_2\text{FeBr}_4$ salt, have stimulated the interest for the investigation of the interplay between the conductivity and magnetism in the research for new organic conductors. From the view point of realization of metallic conductivity, we supposed a molecular design as a fusion of a stable TEMPO radical part to the DTET-TTF [methylidene-1,3-dithiolo[4,5-*d*]-4,5-ethylenedithio-TTF] skeleton, which is a promising building block for realizing stable metallic behavior down to low temperature, such as the cases of MeDTET and CPDTET salts. We have examined the structure and physical properties of the $\text{Au}(\text{CN})_2^-$ salt of TEMPOET. The $\text{Au}(\text{CN})_2^-$ salt was electrochemically prepared. X-

Ray crystallographic analysis revealed that the D:A ratio of this salt is 2:3 and the TEMPOET donors form sheet-like structures. There is short O...O contacts (3.24(2) Å) between donor sheets. The room temperature electrical conductivities is low value of $10^{-3} \text{ S cm}^{-1}$ due to the highly oxidized state and undesirable stacking of donors. The small room temperature magnetic susceptibility ($9.6 \times 10^{-4} \text{ emu mol}^{-1}$ for 2:3 salt) suggests the existence of intramolecular spin singlet formation and/or intermolecular strong antiferromagnetic spin configuration.

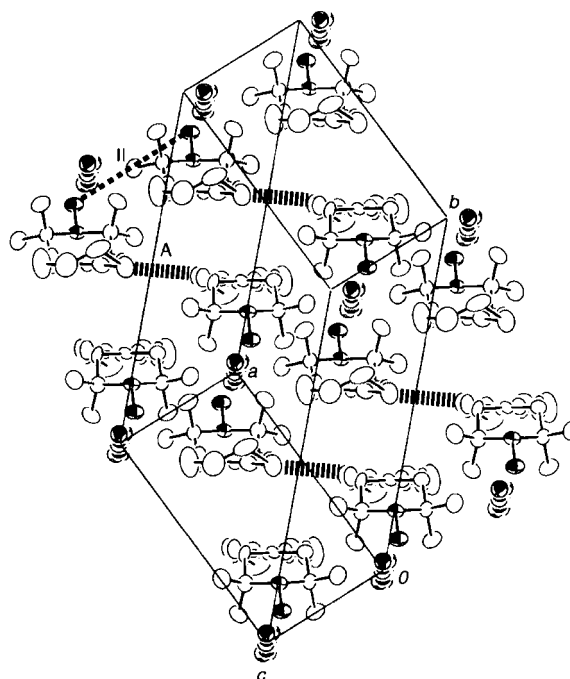


Figure 1. Crystal structure of $(\text{TEMPOET})_2[\text{Au}(\text{CN})_2]_3$.

IV-I-4 Synthesis and Properties of New Organic Donor Containing Two Stable TEMPO Radical Parts

FUJIWARA, Hideki; KOBAYASHI, Hayao

Organic molecular magnetism has become very active field of research for the material chemistry and physics since the discovery of the first pure organic ferromagnet in *p*-nitrophenyl nitronyl nitroxide (β -NPNN) in 1991 and successive development of several ferromagnets based on aminoxyl radicals such as 2,2,6,6-tetramethylpiperidinyloxy (TEMPO) and 4,4,5,5-tetramethyl-2-imidazoline-1-oxyl-3-oxide (NN) radicals. On the other hand, recent studies on the molecular conductors and superconductors containing magnetic transition metal anions have stimulated the interest for the investigation of the interplay between the conductivity and magnetism in the research for new organic conductors. Recently we have synthesized a donor molecule containing a stable TEMPO radical part and reported its electrochemical and magnetic properties. Furthermore we have prepared several cation radical salts and investigated their conducting and magnetic properties. In this context, further development of such stable radical-containing donor molecules

is of interest. In this work, we synthesized a new donor molecule containing two TEMPO radical parts **1** and investigated its ESR spectra and magnetic susceptibility.

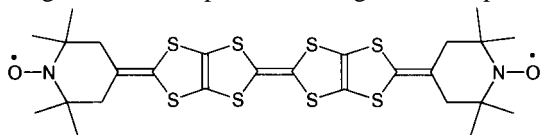


Figure 1. Structure of **1**.

IV-I-5 Origin of the High Electrical Conductivity of Neutral $[\text{Ni}(\text{ptdt})_2]$ —A Route to Neutral Molecular Metal

KOBAYASHI, Akiko¹; TANAKA, Hisashi¹; KUMASAKI, Mieko¹; TORII, Hajime¹; NARYMBETOV, Bakhyt²; ADACHI, Takafumi³
(¹Univ. Tokyo; ²IMS and Uzbek Acad. Sci.; ³IMS and Electrotech. Lab.)

[*J. Am. Chem. Soc.* in press]

A novel neutral nickel complex molecule with the extended TTF dithiolato ligand, propylenedithiotetrathiafulvalenedithiolate [$\text{ptdt}^{2-} = (\text{S}_8\text{C}_9\text{H}_6)^{2-}$], was synthesized. In the $[\text{Ni}(\text{ptdt})_2]$ crystal, $[\text{Ni}(\text{ptdt})_2]$ molecules form one-dimensional columns along the *a* axis, having short intermolecular transverse $\text{S}\cdots\text{S}$ contacts. The crystal exhibited an extremely high electrical conductivity (7 S cm^{-1}) at room temperature as a neutral molecular crystal. High-pressure resistivity measurements was made up to 72 kbar. But contrary to usual low-dimensional organic conductors, the resistivity could not be suppressed by applying high pressure. The tight-binding band structure calculation indicated that the HOMO (highest occupied molecular orbital) and LUMO (lowest unoccupied molecular orbital) form "the crossing bands," whose Fermi surfaces tend to be vanished by HOMO-LUMO interactions. Only very small electron and hole pockets appear in the Fermi surface owing to the transverse interactions between neighboring columns. Based on these analyses, the requirements for the design of molecular metals composed of single molecules have been clarified.

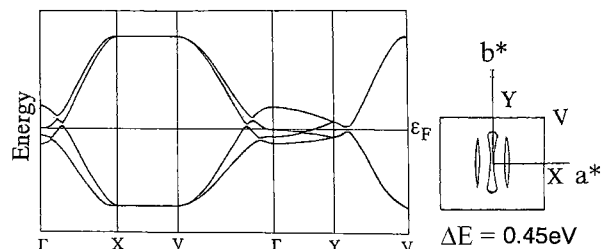


Figure 1. Tight-binding band of neutral $[\text{Ni}(\text{ptdt})_2]$ crystal. The Energy difference between HOMO and LUMO is tentatively assumed to be 0.45 eV.

IV-I-6 Structural, Electrical and Magnetic Properties of Low-dimensional Conductors Based on Unsymmetrical π Donor EDT-TTF and Analogous Selenium-substituted Molecules

SATO, Akane; KOBAYASHI, Hayao; KOBAYASHI, Akiko¹
(¹Univ. Tokyo)

[*J. Mater. Chem.* **9**, 2365 (1999)]

Organic conductors based on unsymmetrical π donor molecules EDT-TTF (ethylenedithiotetrathiafulvalene) or its selenium-substituted analogs (EDST, EDTS) and tetrahedral anions GaCl_4^- were prepared. The crystal structure determinations and the extended Hückel tight-binding band calculations indicated these systems to be quasi-one dimensional conductors similar to TMTTF or TMTSF systems (TM systems). Electrical resistivity and magnetic susceptibility measurements and low-temperature X-ray diffraction experiments suggested the spin-Peierls ground state of $(\text{EDT-TTF})_2\text{GaCl}_4$. $(\text{EDST})_2\text{GaCl}_4$ and $(\text{EDTS})_2\text{GaCl}_4$ exhibited metallic behavior down to *ca.* 40 K. The electric and magnetic properties of $(\text{EDST})_2\text{GaCl}_4$ suggested a semimetallic state at low temperature. In spite of the similarity in the crystal and electronic band structures between TM and EDT systems, these two series of quasi-one dimensional conductors do not share the same "generalized phase diagram." The electron-lattice interaction seems to be important in EDT conductors. The electric and magnetic properties of the isostructural systems with magnetic FeCl_4^- anions were also examined. The magnetic interaction between the high-spin Fe^{3+} ions was found to be very weak.

IV-J Development of Pulsed Field Gradient NMR Spectroscopy

Pulsed field gradient spin echo (PGSE) nuclear magnetic resonance (NMR) is a powerful method for the study of dynamics in condensed matter since it probes translational motion of molecules selectively, without being affected by vibrational or rotational motions. Due to this advantage it has been widely applied to the dynamics of molecules in liquids. However, applications of this technique to strongly dipole-coupled spin systems with short T_2 or to the study of slow and anisotropic self-diffusion are still challenging works because combined techniques of line-narrowing, pulsing of sharp and intense field gradients, and two-dimensional field-gradient generation are necessary.

In the present study we applied the technique to the study of anisotropic self-diffusion in liquid crystals, with the use of the laboratory-made spectrometer equipped with a rotatable quadrupole gradient coil.

IV-J-1 Self-diffusion Coefficients of a Reentrant Liquid Crystal CBOBP

OISHI, Osamu; MIYAJIMA, Seichi

Self-diffusion coefficient tensors of a reentrant liquid crystal CBOBP were measured in the high and low temperature S_A phases. In the high temperature S_A phase, the diffusion coefficient component $D_{//}$ is larger than D_{\perp} . The two activation energies are similar. This property resembles that of the nematic phase, and indicates that the layer structure of the high temperature S_A phase is disordered remarkably. In the low temperature S_A phase, absolute values of the self-diffusion coefficient components, $D_{//}$ and D_{\perp} , are close to each other, in contrast with the diffusion coefficient components in the high temperature S_A phase. The activation energy for $D_{//}$ is much higher than that for D_{\perp} . This suggests a firm layer structure. It is also interesting to note that the activation energies for D_{\perp} are similar in the high and low temperature S_A phases, and the values of D_{\perp} are found on one straight line through both phases. Taking these in mind there seems to be no change in molecular interaction and molecular arrangement in the two S_A phases, as far as the perpendicular components concern. The change in molecular interaction and structure seemed to have occurred in the parallel components.

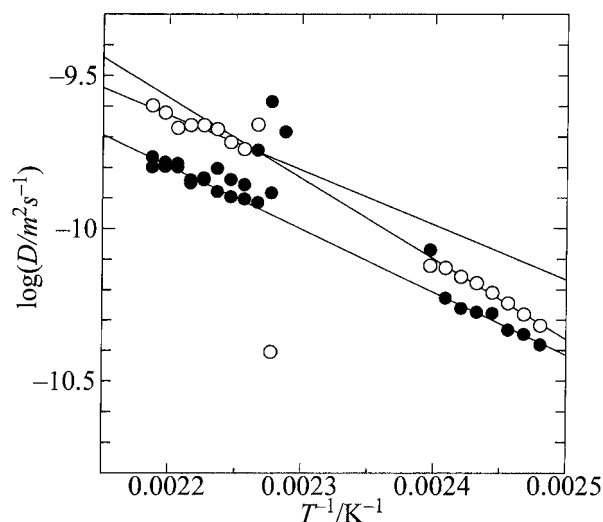


Figure 1. Anisotropic self-diffusion coefficients of CBOBP in smectic A phases (○ $D_{//}$, ● D_{\perp}).

IV-J-2 Self-diffusion Coefficients of OBBC and OBBF

OISHI, Osamu; MIYAJIMA, Seichi

OBBC is a reentrant liquid crystal. OBBF is a derivative of OBBC, where the terminal cyano group in OBBC is replaced by fluorine, and shows no reentrant phases. In the S_A phase of OBBC between the two nematic phases, the self-diffusion coefficient component $D_{//}$ is larger than D_{\perp} . The activation energies for both $D_{//}$ and D_{\perp} are low, and similar in magnitudes.

OBBF exhibits a remarkable feature. $D_{//}$ is higher than D_{\perp} , and the relative magnitudes of $D_{//}$ and D_{\perp} reverses with the change of temperature. The self-diffusion property in the S_A phase of OBBC resembles that in the high temperature phase of CBOBP, and the self-diffusion property of OBBF is close to that of the low temperature phase of CBOBP.

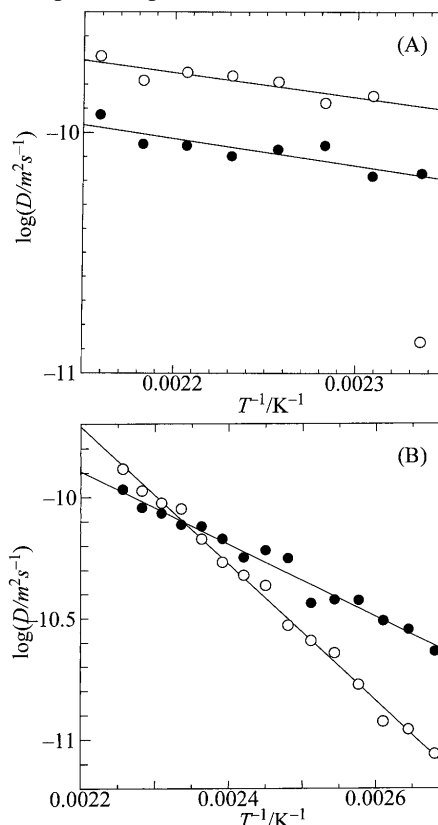


Figure 1. Anisotropic self-diffusion coefficients of OBBC(A) and OBBF(B) in smectic A phases (○ $D_{//}$, ● D_{\perp}).

IV-J-3 Self-Diffusion Coefficients of an Anti-Ferroelectric Liquid Crystal MHPOBC

OISHI, Osamu; MIYAJIMA, Seiichi

The anti-ferroelectric liquid crystal MHPOBC shows various phase structures with temperature change. It was found that the activation energy for $D_{//}$ was much higher than that for D_{\perp} even in the para-electric S_A phase, and so the formation of a firm layer structure was indicated. Smaller values of $D_{//}$ indicate that diffusion across the layers is difficult.

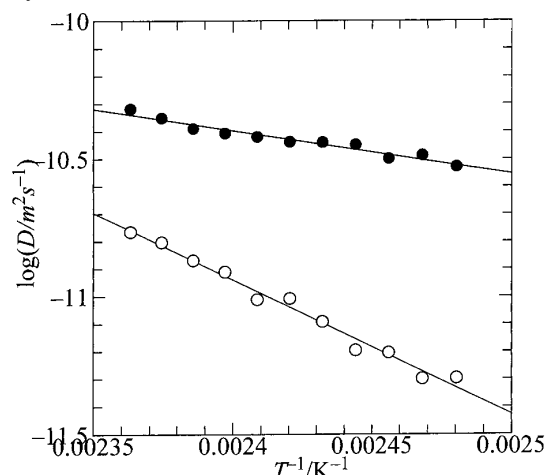


Figure 1. Anisotropic self-diffusion coefficients of MHPOBC in smectic A phase (\circ $D_{//}$, \bullet D_{\perp}).

IV-J-4 Self-diffusion Coefficients of a Hexatic Liquid Crystal PHOAB

OISHI, Osamu; MIYAJIMA, Seiichi

PHOAB exhibits a phase transition sequence, S_A — hexatic smectic B — crystalline smectic B, on lowering the temperature. In the S_A phase, the activation energy for $D_{//}$ is much higher than that for D_{\perp} . This fact shows that a firm layer structure is formed. At the phase transition from S_A to hexatic B, the self-diffusion coefficients become small to a level where even the perpendicular component was immeasurable. The diffusion properties of PHOAB and OBBF are similar: $D_{//}$ and D_{\perp} have similar values at high temperature, but

$D_{//}$ becomes smaller in comparison with D_{\perp} at low temperature.

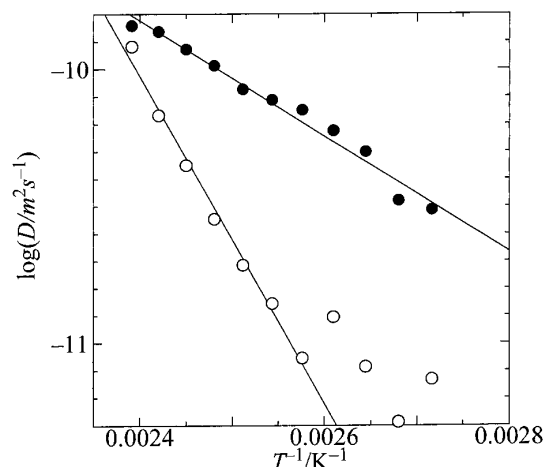


Figure 1. Anisotropic self-diffusion coefficients of PHOAB in smectic A phase (\circ $D_{//}$, \bullet D_{\perp}).

IV-J-5 Calculation of Dipole Moments by MOPAC7

OISHI, Osamu; MIYAJIMA, Seiichi

Dipole moments were calculated with the MOPAC7 program. The calculated values are 5.8 (OBBC), 4.2 (OBBF), 6.4 (CBOBP), 2.5 (MHPOBC), and 4.3 (PHOAB) Debyes. The reentrant nematic liquid crystals, OBBC and CBOBP, have larger dipole moments.

IV-J-6 Measurement of Anisotropic Self-Diffusion Coefficient Tensors by PGSE-NMR

MIYAJIMA, Seiichi; OISHI, Osamu

[*DIM Newsletter* **12**, 16 (1998)]

A review account is given for the pulsed field gradient spin echo (PGSE) NMR technique, which has been applied to the determination of anisotropic self-diffusion coefficient tensors. Principles and methods are explained, and their applications to the translational dynamics of liquid crystals is presented.

IV-K Phase Transitions and Dynamical Ordering in Liquid Crystals

Extensive high resolution NMR studies were conducted to reveal the dynamics and the microscopic origin of antiferroelectricity in liquid crystals.

IV-K-1 A Bent and Asymmetrically Hindered Chiral Alkyl Chain of an Antiferroelectric Liquid Crystal as Observed by ^2H NMR

YOSHIDA, Shohei¹; JIN, Bo¹; TOKUMARU, Koh¹; TAKANISHI, Yoichi¹; ISHIKAWA, Ken¹; TAKEZOE, Hideo¹; FUKUDA, Atsuo²; KUSUMOTO, Tetsuo³;

NAKAI, Toshihito⁴; MIYAJIMA, Seiichi
(¹Tokyo Inst. Tech.; ²Shinshu Univ.; ³Sagami Cent. Res. Cent.; ⁴Tokyo Univ. Agric. Tech.)

[*J. Phys. Soc. Jpn.* **68**, 46 (1999)]

The structure and dynamics of the alkyl chains are

investigated by ^2H -NMR for specifically deuterated samples of an antiferroelectric liquid crystal MHPOBC. The ^2H -NMR spectrum for the chiral alkyl chain exhibits very small quadrupolar splittings, and the methylenes close to the chiral center give double splittings, which are ascribable to two different quadrupolar splittings for each methylene unit. The unusual nature of the chiral chain is revealed; the chain is bent from the molecular long axis, and its motion is asymmetrically hindered.

IV-K-2 Experimental Spectroscopy of Liquid Crystals, No. 4-6. NMR Spectroscopy, Pt. 1-3

MIYAJIMA, Seiichi; NAKAI, Toshihito¹
(¹Tokyo Univ. Agric. Tech.)

[EKISHO 3, 43, 124 and 205 (1999)]

NMR study of liquid crystals is outlined in a series of lectures, with special emphasis on its methodological

aspects. Pt. 1 describes the theoretical framework for the spectral analysis, in connection with the orientational order parameters. Pt. 2 deals with various aspects of experimental ^{13}C NMR spectroscopy. Determination of the order parameters by the alignment-induced shifts, and determination of the nuclear shielding tensor elements by two-dimensional (2-D) site-separated spinning sideband spectroscopy are described. Use of partially averaged ^{13}C - ^1H dipolar interactions is shown in the experiments of transient oscillation in cross-polarized magnetization, and 2-D dipolar separated-local field spectroscopy. Analysis of molecular rotational motion by relaxation measurements is also shown. Pt. 3 describes how ^2H NMR is applied to solve various important problems of liquid crystals, such as determination of segmental order parameters, detection of asymmetrical hindrance in rotational motions, and detection of the phase biaxiality. Finally the pulsed field gradient spin-echo NMR technique is explained, and it is shown how the translational self-diffusion coefficient tensor elements are determined.

IV-L Electronic Properties of Alkali-Hydrogen-Carbon Systems

In alkali-hydrogen-carbon ternary systems, hydrogen or alkali metal elements exhibit a variety of electronic states when doped or intercalated in the host crystal lattice. An interesting feature is how the hydrogen 1s state contribute to the bulk electronic properties. Structural and electronic properties were studied for stage-6 sodium-hydrogen-graphite ternary compound by means of solid state NMR. New alkali-hydrogen- C_{70} compounds were synthesized by detecting and controlling the reaction of alkali hydrides with C_{70} crystal with *in-situ* ^1H NMR measurements and characterized the structures and the magnetic properties by powder X-ray diffraction, ESR and magnetic susceptibility measurements. New alkali-hydrogen-single-walled carbon nanotube aggregates were synthesized and characterized by solid state NMR.

IV-L-1 NMR Study of Stage-6 Sodium-Hydrogen-Graphite Intercalation Compound

OGATA, Hironori; MIYAJIMA, Seiichi; ENOKI, Toshiaki¹; ANTOINE, Laurence²; GUERARD, Daniel²
(¹Tokyo Inst. Tech.; ²Univ. Nancy I)

^{23}Na , ^1H and ^{13}C NMR have been carried out for stage-6 sodium-hydrogen-graphite intercalation compound (NaH-GIC). Figure 1 shows the ^1H decoupled ^{13}C NMR spectra in stage-6 NaH-GIC with the external field (B_0) perpendicular (a) and parallel (b) to the c -axis. The lines 1α and 1β correspond to the inequivalent two carbon atoms on the bounding layer (layer 1), and 2α , 2β and 3α , 3β correspond to those on middle and interior layer (layer 2 and 3), respectively. From the anisotropic values of ^{13}C NMR shifts, the charge transfer rates per one carbon atom were estimated to be 0.028, 0.005 and 0.001 for layer 1, 2 and 3, respectively. Figure 2 shows the angular dependence of the ^1H NMR second moment $\langle\Delta\nu^2\rangle$ measured at room temperature. $\langle\Delta\nu^2\rangle$ has its minimum at around 40° , which suggests that hydrogen forms two-dimensional lattice in the intercalate. However, the values of $\langle\Delta\nu^2\rangle$ obtained were much larger than those expected from the model calculation. This fact suggests

the existence of paramagnetic defects in the intercalate, which was reported for higher stage NaH-GIC sample by ESR measurement. The angular dependence of ^{23}Na NMR spectrum showed the existence of two Na^+ sites with different electric field gradient tensors.

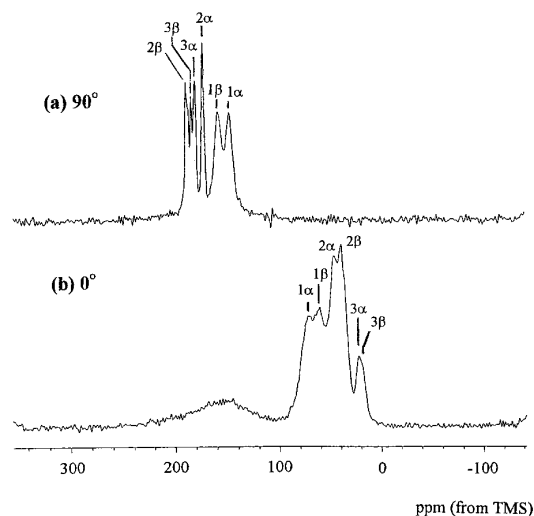


Figure 1. ^1H decoupled ^{13}C NMR spectra in stage-6 NaH-GIC with the external field (B_0) perpendicular (a) and parallel (b) to the c -axis.

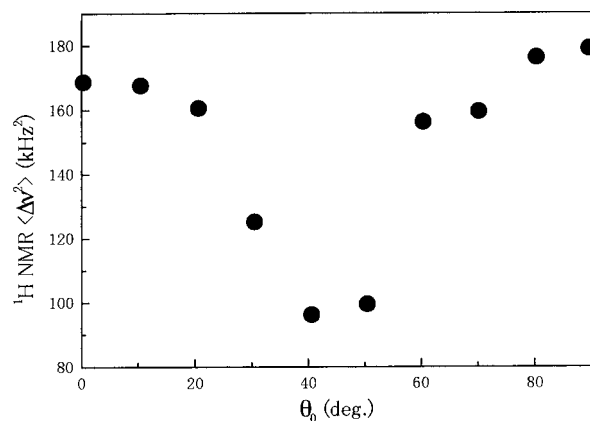


Figure 2. Angular dependence of the ^1H NMR second moment in stage-6 NaH-GIC measured at room temperature.

IV-L-2 *In-situ* NMR Study of the Reaction Process in Alkali-Hydrogen-Fullerene Systems

OGATA, Hironori

In the previous work, we have reported the attempts at detecting and controlling the reaction of potassium hydride (KH) or sodium hydride (NaH) with C_{60} crystal with *in-situ* ^1H NMR measurements. We also conducted with those of NaH or KH with C_{70} crystal. Figure 1 shows the time dependence of ^1H NMR spectra for a mixture of stoichiometric amounts (3:1) of NaH and C_{70} reacted at 503 K (a) and of KH and C_{70} at 450 K (b), respectively. After several minutes' reaction, a signal at about -4 ppm appeared, which may be ascribable to decomposition of KH or NaH. Just after the intensity of this peak became maximum, the sample was cooled rapidly to 150 K to stop the reaction. After cooling, the hydrogen peak disappeared for NaH- C_{70} sample but stabilized as hydrogen anion for KH- C_{70} sample. This peak intensity, however, gradually decreased after the sample was heated up to room temperature and disappeared within 24 hrs. Powder X-ray diffraction profile of the KH- C_{70} sample just after the reaction showed that these crystals form fcc structure with lattice constant $a = 15.04$ Å at room temperature. This value is larger than that of fcc K_3C_{70} ($a = 14.96$ Å at room temperature). These facts suggest that hydrogen anion is occupied in the interstitial site of the K_3C_{70} crystal just after the reaction. Figure 2 shows the temperature dependence of the magnetic susceptibility of $\text{K}_3\text{H}_x\text{C}_{70}$ just after the reaction. A small but distinct anomaly, which was not reported for K_3C_{70} was observed at 120 K. This anomaly was also observed in the temperature dependence of ESR peak-to-peak linewidth ($\Delta H_{\text{p-p}}$) for $\text{K}_3\text{H}_x\text{C}_{70}$ (Figure 3). The value of Pauli-paramagnetic susceptibility was evaluated to be about 7×10^{-4} emu/mole from ESR and magnetic susceptibility measurements.

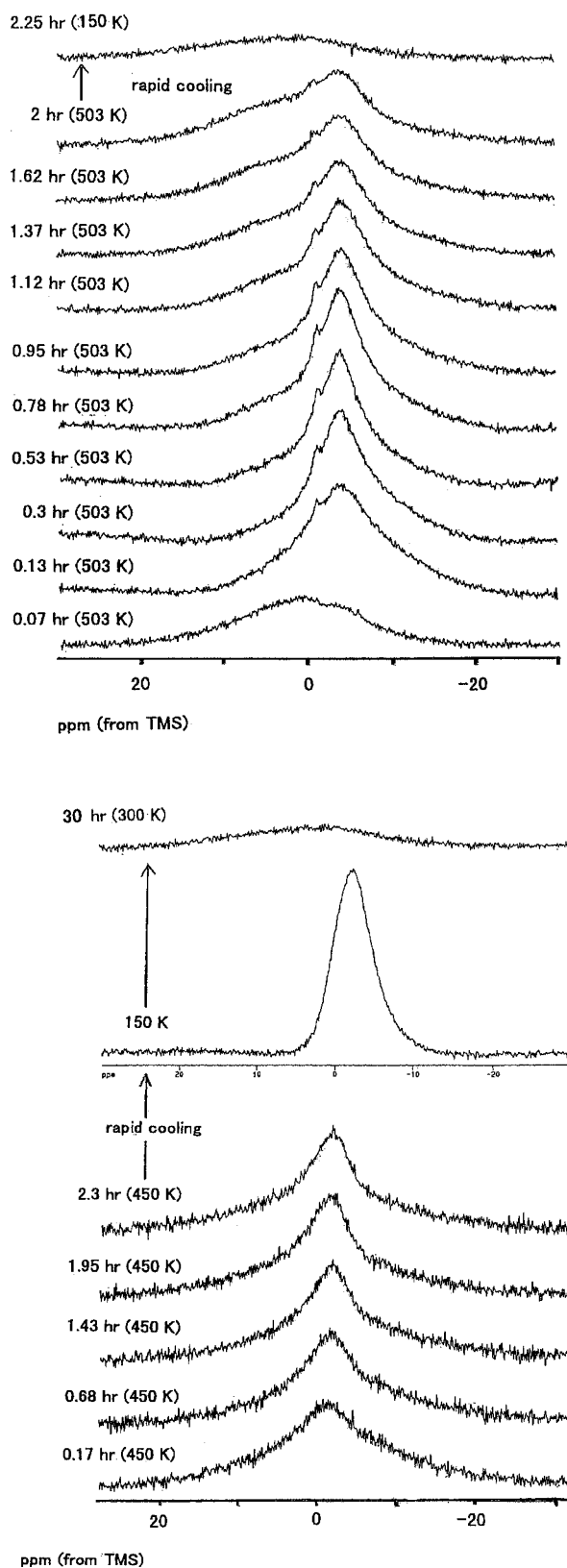


Figure 1. Time dependence of *in-situ* ^1H NMR spectra for the mixture of (a) NaH and C_{70} and of (b) KH and C_{70} .

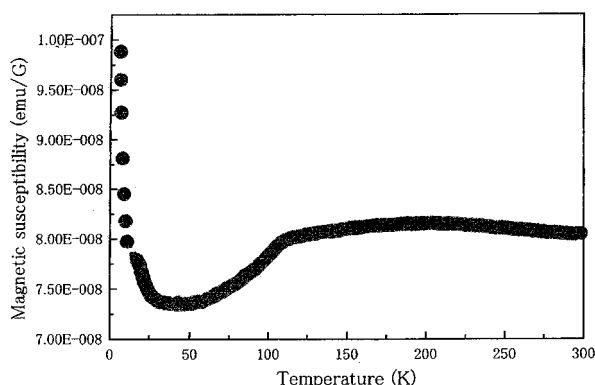


Figure 2. Temperature dependence of static magnetic susceptibility of $K_3H_xC_{70}$ just after the reaction.

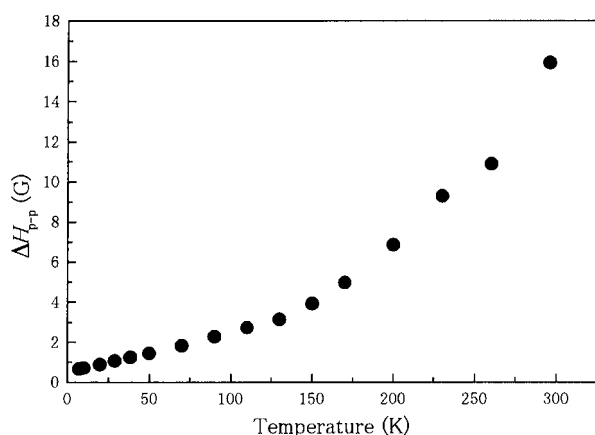


Figure 3. Temperature dependence of ESR peak-to-peak linewidth for $K_3H_xC_{70}$ just after the reaction.

IV-L-3 Synthesis and NMR study of Alkali-Hydrogen-Single-Walled Carbon Nanotubes

OGATA, Hironori; BANDOW, Syunji¹; KUNO, Syougo²; SAITO, Yahachi²
(¹ICORP-JST; ²Mie Univ.)

Potassium-hydrogen-single-walled carbon nanotubes (K-H-SWNTs) aggregates were synthesized first and their states of hydrogen were studied by solid state 1H NMR. Rh-Pt mixed catalysts and hydrogen peroxide were used to produce SWNTs and remove amorphous carbon particles in the raw soot. Two kinds of SWNTs were prepared as starting sample, one was the SWNTs with caps and the other was those without caps obtained by a heating treatment in dried air. K-H-SWNTs samples were synthesized by both (a) the direct reaction of potassium hydride (KH) and SWNTs and (b) the absorption of H_2 gas on K-doped SWNTs. 1H NMR measurements proved that a singlet 1H spectrum with the value of the second moment of about 40 kHz^2 at -10 ppm (from TMS) was observed only by using uncapped SWNTs as starting samples, independently of the way of synthesis. This fact suggests that hydrogen anion is condensed inside SWNTs for K-H-SWNTs (uncapped) system.

IV-M Structural and Electronic Properties of New Carbon Materials

Electronic properties and the function of micropores were studied for new carbon materials in this project. ^{13}C NMR were performed first for single-walled carbon nanotubes (SWNTs) to investigate the electronic structure in the magnetic field. The behavior of water molecules absorbed in activated carbon fiber (ACF) was studied by solid state 1H NMR.

IV-M-1 ^{13}C NMR Study of Single-Walled Carbon Nanotubes

OGATA, Hironori; BANDOW, Syunji¹; KUNO, Syougo²; SAITO, Yahachi²
(¹ICORP-JST; ²Mie Univ.)

^{13}C NMR experiments have been carried out for single-walled carbon nanotubes (SWNTs), which were produced by using non-ferromagnetic Rh-Pt mixed catalysts. Hydrogen peroxide was used to remove amorphous carbon particles in the raw soot almost perfectly. Figure 1 shows the ^{13}C NMR spectrum at 298 K. From the line shape analysis of the ^{13}C spectrum, the shift tensor was evaluated to be $(\delta_{11}, \delta_{22}, \delta_{33}) = (192, 186, 132) \text{ ppm}$. Small anisotropic value ($\Delta\delta = -57 \text{ ppm}$) compared with that reported for MWNTs¹⁾ suggests that this SWNTs sample contains metallic tubes with larger electronic density of states at the Fermi level than that

of MWNTs sample. Furthermore, the intensity of ^{13}C signal was found to be weak for the amount of the sample, suggesting that the ^{13}C signal observed was only from metallic tubes. The ^{13}C NMR signal of semi-conducting tubes was broadened and could not be observed virtually due to the large anisotropy of diamagnetic susceptibility, which is theoretically predicted.²⁾

To obtain more detailed information about the electronic state of SWNTs, we performed ^{13}C spin lattice relaxation time (T_1) measurement at 100.1 MHz (9.4 T). Figure 2 shows the temperature dependence of spin-lattice relaxation time at 9.4 T. It is found that SWNTs follows a Korringa-like behavior ($T_1 \times T = 940 \pm 60 \text{ (sec.K)}$) in the temperature region between 4.2 K and 100 K, which is different largely with that of graphite sample.³⁾ This fact suggests that metallic tubes exist at the magnetic field of 9.4 T.

References

- 1) Y. Maniwa *et al.*, *Proc. XII Int. Winterschool* (Kirchberg, Austria) 87 (1998).
- 2) Ajiki and Ando, *J. Phys. Soc. Jpn.* **62**, 2470 (1993).
- 3) K. Kume *et al.*, *Synth. Met.* **12**, 307 (1985).

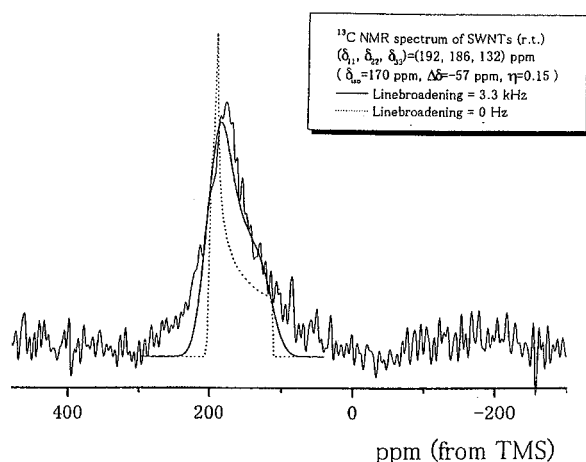


Figure 1. ^{13}C NMR spectrum of SWNTs at 298 K.

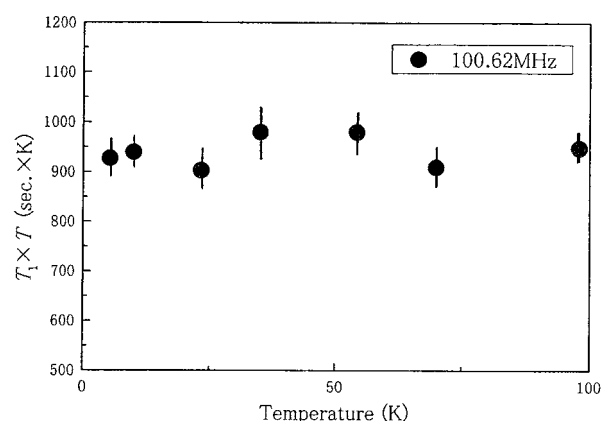


Figure 2. Temperature dependence of ^{13}C $T_1 \times T$ of SWNTs at 9.4 T.

IV-M-2 Dynamics of Water Molecules Confined in Activated Carbon Fiber

OGATA, Hironori; MIYAJIMA, Seichi; YOSHIKAWA, Yuuhi¹; SATO, Hirohiko¹; ENOKI, Toshiaki¹
(¹Tokyo Inst. Tech.)

Water molecules adsorbed in microporous carbon materials are expected to show distinctive characteristics different from those in the bulk state. For example, since micrographite surfaces in carbon materials are hydrophobic, if water is adsorbed, its structure is essentially affected by either the confinement effect or the hydrophobic effect originating in the interaction with carbon surfaces. ^1H NMR measurements were conducted for water molecules adsorbed in activated carbon fiber (ACF). At room temperature the lineshape of the ^1H NMR spectrum for this system consists of two peaks at -0.4 ppm and -3.9 ppm (from TMS) with

inhomogeneous broadenings, which are considered to be attribute to the difference of the adsorption sites of water molecules. The temperature dependence of the value of the ^1H NMR second moment ($\langle \Delta v^2 \rangle$) is shown in Figure 1. With decreasing temperature, $\langle \Delta v^2 \rangle$ increased drastically at about 190 K and a plateau of 55 kHz^2 was observed below 160 K, which was much smaller than that of bulk ice (about 345 kHz^2 at 200 K). The peak position of the ^1H NMR spectrum at 160 K was $+10$ ppm. These facts suggests that water molecules confined in ACF micropores freeze and form a hydrogen-bonded network at 160 K and that strong interaction between water molecules and ACF micropores surface hinders the the growth of three-dimensional hydrogen-bonded network. Figure 2 shows the temperature dependence of ^1H NMR spin-lattice relaxation time (T_1) for this system. The distinct minimum of the T_1 at 225 K was observed, which is thought to be associated with the self-diffusion of the water molecules. The activation energy (E_a) and the correlation time (τ_c) at 298 K were evaluated to be 2.7 kcal/mole, and 5.5×10^{-11} sec., respectively. The value of E_a obtained is almost same as that of the self-diffusion for bulk water (4 kcal/mole), however, the value of τ_c is much larger than that of bulk water (2.5×10^{-12} sec. at 298 K) due to the confinement effect.

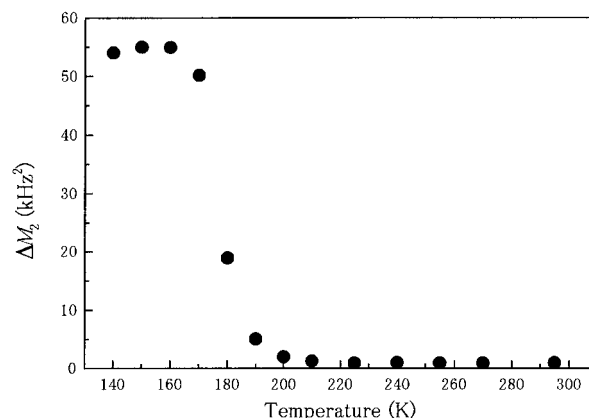


Figure 1. Temperature dependence of ^1H NMR second moment for water adsorbed activated carbon fiber.

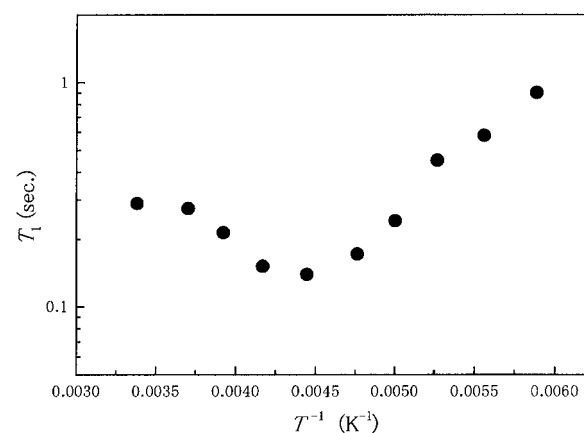


Figure 2. Temperature dependence of ^1H NMR spin-lattice relaxation time for water adsorbed activated carbon fiber.

IV-N Structural and Electronic Properties of Fullerene-Based Compounds

Structural and electronic properties were studied for several types of fullerene-based compounds in this project. Electronic and magnetic properties of $\text{Na}_x(\text{THF})_y\text{C}_{60}$ single crystals were studied by magnetic susceptibility, ESR and Raman scattering measurements. ^1H , ^{23}Na and ^{13}C NMR studies were conducted for $\text{Na}_x(\text{THF})_y\text{C}_{60}$ single crystals to reveal the microscopic origins of the phase transitions and the structural and electronic states at low temperature. Attempts at doping Ce into C_{60} crystal were conducted and structural and magnetic properties of the products were investigated. Raman scatterings and X-ray powder diffractions for a pressure induced superconductor Cs_3C_{60} were studied under some pressures.

IV-N-1 Electronic Properties of Alkali-THF- C_{60} Single Crystals

OGATA, Hironori; KOBAYASHI, Hayao; YAKUSHI, Kyuya; MORIYAMA, Hiroshi¹
(¹Toho Univ.)

The electronic and magnetic properties of $\text{Na}_x(\text{THF})_y\text{C}_{60}$ single crystals were studied by means of ESR, magnetic susceptibility, and Raman scattering measurements. Figure 1 shows the temperature dependence of ESR peak-to-peak linewidth ($\Delta H_{\text{p-p}}$) for $\text{Na}_x(\text{THF})_y\text{C}_{60}$. The value of $\Delta H_{\text{p-p}}$ decreases monotonically with decreasing temperature in the temperature region between 300 K and 10 K with sudden drop at 180 K. This drop is attributed to be metal-metal phase transition previously reported for this compound.¹⁾ Pauli susceptibility at room temperature was evaluated to be $\chi_{\text{P}} = 3.6 \times 10^{-4}$ (emu/mol) from ESR measurement. Figure 2 shows the temperature dependence of magnetic susceptibility for $\text{Na}_x(\text{THF})_y\text{C}_{60}$. Two small reduction in the magnetic susceptibility were observed below 180 K and 50 K, the former is attributed to be metal-metal phase transition above-mentioned. The temperature dependence of the peak position of the $A_g(2)$ mode of C_{60} in $\text{Na}_x(\text{THF})_y\text{C}_{60}$ revealed that the molecular valence of C_{60} was -1 in the temperature region between 298 K and 4.2 K. In conclusion, it was found that $\text{Na}_x(\text{THF})_y\text{C}_{60}$ is a metal down to 4.2 K, which is composed of C_{60}^{1-} anions.

Reference

1) H. Kobayashi *et al.*, *J. Am. Chem. Soc.* **116**, 3153 (1994).

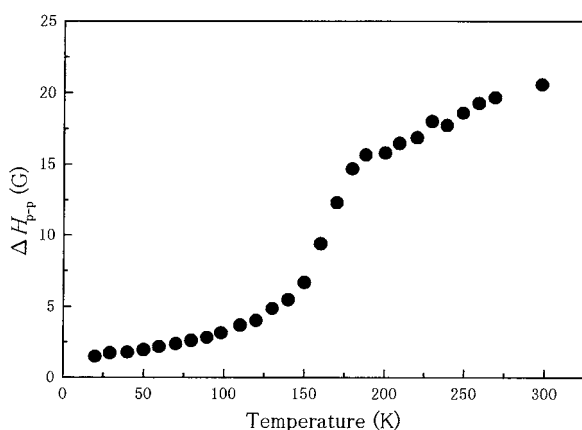


Figure 1. Temperature dependence of ESR peak-to-peak linewidth ($\Delta H_{\text{p-p}}$) for $\text{Na}_x(\text{THF})_y\text{C}_{60}$ single crystals.

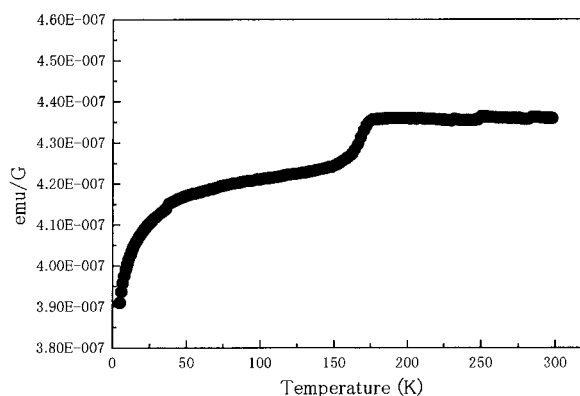


Figure 2. Temperature dependence of magnetic susceptibility for $\text{Na}_x(\text{THF})_y\text{C}_{60}$ single crystals.

IV-N-2 NMR Study of Sodium-THF- C_{60} Single Crystals

OGATA, Hironori; KOBAYASHI, Hayao; MORIYAMA, Hiroshi¹
(¹Toho Univ.)

^1H , ^{23}Na and ^{13}C NMR measurements were performed for $\text{Na}(\text{THF})_y\text{C}_{60}$ single crystals to elucidate the microscopic origins of the phase transitions at 180 K and 50 K and the electronic state at low temperature. Figure 1 shows the temperature dependence of ^{23}Na NMR spectrum for $\text{Na}(\text{THF})_y\text{C}_{60}$. A singlet spectrum appearing at -7 ppm (from 1.0 M NaCl aq. sol.) at 297 K suggests that more than four THF molecules are coordinated around the Na^+ ions. The ^{23}Na linewidth does not undergo the remarkable change at 180 K, while the line broadening is observed below 50 K. Figure 2 shows the temperature dependence of ^1H NMR spectrum for $\text{Na}(\text{THF})_y\text{C}_{60}$. The ^1H linewidth changed clearly at 180 K. At 160 K, the linewidth of ^1H NMR spectrum ($\Delta H_{1/2}$) is evaluated to be about 8 G, which is smaller than that of motionless THF molecules (~ 15 G). No significant change was observed at 180 K in the temperature dependence of the line shape of ^{13}C NMR spectrum. These facts are explicable by assuming that the librational motion around the axis connecting between sodium cation and the oxygen of the THF molecule freezes below 180 K and the hydrogen of the $-\text{CH}_2-$ group becomes motionless below 50 K in the time scale of NMR. The temperature dependence of the ^{13}C nuclear spin-lattice relaxation rate, T_1^{-1} , exhibited Korringa-like behavior ($T_1 \times T = 550$ (sec \times K)) in the temperature region between 50 K and 6 K. This facts suggests that $\text{Na}(\text{THF})\text{C}_{60}$ is metallic down to 6 K. The

electronic density of states at Fermi level of this compound was evaluated to be about 30% of that of K_3C_{60} superconductor, provided that these electronic correlation effects are equal.

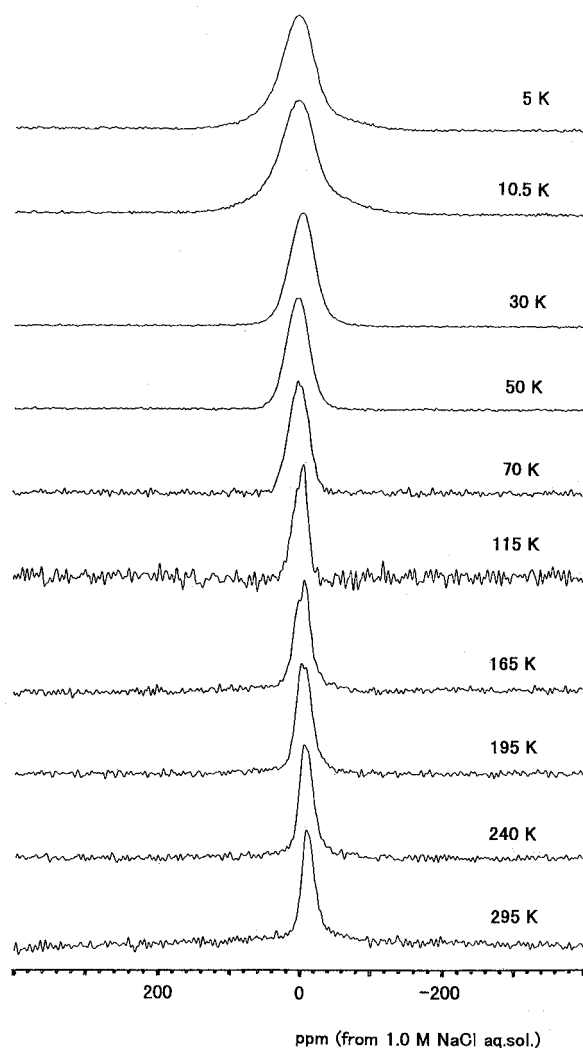


Figure 1. Temperature dependence of ^{23}Na NMR spectrum for $\text{Na}(\text{THF})_y\text{C}_{60}$ single crystals.

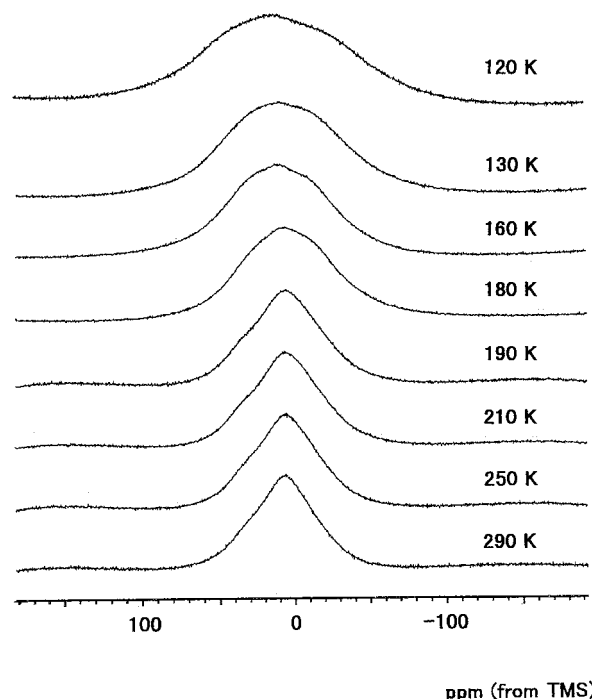


Figure 2. Temperature dependence of ^1H NMR spectrum for $\text{Na}(\text{THF})_y\text{C}_{60}$ single crystals.

IV-N-3 Magnetic Behaviors of High-Temperature Reaction Products of Cerium Metal and C_{60} Solid

MARUYAMA, Yusei¹; SUZUKI, Kenji¹; TAKAGI, Sigenori¹; MOTOHASHI, Satoru¹; OGATA, Hironori
(¹Housei Univ.)

Exohedral metal doping or intercalation to C_{60} solids has been known to be a very important method to modify the solid state properties of C_{60} dramatically. In this study we have used Ce metal as the dopant which has the lowest melting point, 1072 K, among the lanthanide elements and has relatively low ionization potential, 5.54 eV, because it might react with C_{60} solid in the liquid state. Ce metal powder and C_{60} powder were mixed at the nominal stoichiometry of (1.5-1.8):1 in a quartz tube under argon atmosphere and sealed off with 50 Torr He gas after evacuation. The samples were heated in an electric furnace at 650, 700, 750, 800, 850, 900 and 1100 °C for several to 10 hours respectively. The temperature dependence of the magnetizations clearly shows the existence of ferromagnetism in these samples which could be originated in the $4f^1$ electrons of Ce^{3+} ions. Figure 1 shows the M - T curve for 650 °C sample. The ZFC curve in Figure 1 is indicating the diamagnetic contribution in the temperature region of 5–15 K against the ferromagnetic uptake of the magnetization. The M - T curve for 1100 °C sample is shown in Figure 2. Negative magnetization is clearly observed below 10.5 K in the ZFC curve as shown in Figure 2, which may indicate the occurrence of superconductivity in this system.

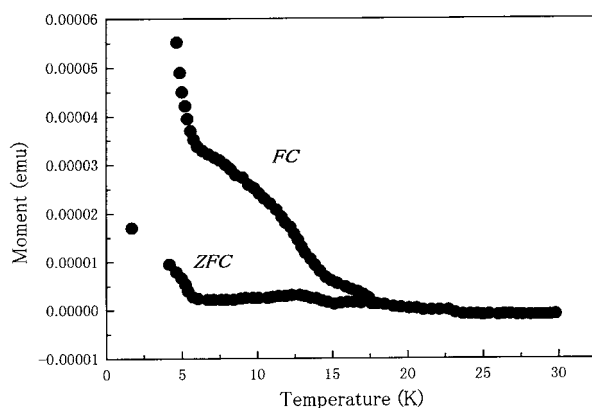


Figure 1. M - T curve of $\text{Ce}_{1.5}\text{C}_{60}$ reacted at 650 °C.

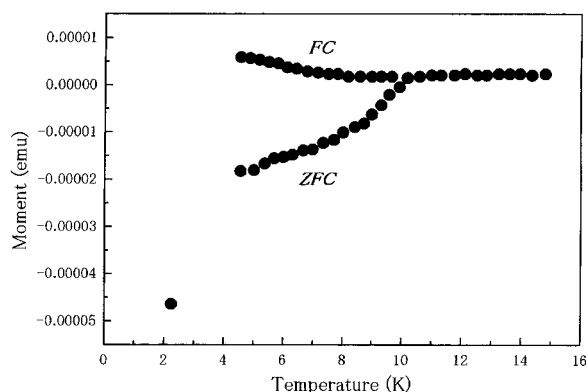


Figure 2. M - T curve $\text{Ce}_{1.5}\text{C}_{60}$ reacted at 1100 °C.

IV-N-4 Structure and Raman Scatterings of Cs_3C_{60} under High Pressure

FUJIKI, Satoshi¹; KUBOZONO, Yoshihiro¹; TAKABAYASHI, Yasuhiro¹; KASHINO, Setsuo¹; EMURA, Shuichi²; FUJIWARA, Akihiko³; ISHII, Kenji³; SUEMATSU, Hiroyoshi³; MURAKAMI, Youichi⁴; IWASA, Yoshihiro⁵; MITANI, Tadaaki⁵; OGATA, Hironori

(¹Okayama Univ.; ²Osaka Univ.; ³Univ. Tokyo; ⁴KEK-PF; ⁵JAIST)

Raman scatterings for a pressure induced superconductor Cs_3C_{60} were studied in a pressure region from 1 bar to 62 kbar. The center frequency ω_0 for $H_g(1)$ and $H_g(2)$ Raman peaks increased by applying pressure, but it showed a saturation in high pressure region. On the other hand, the ω_0 for $A_g(1)$ and $A_g(2)$ modes increased straightforwardly in all pressure region. The electron-phonon coupling constant for Cs_3C_{60} showed no increase at high pressures. X-ray powder diffraction patterns at 11 K under a pressure of 40 kbar showed that a superconducting phase for Cs_3C_{60} was body-centered orthorhombic.

IV-O Magnetic Local Structure and Magnetic Interactions in Molecule Based and Organic-Inorganic Hybrid Magnets

Organic ferromagnet is one of the realizations of great possibilities of organic molecules which can be designed to exhibit a variety of functions by chemical modifications and attracts interest of chemists in broad areas such as organic, physical, and theoretical chemistry, *etc.* Ferromagnetism of organic materials is of current interest. It is desired to clarify the mechanism of intermolecular magnetic interaction in a microscopic viewpoint to establish a leading principle to produce the ferromagnetic ordering in the crystalline phase of molecule based materials and to understanding the characters and the functions of open-cell molecules. Solid state high resolution NMR techniques provide an unique information of the magnetic local structure and the magnetic interactions in a microscopic view point. We have investigated the magnetic local structure and magnetic interaction for a variety of magnetic materials including a class of organic-inorganic hybrid magnetic materials. Botallackite-type compounds $\text{Cu}_2(\text{OH})_3\text{X}$ (X = exchangeable anion) exhibit layered structures, in which a nonequilateral planar triangular lattice of copper ions is constructed. The copper ions are bridged by hydroxide ions and exchangeable anions X to form infinite layers. A variety of anions X can be incorporated by anion-exchange in suspended solution and the bulk magnetism of $\text{Cu}_2(\text{OH})_3\text{X}$ is controlled by the property of X .

IV-O-1 Solid State High Resolution Deuterium NMR Study of Electron Spin Density Distribution of Hydrogen-bonded Organic Ferromagnetic Compound 4-Hydroxyimino-TEMPO

MARUTA, Goro¹; TAKEDA, Sadamu^{2,3}; IMACHI, Ron⁴; ISHIDA, Takayuki⁴; NOGAMI, Takashi⁴; YAMAGUCHI, Kizashi¹

(¹Osaka Univ.; ²Gunma Univ.; ³IMS; ⁴Univ. Electro-Commun.)

[*J. Am. Chem. Soc.* **121**, 424 (1999).]

Electron spin density distribution at hydrogen atoms of 4-hydroxyimino-2,2,6,6-tetramethylpiperidin-1-ylloxyl (4-hydroxyimino-TEMPO), which has been recently found to be a molecular ferromagnet at low temperature, was determined in the crystalline phase from the temperature dependence of the Fermi contact shifts of magic angle spinning deuterium NMR spectrum to elucidate the mechanism of intermolecular magnetic interaction. There are two kinds of close contacts among neighboring radical molecules in the crystalline phase. An axial methyl hydrogen atom locates closely to a neighboring N-O radical group and the hydroxyl group forms hydrogen-bonding with another neighboring N-O radical group. The plus and minus signs of observed hyperfine coupling constants A_D of methyl deuteriums indicate that two different mechanisms of electron spin density distribution exist. Equatorial CD_3 groups show negative coupling constants ($A_D = -0.24$ MHz) induced by the intramolecular spin polarization mechanism, whereas positive hyperfine coupling constants ($A_D = +0.12$ MHz) of axial CD_3 groups indicate that a single occupied MO spreads out partly toward the axial CD_3 groups by the mechanism of hyperconjugation. The small positive hyperfine coupling constant of the axial methyl group is brought about from averaging among one positive and two negative values of the three deuterium atoms of the methyl group due to rapid rotation. The intermolecular magnetic interaction through the axial methyl group seems to be sensitive to the orientation of the methyl group and it can be ferromagnetic in the crystal of 4-hydroxyimino-TEMPO. A large negative hyperfine

coupling constant ($A_D = -0.45$ MHz) observed for the NOD group strongly implies that the hydrogen-bonding mediates the intermolecular magnetic interaction in the crystalline phase. The experimental results and the molecular orbital calculations indicate that the ferromagnetic interaction exists in the hydrogen-bonded chains running along the crystallographic *c* axis and that the two chains are considered to be coupled ferromagnetically through the axial methyl groups to form a double chain. In the directions of crystallographic *a* and *b* axes, weak ferromagnetic interactions are expected from the measured spin density distributions of the deuterium atoms of the equatorial methyl and of the methylene groups which participate in inter-chain contacts in a crystallographic *a-b* plane.

IV-O-2 Magic Angle Spinning ¹H-NMR Study of the Spin Density Distribution of Pyridyl Nitronyl Nitroxides in the Crystalline Phase

MARUTA, Goro¹; TAKEDA, Sadamu^{2,3}; YAMAGUCHI, Akira⁴; OKUNO, Tsunehisa⁴; AWAGA, Kunio⁴; YAMAGUCHI, Kizashi¹

(¹Osaka Univ.; ²Gunma Univ.; ³IMS; ⁴Univ. Tokyo)

[*Mol. Cryst. Liq. Cryst.* **334**, 295 (1999)]

Electron spin density distribution was investigated for *p*- and *m*-pyridyl nitronyl nitroxides (*p*-PYNN and *m*-PYNN) in the crystalline phase by the temperature dependence of the solid state high-resolution ¹H-MAS NMR spectrum. The results were compared with that of phenyl nitronyl nitroxide (PNN) for elucidating the effect of incorporation of a nitrogen atom into the aromatic group. For *p*-PYNN, the magnitude of the negative spin density at 3 and 5 positions of the pyridyl group was suppressed by 30% in comparison with that of PNN and the positive spin density at 2 and 6 positions was slightly enhanced by 10%. On the other hand, the positive spin density at 2, 4 and 6 positions of pyridyl group of *m*-PYNN was suppressed by 30% in average and the negative one at 5 was also suppressed by 20%. The DFT calculation at UBLYP/6-31G(d,p) level suggested that the molecular geometry largely contributed to the change of the spin density in addition

to the effect of incorporation of the nitrogen atom. In fact, the spin density distribution of the aromatic ring of *p*-PYNM was remarkably reduced in solution compared with that in the crystalline phase.

IV-O-3 Local Magnetic Structure of Layered Compounds $\text{Cu}_2(\text{OD})_3\text{X}$ with Exchangeable Acid Anion X Studied by Solid State High Resolution Deuterium NMR

TAKEDA, Sadamu^{1,2}; MARUTA, Goro²; TERASAWA, Katsumasa; FUKUDA, Nobuya; YAMAGUCHI, Kizashi³

(¹Gunma Univ.; ²IMS; ³Osaka Univ.)

[*Mol. Cryst. Liq. Cryst.* **335**, 723 (1999)]

The microscopic magnetic local structure of Botallackite-type layer structured compounds $\text{Cu}_2(\text{OD})_3\text{X}$ ($\text{X} = \text{NO}_3^-$ and HCOO^-) exhibiting non-equilateral planar-triangular magnetic lattice was determined by the solid-state high-resolution deuterium NMR of deuterated hydroxy groups in the high temperature region above 190 K. The magnetic interactions in a copper ion layer were probed by the paramagnetic NMR shifts of the two chemically distinct hydroxy groups. Isotropic NMR shift of each hydroxy group showed different temperature dependence, suggesting non-uniform magnetic interaction. It appeared that the magnetic interaction in the copper layer could be decomposed to a sum of 1D-Heisenberg ferro- and antiferromagnetic chains in the high temperature region. Two distinct copper chains with ferro- and antiferromagnetic exchange interactions $J = +19 \pm 11$ and -21 ± 3 K were found for $\text{X} = \text{NO}_3^-$ from the temperature dependence of the two distinct NMR signals, while $J = +13 \pm 7$ and -13 ± 5 K for $\text{X} = \text{HCOO}^-$. The derived values of J almost reproduced the temperature behavior of the magnetic susceptibility χ_{AT} vs. T .

IV-O-4 Solid State High Resolution NMR Studies of Electron Spin Densities in Charge-Transfer Complex-Based Organic Ferromagnets

MARUTA, Goro¹; TAKEDA, Sadamu^{2,3}; YAMAGUCHI, Kizashi¹; UEDA, Kazumasa⁴; SUGIMOTO, Toyonari⁴

(¹Osaka Univ.; ²Gunma Univ.; ³IMS; ⁴Osaka Pref. Univ.)

[*Synth. Met.* **103**, 2333 (1999)]

A variety of purely organic ferromagnets, which consist of stable neutral radical species, have been developed. Charge-transfer complex-based organic ferromagnets are particularly of current interest because

of their potential to exhibit ferromagnetism at high temperatures. In these compounds, donor ($D^{\bullet+}$) and acceptor ($A^{\bullet-}$) can be designed to bear electron spins and electronic conduction can be also expected, so that the magnetic interaction in these salts may be different from those in neutral radical-based magnetic crystals and a novel magnetism is expected. A series of 4,4,5,5-tetramethylimidazolin-1-oxyls with 4-(*N*-R-pyridinium) groups at the 2-position (**1**^{•+}: R = methyl, **2**^{•+}: R = ethyl, **3**^{•+}: R = *n*-propyl) form stable charge transfer complexes with the radical anion of TCNQF₄. It has been revealed by the magnetic susceptibility measurements that **1**^{•+}·TCNQF₄^{•-} and **3**^{•+}·TCNQF₄^{•-} are ferromagnets at low temperature ($T_c \sim 0.5$ K), whereas **2**^{•+}·TCNQF₄^{•-} exhibits antiferromagnetic behavior. It is interesting to study the mechanism of magnetic interaction of these CT complexes. The mechanism can be elucidated from the electron spin density distribution in the magnetic crystals. In this work, we have determined the electron spin density distribution and the magnetic local structure in the salts of **1**^{•+}·TCNQF₄^{•-}, **2**^{•+}·TCNQF₄^{•-} and **3**^{•+}·TCNQF₄^{•-} by solid state high resolution ¹H, ¹³C and ¹⁹F-NMR.

IV-O-5 Variable Magnetism of Layer-Structured Compounds $\text{Cu}_2(\text{OD})_3\text{X}$ with Exchangeable Anion X: Magnetic Local Structure and Magnetic Interactions Determined by Solid-State High-Resolution Deuterium NMR

TAKEDA, Sadamu^{1,2}; ARAI, Masahiro¹; MARUTA, Goro³; YAMAGUCHI, Kizashi³

(¹Gunma Univ.; ²IMS; ³Osaka Univ.)

[*Mol. Cryst. Liq. Cryst.* in press]

The microscopic magnetic local structure of Botallackite-type layer-structured compounds $\text{Cu}_2(\text{OD})_3\text{X}$ ($\text{X} = \text{C}_6\text{H}_5\text{COO}^-$) was determined by the solid-state high-resolution deuterium NMR above 190 K. The magnetic interaction in a copper layer was probed by the isotropic NMR shifts of OD⁻ groups and could be approximated by a sum of 1D-Heisenberg chains in the high temperature region. Two copper chains with different exchange interactions $J = -54 \pm 4$ and -92 ± 3 K were found for $\text{Cu}_2(\text{OD})_3\text{C}_6\text{H}_5\text{COO}$ from the temperature dependence of the three distinct NMR signals. The derived values of J almost reproduced the high temperature behavior of the magnetic susceptibility χ_{AT} vs. T . The magnetic susceptibility of isotopic analogue $\text{Cu}_2(\text{OH})_3\text{C}_6\text{D}_5\text{COO}$ showed ferromagnetic interaction below 50 K. Electron spin distribution in a phenyl ring of a benzoate anion is governed by spin polarization mechanism and its magnitude is very small. Magnetic interaction between the layers through the benzoate anion is very weak.

IV-P Proton Transfer Tunneling in Interacting Hydrogen Bonds in the Solid State

Control of functional interactions, such as electronic and dynamic one, is a key to produce new functional materials. It is important to study the possibility of the functional interactions in the solid state. The nuclear magnetic resonance provides microscopic aspects of the functional interactions in the solid state. Hydrogen bond has a great capability for mediating a variety of interactions. We have investigated proton transfer dynamics in the interacting hydrogen bonds in organic quasi-conjugated π -system. Interaction between the hydrogen bonds is a key point for propagating an information of one hydrogen bond to the other hydrogen bond through molecular frame.

IV-P-1 Proton Dynamics in Interacting Hydrogen Bonds in the Solid State: Proton Tunneling in the NHO Hydrogen Bonds of N,N'-Di(2-Hydroxy-1-Naphthylmethylene)-p-Phenylenediamine

TAKEDA, Sadamu^{1,2}; INABE, Tamotsu³; BENEDICT, Claudia⁴; LANGER, Uwe⁴; LIMBACH, Hans-Heinrich⁴
(¹Gunma Univ.; ²IMS; ³Hokkaido Univ.; ⁴Freie Univ., Berlin)

[*Ber. Bunsen-Ges.* **102**, 1358 (1998)]

Combination of comprehensive investigations of the spin-lattice relaxation rate of proton and low temperature ¹⁵N-CP/MAS NMR spectrum provides unique information of proton dynamics in two interacting NHO hydrogen bonds of solid N,N'-di(2-hydroxy-1-naphthylmethylene)-p-phenylenediamine (DNP). It was evidenced from the ¹H-NMR relaxation measurement that tunneling mechanism operates for the proton transfer in the hydrogen bonds. The tunneling phenomenon is closely related to the very small energy differences among the four tautomeric states accompanied with the proton transfer in the two NHO hydrogen bonds. The very small values of the energy difference, in spite of the chemically asymmetric NHO hydrogen bond, were revealed by the ¹⁵N-CP/MAS NMR spectrum. This is a unique character of solid DNP. It was also suggested from the derived energy scheme of the four tautomers and activation energies of the proton transfer that an interaction exists between the two NHO hydrogen bonds linked by π -electronic molecular frame. This means that the information of one NHO hydrogen bond, *e.g.* OH-form or NH-form, propagates to the other hydrogen bond and the proton transfer in one hydrogen bond induces the change of the potential function for the proton transfer in the other hydrogen bond.

IV-Q Systematic Study of Organic Conductors

Thanks to the systematic view to structure-property relationship studied particularly in BEDT-TTF-based conductors, recently our understanding of organic conductors has made a great progress. From the concept of “universal phase diagram” in the θ -phase, we can predict metal-insulator transition temperatures of a large number of organic conductors. The underlying logic behind this universal view has been explained by the change of orbital overlap between adjacent molecules. Systematization of detailed stacking patterns in the β - and β' -phases has attempted, from which we can make a fairly good prediction to superconducting phases. These universal views are applied to individual cases, in particular to β -(BEDT-TTF)₂PF₆ family salts with twisted overlap mode, and to α' -phase salts, which are regarded as hybrid of the θ - and β' -phases, and actually whose properties are a complicated mixture of these parent phases.

IV-Q-1 Structural Genealogy of BEDT-TTF-Based Organic Conductors I. Parallel Molecules: β and β' Phases

MORI, Takehiko
(Tokyo Inst. Tech. and IMS)

[Bull. Chem. Soc. Jpn. **71**, 2509 (1998)]

A method is proposed to systematize a number of structural modifications of BEDT-TTF (bis(ethylenedithio)tetrathiafulvalene)-based organic conductors and related materials. Analysis of actual crystal structures indicates that most crystal structures are constructed of two essential building blocks: ring-over-bond (RB) and “ring-over-atom” (RA) overlap modes. Several different ways to pile up these elements lead to various structures which are conventionally designated as β , β' , β'' , θ , α , and α' -phases (Figure 1). In the β - and β' -phases, introduction of “dislocations” along the stacking axis generates a number of modifications, where dislocations are interactions of two donor molecules which have larger displacements along the molecular long axis than the standard RB and RA modes. Systematic nomenclature to distinguish these modifications are proposed. Transfer integrals are, however, not very sensitive to the existence of dislocations, so that the Fermi surfaces of these multiple phases are derived from the fundamental structure by folding the first Brillouin zone.

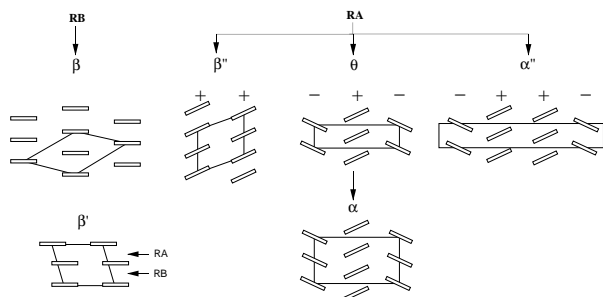


Figure 1. Genealogy of β , β' , β'' , θ , α , and α' -phases; the packing patterns of the donor sheets are viewed along the molecular long axis.

IV-Q-2 Structural Genealogy of BEDT-TTF-Based Organic Conductors II. Inclined Molecules: θ , α , and κ Phases

MORI, Takehiko¹; MORI, Hatsumi²; TANAKA, Shoji²

(¹Tokyo Inst. Tech. and IMS; ²ISTEC)

[Bull. Chem. Soc. Jpn. **72**, 179 (1999)]

Overlap integrals between HOMO's of two non-parallel BEDT-TTF (bis(ethylenedithio)tetrathiafulvalene) molecules have been calculated. As the dihedral angle between the molecular planes decreases from 180° (parallel) to 90° (perpendicular), the overlap integral increases and attains a maximum around 90°. This accounts for the “universal phase diagram” of the θ -phase; θ -salts vary from an insulator to a metal with decreasing the dihedral angle (Figure 1). The ratio of the lattice constants in the conducting plane, c/a , changes in proportion to the dihedral angle. Thus c/a can be used instead of the dihedral angle. A similar universal phase diagram is applicable to analogous phases like α and α' , and also to the corresponding phases of other donors. The properties of κ -phase salts are similarly scaled by c/a . As c/a increases, the intradimer overlap integral decreases owing to the increase of the intradimer spacing, and correlated insulator, superconductor, and simple-metal phases appear in succession. When c/a increases further, another insulating phase emerges due to the decrease of the interdimer overlaps. Chemical pressure in both θ - and κ -phases reduces c/a , and stabilizes the insulating state. Hydrostatic physical pressure gives the same influence in the θ -phase, but enhances the interdimer interaction in the κ -phase to result in the opposite effect. A diagram is proposed to illustrate which structures of β , β' , θ , and κ are favored by BEDT-TTF and other donors.

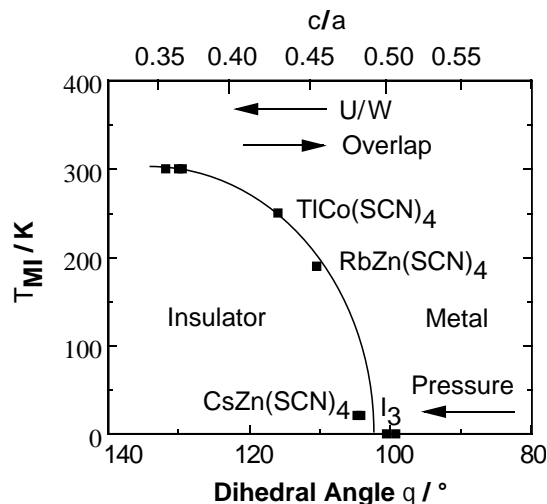


Figure 1. Universal phase diagram of the θ -phase.

IV-Q-3 $2k_F$ CDW Transition in β -(BEDT-TTF) $_2$ -PF $_6$ Family Salts

SENADEERA, G. K. Rohan¹; KAWAMOTO, Tadashi¹; MORI, Takehiko²; YAMAURA, Junichi¹; ENOKI, Toshiaki¹

(¹Tokyo Inst. Tech.; ²Tokyo Inst. Tech. and IMS)

[J. Phys. Soc. Jpn. **67**, 4193 (1998)]

In an attempt to clarify the nature of the metal insulator transition of β -(BEDT-TTF) $_2$ PF $_6$ family salts, temperature dependence of the static magnetic susceptibility, resistivity under various pressures, lattice parameters and the intensity of X-ray superlattice reflections have been measured for β -(BEDT-TTF) $_2$ PF $_6$ and β -(BEDT-TTF) $_2$ AsF $_6$. The transition temperature (T_{MI}) of these salts is shifted to higher temperatures with an increase of pressure. A sharp drop of the activation energy is observed at 5 kbar for the PF $_6$ salt and 6 kbar for the AsF $_6$ salt (Figure 1). Above these pressures, resistivity becomes almost flat down to low temperatures though the resistivity again increases below 50 K. Phase diagrams were constructed for both materials. Static magnetic susceptibilities of both salts exhibit abrupt drops below T_{MI} . A noticeable drop of the lattice parameters, lattice volumes and the X-ray intensities around T_{MI} indicate that the M-I transition is associated with the structural transition. The existence of the 2-fold structural changes is established by observing the superlattice reflections corresponding to (a , b , $2c$) below T_{MI} .

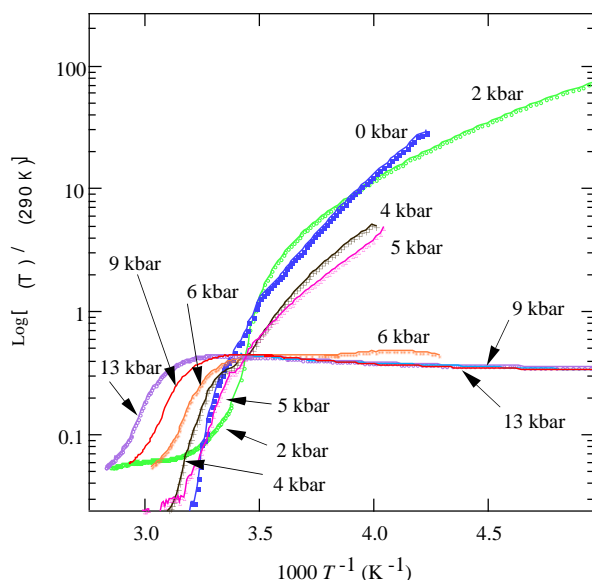


Figure 1. Temperature dependence of normalized resistivity for the PF $_6$ salt at different pressures: Arrhenius plots.

IV-Q-4 Transport Properties of α' -Phase Organic Conductors, (BEDT-TTF) $_2$ CsHg(SCN) $_4$ and (BEDT-TTF) $_2$ K $_{1.4}$ Co(SCN) $_4$

HANAZATO, Shiogo¹; MORI, Takehiko²; MORI, Hatsumi³; TANAKA, Shoji³

(¹Tokyo Inst. Tech.; ²Tokyo Inst. Tech. and IMS; ³ISTEC)

[Physica C **316**, 243 (1999)]

Under pressure, the metal-insulator transition temperature T_{MI} (210 K) of α' -(BEDT-TTF) $_2$ CsHg(SCN) $_4$ (BEDT-TTF: bis(ethylenedithio)tetrathiafulvalene) decreases up to 7 kbar, whereas above this pressure the system becomes more insulating as the pressure increases (Figure 1). This behavior is interpreted in view of the mixed β' -like and θ -like characters of the α' -phase. In this compound two-fold lattice modulation appears much above T_{MI} , even at room temperature. This indicates that the lattice modulation is not the direct origin of the M-I transition. In α' -(BEDT-TTF) $_2$ -K $_{1.4}$ Co(SCN) $_4$, T_{MI} (130 K) rises very slowly under pressure.

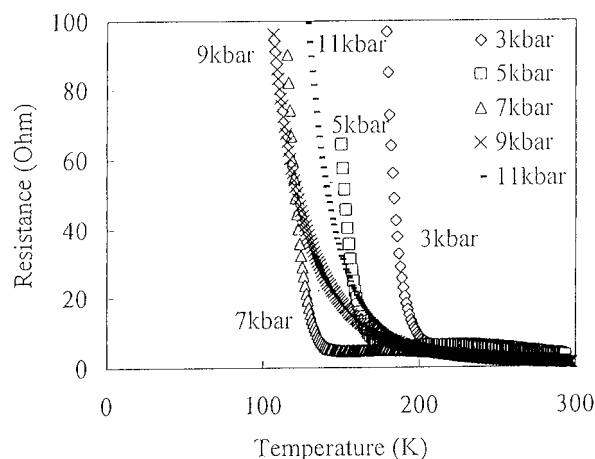


Figure 1. Temperature dependence of electrical resistance of α' -(BEDT-TTF) $_2$ CsHg(SCN) $_4$ under applied pressures.

RESEARCH ACTIVITIES V

Department of Applied Molecular Science

V-A Molecular Mechanisms of Oxygen Activation by Heme Enzymes

By sharing a common prosthetic group, the heme enzymes such as cytochrome P450s, peroxidases, and catalases catalyze their own unique biological functions; monooxygenation, hydrogen peroxide dependent oxidation, and dismutation of hydrogen peroxide, respectively. Our efforts have been focused on the elucidation of the structure-biological function relationship of those heme enzymes by employing both enzymic systems including mutants and their model systems.

V-A-1 Formation and Catalytic Roles of Compound I in the Hydrogen Peroxide-Dependent Oxidation by His64 Myoglobin Mutants

MATSUI, Toshitaka; OZAKI, Shin-ichi; WATANABE, Yoshihito

[*J. Am. Chem. Soc.* in press]

A His64 → Asp mutant of sperm whale myoglobin (Mb), H64D Mb, has been prepared to mimic the active site of chloroperoxidase from the marine fungus *Caldariomyces fumago*, in which distal glutamic acid is suggested to enhance the compound I formation by H₂O₂. The H64D mutant allows us to see the accumulation of compound I in the reaction of Mb with H₂O₂ for the first time (Figure 1). The successful observation of compound I is due to at least 50-fold improvement in the formation rate of compound I as well as its stabilization upon the His64 → Asp replacement. Catalytic activity of wild type Mb and a series of His64 Mb mutants (H64A, H64S, H64L, and H64D Mb) are examined for one-electron oxidation and oxygenation by using H₂O₂ as an oxidant. The H64D mutant is the best catalyst among the myoglobins and shows 50 ~ 70-fold and 600 ~ 800-fold higher activity than the wild type in the one-electron oxidations and peroxygenations, respectively. The origin of the varied activity upon the mutations are discussed on the basis of the formation rate and stability of compound I.

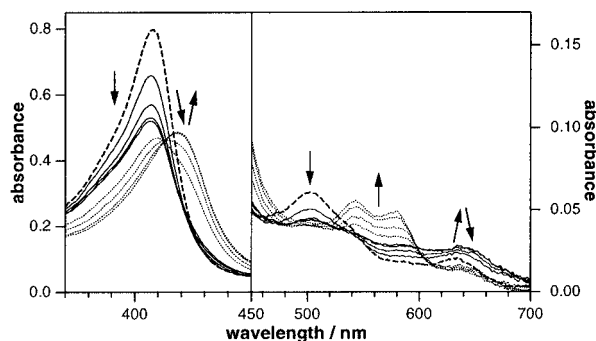


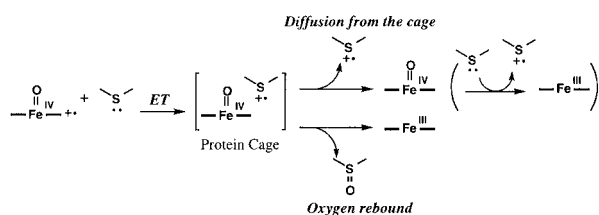
Figure 1. Spectral changes of H64D Mb in the reactions with 1 mM H₂O₂ at pH 7.0 and 20 °C. The spectra were recorded before mixing (broken line), at 10, 30, 60, 100, and 150 ms (solid lines), and at 1, 2, 4, and 6 sec (dotted lines) after mixing. For clarity, Soret and Visible regions are expanded and magnified, respectively.

V-A-2 The Mechanisms of *N*-Demethylation Catalyzed by Heme Enzymes: Mechanisms of Sulfoxidation Catalyzed by High-Valent Intermediates of Heme Enzymes: Electron Transfer vs Oxygen Transfer Mechanism

GOTO, Yoshio; MATSUI, Toshitaka; OZAKI, Shin-ichi; WATANABE, Yoshihito; FUKUZUMI, Shunichi¹ (¹Osaka Univ.)

[*J. Am. Chem. Soc.* in press]

Mechanisms of sulfoxidation catalyzed by high-valent intermediates of heme enzymes have been investigated by direct observation of sulfide induced reduction of three different compound I species including HRP (horseradish peroxidase), the His64Ser myoglobin (Mb) mutant and O=Fe^{IV}TMP⁺ (**1**) (TMP = 5,10,15,20-tetramesitylporphyrin dianion). The reaction of thioanisole and compound I of HRP (10 mM, pH 7.0, 298 K) gives the resting state of HRP with accumulation of compound II as an intermediate. The yield of sulfoxide by a stoichiometric reaction of HRP compound I with thioanisole was only 25 ± 5%. On the other hand, the same sulfoxidation by both **1** and His64Ser Mb compound I exclusively exhibited a two-electron process resulting in quantitative formation of sulfoxide. When 1,5-dithiacyclooctane (DTCO) is employed as a substrate, the reaction of His64Ser Mb compound I with DTCO exhibits rapid formation of compound II which decays to the ferric state due to the low oxidation potential of DTCO. The observed rate constants (log *k*_{obs}) of the reactions of **1** and compounds I of HRP and His64Ser Mb with a series of *p*-substituted thioanisoles correlate with the one-electron oxidation potentials (*E*⁰_{ox}) of the sulfides. A comparison of these correlations with the established correlation between log *k*_{obs} and *E*⁰_{ox} for the corresponding electron transfer reactions of substituted *N,N*-dimethylanilines has revealed that the sulfoxidation reactions of compound I of HRP with the sulfides proceed via electron transfer while the sulfoxidations catalyzed by **1** and compound I of His64Ser Mb occur via direct oxygen transfer.



Scheme 1. Electron Transfer vs. Direct Oxygen Transfer.

V-A-3 Effects of the Arrangement of a Distal Catalytic Residue on Regioselectivity and Reactivity in the Coupled Oxidation of Sperm Whale Myoglobin Mutants

MURAKAMI, Tatsuya¹; MORISHIMA, Isao¹; MATSUI, Toshitaka; OZAKI, Shin-ichi; HARA, Isao; YANG, Hui-Jun; WATANABE, Yoshihito (¹Kyoto Univ.),

[*J. Am. Chem. Soc.* **121**, 2007 (1999)]

Heme oxygenase is a central monooxygenase of the heme catabolism and forms a stoichiometric complex

with protoheme IX. The enzyme utilizes electrons and molecular oxygen for the regioselective heme degradation to afford α -biliverdin and carbon monoxide (CO) through three sequential oxygenase reactions. To understand factors which control the high regioselectivity, the regiospecific heme degradation of sperm whale myoglobin (Mb) mutants has been performed L29H/H64L myoglobin (Mb) almost exclusively gives biliverdin IX γ although H64L and wild type Mb mainly affords the α -isomer. Relocation of the distal histidine at the 43, and 107 position increases the amount of γ -isomer to 44 and 22%, respectively. Interestingly, the increase in the ratio of γ -isomer is also observed by a single replacement of either His-64 with Asp or Phe-43 with Trp. It appears that the polarity of the active site as well as hydrogen bonding between oxygen molecule bound to the heme iron and His or Trp is important in controlling the regioselectivity. The results of coupled oxidation kinetics, autooxidation kinetics, and redox potential of $\text{Fe}^{3+}/\text{Fe}^{2+}$ couple are discussed with regards to their implications for the active site and mechanism of heme oxygenase.

V-B Model Studies of Non-Heme Proteins

Non-heme proteins play important roles in biological redox processes. Many reactions catalyzed by the non-heme enzymes are quite similar to those by hemoproteins. We are interested in the active intermediates responsible for oxidation and oxygenation by non-heme enzyme, especially the similarity and differences.

V-B-1 A Model for Peroxo Intermediates in Reactions Catalyzed by Non-Heme Iron Enzymes

WADA, Akira¹; OGO, Seiji; WATANABE, Yoshihito; MUKAI, Masahiro; KITAGAWA, Teizo; JITSUKAWA, Koichiro¹; MASUDA, Hideki¹; EINAGA, Hisahiko¹ (¹Nagoya Inst. Tech.)

[*Inorg. Chem.* **38**, 3592 (1999)]

Thermodynamically extremely stable alkylperoxo-iron(III) complexes have first been prepared from reaction of the ternary iron(III) complex with a tripodal pyridylamine ligand, bis(6-pivalamido-2-pyridylmethyl)(2-pyridylmethyl)amine (BPPA), and trimethylacetate with alkylperoxide (*t*BuOO or $\text{C}_6\text{H}_5\text{C}(\text{CH}_3)\text{OO}$) in MeCN. The structure of the starting complex $[\text{Fe}(\text{bppa})(\text{tBuCOO})](\text{ClO}_4)_2$ (**1**) was determined by X-ray diffraction method. The electronic absorption spectra obtained by addition of aqueous solutions containing *t*BuOOH (TBHP) (69 w/w%) or $\text{C}_6\text{H}_5\text{C}(\text{CH}_3)\text{OOH}$ (CHP) (80 w/w%) to **1** showed characteristic bands at 613 nm ($\epsilon = 2000 \text{ M}^{-1}\text{cm}^{-1}$) or 585 nm ($\epsilon = 2200 \text{ M}^{-1}\text{cm}^{-1}$) assignable to an alkylperoxide-iron(III) charge transfer transition, respectively. The resonance Raman spectra revealed strong resonance-enhanced Raman features at 873, 838, 629, and 469 cm^{-1} and 878, 838, 639, 548, and 493 cm^{-1} , respectively. The ESI-mass spectra afforded positive and negative ion peaks at $m/z = 316.5$ and 932 corresponding to the ions, $[\text{Fe}(\text{bppa})(\text{tBuOO})]^{2+}$ and $\{[\text{Fe}(\text{bppa})(\text{tBuOO})](\text{ClO}_4)_3\}^-$, and at $m/z = 347.5$

and 994 assignable to $[\text{Fe}(\text{bppa})(\text{C}_6\text{H}_5\text{C}(\text{CH}_3)\text{OO})]^{2+}$ and $\{[\text{Fe}(\text{bppa})(\text{C}_6\text{H}_5\text{C}(\text{CH}_3)\text{OO})](\text{ClO}_4)_3\}^-$, respectively. The ESR spectra at 77 K demonstrated a typical high spin iron(III) state with small rhombic distortion ($g = 7.58, 5.81, 4.25, 1.82$, $E/D = 0.067$ and $g = 7.76, 5.65, 4.20, 1.78$, $E/D = 0.070$, respectively). The cyclic voltammetry of the starting complex **1** exhibited a quasi-reversible redox wave of the $\text{Fe}^{3+/2+}$ couple at +700 mV vs NHE that is fairly agreement with that in lipoxygenase. Their alkylperoxide complexes were successfully isolated as powder precipitates, and the UV-Vis, ESR, and ESI-mass spectra of the acetone or MeCN solutions containing the precipitates were almost the same as those in solution. The above findings strongly suggest that the reaction of **1** with alkylperoxide generated the extremely stable iron(III)-alkylperoxide complexes with seven-coordinate.

V-B-2 An Unusual Conversion of a $\text{Ni(III)}_2(\mu\text{-O})_2$ Core into a $\text{Ni(II)}_2(\mu\text{-OO})_2$ Core by H_2O_2 and Oxygenation of Ligand

SHIREN, Kazushi¹; OGO, Seiji; FUJINAMI, Shuhei¹; HAYASHI, Hideki¹; SUZUKI, Masatatsu¹; UEHARA, Akira¹; WATANABE, Yoshihito; MORO-OKA, Yoshihiko² (¹Kanazawa Univ.; ²Tokyo Inst. Tech.)

[*J. Am. Chem. Soc.* in press]

A six-coordinate bis(μ -oxo)nickel(III) complex, $[\text{Ni}_2(\mu\text{-O})_2(\text{Me}_3\text{-tpa})_2]^{2+}$ (**1**), was synthesized by

reaction of $[\text{Ni}_2(\mu\text{-OH})_2(\text{Me}_3\text{-tpa})_2]^{2+}$ (**2**) with 1 equiv. of hydrogen peroxide in methanol at -90°C , where $\text{Me}_3\text{-tpa}$ = tris(6-methyl-2-pyridylmethyl)amine. The 6-methyl groups of $\text{Me}_3\text{-tpa}$ have a significant influence on the formation and stabilization of the high-valent bis(μ -oxo)dinickel(III) species. Reaction of **2** with a large excess of hydrogen peroxide (> 10 equiv.) afforded a novel bis(μ -superoxo)dinickel(II) complex, $[\text{Ni}_2(\mu\text{-O}_2)_2(\text{Me}_3\text{-tpa})_2]^{2+}$ (**3**). The reaction demonstrates a unique conversion of a $\text{Ni}^{\text{III}}(\mu\text{-O})_2\text{Ni}^{\text{III}}$ core into a $\text{Ni}^{\text{II}}(\mu\text{-OO})_2\text{Ni}^{\text{II}}$ core upon exposure to hydrogen peroxide. Complexes **1**, **2**, and **3** were characterized by X-ray crystallography and various physicochemical techniques. Complex **1** has an edge-shared bioctahedral structure with a $\text{Ni}(\mu\text{-O})_2\text{Ni}$ core. Each nickel atom is coordinated by $\text{Me}_3\text{-tpa}$ to complete a distorted octahedral coordination sphere. The average Ni–O and Ni–N bond distances of **1** (1.871 and 2.143 Å, respectively) are significantly shorter than those of **2**, (2.018 and 2.185 Å, respectively), suggesting that **1** is a bis(μ -oxo)dinickel(III) complex. The crystal structure of **3** consists of a centrosymmetric $\text{Ni}(\mu\text{-OO})_2\text{Ni}$ core with $\text{Me}_3\text{-tpa}$ nitrogens. The nickel centers are in a distorted octahedral structure and linked by two μ -1,2-O–O bridges to form a six-membered ring with a chair conformation. The O–O bond distance is 1.345(6) Å, which is intermediate between those of the typical peroxo and superoxo complexes. The resonance Raman spectrum of a powdered sample of **3** measured at 110 K showed an isotope-sensitive band at 1096 cm^{-1} (1044 cm^{-1} for an ^{18}O labeled sample), indicating that **3** is a bis(μ -superoxo) $\text{Ni}_2(\text{II})$ complex. Thermal decomposition of both **1** and **3** in acetone at -20°C under N_2 atmosphere resulted in a partial hydroxylation of a methyl group of $\text{Me}_3\text{-tpa}$ in yield of 21–29% for both complexes. A carboxylate complex, $[\text{Ni}(\text{Me}_2\text{-tpaCOO})](\text{OH}_2)^+$ (**4**), where one of the three methyl groups of $\text{Me}_3\text{-tpa}$ is oxidized to carboxylate, was isolated from the decomposition under N_2 atmosphere. During the decomposition process, dioxygen evolution was simultaneously observed in yield of $35 \pm 4\%$. Thermal decomposition of **1** under O_2 atmosphere also gave **4**. The Electrospray ionization mass spectrometry (ESIMS) of **3** revealed the formation of **1** during the decomposition process. These results suggest that one possible decomposition pathway of **3** is a disproportionation of two coordinated superoxides to dioxygen and peroxide followed by the O–O bond scission of peroxide to regenerate **1**, which is responsible to the hydroxylation and the oxidation of the 6-methyl group of $\text{Me}_3\text{-tpa}$.

V-B-3 Structural and Functional Model Complexes for the Catechol-Bound Intermediate of Intradiol-Cleaving Catechol Dioxygenases

YAMAHARA, Ryo¹; OGO, Seiji; WATANABE, Yoshihito; FUNABIKI, Takuzo²; JITSUKAWA,

Koichiro¹; MASUDA, Hideki¹; EINAGA, Hisahiko¹
(¹Nagoya Inst. Tech.; ²Kyoto Univ.)

[*Inorg. Chim. Acta* in press]

This paper reports the synthesis and structures of (catecholato)iron(III) complexes with tetradentate tripodal ligands ($\text{L}_{\text{R}',\text{R}''} = \{2\text{-hydroxy-3-R}'\text{-5-R}''\text{-phenyl-bis(2-pyridylmethyl)amine}\}$) containing substituted phenol and pyridine units: $[\text{Fe}^{\text{III}}(\text{L}_{\text{R}',\text{R}''})(\text{DBC})]$ (**1a**: $\text{R}',\text{R}'' = \text{H,H}$, **1b**: $\text{R}',\text{R}'' = \text{Me,Me}$, and **1c**: $\text{R}',\text{R}'' = \text{H,Cl}$, $\text{DBC} = 3,5\text{-di-}t\text{-butylcatechol}$). X-ray structure analysis has revealed that the coordination arrangement around the iron atom of **1a** is very similar to that proposed for the active site of the catechol-bound intermediate of protocatechuate 3,4-dioxygenase (3,4-PCD). The series of complex **1** derivatives has been synthesized by two different methods: (i) reaction of $[\text{Fe}^{\text{III}}(\text{L}_{\text{R}',\text{R}''})(\text{acac})]^+$ (**2a**: $\text{R}',\text{R}'' = \text{H,H}$, **2b**: $\text{R}',\text{R}'' = \text{Me,Me}$, and **2c**: $\text{R}',\text{R}'' = \text{H,Cl}$, $\text{acac} = \text{acetylacetonate}$) with 1 equiv. of DBC and 1 equiv. of Et_3N in *N,N*-dimethylformamide, and (ii) reaction of $[\text{Fe}^{\text{III}}(\text{L}_{\text{R}',\text{R}''})\text{Cl}_2]$ (**3a**: $\text{R}',\text{R}'' = \text{H,H}$, **3b**: $\text{R}',\text{R}'' = \text{Me,Me}$, and **3c**: $\text{R}',\text{R}'' = \text{H,Cl}$) with 2 equiv. of AgOTf ($\text{OTf} = \text{O}_3\text{SCF}_3^-$), 1 equiv. of the catechols, and 2 equiv. of Et_3N in DMF. The exogenous acac ligand of **2** acts as a Lewis-base like the Tyr447 ligand in the active site of 3,4-PCD in the formation of the catechol-bound intermediate. Complexes **1**, **2**, and **3** have been characterized by X-ray analysis, visible and EPR spectroscopies, and cyclic voltammetry. Oxygenation of the bound DBC on **1** in the presence of O_2 has also been investigated and is discussed based on the Lewis basicity of the tripodal ligand containing the substituted phenolato group which is introduced to mimic the Tyr408 ligand of 3,4-PCD.

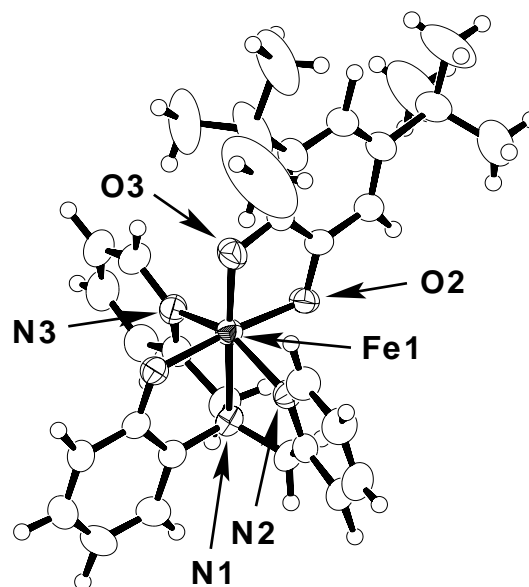


Figure 1. ORTEP drawing of **1a**.

V-C Transition Metal Oxide Clusters

Organometallic oxide clusters with cubic and incomplete cubic frameworks have useful applications as homogeneous and heterogeneous catalysts for reactions such as the oxidation and metathesis of propene. Understanding of the formation mechanisms of such oxide clusters may lead to the further development of synthetic methodologies for the construction of desired clusters having efficient catalytic ability for hydrocarbon transformations.

V-C-1 Direct Observation by Electrospray Ionization Mass Spectrometry of a Key Intermediate in the Formation of a Double Bookshelf-Type Oxide Cluster

TAKARA, Satoshi¹; OGO, Seiji; NISHIKAWA, Koji¹; KINOSHITA, Isamu¹; ISOBE, Kiyoshi¹; WATANABE, Yoshihito
(¹Osaka City Univ.)

[*Angew. Chem., Int. Ed. Engl.* in press]

We have found that a 1:4 reaction of [$[\text{Cp}^*\text{Rh}(\text{m-Cl})\text{Cl}]_2$] (**1**) and [$(n\text{Bu})_4\text{N}]_2[\text{Mo}_2\text{O}_7]$] (**2**) in MeOH

quantitatively yields a double bookshelf-type oxide cluster [$(n\text{Bu})_4\text{N}]_2[(\text{Cp}^*\text{Rh})_2\text{Mo}_6\text{O}_{20}(\text{OMe})_2]$ (**3**) with a multi-incomplete cubic framework. We have investigated the formation mechanism of **3** by electrospray ionization mass spectrometry (ESI-MS) which allows us to detect unstable species generated in solution. Herein, we report a direct observation by ESI-MS of $[\text{Cp}^*\text{RhMo}_3\text{O}_8(\text{OMe})_5]^-$ (**3_{im}**; m/z 809), a key intermediate in the formation of **3** from the reaction of **1** and **2** in MeOH at -78°C . Time dependent-behavior of selected ions during the reaction of **1** and **2** was monitored by rapid scanning of ESI-MS. The existence of the methoxo ligands in **3_{im}** was confirmed by isotopic labeling experiments.

V-D Aqueous Organometallic Chemistry

In recent years, aqueous organometallic chemistry has been widely studied because of industrial advantages and environmental concerns. Few organometallic aqua complexes have been, until now, isolated and used as water-soluble reagents in aqueous media. We have investigated a homogeneous hydrogenation in aqueous media using organometallic aqua complexes whose structures and properties drastically change as a function of pH because of deprotonation of the aqua ligands.

V-D-1 A Unique pH-Dependent Transfer Hydrogenation of Water-Soluble Carbonyl Compounds with an Organometallic Aqua Complex as a Catalyst Precursor in Water

OGO, Seiji; MAKIHARA, Nobuyuki; WATANABE, Yoshihito

[*Organometallics* in press]

This paper reports a unique pH-dependent hydrogen transfer from HCOONa to water-soluble carbonyl compounds with an organometallic aqua complex $[\text{Cp}^*\text{Ir}^{\text{III}}(\text{H}_2\text{O})_3]^{2+}$ (**1**, $\text{Cp}^* = \eta^5\text{-C}_5\text{Me}_5$) as a catalyst precursor in water. The structure of **1** was unequivocally determined by X-ray analysis. Complex **1** is deprotonated to form a dinuclear complex $[(\text{Cp}^*\text{Ir}^{\text{III}})_2(\mu\text{-OH})_3]^+$ (**2**) at pH 3.2. ^1H NMR, IR, and electrospray ionization mass spectrometry (ESI-MS) experiments show that the active species in this catalytic reaction is a dinuclear μ -hydride complex $[(\text{Cp}^*\text{Ir}^{\text{III}})_2(\mu\text{-H})(\mu\text{-OH})(\mu\text{-HCOO})]^+$ (**3**). The rate of this transfer hydrogenation shows a sharp maximum at pH 3.2. The series of carbonyl compounds used in this catalytic reaction are a straight chain aldehyde (*n*-butyraldehyde), a cyclic aldehyde (cyclopropanecarboxaldehyde), a ketone (2-butanone), an aldehyde-acid (glyoxylic acid), and a keto-acid (pyruvic acid).

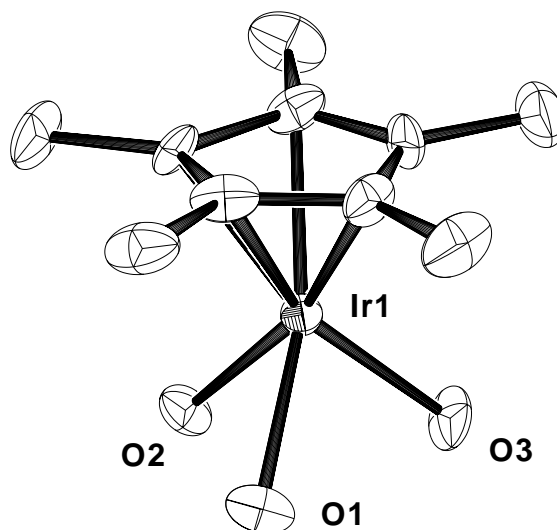


Figure 1. ORTEP drawing of **1**.

V-E Synthesis of New High-spin Molecule

Design and synthesis of organic molecules with high-spin ground states are current subjects of great importance. When three unpaired electrons are placed in proximity and allowed to interact magnetically, 1,3,5-Benzenetriyl unit can be deemed superior to *m*-phenylene unit in assembling organic free radical centers in higher concentrations within a molecule and aligning those spins in parallel for the purpose of designing and constructing very high-spin organic molecules. While some 1,3,5-trisubstituted benzene derivatives having nitronyl nitroxides, diarylmethyl radicals, diphenylamine cation radicals, phenylcarbene, and nitrenes as substituents are reported to be with high-spin ground states, they are either not persistent under ambient conditions or the intraradical couplings are not strong enough in magnitude.

V-E-1 Structure and Magnetic Property of the Organic Triradical with Triazine Skeleton; 1,3,5-Tris[*p*-(*N*-oxy-*N*-*tert*-butylamino)-phenyl]triazine

HAYAMI, Shinya; INOUE, Katsuya

[*Chem. Lett.* 545 (1999)]

1,3,5-tris[*p*-(*N*-oxy-*N*-*tert*-butylamino)phenyl]benzene has been known as persistent triradical with quartet ground state. New triradical with triazine skeleton was synthesized and characterized. Nitroxide triradical with triazine derivative 1,3,5-tris[*p*-(*N*-oxy-*N*-*tert*-butylamino)phenyl]triazine (**1**) exhibits stronger intramolecular ferromagnetic interaction than that with benzene derivative 1,3,5-tris[*p*-(*N*-oxy-*N*-*tert*-butylamino)phenyl]-benzene (**2**), the magnitude of the interactions depends on the planarity of the structures and/or on the spin density of center skeletons. Temperature dependence of the effective magnetic moments values observed for crystalline **1** in 1.8–350 K. The simulation of an isosceles-triangular exchange coupling model gave $J_1/k_B = 14.7$ K, $\gamma = 0.87$, and $\theta = -5.43$ K.

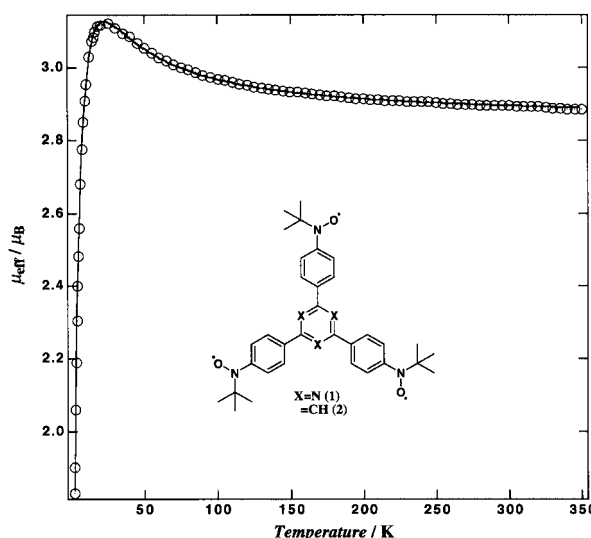


Figure 1. Temperature dependence of effective magnetic moment μ_{eff} values of **1** in neat crystals. Solid curve is a theoretical one.

V-F Construction of New Molecule-Based Magnets

Construction of molecular based magnetic materials which have well-defined one- or two-dimensional magnetic structure is a scientific subject of increasing interest. Heterospin systems consisting of paramagnetic transition metal ions and organic free radicals as ligands constitute one of the mainstreams of such studies. Several of these materials have been established to have finite critical temperature of a ferro- or ferrimagnetic transition.

We have introduced a new strategy of employing π -conjugated polyaminooxyls as ligands in which the $2p$ -spins of the NO groups interact ferromagnetically ($J_1 > 0$). The dimensionality of the complex and the sign and magnitude of the exchange coupling between the neighboring spins may be readily tuned by this strategy. Depending on the nature of the additional interchain or interlayer interaction, the polymers are expected to become an antiferromagnet or ferri/ferromagnet. By modifying and extending this design strategy to bis- and tris(aminooxyl) radicals having triplet and quartet ground states, respectively, we have been able to construct with the aid of magnetic metal ions one-dimensional (1D) chain, two-dimensional (2D) network and three-dimensional (3D) parallel-crosses structures in which both the organic $2p$ and metallic $3d$ spins have been ordered in macroscopic scales. Since such a rational approach by self-assembly to the tailored extended systems having relevant physical properties is of great importance in materials synthesis.

V-F-1 One-Dimensional Ferro- and Ferri-magnetic Chains Made up of an Alternating Array of 1,3-Bis(*N*-*tert*-Butyl-*N*-oxy-amino)-benzene Derivatives and Mn(II)(hfac)₂

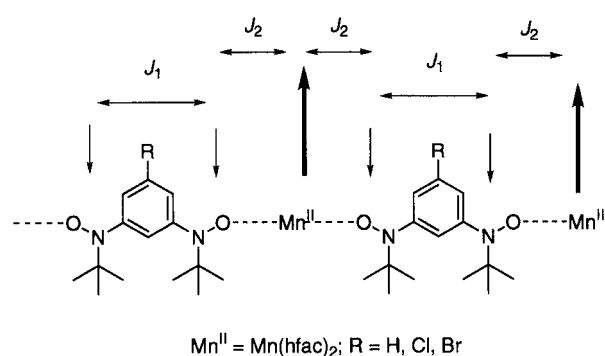
INOUE, Katsuya; IWAHORI, Fumiyasu¹; MARKOSYAN, Ashot S.^{2,3}; IWAMURA, Hiizu⁴
(¹GUAS.; ²M. V. Lomonosov Moscow State Univ.; ³IMS;

⁴Kyushu Univ.)

[*Coord. Chem. Rev.* in press]

Bis(hexafluoroacetylacetonato) manganese (II), Mn(hfac)₂, reacts with the bisnitroxide radicals, 5-R-1,3-Bis(*N*-*tert*-butyl-*N*-oxyamino)benzene **1_R** (R = H, Cl and Br), yielding 1-dimensional polymeric complexes

of formula $[\text{Mn}(\text{hfac})_2\mathbf{1}_R]_n$. X-ray analysis of the complexes has shown that they crystallize in the monoclinic, space group $P2_1/n$. In this structure, the manganese(II) ions and $\mathbf{1}_R$ molecules make up 1-D chains with the bisnitroxide radical serving as a bidentate ligand to $\text{Mn}(\text{II})(\text{hfac})_2$. The $\mathbf{1}_H$ complex orders antiferromagnetically at 5.5 K, while the $\mathbf{1}_{Cl}$ and $\mathbf{1}_{Br}$ complexes show ferrimagnetic order at 4.8 and 5.3 K, respectively. The intrachain exchange interaction parameters for a model of $S = 3/2$ ferromagnetic chains were found to be, $2J_{\text{eff}}/k = 23 \pm 2$ K in all the compounds. J_{eff} means effective magnetic exchange interaction between units of NO–Mn–NO. A change in the sign of the interchain exchange interaction is referred to the change of the shortest exchange path, from the Mn–F–N(*tert*-Bu)O·($\mathbf{1}_{Cl}$ and $\mathbf{1}_{Br}$) to N(*tert*-Bu)O–F–N(*tert*-Bu)O·($\mathbf{1}_H$).



Scheme 1.

Figure 1. Schematic drawing of magnetic structure for the complex a) $\text{Mn}(\text{hfac})_2\mathbf{1}_H$, b) $\text{Mn}(\text{hfac})_2\mathbf{1}_{Cl}$ and $\text{Mn}(\text{hfac})_2\mathbf{1}_{Br}$.

V-F-2 Influence of the Thermal Excitations of the Ferrimagnetic ($\bar{1}/2, 5/2, \bar{1}/2$) Linear Trimer on the Paramagnetic Behavior of the Layered Metal-Radical Complex $\{\text{Mn}(\text{hfac})_2\}_3(\mathbf{R}_N)_2 \cdot n\text{-C}_7\text{H}_{16}$

HOSOKOSHI, Yuko; INOUE, Katsuya; MARKOSYAN, Ashot S.^{1,2}
(¹IMS; ²M. V. Lomonosov Moscow State Univ.)

[Phys. Lett. A in press]

The complex $\{\text{Mn}(\text{hfac})_2\}_3(\mathbf{3R}_\Delta)_2 \cdot n\text{-C}_7\text{H}_{16}$ forms a two-dimensional honeycomb-like spin network. It is shown that the spins of Mn(II) form with the two $1/2$ -spins of different adjacent triradicals $\mathbf{3R}_\Delta$ linear ($\bar{1}/2, 5/2, \bar{1}/2$) ferrimagnetic trimers, which determine the paramagnetic properties of the complex. The intratrimer excitations result in the decay of the trimers above 140 K.

The experimental data can well be described within this model both at high and low temperatures thus proving the importance of the thermal excitations within the trimers. The best agreement was obtained at $J_{\text{TR}}/k_B = -176.4$ K and $= +0.333$ emu/mol. The power series expansion for the 2D honeycomb network gives $J_{\text{TR}}/k_B = -175.4$ K and $J_1/k_B = +0.226$ K.

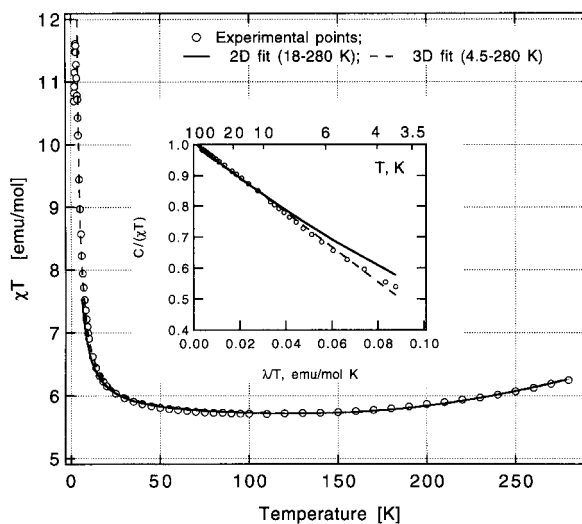


Figure 1. The temperature dependence of $\chi_m T$ for the 2D complex $\{\text{Mn}(\text{hfac})_2\}_3(\mathbf{3R}_\Delta)_2 \cdot n\text{-C}_7\text{H}_{16}$. Open circles are the experimental data, the solid and the dashed lines are the least squares fits for a 2D and 3D lattice, respectively. The inset shows the details of the low temperature behavior in the $C/\chi T$ versus λ'/T form.

V-G Mn(II)-Induced Formation of a [3+3] Benzene Dimer Derivatives

A number of studies have been conducted on the dimerization of aromatic compounds. Most of these compounds are formed by a Diels-Alder-type cycloaddition reaction, *i.e.* [2+2] or [2+4]. We found a unique aromatic [3+3] cycloaddition in the presence of Mn(II) ion. In the course of our study of self-assembly of magnetic metal ions and bis- and tris(aminoxyl) radicals described in V-F, we found the formation of a unique [3+3] benzene dimer structure as a side reaction. Some reports have described the [3+3] cycloaddition of organic molecules but not of aromatic compound. Our crystallographic characterization would help shed light on the mechanistic detail of Lewis acid-catalysed cycloaddition and free-radical reactions.

V-G-1 Mn(II)-Induced Formation and Structural Elucidation of a [3+3] Benzene Dimer Derivative from *m*-Phenylenebis(*N*-*tert*-butylaminoxyl)

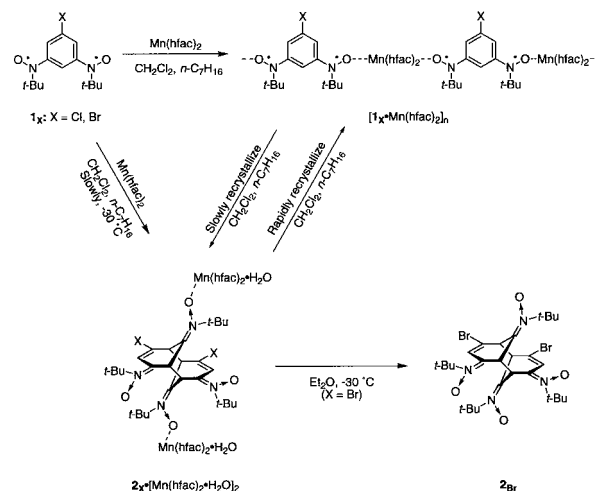
IWAHORI, Fumiyasu¹; INOUE, Katsuya;
IWAMURA, Hiizu²

(¹GUAS; ²Kyushu Univ.)

[*J. Am. Chem. Soc.* **121**, 7264 (1999)]

One-dimensional ferrimagnetic complexes, $[\text{Mn}(\text{hfac})_2 \cdot \mathbf{1}_X]_n$ ($X = \text{Cl}$ or Br), are typically obtained by the reaction of $\text{Mn}(\text{hfac})_2$ with $\mathbf{1}_X$. When it takes a few days for crystallization, however, black solutions often turn yellow in about one day and yellow crystalline precipitates are obtained. A solution of $\mathbf{1}_{\text{Br}}$ in CH_2Cl_2 was added to a suspension of $\text{Mn}(\text{hfac})_2$ in *n*- C_7H_{16} at 0 °C and the mixture was stored at -30 °C. After a few days, yellow needles of $\mathbf{2}_{\text{Br}} \cdot [\text{Mn}(\text{hfac})_2 \cdot \text{H}_2\text{O}]_2 \cdot \text{CH}_2\text{Cl}_2$ were obtained (85.2%). An X-ray structure analysis revealed that $\mathbf{2}_X \cdot [\text{Mn}(\text{hfac})_2 \cdot \text{H}_2\text{O}]_2 \cdot \text{CH}_2\text{Cl}_2$ has a [3+3] benzene-dimer structure $\{X = \text{Cl}$ or Br ; $\mathbf{2}_X = 3,10$ -dihalo-5,8,11,12-tetrakis(*N*-*tert*-butylimino)-tricyclo[5,3,1,1^{2,6}]dodeca-3,9-diene *N,N',N'',N'''*-tetraoxide}. When $\mathbf{2}_{\text{Br}} \cdot [\text{Mn}(\text{hfac})_2 \cdot \text{H}_2\text{O}]_2 \cdot \text{CH}_2\text{Cl}_2$ was dissolved in Et_2O and the solution was stored at -30 °C, white powder of $\mathbf{2}_{\text{Br}} \cdot 2\text{H}_2\text{O}$ free of $\text{Mn}(\text{hfac})_2$ precipitated

out in 30 minutes (68.8%). Spectroscopic data on $\mathbf{2}_{\text{Br}}$ are in good agreement with its structure. The spectra of $\mathbf{2}_{\text{Br}}$ in CH_2Cl_2 is time-dependent and converted eventually to that of monomeric biradical $\mathbf{1}_{\text{Br}}$ by showing four isosbestic points. The result indicates that the dissociation process of $\mathbf{2}_{\text{Br}}$ into two molecules of $\mathbf{1}_{\text{Br}}$ is very clean.



Scheme 1. Transverse scheme between [3+3] benzene derivatives and ID ferrimagnetic complexes.

V-H Synthesis of Chiral Molecule-Based Magnets

There is a phenomenological resemblance between natural and magnetic optical activity. The former is due to the handedness of molecular structure, whereas the latter is due to the magnetic field-induced circular dichroism. In 1984 Barron and Vrbancich call “magneto-chiral dichroism” (MChD) for a link between two phenomena. In 1997, Rikken and Raupach observed the MChD effect of tris(3-trifluoroacetyl- \pm -camphorato)europium (III) in the paramagnetic state. However, the MChD effect in the paramagnetic state is small. It's important to make the fully chiral molecule-based magnets, which expected to be strong MChD effect. There are still no examples of molecule-based chiral magnet. Novel properties are expected for such compounds.

The design of molecular materials with interesting electrical and/or magnetic properties is one of the major challenges of science in the last few years. It's possible to modify the molecular structure in the molecule-based magnetic materials. Recently, we introduced a strategy of using π -conjugated polyaminoxyl radicals with high-spin ground states as bridging ligands for magnetic metal ions in order to assemble and align the electron spins on a macroscopic scale. The crystal structures of these complexes are known, and some cases, the magnetic structures are analyzed. The dimensionality of the complex and the sign and magnitude of the exchange coupling between the neighboring spins may be readily tuned by this strategy. When we use a bidendate bisaminoxyl radicals as ligand and manganese(II) hexafluoroacetylacetonate, $\text{Mn}(\text{II})(\text{hfac})_2$, we can make one-dimensional complexes. If we use chiral triplet bisaminoxyl radicals for the construction of one-dimensional magnet, we can expect to make chiral molecule-based magnets.

V-H-1 A Chiral Molecule-based Metamagnet Made by a Chiral Triplet Organic Radical and Manganese Ion

KUMAGAI, Hitoshi; INOUE, Katsuya

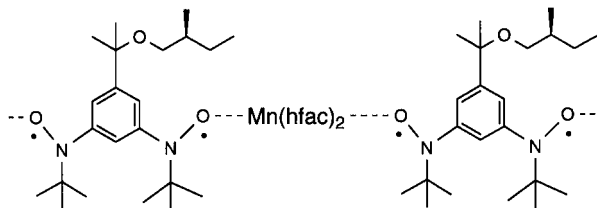
[*Angew. Chem., Int. Ed. Engl.* **38**, 1601 (1999).]

The chiral biradical, 1,3-bis(*N*-*tert*-butylamino-*N*-oxyl)-5-[1'-methyl-1'-{(*S*)-2''-methylbutoxy}]-ethylbenzene (**1**) was prepared and was mixed with an equimolar amount of dehydrated $\text{Mn}(\text{hfac})_2$ in diethyl ether/*n*-heptane and the mixture was evaporated. Deep brown block crystals were obtained in 1 day at -30 °C.

X-ray crystal structure analysis of the complex revealed the formation of a one-dimensional structure. (Scheme 1) The oxygen atoms of the terminal aminoxyl radicals of biradical **1** are ligated to two different manganese ions in *trans* position to form a one-dimensional helical chain along the *c* crystal axis. The bisaminoxylbenzene unit is in a chiral conformation and forms a (*R*)-helical structure.

The magnetization at 1.8 K revealed metamagnetic behavior (Figure 1); while the response of the magnetization was not sensitive to the weak applied magnetic field below *ca.* 500 Oe, a behavior characteristic of an antiferromagnet. A sharp rise and approach to saturation of magnetization characteristic of a ferromagnet was

observed at higher applied magnetic field. A saturation magnetization value of *ca.* 2.7 μ_B was reached at 1.8 K at 3 Tesla, which suggests the antiferromagnetic coupling between the manganese(II) ion and **1**.



Scheme 1. Polymeric chain structure of $[1 \cdot \text{Mn}(\text{hfac})_2]_n$.

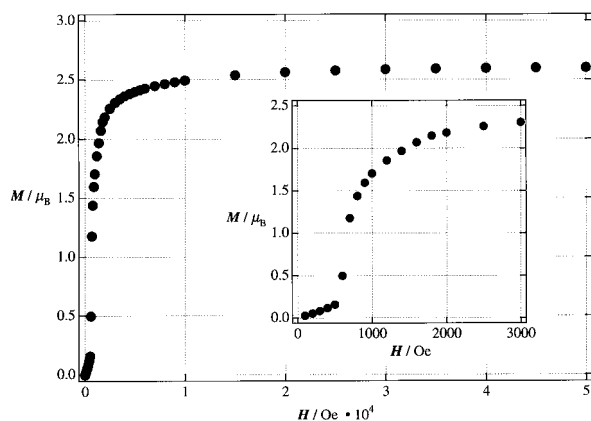


Figure 1. Field dependencies of the magnetic moment of a polycrystalline sample of $[1 \cdot \text{Mn}^{\text{II}}(\text{hfac})_2]_n$ at 1.8 K. Inset shows magnetic field range of 0 to 3000 Oe.

V-H-2 Synthesis and Characterization of a Novel Chiral Molecular-based Ferrimagnet Prepared from a Chiral Nitronyl Nitroxide Radical and Manganese(II) Ion

KUMAGAI, Hitoshi; INOUE, Katsuya

The chiral radical **2** was synthesized and was mixed with an equimolar amount of dehydrated $\text{Mn}(\text{hfac})_2$ in diethyl ether/*n*-heptane and the mixture was evaporated to *ca.* 10 ml. Green block crystals were obtained at -30°C in 1 week.

The X-ray crystal structure analysis revealed that both crystals of **2** and complex $[2 \cdot \text{Mn}^{\text{II}}(\text{hfac})_2]_n$ belongs to the same chiral space group $P2_12_12_1$ (No. 19). The molecular structure of $[2 \cdot \text{Mn}^{\text{II}}(\text{hfac})_2]_n$ is depicted in Figure 1. One-dimensional chain elongates along the crystal *a*-axis. The radicals are bound to the $\text{Mn}(\text{II})$ ion in cis-coordination to each other. In this complex, the metal center exhibits the all Δ configuration. Because of the use of the chiral ligand, the complex crystallized in chiral space group and no Λ chirality of the $\text{Mn}(\text{II})$ are existed in this crystal. Since no inversion centers are present in this space group, chains are isotactic as all units and the crystal lattice as a whole is chiral.

Magnetization measurements have been performed at 2 K. The magnetization increases very rapidly, and reaches a plateau about 3.6 B.M. at 1.5 T. This value suggests the antiferromagnetic coupling between the manganese(II) ion and **2** (Theoretical value is 4 B.M. ($5/2 - 1/2 = 4/2$)). AC susceptibility measurements revealed that $[2 \cdot \text{Mn}^{\text{II}}(\text{hfac})_2]_n$ behaves as ferrimagnet below 4.5 K. The existence of weak ferromagnetic interchain interaction is suggested.

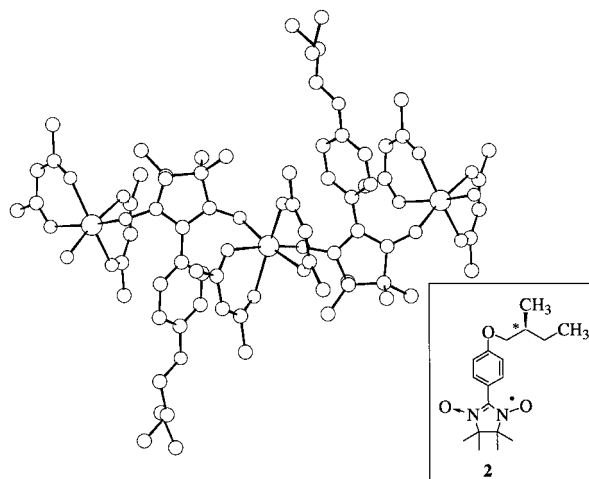


Figure 1. View of a helical chain formed by chiral nitronyl nitroxide **2** and $\text{Mn}(\text{II})(\text{hfac})_2$. Hydrogen atoms and fluorine atoms are omitted for clarity

V-I Synthesis and Characterization of Quantum-Spin Systems

Quantum spin systems have been much attracted for several decades. Haldane's conjecture in 1983 on the difference between a Heisenberg antiferromagnetic chain of integer-spin magnitude and that of half-integer-spin magnitude called renewed interest. The properties of $S = 1$ spin chain with a finite energy gap between the ground state and excited states have been extensively studied both theoretically and experimentally. Then, interested is the crossover between the dimer state and Haldane state, for example, in the $S = 1/2$ alternating chain with ferromagnetic and antiferromagnetic interactions. We have designed and synthesized two types of $S = 1/2$ chains with ferromagnetic and antiferromagnetic interactions. Moreover, we made a two-dimensional antiferromagnetic lattice of the ferromagnetic spin pairs. Another topic is the double chain systems, which is interesting from the aspect of the Haldane state and high T_C superconductivity. We designed and synthesized a railroad trestle compound and observed the existence of an energy gap above the singlet ground state.

V-I-1 Magnetic Properties of Low Dimensional Quantum Spin Systems Made of Stable Organic Biradicals PNNNO, F₂PNNNO and PIMNO

HOSOKOSHI, Yuko; NAKAZAWA, Yasuhiro; INOUE, Katsuya; TAKIZAWA, Kohichi¹; NAKANO, Hiroki¹; TAKAHASHI, Minoru¹; GOTO, Tsuneaki¹
(¹ISSP, Univ. Tokyo)

[Phys. Rev. B in press]

Stable organic biradical crystals PNNNO, F₂PNNNO and PIMNO of the PNNNO family were synthesized. (PNNNO = 2-[4'-(*N*-*tert*-butyl-*N*-oxyamino)phenyl]-4,4,5,5-tetramethyl-4,5-dihydro-1*H*-imidazol-1-oxyl 3-oxide, F₂PNNNO = 2-[2',6'-difluoro-4'-(*N*-*tert*-butyl-*N*-oxyamino)phenyl]-4,4,5,5-tetramethyl-4,5-dihydro-1*H*-imidazol-1-oxyl 3-oxide, PIMNO = 2-[4'-(*N*-*tert*-butyl-*N*-oxyamino)-phenyl]-4,4,5,5-tetramethyl-4,5-dihydro-1*H*-imidazol-1-oxyl) PNNNO and PIMNO crystallize to form quasi-one-dimensional lattices, but F₂PNNNO to form a quasi-two-dimensional lattice. The temperature dependences of the susceptibility and the high-field magnetization process up to 34 T were measured down to 0.5 K. The results are analysed by comparing with the theoretical calculations based on the crystal structures. PNNNO and PIMNO are considered to be antiferromagnetic Heisenberg spin chains consisting of $S = 1/2$ spin pairs (dimers) in which the two spins are coupled ferromagnetically. Both compounds undergo antiferromagnetic phase transitions at 1.1 and 2.5 K, respectively due to weak interchain interactions. The three-dimensional nature of the transition is examined by the thermodynamic discussion through specific heat measurements. On the other hand, F₂PNNNO is thought to be a two-dimensional Heisenberg system, in which the spin pairs are connected by two types of antiferromagnetic interactions. The magnetism of F₂PNNNO is characterized by the singlet ground state and a plateau in the magnetization isotherm.

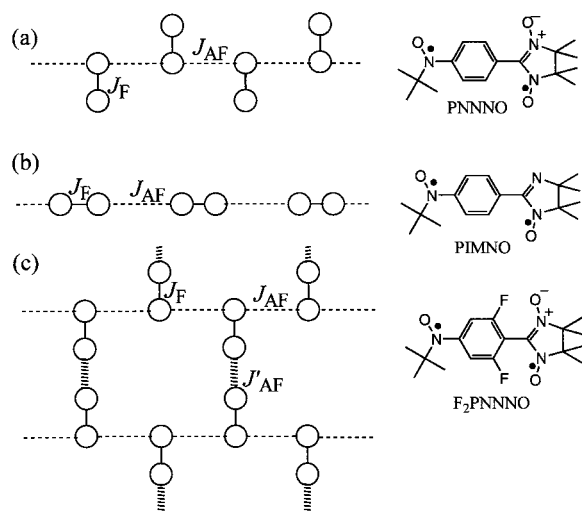


Figure 1. Scheme of the magnetic interactions in (a) PNNNO, (b) PIMNO and (c) F₂PNNNO with their molecular structures.

V-I-2 Construction of a Quantum-Spin System of $S = 1/2$ Antiferromagnetic Chain with the Next-Nearest-Neighbor Interactions

HOSOKOSHI, Yuko; KATOH, Keiichi¹; INOUE, Katsuya; GOTO, Tsuneaki¹
(¹ISSP, Univ. Tokyo)

[J. Phys. Soc. Jpn. **68**, 2910 (1999)]

We have succeeded in synthesizing a new compound with a railroad trestle structure, *i.e.*, a zigzag chain with next-nearest-neighbor interactions. We have newly synthesized organic radicals F₂PIMNH and Cl₂PIMNH, where F₂PIMNH = 2-[4'-*N*-*tert*-butylamino-2',6'-difluorophenyl]-4,4,5,5-tetramethyl-4,5-dihydro-1*H*-imidazol-1-oxyl and Cl₂PIMNH = 2-[4'-*N*-*tert*-butylamino-2',6'-dichlorophenyl]-4,4,5,5-tetramethyl-4,5-dihydro-1*H*-imidazol-1-oxyl. Both crystals include zigzag uniform chains made of hydrogen bondings. The magnetism of Cl₂PIMNH is explained by the Heisenberg antiferromagnetic uniform chain model with $2J/k_B = -3.6$ K and gapless ground state is suggested. On the other hand, static magnetic measurements of F₂PIMNH suggest the nonmagnetic ground state and the existence of a finite gap in its excitation spectrum. In this crystal, the next-nearest-neighbor contacts are seen, which are believed to be the origin of the energy gap.

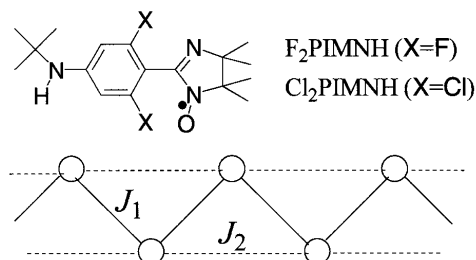


Figure 1. Scheme of the magnetic interactions in F₂PIMNH. Uniform chain with the next nearest neighbor interactions.

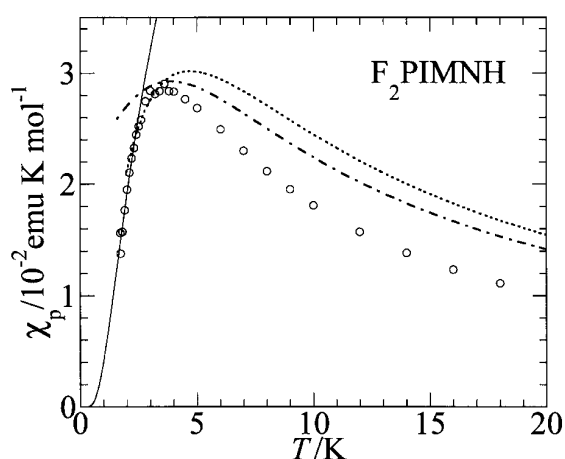


Figure 2. (a) Temperature dependence of χ_p of F₂PIMNH. The solid curve is the fit of $\chi \propto \exp\{-\Delta/T\}$ with $\Delta = 3.1$ K. The dotted broken curve is the calculation for the uniform chain with $2J/k_B = -6$ K, the interchain interactions by the mean-field treatment of $2zJ'/k_B = -5.2$ K are adopted. The dotted curve represents the calculation for the alternating chain with $2J_1/k_B = -7.9$ K and $2J_2/k_B = -6.3$ K.

V-J Pressure Effects on Magnetic Materials

“Pressure” is a powerful tool to control the molecular packings and physical properties. The molecule-based materials with small densities are “soft” and can be expected to exhibit large pressure effects. For the magnetic measurements with high-accuracy, we have developed a small high-pressure clamp cell made of Cu-Ti alloy which can be equipped to a Quantum Design SQUID magnetometer for the dc and ac magnetic measurements. The inner pressure of the clamp cell has been calibrated by the superconducting transition temperature of Pb. The maximum pressure maintained is *ca.* 7 kbar, the reproducibility is good, and the temperature variation of pressure in the cell is within *ca.* 0.3 kbar.

We study the pressure effects on the molecule-based chain compounds. We have observed the pressure-induced phenomena of (1) crossover from an alternating chain to a uniform chain, (2) dimensional-crossover from 2D to 1D, and (3) change of the sign of the interchain interactions. We also apply the pressure to some intermetallic compounds which show large volume effects.

V-J-1 Pressure-Induced Crossover from Alternating to Uniform Interaction in an $S = 1/2$ One-Dimensional Heisenberg Antiferromagnet

MITO, Masaki¹; KAWAE, Tatsuya¹; HOSOKOSHI, Yuko; INOUE, Katsuya; KINOSHITA, Minoru²; TAKEDA, Kazuyoshi¹
(¹Kyushu Univ., ²Sci. Univ. Tokyo in Yamaguchi)

[*Solid State Commun.* **111**, 607 (1999)]

We have confirmed the pressure-induced crossover from the alternating to the uniform one-dimensional (1D) spin system in an organic compound as a function of applied pressure (*p*) by the measurements of heat capacity. The pentafluorophenyl nitronyl nitroxide radical (F₅PNN), which is the 1D alternating Heisenberg antiferromagnet of spin $S = 1/2$ with $\alpha = J_2/J_1 \sim 0.4$ at ambient pressure, has transformed into the uniform one ($\alpha = 1$) at *p* = 6.5 kbar. This pressure induced crossover was made clear by observing the change of initial gradient of heat capacity, which transformed from exponential to linear at low temperature. The crystal structure of F₅PNN at the room temperature and ambient pressure is of the uniform spin chain, and the pressure must play the role of suppressing the structural transition into the alternating system.

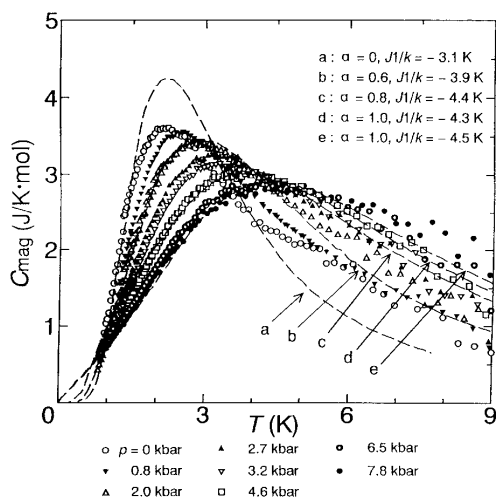


Figure 1. Temperature dependence of C_{mag} of F₅PNN under the pressure up to 7.8 kbar. The broken lines (a-e) express Duffy *et al.*'s theoretical curves of C_{mag} up to 7.8 kbar with such two parameters as α and J_1/k_B .

V-J-2 Pressure Effects on Organic Radicals with Ferromagnetic and Antiferromagnetic Interactions

HOSOKOSHI, Yuko; INOUE, Katsuya

[*Synth. Met.* **103**, 2323 (1999)]

Magnetic properties of stable organic biradicals under pressure are presented. The dimensional crossover from two-dimension to one-dimension is induced by pressure in F₂PNNNO, whereas the properties of the corresponding one-dimensional material, PNNNO is almost independent of the pressure. The phase transition temperature of the quasi-one-dimensional antiferromagnet, PIMNO become higher with applied pressure. The increase of the interchain interactions by pressurization has been observed, whereas the intrachain interactions are almost independent of the pressure.

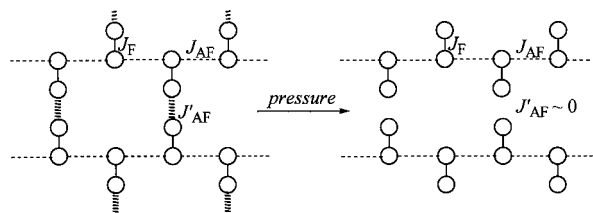


Figure 1. Scheme of the magnetic interactions in F₂PNNNO. Pressure-induced dimensional crossover from 2D to 1D.

V-J-3 Pressure Effect on Mn Complexes of Bisaminoxyl Radicals

HOSOKOSHI, Yuko; SUZUKI, Kentaro¹; INOUE, Katsuya; IWAMURA, Hiizu²
(¹GUAS; ²Kyushu Univ.)

[*Mol. Cryst. Liq. Cryst.* in press]

The pressure effects on magnetic properties of one-dimensional Mn complexes with 1,3-bis(*N-tert*-butylaminoxyl)benzene and 5-chloro-1,3-bis(*N-tert*-butylaminoxyl)benzene have been studied. These complexes have weak interchain interactions with different signs and the former is a metamagnet and the latter is a ferrimagnet at ambient pressure. The interchain interactions of the former is enhanced by pressurization. The transition temperature becomes higher and the critical

field becomes larger with applying pressure. The closer spacing of each chains caused by pressurization, yields larger antiferromagnetic interchain interactions in this compound.

On the other hand, the response to the pressure of the latter ferrimagnet, is rather complicated. The transition temperature becomes higher and the antiferromagnetic interchain interactions are induced by pressurization. The interchain exchange coupling in this compound should be sensitive to the relative orientation of the chain structure. The decrease of the ferromagnetic contribution and/or the increase of the antiferromagnetic one in the interchain interactions is brought about by pressurization.

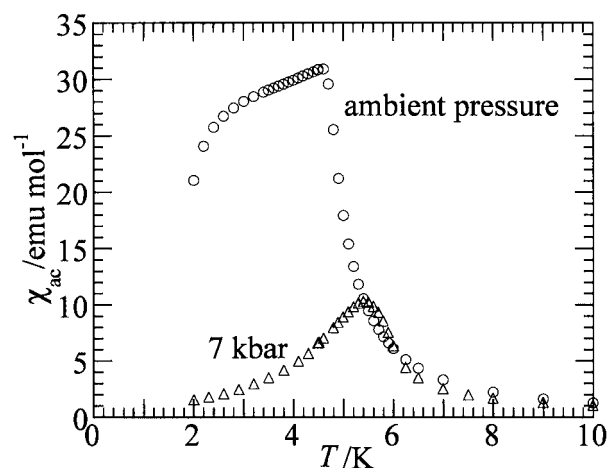


Figure 1. Temperature dependence of the ac susceptibilities of $[\text{Mn}(\text{hfac})_2] \cdot \{5\text{-chloro-1,3-bis}(N\text{-tert-butylaminoxyl})\text{benzene}\}$ at ambient pressure and under 7 kbar.

V-J-4 The Magnetic Phase Diagram and Pressure Effect on the Magnetic Properties of the $\text{Y}_{1-x}\text{Gd}_x\text{Mn}_2$ Intermetallic Compounds

DUBENKO, Igor S.¹; GAIDUKOVA, Irina Yu.²; HOSOKOSHI, Yuko; INOUE, Katsuya; MARKOSYAN, Ashot S.^{2,3}

(¹Moscow Inst. Radioeng. Electron. Autom.; ²M. V. Lomonosov Moscow State Univ.; ³IMS)

[*J. Phys.: Condens. Matter* **11**, 2937 (1999)]

Magnetization up to 50 kOe, magnetic susceptibility under external pressure up to 5 kbar and thermal expansion of the cubic Laves phase compounds $\text{Y}_{1-x}\text{Gd}_x\text{Mn}_2$ were studied in a wide temperature range. Two well defined concentration regions were isolated in the x - T phase diagram: $0 \leq x < 0.2$, in which the antiferromagnetic structure is primarily determined by the d-d interaction (YMn_2 -type), and $0.2 < x \leq 1$, in which the f-d interaction plays a dominant role (GdMn_2 -type). It is concluded that both the Gd and Mn sublattices are ordered in GdMn_2 below $T_N = 108$ K, the change in the magnetic characteristics at 40 K interpreted as an antiferromagnetism – non-collinear ferrimagnetism transition. The intermediate $\text{Y}_{0.8}\text{Gd}_{0.2}\text{Mn}_2$ compound shows a freezing and time dependent effects at low temperatures characteristic for short range order. The effects can also be induced by external pressure at

higher Gd concentrations.

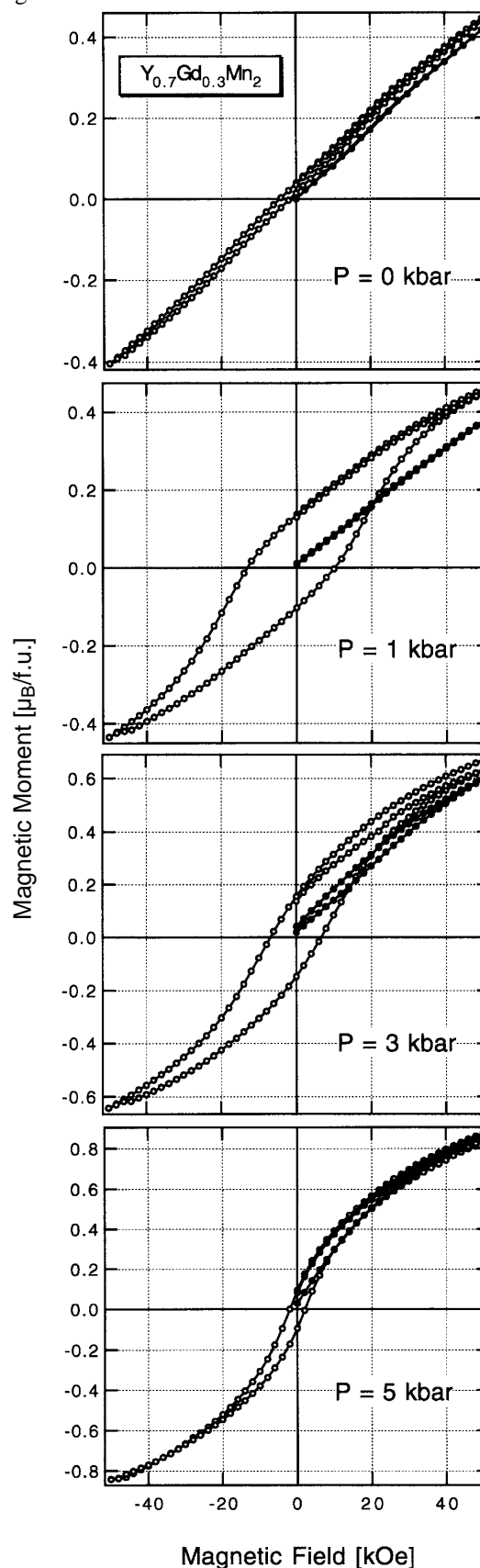


Figure 1. The hysteresis loops of $\text{Y}_{0.7}\text{Gd}_{0.3}\text{Mn}_2$ at 4 K under pressures 0, 1, 3 and 5 kbar. Full and open symbols correspond to the z.f.c. and f.c. (50 kOe) sample, respectively.

V-J-5 Concentration and Pressure Dependence of the Magnetic Ordering in the $Y(Mn_{1-x}Me_x)_2$ Compounds with Me = Al, Fe and Ni

DUBENKO, Igor S.¹; GAIDUKOVA, Irina Yu²; HOSOKOSHI, Yuko; INOUE, Katsuya; MARKOSYAN, Ashot S.^{2,3}

(¹Moscow Inst. Radioengin. Electron. Autom.; ²M. V. Lomonosov Moscow State Univ.; ³IMS)

[*J. Magn. Magn. Mater.* **195**, 687 (1999)]

Magnetic susceptibility of the $Y(Mn_{1-x}Me_x)_2$ (Me = Al, Fe and Ni) compounds was measured in the temperature range 2 ÷ 400 K under external pressure up to 5 kbar. The role of the interatomic Mn-Mn spacing in stabilising the antiferromagnetic transformed phase has been revealed. The value of $\partial T_N/\partial P \approx -50$ K/kbar was found essentially higher than in the mother compound YMn_2 . A freezing effect was observed in the non-transformed phase which was related to the break-down of the quantum spin liquid state.

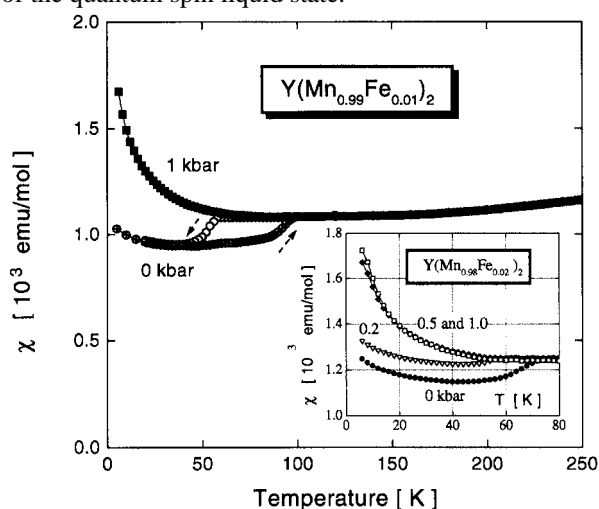


Figure 1. The temperature dependence of χ_{DC} for $Y(Mn_{0.99}Fe_{0.01})_2$ at 1 kbar and ambient pressure. The inset shows the variation of χ_{DC} vs. T on cooling for $Y(Mn_{0.98}Fe_{0.02})_2$ at different pressures.

V-K Desorption Induced by Electronic Transitions at the Surface of van der Waals Condensates

The electronic excitation on the surface of a van der Waals condensate may lead the desorption of neutral and charged molecules, either in the ground state or in excited ones. The phenomena discussed here are neither thermal desorption nor direct mechanical sputtering but processes through a transformation of an electronic excitation energy into a kinetic energy of a desorbing particle. Close investigation of this DIET (Desorption Induced by Electronic Transitions) phenomena will reveal the dynamical aspect of the electronic excitation and its relaxation process at the surface. In this research project, we have determined the absolute total desorption yield at the surface of solid Ne and have investigated the desorption of the excimer, Ne_2^* .

V-K-1 Absolute Measurement of Total Photo Desorption Yield of Solid Ne in Vacuum Ultraviolet Range

[to be submitted]

ARAKAWA, Ichiro^{1,2}; ADACHI, Takashi²; HIRAYAMA, Takato²; SAKURAI, Makoto³
(¹IMS; ²Gakushuin Univ.; ³Kobe Univ.)

[Surf. Sci. submitted]

Absolute yields of photo-induced desorption at the surface of solid Ne have been measured between 25 and 100 nm of wavelength of incident light. There are strong dependence of the total desorption yield of Ne both on the excitation energy and on the thickness of Ne films. On a thick film, the desorption yield is 1–2 atoms/photon by the bulk exciton excitation and 2–10 atoms/photon by the bulk ionization. The main component in the desorbed species is neutral Ne molecules in the ground state; the absolute yield of metastable desorption at the excitonic excitation is the order of 10^{-3} metastable/photon.¹⁾ The absolute yield of the order of unity for the total desorption by the bulk exciton excitation can quantitatively be understood by the following internal sputtering model. From optical absorption data, the number of excitons created per photon per layer is estimated at about 0.1. The kinetic energies of the particles desorbed through the cavity ejection mechanism is about 0.2 eV and those by the excimer dissociation one 1 eV. Because the cohesive energy of Ne is 0.019 eV, the desorbing particle, which is originated from the 2nd or 3rd layer, can blow 10 or more neutral Ne atoms in the overlayer off. The product of these values results in an order of unity of absolute yield of the total desorption. By the surface exciton excitation, the yield is 0.1–0.3 atoms/photon, which value means that the desorption probability of the surface exciton is almost unity.

Reference

- 1) T. Hirayama, A. Hayama, T. Koike, T. Kuninobu, I. Arakawa, K. Mitsuke, M. Sakurai and E. V. Savchenko, *Surf. Sci.* **390**, 266 (1997).

V-K-2 Desorption of an Excimer from the Surface of Solid Ne by Low Energy Electron or Photon Impact

HIRAYAMA, Takato¹; HAYAMA, Akira¹; ADACHI, Takashi¹; ARAKAWA, Ichiro^{1,2}; SAKURAI, Makoto³
(¹Gakushuin Univ.; ²IMS; ³Kobe Univ.)

Desorption of excited dimers Ne_2^* in $^3\Sigma_u$ state from the surface of solid Ne initiated by the creation of a valence exciton was confirmed experimentally using low energy electron or monochromatic VUV light as excitation sources. The kinetic energy of desorbed excimer ($\text{Ne}_2^* \ ^3\Sigma_u$) was (0.2 ± 0.1) eV, which is consistent with a recent quantum mechanical calculation.¹⁾ It is found that the vibrational relaxation of a molecular type exciton is a slow process compared to the time scale of desorption. Desorption of excimers at the excitation of the first order surface exciton was found to be inefficient compared to that by the creation of bulk excitons, which is in striking contrast to the case of the excited atom desorption. The mechanism of excimer desorption can be explained by a cavity ejection model as in the atomic desorption case.

Reference

- 1) L. F. Chen, G. Q. Huang and K. S. Song, *Nucl. Instrum. Methods Phys. Res., Sect. B* **116**, 61 (1996).

V-L Synthesis and Physical Properties of Novel Molecular Metals

Development of organic materials which exhibit interesting electrical properties such as metallic conductivity and superconductivity has received considerable attention. A bis-fused TTF, 2,5-bis(1,3-dithiol-2-ylidene)-1,3,4,6-tetrathiapentalene (TTP) is a promising π -electron framework for preparation of stable metals down to low temperatures, because it has a ladder-like array of sulfur atoms indispensable for constructing two-dimensional network of the donors. In fact, we have found that the unsubstituted TTP has a strong tendency to afford highly conducting radical cation salts retaining metallic conductivity down to ≤ 1.2 K regardless of shape and size of counter anions. In the present study, we have developed several organic metals by means of comprehensive modification of TTP, namely i) introduction of substituents, ii) exchange of sulfur atoms in the TTP framework with selenium, iii) synthesis of TTP analogs possessing non-TTF donor unit.

V-L-1 (CPDT-STF)(TCNQ): A New Charge-Transfer Complex Metallic Down to Low Temperature

TANIGUCHI, Masateru¹; MISAKI, Yohji^{1,2}; TANAKA, Kazuyoshi¹; YAMABE, Tokio¹; MURATA, Kyoji³; MORI, Takehiko³

(¹Kyoto Univ.; ²IMS; ³Tokyo Inst. Tech.)

[Solid State Commun. **111**, 559 (1999)]

A new charge transfer complex (CPDT-STF)-(TCNQ) has been prepared. An X-ray crystal structure analysis revealed that this complex is composed of the donor and acceptor sheets orthogonally arranged to each other (Figure 1), which is similar to (ET)(TCNQ) and (ET)(TCNQF₄). The band calculations indicate that the CPDT-STF layer has significantly two-dimensional interaction, while the TCNQ one has one-dimensional Fermi surface. The electrical resistivity of the present complex showed metallic temperature dependence down to 0.6 K. The thermoelectric power was negative and changed from the positive to the negative gradient at 60 K. The static magnetic susceptibility and transport properties indicate coexistence of local and itinerant electrons in the present complex.

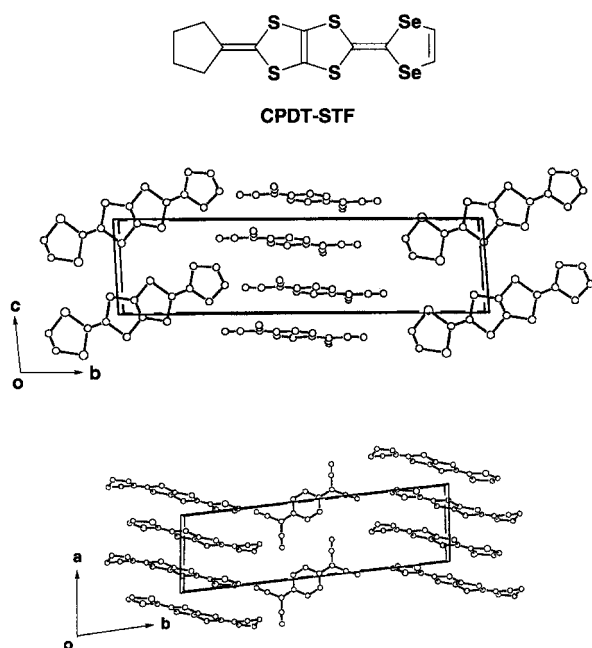


Figure 1. Crystal structure of (CPDT-STF)(TCNQ).

V-L-2 Structures and Electrical Properties of (EO-TTP)₂AsF₆

MISAKI, Yohji^{1,2}; TANAKA, Koji¹; TANIGUCHI, Masateru¹; YAMABE, Tokio¹; KAWAMOTO, Tadashi³; MORI, Takehiko³

(¹Kyoto Univ.; ²IMS; ³Tokyo Inst. Tech.)

Tetrahedral and octahedral anions based on EO-TTP, where EO-TTP is 2-(4,5-ethylenedioxy-1,3-dithiol-2-ylidene)-5-(1,3-dithiol-2-ylidene)-1,3,4,6-tetrathiapentalene, afforded radical cation salts retaining metallic conductivity down to low temperature (1.5–4.2 K). X-Ray structure analysis of the AsF₆ salt (EO-TTP)₂AsF₆ reveals that it has the so-called b-type array of donors (Figure 1). A tight binding band calculation suggested that this salt has a two-dimensional closed Fermi surface.

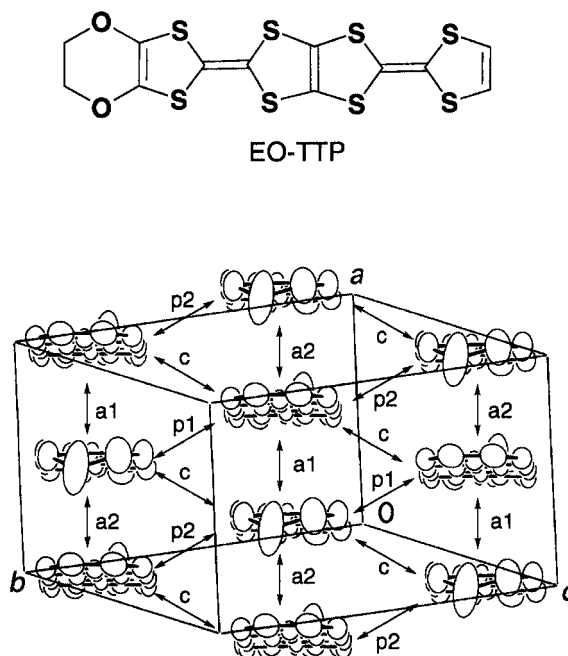


Figure 1. Donor sheet structure of (EO-TTP)₂AsF₆; The intermolecular overlap integrals are $a_1 = 26.9$, $a_2 = 25.2$, $p_1 = 0.47$, $p_2 = 0.11$, $c = -9.07 \times 10^{-3}$.

V-L-3 A Quasi Three-Dimensional Organic Conductor Based on a TTP Analogue Containing Thiopyran-4-ylidene

MISAKI, Yohji^{1,2}; KAIBUKI, Tadahiro¹; TANIGUCHI, Masateru¹; TANAKA, Kazuyoshi¹; TAKIMIYA, Kazuo³; MORIKAMI, Atsushi³; OTSUBO, Tetsuo³; MORI, Takehiko⁴

(¹Kyoto Univ.; ²IMS; ³Hiroshima Univ.; ⁴Tokyo Inst. Tech.)

We have demonstrated that a bis-fused TTP, 2,5-bis-(1,3-dithiol-2-ylidene)-1,3,4,6-tetrathiapentalene (TTP) has afforded many metallic radical-cation salts stable down to liquid helium temperature regardless of shape and size of counter anions, in which the donors have a two-dimensional array. In contrast, (TM-TPDS)₂AsF₆, where TM-TPDS is 2-[4,5-bis(methylthio)-1,3-diselenol-2-ylidene]-5-(thiopyran-4-ylidene)-1,3,4,6-tetrathiapentalene has no two-dimensional conducting sheet in contrast to usual TTP conductors. The donors are arranged in a "windmill" manner in the *bc* plane (Figure 1). The anion is located on the center of "windmill," and are surrounded by methylthio groups in the donors. The donors are alternately stacked along the *a* axis. There are many sulfur-sulfur contacts shorter than the sum of van der Waals radii (3.70 Å) between the central tetrathiapentalene moiety and the thiopyrane ring or methylthio groups. Thanks to a relatively large atomic coefficient of the sulfur atom in the thiopyrane ring, which is comparable to those of the others in the 1,3-dithiole rings, the calculated overlap integrals of the intercolumn interaction are comparatively large of about 10% of the intracolumn one. As a result, the Fermi surface of the present salt is indeed one-dimensional, however, interactions in the *bc* plane is isotropic, namely this salt may be regarded to be a quasi three-dimensional metal. This salt showed high conductivity of 240 S cm⁻¹ at room temperature, and exhibited metal-like temperature dependence down to 100 K. Below this temperature, the resistivity gradually increased.

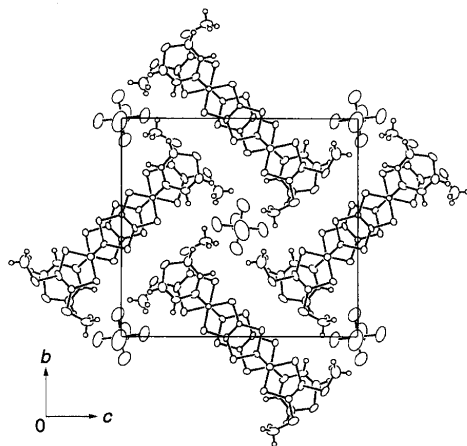
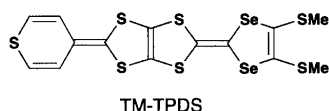


Figure 1. Crystal structure of (TM-TPDS)₂AsF₆.

V-L-4 Structures and Properties of Organic Metals Based on Dimethyl Substituted TTP Analogue

TANIGUCHI, Masateru¹; MISAKI, Yohji^{1,2}; TANAKA, Kazuyoshi¹; YAMABE, Tokio¹; MORI, Takehiko³

(¹Kyoto Univ.; ²IMS; ³Tokyo Inst. Tech.)

[*Synth. Met.* **102**, 1721 (1999)]

A selenium analogue of dimethyl substituted TTP (DM-TS-TTP) was prepared. (DM-TS-TTP)₂PF₆ showed metallic temperature dependence down to 4.2 K. X-Ray crystal structure analysis of this salt reveals that the donors form two-dimensional conducting sheets as is observed in most TTP type metals (Figure 1). The arrangement of donors is classified as the so-called β -type. The band structure calculated by a tight-binding method suggests that it has a quasi one-dimensional Fermi surface.

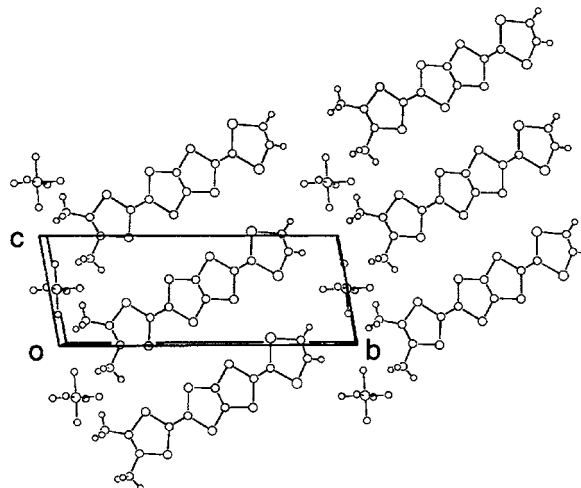
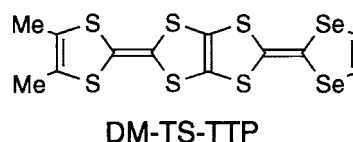


Figure 1. Crystal structure of (DM-TS-TTP)₂PF₆.

V-L-5 Synthesis and Properties of Methylthio Substituted ST-TTP Derivatives

MISAKI, Yohji^{1,2}; KAIBUKI, Tadahiro¹; MONOBE, Tae¹; TANAKA, Koji¹; TANIGUCHI, Masateru¹; TANAKA, Kazuyoshi¹; YAMABE, Tokio¹; TAKIMIYA, Kazuo³; MORIKAMI, Atsushi³; OTSUBO, Tetsuo³; MORI, Takehiko⁴

(¹Kyoto Univ.; ²IMS; ³Hiroshima Univ.; ⁴Tokyo Inst. Tech.)

[*Synth. Met.* **102**, 1781 (1999)]

A new ST-TTP donor TMEO-ST-TTP, where TMEO-ST-TTP is 2-[4,5-bis(methylthio)-1,3-diselenol-2-ylidene]-5-(4,5-ethylenedioxy-1,3-dithiol-2-ylidene)-1,3,4,6-tetrathiapentalene, has been prepared. It affords highly conducting PF₆⁻ and AsF₆⁻ salts retaining

metallic conductivity down to 4.2 K, while the TCNQ complex and ClO_4^- salt are low conductive semi-conductors. X-Ray structure analyses reveal that (TMEO-ST-TTP)(TCNQ)(PhCl) has a DA type mixed stack, and that the donor array of (TMEO-ST-TTP)₂- ClO_4^- (DCE) in the conducting sheet resembles β -BEDT-TTF salts (Figure 1).

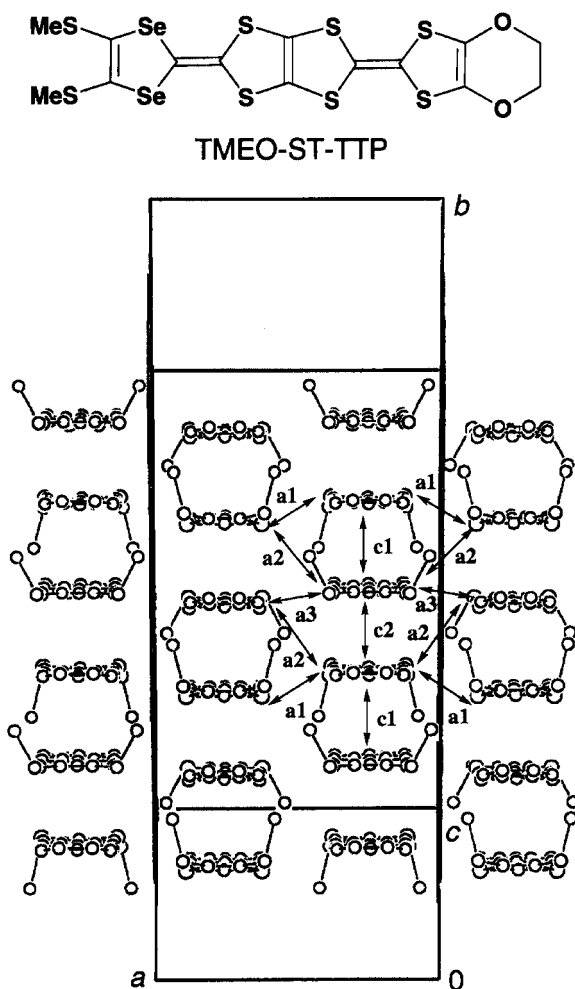


Figure 1. Donor sheet structure of (TMEO-ST-TTP)₂ ClO_4^- (DCE).

V-M Development of Model Core Potentials and Post Hartree-Fock Calculations to Atoms and Molecules

We have developed various types of model core potentials for various elements and applied the MCPs to investigate the electronic structures of atoms, molecules, and clusters at levels of post Hartree-Fock calculations.

V-M-1 Theoretical Study of Low-Lying Electronic States of TiCl and ZrCl

SAKAI, Yoshiko¹; MOGI, Kouichi¹; MIYOSHI, Eisaku
(¹Kyushu Univ.)

[*J. Chem. Phys.* **111**, 3989 (1999)]

Low-lying electronic states of TiCl and ZrCl were investigated by the complete active space SCF (CASSCF), multi-reference singly and doubly excited configuration interaction (MRSDCI), and multi-reference coupled pair approximation (MRCPA) calculations using the model core potential (MCP) method. The relativistic effects were incorporated in the MCP and basis sets for Zr at the level of Cowan and Griffin's quasirelativistic Hartree Fock method. The $^4\Phi$ state was found to be the ground state of TiCl whereas the $^2\Delta$ state was the ground state of ZrCl at all levels of calculations. Two low-lying excited states were very close in energy to the ground state. The excited $^4\Sigma^-$ and $^2\Delta$ states of TiCl were higher than the ground state by 0.102 eV and 0.458 eV, respectively, and the excited $^4\Phi$ and $^4\Sigma^-$ states of ZrCl were higher by 0.094 eV and 0.110 eV, respectively, at the MRCPA calculations.

V-M-2 Benchmarking of Model Core Potentials: Application to the Group 4 Metal Halogen Complexes (MX₄: M = Ti, Zr, Hf and X = F, Cl, Br, I)

DECKER, Stephan A.¹; KLOBUKOWSKI, Mariusz¹; SAKAI, Yoshiko²; MIYOSHI, Eisaku
(¹Univ. Alberta; ²Kyushu Univ.)

The reliability of the model core potential method was probed in a systematic study of the group 4 metal halogen complexes (MX₄; M = Ti, Zr, Hf and X = F, Cl, Br, I). In the first phase of the study we focused on the geometries of these tetrahedral complexes. The computed M-X distances were compared with experimental values, as well as those predicted using a variety of effective core potentials. The reaction energies for a

simple set of halogen diatomic substitution reactions of the MX₄ complexes leading to the mixed halogen complex, MX₂Y₂, were studied in the second part of this work. Although no experimental values are available for these reactions, comparison was again made with the values computed using a number of effective core potential methods. All of the calculations were carried out at the RHF and MP2 levels of theory. Discussion focuses on the predictability of the different pseudopotential techniques and the extent of the metal atom valence space. Furthermore, we comment on the importance of the metal atom valence basis set contraction scheme and polarization space.

V-M-3 Configuration Interaction Study of Differential Correlation Energies in Ca⁺, Ca and Ca⁻

OSANAI, You¹; NORO, Takeshi²; MIYOSHI, Eisaku
(¹Aomori Univ.; ²Hokkaido Univ.)

Configuration interaction (CI) calculations have been carried out for Ca⁺ (4s 2S , 3d 2D and 4p $^2P^o$), Ca (4s $^2^1S$ and 3d4s 1D) and Ca⁻ (4s²4p $^2P^o$) using very large Slater-type orbitals. The effect of Ar-like core was included by allowing the excitation from the most important subshells of the core, 3s and 3p, explicitly. A series of multi-reference single and double excitation CI calculations was performed adding important configurations representing valence correlation to the reference space, and convergence of CI energies and wavefunctions was investigated. Valence correlation can be described adequately only when the reference space is expanded so largely that valence correlation is almost completely described by reference functions alone. The relativistic effects were estimated by carrying out Dirac-Fock calculations. The present calculations gave the ionization potentials to 4s 2S , 3d 2D and 4p $^2P^o$ to be 6.079, 7.819 and 9.179 eV, respectively, and the excitation energy to 3d4s 1D to be 2.805 eV. All these calculated values are in good agreement with the observed values. The electron affinity was obtained to be 17.7 meV, which is in excellent agreement with the recent observed values, 17.5 ~ 21.5 meV.

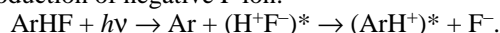
V-N Theoretical Study of the Electronic Structures of Weakly Bound Molecules

The electronic structures of weakly bound molecules such as van der Waals molecules are investigated by using sophisticated methods for electronic states, *i.e.*, multi-reference single and double excitation configuration interaction (MRSDCI) and multi-reference coupled pair approximation (MRCPA) calculations.

V-N-1 *Ab initio* Study of the van der Waals Molecule ArHF

GHOSH, Tapas Kumar; MIYOSHI, Eisaku; TANAKA, Kiyoshi¹
(¹Hokkaido Univ.)

Ab initio calculations were performed for the van der Waals complex ArHF using the multi-reference single and double excitation configuration interaction (MRSDCI) and multi-reference coupled pair approximation (MRCPA) methods to determine the spectroscopic parameters and potential energy surfaces of the ground $X^1\Sigma^+$ and first excited $2^1\Sigma^+$ states. The calculated ground-state equilibrium constants compared well with the available data. This is the first report of spectroscopic data for the excited state. Another subject of this study was the possibility of a fluorine anion from an excited ionic state (ArHF)* produced by Ar colliding with an excited ionic state of HF. The excited $2^1\Sigma^+$ state is of ionic type (H^+F^-) and dissociates to a negative fluorine ion. This enlightens the photochemical reaction of the ionic excited HF with Ar correlating to the production of negative F ion:

**V-N-2 *Ab initio* Molecular Orbital Study of Fe(CO)_n (n = 1, 2 and 3)**

HONDA, Hiroaki¹; NORO, Takeshi¹; MIYOSHI, Eisaku
(¹Hokkaido Univ.)

Various unsaturated iron carbonyl complexes $\text{Fe}(\text{CO})_n$ ($n = 1$ to 4) have been produced by the UV photolysis of iron pentacarbonyl $\text{Fe}(\text{CO})_5$.¹⁾ Among them the spectroscopic studies of the FeCO radical has been extensively performed from both experimental and theoretical points of view and there have been a few experimental spectroscopic constants of $\text{Fe}(\text{CO})_2$ and $\text{Fe}(\text{CO})_3$.

Although there have been published several theoretical studies for $\text{Fe}(\text{CO})_2$ and $\text{Fe}(\text{CO})_3$, there are few comprehensive studies for the change of bonding nature in the $\text{Fe}(\text{CO})_n$ ($n = 1$ to 3) radicals. In this study we have carried out MCSCF calculations for the $\text{Fe}(\text{CO})_n$ ($n = 1$ to 3) to investigate the nature of bonding respect to change in the number of CO ligands. The calculated bond lengths of R(Fe-C) are reasonably in agreement with experimental values and more sophisticated theoretical results. From the Mulliken population analysis, the traditional donation and back donation mechanism is valid for FeCO through $\text{Fe}(\text{CO})_3$.

Reference

- 1) K. Tanaka, K. Sakaguchi and T. Tanaka, *J. Chem. Phys.* **106**, 2118 (1997).

V-N-3 *Ab initio* Study on the Ground State of the C₃O₂ Molecule

MIYOSHI, Eisaku; SHIDA, Norihiro¹
(¹Nagoya Inst. Tech.)

[*Chem. Phys. Lett.* **303**, 50 (1999)]

Restricted Hartree-Fock (RHF) and single-reference coupled pair approximation (SRCPA) calculations were performed for the ground state of the C_3O_2 molecule. The SRCPA calculations revealed that C_3O_2 is quasi-linear with a global minimum in a W-shaped structure (C_{2v} symmetry) with $\angle\text{C-C-C} = 153.6^\circ$ and $\angle\text{C-C-O} = 176.4^\circ$. To obtain the qualitatively correct description that the C_3O_2 molecule has a global minimum in the W-shaped structure, basis sets of higher quality than double-zeta with double polarization functions are indispensable. The observed very low frequency of 18.2 cm^{-1} is not a fundamental vibrational frequency along the ν_7 mode, but should rather be assigned to the transition between two vibrational states which are split by the interaction of two ground vibrational state in the double minima.

V-N-4 On the Calculation of Binding Energy of the (C₆H₆)³⁺ Ion

GHOSH, Tapas Kumar; MIYOSHI, Eisaku

The benzene trimer cation, $(\text{C}_6\text{H}_6)^{3+}$, has become an important system in the cluster ion spectroscopy because of the identification of core in the ion. It is yet controversial whether the benzene trimer cation has charge delocalized or localized structure. We performed *ab initio* CASSCF followed by MRSDCI as well as SRSDCI calculations for the benzene trimer cation $(\text{C}_6\text{H}_6)^{3+}$ in its ground state assuming a sandwich-like structure. The total number of generated CSFs in MRSDCI calculations was 7,131,105. The equilibrium distances between two consecutive rings at the global minimum of the trimer cation in its ground state calculated by CASSCF in C_{2v} symmetry were 7.299 a.u. The dissociation energy (D_e) for the ground state of benzene trimer cation relative to $(\text{C}_6\text{H}_6)^{2+} + \text{C}_6\text{H}_6$ was calculated to be 195 meV at the CASSCF level and 349 meV at the MRSDCI including Davidson's correction in comparison to the experimental value (D_0) of 338 meV. The total binding energy relative to $2\text{C}_6\text{H}_6 + \text{C}_6\text{H}_6^+$ was calculated to be 757 meV at the MCSCF level and 984 meV at the MRSDCI including Davidson's correction, which is in agreement with a recent experimental upper limit of 990 ± 50 meV. It has been concluded from our calculation that in the trimer cation charge is localized at the central benzene ring, not that the charge is localized on a dimer core as was suggested by some experimentalists.

V-O Molecular Dynamics Study Using Potentials by *ab initio* Molecular Orbital Calculations

Using potentials obtained by *ab initio* molecular orbital calculations, molecular dynamics calculations were performed to investigate physical properties of liquid mercury.

V-O-1 Molecular Dynamics Study of Liquid Mercury in the Density Region between Metal and Nonmetal

SUMI, Tomonari; MIYOSHI, Eisaku; TANAKA, Kiyoshi¹

(¹Hokkaido Univ.)

[*Phys. Rev. B* **59**, 6153 (1999)]

We performed SDCI, SDCI(+Q), and CPA calculations for the ground $^1\Sigma_g^+$ state of Hg_2 incorporating the 5d and 6s electron correlations and major relativistic effects. The many-electron-excitation effect produces spectroscopic constants close to the experimental values. Although the metal-nonmetal (M-NM) transition can be explained as a simple band-crossing transition in one-electron theory, the many-electron-excitation effect is very important for describing the interaction between mercury atoms.

MD calculations for expanded liquid mercury were performed using the potential energy curve of Hg_2 , in the regions including the M-NM transition range. The volume (V) dependence of the thermal pressure coefficient, γ_v , and the internal pressure, P_0 , estimated by the MD calculations agree well with experimental results. Thus, many-body interactions or the qualitative change in the form of interatomic interactions arising from density dependence are not necessarily essential to explain the behavior of the γ_v vs. V and the P_0 vs. V curves. The change of calculated pair distribution function between metallic and nonmetallic state qualitatively demonstrates the change of experimental ones. The temperature dependence of the isochoric electrical conductivity was estimated using interatomic distances obtained from the calculated pair distribution functions. It was shown that the increase of the isochoric electrical conductivity accompanying an increase in temperature can be realized through the increase of the density of states at the Fermi energy. In the preceding paper,¹⁾ we reported that the MD calculations near the melting point using the potential curve of Hg_2 reproduce the cooperative motion corresponding to the collective short-wavelength excitations in the dynamic structure factor. These results suggest that pair-potential approximation using the potential curve of the dimeric molecule gives a good qualitative description of the metallic interatomic force for liquid mercury, and MD calculations using this approximation demonstrate the characteristic change of force fields between liquid metal and liquid semiconductor. However, the both γ_v vs. V and P_0 vs. V curves estimated by the MD calculations seem to deviate from the observed values slightly in the high-density metallic region. These differences between the observed and calculated values may be attributed to the lack of the many-body effects.

It has been pointed out²⁾ that the relative importance

of three-body interactions compared with two-body interactions in the liquid-vapor critical range for mercury is larger than for other van der Waals molecules. The boiling point determined by the present MD calculations is much higher than the observed value. This higher temperature should be corrected by considering three-body effects, such as the Axilrod-Teller interaction, because the three-body dispersion forces are repulsive while the two-body dispersion force is a long-range attractive force. It is interesting to determine the liquid-vapor coexistence curve with pair-potential approximation using the potential energy curve of Hg_2 and to investigate the contribution of three-body effects to the liquid-vapor transition phenomena, especially in liquid-vapor critical range.

References

- 1) T. Sumi, E. Miyoshi, Y. Sakai and O. Matsuoka, *Phys. Rev. B* **57**, 914 (1998).
- 2) M. W. Pestak, R. E. Goldstein, M. W. Chan, J. R. de Bruyn, D. A. Balzarini and N. W. Ashcroft, *Phys. Rev. B* **36**, 599 (1987).

V-O-2 The Liquid-Vapor Coexistence Curves of Fluid Mercury

SUMI, Tomonari; MIYOSHI, Eisaku

It has been known that the liquid-vapor coexistence curve of mercury is different from those of alkali metals (Rb, Cs) and inert gases (Ar, Xe).¹⁾ The followings have been established for these liquid-vapor coexistence curves and the rectilinear diameters, $r_d = (r_L + r_V)/2r_c$, where r_L , r_V , and r_c is the coexisting liquid density, vapor density, and the critical density, respectively: (1) The two phase region of mercury is narrower than those of alkali metals and inert gases; (2) The r_d of inert gases is a linear function of temperature, T , which is the law of rectilinear diameter, except for the near critical point, while the r_d of alkali metals and mercury deviate from the law of rectilinear diameter in wide temperature region. It has been suggested that the evidence in (2) might be attributed to many body effects.²⁾

We have performed molecular dynamics (MD) calculations for liquid mercury using the potential energy curve of dimeric mercury (Hg_2), which was obtained by molecular orbital calculations, in order to study the properties of mercury at the various temperature and density regions. In particular, the MD calculations using this approximation qualitatively reproduced the volume dependence of the thermal pressure coefficient and the internal pressure in the density regions including the metal-nonmetal transition range.³⁾ In this study, the MD calculations of fluid mercury are performed to determine the liquid-vapor phase transition points of mercury, and the relationship between the pair potential and liquid-vapor coexistence

curve is discussed.

The pair potential have been obtained from the CPA calculations developed by Tanaka and co-workers. The MD calculations were performed using a Verlet algorithm with 864 particles in an isothermal and isobaric ensemble with a time step of 0.005 fs. The physical quantities near the transition points were determined from the statistical averages over 2 000 000 to 10 000 000 intervals.

The results of MD calculations are as follows: (1) Our calculations qualitatively reproduced the liquid-vapor coexistence curve of mercury which is mentioned above; (2) Calculated r_d is not a linear function of T . Thus, our results suggest that the law of rectilinear diameter breaks down in the pair potential approximation.

References

- 1) F. Hensel, *J. Phys. C* **2**, SA33 (1990).
- 2) R. Goldstein and N. E. Ashcroft, *Phys. Rev. Lett.* **55**, 2164 (1985).
- 3) T. Sumi, E. Miyoshi and K. Tanaka, *Phys. Rev. B* **59**, 6153 (1999).

V-P Millimeter-Wave Spectroscopy Combined with Pulsed-Jet Expansion Technique for the Detection of the Novel Unstable Species and the van der Waals Mode Transitions of Molecular Clusters

Molecular clusters have inherently low-frequency vibrations, so called van der Waals (vdW) vibrational modes, which are characteristic of the weakly bound complexes. The frequency of the vdW mode usually falls in the far-infrared region ($30\text{--}300\text{ cm}^{-1}$). However, if a cluster is extremely floppy, it sometimes falls in the submillimeter-wave (SMMW) region below 30 cm^{-1} .

The ArHCN cluster is a typical example which has extremely low-frequency vdW bending vibrations. Although the frequency of the vdW stretching is estimated to be 23.8 cm^{-1} , those for the bending vibrations are calculated to be as low as $4\text{--}7\text{ cm}^{-1}$. Following the observation of the pure rotational spectra in the microwave region below 20 GHz, the vdW bending transitions of ArHCN have been measured in the millimeter-wave region near 180 GHz by molecular beam electric resonance optothermal spectroscopy (EROS).

In this project, a millimeter-wave absorption spectrometer combined with pulsed-jet expansion technique has been devised and applied to the direct observation of the rovibrational transitions of the vdW bending band of molecular clusters. We have applied this technique to observe the vdW bending bands of the ArHCN ($j = 1\text{--}0$ and $2\text{--}1$) and ArDCN ($j = 1\text{--}0$) clusters as well as the ArHBr ($\Sigma_1\text{--}\Sigma_0$) and OCO·HF ($1^1\text{--}0^0$ (ν_b)) clusters.

In the supersonic jet expansions short lived species can survive thanks to the collision-less environment and ultra low rotational as well as vibrational temperature. The millimeter-wave spectrometer combined with supersonic jet nozzle and glow discharge electrodes, as well as the UV excimer laser photolysis devices, also have been set up for the detection of novel unstable species, such as radicals, molecular ions, and ionic and radical clusters.

V-P-1 Millimeter-Wave Spectroscopy of the van der Waals Bending Band of the ArDCN Cluster

BAILLEUX, Stephane; MIZOGUCHI, Asao; HARADA, Kensuke; BABA, Takeshi¹; SHIRASAKA, Mitsuaki¹; TANAKA, Keiichi²

(¹Kyushu Univ.; ²IMS and Kyushu Univ.)

Millimeter-wave absorption spectroscopy combined with pulsed-jet expansion technique was applied to the measurement of the rovibrational transitions in the van der Waals bending band of the ArDCN cluster in the frequency region of 182–294 GHz. Sixteen and thirty-seven rovibrational lines were observed for the $\Sigma_1\text{--}\Sigma_0$ and $\Pi_1\text{--}\Sigma_0$ bands, respectively, split into hyperfine structure due to the nitrogen nucleus. The spectrum of the $R(1)$ line of the $\Sigma_1\text{--}\Sigma_0$ band observed at 196 GHz is shown in Figure 1.

An accurate set of molecular constants, including the band origins, rotational constants, quadrupole coupling constants, and the Coriolis coupling constant between the Σ_1 and Π_1 bending substates, was determined. The rotational and quadrupole coupling constants for the excited states are much different from those of the ground state indicating the change in average molecular structure, from the linear form in the ground state to the T-shaped form in the first excited ($j = 1$) state. The band origins for the $\Sigma_1\text{--}\Sigma_0$ and $\Pi_1\text{--}\Sigma_0$ bands, 189.017 391 (7) GHz and 195.550 737 (12) GHz, are larger by 24.126 596 (9) and 13.566 315(16) GHz than the corresponding values of ArHCN.¹ The abnormal isotopic effect on the vibrational frequencies is attributed to the characteristic potential energy surface of ArH(D)CN, which have two minima corresponding to linear and T-shaped configurations with similar well depth and connected with a shallow channel. The determined molecular constants were compared with those calculated with potential energy surface given by CCSD(T) level *ab initio* calculation.²

References

- 1) K. Uemura, A. Hara and K. Tanaka, *J. Chem. Phys.* **104**, 9747 (1996).
- 2) S. M. Cybulski, J. Couvillion, J. Klos and G. Chalasinski, *J. Chem. Phys.* **110**, 1416 (1999).

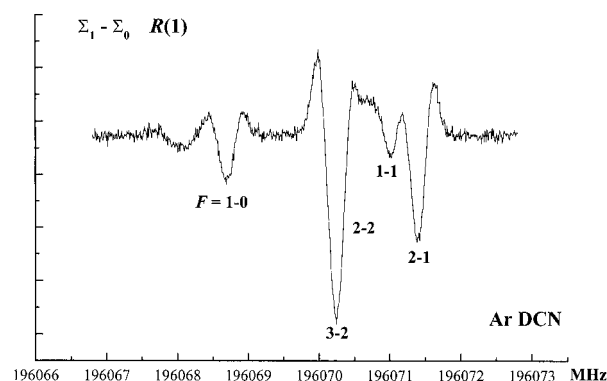


Figure 1. Hyperfine structure of the $R(1)$ line of the $\Sigma_1\text{--}\Sigma_0$ subband of the $j = 1\text{--}0$ vdW bending band of ArDCN.

V-P-2 Direct Observation of the van der Waals Bending Hot Bands of the Ar-HCN Cluster by Millimeter-Wave Spectroscopy

MIZOGUCHI, Asao; HARADA, Kensuke; TANAKA, Keiichi¹

(¹IMS and Kyushu Univ.)

The previous spectroscopic studies of the “ball and ball”-type cluster such as the Ar-HCl and Ar-H₂O clusters gave the computational techniques for evaluating the experimental potential energy surface (PES). As a next target, many experimentalists and theoreticians have investigated the Ar-HCN cluster because it is one of the simplest “ball and rod”-type cluster.

Since the first observation of the rotational spectrum of Ar-HCN was carried out by Leopold *et al.*,¹ many

studies have been reported. The observation of the vdW vibration is important to determine the intermolecular PES. The vdW bending fundamental bands were observed by Drucker *et al.*²⁾ These experimental results showed that this cluster has abnormally large centrifugal distortion constants and isotopic effect on the molecular constants of the normal and deuterated species. *Ab initio* calculation by Tao *et al.*³⁾ and Cybulski *et al.*⁴⁾ showed that this abnormality is due to the characteristic PES of Ar-HCN (Figure 1), which has large angular-radial coupling and anisotropy in the vdW vibration.

In the present work, the vdW bending hot bands of Ar-HCN have been observed by using the millimeter-wave absorption spectroscopy combined with the pulsed supersonic jet expansion technique. In the frequency region of 150–290 GHz, the six bands correlated to the $j = 2-1$ transition in the free rotor limit were assigned and least-squares fitted simultaneously to the effective Hamiltonian including the Coriolis interaction (Figure 2). The order of the sublevels in the $j = 2$ state is reversed to that of $j = 1$ state, which is consistent with the vibrational analysis with the PES by Cybulski *et al.* Since the observed rotational constants in the $j = 2$ state have almost the same values as those of the $j = 1$ state, the average distance between Ar and center of mass of HCN in the $j = 2$ state is not changed so much. The signs of nuclear quadrupole coupling constants in the $j = 2$ state are the same as those of the coupling constants predicted in the free rotor limit.

References

- 1) K. R. Leopold, G. T. Fraser, F. J. Lin, D. D. Nelson, Jr. and W. Klemperer, *J. Chem. Phys.* **81**, 4922 (1984).
- 2) S. Drucker, A. L. Cooksy and W. Klemperer, *J. Chem. Phys.* **98**, 5158 (1993).
- 3) F. M. Tao, S. Drucker and W. Klemperer, *J. Chem. Phys.* **102**, 7289 (1995).
- 4) S. M. Cybulski, J. Couvillion, J. Kłots and G. Chałasiński, *J. Chem. Phys.* **110**, 1416 (1999).

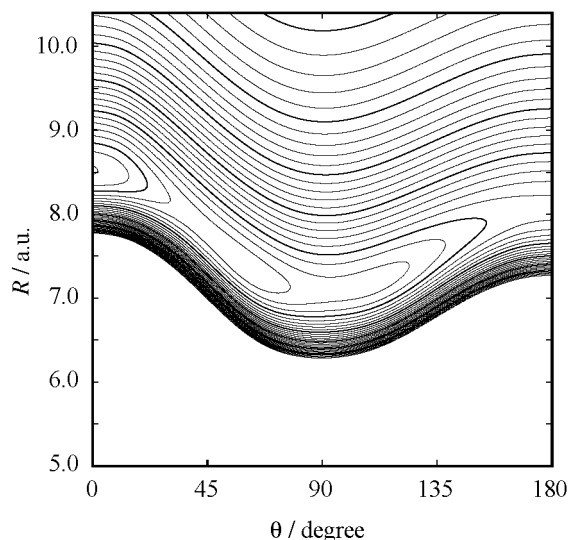


Figure 1. The PES of Ar-HCN. This PES was obtained by the high-level *ab initio* calculation with CCSD(T)/aug-cc-pVTZ+bf method.⁴⁾

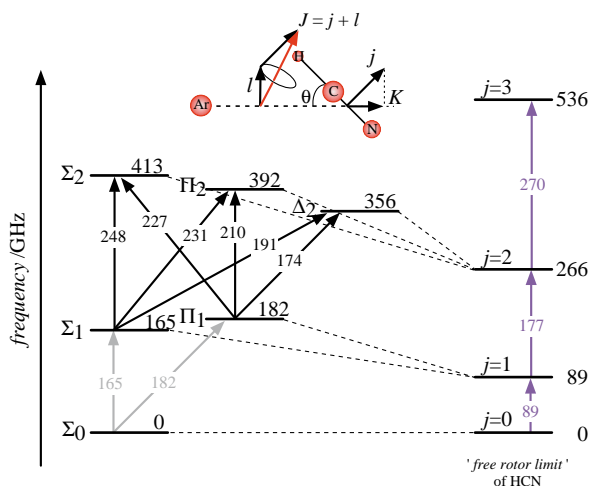


Figure 2. Energy level diagram of Ar-HCN. Since each vibrational energy level correlates to the free rotor energy levels of HCN, the vdW vibrational levels are labeled with $|K|_j$.

V-P-3 Submillimeter-Wave Spectroscopy of the van der Waals Bending Band of Ar-HBr

HARADA, Kensuke; MIZOGUCHI, Asao; TANAKA, Keiichi¹

(¹IMS and Kyushu Univ.)

The Ar-HBr cluster has a large amplitude intermolecular bending motion. It has nearly a “linear” structure of Ar-HBr in the ground state (Σ_0 state), while nearly an “anti-linear” structure of Ar-BrH in the first excited state (Σ_1 state) by the calculation of Hutson.¹⁾ Recently, the excited states of the van der Waals vibrations were observed by infrared²⁾ and far infrared³⁾ laser spectroscopy. The energy difference between the Σ_1 and Σ_0 state was determined to be 10.995 cm^{-1} from the combination difference of the infrared data.²⁾ In the present study, we have observed direct submillimeter-wave transitions of the $\Sigma_1-\Sigma_0$ band of Ar-HBr generated in a pulsed supersonic jet expansion.

The millimeter-wave jet spectrometer have been used for the experiment. The 8 atm mixed gas of 1% HBr, 49% Ar, and 50% Ne was injected to the vacuum chamber from a pulsed nozzle. In the frequency region of 318–335 GHz, the 14 rovibrational transition of P(12)-P(1), R(0), and R(1) have been observed for both Ar-H⁷⁹Br and Ar-H⁸¹Br isotopic species. Since the van der Waals bond length in the Σ_1 states is 0.2 \AA shorter than that in the ground state, the spectrum has a band head at P branch side. Figure 1 shows the P(8) and P(10) lines near the band head at 319 GHz, split due to the nuclear quadrupole interaction of the bromine nucleus.

The eQq constants in the the Σ_1 state were determined to be 260.90(12) and 217.854(98) MHz for Ar-H⁷⁹Br and Ar-H⁸¹Br, respectively, which are 51% larger than the values in the ground state. The rotational dependence of the eQq constant, eQq_J in the the Σ_1 state has reverse sign to that in the ground state. The big change of the eQq constant and the reverse sign of the eQq_J indicate that the cluster is in the different minima of the potential surface at the “linear” and “anti-linear” structures, in the Σ_0 and Σ_1 state, respectively.

References

- 1) J. M. Hutson, *J. Chem. Phys.* **91**, 4455 (1989).
- 2) J. Han, A. L. McIntosh, Z. Wang, R. R. Lucchese and J. W. Bevan, *Chem. Phys. Lett.* **265**, 209 (1997).
- 3) D. W. Firth, M. A. Dvorak, S. W. Reeve, R. S. Ford and K. R. Leopold, *Chem. Phys. Lett.* **168**, 161 (1990).

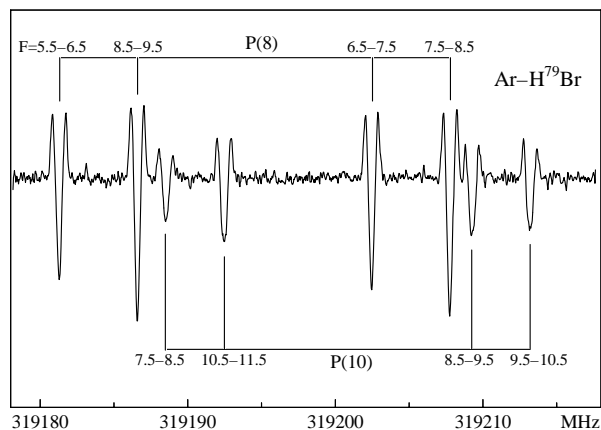


Figure 1. The observed spectrum of the $\Sigma_1-\Sigma_0$ vdW bending band of Ar-HBr.

V-P-4 Millimeter-Wave Spectroscopy of the van der Waals Bending Band of OCO-HF with a Supersonic Jet Expansion Technique

HARADA, Kensuke; ISHIGURO, Masazumi¹; TANAKA, Takehiko¹; TANAKA, Keiichi²
(¹Kyushu Univ.; ²IMS and Kyushu Univ.)

The OCO-HF is a hydrogen-bonded quasi-linear cluster with a dissociation energy of 672 cm^{-1} . The intermolecular potential is double minimum at a bend structure of the COH angle of 22° and a potential barrier of about 1 cm^{-1} is expected in the linear configuration.¹⁾ The rotational spectrum²⁾ and infrared spectrum³⁾ have been already reported. In the present study, we have measured the van der Waals (vdW) bending 1^1-0^0 (ν_b) band by the millimeter wave jet spectroscopy.

The 8 atm mixed gas of 1% HF, 5% CO₂, 31% Ar, and 63% Ne was injected into the vacuum chamber by a pulsed nozzle. In the 250–325 GHz region, 30 rovibrational transitions, P(2)–P(5), Q(1)–Q(15), and R(0)–R(10), were assigned to the 1^1-0^0 (ν_b) fundamental band. Figure 1 shows the stick diagram of the observed spectrum. The band has intense Q and R branch lines, while the P branch lines are rather weak.

An usual linear molecule Hamiltonian with the (2,2) interaction was used for the analysis. The band origin of the 1^1-0^0 band was determined to be 272548.8017 (49) MHz. The rotational constant, centrifugal distortion constant, *l*-type doubling constant, and its higher order term were determined precisely. In order to determine the two dimensional intermolecular bending potential surface, the measurement of the vdW hot band and vdW band of the deuterated species will be important.

References

- 1) D. J. Nesbitt and C. M. Lovejoy, *J. Chem. Phys.* **96**, 5712 (1992).
- 2) F. A. Baiocchi, T. A. Dixon, C. H. Joyner and W.

Klemperer, *J. Chem. Phys.* **74**, 6544 (1981).

- 3) D. J. Nesbitt and C. M. Lovejoy, *J. Chem. Phys.* **93**, 7716 (1990).

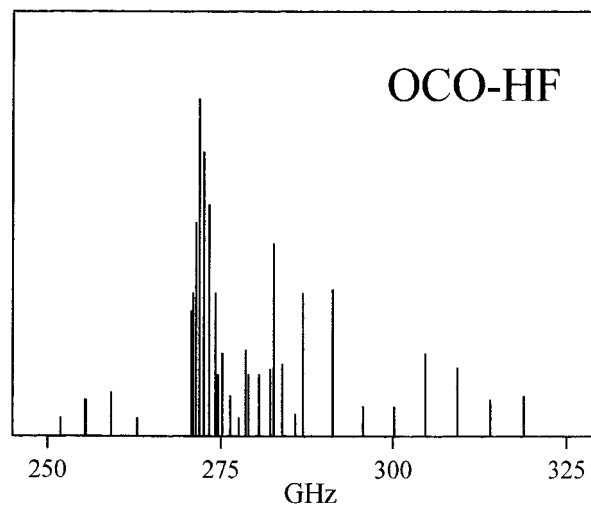


Figure 1. The stick diagram of the observed spectrum of the vdW bending band of OCO-HF.

V-Q Ion-Molecule Reactions in the Troposphere

Ion chemistry in the troposphere is the most complicated among all level of earth's atmosphere because of the presence of a variety of trace compounds. We have been studying ion-molecule reactions in the troposphere by investigating ion mobility distribution and its dependence on reaction time, pressure and temperature using an ion mobility spectrometer.^{1,2)} In order to confirm the ion-molecule reactions occurring in the troposphere, we developed a high-resolution ion mobility/mass spectrometer which is capable of chemical identification of ion species forming ion peaks in mobility spectra. Using this spectrometer, we investigate the ion processes in conditioned laboratory air as well as in natural air.

References

- 1) K. Nagato and T. Ogawa, *J. Geophys. Res.* **103**, 13917 (1998).
- 2) K. Nagato, D. J. Tanner, H. R. Friedli and F. L. Eisele, *J. Geophys. Res.* **104**, 3471 (1999).

V-Q-1 Measurements of Mobility and Mass Spectra of Tropospheric Ions

NAGATO, Kenkichi

We have developed a high-resolution ion mobility/mass spectrometer that can make simultaneous measurements of mobility and mass spectra of cluster ions generated by ion-molecule reactions under atmospheric pressure. The spectrometer consists of a drift tube, a mass analyzer, and an interface chamber between the drift tube and the mass analyzer. Both positive and negative ions, which are generated by irradiation of laboratory air with an americium source, are investigated by measuring mobility spectra, mass spectra, and mass-resolved mobility spectra. The results provide new information on the tropospheric ion evolution. In the positive ion spectra, ammonium ions dominate at around a few tenth milliseconds after ionization. Then, they are converted into other ion species that have higher proton affinities than that of ammonia. Such ion species include pyridine, methylpyridine, methylamine, dimethylamine, trimethylamine, and isobutylamine. In addition, several ions are found in the mass spectra at masses 135, 149, 152, and 279, which have not been identified. In the negative ion mass spectra, we found new ion species at masses 45, 46, and 89, which were identified as ions of formic acid, nitrous acid, and oxalic acid, respectively.

RESEARCH ACTIVITIES VI

Department of Vacuum UV Photoscience

VI-A Electronic Structure and Decay Mechanism of Inner-Shell Excited Molecules

This project is being carried out in collaboration with Fritz-Haber Institute, McMaster University, University of Alberta, and Photon Factory. We are experimentally interested in ionic fragmentation and electron emission via inner-shell excitation of molecules and in their linear polarization dependence. Recently we are also developing a theoretical approach based on quantum chemistry for inner-shell spectroscopy and dynamics.

VI-A-1 Partial Electron Yield Spectrum of N₂: Doubly Excited States at the K-Shell Threshold

NEEB, Matthias¹; BRADSHAW, Alexander M.¹; KOSUGI, Nobuhiro
(¹Fritz-Haber Inst.)

[*Chem. Phys. Lett.* in press]

Doubly excited states have been revealed both below and immediately above the core ionization threshold in N₂ by measuring a partial electron yield spectrum at the kinetic energy corresponding to the Auger decay of the double excitations. In this partial yield spectrum the core-to-Rydberg transitions and the σ^* shape resonance are absent from this absorption spectrum. The calculated potential energy curves suggest a strongly dissociative nature of the molecular-type double excitations. This agrees well with the observed width of the absorption feature in the partial yield spectrum.

VI-A-2 Inner-Shell Excitation of PF₃, PCl₃, PCl₂CF₃, OPF₃ and SPF₃

NEVILLE, John J.¹; JÜRGENSEN, Astrid²; CAVELL, Ronald G.²; KOSUGI, Nobuhiro; HITCHCOCK, Adam P.¹
(¹McMaster Univ.; ²Univ. Alberta)

[*Chem. Phys.* **238**, 201 (1998)]

Total ion yield spectra of PF₃, PCl₃, PCl₂CF₃, OPF₃ and SPF₃ were recorded in the region P 2p, P 2s, S 2p, S 2s and halogen (Cl 2p, F 1s) excitation using synchrotron radiation. The theoretical calculations indicate that several of the discrete states are best described as LS-coupled states because the core-valence electron exchange is very large and thus the singlet-triplet splitting is larger than the spin-orbit splitting. Aspects of partial ion yield measurements support this interpretation by revealing isolated single states without a corresponding partner at the spin-orbit splitting. The partial ion yields help clarify spectral interpretation by removing interference from overlap with adjacent states having the normal (j,j)-coupled ion core character.

VI-A-3 The Sulphur 2p Photoabsorption Spectrum of NSF₃

JÜRGENSEN, Astrid¹; KOSUGI, Nobuhiro;

CAVELL, Ronald G.¹
(¹Univ. Alberta)

[*Chem. Phys.* in press]

The Sulfur 2p photoabsorption spectrum of gaseous NSF₃ has been measured at high resolution using synchrotron radiation. Similar to isoelectronic OPF₃ and other pyramidal phosphorus compounds there exist two states, best described as LS-coupled because of a very large core-valence electron exchange. The post-edge features, corresponding to outer well p and d shape resonances, were assigned.

VI-A-4 Jahn-Teller Effect and Rydberg-Valence Mixing in the C1s → 3p_{t2} and 3d_{t2} Rydberg Excited States of CH₄

ADACHI, Jun-ichi; TAKATA, Yasutaka; SHIGEMASA, Eiji; KOSUGI, Nobuhiro; YAGISHITA, Akira¹
(¹KEK-PF)

Figure 1 shows angle-resolved photoion-yield spectra for the C1s excited states of CH₄ using linearly polarized synchrotron radiation. The angular distributions of fragment ions emitted from the C1s → 3p_{t2} and 3d_{t2} Rydberg excited states of CH₄ are anisotropic; the anisotropy parameter β_{3V} deviates from zero. This means that the bond angle on the fragmentation is distorted. The anisotropic photoabsorption is attributed to the Jahn-Teller effect in the excited states with ¹T₂ symmetry. The bond angle distortion on the fragmentation is related to the Jahn-Teller distortion along the bending modes (ν_2 and ν_4). The Jahn-Teller effect in the Rydberg excited states is expected to be so weak that the T_d geometry is hardly changed. We have to take into account the Rydberg-valence mixing in order to explain the present result, that is, the 2t₂* valence orbital may be mixed with the 3p_{t2} and 3d_{t2} Rydberg orbitals in the distorted geometry.

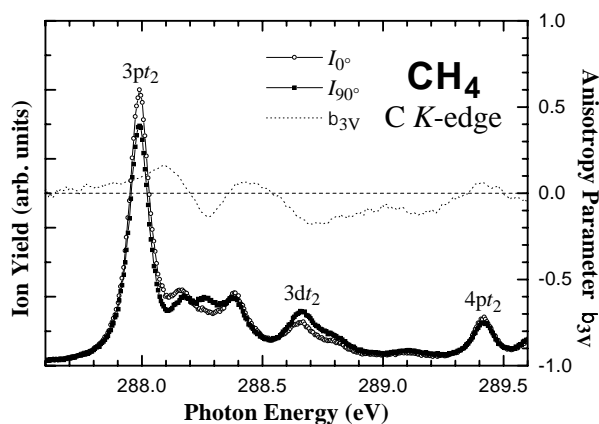


Figure 1. Angle-resolved ion-yield spectra for the C1s \rightarrow $3pt_2$ and $3dt_2$ Rydberg excited states of CH_4 .

VI-A-5 Renner-Teller Splitting in the $1s \rightarrow 1\pi_g^*$ Excited States of C_2H_2

ADACHI, Jun-ichi; TAKATA, Yasutaka; SHIGEMASA, Eiji; KOSUGI, Nobuhiro; YAGISHITA, Akira¹
(¹KEK-PF)

Figure 1 shows high-resolution angle-resolved photoion-yield spectra for the $\text{C}1s \rightarrow 1\pi_g^*$ excited states of C_2H_2 . The π^* peak shows fine structures on the lower energy side with a spacing of about 0.11 eV. The fine structures of the lower energy side are dominated by the bending modes (cis- and trans-bending modes), which are induced by the Renner-Teller effect. The fragment ions at the π^* peak are observed not only in the 90° direction but also in the 0° direction (I_{0°) respective to the electric vector of the incident light (I_{90°); the anisotropy parameter β_{3v} deviates from -1 . In addition, the I_{0° yield is slightly enhanced on the lower energy side of the peak. The result agrees with the Renner-Teller splitting, that is, the lower π^* excited state has a stable bent structure. The π^* peak has a clear shoulder structure on the higher energy side with its spacing of about 0.46 eV. This shoulder is mainly attributed to the C-H stretching mode.

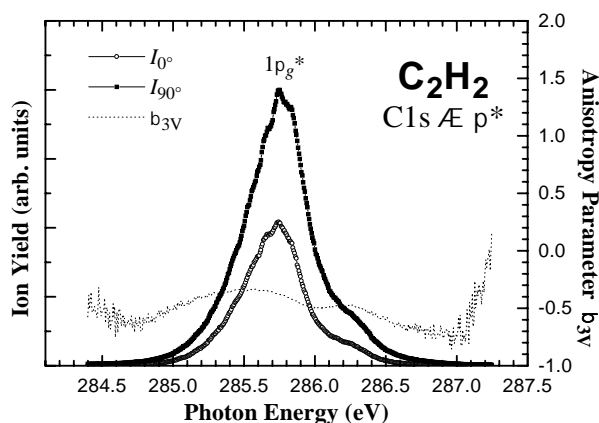


Figure 1. Angle-resolved ion-yield spectra for the $\text{C}1s \rightarrow \pi^*$ states of C_2H_2 .

VI-A-6 Enhancement of the $\text{O}1s \rightarrow n\sigma_g$ Rydberg Series of CO_2 through the $5\sigma_g$ -Valence Mixing

ADACHI, Jun-ichi; TAKATA, Yasutaka; SHIGEMASA, Eiji; KOSUGI, Nobuhiro; YAGISHITA, Akira¹
(¹KEK-PF)

We have measured high-resolution angle-resolved ion-yield spectra for the $\text{O}1s$ excited states of CO_2 using linearly polarized synchrotron radiation. The spectra show the $2\pi_u^*$ peak at 535.4 eV, the Rydberg series between 536 and 540.8 eV, the broad peak just above the $\text{O}1s$ ionization threshold, and the shape resonance ($4\sigma_u^*$) at 559 eV. It is found that the $\text{O}1s \rightarrow 3s\sigma_g$ Rydberg peak overlaps with the higher energy-side component of the π_u^* peak. The present spectra show that the $n\sigma_g$ Rydberg series is the stronger than the other Rydberg series. In addition, the intensity of the $4s\sigma_g$ Rydberg peak is stronger than that of the $3s\sigma_g$ Rydberg peak. These results are explained by the $n\sigma_g$ Rydberg- $5\sigma_g^*$ valence mixing as in the case for the terminal N and $\text{O}1s$ excited states of N_2O .¹⁾ On the other hand, the $5\sigma_g^*$ valence excited state may raise its energy just above the $\text{O}1s$ ionization threshold through the mixing.

Reference

- 1) J. Adachi *et al.*, *J. Chem. Phys.* **102**, 7369 (1995).

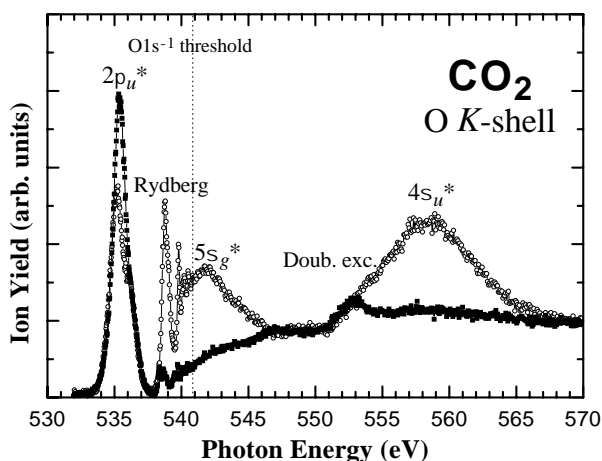


Figure 1. Angle-resolved ion-yield spectra for the $\text{O}1s$ excited states of CO_2 .

VI-A-7 Vibronic Coupling and Valence Mixing in the $1s \rightarrow \text{Rydberg}$ Excited States of C_2H_2 in Comparison with N_2 and CO

ADACHI, Jun-ichi; SHIGEMASA, Eiji; KOSUGI, Nobuhiro; YAGISHITA, Akira¹
(¹KEK-PF)

[*Chem. Phys. Lett.* in press]

The angle-resolved ion-yield spectra are reported for the $\text{C}1s \rightarrow \text{Rydberg}$ excitations of linear acetylene, C_2H_2 , in comparison with N_2 and CO . The $3\sigma_u^*$ valence state is observed in the $3s\sigma_g$ Rydberg region with no mixing. The $3p\sigma_u$ state is found in the same region as the $\text{C}1s\sigma_g \rightarrow 3p\pi_u$ state, which shows only totally symmetric vibrations. This is the first to observe that the Rydberg state in C_2H_2 keeps gerade and ungerade symmetries without vibronic coupling through

antisymmetric stretching vibrations related to core hole localization. On the other hand, the lowest $1\pi_g^*$ valence

state induces vibronic coupling through bending vibrations in the $3\sigma_u^*$ and $3s\sigma_g$ states.

VI-B Soft X-Ray Photoelectron-Photoabsorption Spectroscopy and Electronic Structure of Transition Metal Compounds

We are investigating electronic structure of molecular Ni complexes with planar structure by means of inner-shell photoabsorption and photoelectron spectra at the soft X-ray double crystal monochromator beamline BL1A of the UVSOR facility. We have found that a one-electron picture is appropriate to interpret the Ni 2p photoabsorption and resonant photoelectron spectra of the molecular Ni complexes, and that the metal-to-ligand charge transfer (MLCT) is essential to describe the photoexcited states. This year, we extend our study to resonant X-ray emission spectra, and also to another Ni compounds with Ni-Ni bonding.

VI-B-1 Ni 2p-3d Photoabsorption and Strong Charge Transfer Satellites in Divalent Ni Complexes with Molecular Ligands. Evaluation of π -Back Donation Based on the DFT Approach

PETTERSSON, Lars G. M.; HATSUI, Takaki¹;
KOSUGI, Nobuhiro
(¹GUAS)

[Chem. Phys. Lett. in press]

Density functional theory within a transition potential approach (DFT-TP) is applied to interpret remarkably strong π -type MLCT (metal-to-ligand charge transfer) satellites in the Ni 2p photoabsorption of planar low-spin Ni^{II} complexes, $K_2Ni(CN)_4 \cdot H_2O$ and bis(dimethylglyoximate)nickel. The MLCT intensities calculated with DFT-TP are in good agreement with experiment, whereas the HF-STEX (Hartree-Fock based static exchange approximation) approach underestimates the intensities. The DFT-TP approach gives more reasonable π -back donation due to a better description of the strong covalency hybridization of the ligand π^* orbitals with the occupied 3d orbitals. The DFT analysis indicates that we can evaluate π -back donation qualitatively by experimentally examining the MLCT satellites.

VI-B-2 Ni-Ni Chemical Bond in $[Ni_2(napy)_4Br_2][B(C_6H_5)_4]$ Studied by Linearly Polarized Ni 2p Photoabsorption

HATSUI, Takaki¹; TAKATA, Yasutaka; KOSUGI, Nobuhiro
(¹GUAS)

The Ni-Ni bonding is not well characterized in contrast to the metal-metal bonds of early transition metals. In order to elucidate the character of Ni-Ni bonding, linearly polarized Ni 2p photoabsorption spectra of $[Ni_2(napy)_4Br_2][B(C_6H_5)_4]$ (napy: 1,8-naphthyridine) were measured (Figure. 1). For $[Ni_2(napy)_4Br_2]^{1+}$ cation with Ni atoms of the formal oxidation number +1.5, there are 3 holes in σ -, δ -, and π -symmetry orbitals produced mainly by Ni 3d orbitals. The lowest band A is strong in the $E \perp z$ direction, and very weak in the $E \parallel z$ direction, where E and z denote

the electric vector of the incident photon and the molecular axis parallel to the Ni-Ni bond, respectively. This indicates that some holes are located in δ orbitals. On the contrary, band B is strong in the $E \parallel z$ direction and weak in the $E \perp z$ direction, indicating that the other holes are located in the σ^* orbital. The intensity ratio of band A to B is estimated to be about 2 from the spectrum of the powder sample. Therefore, one hole is located in the σ^* orbital and two holes in δ -symmetry orbitals, though we cannot distinguish between $\delta^3\delta^{*3}$ and $\delta^4\delta^{*2}$ configurations.

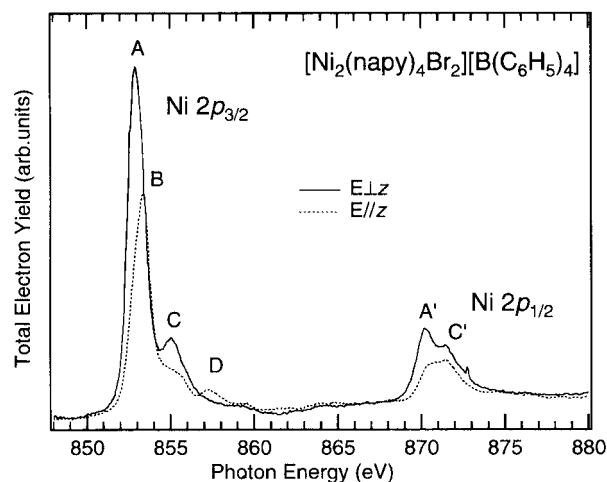


Figure 1. Linearly polarized Ni 2p photoabsorption spectra of a single crystalline $[Ni_2(napy)_4Br_2][B(C_6H_5)_4]$ for the $E \parallel z$ and $E \perp z$ directions, where E and z denote the electric vector of the incident photons and the molecular axis z parallel to the Ni-Ni bond, respectively.

VI-B-3 Valence Band Excitation Observed in Resonant Soft X-Ray Emission Spectra of $K_2Ni(CN)_4 \cdot H_2O$ at the Ni 2p Edge

TAKATA, Yasutaka; HATSUI, Takaki¹; KOSUGI, Nobuhiro; AGUI, Akane²; MAGNUSON, Martin²; SATHE, Conny²; RUBENSSON, Jan-Erik²; NORDGREN, Joseph²
(¹GUAS; ²Uppsala Univ.)

In order to investigate the valence band structure of a planar nickel complex $K_2Ni(CN)_4 \cdot H_2O$, which shows

characteristic MLCT (metal-to-ligand charge transfer) bands in the Ni 2p photoabsorption spectra, resonant soft X-ray emission spectra at the Ni 2p edge have been measured. The experiments were performed at the undulator beamline BW3 in HASYLAB (Germany).

Soft x-ray emission spectra of $\text{K}_2\text{Ni}(\text{CN})_4 \cdot \text{H}_2\text{O}$ at some Ni 2p resonant excitation are plotted in Figure 1 as a function of the energy difference between excitation and emission energies. At resonance A assigned to the intra-atomic Ni 2p $\rightarrow 3d^*$ excitation, three structures are observed in addition to the elastic peak at 0 eV. These peaks correspond to the $d \rightarrow d^*$ valence excitation with different symmetry. On the other hand, at t resonances B and C, the spectra drastically changed and give the single peak with narrow band width. We have assigned resonances B and C to the excitation to ligand π^* orbitals with different symmetry; therefore, the emission peaks correspond to the $d \rightarrow \pi^*$ or $\pi \rightarrow \pi^*$ valence excitation.

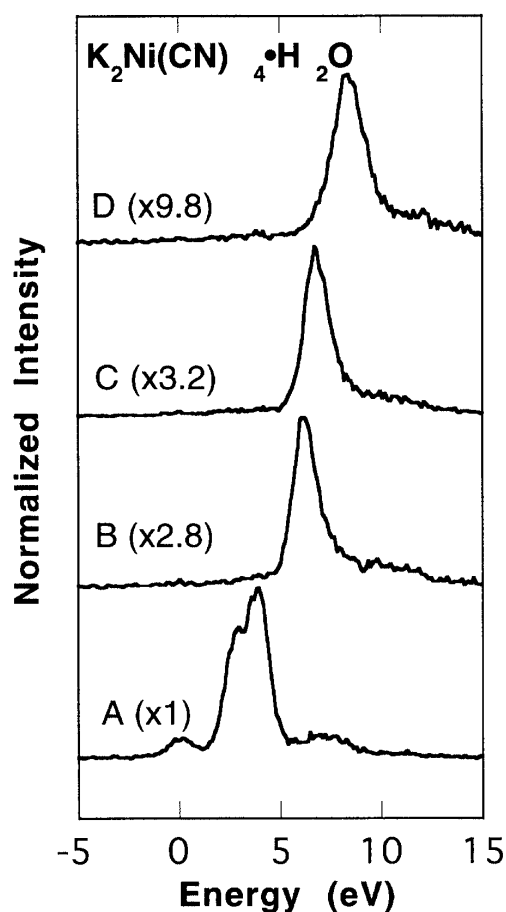


Figure 1. Soft x-ray emission spectra of $\text{K}_2\text{Ni}(\text{CN})_4 \cdot \text{H}_2\text{O}$ at some Ni 2p resonant excitation. The energy (lateral axis) is obtained by subtracting the emission energy from the excitation energy.

VI-B-4 Resonant X-Ray Emission Spectra of $\text{K}_2\text{Ni}(\text{CN})_4 \cdot \text{H}_2\text{O}$ at the Ni 1s Edge

TAKATA, Yasutaka; HATSUI, Takaki¹; SHOJI, Hironobu²; IWAZUMI, Toshiaki³; KOSUGI, Nobuhiro (¹GUAS; ²Univ. Tokyo; ³KEK-PF)

Recently, we have reported that the electronic

structure of nickel planar complexes can be described within a one-electron picture from the Ni 2p photoabsorption and resonant photoelectron spectra. This is different from the interpretation for the strongly correlated system such as NiO. In order to confirm our interpretation experimentally, resonant X-ray emission spectra of $\text{K}_2\text{Ni}(\text{CN})_4 \cdot \text{H}_2\text{O}$ at the Ni 1s edge were measured at the beamline BL-8B in Photon Factory.

Figure 1 shows resonant X-ray emission spectra at the Ni 1s excitation. The spectrum A was measured at a quadrupole transition to Ni $3d_{x^2-y^2}$, and B, C are at dipole transitions to Ni $4p\pi^*$. The elastic peak is shifted to the higher energy side with increase of the excitation energy. Nearby the peak, no extra feature with energy loss was observed. This is quite different from the results for NiO. In NiO, two peaks with the energy loss of 4.9 and 7.8 eV were observed and assigned to the deexcitation to an LMCT (ligand-to-metal charge transfer) state $3d^9\bar{L}$ (\bar{L} : ligand hole). The absence of the energy loss feature clearly indicates that LMCT is not important and the one-electron picture is appropriate for the nickel planar complexes. For the Ni $K\beta$ line, the energy shift is observed, depending on the photoexcited states. Narrowing of the peak width due to the Raman effect was observed.

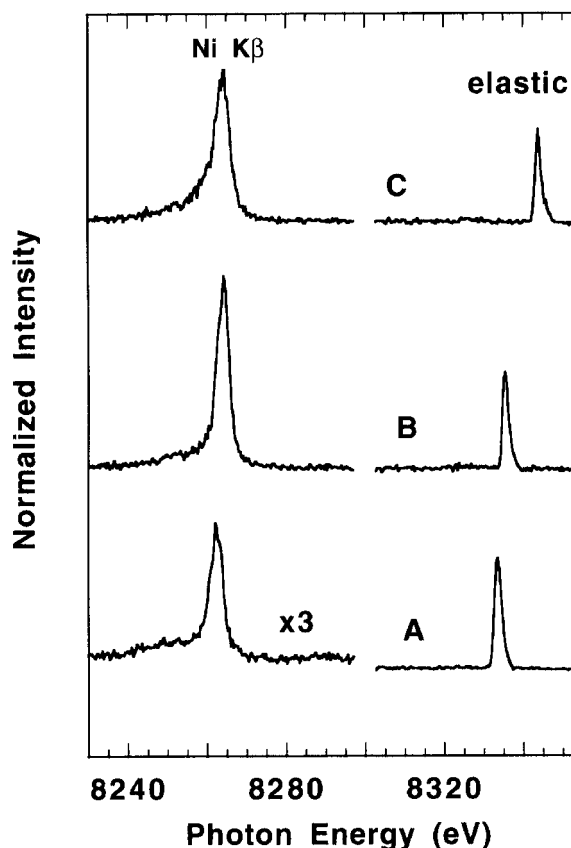


Figure 1. X-ray emission spectra of $\text{K}_2\text{Ni}(\text{CN})_4 \cdot \text{H}_2\text{O}$ at Ni 1s edge.

VI-C Generation of Ultrashort Optical Pulse for Time-Resolved Spectroscopy

It is important to improve time-resolution of time-resolved spectroscopy because higher time-resolution gives us a chance to observe new "fast" phenomena that can not be recognized with lower time-resolution. Nowadays, we can generate sub-10 fs pulses using modern laser technology. Although it is not easy task to handle such short optical pulses and to employ them for the study in molecular science, time-resolved spectroscopy utilizing such pulses are very important and desirable. We constructed two optical setups to generate ultrashort optical pulses whose duration is in the range from ten to a few tens of femtoseconds.

VI-C-1 Development of UV-Excited Transient Absorption Spectrometer Based on 10-fs Pulses

TAKEUCHI, Satoshi; TAHARA, Tahei

Ultrashort optical pulses have been widely used in time-resolved spectroscopic studies of the excited state properties and the reaction dynamics of molecules. The time-resolution in most of these studies, however, has been so far limited to the range of 200–500 fs. Particularly in experiments using ultraviolet pulses, the time-resolution tends to become worse due to broadening of the pulse duration in the frequency conversion process to the ultraviolet. In this project trying to achieve better time-resolution in molecular spectroscopy, we have constructed a high-power optical parametric amplifier (OPA) producing 10-fs pulses in the visible region, and utilized it for the transient absorption measurements (Figure 1). In the OPA, a femtosecond white-continuum seed pulse is amplified twice in a BBO nonlinear crystal, which is pumped by the second harmonic (400 nm) of the amplified Ti:sapphire laser pulse. The output pulse is then sent to a double-pass prism compressor to correct its phase dispersion. The autocorrelation of the compressed pulse (Figure 2A) indicates that the pulse duration is as short as 9.6 fs. The OPA is tunable in the wavelength region of 500–750 nm, and the typical pulse energy is 10–15 μJ at a 1 kHz repetition rate. Next, in the transient absorption spectrometer, most of the 10-fs pulse energy from the OPA is focused into a thin BBO crystal to generate the second harmonic tunable in the near-ultraviolet (250–375 nm). After the phase-dispersion compensation with a prism pair, the second harmonic is used as a pump pulse for photoexcitation of the sample. The minor rest of the 10-fs pulse is used as a probe and a reference pulse. The time-resolution of this spectrometer is evaluated as 35 fs from a cross-correlation trace between the pump and probe pulses (Figure 2B). This value is an order of magnitude better than that of a conventional transient absorption spectrometer using femtosecond white-continuum pulses. Observation of the excited state dynamics in a very early time region is now in progress by using this spectrometer.

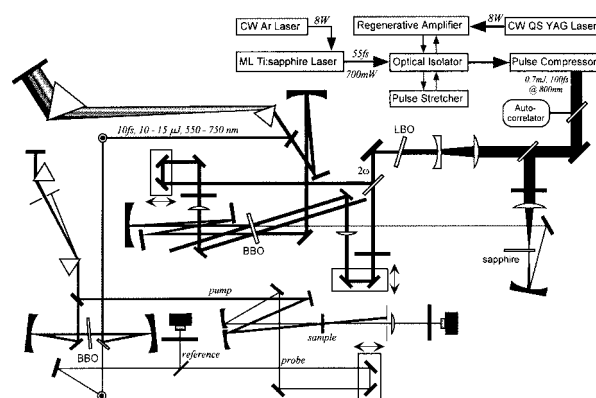


Figure 1. Experimental setup for uv-excited transient absorption measurements using 10-fs pulses.

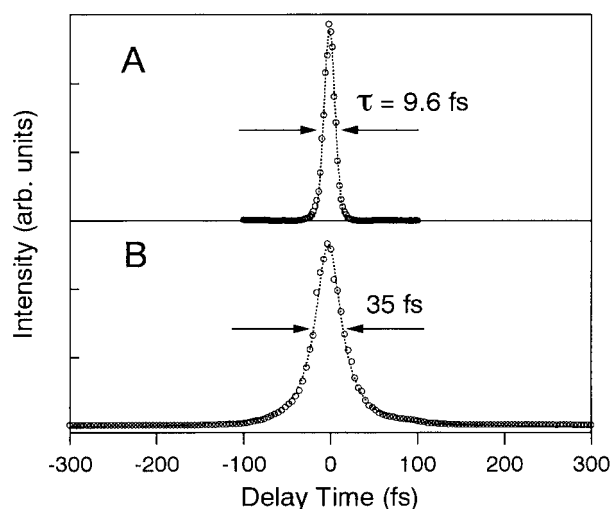


Figure 2. Autocorrelation of the OPA output pulse (A), and cross-correlation trace between the pump and probe pulses used in the transient absorption spectrometer (B).

VI-C-2 Generation of Ultra-Short Pulses Using a Krypton Gas-Filled Hollow Fiber

FUJIYOSHI, Satoru; TAKEUCHI, Satoshi; TAHARA, Tahei

We have constructed an apparatus to generate ultra-short pulses using a krypton gas-filled hollow fiber.¹⁾ This apparatus consists of two parts. In the first part, the femtosecond pulse from a Ti:sapphire regenerative amplifier (100 fs, 800 nm, 210 μJ , 1 kHz) is coupled into a hollow fiber that is filled with krypton gas. The input pulse spectrum becomes broader due to the self phase modulation in the gas while the pulse passes

through the fiber. The spectrum of the input pulse and that of the output pulse from the hollow fiber are shown in Figure 1a. Spectral width of the input pulse is 12 nm (FWHM) and that of the output pulse covers a wide range from 770 to 870 nm. In the second part, the broadened output pulse is sent to a prism compressor to correct its group velocity dispersion. Autocorrelation of the final compressed pulse is shown in Figure 1b. The pulse duration is as short as 30 fs as well as pulse energy of 5 μ J has been obtained.

Reference

1) M. Nisoli *et al.*, *Opt. Lett.* **22**, 522 (1997).

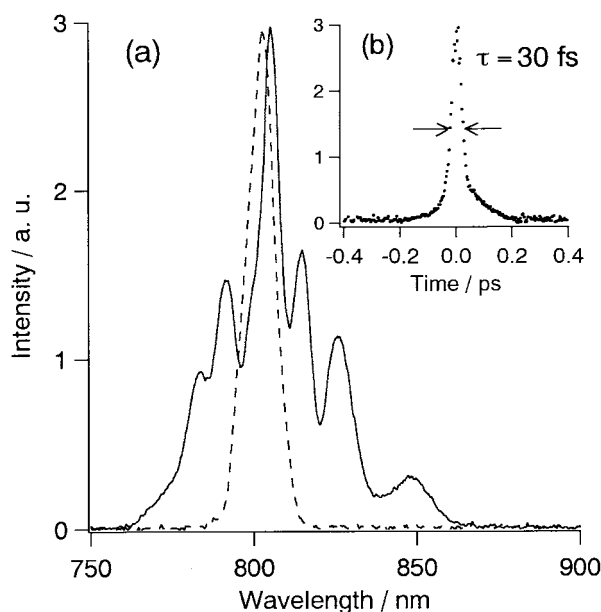


Figure 1. (a) Spectra of input pulse (dashed line) and output pulse (solid line) of hollow fiber. (b) Auto-correlation trace. The pulse duration (FWHM) is 30 fs.

VI-D Studies of Primary Photochemical/Physical Processes Using Femtosecond Fluorescence and Absorption Spectroscopy

Ultrafast spectroscopy is playing an essential role in elucidation of photochemical reactions. Thanks to the recent advance in laser technology, we are now able to observe the dynamics of chemical reactions taking place in the femtosecond time region. In this project, we are studying primary photochemical/physical processes in the condensed phase using time-resolved fluorescence and absorption spectroscopy with a few hundreds femtoseconds time-resolution. Time-resolved fluorescence and absorption spectroscopy are complimentary to each other. The advantage of fluorescence spectroscopy lies in the fact that fluorescence originates from the transition between the “well-known” ground state and the excited state in question. Thus time-resolved fluorescence spectroscopy can afford unique information not only about the dynamics but also other properties of the excited singlet states such as their energies and oscillator strengths. On the other hand, however, time-resolved absorption spectroscopy is considered to be more versatile because it can detect not only fluorescent excited singlet states but also other “dark” transients. In this year, we investigated the ultrafast proton transfer reaction and the relaxation process of the highly excited states of several fundamental molecules, with use of these time-resolved electronic spectroscopy.

VI-D-1 Vibronic Relaxation of Polyatomic Molecule in Non-polar Solvent: Femtosecond Anisotropy/Intensity Measurements of the S_n and S_1 Fluorescence of Tetracene

SARKAR, Nilmoni; TAKEUCHI, Satoshi; TAHARA, Tahei

[*J. Phys. Chem. A* **103**, 4808 (1999)]

The electronic and vibrational relaxation of tetracene have been studied in solution by femtosecond time-resolved fluorescence spectroscopy. Tetracene was initially photoexcited to the highly excited singlet (S_n) state, 1B_b , and the dynamics of the fluorescence from the 1B_b state and the 1L_a state (S_1) were investigated by fluorescence up-conversion. The fluorescence from the 1B_b state was observed in the ultraviolet region, and its lifetime was determined as ~ 120 fs. The anisotropy of

the 1B_b fluorescence was close to 0.4, which assured that the fluorescence is emitted from the excited state that was prepared by photoexcitation. The visible fluorescence from the 1L_a state showed a finite rise that agreed well with the decay of the 1B_b fluorescence (Figure 1A). Negative anisotropy was observed for the 1L_a fluorescence, reflecting that the 1L_a transition moment is parallel to the short axis of the molecule and hence perpendicular to the 1B_b transition moment. The anisotropy of the 1L_a fluorescence, however, showed a very characteristic temporal behavior in the femtosecond time region: it exhibited a very rapid change and reached a certain value that is deviated from -0.2 (Figure 1B). The anisotropy data indicate that the 1L_a fluorescence contains not only short-axis polarized component but also long-axis polarized component and that the ratio between the two components depends on both time and wavelength. The long-axis polarized component in the 1L_a fluorescence was assigned to the

1B_b -type fluorescence that appears as the result of the vibronic coupling between the 1L_a state and the 1B_b state. The observed initial rapid change of the anisotropy suggests that the highly excited vibrational states in the 1L_a state which are strongly coupled with the 1B_b state are first populated preferentially when the molecule is relaxed from the 1B_b state to the 1L_a state. The visible fluorescence anisotropy vanishes gradually due to the rotational diffusion in a few tens of picoseconds. In the picosecond region, we also observed additional dynamics in the fluorescence intensity whose time constant was about 12 ps. This dynamics was assigned to the vibrational relaxation (cooling) in the 1L_a state. The observed relaxation processes that take place after photoexcitation of tetracene are sketched in Figure 2.

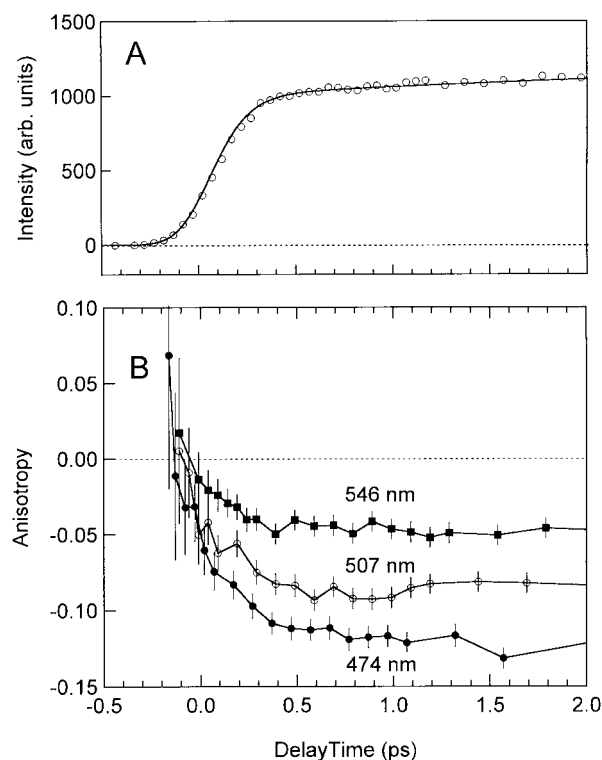


Figure 1. Early-time dynamics of the fluorescence intensity and anisotropy obtained from tetracene in hexadecane (273 nm excitation). (A) Time-resolved fluorescence signal at 507 nm measured with the magic angle condition. (B) Time-resolved fluorescence anisotropy measured at three different wavelengths (474, 507 and 546 nm).

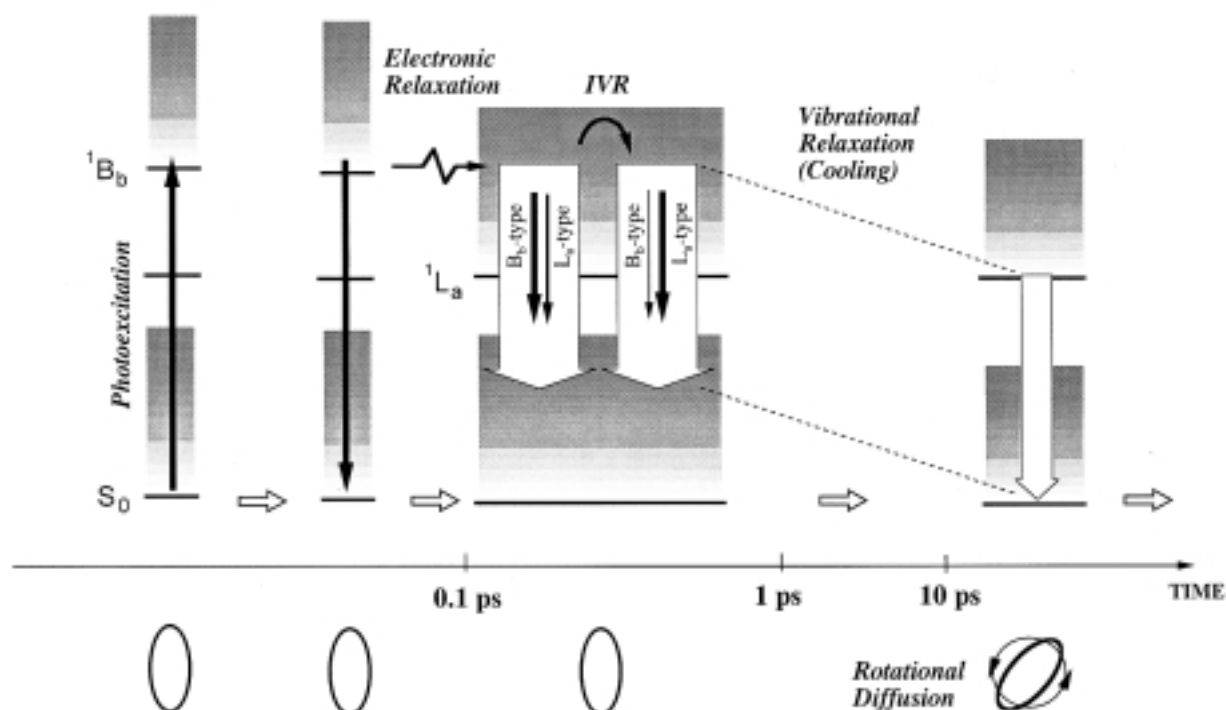


Figure 2. Schematic diagram depicting the relaxation processes of tetracene in solution following the direct photoexcitation to the high excited singlet (S_1) state.

VI-D-2 Determination of the Excited-State Transition-Moment Directions of 7-Aza-indole Dimer by Femtosecond Fluorescence Anisotropy Measurements

TAKEUCHI, Satoshi; TAHARA, Tahei

Time-resolved fluorescence anisotropy data can afford much information not only about the orientational diffusion of molecules in solution but also about the transition moment of the fluorescing state. In fact, the anisotropy change observed in the femtosecond time region does not arise from the orientational diffusion but is mainly caused by changes in the transition-moment direction, because the molecular motion is almost neglected in this short time region. Femtosecond fluorescence anisotropy measurement is, therefore, a powerful method which enables us to determine the transition-moment directions. In order to know the transition-moment directions of the three excited states (dimer L_b , dimer L_a , and tautomer L_a) which appear successively in the proton transfer reaction of 7-azaindole dimer, we measured fluorescence anisotropy of this dimer at three visible wavelengths with a 230-fs time-resolution (Figure 1). The anisotropy shows a rapid decay within one picosecond, and its feature depends on the observation wavelength. An additional slow component (12 ps) observed in every wavelength is due to the orientational diffusion of the dimer. We have simulated the time-dependence of the anisotropy on the basis of a model that includes the three excited states, and determined relative angles of the transition moments of each excited state by a fitting procedure (dotted curves). It was found that the wavelength dependence of the observed anisotropy can be explained by spectral difference of the fluorescences from the three excited states and that relative angle obtained from the data taken at the three wavelengths agreed very well with one another. We concluded that the relative transition-moment directions of the dimer L_a and tautomer L_a states with respect to the initially-populated dimer L_b state are 39° and 42° , respectively. It was reported by a rotational contour analysis of 7-azaindole in gas phase that the transition moment of the L_b state is 16° tilted from the inertial axis. Consequently, we can finally determine the absolute direction of the transition moments with respect to the inertial axis as 16° , 55° , and 58° for the dimer L_b , dimer L_a , and tautomer L_a states, respectively.

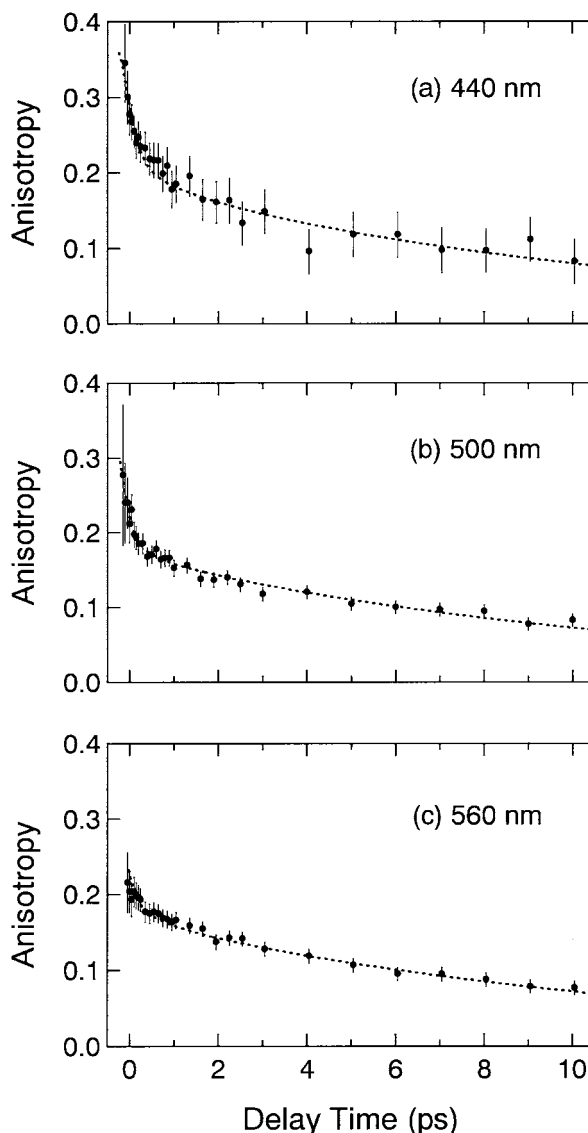


Figure 1. Time-resolved fluorescence anisotropy of 7-azaindole dimer in hexane measured at 440 (a), 500 (b), and 560 nm (c). Calculated anisotropy is also shown by a dotted curve.

VI-D-3 Investigation of Excited State Intramolecular Proton Transfer in Anthralin by Femtosecond Time-Resolved Fluorescence Spectroscopy

ARZHANTSEV, Sergei; TAKEUCHI, Satoshi; TAHARA, Tahei

Numerous elementary photoreactions in condensed phase occur on ultrafast time scale and femtosecond spectroscopy provides direct insight into the dynamics of such processes. The photoinduced intramolecular proton transfer of hydrogen-bonded molecules is a topic of current interest. Anthralin (1,8-dihydroxy-9(10H)-anthracenone) is of biological and pharmacological importance as antipsoriatic drug. Steady-state fluorescence excitation and emission spectra display an unusually large Stokes shift, indicating intramolecular proton transfer. The proposed scheme of photoinduced reaction is shown in Figure 1. Time-resolved fluorescence measurements were performed in a wide spectral

region from 480 nm to 690 nm. Several time-resolved fluorescence traces are presented in Figure 2. We observed the fast decays in blue side and coinciding fast rises in red side of the spectrum in (sub)picosecond time region, which gave us the information about the proton transfer rate. The global fit procedure was applied for quantitative analysis of experimental data. As results of fitting procedure, characteristic time constants ($\tau_1 = 0.1$ ps, $\tau_2 = 1.4$ ps, $\tau_3 = 120$ ps) of excited state dynamics were obtained. The excited state dynamics were discussed in terms of excited-state intramolecular proton transfer and other pathways of the energy relaxation.

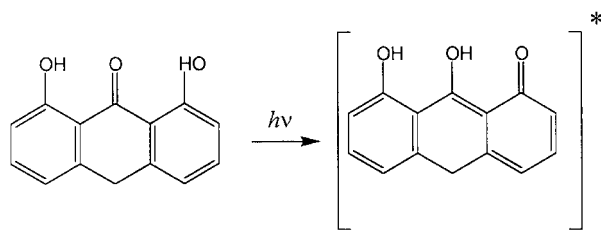


Figure 1. The proposed scheme of proton transfer in anthralin.

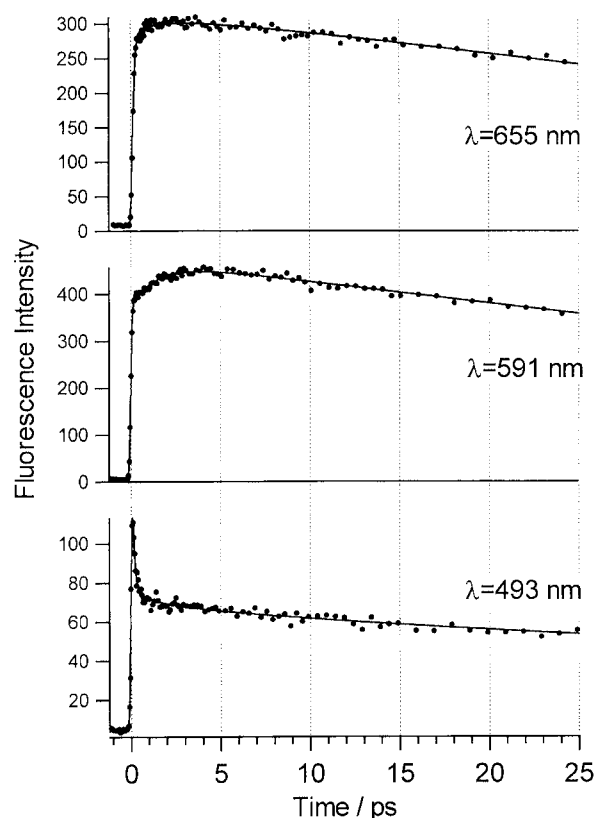


Figure 2. Time-resolved fluorescence traces obtained from anthralin at 655, 591 and 493 nm. The dots are experimental data and the solid curves are the results of the fitting analysis.

VI-D-4 Relaxation Kinetics of the S_n and S_1 States of Biphenyl Probed by Femtosecond Fluorescence Anisotropy

IWATA, Koichi¹; TAKEUCHI, Satoshi; TAHARA, Tahei
(¹Univ. Tokyo)

Fluorescence intensity and its anisotropy decay of biphenyl were measured in hexane solution. The sample solution was photoexcited with a linearly polarized femtosecond light pulse at 270 nm. Time dependence of the fluorescence intensity as well as its anisotropy was measured with the up-conversion method. The observed fluorescence decay curve showed a fast decay component of 0.4 ps, in addition to a slow component corresponding to the reported fluorescence decay of 16 ns. The observed fluorescence anisotropy value at time 0 was approximately 0.4, indicating that the direction of the fluorescence transition dipole at time 0 is same as the S_n - S_0 absorption at 270 nm. The observed anisotropy change was well fitted by a double exponential decay function, with time constants of 0.2 ps and 9 ps. The fast component represents the S_n - S_1 internal conversion process, while the slow component corresponds to the rotational diffusion of the S_1 state. From the extrapolated value of the slow component at time 0, the angle between the effective transition dipoles of the S_n - S_0 transition and the S_1 - S_0 transition was estimated to be 27 degrees.

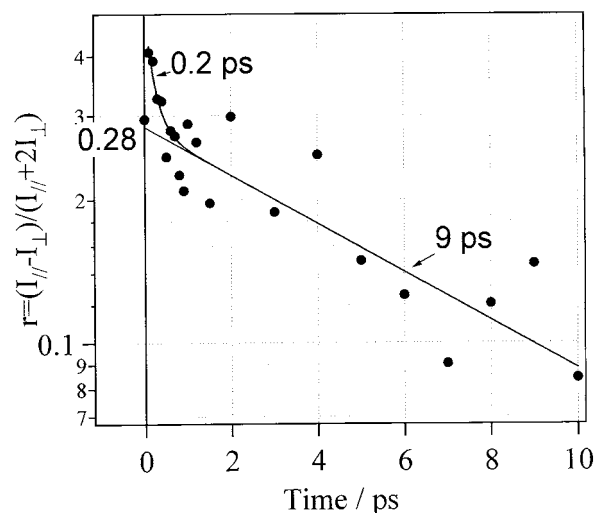


Figure 1. Time dependence of femtosecond fluorescence anisotropy of biphenyl.

VI-D-5 Lifetime Measurements of S_2 Emission from Zinc(II) Porphyrins by the Femtosecond Up-Conversion Method

ASANO-SOMEDA, Motoko¹; ARZHANTSEV, Sergei; TAHARA, Tahei
(¹Tokyo Inst. Tech.)

In violation of Kasha's rule, upper excited-state emission has been observed for some polyatomic molecules. For instance, a variety of diamagnetic metalloporphyrins exhibit fluorescence from the secondary excited singlet (S_2) state even under the steady-state condition. Relatively intense S_2 emission of metalloporphyrins must be related with their characteristic electronic structure. In the typical diamagnetic metalloporphyrins, the S_1 and S_2 states are described as a 50-50 admixture of two common (π, π^*) configurations, and this leads to almost parallel surfaces in the S_1 and S_2 states. In addition, there is a reasonably

large energy gap between the S_1 and S_2 states. Such features of metalloporphyrins slow $S_2 \rightarrow S_1$ internal conversion rates, thus allowing observation of S_2 emission.

Zinc(II) porphyrin is one of the typical diamagnetic metalloporphyrins and exhibits S_2 fluorescence. While subpicosecond lifetimes are estimated for such porphyrins from the quantum yields of S_2 emission, it is crucial to determine the lifetimes by means of time-resolved measurements. We have applied the femto-second up-conversion method to a series of zinc(II) porphyrins. Figure 1 shows the decay of S_2 and rise of S_1 emission signals of TMPZn(II) (TMP denotes tetramesitylporphin) measured with 400 nm excitation. Both kinetic traces give the same time constant of 1.6 ps, which corresponds to the S_2 lifetime.

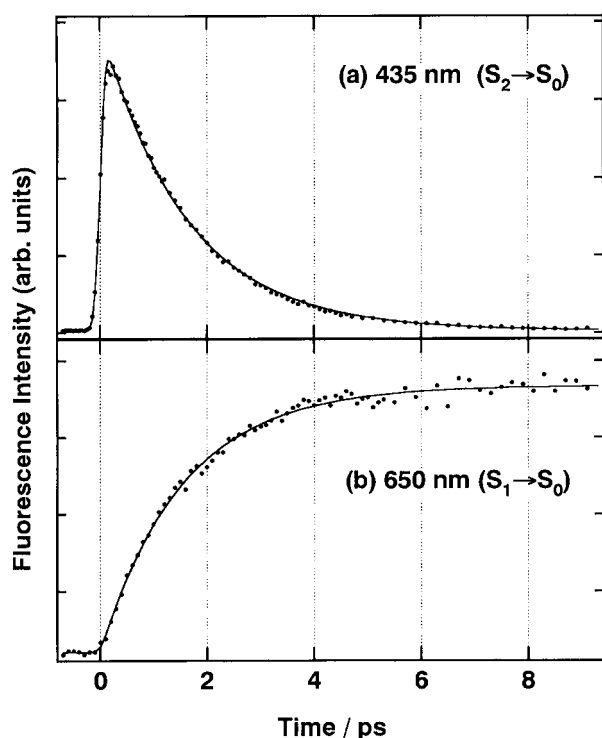


Figure 1. (a) Decay of S_2 and (b) rise of S_1 emission signals of TMPZn in toluene upon femtosecond laser irradiation at 400 nm. Experimental results are given by dots along with the best fitting curves in solid lines.

VI-D-6 Femtosecond Absorption Study on Ultrafast Decay Dynamics of Photoexcited Cu(II)(TMpy-P4) in Water Solvent

JEOUNG, Sae Chae; TAKEUCHI, Satoshi; TAHARA, Tahei; KIM, Dongho¹
(¹KRISS)

[Chem. Phys. Lett. **309**, 369 (1999)]

Femtosecond time-resolved absorption spectroscopy was employed to investigate the relaxation dynamics of photoexcited copper(II) tetrakis(4-N-methylpyridyl)-porphyrin (Cu(II)(TMpy-P4)) in neat water. It was found that the transient absorption spectra as well as their temporal profiles exhibit a strong pump-power dependency, which is probably the cause of the

discrepancy in the previous reports about dynamics of this molecule. It was concluded that the multiphoton ionization of solvent water takes place under the high pump-power condition. Time-resolved absorption spectra of Cu(II)(TMpy-P4) were measured with the pump power as low as 0.03 mJ/cm², and it was confirmed that the relaxation process finishes within 100 ps. We observed temporal changes of the excited-state(s) absorption in the picosecond region as well as the double exponential recovery of the ground state bleaching. The obtained time-resolved absorption data revealed that the relaxation process of photoexcited Cu(II)(TMpy-P4) in water is rather complicated and they suggested that several transient species (excited states) appear in the course of the relaxation. The relaxation mechanism of photoexcited Cu(II)(TMpy-P4) as well as the interaction with solvent water was discussed.

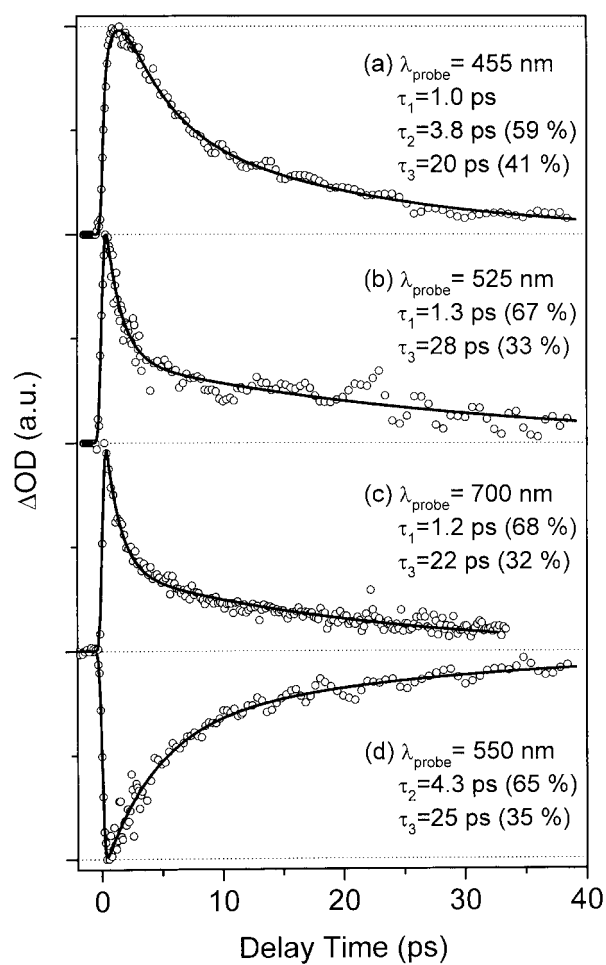


Figure 1. The time-resolved absorption changes of photoexcited Cu(II)(TMpy-P4) in water at three wavelengths of 455 (a), 525 (b) and 700 nm (c). The temporal change of the Q-band bleaching at 550 nm (d) was determined after correcting the baseline variation due to the photoinduced absorption.

VI-E Studies of Photochemical Reactions Using Picosecond Time-Resolved Vibrational Spectroscopy

Time-resolved vibrational spectroscopy is a very powerful tool for the study of chemical reactions. It often affords detailed information about the molecular structure of short-lived intermediates, which is not obtainable with time-resolved electronic spectroscopy. However, for molecules in the condensed phase, we need energy resolution as high as 10 cm^{-1} in order to obtain well-resolved vibrational spectra. This energy resolution is compatible only with time-resolution slower than picosecond because of the limitation of the uncertainty principle. In this sense, picosecond measurements are the best compromise between energy resolution and time resolution for time-resolved frequency-domain vibrational spectroscopy. In this project, we study photochemical processes and short-lived transient species by using picosecond time-resolved Raman spectroscopy. In this year, we focused on trans-azobenzene that is a prototypical molecule showing fast cis-trans isomerization. We studied the electronic and vibrational relaxation processes as well as the structure of the S_1 state of this molecule. In addition, while doing time-resolved Raman work, we recently noticed that amplified picosecond pulses are suitable for the excitation of hyper-Raman scattering.

VI-E-1 Picosecond Time-Resolved Raman Study of Trans-Azobenzene

FUJINO, Tatsuya; TAHARA, Tahei

[*J. Phys. Chem. A* in press]

The electronic and vibrational relaxation of photoexcited trans-azobenzene were investigated by picosecond time-resolved Raman spectroscopy. The second and third harmonic pulses of the regeneratively amplified output of a Ti:sapphire laser were used as the probe (410 nm) and the pump (273 nm). The frequency resolution of the measurement was approximately 10 cm^{-1} and time resolution was about 2 ps. With the 273-nm pumping pulse, the molecule is initially excited to the $S_2(\pi\pi^*)$ state, and the 410-nm probing wavelength is in resonance with the $S_n \leftarrow S_1$ transient absorption that appears in accordance with the decay of the S_2 state. Several transient Raman bands assignable to the S_1 state were observed immediately after photoexcitation. The lifetime of the S_1 state showed a significant solvent dependence and it was determined as $\sim 12.5\text{ ps}$ in ethylene glycol and $\sim 1\text{ ps}$ in hexane. Time-resolved anti-Stokes Raman measurements were also carried out for hexane solution to obtain information about vibrational relaxation process (Figure 1). We observed almost all S_1 Raman band in the anti-Stokes spectra, which implies that the S_1 state is highly vibrationally excited. In addition, several anti-Stokes Raman bands due to the S_0 state were observed after the decay of the S_1 state, indicating that the vibrationally excited S_0 azobenzene was generated after electronic relaxation in hexane. The lifetime of vibrationally excited S_0 azobenzene was evaluated as $\sim 16\text{ ps}$ by the analysis for the intensity change of the anti-Stokes NN stretching band. The relaxation process of photoexcited trans-azobenzene clarified in the present study is depicted in Figure 2.

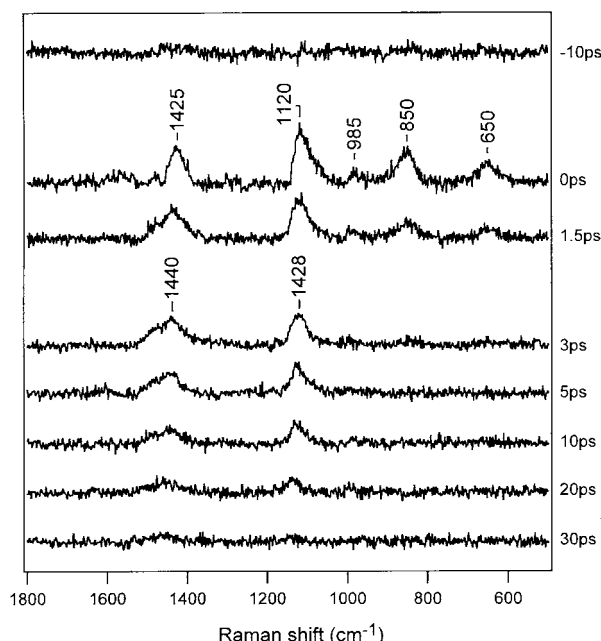


Figure 1. Picosecond time-resolved anti-Stokes Raman spectra of azobenzene in hexane in the delay time range from -10 ps to 30 ps ($1.5 \times 10^{-2}\text{ mol dm}^{-3}$; pump at 273 nm ; probe at 410 nm).

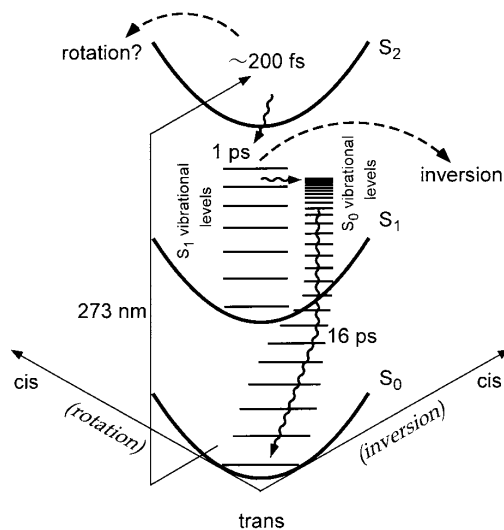


Figure 2. The relaxation mechanism of photoexcited trans-azobenzene (in hexane).

VI-E-2 Molecular Structure of S_1 Azobenzene: Vibrational Frequency of the NN Stretch Mode in the S_1 and S_0 State

FUJINO, Tatsuya; TAHARA, Tahei

Time-resolved vibrational spectra contain much information about the molecular structure of transient species. Concerning the S_1 state of azobenzene, information about the structure around the central NN bond is the most important because it can afford a clue to understand how the S_1 state participates in the photoisomerization process. In this sense, the assignment of the NN stretching vibration is crucial. We synthesized a ^{15}N -substituted analogue and measured S_1 Raman spectra in order to make unambiguous assignment about this key vibration and to discuss the molecular structure of the S_1 state.

Figure 1 shows transient Raman spectra of the normal species and the ^{15}N analogue ($(\text{C}_6\text{H}_6^{15}\text{N})_2$) of the S_1 state of azobenzene. The spectra were measured for ethylene glycol solutions. The Raman spectra of the S_0 state are also shown in this figure for the comparison. In the S_1 spectra, it is clearly recognized that the Raman band at 1428 cm^{-1} shows a 27-cm^{-1} downshift with ^{15}N substitution. This S_1 band is straightforwardly attributable to the NN stretching vibration in the S_1 state. The NN stretching frequency in the S_1 state is almost same as that in the S_0 state (1440 cm^{-1}), which manifests that the NN bond in S_1 azobenzene retains a double bond character. The double bond nature of the NN bonding as well as high similarity in the spectral feature between S_1 Raman and S_0 Raman suggests that the observed S_1 azobenzene has a planar structure around the central NN bond.

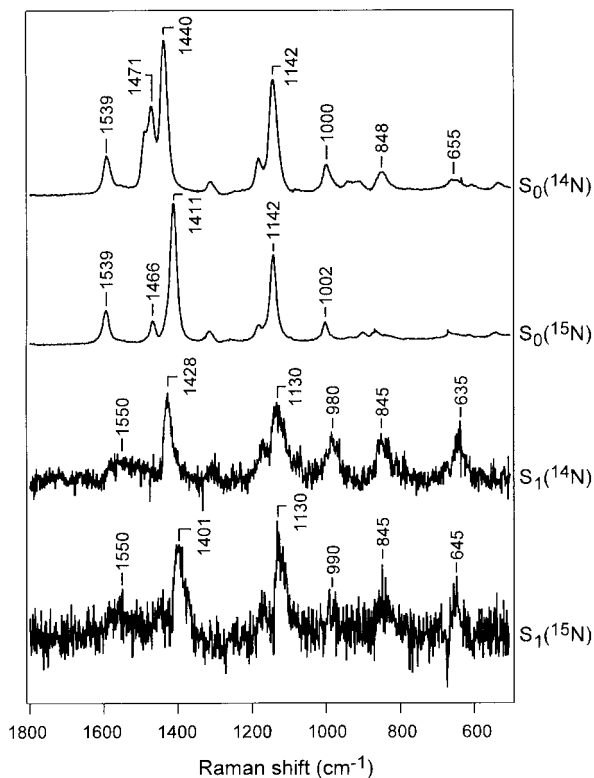


Figure 1. Raman spectra of azobenzene in the S_1 state and the S_0 state (in ethylene glycol). From the top to the bottom, normal species in the S_0 state, ^{15}N analogue in the S_0 state, normal species in the S_1 state, and ^{15}N analogue in the S_1 state. The S_1 spectra were taken at 0 ps. ($1.5 \times 10^{-2}\text{ mol dm}^{-3}$; pump at 273 nm; probe at 410 nm).

VI-E-3 Observation of Resonance Hyper-Raman Scattering of *all-trans* Retinal

MIZUNO, Misao; TAHARA, Tahei; HAMAGUCHI, Hiro-o¹
(¹Univ. Tokyo)

High peak powered ultrafast lasers allow us to observe a variety of higher order optical processes. We recently found that a fairly strong hyper-Raman scattering of *all-trans* retinal can be observed by using the excitation with amplified picosecond pulses under a resonance condition, even from a diluted solution. A typical resonance hyper-Raman spectrum excited at 800 nm (ω) is shown in Figure 1(a). The probe pulse was the output of the picosecond regenerative amplifier of a Ti:sapphire laser system. The pulse width and the pulse energy were about 2 ps and 10 μJ , respectively. The resonance Raman spectrum excited at 400 nm (2ω) is shown in Figure 1(b), for comparison. The spectral pattern of the hyper-Raman and the Raman spectra is very similar to each other, although the intensity enhancement arises from two-photon resonance in hyper-Raman process while it is due to one-photon resonance in ordinary Raman. The similarity of these spectra suggests that resonance mechanism of hyper-Raman scattering is attributed to the A-term of the resonance hyper-Raman theory.¹⁾ We also measured resonance hyper-Raman spectra of *all-trans* retinal by probing at every 10 nm from 770 nm to 840 nm, and examined the excitation profiles.

Reference

- 1) Y. C. Chung and L. D. Ziegler, *J. Chem. Phys.* **88**, 7287 (1988).

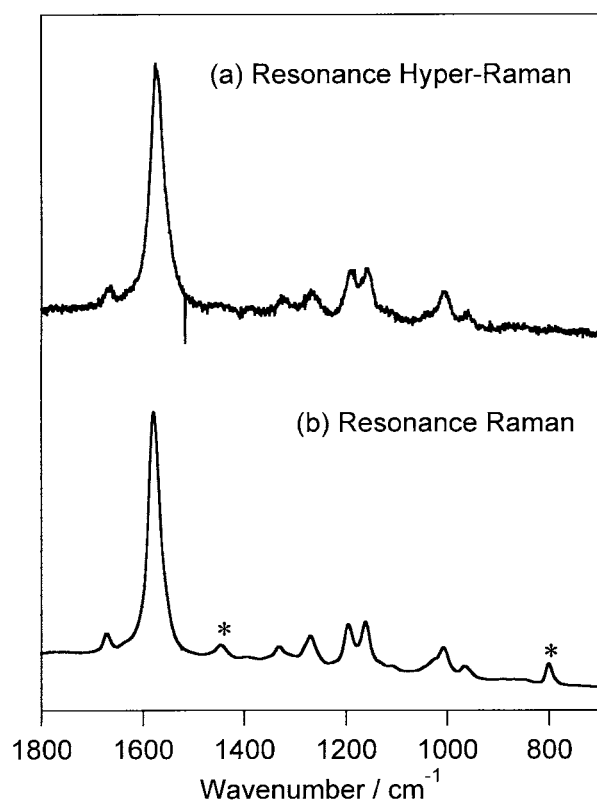


Figure 1. Comparison of (a) resonance hyper-Raman and (b) resonance Raman spectra of all-trans retinal in cyclohexane (1×10^{-3} mol dm⁻³). Excitation wavelength is 800 nm for resonance hyper-Raman, and 400 nm for resonance Raman. The asterisks (*) indicate solvent bands.

VI-F Synchrotron Radiation Stimulated Surface Reactions

Study of synchrotron radiation (SR) stimulated surface reaction is a promising topic in fundamental science, because dynamical processes induced by the photostimulated core electron excitations on surfaces are scarcely explored so far. This field is important also in applied science, since the fundamental study is expected to develop the new techniques for semiconductor processing such as SR stimulated etching and SR stimulated epitaxial growth.

VI-F-1 Vibration Analysis of SiH_n Bending Modes on Hydrogenated Si(100) Surface Using Infrared Reflection Absorption Spectroscopy

NODA, Hideyuki; URISU, Tsuneo; HIRAMATSU, Mineo¹
(¹Meijo Univ.)

Detailed analyses have been successfully made for the SiH_n stretching vibration mode on hydrogenated Si(100) surface, which is of great scientific and technological interest.¹⁾ However, concerning the bending vibration region, which gives important information about SiH_2 and SiH_3 species, very little work has been done. Recent developments of buried metal layer-infrared reflection absorption spectroscopy (BML-IRRAS) have made the high-resolution vibration analysis of the bending region easy. In this work, adsorption and desorption of hydrogen on Si(100) surfaces have been investigated by measuring BML-IRRAS covering a wide spectral range (800–2200 cm^{-1}). In both 3×1 and 1×1 phases observed with reflection high-energy electron diffraction (RHEED), a doublet peak (902 and 913 cm^{-1}) has been clearly observed and assigned to the SiH_2 scissors mode. The splitting of the peak is most likely due to the frequency difference of SiH_2 scissors vibration between single SiH_2 (ordered 3×1 units; H-Si-Si-H H-Si-H H-Si-Si-H) and neighboring SiH_2 (disordered 3×1 units; H-Si-Si-H H-Si-H H-Si-H H-Si-Si-H). Coverage and annealing temperature dependence of this doublet peak have also been investigated.

Reference

1) Y. J. Chabal and K. Raghavachari, *Phys. Rev. Lett.* **54**, 1055 (1985).

VI-F-2 Scanning Tunneling Microscopy for the Study of the Synchrotron-Radiation Stimulated Processes; Synchrotron-Radiation Stimulated Desorption of SiO_2 Films on Si(111) Surface

MIYAMAE, Takayuki; URISU, Tsuneo; UCHIDA, Hironaga¹; MUNRO, Ian H.²
(¹Toyohashi Univ. Tech.; ²UMIST)

[*Jpn. J. Appl. Phys.* **38**, 249 (1999)]

We have constructed a scanning tunneling microscopy (STM) system for the study of synchrotron radiation (SR) stimulated photochemical reactions. In order to eliminate the vibration and acoustic noise, the entire UHV chamber is mounted on a high-performance air-suspended vibration isolation table and was also covered by the soundproof mat. The mechanisms for SR stimulated desorption of SiO_2 thin films on the Si (111)

surfaces have been investigated using the STM, low energy electron diffraction (LEED), and Auger electron spectroscopy. An atomically flat and clean Si(111)-(7 \times 7) surface was obtained after two hours SR irradiation at a surface temperature of 700 °C. The STM topograph suggests that the desorption mechanism may be completely different between thermal and SR stimulated desorption of SiO_2 film.

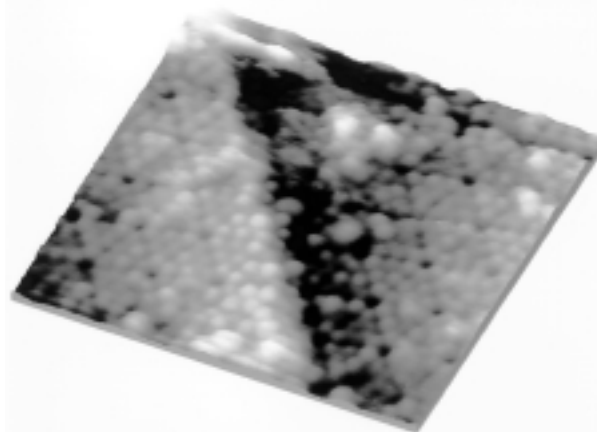


Figure 1. Three-dimensional STM image of 2 hours SR-irradiation to the samples at the sample temperature of 700 °C. Image size = 15 \times 15 nm.

VI-F-3 Synchrotron-Radiation Stimulated Desorption of SiO_2 Thin Films on Si(111) Surfaces Observed by Scanning Tunneling Microscopy

MIYAMAE, Takayuki; UCHIDA, Hironaga¹; MUNRO, Ian H.²; URISU, Tsuneo
(¹Toyohashi Univ. Tech.; ²UMIST)

[*J. Vac. Sci. Technol., A* **17**, 1733 (1999)]

Synchrotron radiation (SR) stimulated desorption of silicon dioxide thin films was studied using scanning tunneling microscopy (STM), low energy electron diffraction (LEED), and Auger electron spectroscopy. Reconstructed Si(111)-7 \times 7 patterns were observed by LEED after 2 h SR irradiation at a surface temperature of 700 °C. The STM images show an atomically flat Si(111)-(7 \times 7) surface. STM topographs of SR-irradiated surfaces suggest that the oxide desorption mechanism is completely different from that of thermal desorption of SiO_2 film. These results indicate that the atomically flat Si surface can be obtained at low temperatures by using this technique.

VI-F-4 Direct Observation of Synchrotron Radiation Stimulated Desorption of Thin SiO₂ Films on Si (111) by Scanning Tunneling Microscopy

MIYAMAE, Takayuki; UCHIDA, Hironaga¹; MUNRO, Ian H.²; URISU, Tsuneo
(¹Toyohashi Univ. Tech.; ²UMIST)

[*Surf. Sci. Lett.* **437**, L755 (1999)]

This is the first report of the use of scanning tunneling microscopy (STM) to study changes in the surface morphology during synchrotron radiation (SR) stimulated desorption of SiO₂ films on Si(111). An atomically flat surface was obtained after two hours SR irradiation at a surface temperature of 700 °C. The STM topograph indicates that the SR desorption mechanism is quite different for the thermal desorption of SiO₂. The non-formation of multistep holes on the exposed Si surface indicates that the desorption of oxygen atoms and molecules by SR excitation leaving volatile SiO is an important mechanism.

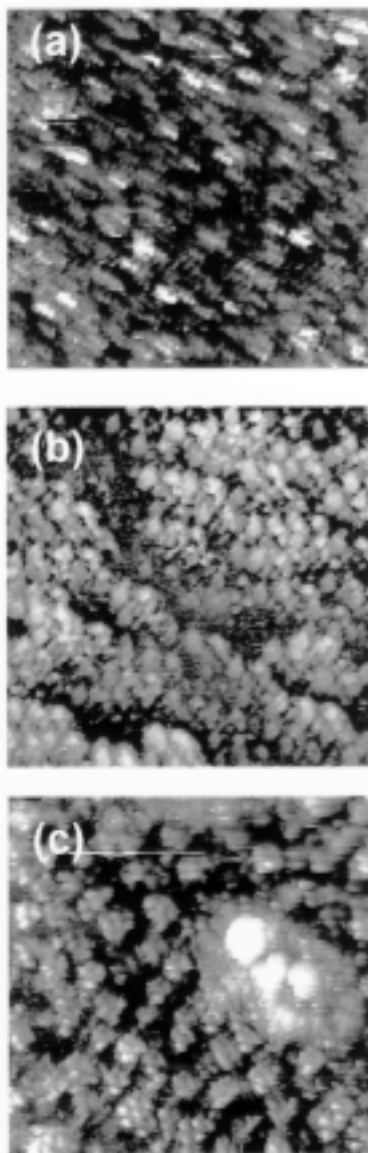


Figure 1. (a) STM image of Si (111) sample after 2.5 h SR-irradiation at the sample temperature of 650 °C. Image size = 2000 × 2000 Å. (b) STM image of 1 h SR-irradiation to the samples at the sample temperature of 700 °C. Image size = 5000 × 5000 Å. (c) STM image of 2 h SR-irradiation to the samples at the sample temperature of 700 °C.

VI-F-5 Scanning Tunneling Microscopy Study of Surface Morphology of Si(111) after Synchrotron Radiation Illumination

GAO, Yongli¹; MEKARU, Harutaka; MIYAMAE, Takayuki²; URISU, Tsuneo
(¹Univ. Rochester; ²Natl. Inst. Mater. Chem. Res.)

The surface morphology of Si(111) was investigated using scanning tunneling microscopy the after illumination by synchrotron radiation. The surface shows large regions of atomically flat Si(111)-7×7 structure, and is characterized by the formation of bilayer atomic steps nicely registered to the crystal structure. The pinning of the steps by nanometer scale dust is evident. This is in sharp contrast to Si(111) surfaces after thermal desorption of SiO₂ at temperatures 880 °C and above, where the surface steps are much more irregular. The registration of the surface steps to the underlying crystal structure indicates that the bilayer atomic steps reach thermodynamic equilibrium under synchrotron radiation at temperatures much lower than that necessary for thermal desorption.

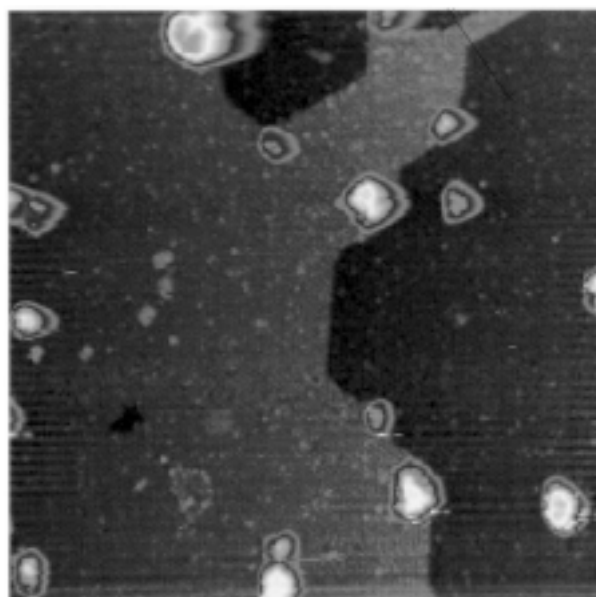


Figure 1. 1000 × 1000 Å² topograph of a Si(111) surface after 5 hours of SR irradiation at 650 °C. The most striking feature of the topography is the bilayer steps in alignment to the high symmetry axes of the surface.

VI-F-6 Construction of the Multilayered-mirror Monochromator Beam Line for the Study of Synchrotron Radiation Stimulated Process

MEKARU, Harutaka; TSUSAKA, Yoshiyuki¹; MIYAMAE, Takayuki; KINOSHITA, Toyohiko; URISU, Tsuneo; MASUI, Shin²; TOYOTA, Eijiro²;

TAKENAKA, Hisataka³¹Himeji Inst. Tech.; ²Sumitomo Heavy Ind. Ltd.; ³NTT-AT)[Rev. Sci. Instrum. **70**, 2601 (1999)]

A multilayered-mirror (MLM) monochromator beam line designed specially for synchrotron radiation (SR) stimulated process experiments has been constructed for the first time. The beam line was designed by the criteria; a beam spot size on the sample surface $\geq 3 \times 3 \text{ mm}^2$, a density of total irradiated photons $\geq 10^{18} \text{ photons/cm}^2$ (for an irradiation time of a few tens of minutes to a few hours) and low-energy background $\leq 1\%$ of the output. The performance of the beam line was evaluated by measuring the transmitted photon flux of an Al filter around the Al $L_{2,3}$ absorption edge and by measuring the photo-emission spectra of Ta using the output beam as an excitation light source. The Al thin film deposition was successfully demonstrated by using the monochromatized output beam. We conclude that this MLM monochromator performs sufficiently well to study the excitation energy dependence in SR-stimulated processes.

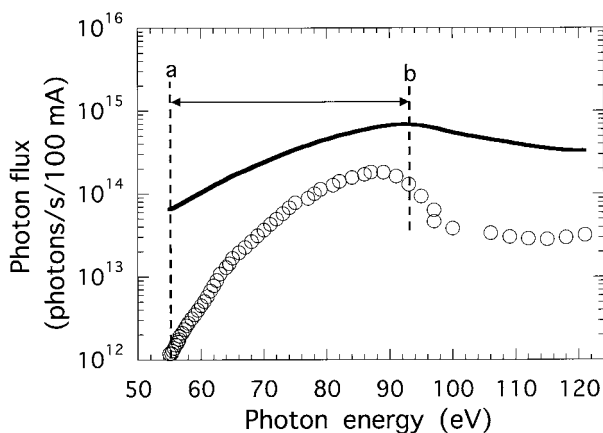


Figure 1. The dependence on the photon energy of the photon flux of output beam. The solid line shows calculated values and "○" shows measured values. The dotted lines a and b show the working region of the monochromator.

VI-F-7 Excitation Energy Dependence on Composition of an Al Deposited-thin Film Stimulated by Monochromatized SR

MEKARU, Harutaka; URISU, Tsuneo

The output beam of a multilayered-mirror monochromator beam line (BL4A1) at the UVSOR of the IMS was applied to an Al thin film deposition using dimethylaluminum hydride (DMAH) low temperature condensed layer. After cooling Si(100) substrate to about 100 K, the DMAH gas was introduced and deposited on the substrate (10–20 monolayers). The surface of the substrate was irradiated by the monochromatized SR beam tuned to the Al 2p core electron excitation energy, and the composition of the deposited film was measured by XPS at room temperature. An interesting point is the C concentration of the deposited film. By assuming C/Al = 2 for DMAH

condensed layer before irradiation, the minimum composition C/Al of the deposited film is estimated to be about 0.65. This value is quite small compared with those of films obtained by the white or filtered white SR beams irradiations. This may be due to that the Al-C bond is preferentially broken by the Al core electron excitations.

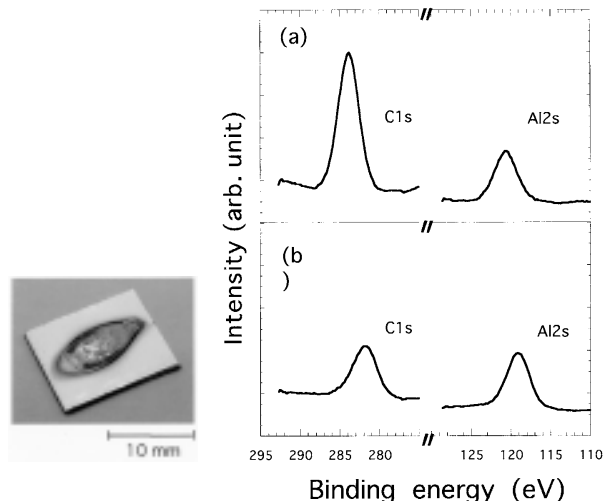


Figure 1. Photograph of the deposited Al thin film and the observed XPS spectra for (a) the DMAH condensed layers at 105 K and (b) the deposited Al thin film.

VI-F-8 SR-stimulated Etching and OMVPE Growth for Semiconductor Nano-structure Fabrication

NONOGAKI, Youichi¹; HATATE, Hitoshi¹; OGA, Ryo¹; YAMAMOTO, Shunsuke¹; FUJIWARA, Yasufumi¹; TAKEDA, Yoshikazu¹; NODA, Hideyuki; URISU, Tsuneo
(¹Nagoya Univ.)

We proposed a new method to form ordered array of the quantum dots using SR-stimulated etching and selective area growth by OMVPE. The SR etching has a great potential for fabrication of semiconductor devices, because side wall is very vertical and the induced damage of the etched surface is extremely low. Neither of them can be achieved by wet chemical etching or RIE. We report here preliminary results on SR etching of SiO₂ on InP substrate and growth of InP on the patterned substrate. SR etching was performed by exposing SiO₂ to SR irradiation in SF₆ ambient. The etched depth dependence on SF₆ pressure ranging from 5×10^{-8} Torr to 0.5 Torr was investigated at SR irradiation dose of 10,000 mA·min. The maximum etching rate in this study was $4.7 \times 10^{-3} \text{ nm/(mA·min)}$ at SF₆ pressure of 0.05 Torr. Using the SR etching, we patterned SiO₂ with 0.4 μm opening on the InP substrate. Selective area growth of InP was successfully observed on the patterned substrate. In the low-temperature PL measurement, exciton related emission lines were clearly observed.

VI-G Ion Desorption Induced by Core-Electron Transitions Studied by Electron Ion Coincidence Spectroscopy Combined with Synchrotron Radiation

Ion Desorption Induced by Core-Electron Transitions has been studied using energy-selected electron ion coincidence spectroscopy combined with synchrotron radiation. Auger electron photo-ion coincidence (AEPICO) and photoelectron photo-ion coincidence (PEPICO) spectroscopy proved to be an ideal tool for investigations of the ion desorption induced by core-level excitations. AEPICO results show that the character of the orbitals where holes are created, as well as the effective hole-hole Coulomb repulsion are important factors in the Auger-stimulated ion desorption from covalent molecules. The PEPICO spectroscopy, on the other hand, provided direct evidences of site-specific ion fragmentation induced by core-level excitations.

VI-G-1 Study of Ion Desorption Induced by a Resonant Core-Electron Transition of Condensed H₂O by Using Auger Electron Photoion Coincidence (AEPICO) Spectroscopy Combined with Synchrotron Radiation

MASE, Kazuhiko; NAGASONO, Mitsuru; TANAKA, Shin-ichiro; URISU, Tsuneo; IKENAGA, Eiji; SEKITANI, Tetsuji; TANAKA, Kenichiro¹
(¹Hiroshima Univ.)

Auger stimulated ion desorption mechanism is responsible at photon energies above the O:1s ionization. These results and conclusions are consistent with the previous study carried out by low-resolution AEPICO spectroscopy.¹⁾

Reference

1) K. Mase, *et al.*, *J. Chem. Phys.* **108**, 6550 (1998).

Proton desorption mechanism in the region of resonant excitations of Oxygen 1s core-electron of condensed water is studied using Auger electron photoion coincidence (AEPICO) spectrometer with an improved resolution of the electron kinetic energy of $E/\Delta E = 100$. The spectrum of total ion yield divided by Auger electron yield (AEY, electron kinetic energy: 490 eV) exhibited a characteristic threshold peak at the $4a_1 \leftarrow \text{O:1s}$ resonance ($h\nu = 532.3$ eV) and a suppression at the $3p \leftarrow \text{O:1s}$ resonance ($h\nu = 535.5$ eV). The electron kinetic energy dependence of the AEPICO yield (AEPICO yield spectra) were measured at $h\nu = 532.6, 533.6, 335.4, 540.6, 547.6$ and 557.8 eV. At the $4a_1 \leftarrow \text{O:1s}$ resonance ($h\nu = 532.6$ eV) and $2b_2 \leftarrow \text{O:1s}$ resonance ($h\nu = 533.6$ eV), the AEPICO yield spectrum exhibited major, medium and minor peaks at the electron kinetic energies of 502.5, 485 and 465 eV, which are assigned to $(\text{O:2p})^{-2}(4a_1 \text{ (or } 2b_2))^{-1}$, $(\text{O:2s})^{-1}(\text{O:2p})^{-1}(4a_1 \text{ (or } 2b_2))^{-1}$, and $(\text{O:2s})^{-2}(4a_1 \text{ (or } 2b_2))^{-1}$ spectator Auger final states, respectively. These results shows that ultrafast ion desorption (UFID) mechanism is predominant at the $4a_1$ and $2b_2$ resonances. The enhancement of the H⁺ AEPICO yield was attributed to the strongly O-H antibonding character of $4a_1$ and $2b_2$ orbitals. At the $3p$ resonance ($h\nu = 535.4$ eV), the AEPICO yield spectrum exhibited major, medium and minor peaks at the electron kinetic energies of 460, 475 and 490 eV, which are assigned to $(2a_1)^{-2}(3p)^{-1}$, $(2a_1)^{-1}(1b_2)^{-1}(3p)^{-1}$, and $(1b_2)^{-2}(3p)^{-1}$ spectator Auger final states, respectively. This result indicates that spectator Auger stimulated ion desorption (SASID) mechanism is responsible at the $3p$ resonance. The suppression of the H⁺ AEPICO yield was attributed to the reduction of the hole-hole Coulomb repulsion due to the $3p$ electron. At $h\nu = 540.6, 547.6$ and 557.8 eV, the AEPICO yield spectrum exhibited three peaks at the electron kinetic energy of 460, 475 and 490 eV, which are assigned to $(2a_1)^{-2}$, $(2a_1)^{-1}(1b_2)^{-1}$, and $(1b_2)^{-2}$ normal Auger final states, respectively. This result indicates that the normal

VI-H Photoionization Dynamics Studied by Electron Spectroscopy Combined with a Continuous Synchrotron Radiation Source

Molecular photoionization is a major phenomenon in vacuum UV excitation and provides a large amount of information on fundamental electron-core interactions in molecules. Especially, neutral resonance states become of main interest, since they often dominate photoabsorption cross sections and lead to various vibronic states which are inaccessible in direct ionization. We have developed a versatile machine for photoelectron spectroscopy in order to elucidate dynamical aspects of superexcited states such as autoionization, resonance Auger decay, predissociation, vibronic couplings, and internal conversion. Introduction of a new methodology, two-dimensional photoelectron spectroscopy, allows us to investigate superexcited states in the valence excitation region of acetylene, nitric oxide, carbonyl sulfide, sulfur dioxide and so on. In this method, the photoelectron yield is measured as a function of both photon energy and electron kinetic energy (binding energy). The spectrum, usually represented as a contour plot, contains rich information on photoionization dynamics.

VI-H-1 Autoionization of a Dipole-Forbidden Superexcited State of CS₂

MITSUKE, Koichiro; HIKOSAKA, Yasumasa¹
(¹Inst. Mater. Struct. Sci.)

Two-dimensional photoelectron spectroscopy of CS₂ has been employed to study excitation and autoionization mechanism of Rydberg states with the aid of analyses of the vibrational branching ratios of the final ions. The photoelectron yield is measured as a function of both photon energy $E_{h\nu}$ and ionization energy I_E . Figure 1 shows a spectrum in the $E_{h\nu}$ range of 14.6-15.3 eV. The Rydberg state at $E_{h\nu} = 14.88$ eV shows anomalously intense patterns at $I_E = 10.23$ and 10.28 eV, which are identified as the $\nu_3 = 1$ vibrational levels of the antisymmetric stretching mode ν_3 of the two spin-orbit components of CS₂⁺ [(2 π_g)⁻¹ X ² $\Sigma_{g,\Omega}$, $\Omega = 1/2$ and $3/2$]. Similar enhancement of the $\nu_3 = 1$ level has been also observed for autoionization of the Rydberg state at 14.88 eV to CS₂⁺ [(5 σ_u)⁻¹ B ² Σ_u^+]. This Rydberg state is considered to be the $\nu_3 = 1$ level of the (6 σ_g)⁻¹(3d σ_g)¹ ² Σ_g^+ state converging to CS₂⁺ [(6 σ_g)⁻¹ C ² Σ_g^+]. The electronic dipole transition is forbidden from the ground state CS₂ (X ¹ Σ_g^+) to this Rydberg state, but comes to have a substantial oscillator strength through vibronic coupling involving the ν_3 vibration. Conceivably, the transition to the (6 σ_g)⁻¹(3d σ_g)¹ ² Σ_g^+ , $\nu_3 = 1$ vibronic state borrows the intensity from a nearby dipole-allowed transition. From a broad line profile and a shift in the quantum defect, we conclude that the intensity is

borrowed from the transition to the vibrational ground state of (6 σ_g)⁻¹(5p σ_u)¹ ² Σ_u^+ observed at $E_{h\nu} = 14.951$ eV.

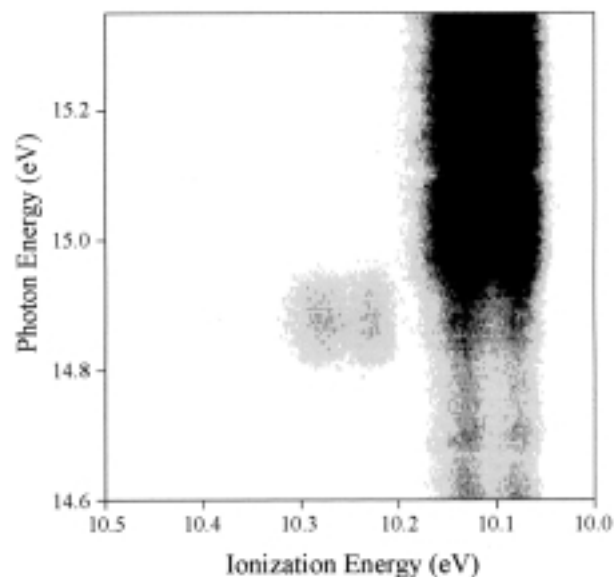


Figure 1. First band in the two-dimensional photoelectron spectrum of CS₂ corresponding to the formation of CS₂⁺ (X ² $\Pi_{g,1/2}$, ² $\Pi_{g,3/2}$). The electron intensity is plotted with eight tones from light to dark on a linear scale. The photon wavelength resolution is 0.8 Å (15 meV at $E_{h\nu} = 15$ eV) and the overall electron energy resolution is set to 40 meV.

VI-I Laser Photionization of Polarized Atoms Produced by Excitation with Synchrotron Radiation

In conventional photoionization experiments, the most standard method has generally been taken to be measurement of energy and angular distributions of photoelectrons from randomly oriented (unpolarized) atoms or molecules. However, information obtained from these experiments is insufficient, since the initial state constituted of atoms and photons is not selected and the internal properties of final photoions and electrons are not analyzed. In this project, we have performed photoelectron spectroscopy of polarized atoms using linearly-polarized laser light, aiming at complete quantum-mechanical photoionization experiments. Initial excitation with a linearly polarized synchrotron radiation permits ensemble of atoms to be aligned along the electric vector of the light. From an angular distribution of photoelectrons from polarized atoms, we are able to gain insight into the magnitude and phase shift difference of transition dipole matrix elements of all final channels which are allowed by selection rules.

VI-I-1 Laser Photoionization Electron Spectroscopy of Polarized Rare Gas Atoms Excited with Synchrotron Radiation

IWASAKI, Kota; HIKOSAKA, Yasumasa¹;
MITSUKE, Koichiro
(¹Inst. Mater. Struct. Sci.)

Laser photoionization processes of polarized rare gas atoms have been observed in order to study spin-orbit interactions of many electron systems and exploit the possibility of the complete photoionization experiment. Photoelectrons emitted in the direction perpendicular to both the laser and synchrotron radiation are detected with a 160° spherical electrostatic analyzer. In Figure 1(a), the photoelectron yield for $\text{Ar}(5s'[1/2]_1) \rightarrow \text{Ar}^+(^2P_{1/2}) + e^-$ ($l = 1; j = 1/2, 3/2$) is plotted as a function of the angle φ_e between the electric vector of the laser and the direction of the linear momentum of photoelectrons. The angular distribution should be interpreted in terms of a p partial wave from excited Ar atoms aligned toward the electric vector of synchrotron radiation. We have obtained an asymmetry parameter β of 1.7 ± 0.2 from Figure 1(a). The angular distributions have also been measured for photoelectrons produced by the process $\text{Ar}(3d[1/2]_1) \rightarrow \text{Ar}^+(^2P_{1/2}) + e^-$ ($l = 1$ or $3; j = 1/2, 3/2$ or $5/2, 7/2$) with $J_f = 1/2$ and $3/2$ as illustrated in Figure 1(b). Here, J_f is the total angular momentum quantum number of Ar^+ . The β values for these distribution curves were found to be 0.64 ± 0.04 and 0.90 ± 0.07 for the $J_f = 3/2$ and $1/2$ states of Ar^+ , respectively. We are planning to perform the complete photoionization experiment to determine dipole matrix elements and phase shift differences for all final open channels.

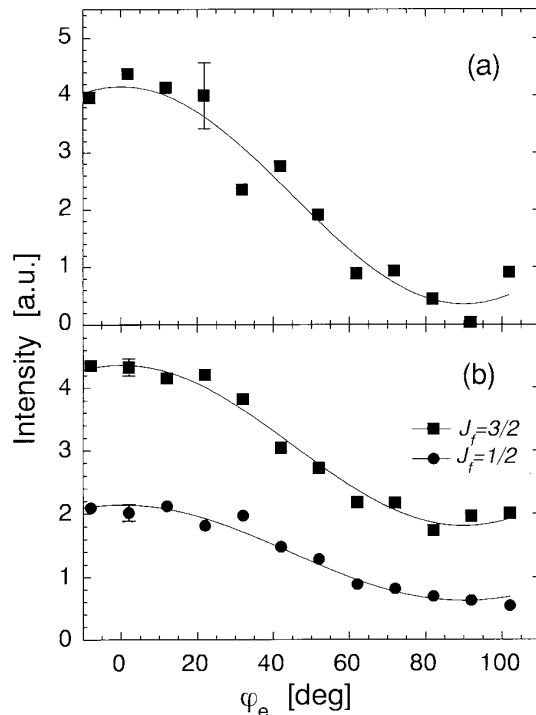


Figure 1. Angular distributions of photoelectrons: (a) $\text{Ar}(5s'[1/2]_1) \rightarrow \text{Ar}^+(^2P_{1/2}) + e^-$ ($l = 1; j = 1/2, 3/2$), (b) $\text{Ar}(3d[1/2]_1) \rightarrow \text{Ar}^+(^2P_{1/2,3/2}) + e^-$ ($l = 1$ or $3; j = 1/2, 3/2$ or $5/2, 7/2$).

VI-I-2 Theoretical Angular Distribution of Photoelectrons from Polarized Ar Atoms

MITSUKE, Koichiro; HIKOSAKA, Yasumasa¹;
IWASAKI, Kota
(¹Inst. Mater. Struct. Sci.)

The photoelectron angular distribution of Ar Rydberg atoms produced by excitation with linearly polarized synchrotron radiation is given under the present experimental geometry by

$$\frac{d\sigma}{d\Omega} = \frac{\sigma^{(\text{iso})}}{4\pi} \left[1 + \sqrt{\frac{5}{3}} \overline{A}_{20} \beta_{220} - \left(\sqrt{\frac{5}{6}} \beta_{022} + \sqrt{\frac{5}{6}} \overline{A}_{20} \beta_{202} - \frac{5}{\sqrt{21}} \overline{A}_{20} \beta_{222} + \sqrt{\frac{15}{7}} \overline{A}_{20} \beta_{242} \right) \times \frac{1}{2} (1 + 3 \cos 2\varphi_e) \right]$$

where the normalized statistical tensor of the initial state \overline{A}_{20} is proportional to the zero component of the statistical tensor in a coordinate frame with the z -axis directed along the symmetry axis for the pumping process producing the polarized atoms. We have derived the expression¹⁾ which connects generalized asymmetric coefficients $\beta_{k_0 k k_y}$ for the angular distribution with theoretical dynamic parameters involving reduced forms of transition dipole matrix elements, $\exp(i\delta_{lj}) \langle \epsilon | j:J || D || n_0 | 0 \rangle$. Here, J is the total angular momentum quantum number of the final state. In the case of photoionization of $\text{Ar}(5s'[1/2]_1)$, accessible open channels are four, which are designated as $(j, J) = (1/2, 0), (1/2, 1), (3/2, 1)$, and $(3/2, 2)$. Hence, the number of independent theoretical dynamic parameters is seven: four reduced dipole matrix elements, $D_{jJ} = \langle \epsilon, l = 1j:J || D || n_0 = 5, l_0 = 0 \rangle$, and three phase shift differences, $\delta_{l=1jJ} - \delta_{l=1j'J}$. The anisotropy of the observed angular distribution can be reasonably explained, assuming that the matrix elements and phase shift differences are essentially independent of J and that the spin-orbit interaction in the continuous spectrum is small.

Reference

- 1) K. Mitsuke, Y. Hikosaka and K. Iwasaki, *J. Phys. B* submitted.

VI-J Vacuum UV Spectroscopy Making Use of a Combination of Synchrotron Radiation and a Mode-Locked or Pulsed UV Laser

An ultraviolet laser system has been developed which synchronizes precisely with the synchrotron radiation (SR) from the storage ring of the UVSOR facility. A mode-locked Ti:sapphire laser is made to oscillate at the frequency of the ring in a multibunch operation mode. The delay timing between SR and laser pulses can be changed from 0 to 11 ns. We have developed another system, a pulsed dye laser pumped by an excimer laser, for SR-laser combination experiments. The second harmonic of the dye laser is tunable at 265–280 nm with a pulse energy of *ca.* 2 mJ pulse⁻¹ at a repetition rate of 10–100 Hz. This laser system is mainly devoted to observing neutral species produced by neutral or ionic photofragmentation induced by SR excitation of molecules. The following three combination studies have been performed: (1) two-photon ionization of helium atoms studied as the prototype of the time-resolved experiment, (2) laser induced fluorescence (LIF) excitation spectroscopy of $N_2^+(X^2\Sigma_g^+)$ ions produced by synchrotron radiation photoionization of N_2 or N_2O , and (3) resonance enhanced multiphoton ionization (REMPI) spectroscopy of $S(3s^23p^4\ ^3P_J, J'' = 0, 2)$ dissociated from Rydberg states of OCS. Among these topics LIF spectroscopy of ions is making marked progress in improvements of spectral resolution and fluorescence counts. These improvements are brought about by introducing an RF ion trap and by narrowing the laser band-width. As a consequence, we can obtain reliable rotational distribution curves of $N_2^+(X^2\Sigma_g^+)$.

VI-J-1 Improvement in the Energy Resolution of Laser Induced Fluorescence Excitation Spectroscopy of Ionic Species Produced by SR Photoexcitation

NIIKURA, Hiromichi¹; MIZUTANI, Masakazu; MITSUKE, Koichiro
(¹GUAS)

Pump-probe spectroscopy making use of a combination of laser and synchrotron radiation has been performed at the beam line BL3A2 in UVSOR to study ionization and dissociation dynamics in the vacuum UV energy region. The fundamental light emitted from the planar-type undulator was dispersed by a 2.2 m grazing incidence constant deviation monochromator in the photon energy range 15.5–19 eV. The second harmonic of a mode-locked Ti:sapphire laser was used to probe cations produced by SR photoionization. Fluorescence was collected in the perpendicular direction to the two light beams and dispersed by another monochromator and detected with a photomultiplier tube. To increase the number density of ions, we employed a cylindrical ion trap, in which collisional quenching of the rotational distribution of ions can be disregarded. Figure 1 shows an LIF spectrum of $N_2^+(X^2\Sigma_g^+, v = 0, N)$ produced by the photoexcitation of N_2 at the SR photon energy of 15.983 eV. This energy is equal to the excitation energy for the formation of the $4d\sigma_g\ ^1\Pi_u$ Rydberg state converging to $N_2^+(A^2\Pi_u, v = 0)$. We can clearly resolve the rotational structures of the *R*-branch resulting from the transition of $N_2^+(B^2\Sigma_u^+, v = 0, N + 1) \leftarrow (X^2\Sigma_g^+, v = 0, N)$. The spectral resolution of 1.6 cm⁻¹ (0.2 meV) has been achieved.

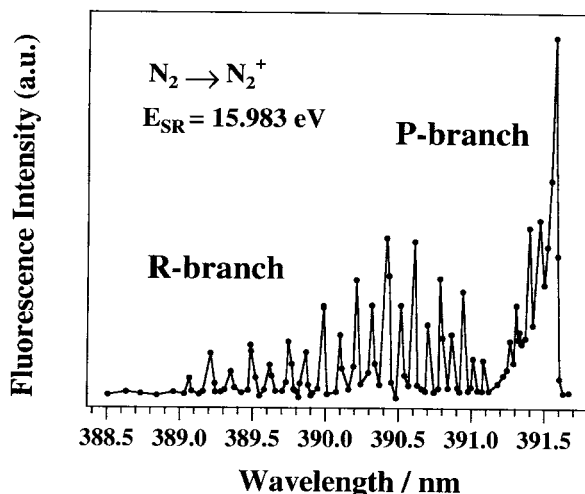


Figure 1. LIF excitation spectrum of the $(B^2\Sigma_u^+, v = 0, N') \leftarrow (X^2\Sigma_g^+, v = 0, N'')$ transition of N_2^+ produced by SR photoionization of N_2 .

VI-J-2 Rotational State Distribution of N_2^+ Produced from N_2O

NIIKURA, Hiromichi¹; MIZUTANI, Masakazu; MITSUKE, Koichiro
(¹GUAS)

We have measured LIF spectra of $N_2^+(X^2\Sigma_g^+, v = 0, N)$ produced by SR excitation of N_2O . The spectral resolution of the probing laser was set to 11 cm⁻¹. Figure 1 shows an LIF spectrum of N_2^+ obtained at the photon energy of 18.556 eV, which value accords with the excitation energy for the formation of the $3d\pi$ Rydberg state converging to $N_2O^+(C^2\Sigma)$. Auto-ionization to the vibrational manifolds of $N_2O^+(B^2\Pi)$ is followed by the dissociation into $N_2^+(X^2\Sigma_g^+) + O(^3P^e)$. Two maxima centered at 391.54 and 390.8 nm are ascribed to the *P* and *R* branches, respectively, for the $(B^2\Sigma_u^+, v = 0, N') \leftarrow (X^2\Sigma_g^+, v = 0, N'')$ transition. The rotational temperature of N_2^+ is estimated to be 200–230 K by fitting observed data points with the

theoretical intensity distribution with changing the temperature as a parameter. For the purpose of comparison, the average rotational energy of the $N_2^+(X^2\Sigma_g^+)$ fragment was calculated as a function of the $\angle NNO$ angle on the basis of the *modified impulsive model*. We assumed a stiff NN bond and no vibrational excitation of the N_2^+ fragment. This analysis suggests that the $\angle NNO$ angle of $N_2O^+(B^2\Pi)$ in the equilibrium geometry is larger than 160° .

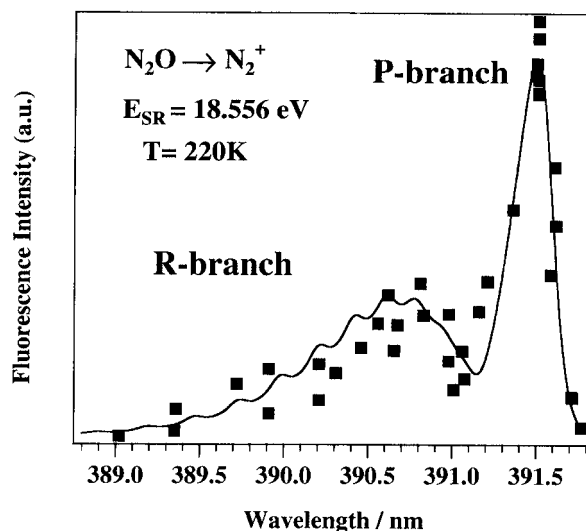


Figure 1. LIF spectrum of the $(B^2\Sigma_u^+, v=0, N') \leftarrow (X^2\Sigma_g^+, v=0, N'')$ transition of N_2^+ produced by SR photoionization of N_2O . The solid line represents the calculated rotational distribution at the temperature of 220 K.

VI-K Monochromator Newly Developed on the Beam Line BL2B2 in UVSOR

A grazing incidence monochromator has been constructed which supplies photons in the energy region from 20 to 200 eV. This monochromator will bridge the energy gap between the beam lines BL3A2 and BL8B1, thus providing for an accelerating demand for the high-resolution and high-flux photon beam from the research field of photoexcitation of inner-valence electrons or *L*-shell electrons in the third-row atom.

VI-K-1 First Performance Test of the 18 m-Spherical Grating Monochromator

ONO, Masaki; HATTORI, Hideo; YOSHIDA, Hiroaki¹; MITSUKE, Koichiro
(¹Hiroshima Univ.)

This monochromator of Dragon type has been designed to cover the energy range of 20–200 eV with three gratings (G1, 80–200 eV; G2, 40–100 eV; G3, 20–50 eV). The resolving power ($E/\Delta E$) of 5000 and the photon flux of more than 1×10^{10} photons s^{-1} are expected at a 100 mA ring current.¹⁾ The performance is now being examined by measuring photoionization efficiency curves of rare gas samples introduced into a differentially pumped chamber at the end station.

Figure 1 shows a He^+ efficiency curve in the region of the $2snp \pm 2pns$ series resulting from doubly excited He. The widths of the entrance and exit slits of the monochromator were set to 50 μm . The members up to $n = 14+$ of the series are clearly observed. The spectral width of the $14+$ line is about 6.5 meV (FWHM). We therefore evaluate that $E/\Delta E$ of approximately 10^4 has been achieved at 65 eV. When $E/\Delta E$ is lowered to 6500 by changing the slit widths to 100 μm , the photon flux at 65 eV is estimated to be 1×10^{10} photons s^{-1} . Next, the photon energy is tuned at 91.2 eV which agrees with the excitation energy of the $5p \leftarrow 3d_{5/2} 5p[3/2]_1$ state of Kr. From the band width of its resonance peak, $E/\Delta E$ is estimated to be 4500 with the slit widths of 50 μm .

Reference

- 1) H. Yoshida and K. Mitsuke, *J. Synchrotron Radiat.* **5**, 774 (1998).

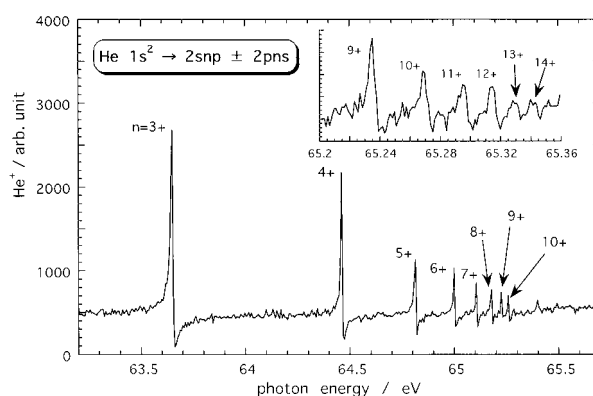


Figure 1. Photoionization efficiency curve exhibiting the $2snp \pm 2pns$ series of the doubly-excited He atom measured with the slit widths of 50 μm . Inset shows an enlarged spectrum in the region of $n \geq 9+$.

VI-L Ultraviolet Photoelectron Spectroscopy on Organic Thin Films Using Synchrotron Radiation

The electronic structure and molecular orientation of organic thin films were investigated by angle-resolved UPS with synchrotron radiation. Furthermore corresponding spectroscopies, such as low energy electron transmission spectroscopy, electron energy loss spectroscopy and Penning ionization electron spectroscopy were used in investigating the electronic states of the thin films.

VI-L-1 Origin of Photoemission Intensity Oscillation of C₆₀ (*Chiba Univ.)

HASEGAWA, Shinji; MIYAMAE, Takayuki; YAKUSHI, Kyuya; INOKUCHI, Hiroo; SEKI, Kazuhiko¹; UENO, Nobuo
(¹Nagoya Univ.)

The photon-energy dependences of photoemission intensities of C₆₀ were quantitatively calculated by the single-scattering approximation for the final state and the ab initio molecular orbital calculation for the initial state. The calculated results agreed well with the measured intensity oscillation in the photon-energy range of $h\nu = 18\text{--}110$ eV. The calculation by the plane-wave approximation for the final state also gave similar oscillations, which suggests that the oscillations are independent of the accuracy of the final state. These results indicated that the oscillations originate from the interference of photoelectron waves emanating from the 60 carbon atoms, *i.e.*, the multicentered photoemission with the phase difference of each wave. Further, the analytical calculation with a simplified spherical shell-like initial state revealed that the spherical structure of C₆₀ molecule and its large radius dominate the oscillations.

VI-L-2 Penning Ionization Electron Spectroscopy on Self-Assembled Monolayer of 1-Mercapto-8-Bromooctane on Au(111)

ABDUREYIM, Abduaini¹; KERA, Satoshi¹; SETOYAMA, Hiroyuki¹; SUZUKI, Ryouichi²; AOKI, Masaru²; MASUDA, Shigeru²; OKUDAIRA, Koji K.¹; YAMAMOTO, Makoto¹; UENO, Nobuo; HARADA, Yoshiya¹
(¹Chiba Univ., ²Univ. Tokyo)

Penning ionization electron spectroscopy (PIES) and ultraviolet photoelectron spectroscopy (UPS) were used to characterize self-assembled monolayers (SAMs) of 1-mercapto-8-bromooctane adsorbed on Au(111) from aqueous solution. The analysis of the relative band intensity of Penning spectrum indicates that the molecule stand up right to the substrate surface at room temperature. Upon heating, the molecule becomes tilted in the layer.

VI-L-3 Thickness-Dependent Orientation of the Pendant Phenyl Group at the Surface of Polystyrene Thin Films

UENO, Nobuo; AZUMA, Yasushi; TSUTSUI, Masahiko¹; OKUDAIRA, Koji K.¹; HARADA, Yoshiya¹

This paper reports on experimental evidence showing that the take-off angle dependence of the photoelectron intensity from the top π band of a polystyrene thin film, originating from the pendant phenyl group, depends on the film thickness. The result indicates that the orientation of the phenyl group at the film surface changes with the film thickness. Theoretical analysis of the observed angular distribution using the single scattering approximation combined with molecular orbital calculation (SS/MO) showed that the phenyl groups at the film surface become perpendicular oriented for a thicker film. The present finding suggests the possibility that the surface property of a thin film of a pendant group polymer can be controlled by changing the film thickness.

VI-L-4 Structure of Copper- and H₂-phthalocyanine Thin Films on MoS₂ Studied by Angle Resolved Ultraviolet Photoelectron Spectroscopy and Low Energy Electron Diffraction

OKUDAIRA, Koji K.¹; HASEGAWA, Shinji; ISHII, Hisao²; SEKI, Kazuhiko²; HARADA, Yoshiya; UENO, Nobuo
(¹Chiba Univ., ²Nagoya Univ.)

Angle-resolved ultraviolet photoelectron spectra (ARUPS) of copper phthalocyanine (CuPc) and metal-free phthalocyanine (H₂Pc) films (thickness from monolayer to 50–80 Å) on cleaved MoS₂ substrates were measured using monochromatic synchrotron radiation. Observed take-off angle (θ) and azimuthal angle (ϕ) dependencies of the top π band intensity were analyzed quantitatively by the single-scattering approximation theory combined with molecular orbital calculations. The analysis indicated that the molecules lie flat on the MoS₂ surface in monolayer films of CuPc and H₂Pc. The azimuthal orientation of the molecules (angle between molecular axis and surface crystal axis of MoS₂), was found to be about -7° , -37° , or -67° for both monolayer films of CuPc and H₂Pc. In the azimuthal orientation, the analyses indicated that there are only molecules with counterclockwise rotation, although both clockwise and counterclockwise rotations are expected. From the low energy electron diffraction, the two-dimensional lattice structure of the monolayer film was obtained. On the basis of these two kinds of experimental results, the full structure of the monolayer film, the two dimensional lattice and the molecular orientation at the lattice points, was determined. Furthermore, for the thick films it is found from the analyses of ARUPS that CuPc and H₂Pc molecules tilt about 10° from the surface plane.

VI-L-5 Electronic Structure of Poly(1,10-phenanthroline-3,8-diyl) and Its K-doped State Studied by Photoelectron Spectroscopy

MIYAMAE, Takayuki; UENO, Nobuo; HASEGAWA, Shinji; SAITO, Yutaka¹; YAMAMOTO, Takakazu¹; SEKI, Kazuhiko²

(¹Tokyo Inst. Tech., ²Nagoya Univ.)

Ultraviolet photoelectron spectra were measured using synchrotron radiation for thin films of poly(1,10-phenanthroline-3,8-diyl) (PPhen) and its potassium-doped state. Upon potassium doping of PPhen, two new states, which could be assigned to bipolaron bands, appear in the originally empty energy gap. The electronic structure of the neutral and potassium-doped states was theoretically analyzed using single-scattering approximation combined with semiempirical molecular orbital calculations.

VI-L-6 A Differential Thermal Analysis and Ultraviolet Photoemission Study on Surface Freezing of n-Alkanes

YAMAMOTO, Yasushi¹; OHARA, Hideaki¹; KAJIWARA, Kotaro¹; ISHII, Hisao¹; UENO, Nobuo; SEKI, Kazuhiko¹; OUCHI, Yukio¹

(¹Nagoya Univ.)

The surface-freezing effect of pentacontane (*n*-C₅₀H₁₀₂) and tetratetracontane (*n*-C₄₄H₉₀) films evaporated on a copper substrate has been investigated by differential thermal analysis (DTA) simultaneously with measurements of surface-specific ultraviolet (UV) photoemission. Two anomalies in the DTA curve were observed near the bulk melting temperature, one of which has been attributed to bulk melting. Since the temperature dependence of the surface-specific UV photoemission measurement showed a corresponding stepwise increase and decrease in the photoemission current at the two anomalies observed in the DTA, we have concluded that the other phase transition peak originates from surface freezing.

VI-L-7 Angle-Resolved UPS Studies of Organic Thin Films

UENO, Nobuo

This paper describes recent progress of angle-resolved photoelectron spectroscopy using synchrotron radiation (SR-ARUPS) on organic thin films. SR-ARUPS has been growing to a new surface analysis technique which can offer concrete information on the molecular orientation at the film surface as well as on the origin of the electronic structure, both of which are important in understanding functions of organic thin films. Some examples of the experimental determination of the molecular orientation by SR-ARUPS are shown for epitaxial ultrathin films of phthalocyanines and bis(1,2,5-thiadiazolo)-*p*-quinobis (1,3-dithiole) (BTQBT). The orientation of pendant naphthalene groups at the surface of thin film of poly(2-vinyl-naphthalene) is also shown, where the comparison

between the results obtained by SR-ARUPS and near edge X-ray absorption fine structure (EXAFS) spectroscopy is made in order to understand an advantage of SR-ARUPS. Furthermore, it is pointed out by showing the result on C₆₀ thin film that the multicentered photoemission dominates the photoelectron intensity of thin films of large organic molecules.

VI-M Thin Film Preparation of SiO₂ by Photo-Chemical Vapor Deposition Using Vacuum Ultraviolet Radiation

Silicon dioxide has been extensively used and studied in semiconductor manufacturing applications. For such a material, conventional pyrolytic deposition occurs above 600 °C while traditional oxidation occurs at temperatures around and above 900 °C. Low temperature processing has become much more important mainly in the semiconductor industry, according to the continued reduction in device geometry. Photo-stimulated processing is very promising since the processed surfaces and growing films are not subjected to damaging ionic bombardment unavoidable in plasma-assisted processing systems. The aims of this project are to exploit the fundamental processes and to demonstrate the possibility and inherent advantages of depositing silicon dioxide at room temperature from tetraethoxyorthosilicate (TEOS: Si-(OC₂H₅)₄) with the use of vacuum ultraviolet radiation.

VI-M-1 SiO₂ Thin Film Preparation Using Dielectric Barrier Discharge-Driven Excimer Lamps

(¹Miyazaki Univ.)

[Hyomen Kagaku 20, 401 (1999)]

TAKEZOE, Noritaka; YOKOTANI, Atsushi¹; KUROSAWA, Kou; SASAKI, Wataru¹; IGARASHI, Tatsushi²; MATSUNO, Hiromitsu²
(¹Miyazaki Univ.; ²USHIO Inc.)

[Appl. Surf. Sci. 138-139, 340 (1999)]

By using a photochemical vapor deposition method with a Xe₂ excimer lamp (172 nm, 20 mW/cm² output power), silica films have been prepared by means of a single precursor from tetraethoxyorthosilicate (TEOS) at room temperature. Transparent thin films of SiO₂ obtained on sapphire and quartz single crystal substrates with a deposition rate of 0.9 nm/min. They were mainly composed of amorphous SiO₂, although small amounts of residual organic materials were contained. The refractive index was 1.476 at 632.8 nm. The surface roughness decreased with the film thickness and reached 0.2 nm-rms. These findings indicate that the VUV excimer lamp CVD is a promising method for preparing smooth, dense and fine thickness-controllable films of SiO₂ at room temperature.

VI-M-2 SiO₂ Film Coatings with VUV Excimer Lamp CVD

KUROSAWA, Kou; TAKEZOE, Noritaka; YANAGIDA, Hideaki; NOMURA, Ryo¹; YOKOTANI, Atsushi¹
(¹Miyazaki Univ.)

[Mater. Res. Soc. Symp. Proc. 555, 167 (1999)]

Silica film coatings were demonstrated using photochemical vapor deposition with a 172-nm Xe excimer lamp. Tetraethoxyorthosilicate (TEOS) molecules were successfully dissociated into SiO₂ + 2C₂H₅-OH + (residual C and H) with the 7.2-eV photons. The films were deposited onto quartz or Al₂O₃ single crystal substrates with the deposition rate of 1 nm/min. The films were uniform and smooth enough for optical applications.

VI-M-3 Thin Film Preparation Using Vacuum Ultraviolet Rare Gas Excimer Lamps

TAKEZOE, Noritaka; YOKOTANI, Atsushi¹; KUROSAWA, Kou

Rare gas excimer lamps using dielectric-barrier discharge are new type of compact and high-efficient light source for vacuum ultraviolet wavelength region. Since the lamps produce incoherent and quasi-continuous radiation, uniform processing over large sample areas is expected to be possible without thermal effects and speckling or interference fringes. The purpose of this paper is to exploit a new technique of material processing by use of the newly developed incoherent rare gas excimer lamps. We will describe some findings obtained by applying the excimer lamps to preparation of silica films. A photochemical vapor deposition using Xe₂* excimer lamp has made it possible to prepare silica films by means of a single precursor process from tetraethoxyorthosilicate (TEOS) at room temperature. Transparent SiO₂ thin films were obtained with a deposition rate of 0.9 nm/min. The refractive index was 1.476 at 632.8 nm and the surface roughness reached 0.2 nm-rms. These findings indicate that the VUV excimer lamp CVD is promising method for preparing smooth and fine thickness-controllable films of SiO₂ at room temperature. We confirmed that this technique provides a very promising photo-quantum process for the fabrication of semiconductors and optoelectronic devices, and others.

VI-M-4 Photo-Dissociation Process of Tetraethoxyorthosilicate (TEOS) Induced by Synchrotron Radiation

YANAGIDA, Hideaki; TAKEZOE, Noritaka; KUROSAWA, Kou; YOKOTANI, Atsushi¹; KAWASAKI, Yasuhiro¹; MAESONO, Yoshihiro¹; NOMURA, Ryo¹
(¹Miyazaki Univ.)

Tetraethoxyorthosilicate (TEOS: Si-(OC₂H₅)₄) is one of the promising materials for preparing insulating SiO₂ thin layer in semiconductor industry. Photo-chemical vapor deposition using vacuum ultraviolet radiation provides the thin film preparation at room temperature. However the photo-dissociation process has never been exploited yet. We have a plan to exploit the detailed process, to find the most appropriate conditions, in particular for wavelength, and to make high quality SiO₂ thin film using synchrotron radiation (at the beam lines of BL-1B and BL-7B of UVSOR).

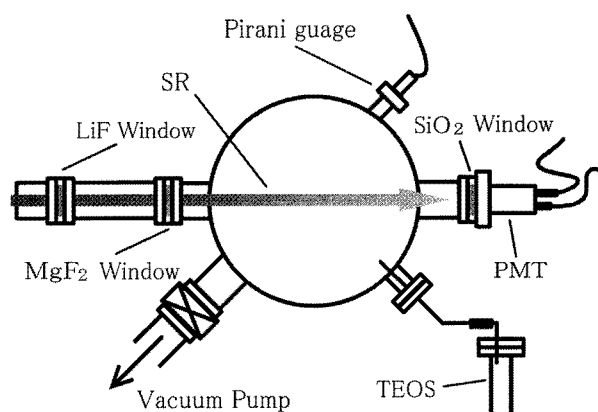


Figure 1. Schematic drawing of reaction chamber for TEOS.

VI-N Vacuum Ultraviolet Lasers and Their Applications to Surface Modification of Silica Glass

Rare gas excimers are most promising materials for coherent light sources in vacuum ultraviolet spectral region. Among them, an argon excimer laser which provides 126-nm photons has been realized only by high-energy electron beam pumping. The photon energy surmounts the band-gap energy of almost all solid-state materials and thus has a strong interaction with the materials. For an example, we have demonstrated that the 9.8-eV photons excite electrons from the valence band to the conduction band via one-photon process, resulting in desorption of oxygen atoms and crystal growth of silicon in the surfaces of silica glass and quartz crystals.

VI-N-1 The State of the Art of Rare Gas Excimer Lasers and Lamps as a Light Source for Giga-Bit Lithography

SASAKI, Wataru¹; KUROSAWA, Kou; KUBODERA, Shoichi¹; KAWANAKA, Jyunji¹
(¹Miyazaki Univ.)

[*J. Photopolymer Sci. Tech.* **11**, 361 (1998)]

Coherent and incoherent light sources using rare gas excimers are reviewed from a point of view of post ArF lithography. Present status of electron beam pumped rare gas excimer lasers is reported. Potentialities of rare gas excimer lasers by discharge pumping are discussed. We have obtained laser gain of $2.2 \times 10^{-3} \text{ cm}^{-1}$ in Kr discharge that was very close to the threshold gain. It is pointed out that gas excimer lasers are suitable for light sources for next generation lithography after ArF lithography in the 21st century, when a compact excitation method is established. Jet discharge excimer lamps are also discussed from a point of view of an incoherent light source for lithography.

VI-N-2 Radiation Effects of Vacuum Ultraviolet Lasers on Silica Glasses

KUROSAWA, Kou; HERMAN, Peter¹; SASAKI, Wataru²
(¹Univ. Toronto; ²Miyazaki Univ.)

[*J. Photopolymer Sci. Tech.* **11**, 367 (1998)]

Excimer-laser processing can be extended to a broader and more diverse range of materials by moving to vacuum-ultraviolet (100–200 nm) laser sources such

as the molecular fluorine and argon excimer lasers. The 126-nm and 157-nm output wavelengths from the argon excimer and fluorine lasers take advantages of the extremely high photon-energy, the high opacity in most materials, and short pulse duration to minimize thermal loading of target surfaces. The lasers readily drive photochemical interactions. The 126-nm photons induce oxygen desorption and silicon precipitation both in high purity silica glass and crystalline quartz. The 157-nm photons readily etch off the surfaces in vacuum ultraviolet-grade silica glass and crystalline quartz.

VI-N-3 X-Ray Emission Spectroscopic Studies of Silicon Precipitation in Surface Layer of SiO₂ Induced by Argon Excimer Laser Irradiation

KUROSAWA, Kou; HERMAN, Peter¹; KURMAEV, E.²; SHAMIN, S.²; GALAKHOV, V.²; TAKIGAWA, Yasuo³; YOKOTANI, Atsushi³; KAMEYAMA, Akihiro³; SASAKI, Wataru³
(¹Univ. Toronto; ²Inst. Met. Phys., Russia; ³Miyazaki Univ.)

[*Appl. Surf. Sci.* **126**, 83 (1998)]

The ultra-soft X-ray emission spectra were taken from surfaces of bulk silica glass and silica glass films exposed to an argon excimer laser ($\lambda = 126 \text{ nm}$) and composed with the spectra taken from the virgin surfaces. The precipitation of crystalline silicon is found to take place in thin surface layers of the irradiated bulk silica glass and 15 nm film. An estimation of concentration of crystalline silicon precipitation with the depth is given on the basis of the measurements of Si L_{2,3} X-ray emission spectra obtained at different accelerating voltages of the electron beam on the X-ray

tube. Based upon the precipitation conditions for these samples, we discuss the crystalline silicon precipitation mechanisms: the electronic excitation induces the bond-breaking between Si and O atoms, although there is a critical density of photons for the bond-breaking and temperature rise enhances the crystalline silicon precipitation.

VI-N-4 Polycrystalline Silicon Precipitation on SiO₂ Using an Argon Excimer Laser

OHMUKAI, Masato¹; TAKIGAWA, Yasuo²; KUROSAWA, Kou

(¹Akashi College Tech.; ²Osaka Electro-Commun. Univ.)

[*Appl. Surf. Sci.* **137**, 78 (1999)]

We are developing an argon excimer laser that oscillates at 126 nm (9.8 eV). Since the photon energy of the laser is as high as 9.8 eV, the laser can induce bond breaking in most of materials without any reactive gas or solution. We performed irradiation of an argon excimer laser on crystal and glass SiO₂, and then investigated the surfaces by means of X-ray photoelectron spectroscopy, Raman scattering, X-ray diffraction and reflection of high-energy electron diffraction measurements. The results indicate that polycrystalline silicon precipitates on the surface with a preferential orientation.

VI-O Photo-Stimulated Luminescence as Data Storage in UV to Vacuum UV Regions

Photo-stimulated luminescence is a promising process for data storage in X-ray radiation with the advantages of linear response and wide dynamic range. The fundamental mechanisms under the data storage in imaging plates using BaFBr:Eu as the photo-stimulated luminescence material have been explained to trapping electrons released from Eu impurity atoms at least for X-ray radiation. Viewing the energy diagram, we can expect the photo-stimulated process occurring even for Vacuum UV and UV radiation. We have exploited the fundamental mechanism for data storage in the imaging plate particularly for VUV and UV radiation.

VI-O-1 Response Characteristics of Imaging Plate in UV Region

YAMASHITA, Hiroshi¹; KATTO, Masahoto¹; OHNISI, Shunshiro¹; KURIOKA, Yutaka¹; TAKIGAWA, Yasuo²; KUROSAWA, Kou; YAMANAKA, Tatsuhiko³; MIYAHARA, Jyunji⁴

(¹Kinki Univ.; ²Osaka Electro-Commun. Univ.; ³Osaka Univ.; ⁴Fuji Photo Film Co. Ltd.)

[*Rev. Laser Eng.* **26**, 812 (1998)]

An imaging plate (IP) has been developed as an image-storing medium for use in medical X-ray

diagnosis. We confirmed the IP to be a good medium not only for X-ray radiation but also vacuum ultraviolet (VUV) and ultraviolet (UV) radiation. We found that the photo-stimulated luminescence (PSL) intensity showed a linear response to UV photon numbers in the range of 10⁴⁻⁵, and that showed saturation as the irradiated photon number increased. The sensitivity curve of the IP showed a peak at the wavelength of 200 nm and decreased at longer wavelengths. When the wavelength of the irradiated UV radiation was longer than 320 nm, the PSL intensity was too low to detect with our system. This means that the cut-off wavelength of the sensitivity was measured as 310 nm.

VI-P Nano-Structure Fabrication Using Synchrotron Radiation Stimulated Processing

Nano structures must open new windows not only for surface physics and chemistry but also for electronic and photonic devices. Synchrotron radiation stimulated surface chemical reactions have been a most promising way to fabricate nano structures, because they offer a process with the advantages of high-site selectivity by core electron excitation and also free-of damage with atomic scale. Since a new beam line with higher flux is required for the processings, we have been designing and constructing BL-4A2 beam line for the nano structure fabrication.

VI-P-1 Design and Construction of BL-4A2 Beam Line for Nano-Structure Processing

TAKEZOE, Noritaka; YANAGIDA, Hideaki¹; KUROSAWA, Kou; URISU, Tsuneo; MEKARU, Harutaka; NODA, Hideyuki; MATSUI, Shinji²; KANDA, Kazuhiro²; UCHIDA, Hiroyuki³

(¹Miyazaki Univ.; ²Himeji Inst. Tech.; ³Toyohashi Univ.

Tech.)

We have been constructing a new beam line BL-4A2 which consists of white ray beam, ultra-high vacuum scanning tunneling microscope (UHV-STM) and photo-stimulated reaction chamber. In near future, we are going to join a near field optical microscope for monitoring optical properties with the atomic scale to

them. Figure 1 shows the outline of the beam line, which consists of pre-focusing mirror (M1), secondary mirror (M2), monitor port, two differential pumping ports, reaction chamber and STM. An elliptically bent cylindrical mirror made of a quartz coated with platinum is used as the pre-mirror. The reflected beam is focused at a point of 12.7 m down stream from the center of the pre-mirror and has a spot size of 8×6

mm². Low energy electron diffraction (LEED) is installed in the reaction chamber for in-situ characterization of substrate surfaces and also STM is for observation of the surface processes with atomic scale. We have a plan to make a photonic band-gap structures in a SiO₂ planer waveguide and study evanescent light from the waveguide surfaces with near field optical microscope.

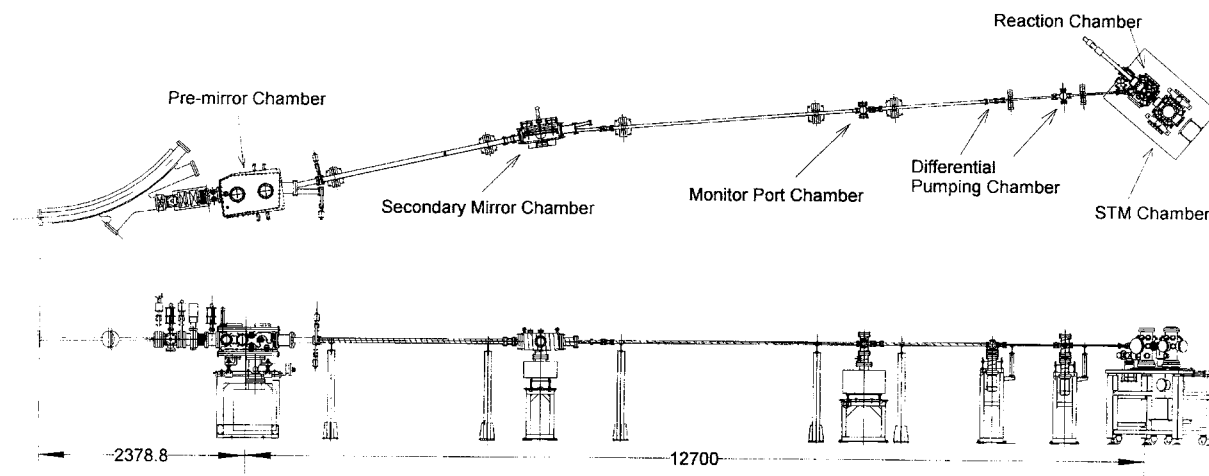


Figure 1. Schematic drawings of the BL-4A2 beam line with a reaction chamber and STM.

VI-Q Desorption Induced by Electronic Transitions from Cryogenic Surfaces

Desorption process of particles from cryogenic surfaces are studied using synchrotron radiation in vacuum ultraviolet region. As a result of decay processes after an electronic excitation of surface layers by synchrotron radiation, various kinds of particles are released from the surface. Cryogenic substrates such as solid rare gases have particular excitation channels for the desorption of electronically excited neutral particles that are pronounced at the creation energy region of exciton. Experiments are performed at BL2B1 and BL5B of UVSOR. We discuss the mechanisms of excitation, energy and angular distribution of desorbed species, incident energy dependence of desorption yield, correlation between particle emission and photon emission, and so on.

VI-Q-1 Desorption of Excimers from the Surface of Solid Ne by Low Energy Electron or Photon Impact

HIRAYAMA, Takato¹; HAYAMA, Akira¹; ADACHI, Takashi¹; ARAKAWA, Ichiro^{1,2}
(¹Gakushuin Univ.; ²IMS)

Desorption of excited dimers Ne_2^* in $^3\Sigma_u$ state from the surface of solid Ne initiated by the creation of a valence exciton was confirmed experimentally using low energy electron and monochromatic VUV light as excitation sources. The kinetic energy of desorbed excimer ($\text{Ne}_2^* \ ^3\Sigma_u$) was (0.2 ± 0.1) eV, which is consistent with a recent quantum mechanical calculation. It is found that the vibrational relaxation of a molecular type exciton is a slow process compared to the time scale of desorption. Desorption of excimers at the excitation of the first order surface exciton was found to be inefficient compared to that by the creation of bulk excitons, which is in striking contrast to the case of the excited atom desorption. The mechanism of excimer desorption can be explained by a cavity ejection model as in the atomic desorption case.

VI-Q-2 Photon Stimulated Ion Desorption from Solid Rare Gases in the Core Excitation Region

SAKURAI, Makoto; MASE, Kazuhiko; NAGASONO, Mitsuru; TANAKA, Shin-ichiro

Ion desorption from solid rare gases was measured by the irradiation of synchrotron radiation in the core excitation region. Experiments were performed in a UHV chamber at BL-2B1. Solid rare gases were prepared on gold-plated copper substrate, which was attached at the end of a flow type liquid He cryostat. Partial electron yield (PEY) and total ion yield (TIY) spectra of condensed Ar and Xe were measured using an Auger electron-photoion coincidence spectrometer.

Typical PEY and TIY spectra of condensed Ar measured around the energy range of Ar 2p excitation exhibit very similar waveforms, and ion yield is relatively high compared to the intensity of emitted electrons. The measured electron corresponds to LMM Auger electron (~210 eV). The time of flight spectrum of desorbed ions in the coincidence with Auger electrons showed no observable peaks. We obtained similar results for condensed Xe at 3d excitation (~680 eV). These features suggest that ion desorption from solid rare gases in the core excitation region is dominated by the interaction between the secondary electrons and desorbing ions.

VI-R Structure and Vibrational Spectra of Molecules Physisorbed on Metal Surfaces

Molecular layers physisorbed on metal surfaces at low temperature show specific structures which depend on the interaction between molecules and substrate, and vibrational spectra for physisorbed molecules reveal the details of the interaction. We use dynamical analysis of low-energy electron diffraction (LEED) to investigate the structure of adsorbed layers, and high-resolution electron energy loss spectroscopy has been utilized for vibrational spectroscopy for adsorbed molecules. As a complementary method for vibrational spectroscopy of surfaces, infrared reflection absorption spectroscopy will be combined with our experimental system. A new cryogenic sample holder for surface vibrational spectroscopy is also under development in order to provide a substrate at less than 4.2K.

VI-R-1 Upgraded Infrared Beamline BL6A1 at UVSOR

SAKURAI, Makoto; OKAMURA, Hidekazu¹; WATANABE, Katsumi¹; NANBA, Takao¹; KIMURA, Shin-ichi¹; KAMADA, Masao
(¹Kobe Univ.)

BL6A1, a far-infrared (FIR) beamline at UVSOR originally built in 1986, has been upgraded recently. The upgrade included the introduction of a second FT-IR spectrometer, and now it is possible to cover the entire FIR-IR range (3 cm^{-1} to 10000 cm^{-1}) in one sequence of measurements, without having to open the sample chamber; the beamline has become a more convenient and powerful experimental station than before. The upgrade is also expected to enable such experiments as IR studies of molecules adsorbed on the

solid surfaces, and time-resolved IR spectroscopies.

VI-R-2 Development of High Sensitivity EELS

SAKURAI, Makoto

Electron energy loss spectroscopy (EELS) is a powerful tool for the structural analysis of molecules adsorbed on a solid surface. However, since ordinary EELS system uses a single channel electron analyzer, the measurement time for one spectrum usually amount to several minutes. This has been a disadvantage of EELS for real time analysis of surface reaction. We developed a new electron analyzer for EELS. The

analyzer is a simulated hemispherical analyzer with a position sensitive detector. The components are made of aluminum, and mean radius of the deflector is 104 mm. The detector has CR chain type anode, and the signal is stored to a histogramming memory via position analyzer. The spectrum can be measured as frequent as every 10ms. This feature makes it possible to perform a time-resolved measurement of repetitive reaction processes. The analyzer and an cylindrical double pass monochromator are mounted on a rotatable stage, and they are installed in a vacuum chamber (600 ϕ). Control program written in Visual Basic for the data acquisition system has been developed.

VI-S Structure and Vibrational Spectra of Molecules on Metal Surfaces

Adsorption structure of the adsorbed molecules is one of the most fundamental information to understand the reaction of the molecules on the surface, which is useful for calculating the electronic structure of the system and understanding the elementary processes such as desorption, dissociation or diffusion. Understanding the elementary processes further enables us to understand more complex reactions such as catalysis. Nitric oxide (NO) on the Pt(111) surface is a prototype of catalytic process of the exhaust gas of automobiles. In spite of many efforts, its adsorption structure has not been determined yet. Dynamical analysis of low-energy electron diffraction (LEED) and direct observation by scanning tunneling microscopy (STM) are utilized to investigate the structures of adsorbed molecules in various conditions. Vibrational spectra, which is closely related to adsorption structure, are also utilized to determine the structures correctly.

VI-S-1 Adsorption Structures of NO on Pt(111) Investigated by Scanning Tunneling Microscopy

MATSUMOTO, Masuaki; TATSUMI, Natsuo¹; FUKUTANI, Katsuyuki¹; OKANO, Tatsuo¹; YAMADA, Toshiyuki²; MIYAKE, Koji²; HATA, Kenji²; SHIGEKAWA, Hidemi²
(¹IIS, Univ. Tokyo; ²Tsukuba Univ. and CREST)

[*J. Vac. Sci. Technol., A* **17**, 1577 (1999).]

The adsorption structure of nitric oxide (NO) on Pt(111) was studied at 10 and 70 K by scanning tunneling microscopy (STM). The island growth modes at both temperatures are similar except for the domain size of the 2 \times 2 structure. In these low temperature region, two phases can coexist at medium coverages. These phases are assigned to the two NO species occurring at different stretching-vibrational frequencies observed in the previous vibrational spectroscopic studies. The relative location of two different species observed by STM and its stretching-vibrational frequencies suggests that the adsorption sites of NO on the Pt(111) surface at low and high coverages correspond to the hollow and the on-top sites, respectively.

VI-S-2 Dynamical LEED Analyses of the Pt(111)-p(2 \times 2)-NO Structures

TATSUMI, Natsuo¹; MATSUMOTO, Masuaki; AIZAWA, Hideaki²; TSUNEYUKI, Shinji³;

FUKUTANI, Katsuyuki¹; OKANO, Tatsuo¹
(¹IIS, Univ. Tokyo; ²Univ. Tokyo; ³ISSP, Univ. Tokyo)

[*J. Vac. Soc. Jpn.* **42**, 572 (1999).]

Adsorption structures of NO molecules on a Pt(111) surface at low temperatures have been studied using low-energy electron diffraction (LEED). At 150 K a 2 \times 2 LEED pattern appears at exposures higher than 0.2 L. With increasing exposure, the LEED spots get sharper, indicating two-dimensional island growth of adsorbed NO. The LEED I-V spectra measured at 0.4 L are different from those at 3 L, suggesting the presence of two kinds of 2 \times 2 structure. The LEED I-V analysis performed for the 2 \times 2 at 0.4 L strongly supports that NO is adsorbed at a threefold fcc hollow site. For the I-V curves of 2 \times 2 at 3 L, the fcc hollow site model calculation does not fit the experimental I-V curve, suggesting that a different 2 \times 2 structure grows after the first 2 \times 2 structure is completed.

VI-T Ultraviolet, Visible and Infrared Spectroscopy of Solids

Work of ultraviolet (UV), visible (VIS) and infrared (IR) spectroscopy of solids have been proceeded. These are mainly performed using synchrotron radiation (beamlines BL7B and BL1B at UVSOR), owing to the wide wavelength continuity of synchrotron radiation with no structure.

VI-T-1 Reconstruction of BL7B for UV, VIS and IR Spectroscopy with a 3 m Normal-Incidence Monochromator

FUKUI, Kazutoshi; NAKAGAWA, Hideyuki¹; SHIMOYAMA, Iwao²; NAKAGAWA, Kazumichi²; OKAMURA, Hidekazu²; NANBA, Takao²; HASUMOTO, Masami; KINOSHITA, Toyohiko³
(¹Fukui Univ.; ²Kobe Univ.; ³Univ. Tokyo)

[*J. Synchrotron Radiat.* **5**, 836 (1998)]

The beamline BL7B at the UVSOR facility for solid-state spectroscopy is currently under reconstruction. This reconstruction mainly involves the replacement of the 1 m Seya-Namioka-type monochromator (50-600 nm) with a 3 m NIM (modified version of McPherson model 2253), which covers the 50-1000 nm range with three gratings. The deviation angle of the gratings is 15°. For linear and circular polarization experiments, the beamline optics consist of a two-grazing-incidence (87.5°) pre-mirror system and a normal-incidence (15°) post-mirror.

VI-T-2 Absorption and Luminescence Spectra of Amorphous CdI₂ Thin Films

FUKUI, Kazutoshi; ASAKURA, Kenji¹; NIIMI, Ken-ichi¹; ISHIZUE, Ikuto¹; NAKAGAWA, Hideyuki¹
(¹Fukui Univ.)

[*J. Electron Spectrosc. Relat. Phenom.* **101-103**, 299 (1999)]

Absorption and luminescence spectra of amorphous CdI₂ thin film were measured at liquid nitrogen

temperature. Two emission bands were observed at 2.3 and 3.1 eV, and the intensity ratio between them depends on the excitation energy. The 3.1 eV emission is explained in terms of the MX₆ model which explains the emission mechanism of the CdI₂ crystal, but the other is not explained.

VI-T-3 Optical Study of the Metal-Nonmetal Transition in Ni_{1-δ}S

OKAMURA, Hidekazu¹; NAITOH, Jun¹; NANBA, Takao¹; MATOBA, Masanori²; NISHIOKA, Masaya²; ANZAI, Shunichiro²; SHIMOYAMA, Iwao¹; FUKUI, Kazutoshi; MIURA, Hiroshi³; NAKAGAWA, Hideyuki³; NAKAGAWA, Kazumichi¹; KINOSHITA, Toyohiko⁴
(¹Kobe Univ.; ²Keio Univ.; ³Fukui Univ.; ⁴Univ. Tokyo)

[*Solid State Commun.* **112**, 91 (1999)]

Optical reflectivity spectra of the hexagonal Ni_{1-δ}S have been measured to study its electronic structures, in particular those associated with the metal-nonmetal transition in this compound. Samples with $\delta \sim 0.002$ and 0.02 are studied, which have transition temperature $T_t \sim 260$ K and 150 K, respectively. Upon the transition, a pronounced dip appears in the infrared region of the reflectivity spectra. The optical conductivity spectra suggest that the nonmetallic phase is a carrier-doped semiconductor with an energy gap of ~ 0.2 – 0.3 eV. The spectra also show that the gap becomes larger with decreasing temperature, and smaller with increasing δ . It is found that the overall spectrum in the nonmetallic phase can be explained in terms of a charge-transfer semiconductor, consistent with recent theoretical and photoemission studies of NiS.

VI-U Electronic Structure and Optical Properties of III-V Nitrides

The III-V nitrides (GaN, AlN and InN) and their alloys (AlGaN, InGaN and AlInN) are promising for optoelectronic device application. They are also the attractive material series which have scientific interest because the band structure, the luminescence mechanisms, excitons, *etc.* are still not well known. We mainly investigate their band structures using vacuum ultraviolet and soft X-ray monochromators combined with synchrotron radiation light source (UVSOR). Since the core levels are strictly localized in space, core absorption spectrum gives us the site-specific information which is a useful method to investigate the binary or ternary compounds.

VI-U-1 Soft X-ray Absorption Study of III-V Nitrides

FUKUI, Kazutoshi; HIRAI, Ryousuke¹; YAMAMOTO, Akio¹; NAOE, Syun-ichi²; TANAKA, Satoru³
(¹Fukui Univ.; ²Kanazawa Univ.; ³Hokkaido Univ.)

[*Jpn. J. Appl. Phys., Part 1* **38**, 538 (1999)]

The soft X-ray absorption measurements around nitrogen K and aluminum K edge of the wurtzite AlN, GaN and their ternary compounds AlGaN have been performed. The incidence light angle dependence of the absorption spectra were clearly observed in all samples. A numerical component analysis is presented to separate the experimental K-absorption spectra into three partial spectra which correspond to in-plane, out-

of-plane and angular independent components of the unoccupied p partial density of states.

Reference

- 1) W. R. L. Lambrecht, S. N. Rashkeev, B. Segall, K. Lawniczak-Jablanska, T. Suski, E. M. Gullikson, J. H. Underwood, R. C. C. Perera, J. C. Rife, I. Grzegory, S. Porowski and D. K. Wickenden, *Phys. Rev. B* **55**, 2612 (1997).

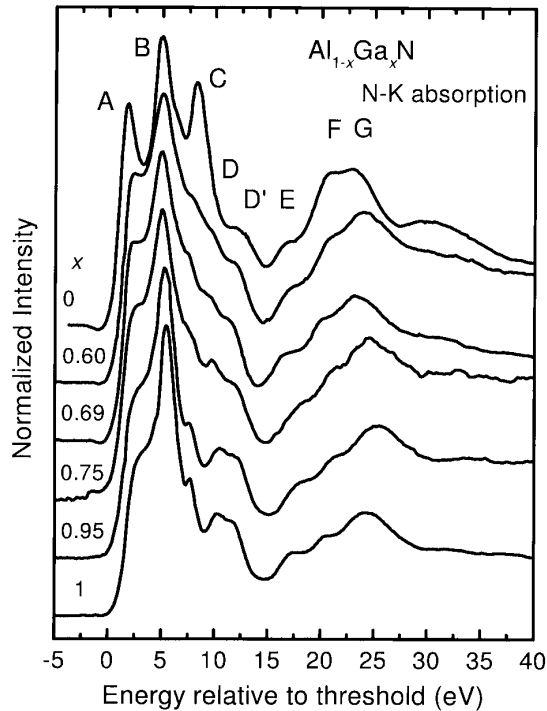


Figure 1. Normal incidence nitrogen K absorption spectra of $\text{Al}_{1-x}\text{Ga}_x\text{N}$. The energy scale is relative to the threshold energy. The labels A to G correspond to those for GaN in Reference 1. The intensity of each spectrum is normalized at the peak B.

VI-V Site-Specific Fragmentation Following Core-Level Photoexcitation

Monochromatized synchrotron radiation can excite core electrons of an atom in a specific chemical environment selectively, discriminating the core electrons from those of like atoms having different chemical environments. This site-specific excitation often results in site-specific fragmentation, which is of importance in understanding localization phenomena in chemical reactions and which is potentially useful for synthesizing materials through selective bond breaking. Synchrotron radiation can indeed play the part of an optical knife for molecules. When bond dissociation around an atomic site is required in the synthesis, one can use the optical knife that has the photon energy corresponding to the specific excitation of that site. To elucidate the site-specific fragmentation, we have used photoemission spectroscopy and the energy-selected-photoemission photoion coincidence method to study site-specific phenomena in the C:1s and Si:2p photoexcitation of organic and organosilicon molecules condensed on a Si surface and in the vapor phase.

VI-V-1 Site-Specific Phenomena in Si:2p Core-Level Photoionization of $X_3Si(CH_2)_nSi(CH_3)_3$ ($X = F$ or Cl , $n = 0-2$) Condensed on a Si(111) Surface

NAGAOKA, Shin-ichi; MASE, Kazuhiko¹; NAGASONO, Mitsuru²; TANAKA, Shin-ichiro³; URISU, Tsuneo; OHSHITA, Joji⁴; NAGASHIMA, Umpei⁵

(¹KEK-PF; ²MAX-lab; ³Nagoya Univ.; ⁴Hiroshima Univ.; ⁵Natl. Inst. Adv. Interdisciplinary)

[Chem. Phys. in press]

We used photoelectron spectroscopy and the energy-selected-photoelectron photoion coincidence (ESPEPICO) method to study site-specific phenomena in the Si:2p photoionization of $X_3Si(CH_2)_nSi(CH_3)_3$ ($X = F$ or Cl , $n = 0-2$) condensed on a Si(111) surface. The site-specific excitation and the occurrence of different chemical shifts at two Si sites were revealed in the total electron-yield spectra and the photoelectron spectra of $F_3Si(CH_2)_nSi(CH_3)_3$ ($n = 1, 2$), although they were not clearly revealed in those of $Cl_3SiSi(CH_3)_3$. We conclude that these site-specific phenomena are easily observed in molecules in which the two Si sites are located far apart and in which electron migration between the two Si-containing groups does not occur. This was supported by our ab initio calculation. Site-specific fragmentation was revealed in the ESPEPICO spectrum of $F_3SiCH_2CH_2Si(CH_3)_3$, although it was negligible for $Cl_3SiSi(CH_3)_3$ and was less remarkable in $F_3SiCH_2Si(CH_3)_3$ than in $F_3SiCH_2CH_2Si(CH_3)_3$. Site-specific fragmentation also occurred when the two Si sites were located far apart.

VI-V-2 Ion Desorption Induced by Core-Electron Transitions Studied with Electron-Ion Coincidence Spectroscopy

MASE, Kazuhiko¹; TANAKA, Shin-ichiro²; NAGAOKA, Shin-ichi; URISU, Tsuneo

(¹KEK-PF; ²Nagoya Univ.)

In a study of $CF_3CH(OH)CH_3$ chemisorbed on a Si(100) surface using photoelectron photoion coincidence (PEPICO) spectroscopy, site-specific ion desorption is directly verified, that is, F^+ desorption is predominant for C:1s photoionization at the CF_3 - site, while H^+

desorption is predominantly induced by C:1s photoionization at the $-CH_3$ site. This study demonstrates that PEPICO spectroscopy combined with synchrotron radiation is a novel and powerful tool for the study of ion desorption induced by core-electron excitations and that it is also a prospective method to investigate the electronic structure of the specific sites responsible for ion desorption.

VI-V-3 Development of Electron-Ion Coincidence Spectroscopy for Study of Surface and Vapor-Phase Dynamics

MASE, Kazuhiko¹; NAGAOKA, Shin-ichi
(¹KEK-PF)

An electron-ion coincidence spectrometer for vapor-phase dynamics study is being built now. The equipment consists of an electron gun, a cylindrical mirror analyzer (CMA) and a time-of-flight ion mass analyzer (TOF-MS). Sample gas is excited with the electron beam and the CMA analyzes energy of emitted or scattered electrons. TOF spectra of desorbed ions are measured with a multichannel scalar taking the energy-analyzed electron signal as the starting trigger.

VI-W Study on RF-Photocathode for Compact X-Ray Sources

Electron storage rings are useful and practical devices as x-ray sources because which produce a number of photons owing to high electron current and various insertion devices. However, these synchrotron radiation facilities usually occupy large area and cost much. So that there have been many works to investigate more compact x-ray sources such as x-ray lasers and free electron lasers. It is also useful to use laser undulator radiation or backward Compton scattering caused by the interactions of electron beams with laser photons, if we provide enough electrons to produce practical intensity of x-rays. RF-photocathode would produce dense electron beam so that it is a useful candidate of a electron source. It is necessary to search good materials as the photocathode for construction of a practical compact x-ray source. Cesium telluride has reported to have a good quantum efficiency, we study about it.

VI-W-1 Measurement of Quantum Efficiency of Cesium Telluride as a Photocathode

TAKASHIMA, Yoshifumi; KOBAYAKAWA, Hisashi¹; KIMURA, Kenichi¹; SUGIYAMA, Harue¹; FURUTA, Fumio¹; NAKANISHI, Tsutomu¹; OKUMI, Shoji¹; TOGAWA, Kazuaki¹; SUZUKI, Chihiro¹; NAKAMURA, Shinsuke¹; WADA, Kouji¹; YAMAMOTO, Masahiro¹; NISHITANI, Tomohiro¹; YOSHIOKA, Masakazu²; MATSUMOTO, Hiroshi²
(¹Nagoya Univ.; ²KEK)

The photocathode for a x-ray source is required to have high quantum efficiency for production of practical intensity of x-rays. There have been a number of works¹⁻⁴⁾ to test materials as photocathode. We used cesium telluride as the photocathode and studied quantum efficiency. Figure 1 shows a picture of the vacuum chamber in which the cathode was installed. Ultraviolet (UV) radiations, generated with a xenon lamp, were guided into diffraction grating. Monochromatic UV radiations from the grating passed through an entrance sapphire window of the vacuum chamber, then focused on the photocathode. Cesium telluride was made on a surface of a molybdenum block by vacuum evaporation method. Negative constant voltage of 100V was supplied to the photocathode.

Electric current flowing into the cathode was measured to derive the quantum efficiency which is shown in Figure 2 with wavelength of injected UV radiations. The maximum quantum efficiency is about 10% and is kept longer than hundred hours. For the further study, we should supply RF voltage and test the cathode whether it has a good performance as this experiment.

Reference

- 1) S. W. Downey, L. A. Buita, D. C. Moir, T. J. Ringler and J. D. Saunders, *Appl. Phys. Lett.* **49**, 911 (1986).
- 2) A. Septier, F. Sabary and J. C. Dudek, *Nucl. Instrum. Methods Phys. Res., Sect. A* **304**, 392 (1991).
- 3) Y. Yamaoka *et al.*, *Proceedings of the 14th Linear Accelerator Meeting* (1989).
- 4) R. A. Powell, W. E. Spicer, G. B. Fisher and P. Gregory, *Phys. Rev. B* **8**, 3987 (1973).

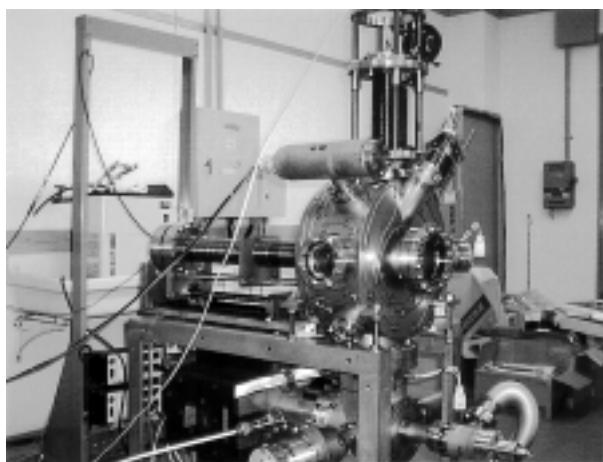


Figure 1. Vacuum chamber in which there is a photocathode. UV radiation is injected on the photocathode through one of a viewing port.

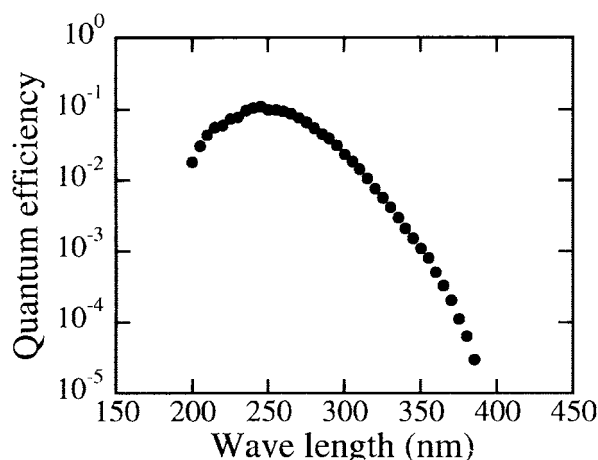


Figure 2. Quantum efficiency of cesium telluride with wavelength of injected UV radiations.

RESEARCH ACTIVITIES VII

Coordination Chemistry Laboratories

Prof. Mitsuhiro Shionoya and Dr. Kentaro Tanaka in laboratory of Complex Catalysis moved to Faculty of Science, Tokyo University in April 1999. Prof. Makoto Fujita and Dr. Takahiro Kusukawa in laboratory of Functional Coordination Chemistry also moved to Faculty of Engineering, Nagoya University in April 1999. Prof. Yuzo Nishida, Prof. Masahiro Ebihara, Dr. Tomohiro Ozawa and Dr. Hiroyuki Kawaguchi continued the position of Synthetic Coordination Chemistry from April 1998. Prof. Ginya Adachi (Osaka University) and Assoc. Prof. Hiromi Tobita (Tohoku University) finished their term as Adjunct Prof. in March 1999 in the Laboratory of Coordination Bond. Their effort during their term is gratefully appreciated. Prof. Hiromu Sakurai (Kyoto pharmacy University) and Assoc. Prof. Yuji Mizobe (Tokyo University) continued their position as Adjunct Prof. of Laboratory of Complex Catalysis. Prof. Takuzo Aida (Tokyo University) and Assoc. Prof. Itaru Hamachi (Kyushu University) took the position of the laboratory of Coordination Bond.

VII-A New Insight into Mechanism of Oxygen Activation in Biological Oxygenases

One of the remaining frontiers in organic chemistry is the direct functionalization of saturated hydrocarbons. The catalytic cycle that oxidizes a hydrocarbon R-H to an alcohol R-OH employing cytochrome P-450 and methane monooxygenase is a well-established process, however no reasonable mechanism for dioxygen activation and for formation of the R-OH is available at present. Recently the present author has proposed a new idea that elucidates many biological oxygenation reactions including monooxygenases and dioxygenases comprehensively. In this new

concept, the importance of electrophilic nature of a metal-peroxide adduct and the role of the substrate as an electron donor to the peroxide adduct were emphasized. This idea suggests that formation of a high-valent iron-oxo species, which has been frequently pointed out by the previous authors, occurs most likely when the metal-peroxide intermediate is activated through electronic interaction with both the substrate and the peripheral organic group; the latter two act as an electron donor to the peroxide adduct (see Figure 1: Y. Nishida, *Trends Inorg. Chem.* **5**, 89 (1998)). We are now continuing the study on the reactivity of the metal-peroxide adducts in order to ascertain that my idea is applicable to other reactions, such as degradation of DNA and proteins by the metal-peroxide adducts.

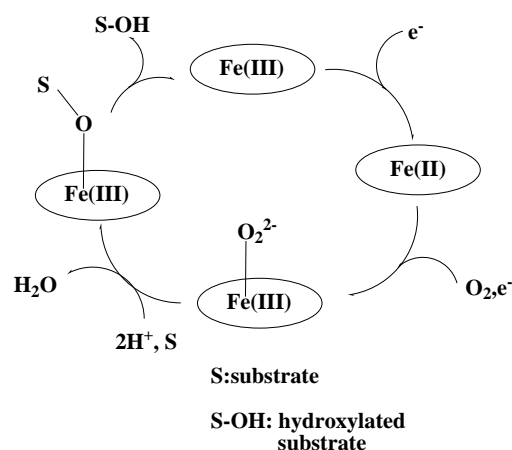


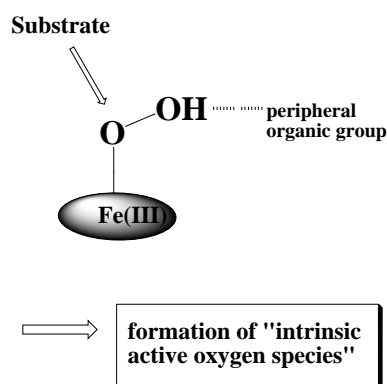
Figure 1. Nishida's mechanism for hydroxylation reaction catalyzed by cytochrome P-450

VII-A-1 Important Role of Substrate in Activation of Dioxygen in Biological Oxygenases

NISHIDA, Yuzo

[*Trends Inorg. Chem.* **5**, 89 (1998)]

In this paper, I have discussed the reaction mechanism of monooxygenases and dioxygenases based on the results obtained for the model systems. Monooxygenases and dioxygenases activate peroxide ion and dioxygen molecule, respectively, and in both cases the substrate plays an important role in the activation of the oxygen species, generating an "intrinsic active oxygen species." (see the Scheme shown below)



My idea is completely different from those of the previous papers; in the latter cases it has been believed that the active oxygen species generates from the reaction between oxygen and the metal enzymes, and then it reacts with a substrate. According to our scheme,

the oxygen atom of the peroxide adduct which is coordinate to the iron(III), is inserted to the substrate in P-450 reaction (see the figure above). On the contrary, terminal oxygen atom of the peroxide adduct is inserted to the porphyrin ring in Heme-oxygenase; in the latter case the substrate is identical to the peripheral group. Thus, it seems quite likely that oxygen atom, which interacts strongly with the substrate is transferred to the organic group, and that electronic interaction between the orbitals of a metal-peroxide and substrate induces heterolytic cleavage of O-O bond, and the electron transfer is not necessary in this process.

In the monooxygenases such as cytochrome P-450 and methane monooxygenase, at first a metal peroxide forms via two electron transfer reduction, and heterolysis of the O-O bond of the metal-peroxide occurs in the presence of substrate and also peripheral organic moiety near the metal ion, and one oxygen atom is incorporated into the substrate.

In the dioxygenases, the metal ion plays a role to bring the substrate near to oxygen molecule and to promote the electron transfer from the substrate to oxygen, giving a C-OOH bond formation. In this case, since the activation of oxygen molecule occurs, O-O bond cleavage does not occur. The substrate in the dioxygenases are generally oxidizable than those in the monooxygenases.

In the case of phenylalanine hydroxylase and tyrosine hydroxylase, which are one of the monooxygenases, dioxygenase reaction proceeds in the first step, and in the next step, monooxygenase, does. In the first step the substrate is pterin, and in the second step, amino acid, such as phenylalanine or tyrosine.

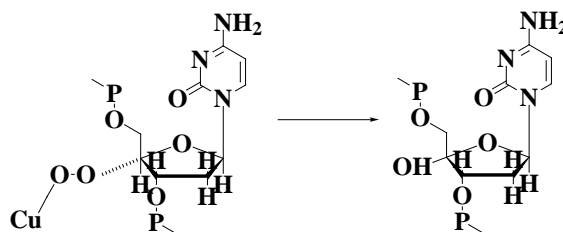
VII-A-2 Structural Variety of Copper(II)-Peroxide Adducts and its Relevance to DNA Cleavage

NISHINO, Satoshi; KOBAYASHI, Teruyuki; KUNITA, Mami; ITO, Sayo; NISHIDA, Yuzo

[*J. Bioscience* **54C**, 94 (1999)]

The reactivity of copper(II) compounds with several tetradentate ligands towards some spin-trapping reagents was studied in the presence of hydrogen peroxide. The compounds used in this study are roughly divided into two groups based on the reactivity towards 2,2,6,6-tetramethyl-4-piperidinol (and also 2,2,6,6-tetramethyl-4-piperidone), which are trapping agents for singlet oxygen, $^1\text{O}_2(^1\Delta_g)$. The A-group compounds exhibited a high activity to form the corresponding nitron radical, which was detected by ESR spectrometry, but the corresponding activity of the B-group compounds was very low. The A-group compounds defined as above exhibited high activity for cleavage of DNA (supercoiled Form I DNA in the presence of hydrogen peroxide, yielding DNA Form II (relaxed circular) or Form III (linear duplex) under our experimental conditions. On the other hand, the B-group compounds effected complete degradation of the DNA (double-strand scission) under the same experimental conditions; formation of Form II or Form III DNA is negligible. Two different DNA cleavage patterns observed for A-

and B-group compounds were elucidated by different structural properties of the copper(II)-peroxide adducts, which is controlled by the interaction through both DNA and the peripheral group of the ligand system. Based on these results, it was assumed that double-strand break by Cu(bdp_g)/H₂O₂ system (one of the B-group compound) may proceed via formation of 4'-OH as shown in Scheme.

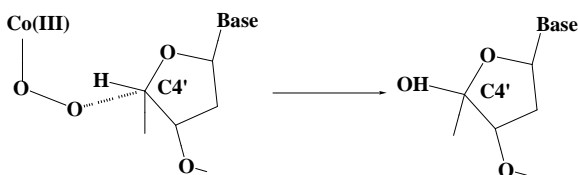


VII-A-3 Mechanism of DNA Cleavage due to Green Cobalt(III)-Bleomycin Hydroperoxide Irradiated by Visible Light

NISHIDA, Yuzo; KUNITA, Mami; NISHINO, Satoshi

[*Inorg. Chem. Commun.* **2**, 156 (1999)]

The origin of the DNA cleavage reaction due to green cobalt(III)-bleomycin hydroperoxide irradiated by visible light (366 nm) was developed on the molecular orbital theory. The importance of the activation of the peroxide ion by transferring an electron from the occupied orbital to σ^* -orbital of the peroxide ion was pointed out. We have proposed that the irradiation of the system by the light (366 nm) induces a direct hydroxylation reaction at the 4' position associated with a concerted heterolytic O-O cleavage reaction (*i.e.*, insertion of an atomic oxygen into the C-H bond) without formation of a C4' radical (see the Scheme shown below). This consideration is quite consistent with the observed results, and a study on the reaction mechanism of hydroxylation by heme-oxygenase, and our previous theoretical consideration.

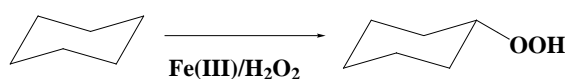


VII-A-4 Selective Dioxygenation of Cyclohexane Catalyzed by Hydrogen Peroxide and Dinuclear Iron(III) Complexes with μ -Alkoxo Bridge

NISHINO, Satoshi; HOSOMI, Hiroyuki; OHBA, Shigeru; MATSUSHIMA, Hideaki; TOKII, Tadashi; NISHIDA, Yuzo

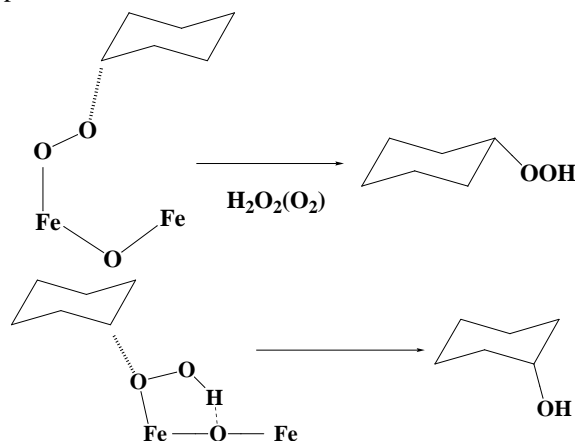
[*J. Chem. Soc., Dalton Trans.* 1509 (1999)]

Several dinuclear iron(III) complexes with μ -alkoxo bridge gave predominantly cyclohexyl hydroperoxide in the reaction with cyclohexane and hydrogen peroxide



and similar results were observed when linear n-alkanes, such as n-nonane and n-octane, were used instead of cyclohexane.

These facts clearly indicate that the Fish's mechanism for the hydroxylation of cyclohexane by Fe(III)/H₂O₂ system is wrong. We have proposed new mechanism for the functionalization of alkanes by Fe(III)/H₂O₂ system; the active species which catalyze dioxygenation and monooxygenation are different from each other, and theoretical elucidation was also provided to our conclusion.

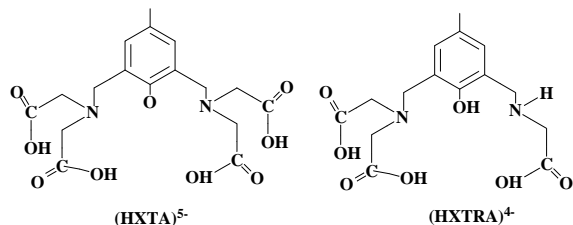


VII-A-5 Interaction between the Peroxide Ion and Acetate Moiety of the Ligand System in a Cobalt(II) Complex with a Binucleating Ligand

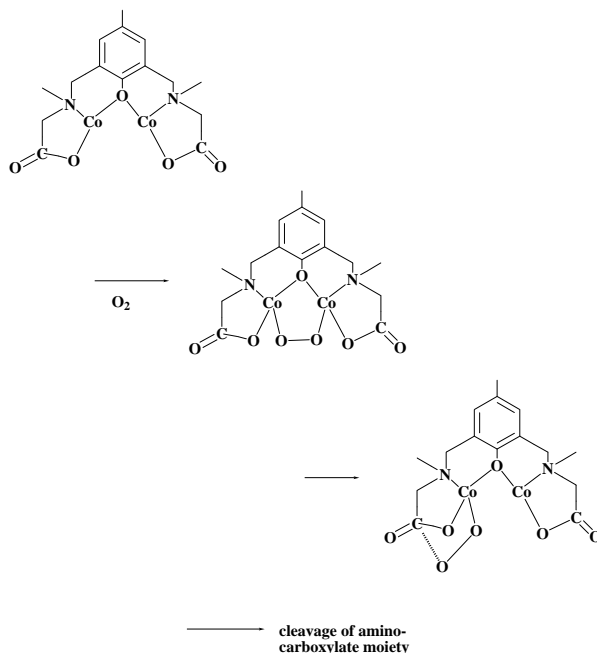
SASAKI, Yumiko; KOBAYASHI, Teruyuki; MASUDA, Hideki; EINAGA, Hisahiko; OHBA, Shigeru; NISHIDA, Yuzo

[*Inorg. Chem. Commun.* **2**, 244 (1999)]

We have found that reaction between Na₃H₂(HXTA) and Na₃Co(CO₃)₃ in an aqueous solution gave a binuclear cobalt(III) complex, Na₂Co₂(HXTRA), where in (HXTRA)⁴⁻ ligand one of the four acetato arms of the original (HXTA)⁵⁻ ligand is lost.



This may be attributed to the oxidative degradation of one acetato arm of (HXTA)⁵⁻ ligand due to an electrophilic peroxide-cobalt(III) species with end-on type, as illustrated in Scheme.



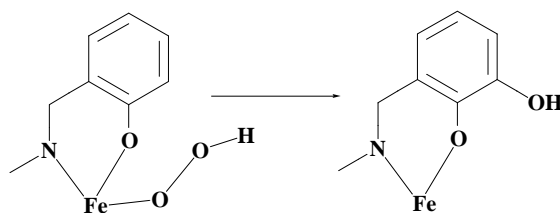
VII-A-6 Electrospray Mass Spectrometry of Peroxide Adduct of Monomeric Fe(III) Complex Containing Phenol Group

OKUTSU, Wataru; ITO, Sayo; NISHIDA, Yuzo

[*Inorg. Chem. Commun.* **2**, 308 (1999)]

Peroxoiron(III) complexes are increasingly being considered as potential intermediates in oxidation catalyzed by both non-heme and heme iron centers. In 1994, Sam *et al.* reported that an "activated bleomycin" is a monomeric iron(III)-peroxide adduct with end-on type, however evidence for the formation of a monomeric iron(III)-peroxide adduct with end-on type is scarce, and their reactivity is unknown at present. In our previous paper, we have reported the preparation, crystal structure determinations of the monomeric iron(III) compounds with ligands containing phenol group, and proposed that the phenol group plays an important role in formation of a peroxide adduct, and in activation of he peroxide ion.

In this study we have confirmed the formation of a peroxide adduct of the monomeric iron(III) complex with end-on type in terms of the electrospray mass spectrometry, and discussed the activation of the peroxide ion and hydroxylation of phenol ring (see Scheme) based on these facts.

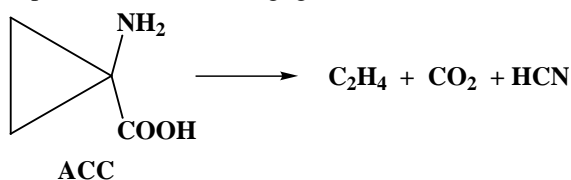


VII-A-7 High Activity of Binuclear Cobalt(II) Complex for Ethylene Evolution from 1-Aminocyclopropane-1-carboxylic Acid in the presence of Hydrogen Peroxide

KOBAYASHI, Teruyuki; SASAKI, Yumiko; AKAMATSU, Tetsuya; ISHII, Toshihiro; MASUDA, Hideki; EINAGA, Hisahiko; NISHIDA, Yuzo

[*Z. Naturforsch., C: Biosci.* **54**, 534 (1999)]

The binuclear Co(II) and Mn(II) complexes with H₅(HXTA), where H₅(HXTA) represents *N,N'*-(2-hydroxy-5-methyl-1,3-xylylene)bis(*N*-carboxylmethyglycine) induced a strong ethylene evolution from 1-aminocyclopropane-1-carboxylic acid (ACC) in the presence of hydrogen peroxide (see Scheme), whereas the activities of the corresponding Fe(III), Ni(II) and V(III) compounds were found negligible.



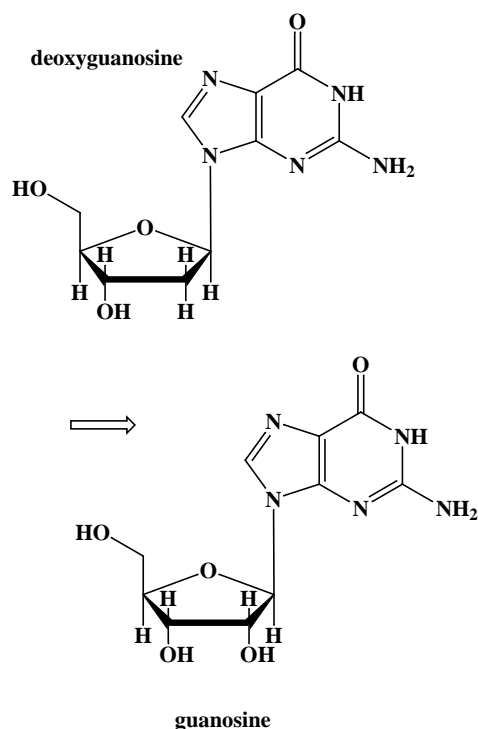
Based on the spectroscopic and mass-spectral data it is proposed that a peroxide adduct of binuclear Co(II) (and Mn(II)) complex with η^1 -coordination mode interacts with ACC, which is chelated to a binuclear cobalt(II) complex leading to facile oxidative degradation of ACC and to evolution of ethylene.

VII-A-8 Oxygenation of Nucleosides by Peroxide Adduct of Binuclear Iron(III) Complex with a μ -Oxo Bridge

ITO, Sayo; SASAKI, Yumiko; TAKAHASHI, Yasuyuki; OHBA, Shigeru; NISHIDA, Yuzo

[*Z. Naturforsch., C: Biosci.* **54**, 554 (1999)]

The (μ -oxo)(μ -carbonato)diiron(III) complex with H₂(tfda) (H₂(tfda) = 2-aminomethyltetrahydrofuran-*N,N*-diacetic acid) exhibited high activity for hydroxylation of 2'-deoxyguanosine in the presence of hydrogen peroxide, giving 8-hydroxydeoxyguanosine, but its hydroxylation activity towards other nucleosides, such as 2'-deoxyadenosine, adenosine, or thymidine was found negligible. In the case of the Fe(III)-(eda) complex (H₂(eda) = 2-methoxyethylamine-*N,N*-diacetic acid), hydroxylation reaction occurred mainly at the sugar site, converting 2'-deoxyguanosine to guanosine (see the Scheme). Based on the spectroscopic and structural properties of these iron(III) compounds, it seems most likely that an intrinsic active species for hydroxylation should be an electrophilic peroxide adduct of the (μ -oxo)diiron(III) core with η^1 -coordination mode, while the contribution of OH• to the hydroxylation reaction of nucleosides is ruled out.



VII-B Electronic Structure and Reactivity of Metal Cluster Complexes

Because trimetal cluster complex is a fundamental framework for constructing high nuclearity cluster, electronic structure and reactivity of trimetal cluster complex is important. We have studied the electronic structure and reactivity of bis(μ_3 -benzylidyne)tris(cyclopentadienylcobalt) complex. It reacts halogens and silver(I) to give halide and silver bridged complexes.

VII-B-1 Synthesis, Structure and Redox Behavior of Tricobalt Cluster with Capping Benzylidyne and Bridging halogen $[\text{Co}_3\text{Cp}_3(\mu_3\text{-CPh})_2(\mu\text{-X})]^+$ ($\text{X} = \text{Cl}, \text{Br}, \text{I}$)

EBIHARA, Masahiro; IIBA, Masami¹; MATSUOKA, Hiroaki¹; KAWAMURA, Takashi¹
(¹Gifu Univ.)

Reactions of the benzylidyne capped tricobalt cluster $[\text{Co}_3\text{Cp}_3(\mu_3\text{-CPh})_2]$ (**1**) with halogens ($\text{X}_2 = \text{Cl}_2, \text{Br}_2, \text{I}_2$) in CH_2Cl_2 gave oxidative addition products of halogen to **1**. X-ray structures of four salts, $[\text{Co}_3\text{Cp}_3(\mu_3\text{-CPh})_2(\mu\text{-Cl})]\text{PF}_6 \cdot \text{CH}_3\text{CN}$ (**2**⁺ $\text{PF}_6^- \cdot \text{CH}_3\text{CN}$), $[\text{Co}_3\text{Cp}_3(\mu_3\text{-CPh})_2(\mu\text{-Br})]\text{SbF}_6$ (**3**⁺ SbF_6^-), $[\text{Co}_3\text{Cp}_3(\mu_3\text{-CPh})_2(\mu\text{-I})]\text{SbF}_6 \cdot \text{CH}_2\text{Cl}_2$ (**4**⁺ $\text{SbF}_6^- \cdot \text{CH}_2\text{Cl}_2$) and $[\text{Co}_3\text{Cp}_3(\mu_3\text{-CPh})_2(\mu\text{-I})]\text{I}_3$ (**4**⁺ I_3^-) were determined. In all structures the halogen atom was in the Co_3 plane. The halogen-bridged Co–Co distance was elongated (**2**⁺ $\text{PF}_6^- \cdot \text{CH}_3\text{CN}$: 2.6072(5) Å, **3**⁺ SbF_6^- : 2.6097(9) Å, **4**⁺ $\text{SbF}_6^- \cdot \text{CH}_2\text{Cl}_2$: 2.621(2) Å) and the Co–Co distances without halogen-bridge remained unchanged (**2**⁺ PF_6^- : 2.4038(9) and 2.3947(7) Å, **3**⁺ SbF_6^- : 2.3902(8) and 2.4015(9) Å, **4**⁺ $\text{SbF}_6^- \cdot \text{CH}_2\text{Cl}_2$: 2.392(2) and 2.388(2) Å) from that of **1** (2.38 Å). Cyclic voltammogram of **2**⁺ PF_6^- in CH_2Cl_2 with 0.1 M $n\text{-Bu}_4\text{NPF}_6$ as supporting electrolyte showed an quasi-reversible oxidation (+0.75 V, potential vs Fc/Fc^+) and an irreversible reduction wave (−0.57 V) (Figure 1). The irreversible reduction caused recovery of neutral cluster complex **1**. The redox properties of **3**⁺ and **4**⁺ were similar to that of **2**⁺. Cyclic voltammetry of **1** in 0.1 M $n\text{-Bu}_4\text{NCl}/\text{CH}_3\text{CN}$ with various scan rates indicated that the formation of **2**⁺ was a multi-step reaction. First **1** was oxidized to **1**⁺ and it was coordinated by Cl^- and immediately oxidized to **2**⁺.

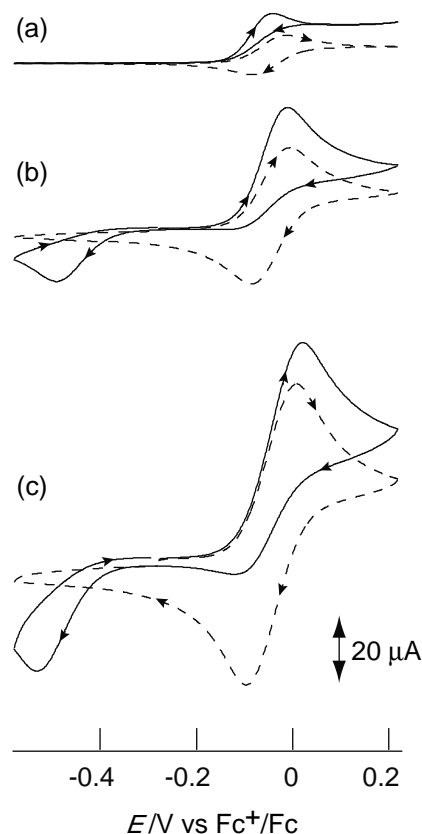


Figure 1. Cyclic voltammograms of **1** (2.0 mM) in CH_3CN with 0.1 M $n\text{-Bu}_4\text{NCl}$. Scan rate (a) 10 mVs^{-1} , (b) 100 mVs^{-1} and (c) 500 mVs^{-1} with cyclic voltammograms of **1** (2.0 mM) in 0.1 M $n\text{-Bu}_4\text{NPF}_6$ (broken line).

VII-B-2 Bis- μ_3 -Benzylidyne Tri(cyclopentadienylcobalt) Cluster with Edge-bridging Silver(I): Synthesis, Structure and Solution Properties of $[\text{Co}_3\text{Cp}_3(\mu_3\text{-CPh})_2\{\mu\text{-Ag(X)}\}]$ ($\text{X} = \text{CF}_3\text{CO}_2, \text{NO}_3$) and $[\text{Co}_3\text{Cp}_3(\mu_3\text{-CPh})_2\{\mu\text{-Ag}(\text{NCCH}_3)\}]\text{PF}_6$

EBIHARA, Masahiro; IIBA, Masami¹; MATSUOKA, Hiroaki¹; KAWAMURA, Takashi¹
(¹Gifu Univ.)

Reactions of the benzylidyne capped tricobalt cluster $[\text{Co}_3\text{Cp}_3(\mu_3\text{-CPh})_2]$ (**1**) with various silver salts are examined. The salts of weakly- or non-coordinating anions (BF_4^- , PF_6^-) oxidize **1** to its cationic radical $[\text{Co}_3\text{Cp}_3(\mu_3\text{-CPh})_2]^+$ (**1**⁺) in CH_2Cl_2 . The reaction with the salts of strongly-coordinating anions (CF_3CO_2^- , NO_3^-) gives silver(I) adducts of **1**, $[\text{Co}_3\text{Cp}_3(\mu_3\text{-CPh})_2\{\mu\text{-Ag(X)}\}]$ ($\text{X} = \text{CF}_3\text{CO}_2^-$ (**2**, Figure 1), NO_3^- (**3**)). Even for AgBF_4 or AgPF_6 the reaction in CH_3CN produces silver(I) adduct $[\text{Co}_3\text{Cp}_3(\mu_3\text{-CPh})_2\{\mu\text{-Ag}(\text{NC-})$

$\text{CH}_3\}}]^{+}$ (4^{+}). The Co_3Ag skeleton in structures of **2**, **3** and 4^{+} resembles each other. The Co–Co bonds bridged by the Ag atom (**2**: 2.4783(9) Å, **3**: 2.481(1) Å, 4^{+} : 2.4600(9) Å) are longer than that of **1** (2.38 Å). The other Co–Co bonds are slightly shorter than that in **1**. The Co_2Ag triangle is not coplanar with the Co_3 triangle; the dihedral angles between these triangles for **2**, **3**, and 4^{+} are 162.7° , 157.8° , and 151.3° , respectively. Dissolution of 4^{+}PF_6^{-} in CH_2Cl_2 causes formation of 1^{+} with deposition of Ag metal. ^1H NMR spectra of **2** and **3** in CD_2Cl_2 indicates partial dissociation of the AgX group. The ^1H NMR spectra of CD_3CN solutions and the ESR spectra in frozen CH_3CN solutions of **2**, **3**, and 4^{+}PF_6^{-} shows generation of 1^{+} without deposition of Ag metal. It suggests that equilibrium of Ag^{+} and **1** with Ag^0 and 1^{+} is established in acetonitrile. Addition of AgO_2CCF_3 to the solution causes disappearance of the ESR signal. It indicates that 1^{+} is generated from 4^{+} or the reaction of **1** with anion-uncoordinated Ag^{+} .

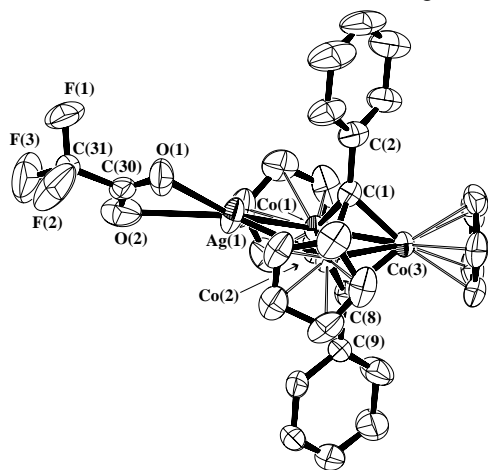


Figure 1. Structure of $[\text{Co}_3\text{Cp}_3(\mu_3\text{-CPh})_2\{\mu\text{-Ag}(\text{O}_2\text{CCF}_3)\}]$.

VII-C Bio-Inspired Molecular Architecture

Nature has produced a limited number of molecular modules such as nucleosides and nucleotides, amino acids, and lipids. However, the chemical diversity of these biomolecules and the different ways they can be polymerized or assembled into precisely-defined three-dimensional shapes provide a wide range of possible structures and functions. Furthermore, owing to advances in chemical synthesis and biotechnology we can combine or chemically modify these molecular building blocks, almost at will, to produce new functional molecules that have not yet been made in Nature. Based on these concepts, we have been working on the following research projects. Our research programs also consciously focus on structures and functions that have been unknown in living, biological systems.

VII-C-1 Synthesis of a Novel Nucleoside for Alternative DNA Base Pairing through Metal Complexation

TANAKA, Kentaro; SHIONOYA, Mitsuhiro

[*J. Org. Chem.* **64**, 5002 (1999)]

A novel artificial nucleoside was synthesized, in which artificial bases are introduced as metal coordination sites for alternative base-pairing through metal complexation instead of hydrogen bonding in natural DNA. The artificial β -C-nucleoside (4-[1,2-dideoxy- β -D-ribofuranos-1-yl]-*o*-phenylenediamine) **1** which has a phenylenediamine moiety as a metal coordination site was prepared by coupling reaction of a lithiated *o*-phenylenediamine derivative and 2,3,5-tri-*O*-benzyl-D-ribofuran- γ -lactone followed by several reactions to remove 2'-hydroxyl group. ^1H NMR and ESI mass spectroscopic studies clearly showed that **1** and Pd^{2+} form a stable 2:1 complex in aqueous media (Figure 1).

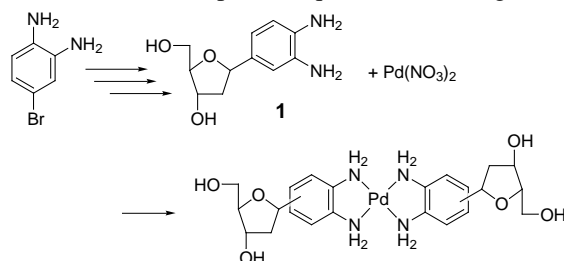


Figure 1. Complex formation of phenylenediamine-nucleoside **1** with Pd^{2+} .

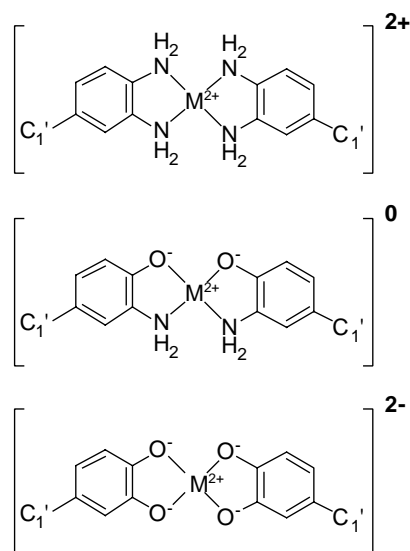
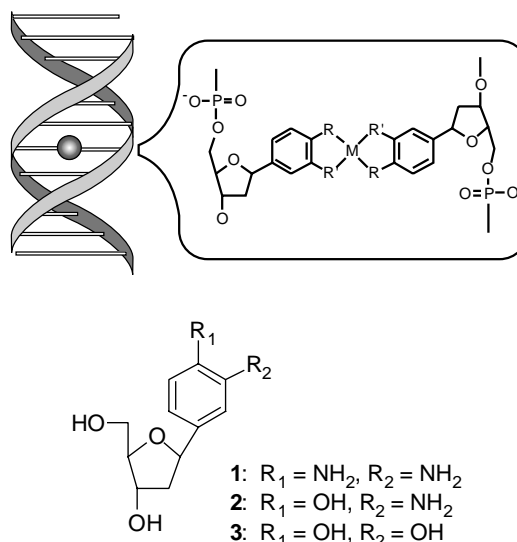
VII-C-2 An Approach to Metal-Assisted DNA Base Pairing: Novel β -C-Nucleosides with a 2-Aminophenol or a Catechol as the Nucleobase

TANAKA, Kentaro; TASAKA, Motoyuki¹; CAO, Honghua¹; SHIONOYA, Mitsuhiro
(¹GUAS)

[*Eur. J. Pharm. Sci.* in press]

The metal-chelating β -C-nucleoside having a phenylenediamine moiety as the nucleobase was previously found to form a stable 2:1 complex with a Pd^{2+} ion in aqueous media, where hydrogen bonding is replaced by metal coordination in the base pairing thereby creating a novel hybridization motif in duplex DNA. In this regard, we have further designed two types of artificial β -C-nucleosides possessing a metal-chelating site (a 2-aminophenol or a catechol) as the

nucleobase moiety. These artificial nucleosides are directed toward controlling the net charges of the metal-assisted base pairs. This paper describes convenient syntheses of the artificial nucleosides bearing a 2-aminophenol or a catechol moiety. Each nucleoside was directly synthesized through 2'-deoxy derivative via a Friedel-Crafts coupling reaction as the key step between the aromatic ring and ribose moiety, whereas the nucleoside having a phenylenediamine moiety was prepared in rather longer steps through an RNA type intermediate followed by the removal of 2'-hydroxy group.



VII-C-3 Cyclic Metallopeptides, *cyclo*[-Gly-L-Cys(terpyPt^{II})]_nCl_n

TANAKA, Kentaro; SHIGEMORI, Kazuki¹; SHIONOYA, Mitsuhiro
(¹GUAS)

[Chem. Commun. in press]

A new efficient synthetic methodology has been developed that can be utilized for the iterative construction of a new family of cyclohexa and cycloocta metallopeptides of the general formula, *cyclo*[-Gly-L-Cys(terpyPt^{II})]_nCl_n, **1** (*n* = 3) and **2** (*n* = 4). The linear peptides, TFA·H-[Gly-L-Cys(terpyPt^{II})]_n-OH(CF₃CO₂)_n, (*n* = 3) and (*n* = 4), were cyclized in H₂O-CH₃CN (7:3) at 25 °C to the corresponding cyclopeptides, **1** and **2**, in the presence of excess HOBt and EDC in 58% yield in both cases. The ring size of each cyclopeptide was determined by high-resolution ESI mass spectroscopy. The cyclohexapeptide **1** selectively separated benzene 1,3,5-tricarboxylate from a mixture of three tricarboxylates (benzene 1,3,5-tricarboxylate and its 1,2,4- and 1,2,3-isomers) in neutral water. The ¹H NMR and ESI mass spectra of the precipitate immediately appeared clearly evidenced the 1:1 complexation of **1** and benzene 1,3,5-tricarboxylate. The Pt^{II}-terpyridine complex moieties of **1** were readily removed by acid treatment to afford the corresponding cyclohexapeptides, *cyclo*[-Gly-L-Cys-]₃. The synthetic strategy developed in this work would provide a powerful tool for arraying functional metal complexes on cyclopeptide frameworks.

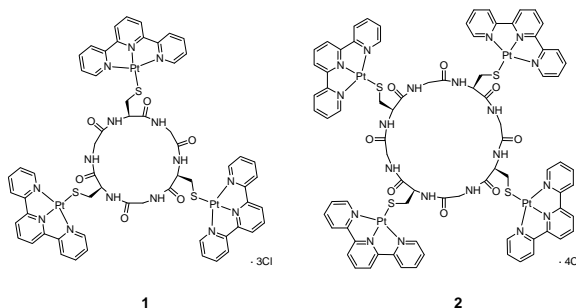


Figure 1. Chemical structures of the cyclic metallopeptides newly synthesized in this study.

VII-C-4 Construction of a Unique Alternating-Chain Array with Copper(II) and a New Diazamesocycle Bearing One Functional Pendant

BU, Xian-He¹; XU, Qiang¹; SHANG, Zhi-Liang¹; ZHANG, Ruo-Hua¹; ZHAO, Qi-Hua¹; TANAKA, Kentaro; SHIONOYA, Mitsuhiro
(¹Nankai Univ.)

[Inorg. Chem. Commun. submitted]

The polymeric Cu^{II} complex of 1-[(1-methylimidazol-2-yl)methyl]-1,5-diazacyclooctane (**L**), {[Cu₂(**L**)₂(μ-Cl)₂](ClO₄)₂]_∞ (**I**), has been constructed from the self-assembling reaction of Cu^{II} perchlorate and **L** in

water; and the X-ray crystallographic analysis of the complex showed that it has a zigzag alternating-chain structure consisting of two distinct coordination geometries.

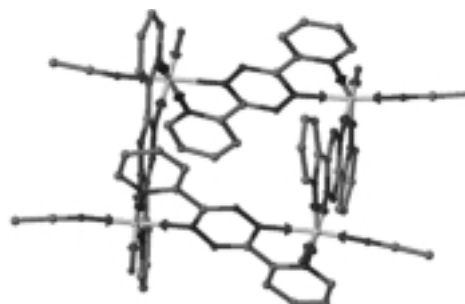
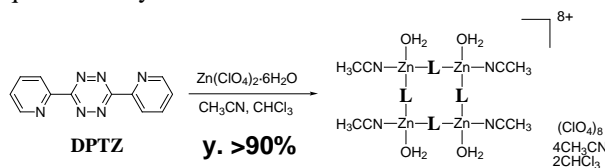
VII-C-5 Spontaneously Resolved Chiral Molecular Box: A Cyclic Tetranuclear Zn(II) Complex with DPTZ (DPTZ = 3,6-Di-2-Pyridyl-1,2,4,5-Tetrazine)

BU, Xian-He¹; MORISHITA, Hiromasa²; TANAKA, Kentaro; BIRADHA, Kumar; SHIONOYA, Mitsuhiro
(¹Nankai Univ.; ²GUAS)

[J. Am. Chem. Soc. submitted]

Interest in coordination architectures constructed by metal ions and bridging ligands has been driven by the expectation of developing new materials with unique electronic, magnetic, and optical properties, or catalytic activities. Their structure and functions have a close relationship with the geometry and chemical properties of the metal ions and bridging ligands used in the architectures. Our recent studies make clear that 3,6-di-2-pyridyl-1,2,4,5-tetrazine (DPTZ) is a promising ligand which can be used in the construction of highly organized supramolecular structures.

We report herein a novel tetranuclear Zn(II) molecular square complex that exhibits a chiral structure in the crystal state. The reaction of Zn(ClO₄)₂·6H₂O with DPTZ in a 1:1 ratio in a mixed solvent of CHCl₃ and CH₃CN at room temperature produced a tetranuclear zinc(II) complex as orange prisms in ca. 90% yield. Its X-ray crystal structure is shown in Figure 1. This compound crystallizes in the chiral space group C222₁. In contrast, a similar reaction of DPTZ with Cd(II) in a 1:1 ratio afforded a linear complex of Cd(II) with 1D chain structure almost quantitatively.



all Δ or all Λ

Figure 1. A chiral molecular box Zn(II) complex.

VII-D Research on the Relationship between Structure of Vanadyl Complex and Insulin-Mimetic Activity

Insulin-dependent diabetes mellitus (IDDM) shows hyperglycemia owing to deficiency of insulin, causing many serious secondary complications. To prevent the complications, IDDM is controlled by daily injections of insulin. Therefore, we have developed orally active insulin-mimetic vanadyl complexes.

VII-D-1 Syntheses, Structure, and Insulin-like Activities of Oxovanadium (IV) Complexes with Tetra- and Penta-Dentate Histidine Derivatives

(PASP), VO(PA) and VO(MPA) complexes have been found to have good insulin-mimetic activities.

KAWABE, Kenji¹; SUEKUNI, Tomonari¹; INADA, Takanori¹; YAMATO, Kazuhiro¹; TADOKORO, Makoto¹; KOJIMA, Yoshitane¹; FUJISAWA, Yae²; SAKURAI, Hiromu³

(¹Osaka City Univ.; ²Kyoto Pharm. Univ.; ³IMS and Kyoto Pharm. Univ.)

[*Chem. Lett.* 1155 (1998)]

[VO(^{pm}H)(ClO₄)], [VO(Me₄)], and [VO(^{pm}H)₂]- (ClO₄) complexes were prepared and their X-ray structures were analyzed. Among them, *in vitro* insulin-mimetic activity of [VO(^{pm}H)(ClO₄)] was found to be higher than that of vanadyl sulfate as a positive control.

VII-D-2 Insulin-Mimetic Vanadyl-Dithiocarbamate Complexes

SAKURAI, Hiromu¹; WATANABE, Hiromi²; TAMURA, Hideyuki²; YASUI, Hiroyuki²; MATSUSHITA, Rokuji³; TAKADA, Jitsuya³

(¹IMS and Kyoto Pharm. Univ.; ²Kyoto Pharm. Univ.; ³Res. Reactor Inst., Kyoto Univ.)

[*Inorg. Chim. Acta* **283**, 175 (1998)]

Five vanadyl-dithiocarbamate complexes with VO-(S₄) coordination mode such as VO-DMD, VO-DED, VO-PYD, VO-MGD and VO-SAD were prepared and their *in vitro* and *in vivo* insulin-like activities were examined. VO-PYD complex was concluded to be a potent agent on daily oral administration to treat insulin-dependent diabetes in experimental animals.

VII-D-3 A New Insulin-mimetic Vanadyl Complex, (N-Pyridylmethylaspartate) Oxovanadium (IV) with VO(N₂O₂) Coordination Mode, and Evaluation of its Effect on Uptake of D-Glucose by Ehrlich Ascites Tumor Cells

TAWA, Riichi¹; UCHIDA, Keiko¹; TANIYAMA, Junko¹; FUJISAWA, Yae¹; FUJIMOTO, Seiki¹; NAGAOKA, Takashi²; KANAMORI, Kan²; SAKURAI, Hiromu³

(¹Kyoto Pharm. Univ.; ²Toyama Univ.; ³IMS and Kyoto Pharm. Univ.)

[*J. Pharm. Pharmacol.* **51**, 119 (1999)]

A new *in vitro* assay method using Ehrlich ascites tumor cells for the insulin-mimetic activity of a compound was proposed. By using this method, VO-

VII-E Syntheses of Transition Metal-Sulfur Clusters and Development of Their Catalysis

This project focuses on the development of the new, reliable synthetic routes towards the transition metal-sulfur clusters with the tailored core structures in high yield, and also on the determination of the detailed structures of the novel clusters prepared in this study by the X-ray crystallography. Activation of the small molecules will be attempted by the use of polynuclear homo- or heterometallic site in these clusters to exploit the new catalytic reactions that are inaccessible by the mononuclear complex catalyst.

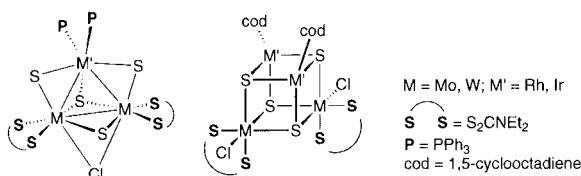
VII-E-1 Syntheses and Structures of Mixed-Metal Sulfido Clusters Containing Incomplete Cubane-Type $M_2M'S_4$ and Cubane-Type $M_2M'_2S_4$ Cores ($M = Mo, W$; $M' = Rh, Ir$)

IKADA, Tomotake¹; KUWATA, Shigeki¹; MIZOBE, Yasushi²; HIDAI, Masanobu¹

(¹Univ. Tokyo; ²Univ. Tokyo and IMS)

[*Inorg. Chem.* **38**, 64 (1999)]

The reactions of sulfido-bridged dimolybdenum and ditungsten complexes $[M_2S_2(\mu-S)_2(S_2CNEt_2)_2]$ ($M = Mo, W$) with an equimolar amount of $[M'Cl(PPh_3)_3]$ ($M' = Rh, Ir$) gave a series of mixed-metal incomplete cubane-type sulfido clusters $[M'(PPh_3)_2(\mu_3-S)(\mu_2-S)_3\{M(S_2CNEt_2)_2\}_2(\mu_2-Cl)]$. On the other hand, mixed-metal cubane-type sulfido clusters $[M'(cod)_2\{MCl(S_2CNEt_2)_2\}_2(\mu_3-S)_4]$ ($M' = Rh, Ir$; $cod = 1,5$ -cyclooctadiene) were obtained by the reactions of **1** with an equimolar amount of $[M'Cl(cod)_2]$. Detailed structures of $[Ir(PPh_3)_2(\mu_3-S)(\mu_2-S)_3\{W(S_2CNEt_2)_2\}_2(\mu_2-Cl)]$ and $[Rh(cod)_2\{MoCl(S_2CNEt_2)_2\}_2(\mu_3-S)_4]$ have been determined by X-ray crystallography.



VII-E-2 Synthesis and Reactivities of Ir_2Ru Heterobimetallic Sulfido Clusters Derived from a Hydrogensulfido-Bridged Diiridium Complex

KOCHI, Takuya¹; NOMURA, Yasuo¹; TANG, Zhen¹; ISHII, Youichi¹; MIZOBE, Yasushi²; HIDAI, Masanobu¹

(¹Univ. Tokyo; ²Univ. Tokyo and IMS)

[*J. Chem. Soc., Dalton Trans.* 2575 (1999)]

The hydrogensulfido-bridged diiridium complex $[ClCp^*Ir(\mu-SH)_2IrCp^*Cl]$ reacted with $[RuH_2(PPh_3)_4]$ to give a mixed-metal trinuclear cluster $[(Cp^*Ir)_2(\mu_3-S)_2RuCl_2(PPh_3)]$ **1**, which was further converted into the cationic diphosphine derivatives $[(Cp^*Ir)_2(\mu_3-S)_2RuCl(L)]Cl$ ($L = dppe = Ph_2PCH_2CH_2PPh_2$ **2** or $depe = Et_2PCH_2CH_2PET_2$ **3**). The reaction of **2** with Me_2CuLi followed by anion metathesis with KPF_6 afforded the methyl cluster $[(Cp^*Ir)_2(\mu_3-S)_2RuMe(dppe)][PF_6]$, while treatment of **2** with $CHCl_2Li$ led to formation of

$[(Cp^*Ir)\{\eta^4-C_5Me_5CHCl_2\}Ir](\mu_3-S)_2RuCl(dppe)]$, in which one of the Cp^* ligands was alkylated by $CHCl_2Li$ to form an η^4 -diene. Clusters **2** and **3** were also transformed into the dihydrido clusters $[(Cp^*Ir)_2(\mu_3-S)_2(\mu-H)_2Ru(L)]$ ($L = dppe$ or $depe$) by the reaction with $NaBH_4$. On the other hand, **1** was converted into the carbonyl cluster $[(Cp^*Ir)_2(\mu_3-S)_2RuCl(CO)(PPh_3)]Cl$, the isocyanide clusters $[(Cp^*Ir)_2(\mu_3-S)_2RuCl(CNXy)(PPh_3)]Cl$ ($Xy = 2,6-C_6H_3Me_2$) and $[(Cp^*Ir)_2(\mu_3-S)_2RuCl(CNXy)_2(PPh_3)][BPh_4]_2$ and the co-ordinatively unsaturated thiolato clusters $[(Cp^*Ir)_2(\mu_3-S)_2Ru(SAr)_2]$ ($Ar = 2,4,6-C_6H_2Pr^i_3$ **12** or Xy) on treatment with CO, $XyNC$ and $LiSAr$, respectively.

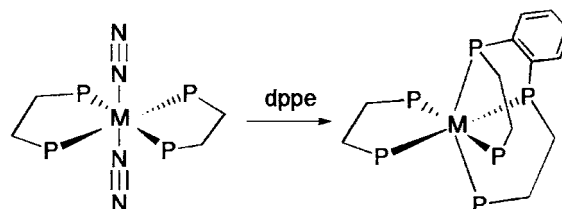
VII-E-3 Formation of Linear Tetradentate Phosphine Ligand $o-C_6H_4(PPhCH_2CH_2PPh_2)_2$ by Coupling of Two Diphosphine Ligands Bound to Low-Valent Mo or W Center. Synthesis and Structure of $[M\{o-C_6H_4(PPhCH_2CH_2PPh_2)_2\}-(Ph_2PCH_2CH_2PPh_2)]$ ($M = Mo, W$)

ARITA, Chirima¹; SEINO, Hidetake¹; MIZOBE, Yasushi²; HIDAI, Masanobu¹

(¹Univ. Tokyo; ²Univ. Tokyo and IMS)

[*Chem. Lett.* 611 (1999)]

A mixture of *trans*- $[M(N_2)_2(dppe)_2]$ ($M = Mo$ or W ; $dppe = Ph_2PCH_2CH_2PPh_2$) and $dppe$ was heated to reflux in benzene or toluene to give the $M(0)$ complex $[M(P_4)(dppe)]$, which contains the novel tetradentate phosphine $o-C_6H_4(PPhCH_2CH_2PPh_2)_2$ (P_4) arising from the coupling of two $dppe$ ligands. The reaction of $[Mo-(P_4)(dppe)]$ with CO afforded the carbonyl complex $[Mo(CO)_2(P_4)]$.



VII-F Activation of Carbon Dioxide and Creation of Reactive Hydroxy- and Oxo-metal Complexes through Activation of Water Molecules on Metals

An electrophilic attack of CO₂ to coordinatively unsaturated low valent metal complexes produces M-η¹-CO₂ complexes, which can be smoothly converted to M-CO ones. Metal complexes with a chelate ring that smoothly opens and closes depending on reaction conditions must be suitable for generation of M-η¹-CO₂ complexes by considering thermal lability of coordinatively unsaturated low valent metal complexes. A major problem of multi-electron reduction of CO₂ in homogeneous reactions is predominant cleavages of metal-CO bonds derived from CO₂ under reductive conditions, because accumulation of too many electrons in the central metals causes reductive cleavage of M-CO bonds. Electro- and photochemical reduction of CO₂ by using ligand localized redox reactions, therefore, may afford a new methodology for multi-electron reduction of CO₂.

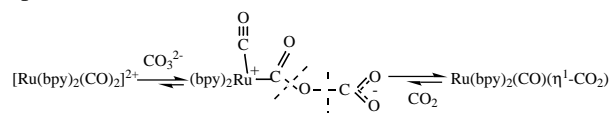
The proton gradient (Δ*p*) between inside and outside of a cell is depicted as the sum of electric activity (Δ*ψ*) and chemical activity (Δ*pH*) components. Δ*p* = Δ*ψ* - ZΔ*pH* (Z = 2.303 *RT/F*) Proton gradient is equivalent to the neutralization energy because the neutralization reaction takes place if the separating membrane is removed. Biological system creates various valuable energies from the neutralization. Although acids or bases generated in industrial process are just wasted as thermal energy, neutralization energy is originated from the binding energy of acid and base, which is able to be converted directly to chemical energy. Along this line, we tried to convert the neutral energy to electronic energy by using ruthenium-aqua complexes.

VII-F-1 Stabilization of [Ru(bpy)₂(CO)(η¹-CO₂)] and Unprecedented Reversible Oxide Transfer Reactions from CO₃²⁻ to [Ru(bpy)₂(CO)₂]²⁺ and from [Ru(bpy)₂(CO)(η¹-CO₂)] to CO₂

NAKAJIMA, Hiroshi; TSUGE, Kiyoshi; TOYOHARA, Kiyotsuna; TANAKA, Koji

[*J. Organomet. Chem.* **561**, 61 (1998)]

Metal complexes with an η¹-CO₂ group, which is formed by overlap of the filled *dz*² orbital of *d*⁸ metals and the empty CO₂ π* orbital, are generally extremely labile to air, moisture and temperature. Unusual thermal stability of [Ru(bpy)₂(CO)(η¹-CO₂)] (**1**) as a metal-η¹-CO₂ complex was examined both in the solid state and in solutions. LiCF₃SO₃ assists solubilization of **1** in CH₃CN due to the interaction between Li⁺ and the η¹-CO₂ group. Electron flow from Ru to the CO₂ ligand induced by Li⁺ also largely stabilizes the Ru-CO₂ bond. Oxide transfer from [Crown·K]₂CO₃ to [Ru(bpy)₂(CO)₂](PF₆)₂ smoothly took place in dry CH₃CN to afford **1** through the 1 : 1 adduct with the RuC(O)-OCO₂ moiety. On the other hand, Li⁺ caused the oxide transfer from **1** to CO₂ giving [Ru(bpy)₂(CO)₂]²⁺ and CO₃²⁻ due to insolubility of the Li₂CO₃ in organic solvents. Unprecedented reversible oxide transfer from **1** to CO₂ and from CO₃²⁻ to [Ru(bpy)₂(CO)₂]²⁺ proceeds via their 1 : 1 adduct, which was confirmed by the NMR spectra.

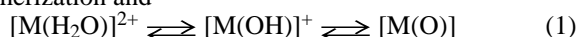


VII-F-2 First Artificial Energy Conversion from Proton Gradient to Electricity

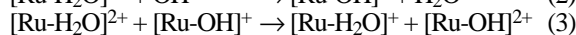
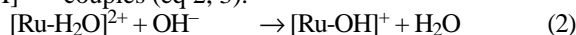
TSUGE, Kiyoshi; TANAKA, Koji

[*Chem. Lett.* 1069 (1998)]

Metal-aqua, -hydroxy and -oxo complexes are expected to exist as equilibrium mixtures depending on proton concentrations in solutions (eq 1) when dimerization and



oligomerization of these complexes can be effectively depressed. Electron withdrawing ligands will decrease nucleophilicity of the terminal hydroxy and oxo groups, which would serve to depress the formation of μ-OH and μ-O bridged oligomers. We, therefore, introduce redox active quinone ligands to stabilize the aqua, hydroxy and oxo complexes to accommodate extra electrons generated deprotonation of the aqua and hydroxy ligands. As a result, the redox potentials of the complexes reversibly change depending on pH in solutions. The cyclic voltammogram (CV) of [Ru(trpy)-(3,5-di-*tert*-butylquinone)(H₂O)]²⁺ ([Ru-H₂O]²⁺) in acetone showed two reversible redox couples at *E*_{1/2} = -0.47 V and *E*_{1/2} = 0.38 V (*E*_{1/2} = (*E*_{pc} + *E*_{pa})/2) assigned to the [Ru-H₂O]^{0/+} and [Ru-H₂O]^{+2/+} couples, respectively. When 0.7 equiv of OH⁻ was added to the solution, the rest potential of the solution (*V*_{rest}) shifted from 0.60 V to 0.30 V across the *E*_{1/2} of the [Ru-H₂O]^{+2/+} couple, and new redox couples appeared at *E*_{1/2} = -0.80 V and 0.00 V assignable to the [Ru-OH]^{0/+} and [Ru-OH]^{+2/+} couples (eq 2, 3).



Further addition of OH⁻ caused deprotonation of [Ru-OH]²⁺ to produce [Ru-O] (eq 4), which equilibrates with the reactant (eq 5).



The energy conversion was conducted with two compartment cells (I and II) separated by an anion exchange membrane filled with an acetone solution of [Ru-H₂O]²⁺ (7.0 μmol/15 ml in each cell). Upon an addition of 1.6 equivalent of OH⁻ to cell(I), [Ru-H₂O]⁺ and [Ru-OH]⁺ formed and *V*_{rest} shifted from 0.60 V to -0.13 V (eqs 2-5). The connection of two cells induced current flow from the cell(II) to cell(I). At the end of the discharge (12 hr later), *V*_{rest} of two cells were 0.33 ±

0.02 V, and 0.50 C of electricity was obtained. Thus the proton gradient is catalytically converted to electricity by ruthenium aqua complex $[\text{Ru}(\text{trpy})(3,5\text{-di-tert-butylquinone})(\text{H}_2\text{O})]^{2+}$.

VII-F-3 Two-Electron Reduction of $[\{(\text{bpy})_2\text{Ru}(\text{dmmbbpy})\}_3\text{Ru}]^{8+}$ from $(\text{BNA})_2$ via Photo-induced Electron Transfer [dmmbbpy = 2,2'-Bis(*N*-Methylbenzimidazole-2-yl)-4,4'-bipyridine]

ALI, Md. Meser¹; SATO, Hiroyasu¹; TANAKA, Koji; HAGA, Masa-aki; YOSHIMURA, Akio²; OHNO, Takeshi²
(¹Mie Univ.; ²Osaka Univ.)

[*Inorg. Chem.* **37**, 6176 (1998)]

Photoirradiation ($\lambda > 500$ nm) of $[\{(\text{bpy})_2\text{Ru}(\text{dmmbbpy})\}_3\text{Ru}]^{8+}$ (**1**⁸⁺) (dmmbbpy = 2,2'-Bis(*N*-methylbenzimidazole-2-yl)-4,4'-bipyridine and bpy = 2,2'-bipyridine) in the presence of dimeric *N*-benzyl-dihydronicotinamide, $(\text{BNA})_2$ produced stable two-electron reduced species (**1**⁶⁺). Laser flash photolysis and emission spectroscopy were used to understand the reductive reaction pathways. The emission quenching k_q value ($4.1 \times 10^9 \text{ M}^{-1}\text{s}^{-1}$) obtained from Stern-Volmer plot is in excellent agreement with the electron transfer rate constant, k_{et} ($4.7 \times 10^9 \text{ M}^{-1}\text{s}^{-1}$) determined from the decay kinetics of transient **31**⁸⁺ triplet-triplet absorption at 650 nm indicating that photoreduction of **1**⁸⁺ proceeds via photoinduced electron transfer from $(\text{BNA})_2$ to **31**⁸⁺. After bimolecular electron transfer process, **1**⁸⁺ was reduced to **1**⁷⁺ and electron donor $(\text{BNA})_2$ was oxidized. Oxidation of $(\text{BNA})_2$ leads to the formation of highly reactive species, BNA^\bullet which then reduces **1**⁷⁺ to **1**⁶⁺. The quantum yield for the formation of the photo-reduction product was 0.026.

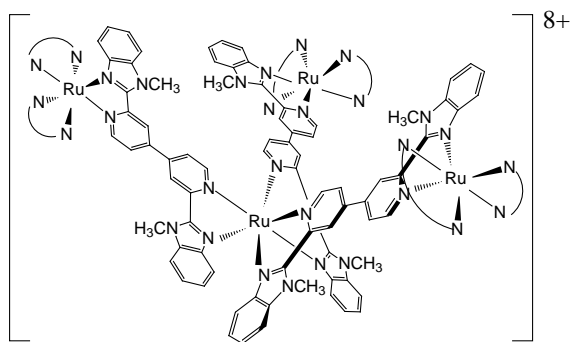


Figure 1. $[\{(\text{bpy})_2\text{Ru}(\text{dmmbbpy})\}_3\text{Ru}]^{8+}$.

VII-F-4 Selective Production of Acetone in Electrochemical Reduction of CO_2 Catalyzed by Ru-naphthyridine Complex

MIZUKAWA, Tetsunori; TSUGE, Kiyoshi; NAKAJIMA, Hiroshi; TANAKA, Koji

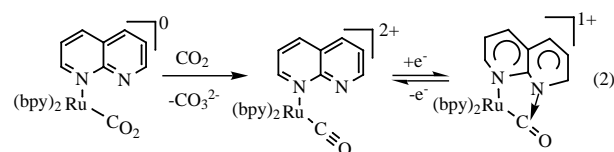
[*Angew. Chem., Int. Ed. Engl.* **111**, 373 (1999)]

Carbon dioxide is smoothly converted to CO on metals by oxide transfer from M-CO_2 to CO_2 , while reductive cleavage of the resultant metal-CO bond (eq

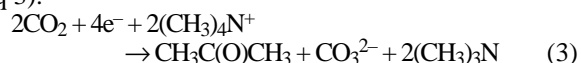
1) is the major problem in utilization of CO_2 as a C1 resource. Acylation of the metal-CO complexes



derived from CO_2 under reductive conditions, therefore, would provide new methodologies for utilization of CO_2 as a starting material in organic synthesis. One and two-electron reductions of $[\text{Ru}(\text{bpy})_2(\text{napy})(\text{CO})](\text{PF}_6)_2$ (napy = 1,8-naphthyridine- κN) take place in napy localized orbitals, which induce nucleophilic attack of the free nitrogen of napy to the carbonyl carbon (eq2). Electron transfer from the reduced form of napy to the CO group in the metallacycle enables reductive activation of the CO group without the



metal-CO bond cleavage and gives rise to electrophilic attack of $(\text{CH}_3)_4\text{N}^+$ to the carbonyl carbon. As a result, $\text{CH}_3\text{C}(\text{O})\text{CH}_3$ and CO_3^{2-} were catalytically produced in the electrochemical reduction of $[\text{Ru}(\text{bpy})(\text{napy-}\kappa\text{N})_2(\text{CO})_2](\text{PF}_6)_2$ in the presence of in CO_2 -saturated DMSO when $(\text{CH}_3)_4\text{NBF}_4$ was used as an electrolyte (eq 3).



VII-F-5 Basicity of $\mu_3\text{-X}$ and $\eta^1\text{-Y}$ Ligands (X, Y = S, Se) of Reduced, Oxidized and Super-Oxidized Forms of $[\text{Fe}_4\text{X}_4(\text{YAd})_4]^{2-}$ (Ad = 1-Adamantane) in Aqueous Solutions

NAKAMOTO, Masami; FUKAISHI, Kenji; TAGATA, Tsuyoshi; KAMBAYASHI, Hide; TANAKA, Koji

[*Bull. Chem. Soc. Jpn.* **72**, 407 (1999)]

Synthetic $4\text{Fe}_4\text{S}$ clusters are subject to hydrolysis under aqueous conditions. A series of $[\text{Fe}_4\text{X}_4(\text{YAd})_4]^{2-}$ (X, Y = S, Se; Ad = 1-adamantane) solubilized in aqueous poly[2-dimethylamino(hexanamide)] (PDAH) solutions were stable due to the embedding effect in hydrophobic environment and inhibition of dissociation of the terminal ligand into the aqueous media. Cyclic voltammetry of the clusters in the solutions showed pH dependent redox potentials of not only $[\text{Fe}_4\text{X}_4]^{+/2+}$ but also $[\text{Fe}_4\text{X}_4]^{2+/3+}$ (X, Y = S and Se) couples, resulting from redox-linked protonation reactions of the three oxidation states of $[\text{Fe}_4\text{X}_4(\text{YAd})_4]^{n-}$ ($n = 1-3$), which enabled to determine the pK of each oxidation state. Computer simulation of the pH dependent redox potentials indicated the basicity of the $\mu_3\text{-X}$ cores (X = S and Se) of $[\text{Fe}_4\text{X}_4(\text{YAd})_4]^{n-}$ ($n = 1, 2, 3$) is stronger than the YAd (Y = S and Se) ligands. In the case of the mono-protonated $[\text{Fe}_4\text{X}_4(\text{YAd})_4]^{3-}(\text{H}^+)$ and $[\text{Fe}_4\text{X}_4(\text{YAd})_4]^{2-}(\text{H}^+)$, the basicity of the $\eta^1\text{-Y}$ ligand of $[\text{Fe}_4\text{X}_4(\text{YAd})_4]^{2-}(\text{H}^+)$ becomes stronger than that of $\mu_3\text{-X}$ cores. On the other hand, the $\mu_3\text{-X}$ of $[\text{Fe}_4\text{X}_4(\text{YAd})_4]^{3-}(\text{H}^+)$ still show strong basicity compared with those of $\eta^1\text{-Y}$ ligands.

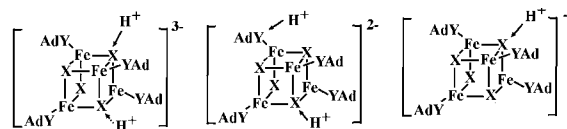


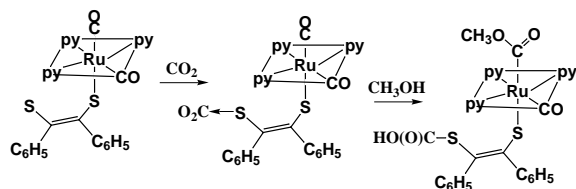
Figure 1. Protonation of $[\text{Fe}_4\text{X}_4(\text{YAd})_4]^{n-}$ ($\text{X}, \text{Y} = \text{S}, \text{Se}$; $n = 2, 1, 0$) in aqueous PDAH solutions: dotted arrow is estimated by computer simulation.

VII-F-6 Double Addition of CO_2 and CH_3OH to Ruthenium Carbonyl Complex with Novel Mono-Dentate Dithiolene

SUGIMOTO, Hideki; TSUGE, Kiyoshi; TANAKA, Koji

[*Chem. Lett.* in press.]

The reaction of $[\text{Ru}(\text{CO})_2\text{Cl}(\text{terpy})]\text{PF}_6$ and Na_2mnt in CH_3OH gave a yellow complex (**1**) with mono-dentate mnt. On the other hand, the reaction between $[\text{Ru}(\text{CO})_2\text{Cl}(\text{terpy})]^+$ and $\text{Cs}_2\text{S}_2\text{C}_2\text{Ph}_2$ in CH_3OH under aerobic conditions gave a complex (**2**) with thio-carboxylic acid and methoxy carbonyl groups rather than the expected $[\text{Ru}(\text{CO})_2(\text{SSC}_2\text{Ph}_2-\kappa^1\text{S})(\text{terpy}-\kappa^3\text{N}, \text{N}', \text{N}'')]^-$. The most characteristic feature of **2** is that the carbonyl and the uncoordinate thiolate of **1** are changed to methoxy carbonyl and thio-carboxylato units, respectively. Although it is not clear that the carboxylato moiety of **2** exists as protonated or deprotonated form by X-ray analysis, the former is deduced from the elemental analysis and the charge balance of **2**. Unprecedented double addition of CO_2 and methanol to thiolate and carbonyl ligands located far from each other is apparently caused by the long-range π - π interaction between basic $\text{Ph}_2\text{C}_2\text{SS}^{2-}$ and acidic carbonyl units through d-orbitals of the ruthenium atom.



VII-G Molecular Self-assembly Through Coordination

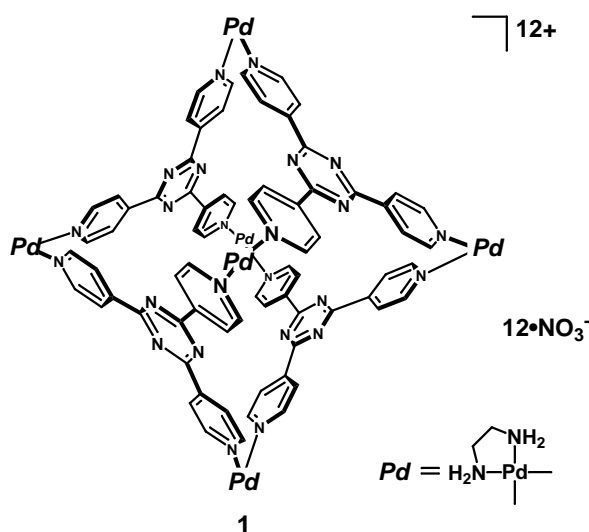
Molecular self-assembly refers to the spontaneous generation of well-defined structures from component molecules under a well-defined set of conditions. Since 1990, we have been studying the self-assembly of discrete structures based on coordination chemistry, where coordinate bonds induce the generation of defined structures. Studies during 1998-1999 are focused on the self-assembly of such three dimensional systems as cages, capsules, tubes, bowls, and 3D-interlocked molecules. Our strategy is characterized by the use of a *cis*-protected Pd(II) unit as a convergent block for molecular assembly, providing 90 degree coordination angle.

VII-G-1 Encapsulation of Large, Neutral Molecules in a Self-Assembled Nanocage Incorporating Six Palladium(II) Ions

KUSUKAWA, Takahiro; FUJITA, Makoto

[*Angew. Chem., Int. Ed. Engl.* **37**, 3142 (1998)]

Cage compound **1** encapsulates as many as four molecules of *o*-carborane (8 Å in diameter). A large guest, 1,3,5-tri-*tert*-butylbenzene, once encapsulated by thermally-activated slippage, cannot escape from the cavity at room temperature since its dimension is slightly larger than that of the cavity window.



VII-G-2 “Ship-in-a-Bottle” Formation of Stable Hydrophobic Dimers of *cis*-Azobenzene and -Stilbene Derivatives in a Self-assembled Coordination Nanocage

KUSUKAWA, Takahiro; FUJITA, Makoto

[*J. Am. Chem. Soc.* **121**, 1397 (1998)]

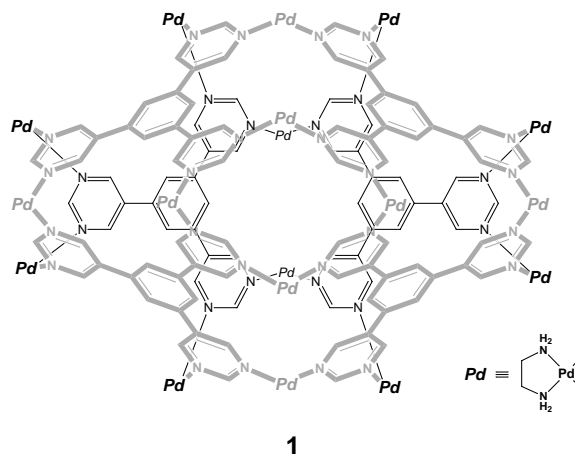
Nano-sized coordination cage **1** (see compound **1** in VII-G-1) has been shown to enclathrate large neutral guest molecules. Here we report the selective enclathration of “C-shaped” molecules such as *cis*-azobenzene and -stilbene derivatives by cage **1**. These guest molecules are enclathrated in the cavity through the “ship-in-a-bottle assembly” into a hydrophobically interacted dimer. The hydrophobic dimers of azobenzene derivatives are considerably stabilized and do not undergo *cis-trans* isomerization.

VII-G-3 A Nonometer-Sized Hexahedral Coordination Capsule Assembled from 24 Components

TAKEDA, Nobuhiro¹; UMEMOTO, Kazuhiko²; YAMAGUCHI, Kentaro³; FUJITA, Makoto
(¹CREST, Jpn. Sci. Tech. Co. (JST); ²GUAS; ³Chiba Univ.)

[*Nature* **398**, 794 (1999)]

Molecular capsules consist of closed, hollow frameworks within which encapsulated molecules are isolated from interaction with external molecules. In this environment, otherwise reactive molecules can be stabilized. Although some molecular capsules have been prepared by conventional synthetic chemistry, recent progress in non-covalent synthesis has allowed the creation of capsules held together by hydrogen bonds. Here we report the use of transition-metal based coordination chemistry to assemble a stable, nanometre-scale capsule **1** from 24 small components: 18 metal ions and six triangular ligands. The capsule is roughly hexahedral and comprises six edge-sharing triangles with two metal ions on each edge. This internal space has a volume of 900 Å³ and is fully closed to all but very small molecules.

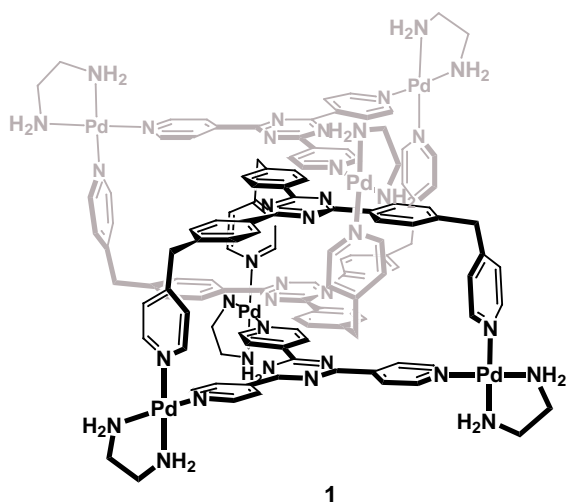


VII-G-4 Spontaneous Assembly of Ten Components into a Two Interlocked, Identical Coordination Cages

FUJITA, Makoto; FUJITA, Norifumi¹; OGURA, Katsuyuki²; YAMAGUCHI, Kentaro²
(¹GUAS; ²Chiba Univ.)

[*Nature* **400**, 52 (1999)]

Supermolecules consisting of interlinked ring-like molecules (catenanes) are an interesting target for chemical synthesis both for their intrinsic interest as non-covalently bound but robust assemblies and because of the perspective they offer on materials chemistry. Catenanes have been prepared by metal-ion templating and self-assembly through other non-covalent interactions. Here we report the synthesis of catenane **1** composed not of two interlocking rings but of two cages. This structure is prepared by metal-mediated self-assembly. The framework of each cage is assembled from five components: two tridentate ligands held together with three metal ions. Because each cage framework can bind an aromatic ring, two cage units will bind one another during their assembly process through the formation of a quadruple aromatic stack, giving rise to the ten-component interlocked supermolecule.

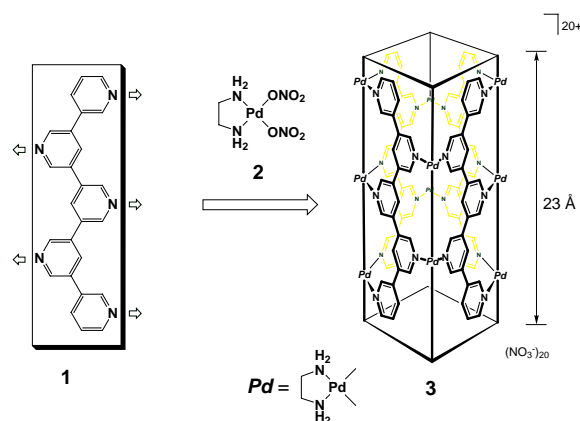


VII-G-5 Quantitative Formation of Coordination Nanotubes Templated by Rod-like Guests

AOYAGI, Masaru¹; BIRADHA, Kumar²; FUJITA, Makoto
(¹GUAS; ²JSPS)

[*J. Am. Chem. Soc.* **121**, 7457 (1999)]

Molecular-based tubular structures have attracted considerable current interest because of their potential abilities for selective inclusion and transportation of ions and molecules and catalysis for specific chemical transformations, by exploiting the interior space of the tubes. In the present study, coordination nanotubes **3** are constructed by linking oligo(3,5-pyridine)s **1** with a cis-protected Pd(II) building block, (en)Pd(NO₃)₂ (**2**, en = ethylenediamine). This transformation was in fact accomplished with the remarkable template effect of biphenyl derivatives. Thus, the reaction of **1** and **2** first resulted in the formation of uncharacterizable products. However, the addition of sodium 4,4'-biphenylene-dicarboxylate to the solution induced the smooth assembly of nanotubes **3** wherein four oligo(3,5-pyridine) molecules were held together with six to ten Pd(II) units. A nanotube structure templated by a guest was confirmed by an X-ray crystallographic analysis.

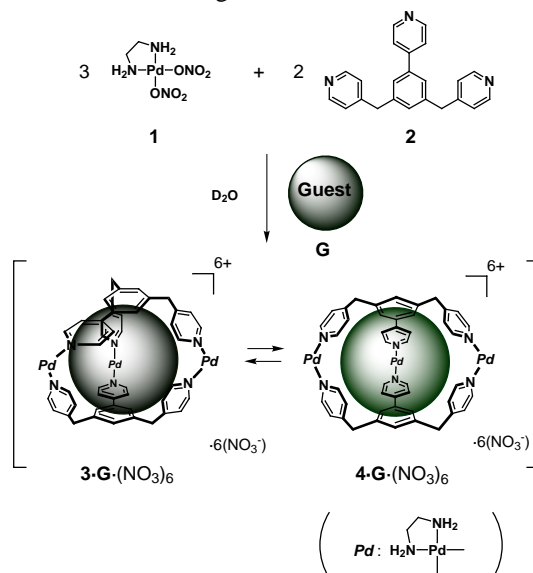


VII-G-6 Guest-Selected Formation of Pd(II)-Linked Cages from a Prototypical Dynamic Library

HIRAOKA, Shuichi¹; FUJITA, Makoto
(¹CREST, Jpn. Sci. Tech. Co. (JST))

[*J. Am. Chem. Soc.* in press]

Biological receptors modulate the shape and size of their recognition sites to bind substrate molecules, generating numerous receptor structures from which the most suitable one is selected (or induced-fit) by their substrates. Modeling such a system is particularly important to develop a new receptor design wherein artificial receptors are constructed through a selection process by their own guests. Although previous examples are dealing with the induced-fit control of receptor conformations, there are only several reports on the control of receptor linkages. Here we report the guest-selected formation of its optimal cage-like receptor from an equilibrium mixture of receptors. In the following scheme, Pd(II)-linked cages, **3** and **4**, and some oligomeric compounds, accessible from the same components **1** and **2**, are in equilibrium. From this thermodynamic mixture, each cage structure is selected upon the addition of appropriate guest molecules. This phenomenon is a prototype for "dynamic receptor library," which represents one of important goals in the field of molecular recognition.



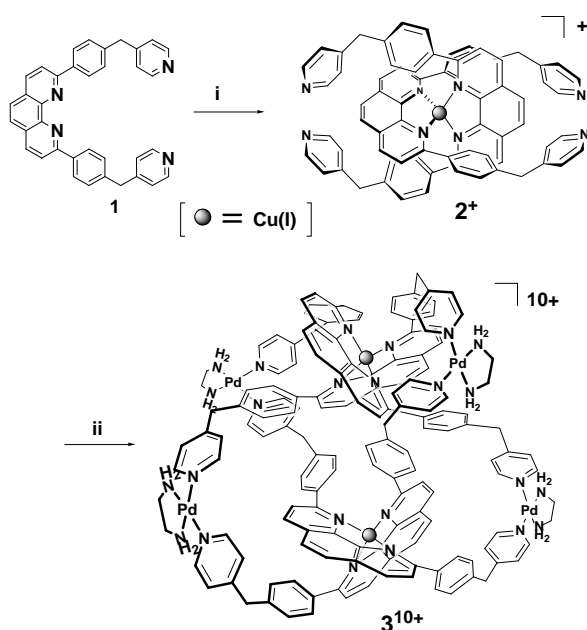
VII-G-7 Quantitative and Spontaneous Formation of a Doubly Interlocking [2]Catenane using Copper(I) and Palladium(II) as Templating and Assembling Centers

IBUKURO, Fumiaki¹; FUJITA, Makoto; YAMAGUCHI, Kentaro²; SAUVAGE, Jean-Pierre³
(¹GUAS; ²Chiba Univ.; ³Univ. Louis Pasteur)

[*J. Am. Chem. Soc.* in press]

A new strategy based on pure coordination chemistry has been used to construct a 4-crossing [2]catenane. The ligand **1** contains a central 1,10-phenanthroline site attached to two pendent/4-pyridyl groups. The central site is used to complex a copper(I) center whereas the lateral pyridine groups are coordinated to palladium(II).

The stepwise complexation procedure is virtually quantitative. It can be carried out both ways (copper(I) followed by palladium(II) or reverse). The final complex **3** is a chiral species incorporation 4 ligands, 2 copper(I) and 4 palladium(II) centres. It has been characterized in solution and its structure has been evidenced by ESI-MS.



VII-G-8 Flexible Coordination Networks with Fluorinated Backbones. Remarkable Ability for Made-to-Order Enclathration of Organic Molecules

KASAI, Kayoko¹; AOYAGI, Masaru²; FUJITA, Makoto
(¹Miyagi Univ. Education; ²GUAS)

We have designed and prepared flexible ligands containing fluorinated aromatic rings: PyCH₂-R_F-CH₂Py; Py = 4-pyridyl, R_F = -C₆F₄-, -C₆F₄-C₆F₄-, and -C₁₀F₆-. Because of very weak intermolecular forces among fluorinated compounds, networks from these ligands and metal ions are not apt to be constricted or interpenetrated, but prefer to interact with guest molecules to form clathrate compounds. In these clathrate complexes,

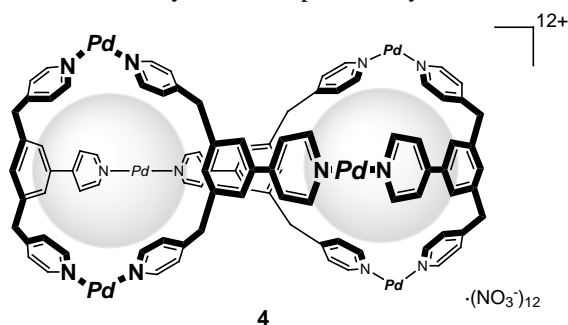
we have found that the network topologies are induced-fit by guest molecules owing to the flexibility of the ligand frameworks giving rise to 1D, 2D, and 3D structures with large cavities. Consequently, we have achieved “made-to-order” enclathration of a variety of organic guests with the flexible, fluorinated coordination networks.

VII-G-9 Kinetic and Thermodynamic Aspects in the Substrate-Induced Assembly of Optimal Receptors from a Dynamic Library

HIRAOKA, Shuichi¹; KUBOTA, Yasuo²; BIRADHA, Kumar³; FUJITA, Makoto
(¹CREST, Jpn. Sci. Tech. Co. (JST); ²Nagoya Univ.; ³JSPS)

Pyridine functionalized C_{2v} ligand **1** (see compound **2** in VII-G-6) has been recently shown to provide a mixture of more than two cage-like receptors upon complexation with (en)Pd²⁺ coordination block. The mixture thus obtained can be termed as “dynamic receptor library” because appropriate substrates induce the assembly of their optimal receptors from the mixture. Further studies on this thermodynamic phenomenon have elucidated some important structural and mechanistic aspects.

We report here that, in addition to M₃L₂ type receptors **2** and **3** (see compounds **3** and **4** in VII-G-6, respectively), dimeric M₆L₄ cage **4** is involved in the equilibrium mixture. Interestingly, **2** and **3** interconvert via the dimeric M₆L₄ form as revealed by a kinetic study. Furthermore, symmetrical M₃L₂ cage **2** and M₆L₄ dimer **4** are isolated and characterized by X-ray crystallography. These results emphasize how easily a variety of host frameworks with different connectivities and stoichiometries are generated from only one ligand component and how precisely the optimal receptor frameworks are selected from the equilibrated cage molecules or a “dynamic receptor library.”



VII-G-10 Dynamic Behavior of Rod-like Guest Accommodated in Coordination Nanotubes

AOYAGI, Masaru¹; FUJITA, Makoto
(¹GUAS)

Oligo(3,5-pyridine) ligands **1** self-assemble into coordination nanotubes **2** with the aid of remarkable template effect of rod-like guest (For the structures of **1** and **2**, see those of **1** and **3** in VII-G-5, respectively). Studies on the dynamic behavior of guest molecules accommodated in the tubes are particularly interesting

because guests are expected to move only in a one-dimensional way within a tightly fitted tubular space and such a restricted guest motion would lead to novel functions of tubular molecules: *e.g.*, shape-selective molecular transportation and (catalytic) chemical transformation. Here, we report NMR studies on the dynamic motion of the guests accommodated in the coordination nanotube. Guest molecules are found to shuttle in the tube without turning their head and tail at room temperature, but intermolecularly exchange at elevated temperature.

VII-G-11 Wacker Oxidation in an Aqueous Phase Through the Reversed Phase-Transfer Catalysis of a Self-Assembled Nanocage

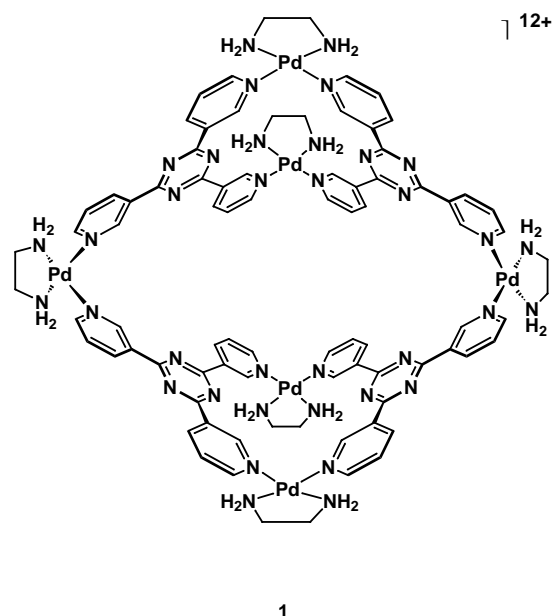
ITO, Hirokazu¹; KUSUKAWA, Takahiro; FUJITA, Makoto
(¹GUAS)

Chemical transformation in aqueous media is a current trend in synthetic chemistry in view of developing clean technology. One of the best approaches to water-based reactions is to develop reversed phase-transfer catalysts which bring organic substrates into aqueous phase, let them react with aqueous reagents, and take out products from the aqueous phase. This paper reports that the coordination nanocage **1** (see compound **1** in VII-G-1) shows the reversed phase-transfer catalysis toward Wacker oxidation of olefins which is a typical Pd(II)-promoted catalytic reaction. Thus, styrene is effectively and catalytically oxidized to acetophenone (86% yield) by treating it with aqueous solution of (en)Pd(NO₃)₂ (10 mol%) and cage **1** (10 mol%).

VII-G-12 Hydrophobic Assembling of a Coordination Nanobowl into a Dimeric Capsule Which can Accommodate upto Six Large Organic Molecules

YU, Shu-Yan¹; KUSUKAWA, Takahiro; KUMAR, Biradha¹; FUJITA, Makoto
(¹JSPS)

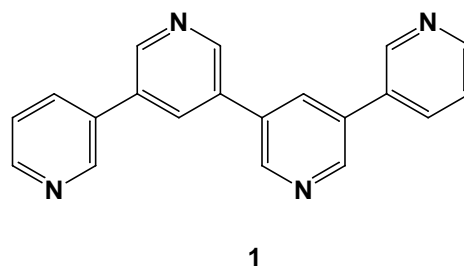
Dimerization of bowl-shaped molecules is an attractive approach to molecular capsules which are capable of accommodating organic molecules within their interior space. Both covalent and non-covalent dimers of bowl-shaped molecules have been studied during the last decade. Recently reported coordination nanobowl **1** provides a unique component for a dimeric capsule because the nature of the bowl is amphiphilic: *i.e.*, the open cavity of **1** is surrounded by 16 aromatic rings and thus hydrophobic, whereas the outside surface of the bowl is hydrophilic due to the exposure of six charged Pd(II) centers. Therefore, bowl **1** is expected to assemble in aqueous media into a dimeric capsule creating a large hydrophobic pocket inside the framework. Reported here is that such a dimeric structure assembles in a solid state accommodating as many as six neutral organic molecules. Spectroscopic studies elucidated that the same structure also exists even in solution.



VII-G-13 Porous Coordination Polytubes

BIRADHA, Kumar¹; AOYAGI, Masaru²; FUJITA, Makoto
(¹JSPS; ²GUAS)

Despite great interest in porous coordination polymers assembled from metals and bridging ligands, there remains difficulty in predicting cavities in the polymer frameworks because of the frequently encountered unfavorable interpenetration of the networks. This problem can be solved by designing organic ligands which are unable to give interpenetrated networks. In this regard, use of a panel-like ligand such as **1** is attractive because its coordination assembly is expected to give polytube structures which are not allowed to interpenetrate. In this report we show that, upon treatment with a transition metal (CuI), ligand **1** assembles into polytube structures which accommodate organic guests in the tubular cavities. Interestingly, the polytube structures are templated by the guest employed; *i.e.*, two polytubes possessing different linkage connectivities with the accessible porosity of *ca.* 30–50% have been obtained by using different organic guests.



VII-G-14 X-Ray And NMR Observation of Encapsulated Molecules in a Self-Assembled Coordination Nanocage

KUSUKAWA, Takahiro; FUJITA, Makoto

Nano-sized coordination cage **1** (see compound **1** in VII-G-1) has been shown to enclathrate “C-shaped” molecules such as *cis*-azobenzene and -stilben derivatives. The dimeric assembly of the guests was evidenced for a diaryl diketone guest **2**, by X-ray crystallography (Figure 1), which showed the formation of M and P helical conformations for the guest molecule. Due to the formation of a desymmetrized M/P meso dimeric structure, the ¹H-NMR showed 12 signals for the pyridine protons of the triazine ligand. This observation indicated that the conformation of guest molecule **2** was fixed as a meso-dimeric form even in a solution.

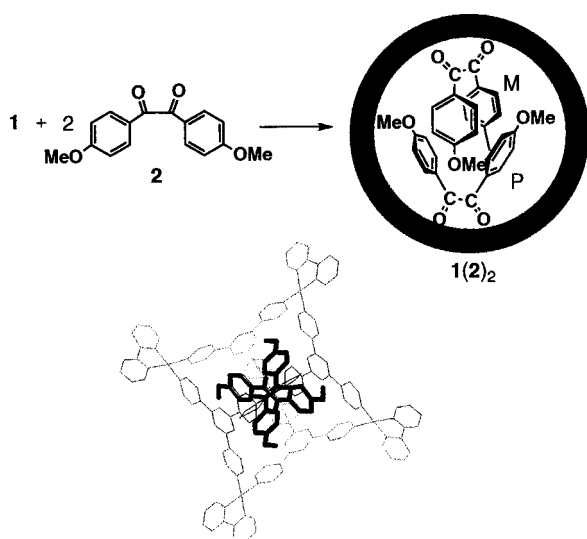


Figure 1. The crystal structure of **1(2)₂**.

VII-H Synthesis and Reactivity of Complexes Containing Peculiar Bonds between Transition Elements and Main Group Elements

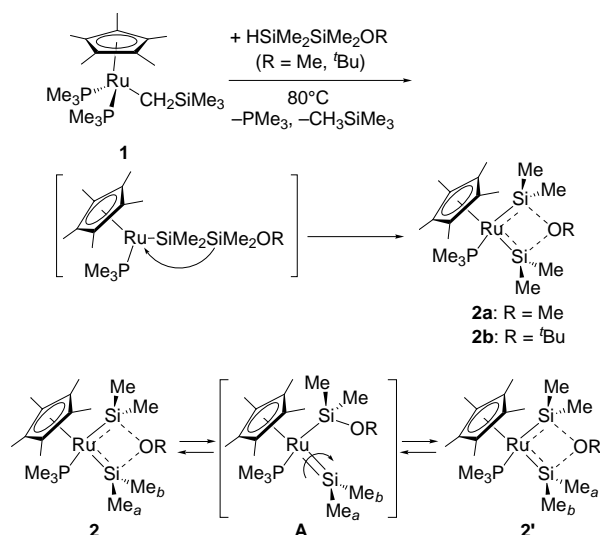
The bonds between transition elements and main group elements are attracting increasing attention in recent years. This is attributable not only to the great variety of the combination of elements but also to the peculiarity of their physical and chemical properties. We are currently focusing on transition metal complexes containing novel and peculiar bonds between transition elements and some main group elements, particularly single and multiple bonds to silyl, silene, and sulfido ligands. We are examining the synthesis, structures, fluxional behaviors, and reactivity of these complexes to gain a better understanding on the characters of these bonds.

VII-H-1 Fluxional Behavior of Alkoxy-Bridged Bis(silylene)ruthenium Complexes $\text{Cp}^*(\text{Me}_3\text{P})\text{-Ru}\{\text{SiMe}_2\cdots\text{O}(\text{R})\cdots\text{SiMe}_2\}$ ($\text{R} = \text{Me}, \text{'Bu}$) Caused by Rotation of the Silylene Ligands

WADA, Hiroaki¹; TOBITA, Hiromi^{1,2}; OGINO, Hiroshi¹
(¹Tohoku Univ.; ²IMS)

[Chem. Lett. 993 (1998)]

Heating a hexane solution of $\text{Cp}^*(\text{Me}_3\text{P})_2\text{RuCH}_2\text{-SiMe}_3$ (**1**; $\text{Cp}^* = \eta^5\text{-C}_5\text{Me}_5$) and $\text{HSiMe}_2\text{SiMe}_2\text{OR}$ ($\text{R} = \text{Me}, \text{'Bu}$) at 80 °C overnight in a sealed tube gave alkoxy-bridged bis(silylene)ruthenium complexes $\text{Cp}^*(\text{Me}_3\text{P})\text{Ru}\{\text{SiMe}_2\cdots\text{O}(\text{R})\cdots\text{SiMe}_2\}$ (**2a**: $\text{R} = \text{Me}$; **2b**: $\text{R} = \text{'Bu}$) in 77 and 39% yields, respectively. The exchange of Si-Me groups in **2a** and **2b** through silylene ligand rotation on the intermediate **A** was observed by variable temperature ¹H NMR spectroscopy. Such a fluxionality was not observed in $\text{CpLRu}\{\text{SiMe}_2\cdots\text{O}(\text{Me})\cdots\text{SiMe}_2\}$ ($\text{L} = \text{PPh}_3, \text{CO}$) nor in the iron analogues. Thus, this fluxionality is considered to be due to the weakened $\text{Si}\cdots\text{O}$ partial bonds caused by the strong electron-releasing effect of Cp^* and PMe_3 ligands.

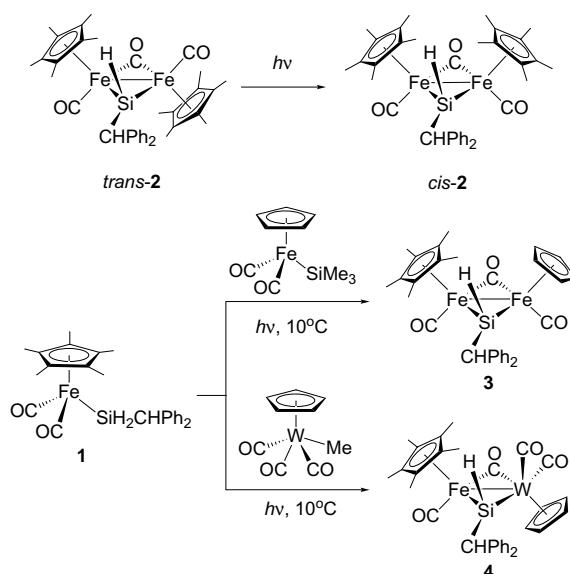


VII-H-2 Preparation of Silanediyl-Bridged Fe-Fe and Fe-W Dinuclear Complexes. X-Ray Structures of $[\text{Cp}^*\text{Fe}(\text{CO})(\mu\text{-CO})(\mu\text{-Si}(\text{H})\text{CHPh}_2)(\text{CO})_n\text{MCp}]$ ($\text{Cp}^* = \text{C}_5\text{Me}_5$, $\text{Cp} = \text{C}_5\text{H}_5$, $\text{M} = \text{Fe}, n = 1$; $\text{M} = \text{W}, n = 2$)

LUH, Lung-Shiang¹; WEN, Yuh-Sheng¹; TOBITA, Hiromi^{2,3}; OGINO, Hiroshi³
(¹Academia Sinica, Taipei; ²IMS; ³Tohoku Univ.)

[Bull. Chem. Soc. Jpn. 71, 2865 (1998)]

Photolysis of a 2:1 mixture of $[\text{Cp}^*\text{Fe}(\text{CO})_2\text{Me}]$ and $\text{Ph}_2\text{CHSiH}_3$ produces the mononuclear silyl complex $[\text{Cp}^*\text{Fe}(\text{CO})_2\{\text{Si}(\text{H})_2\text{CHPh}_2\}]$ (**1**) as a main product in 41% yield together with two silanediyl-bridged diiron complexes, *cis*- and *trans*- $[\text{Cp}^*_2(\text{CO})_2\text{Fe}_2(\mu\text{-CO})\{\mu\text{-Si}(\text{H})\text{CHPh}_2\}]$ (**2**), and $[\text{Cp}^*\text{Fe}(\text{CO})_2]_2$. The *trans*-**2** complex isomerizes to *cis*-**2** photochemically, but no *cis*-*trans* isomerization occurs thermally below 100 °C. Photolysis of $[\text{CpFe}(\text{CO})_2\text{SiMe}_3]$ or $[\text{CpW}(\text{CO})_3\text{Me}]$ in the presence of **1** produces novel unsymmetrical silanediyl-bridged complexes $[\text{Cp}^*\text{Fe}(\text{CO})(\mu\text{-CO})\{\mu\text{-Si}(\text{H})\text{CHPh}_2\}(\text{CO})_n\text{MCp}]$ (**3**: $\text{M} = \text{Fe}, n = 1$; **4**: $\text{M} = \text{W}, n = 2$) in moderate yields. Complexes **3** and **4** have been characterized by X-ray diffraction analysis. To the best of our knowledge, complex **4** is the first example of silanediyl-bridged Fe-W complex. The Cp and Cp^* rings are mutually *cis* with the dihedral angle of 78.7(2)° in complex **3** but they are *trans* with the dihedral angle of 13.1(6)° in complex **4**.

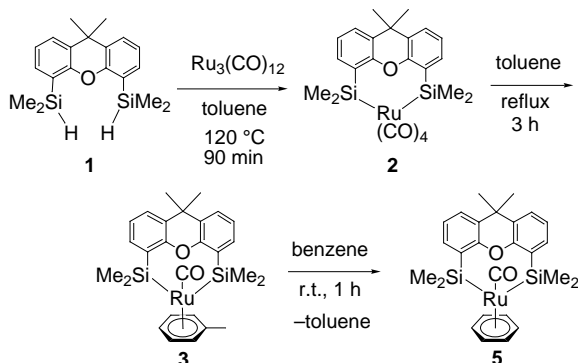


VII-H-3 Extremely Facile Arene Exchange on a Ruthenium(II) Complex Having a Novel Bis-(silyl) Chelate Ligand (9,9-Dimethylxanthene-4,5-diyl)bis(dimethylsilyl) (Xantsil)

TOBITA, Hiromi^{1,2}; HASEGAWA, Kenji²; MINGLANA, Jim Josephus Gabrillo²; LUH, Lung-Shiang³; OKAZAKI, Masaaki²; OGINO, Hiroshi²
(¹IMS; ²Tohoku Univ.; ³Academia Sinica, Taipei)

[*Organometallics* **18**, 2058 (1999)]

Heating a solution of 4,5-bis(dimethylsilyl)-9,9-dimethylxanthene (xantsilH₂) (**1**) and 0.4 molar equivalent of Ru₃(CO)₁₂ in toluene at 120 °C for 90 min afforded a ruthenium complex having a novel bis(silyl) chelate ligand (9,9-dimethylxanthene-4,5-diyl)bis(dimethylsilyl) (xantsil), *cis*-Ru(CO)₄(xantsil) (**2**), as a main product. The X-ray crystal structure analysis showed that the Ru-Si bonds in **2** (2.562(2) and 2.564(2) Å) represent the longest known Ru-Si bonds ever reported probably because of the intramolecular steric repulsion. Isolated **2** reacted with toluene on refluxing for 3 h to give *cis*-Ru(CO)(xantsil)(η⁶-C₆H₅CH₃) (**3**) in 95% yield. When **3** was dissolved in benzene, the η⁶-toluene ligand was cleanly substituted by the solvent at room temperature within 1 h to afford *cis*-Ru(CO)(xantsil)(η⁶-C₆H₆) (**5**) quantitatively.



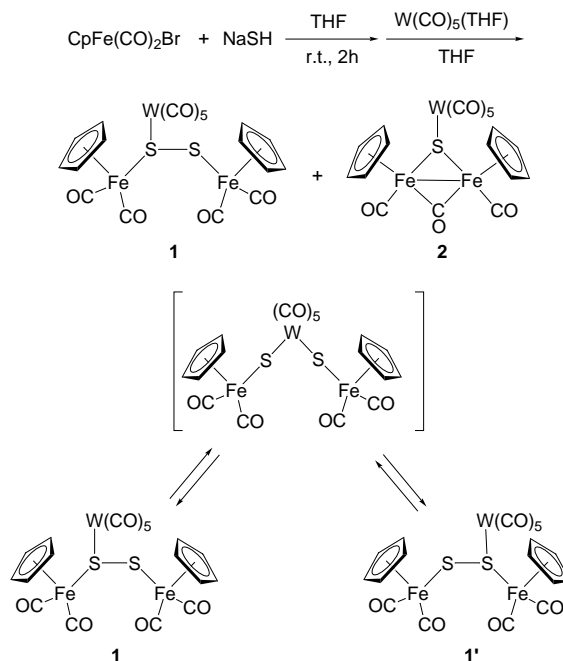
VII-H-4 Synthesis and Structures of Heterometallic Trinuclear Clusters [CpFe(CO)₂]₂(μ₃-S₂)W(CO)₅ and Cp₂Fe₂(CO)₂(μ-CO)(μ₃-S)W(CO)₅ and Kinetic Study of Migration of the W(CO)₅ Moiety in the Disulfido Complex

KUGE, Katsuaki¹; TOBITA, Hiromi^{1,2}; OGINO, Hiroshi¹
(¹Tohoku Univ.; ²IMS)

[*Chem. Commun.* 1061 (1999)]

Reaction of CpFe(CO)₂Br with an excess of NaSH in THF at room temperature resulted in formation of a brown solution. Addition of W(CO)₅(THF) after 2 h to the reaction mixture gave two heterometallic trinuclear clusters [CpFe(CO)₂]₂(μ₃-S₂)W(CO)₅ (**1**) and Cp₂Fe₂(CO)₂(μ-CO)(μ₃-S)W(CO)₅ (**2**) in 30 and 11% yields, respectively. X-ray crystal structures of both **1** and **2** were determined. Complex **1** is the first example of a trinuclear cluster connected by only one disulfido ligand

in an η¹:η¹:η¹ fashion. Variable-temperature ¹H NMR spectroscopy of **1** clearly showed that the W(CO)₅ moiety is migrating between two sulfur atoms faster than the NMR time scale to make the two Cp ligands equivalent. A mechanism involving oxidative addition-reductive elimination of the S-S bond was proposed for this fluxional behavior.



RESEARCH ACTIVITIES VIII

Computer Center

VIII-A Theoretical Studies on Electronic Structure and Dynamics of Electronically Excited States in Polyatomic Molecules

VIII-A-1 Theoretical Study on the Spectroscopy and Dynamics of Electronically Excited States of HCP Molecule

NANBU, Shinkoh; KINOSHITA, Tomoko; GRAY, Stephen K.¹; AOYAGI, Mutsumi
(¹Argonne Natl. Lab.)

Quantum mechanical bound-state calculations for the low-lying electronic excited states of HCP molecule, $1^1A''$, $2^1A'$ and $2^1A''$, were performed using the ab initio global potential energy surfaces. The global potential surfaces were determined by the multi-reference configuration interaction (MRCI) method at DZP basis set level. A large direct-product basis coupled with the standard Lanczos iterative method was employed for computing the rovibrational energy levels. An evenly spaced discrete variable representation (DVR) was used to describe the two radial coordinates of Jacobi coordinates, and the Gauss-Legendre quadrature points was used as an angular DVR for the bending coordinate. The results almost reproduced the low-lying vibrational levels for the $1^1A''$ state measured in the UV absorption spectrum and IR-UV double resonance spectroscopy, and moreover the term energies of the $1^1A''$ and $2^1A''$ states with including the zero point vibrational energy were also in good agreement with the experimental data at aug-cc-pVDZ basis set level. We also performed wave packet calculations on ab initio surfaces to investigate the photodissociation dynamics for $HCP(1^1\Sigma^+) + h\nu \rightarrow H(^2S) + CP(X)$; where $X = 1^2\Sigma^+$ and $2^2\Pi$. It is found that the non-adiabatic transition between $1^1A'$ and $2^1A'$ states in the bent conformations plays an important role in the predissociation process.

VIII-A-2 Development of *Ab Initio* MD Method Based on the Direct Evaluation of CAS-SCF Energy Derivatives

KINOSHITA, Tomoko; NANBU, Shinkoh; AOYAGI, Mutsumi

We have been developing an ab initio molecular dynamics programs to investigate the reaction dynamics of large scale problems, *i.e.*, surface reactions, and biological systems. Since we employed parallelized version of McMurchie-Davidson's algorithm to evaluate both AO integrals and derivatives of AO integrals, the most time consuming step of electronic structure calculations has been carried out in a tractable way. At each time steps of MD calculations, we obtain analytical energy derivatives of complete active space (CAS) wavefunctions. We continue to develop the codes for non adiabatic and spin-orbit coupling matrix elements.

Our direct method can easily extend to apply a number of interesting problems including non adiabatic reactions and spin forbidden processes.

VIII-A-3 Theoretical Study on the Unimolecular Reaction Dynamics of Acetyl Radical $CH_3CO \rightarrow CH_3 + CO$

ITO, Masakatsu; NANBU, Shinkoh; AOYAGI, Mutsumi

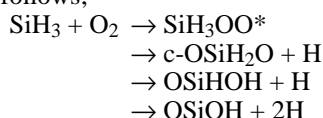
We investigate the dissociation dynamics of acetyl radical with the classical trajectory method using the electronic model hamiltonian based on our ab initio calculations. At each time step in our classical trajectory calculations, the electronic hamiltonian is diagonalized to obtain the instantaneous adiabatic states and then the Hellmann-Feynmann forces are evaluated to drive the nuclear coordinates. Our hamitonian is based on the valence bond (VB) description of the electronic wavefunctions. Since acetyl radical and its dissociative products have different bonding characters, the wavefunctions along the dissociation process are approximately expanded by two corresponding VB bases states. We found that the energy of the CCO bending excitation does not efficiently transfer into the dissociation coordinate (C-C) over the time period of 30 ps. It is suggested that this slow transfer or redistribution of internal energy could be one of the important sources for the discrepancy between the RRKM rate constants and the experimental results.

VIII-A-4 Ab Initio Molecular Orbital Studies of Isomerization Reaction from *c*-OSiH₂O to *t*-OSiOH

KONDO, Shigeo¹; TOKUHASHI, Kazuaki¹; NAGAI, Hidekazu¹; TAKAHASHI, Akifumi¹; SUGIE, Masaaki¹; AOYAGI, Mutsumi
(¹Natl. Inst. Mater. Chem. Res.)

[*J. Mol. Struct. (THEOCHEM)* **469**, 25 (1999)]

We have suggested in a previous study that the reaction route from SiH₃ + O₂ to OSiOH + 2H is a key to understand the spontaneous ignition at room temperature. The whole route of this reaction was found as follows;



In this study, the isomerization reaction from *c*-OSiH₂O to *t*-OSiHOH, a vital reaction to understand the

spontaneous ignition of Silane, has been reinvestigated with Gaussian-2 theory and CAS(6,6) method. It was found that the reaction proceeds through two consecutive steps; *i.e.*, c-OSiH₂O undergoes isomerization to yield w-OSiH₂O, and then the latter is converted to t-OSiHOH. The G-2 energy of the transition state of the latter process is 4.3 kcal/mol higher than that of the former. However, the G-2 energy of this higher transition state plus H atom is still 4.8 kcal/mol lower than that of the original reactants of SiH₃ + O₂.

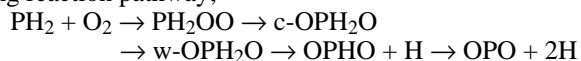
VIII-A-5 Ab Initio Study of PH₂ + O₂ Reaction Relevant to the PH₃ Combustion

KONDO, Shigeo¹; TOKUHASHI, Kazuaki¹; TAKAHASHI, Akifumi¹; SUGIE, Masaaki¹; AOYAGI, Mutsumi

(¹Natl. Inst. Mater. Chem. Res.)

[*J. Phys. Chem. A* in press]

Ab initio calculations have been carried out for the PH₂ + O₂ reaction by using Gaussian-2 theory, which is considered as a key reaction to understand low temperature phosphine combustion. This reaction consists of two main branching routes at low temperatures. One is the reaction to yield OH radicals, and the other to yield hydrogen atoms. Of the two reactions, we found that a long reaction pathway;



has been concluded to be the chain branching process, which enables the spontaneous ignition of phosphine at room temperature.

VIII-A-6 Semiclassical Study of Nonintegrable Systems

TAKAMI, Toshiya

We study nonadiabatic processes in highly excited states of molecules. Although a lot of theoretical works have been published on the subject so far, many of the authors have considered the problem under assumption that avoided crossings are sufficiently small. In the highly excited states, however, the assumption is not always validated. A new approach is desirable in order to study dynamical processes in systems with many levels interacting each other.

Our approach for the problem starts from studying systems with boundaries in the parameter space. We showed that the transition probability in adiabatic limit is dominated by an extra transition on the boundaries, which comes from nonadiabatic couplings between adiabatic states. We also found an iterative method to define a new base in which the extra transition is suppressed and the transition by avoided crossings can be observed locally. The new base can be used to analyze nonadiabatic processes of not only two level systems but also many level ones.

Our final goal is to construct a new framework for investigating many level nonadiabatic transition in realistic systems by using the new base instead of the usual adiabatic or diabatic base, as well as to develop

the higher order asymptotic theories in nonintegrable dynamical systems.

VIII-A-7 A Theoretical Study on Structures and Vibrational Spectra of C₈₄ Fullerene Isomers

NISHIKAWA, Takeshi; KINOSHITA, Tomoko; NANBU, Shinkoh; AOYAGI, Mutsumi

[*J. Mol. Struct. (THEOCHEM)* **461-462**, 453 (1999)]

The C₂, D₂, and D_{2d} isomers of C₈₄ fullerene were investigated by *ab initio* molecular orbital calculations. Optimized geometries, relative stabilities, and vibrational spectra of eleven isomers are determined by restricted Hartree-Fock (RHF) calculations with STO-3G, 3-21G, and D95V basis sets. For the purpose of an assignment on the C₈₄ structures, we discussed a way to distinguish a specific isomer by comparing the calculated vibrational spectra.

We found that the peaks located at higher than 1300 cm⁻¹ are all belonging to the on-surface mode where each carbon atom moves on the surface of C₈₄ skeleton. On the other hand, the peaks below 1000 cm⁻¹ correspond to the breathing mode, in which atoms are moving perpendicularly to the surface. There exists a window region (around 1000–1300 cm⁻¹) in all calculated spectra, which split a character of normal mode vibrations. In D₂ symmetry, the vibrational spectra of isomer No. 1 has a noticeable difference in the locations of three main peaks. The isomer No. 2 with C₂ symmetry also has characteristic vibrational structure, where numbering scheme introduced by Fowler *et al.* is used. For the rest of other isomers examined, it was hard to clearly predict the structure solely with calculated vibrational spectra. We suggested that the difference in the bands around 650 cm⁻¹ and 1670 cm⁻¹ can be used as a finger print of D₂ isomers, and that the vibrational bands below 900 cm⁻¹ and peak around 1880 cm⁻¹ can be used to distinguish C₂ species.

Laser Research Center for Molecular Science

VIII-B Developments of Advanced Lasers for Chemical Reaction Controls and ZEKE Photoelectron Spectroscopy

VIII-B-1 Developments of Liquid Crystal Spatial Light Modulator

SATO, Shin-ichiro; WATANABE, Kazuo

The chemical reaction controls with laser lights are one of the most important subjects of chemistry. The coherence of laser lights has not been considered seriously in the old fashion of the laser controls of chemical reactions. Recent theoretical studies have shown that the more sophisticated controls of chemical reactions. As a first step, we are trying to maximize efficiency of the quantum transition with a chirped ultra short pulsed laser. This technique is based on an adiabatic passage theory of quantum transitions. We are developing a photo waveform shaper of ultra short laser pulses to make an arbitrary shaped pulse, including chirped ones. The spectral components of the incident pulse are spatially dispersed with a grating, modulated or retarded with a liquid crystal array on the Fourier plane and recombined with another grating.

vibrational progression with a spacing of $9\text{--}10\text{ cm}^{-1}$ in the ZEKE spectra of azulene-Ar has been assigned experimentally and theoretically to the vdW bending vibration b_x^{+1} along the long axis of azulene. (4) From the calculated LJ potential energy minima, it has been found that Ar is shifted by 0.10 \AA along the long axis of azulene from the position in the neutral ground state. (5) The observed vdW vibrational progressions have been reproduced by Franck-Condon calculations, suggesting that Ar is shifted by 2° for (azulene-Ar) $^+$ with respect to its neutral S_2 state.

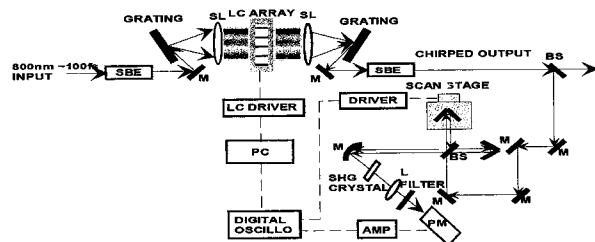


Figure 1. Schematic diagram of liquid crystal spatial light modulator.

VIII-B-2 ZEKE Electron Spectroscopy of Azulene and Azulene-Argon

TANAKA, Daisaku; SATO, Shin-ichiro; KIMURA, Katsumi

Mass-selected ion-current spectra and zero-kinetic-energy (ZEKE) electron spectra were obtained for azulene and its van der Waals (vdW) complex with Ar in supersonic jets by two-photon ($1 + 1'$) resonant ionization through the second singlet electronic excited state (S_2). Ab initio calculations were also carried out to study the optimized geometry and vibrational modes for azulene in the neutral and cation ground states (S_0 and D_0). Lennard Jones (LJ) potential energy calculations including "charge-charge-induced-dipole interactions" were also made for azulene-Ar. The main results may be summarized as follows. (1) The adiabatic ionization energies have been determined as $I_a(\text{azulene}) = 59781 \pm 5\text{ cm}^{-1}$ and $I_a(\text{azulene-Ar}) = 59708 \pm 5\text{ cm}^{-1}$. The difference in I_a is 73 cm^{-1} . (2) Several vibrational frequencies of (azulene) $^+$ have been observed and identified on the basis of ab initio theoretical calculations. (3)

VIII-C Developments and Researches of New Laser Materials

Although development of lasers is remarkable, there are no lasers which lase in ultraviolet and far infrared regions. However, it is expected that these kinds of lasers break out a great revolution in not only the molecular science but also in the industrial world.

In this project we research characters of new materials for ultraviolet and far infrared lasers, and develop new lasers by using these laser materials.

VIII-C-1 Intense THz Radiation from Femtosecond Laser Pulses Irradiated InAs in a Strong Magnetic Field

OHTAKE, Hideyuki; ONO, Shingo¹; KAWAHATA, Eiji; LIU, Zhenlin; SARUKURA, Nobuhiko
(¹Sci. Univ. Tokyo)

Since the first observation of THz radiation from InAs surface irradiated with femtosecond laser pulses, considerable effort have been made to design an intense THz-radiation source and to understand the mechanism for generating THz radiation. However, the problem has not been solved. In this paper, we have investigated the intense THz radiation from InAs by applying a strong magnetic field up to 5 T. We compared several different geometries. Besides quadratic magnetic field dependence, we found saturation of the THz-radiation intensity around 3 T. Furthermore, the intensity decreased dramatically above 3 T. It represented that the most suitable magnetic field was 3 T to design an intense THz-radiation source. We also took spectra by a Polarizing Michelson interferometer. The spectral shapes for the different magnetic field directions were significantly different. The center frequency of these spectra shifted to lower frequency with increasing magnetic field. Through these experiments, we found the best configuration and the most suitable magnetic field to obtain an intense THz radiation for various applications such as imaging, sensing, and spectroscopy. This configuration dependence of the spectral shape and the center frequency is attributed to be the initial carrier acceleration processes modulated by a strong magnetic field.

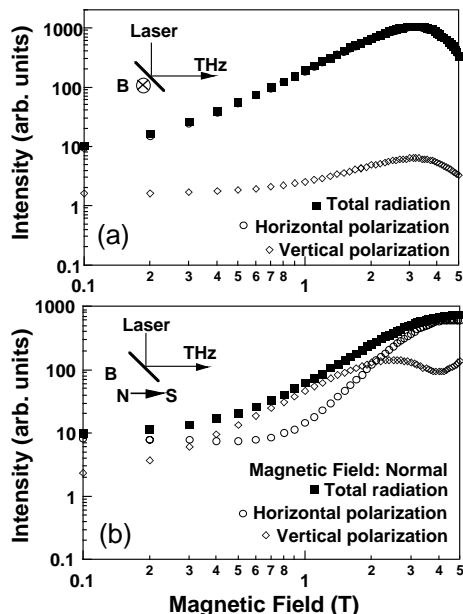


Figure 1. Magnetic field dependence of THz-radiation intensity. Inset indicates the experimental geometry. Closed squares, open circle and diamonds show total radiation, horizontal and vertical polarization, respectively. (a) The saturation of THz radiation intensity is clearly observed. (b) The saturation is not observed.

VIII-C-2 High-Repetition-Rate, High-Average-Power Mode-Locked Ti:sapphire Laser with an Intracavity cw-Amplification Scheme

LIU, Zhenlin; ONO, Shingo¹; KOZEKI, Toshimasa; OHTAKE, Hideyuki; SARUKURA, Nobuhiko
(¹Sci. Univ. Tokyo)

We have demonstrated a high-average-power, mode-locked Ti:sapphire laser with an intracavity cw-amplification scheme. The laser generated 150-fs pulses with 3.4-W average power at a repetition rate of 79 MHz. This simple amplification scheme can be applied for the power scaling of other lasers.

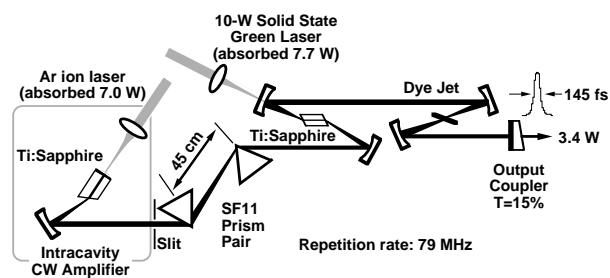


Figure 1. Configuration of high-repetition-rate high-average-power (3.4 W) femtosecond Ti:sapphire laser with an intracavity cw amplifier. The half-cut Brewster Ti:sapphire crystal composed the intracavity cw amplifier.

VIII-C-3 Compact THz-radiation Source Consisting of a Bulk Semiconductor, a Mode-Locked Fiber Laser, and a 2-T Permanent Magnet

ONO, Shingo¹; TSUKAMOTO, Takeyo¹; KAWAHATA, Eiji; LIU, Zhenlin; OHTAKE, Hideyuki; SARUKURA, Nobuhiko; NISHIZAWA, Seizi²; NAKANISHI, Akio³; YOSHIDA, Makoto⁴
(¹Sci. Univ. Tokyo; ²JASCO Co.; ³Sumitomo Special Metals co., Ltd.; ⁴IMRA AMERICA, INC. JLO)

Various THz-radiation sources have been intensively studied including photo conductive switches irradiated with ultrashort optical pulses. An intense, compact, and simple light source is required for applications in sensing or imaging. We have demonstrated the strong enhancement of THz-radiation power with a magnetic

field by using an InAs semiconductor. In this paper, we report on a compact THz-radiation source consisting of a fiber femtosecond laser and a newly designed 2-T permanent magnet shown in Figure 1. A mode-locked frequency doubled Er-doped fiber laser delivered 170-fsec pulses at 780 nm with a 48.5-MHz repetition rate (IMRA model FA7850/10SA) with 30-mW average power and 4.1-kW peak power. The mode-locked fiber laser is a completely turn-key system. It is much smaller than a mode-locked Ti:sapphire laser that requires daily alignment. The used semiconductor sample was undoped bulk InAs with a (100) surface. The 2-T permanent magnet unit consisted of 8 Nd-Fe-B magnet pieces. The remanence magnetic field of the Nd-Fe-B material itself was 1.3 T (NEOMAX-44H). Owing to the new magnetic circuit design, the magnetic field in the center exceeded the remanence magnetic field of the material. The permanent magnet only weighs about 5 kg. The 2-T permanent magnet unit is smaller and much lighter than an electromagnet. At present the average power is estimated to sub-micro watt level. The spectra of the THz radiation were obtained by a Polarizing Michelson interferometer. Many water vapor absorption lines were clearly observed. Therefore, the THz-radiation source is already usable for spectroscopy. Such a simple and compact source will open up new application for THz-radiation.

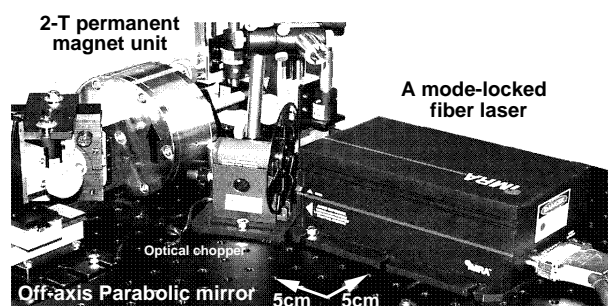


Figure 1. Photograph of a compact THz-radiation source with a bulk semiconductor, a fiber femtosecond laser, and a 2-T permanent magnet. Including the laser, the size is less than 40 × 30 × 15 cm.

VIII-C-4 Spectrum Control of THz Radiation from InAs in a Magnetic Field by Duration and Frequency Chirp of the Excitation Pulses

KAWAHATA, Eiji; ONO, Shingo¹; LIU, Zhenlin; OHTAKE, Hideyuki; SARUKURA, Nobuhiko
(¹Sci. Univ. Tokyo)

The THz-radiation spectrum from InAs in a magnetic field irradiated with femtosecond pulses can be controlled by varying the excitation pulse width and chirp direction of the excitation pulse. A longer excitation pulse width produces lower frequency THz radiation. Also, positively chirped pulse excitation will generate higher power and higher frequency THz radiation, due to the corruption of the impulse response of the semiconductor in the longer pulse width region. The spectral shape of the radiation strongly depends on the chirp direction. This unexpected difference with the same excitation peak power and the same pulse duration

with different chirp direction is rather surprising. This difference of THz-radiation for the chirping of the excitation pulses might be attributed to the difference of the photo-carrier relaxation process in the conduction band with oppositely chirped-pulse excitation.

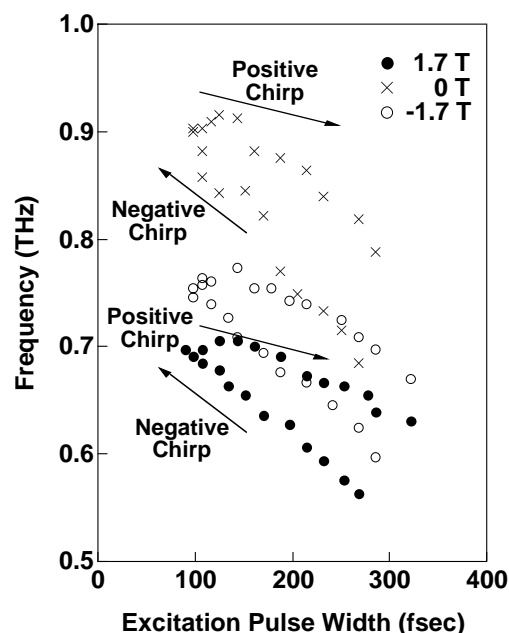


Figure 1. Center frequency spectrum dependence of THz radiation with different excitation chirp, pulse duration and magnetic field. Close circle, open circle and cross show 1.7 T, -1.7 T and 0 T, respectively.

VIII-C-5 LiCAF Crystal as a New Vacuum Ultraviolet Optical Material with Transmission down to 112 nm

KOZEKI, Toshimasa; SAKAI, Masahiro; LIU, Zhenlin; OHTAKE, Hideyuki; SARUKURA, Nobuhiko; SEGAWA, Yusaburo¹; OBA, Tomoru²; SHIMAMURA, Kiyoshi³; BALDOCHI, Sonia L.³; NAKANO, Kenji³; MUJILATU, Na³; FUKUDA, Tsuguo³
(¹RIKEN; ²Optron Inc.; ³Tohoku Univ.)

LiCaAlF₆ (LiCAF) was found to be an ideal optical material for the vacuum ultraviolet region due to its superior transmission characteristic of down to 112 nm, its non hygroscopic nature, and its better mechanical properties compared with LiF.

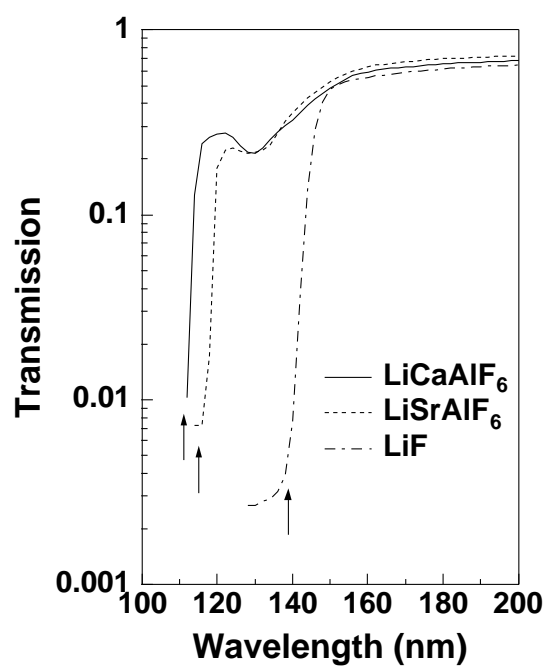


Figure 1. Transmission characteristics of LiCAF, LiSAF, LiF.

VIII-D Development and Research of Advanced Tunable Solid State Lasers

Diode-pumped solid-state lasers can provide excellent spatial mode quality and narrow linewidths. The high spectral power brightness of these lasers has allowed high efficiency frequency extension by nonlinear frequency conversion. Moreover, the availability of new and improved nonlinear optical crystals makes these techniques more practical. Additionally, quasi phase matching (QPM) is a new technique instead of conventional birefringent phase matching for compensating phase velocity dispersion in frequency conversion. These kinds of advanced tunable solid-state light, so to speak Chroma Chip Lasers, will assist the research of molecular science.

In this projects we are developing Chroma Chip Lasers based on diode-pumped-microchip-solid-state lasers and advanced nonlinear frequency conversion technique.

VIII-D-1 Frequency-Doubled Tunable Yb:YAG Microchip Laser for Holographic Volume Memories

SAIKAWA, Jiro; TAIRA, Takunori

Holographic volume memories have provoked a great deal of controversy.¹⁾ Angle and wavelength-multiplexed recordings have excellent potential for a large storage capacity.^{2,3)} However, large cumbersome light sources prevent the research of holographic data storage systems. Lately, we developed diode-pumped single-frequency and tunable Yb:YAG microchip laser.⁴⁾ In this work, we have demonstrated multiplex recording by using an intracavity frequency doubled Yb:YAG green laser.

The experimental configuration is shown in Figure 1. The frequency-doubled Yb:YAG laser consists of 400- μm thickness YAG doped with 25 at.% Yb³⁺ ion assembled on a sapphire substrate. Because the internal surface of the Yb:YAG microchip has partial reflectivity for laser wavelength, this microchip acts as an mode selection etalon. For tuning, a 1 mm thickness quartz plate was inserted into the laser cavity as a birefringent filter. A 2 mm KTP crystal was cut for type-II second-harmonic (SH) phase matching ($\theta = 90^\circ$, $\phi = 50^\circ$). In the frequency doubled Yb:YAG laser, tuning from 514.8 to 525.7 nm (10.9 nm, 12.4 THz) and maximum SH output power of 112 mW were obtained with single-axial-mode.

The recording medium was a 1% Fe-doped LiNbO₃ (Fe:LN) single crystal (3 \times 3 \times 5 mm). The *c*-axis of the crystal was parallel to the grating vector of the hologram. A reference beam *R* and a signal beam *S* irradiated opposite sides of the crystal, both at an angle θ_0 of 10° . A pattern mask with a 10 \times 10 mm² character image, two lenses (diameter: $d = 1\text{-inch}$, focal length $f = 75.5\text{-mm}$), the Fe:LN crystal, and a CCD camera made a Fourier-transform holographic system. We recorded and reconstructed two successive wavelength-multiplexed holograms by using light of two wavelengths that were 0.31 nm apart which corresponds to the FSR of 400- μm Yb:YAG microchip.

References

- 1) J. F. Heanue *et al.*, *Science* **265**, 749 (1994).
- 2) S. Campbell and P. Yeh, *Appl. Opt.* **35**, 2380 (1996).
- 3) T. Kume *et al.*, *Jpn. J. Appl. Phys.* **35**, 448 (1996).
- 4) T. Taira *et al.*, *IEEE J. Sel. Top. Quantum Electron.* **3**, 100 (1997).

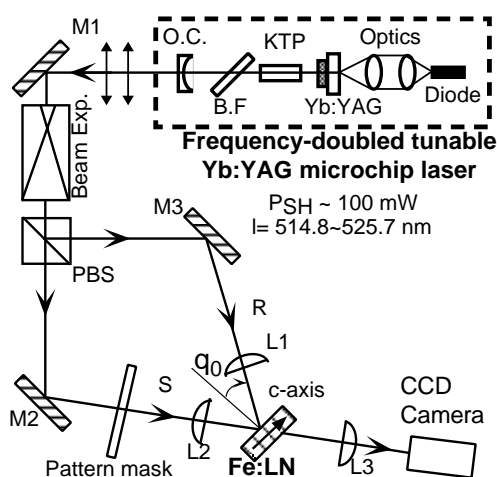


Figure 1. Holographic recording system by using intracavity frequency-doubled Yb:YAG microchip laser.

VIII-D-2 Design Criteria for Optimization of Fiber-Coupled Diode Longitudinally-Pumped Laser Using Pump-beam M^2 Factor

PAVEL, Nicolaie¹; KURIMURA, Sunao; TAIRA, Takunori

(¹*Inst. Atm. Phys., Romania*)

For optimization of longitudinally-pumped solid-state lasers, a model which consider the pump-beam propagation described by its M^2 factor is proposed. Analytical functions for the optimum focusing-position, the optimum pump spot-size, the minimum threshold pump power and the maximum overlap efficiency are given. A simple output to input power relation and previous formula provides a straightforward procedure to design the optimum laser resonator, the coupling-optics and to evaluate the laser output power.

A slope efficiency of 57% with a 53% optical-efficiency at maximum 8-W pump-power was obtained from a fiber-coupled longitudinally-pumped Nd:YAG medium. A very good agreement between experiments and theory was obtained.

References

- 1) R. A. Fields *et al.*, *Appl. Phys. Lett.* **51**, 1885 (1987).
- 2) T. Taira *et al.*, *Opt. Lett.* **16**, 1955 (1991).
- 3) M. D. Selker *et al.*, *CLEO CPD21*, (1996).
- 4) T. Taira *et al.*, *OSA TOPS* **19**, 430 (1998).

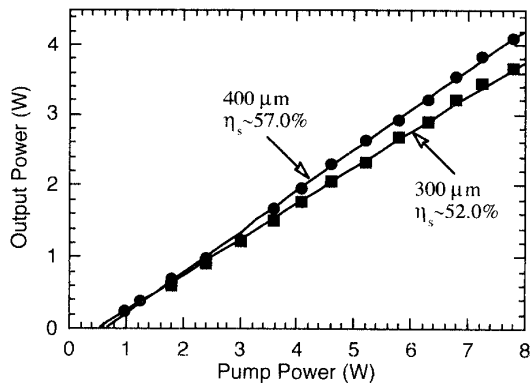


Figure 1. Output power as a function of pump-power.

VIII-D-3 Highly Nd³⁺-Doped YAG Ceramic for Microchip Lasers

TAIRA, Takunori; KURIMURA, Sunao; SAIKAWA, Jiro; IKESUE, Akio¹; YOSHIDA, Kunio²
(¹JFCC; ²Osaka Inst. Tech.)

Nd:YVO₄ offers highly efficiency miniature or microchip lasers due to its high absorption and emission cross-sections.¹⁻⁴ However, its poor thermo-mechanical properties prevent high power laser operation. Much effort has gone into laser material research to find a high absorption coefficient laser medium with high thermal shock parameters. Lately, a high optical quality Nd:YAG laser material of polycrystalline ceramic has been reported.⁵ In this paper, we have demonstrated a highly efficient oscillation in a Nd:YAG ceramic microchip laser.

The YAG ceramic allows highly neodymium-ion doping to overcome low absorption cross-section. The absorption coefficient of the single Nd:YAG crystal was 3.45 cm⁻¹ at 808 nm, while the 9.1 at.% Nd:YAG ceramic has about 10 times higher absorption. The absorption coefficient of the 4.8 at.% Nd:YAG ceramic was 11.7 cm⁻¹. This result indicates that Nd:YAG ceramic has advantages in a microchip or miniature laser system as well as Nd:YVO₄. The thermal conductivity of Nd:YAG ceramic decreases with Nd concentration and thermal conductivity of the 9.1 at.% doped YAG ceramic was 9.0 W/mK.

The 4.8 at.% Nd³⁺ doped YAG ceramic was cut to a 847 μm thickness for microchip laser experiments. The plan-concave resonator configuration has an output mirror radius of 100-mm and a resonator length of 50-mm. The 808 nm pump beam was focused to a diameter of 100 μm in the medium. Figure 1 shows an output power of Nd:YAG ceramic laser as a function of input power. A performance of 0.9 at.% Nd:YAG single crystal also plotted in order to compare. As a result, the maximum output power of Nd:YAG ceramic laser was four times higher than conventional Nd:YAG single crystal laser because the YAG ceramic has over five times higher Nd³⁺ ion doping level. Conventional ceramic laser has highly scattering loss which prevent the highly efficient laser oscillation. We are estimating an internal loss of laser cavity from the slope efficiency.

In summary, we developed highly Nd-doped YAG in ceramic for high power microchip laser. Four times higher laser output power in YAG ceramic compared

with conventional YAG single crystal was demonstrated.

References

- 1) R. A. Fields *et al.*, *Appl. Phys. Lett.* **51**, 1885 (1987).
- 2) T. Taira *et al.*, *Opt. Lett.* **16**, 1955 (1991).
- 3) W. L. Nighan *et al.*, *Conf. Lasers and Electro-Optics*, OSA Tech. Dig.; Washington DC., paper CMD5 (1995).
- 4) M. D. Selker *et al.*, *Conf. Lasers and Electro-Optics*, OSA Tech. Dig.; Washington DC., paper CPD21 (1996).
- 5) T. Taira *et al.*, *TOPS* **19**, 430 (1998).

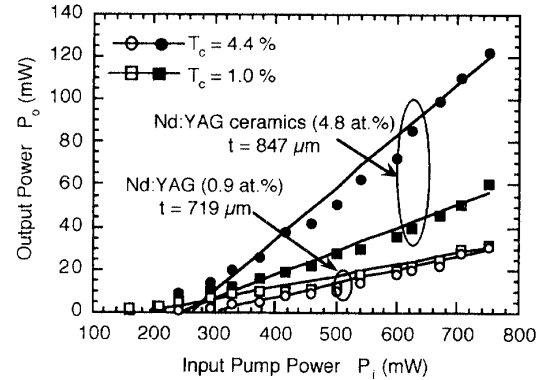


Figure 1. Input-output power characteristics of a diode-pumped Nd:YAG ceramic laser.

VIII-D-4 Nondestructive Characterization of Quasi-Phase-Matched Wavelength Converter

KURIMURA, Sunao; UESU, Yoshiaki¹
(¹Waseda Univ.)

We devised an observation technique of 180° domains in ferroelectric crystals by using Second Harmonic Generation (SHG) Microscope. The phase reversal of the SH wave accompanying inversion of spontaneous polarization is exploited to visualize domains. Interference between SH waves converts the phase information to the SH contrast. Domain mapping is achieved in LiNbO₃ and LiTaO₃ with nonlinear coefficients d_{33} and d_{22} under the microscope, which enables characterization of a periodically-poled structure in quasi-phase-matched wavelength converters in a nondestructive way. The validity of the technique is proved by another characterizing tool of destructive etching.

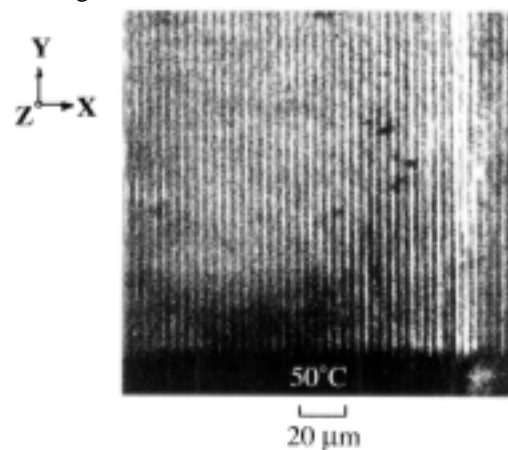


Figure 1. Photo of a Z-cut QPMLT device.

Research Center for Molecular Materials

VIII-E Development of Novel Heterocyclic Compounds and their Molecular Assemblies for Advanced Materials

Heterocycles containing sulfur and/or nitrogen atoms are useful as components of functional materials since heteroatoms in their rings are helpful to stabilize ions or ion-radical species, and extended π -conjugation decreases Coulombic repulsion. In addition intermolecular interactions caused by heteroatom contacts can be expected to form novel molecular assemblies. In this project new electron acceptors, donors, and donor-acceptor compounds based on heterocycles such as 1,2,5-thiadiazole and 1,3-dithiole were synthesized and their properties including those of the charge-transfer complexes or ion-radical salts were investigated. Unique crystal structures were constructed by using weak intermolecular interactions such as hydrogen bonding or heteroatom contacts. Thiophene oligomers with rigid structures were also synthesized for molecular wires.

VIII-E-1 Cation Radical Salts of TTF Vinylogues with $\text{Au}(\text{CN})_2$ Anion

YAMASHITA, Yoshiro; TOMURA, Masaaki; IMAEDA, Kenichi

TTF vinylogues bearing substituents have been easily obtained and the TTF skeletons can be planar when the aryl substituents are twisted from the π -conjugated framework. We have now found that TTF vinylogues **1a-c** containing one halogen atom at the ortho position afford cation radical salts $[\mathbf{1}\cdot\text{Au}(\text{CN})_2]$ as single crystals when they are electrochemically oxidized in dichloromethane in the presence of $\text{Bu}_4\text{N}\cdot\text{Au}(\text{CN})_2$. The X-ray crystal structure analyses of $\mathbf{1b,c}\cdot\text{Au}(\text{CN})_2$ salts were carried out to reveal the unique crystal structures. The molecular and crystal structure of $\mathbf{1b}\cdot\text{Au}(\text{CN})_2$ is shown in Figure 1. The TTF vinylogue skeleton is planar and the phenyl groups are orthogonal from the π -framework. The donor molecules do not take a stacking structure and the 1,3-dithiole parts sandwich the counter anion. The crystal structure of $\mathbf{1c}\cdot\text{Au}(\text{CN})_2$ is very similar to that of $\mathbf{1b}\cdot\text{Au}(\text{CN})_2$. These cation radical salts showed semiconducting behaviour since these have a 1:1 stoichiometry $[\mathbf{1b}\cdot\text{Au}(\text{CN})_2]$; $\sigma = 1 \times 10^{-2} \text{ Scm}^{-1}$, $E_a = 0.11 \text{ eV}$, $\mathbf{1c}\cdot\text{Au}(\text{CN})_2$; $\sigma = 5 \times 10^{-3} \text{ Scm}^{-1}$, $E_a = 0.11 \text{ eV}$].

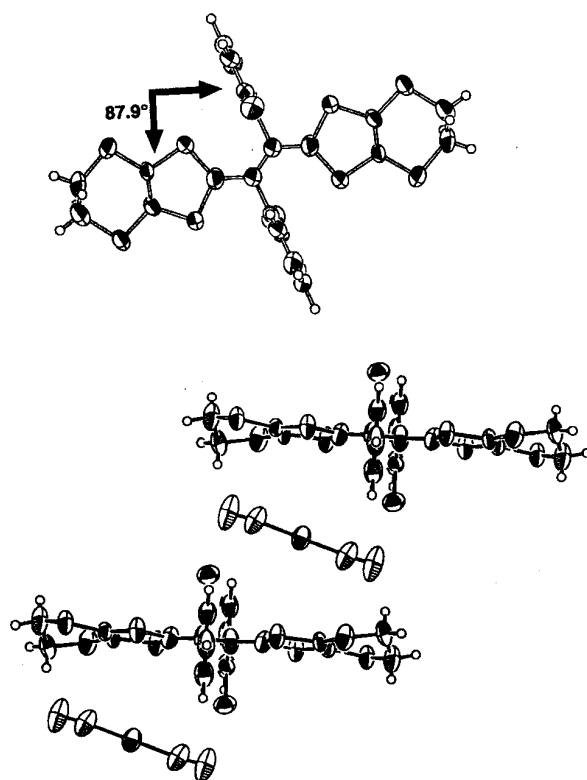
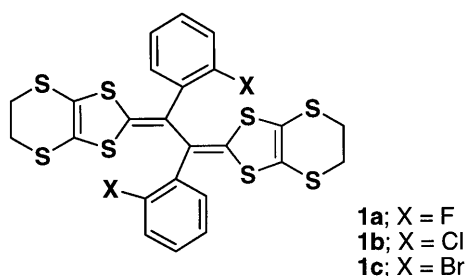


Figure 1. Molecular and crystal structure of $\mathbf{1b}\cdot\text{Au}(\text{CN})_2$.

VIII-E-2 Control of Packing Mode in Crystals of Cation Radical Salts of TTF Vinylogues

TOMURA, Masaaki; YAMASHITA, Yoshiro

Molecular and crystal structures of cation radical salts of novel tetrathiafulvalene (TTF) vinylogues with extended π -conjugation and aryl groups in their vinyl part have been studied by X-ray crystallographic analysis. We reported that the unique conformation with a planar TTF vinylogue framework in $\mathbf{1}\cdot\text{PF}_6$ salt causes an interesting two-dimensional stacking mode where one donor molecule bridges two molecules like a brick wall in the crystal.¹⁾ We have succeeded in controlling the packing mode in the two-dimensional stack by changing the counter anion. In the case of $\mathbf{1}\cdot\text{FeCl}_4$ salt, we observed a partial two-dimensional stacking in the crystal. On the other hand, the zigzag two-dimensional

stacking with an angle of nearly 90° exists in the crystal of **1**-ReO₄ salt, as shown in Figure 1.

Reference

- 1) Y. Yamashita, M. Tomura, M. B. Zaman and K. Imaeda, *Chem. Commun.* 1657 (1998).

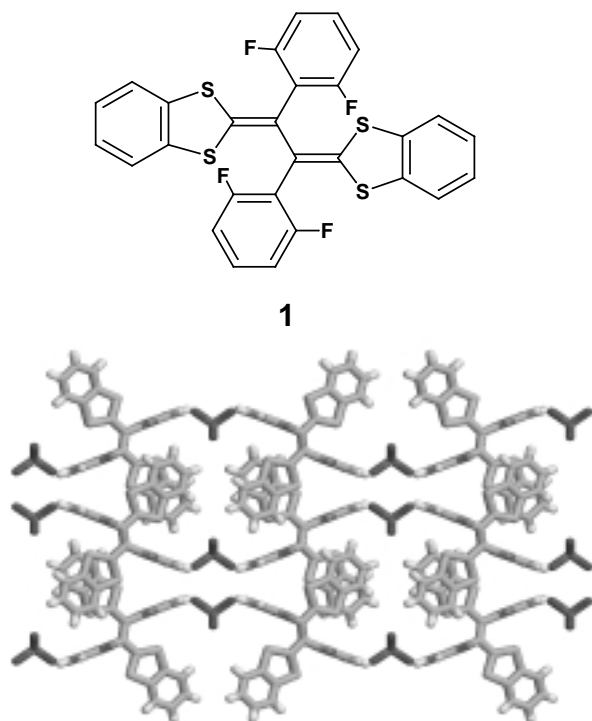


Figure 1. Crystal structure of **1**-ReO₄ salt.

VIII-E-3 Non-Planar BEDT-TTF Derivatives Fused with Tetrahydrofuran Rings Affording Cation Radical Salts with Unusual Structures

YAMASHITA, Yoshiro; TOMURA, Masaaki

Unusual crystal structures are expected from non-planar molecules to avoid steric interactions. Three-component conductors might be prepared from non-planar molecules by inclusion of solvent molecules. We have now designed new electron donors **1** and **2** where tetrahydrofuran (THF) rings are fused to BEDT-TTF. The new donors were prepared using the addition reaction of oligo(1,3-dithiole-2,4,5-trithione) with 2,5-dihydrofuran. The donor **2** gave two cation radical salts [**2**·Au(CN)₂ and **2**·PF₆·(PhCl)_{0.5}] as single crystals when electrochemically oxidized in chlorobenzene. The salts exhibit semiconducting behavior [**2**·Au(CN)₂; $\sigma = 3 \times 10^{-3} \text{ Scm}^{-1}$, $E_a = 0.20$, **2**·PF₆·(PhCl)_{0.5}; $\sigma = 5 \times 10^{-5} \text{ Scm}^{-1}$, $E_a = 0.24 \text{ eV}$]. The X-ray crystal analyses of these salts revealed their unusual crystal structures. The donor molecule is non-planar and the cis-fused THF ring is like a hook. In **2**·Au(CN)₂ one Au(CN)₂ anion is sandwiched between the donor molecules. This sandwiched structure is stacked to give a column. In **2**·PF₆·(PhCl)_{0.5}, instead of a stacking structure, a complicated molecular network is observed, where one neighboring molecule is highly leaned (77°) and the molecules are combined by short S...S contacts as

shown in Figure 1.

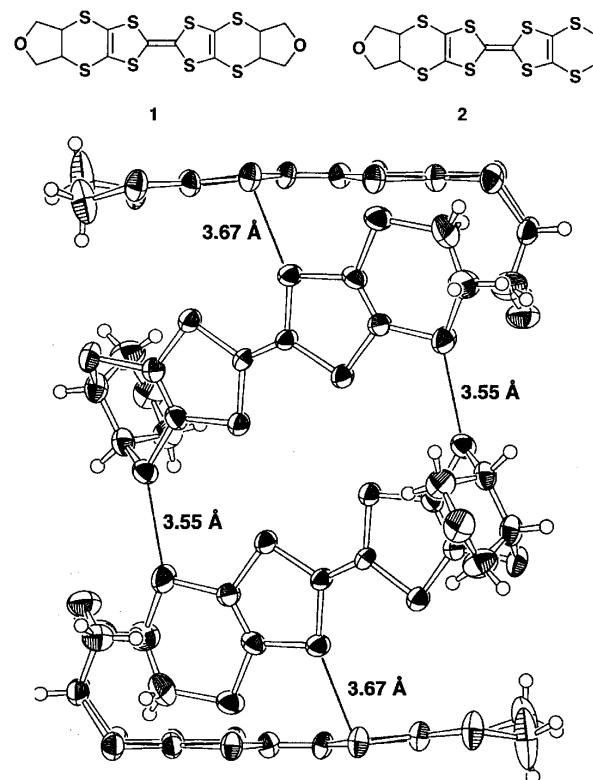


Figure 1. Crystal structure of **2**·PF₆·(PhCl)_{0.5}.

VIII-E-4 Bithiophene-TCNQ Analogue with Fused 1,2,5-Thiadiazole Rings

SUZUKI, Kazuharu; TOMURA, Masaaki; YAMASHITA, Yoshiro

Sulfur containing TCNQ analogues are highly polarized and are expected to have strong intermolecular interactions by heteroatom contacts. We have now prepared π -extended electron acceptor **1** containing fused thiadiazole rings and carried out the X-ray structure analysis to reveal the intermolecular interactions. The acceptor **1** was obtained by the reaction of dibromide **2** with tetracyanoethylene oxide (TCNEO) in 3% yield. However, thiophen-TCNQ analogue **3** could not be isolated in this reaction. The mechanism for the formation of **1** is still ambiguous. In the reaction to give **1**, a small amount of new compound **4** was isolated whose structure was determined by X-ray structure analysis. The dibromide **4** gave **1** upon heating, suggesting that **4** is an intermediate to give **1**. The absorption maximum of **1** is observed at 461 nm in dichloromethane. The reduction potential (-0.31 V vs. SCE) is lower than that of TCNQ, indicating that the interaction between the dicyanomethylene parts is weak in **1**. The X-ray analysis revealed that **1** forms a molecular assembly by heteroatom interactions. The crystal structure is shown in Figure 1. The planar molecules are combined by short S...N contacts to give a three-dimensional network. The distance of S...N contact (3.18 Å) is shorter than the sum of the van der Waals distances (3.35 Å).

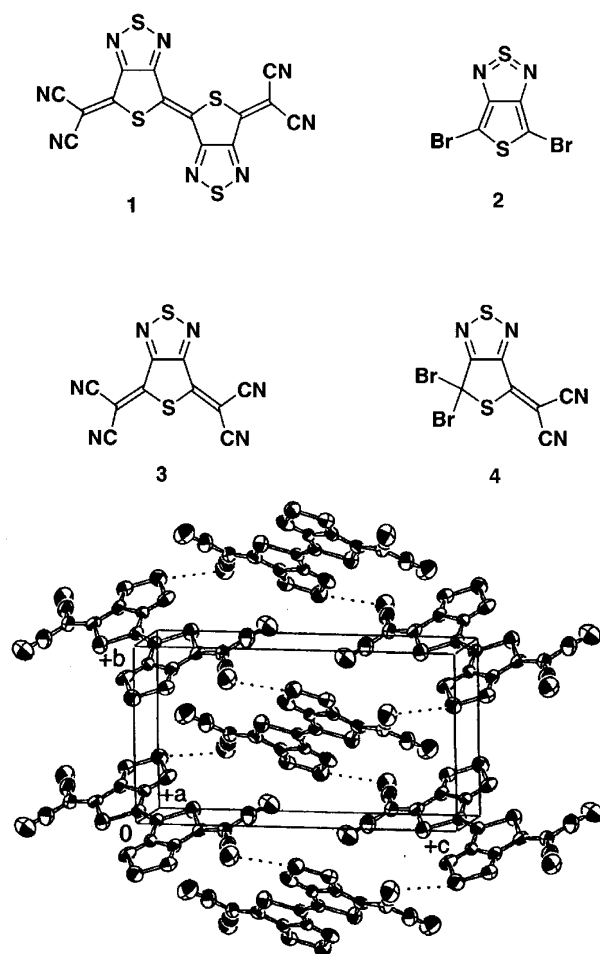


Figure 1. Crystal structure of 1.

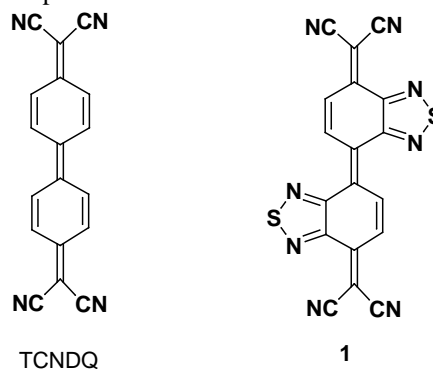
VIII-E-5 First Stable Tetracyanodiphenylquinodimethane with a Completely Planar Geometry: Preparation, X-Ray Structure, and Highly Conductive Complexes of Bis[1,2,5]thiadiazolo-TCNDQ

FUKUSHIMA, Takanori¹; OKAZERI, Nobuharu¹; MIYASHI, Tsutomu¹; SUZUKI, Kazuharu; YAMASHITA, Yoshiro; SUZUKI, Takanori²
(¹Tohoku Univ.; ²Hokkaido Univ.)

[*Tetrahedron Lett.* **40**, 1175 (1999)]

The title tetracyanodiphenylquinodimethane (TCNDQ) derivative **1** was newly designed and prepared as a novel component for highly conductive organic materials. This is the first stable TCNDQ derivative which is a π -extended electron acceptor. The synthesis was achieved by using Pd(0)-catalyzed reaction of the corresponding diiodo compound with NaCH(CN)₂ followed by oxidation. Introduction of thiadiazole rings into the TCNDQ skeleton leads to large stabilization in the neutral state. X-ray analysis has revealed the unique structure, where interatomic interactions (CH \cdots N, S \cdots N) play an important role in determining the molecular and crystal structure. The novel electron acceptor shows strong electron affinity ($E_{\text{red}} = +0.33, +0.12$ V vs. SCE in CH₂Cl₂) comparable with that of TCNQ, and gave highly conductive charge

transfer complexes and anion radical salts.



VIII-E-6 Novel Supramolecular Synthons in Crystal Engineering: Ionic Complexes of 4,4'-Bipyridine and 1,2-Bis(2-pyridyl)ethylene with 2,5-Dichloro-3,6-dihydroxy-1,4-benzoquinone

ZAMAN, Md. Badruz; TOMURA, Masaaki; YAMASHITA, Yoshiro

[*Chem. Commun.* 999 (1999)]

In order to develop a new type of hydrogen-bonding system, we have selected bipyridine (BPY) and 1,2-bis(2-pyridylethylene) (2-PDE) as proton acceptor, and chloranilic acid (2H-CLA) as proton donor. The complexes were prepared by reacting BPY and 2-PDE with an equal amount of 2H-CLA in acetone and/or a mixture of acetone-MeOH. The crystal structure analysis revealed that molecular complexes [BPY-2H]²⁺[CLA]²⁻ **1** and [2-PDE-2H]²⁺[CLA]²⁻ **2** are formed where proton transfer occurs. The component molecules are combined via three-center hydrogen bonded interactions to build a linear molecular chain for **1** and a zigzag molecular tape for **2**. The structure of **1** is shown in Figure 1. In both **1** and **2**, bifurcated interionic [N⁺-H \cdots O⁻ and N⁺-H \cdots O] hydrogen bonds between the nitrogen atoms of the cations and the two oxygen atoms from the anions are observed. This is a new supramolecular synthon motif. In complex **1** alternating DA-type pairs of the cation and anion molecules are observed in the stacking, while complex **2** has a segregated stacking assembly as DD- and AA-type pairs.

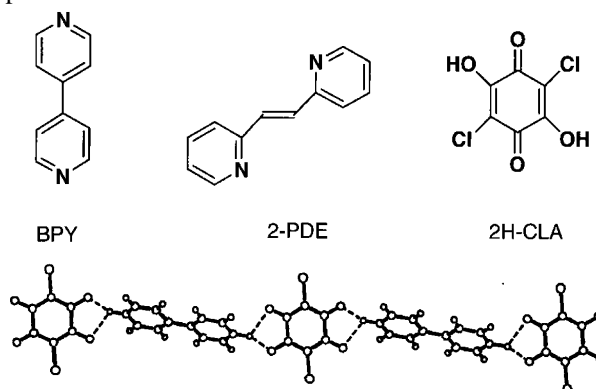


Figure 1. Hydrogen bonding in 1.

VIII-E-7 Design and Synthesis of Soluble Linear Macromolecules with Highly Extended π -Conjugated Backbone

TANAKA, Shoji; YAMASHITA, Yoshiro

The development of soluble linear macromolecules with highly extended π -conjugated system is of crucial importance to establish the structure-conductance relationship in ballistic-type molecular electric wires. Although the introduction of alkyl substituents into the main chain is an effective method to improve the solubility, this modification often results in conjugation defects in the main chain due to the enhanced inter-unit steric repulsion. Here we report on a tactics in molecular design to do well both in solubility and π -conjugation of

linear oligomers. We have synthesized a series of mixed oligomers **1-5**. All of the alkyl-substituted oligomers are more soluble in CH_2Cl_2 , CHCl_3 , and THF compared with the unsubstituted ones. As shown in Figure 1, the hexyl substitution on **1a** induces only a small blue shift of the absorption maximum, indicating a tiny loss of conjugation in spite of the long alkyl-chain substitution. These results suggest that **1b** unit can be used as a building block for soluble and effectively π -conjugated macromolecules. Along this line, we have obtained soluble highly oligomers **1c-d**. The red shift values induced by the chain extension (**1b** \rightarrow **1c** \rightarrow **1d**) are significantly higher than the shift value of the related oligomers (**3c** \rightarrow **3d**). This supports the highly extended π -conjugation in the main chain of **1c-d**.

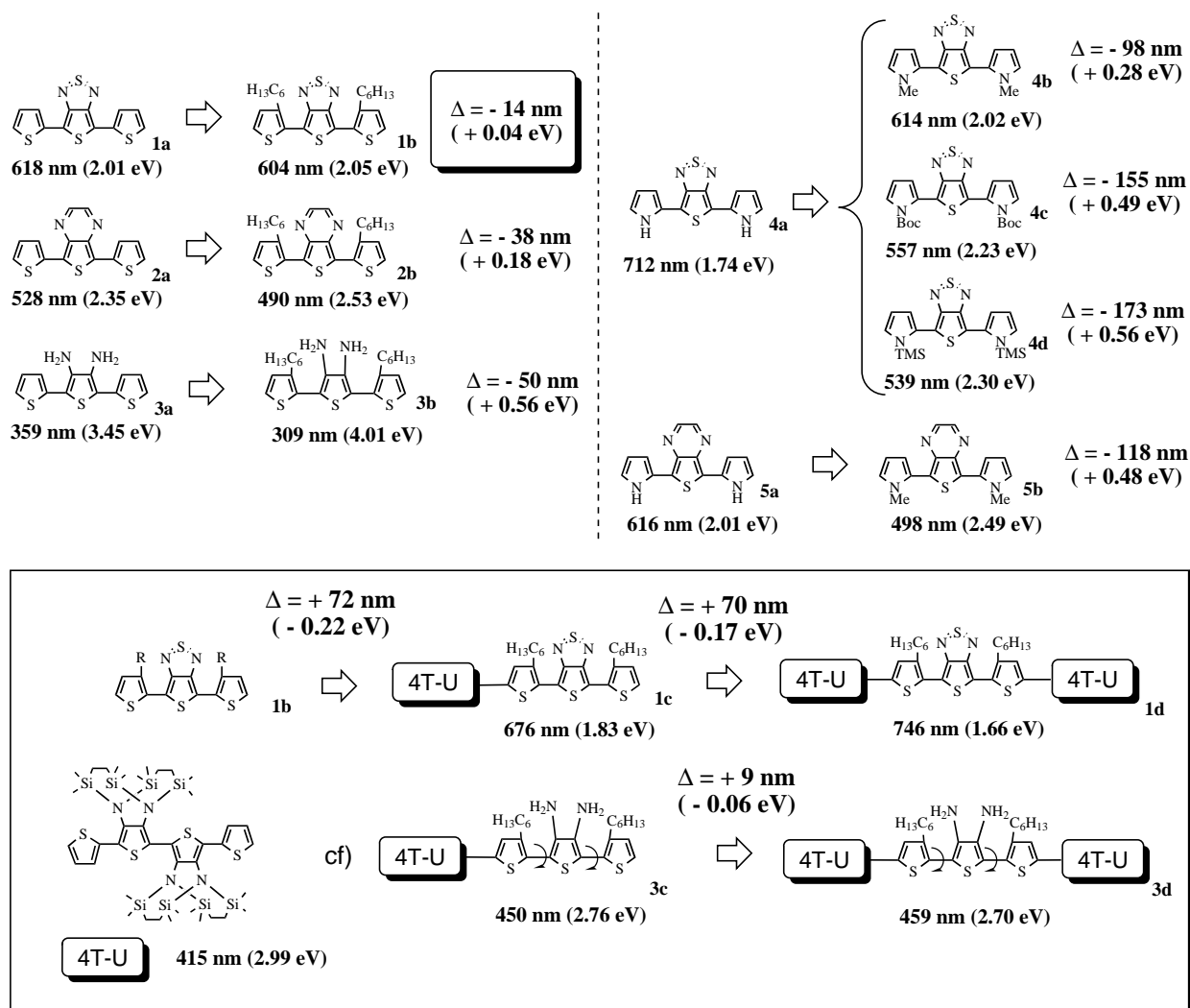


Figure 1. Substituent effects on the absorption maximum of the obtained mixed oligomers.

VIII-F Electronic Structures and Reactivities of Active Sites of Metalloproteins

Metalloproteins are a class of biologically important macromolecules which have various functions such as oxygen transport, electron transfer, oxidation, and oxygenation. These diverse functions of metalloproteins have been thought to depend on the ligands from amino acid, coordination structures, and protein structures in immediate vicinity of metal ions. In this project, we are studying the relationship between the structures of the metal active sites and functions of metalloproteins.

VIII-F-1 High-Spin (meso-Tetraalkylporphyrinato)-iron(III) Complexes As Studied by X-ray Crystallography, EPR, and Dynamic NMR Spectroscopies

IKEUE, Takahisa¹; OHGO, Yoshiki¹; UCHIDA, Akira¹; NAKAMURA, Mikio¹; FUJII, Hiroshi; YOKOYAMA, Masataka²
(¹Toho Univ.; ²Chiba Univ.)

[*Inorg. Chem.* **38**, 1276 (1999)]

¹H-NMR spectra of a series of high-spin (meso-tetraalkylporphyrinato)iron(III) chlorides, [Fe(TRP)Cl] where R = Me, Et, Pr, or iPr, have been measured at various temperatures in CD₂Cl₂ solution. In the case of the Et, Pr, and iPr complexes, either the methyl or the methylene signal split into two signals with equal integral intensities at low temperature. In contrast, the Me complex did not show any splitting even at -100 °C. The results have been ascribed to the hindered rotation of the meso-alkyl groups about Cmeso-C bonds. The activation free energies for rotation have been determined as 8.0 (-72 °C), 8.5 (-60 °C), and 8.9 (-62 °C) kcal·mol⁻¹ for the Et, Pr, and iPr complexes, respectively, at coalescence temperatures given in parentheses. The small activation free energy for rotation of the isopropyl groups observed in the present system is explained in terms of the nonplanarity of the porphyrin ring, which has been verified both by the X-ray crystallographic analysis and by the EPR spectrum taken in a frozen CH₂Cl₂-toluene solution. The success in observing the hindered rotation of less bulky primary alkyl groups such as ethyl and propyl groups at an easily accessible temperature range is attributed to the large difference in chemical shifts of the mutually exchanging protons, *ca.* 3500 Hz in the case of the Et complex, caused by the paramagnetism of the five-coordinated ferric porphyrin complexes.

VIII-F-2 Insensitivity of Vanadyl-Oxygen Bond Strengths to Radical Type (²A_{1u} vs. ²A_{2u}) in Vanadyl Porphyrin Cation Radicals

CZARNECKI, Kazimierz¹; PRONIEWICZ, Leonard M.¹; FUJII, Hiroshi; JI, David²; CZERNUSZEWICZ, Roman S.²; KINCAID, James R.¹
(¹Marquette Univ.; ²Univ. Houston)

[*Inorg. Chem.* **38**, 1543 (1999)]

Resonance Raman (RR) spectra are reported for vanadyl octaethylporphyrin, O=V(OEP), tetramesityl-tetramethylporphyrin, O=V(TMTMP), and tetramesityl-

porphyrin, O=V(TMP), and their corresponding π -cation radicals obtained by chemical and electrochemical oxidation. The behavior of the ν_2 RR porphyrin "marker band," which moves to higher frequency upon oxidation of the O=V(OEP) and O=V(TMTMP) and to lower frequency for O=V(TMP), shows that the resultant cation radicals have predominantly ²A_{1u} and ²A_{2u} ground states, respectively. In contrast to earlier work (K. A. Macor, R. S. Czernuszewicz and T. G. Spiro, *Inorg. Chem.* **29**, 1990 (1996)), it is demonstrated here that the shift of the $\nu(V=O)$ is insensitive to radical type, behavior which is in agreement with similar studies of the ferryl analogues (K. Czarnecki *et al.*, *J. Am. Chem. Soc.* **116**, 2929 and 4680 (1996)). It is suggested that the observed downshifts of the $\nu(V=O)$ previously reported for RR spectra of vanadyl porphyrin π -cation radicals, relative to their neutral parents, are most reasonably ascribed to trans oxo ligand coordination (most probably a water molecule) during low-temperature electrochemical oxidation of the neutral species.

VIII-F-3 Electron Configuration of Ferric Ions in Low-Spin (Dicyano)(meso-tetraarylporphyrinato)-iron(III) Complexes

NAKAMURA, Mikio¹; IKEUE, Takahisa¹; IKEZAKI, Akira¹; OHGO, Yoshiki¹; FUJII, Hiroshi
(¹Toho Univ.)

[*Inorg. Chem.* **38**, 3857 (1999)]

The electron configuration of a series of low-spin (dicyano){meso-tetrakis(2,4,6-trialkylphenyl)-porphyrinato}iron(III) complexes, [Fe(R-TPP)(CN)₂]⁻ where R = Me, Et, or iPr, together with the parent [Fe(TPP)(CN)₂]⁻, has been examined in dichloromethane-methanol solution by ¹H-NMR, ¹³C-NMR, and EPR spectroscopies. While the ferric ion of [Fe(TPP)(CN)₂]⁻ has shown a common (d_{xy})²(d_{xz},d_{yz})³ configuration, the ferric ions of the alkyl-substituted complexes [Fe(R-TPP)(CN)₂]⁻ have exhibited the preference of a less common (d_{xz},d_{yz})⁴(d_{xy})¹ configuration. Spectroscopic characteristics of the complexes in which ferric ions take the (d_{xz},d_{yz})⁴(d_{xy})¹ configuration are (i) axial type EPR spectra, (ii) downfield shifted pyrrole and meta signals in ¹H-NMR spectra, and (iii) downfield shifted meso-carbon signals in ¹³C-NMR spectra. Occurrence of the less common (d_{xz},d_{yz})⁴(d_{xy})¹ configuration in [Fe(R-TPP)(CN)₂]⁻ has been ascribed to the electronic interaction between iron(d) and cyanide(p*) orbitals. The interaction stabilizes the d orbitals and induces (d_{xz},d_{yz})⁴(d_{xy})¹ configuration. Since the electron configuration of (dicyano){meso-tetrakis(2,6-dichloro-

phenyl)porphyrinato}iron(III), $[\text{Fe}(\text{Cl-TPP})(\text{CN})_2]^-$, which carries bulky electronegative chlorine atoms at the ortho positions, is presented as a common $(d_{xy})^2(d_{xz}, d_{yz})^3$, the less common $(d_{xz}, d_{yz})^4(d_{xy})^1$ configuration in $[\text{Fe}(\text{R-TPP})(\text{CN})_2]^-$ can be ascribed, at least partially, to the electron-donating ability of the meso-aryl groups.

VIII-F-4 Resonance Raman Spectra of Legitimate Models for the Ubiquitous Compound I Intermediates of Oxidative heme Enzymes

CZARNECKI, Kazimierz¹; KINCAID, James R.¹; FUJII, Hiroshi
(¹Marquette Univ.)

[J. Am. Chem. Soc. in press]

Resonance Raman (RR) spectra are reported for two models of the compound I intermediates of oxidative heme proteins; namely, the imidazole (Im) and 2-methyl-imidazole (2-MeIm) complexes of the ferryl π -cation radical derivative of iron-(5,10,15,20-tetramesitylporphyrin), $[\text{O}=\text{Fe}(\text{TMP}^{+\bullet})(\text{Im})]^+$ and $[\text{O}=\text{Fe}(\text{TMP}^{+\bullet})(2\text{-MeIm})]^+$, which are stabilized in dichloromethane solution at -80°C . The present study yields high quality RR spectra of these complexes and provides the first opportunity to compare the $\nu(\text{Fe}=\text{O})$ stretching modes and the structure-sensitive core marker modes for a ferrylporphyrin π -cation radical with the corresponding modes of the neutral parent bearing the same trans-axial ligand. While the observed shifts in the frequencies of the core modes are in agreement with those expected upon formation of the π -cation radical, the results suggest that the isolated effect of macrocycle oxidation on the $\text{Fe}=\text{O}$ stretching frequency is rather small; the observed shift being only about 4 cm^{-1} to lower frequency.

VIII-F-5 Newly Designed Iron-Schiff Base Complexes as Models of Mononuclear Non-Heme Iron Active Sites

FUNAHASHI, Yasuhiro; FUJII, Hiroshi

High valent iron-oxo species have been suggested as the active intermediates for catalytic oxygenation

reactions by iron-containing oxygenases. In the reaction mechanisms of heme and binuclear non-heme iron enzymes, an $\text{Fe}^{\text{IV}}=\text{O}$ porphyrin radical species (Compound I) and a $\text{Fe}^{\text{IV}}_2(\mu\text{-O})_2$ species (Intermediate Q) have been found to be responsible oxidant for alkane hydroxylation and alkene epoxidation. Such the high valent iron-oxo species are inferred to involve in hydroxylation of aromatic compounds by mononuclear non-heme iron oxygenases, the reaction processes of which, however, still remains to be established. In order to gain insight into the active intermediates, we try to synthesize iron complexes with bulky schiff-base ligands as biomimetic models of mononuclear non-heme iron active sites. The active oxygen adduct of these complexes, which would be kinetically stabilized by their steric hindrance, might provide a basis for understanding the oxygenation by mononuclear iron sites.

VIII-F-6 ¹⁷O-NMR Study of Oxygen Molecules Bound to Copper Ions of Mononuclear and Dinuclear Copper Complexes

MIZUTANI, Mamoru; FUJII, Hiroshi

The activation of molecular oxygen by transition metals has fascinated chemists for decades. In particular copper-dioxygen complexes are suggested as key reaction intermediates in many enzymatic reactions. The differentiation in the function of these copper enzymes is attributed primarily to the coordination structure of the copper-dioxygen intermediate formed in the protein matrices, depending on the ligand donors, the geometry, and the coordination mode of the dioxygen. However, the correlation between these structural factors and the function/catalysis of the enzymes remains to be elucidated. To this end, there have been reported the structural and/or functional model complexes of copper-dioxygen adducts, such as μ -peroxo complex and μ - η_2, η_2 complex. The copper-bound dioxygen is not activated when it is end-on structure but activated via O-O bond cleavage when it is side-on structure. In order to investigate the relationships between electronic structure and reactivity of copper-dioxygen complex, we have examined ¹⁷O-NMR spectroscopies of several copper-dioxygen complexes.

VIII-G Molecular Mechanism of Heme Degradation and Oxygen Activation by Heme Oxygenase

Heme oxygenase (HO), an amphipathic microsomal proteins, catalyzes the regiospecific oxidative degradation of iron protoporphyrin IX (heme) to biliverdin IX α , carbon monoxide, and iron in the presence of NADPH-cytochrome P-450 reductase, which functions as an electron donor. Heme oxygenase reaction is the biosynthesis processes of bile pigments and CO which is a possible physiological messenger. Recent development in the bacterial expression of a soluble form of heme oxygenase has made it possible to prepare in the large quantities for structural studies. In this project, we are studying the molecular mechanism of heme degradation and the oxygen activation by heme oxygenase using various spectroscopic methods.

VIII-G-1 Molecular Oxygen Oxidizes the Porphyrin Ring of the Ferric α -Hydroxyheme in Heme Oxygenase in the Absence of Reducing Equivalent

MIGITA, Catharina T.¹; FUJII, Hiroshi; MATERA, Kathryn M.¹; TAKAHASHI, Satoshi²; ZHOU, Hong³; YOSHIDA, Tadashi³; IKEDA-SAITO, Masao¹

(¹Case Western Reserve Univ.; ²RIKEN; ³Yamagata Univ.)

[*Biochim. Biophys. Acta* **1432**, 203 (1999)]

Heme oxygenase catalyzes the regiospecific oxidative degradation of iron protoporphyrin IX (heme) to biliverdin, CO and Fe, utilizing molecular oxygen and electrons donated from the NADPH-cytochrome P450 reductase. The catalytic conversion of heme proceeds through two known heme derivatives, α -hydroxyheme and verdoheme. In order to assess the requirement of reduction equivalents, we have prepared the α -hydroxyheme complex with rat heme oxygenase isoform-1 and examined its reactivity with molecular oxygen in the absence of added electrons. Upon reaction with oxygen, a minor portion of the α -hydroxyheme in heme oxygenase is converted to verdoheme with the majority altered to a species which exhibits an optical absorption spectrum with a broad Soret band. The major species, which is EPR-silent, can be converted to the original α -hydroxyheme by addition of sodium dithionite. We have also found that oxidation of the α -hydroxyheme-heme oxygenase complex by ferricyanide or iridium chloride yields a species which exhibits an optical absorption spectrum and reactivity similar to those of the main product of the oxygen reaction. We infer that the oxygen reaction with the ferric α -hydroxyheme-heme oxygenase complex forms a ferric-porphyrin cation radical. We conclude, inconsistent to a previous report (Y. Liu, P. Moenne-Loccoz, T. M. Loehr and P. R. Ortiz de Montellano, *J. Biol. Chem.* **272**, 6909 (1997)), that in the absence of reducing agents, the oxygen molecule functions mainly as an oxidant for the porphyrin ring and has no role in the oxygenation of α -hydroxyheme. This result corroborates our previous conclusion that the catalytic conversion of α -hydroxyheme to verdoheme by heme oxygenase requires one reducing equivalent along with molecular oxygen.

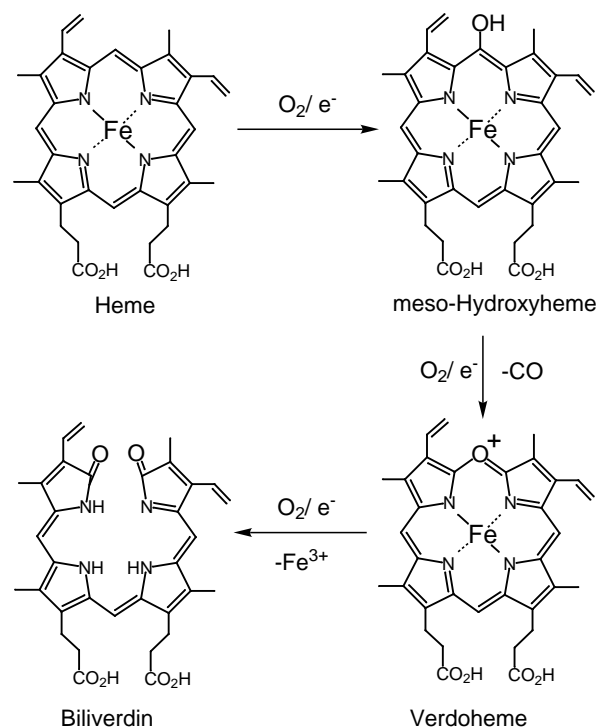


Figure 1. Reaction intermediates in the heme oxygenase catalyzed oxidation of heme to biliverdinIX α .

VIII-H Designing Artificial Photosynthesis at Molecular Dimensions

Photosynthesis is one of the finest piece of molecular machinery that Nature has ever created. Its ultrafast electron transfer and following well-organized sequence of chemical transformation have been, and will continue to be, challenging goals for molecular scientists. We are trying to mimic the function of photosynthesis by assembling molecular units that perform individual physical/chemical action. The molecular units include porphyrins, redox active organic molecules, and transition metal complexes.

Our present efforts focus on chemistry of manganese complexes (which are known to play a key role in oxygenic photosynthesis), and photochemistry of porphyrin/transition metal complex dyads. Our ultimate goal is to design artificial molecular systems that effect multiple chemical reactions triggered by light, on the basis of molecular rationale.

VIII-H-1 Synthesis and Characterization of Manganese Complexes

AIKAWA, Katsuji¹; NAGATA, Toshi
(¹Kyoto Univ.)

In search for rationally designed dimanganese complexes that catalyze four-electron oxidation of water to dioxygen, we developed two xanthene-based dinucleating ligands, XT-btpa and XT-bterpy (Figure 1).

The XT-btpa (xanthene-bis(tris(2-pyridylmethyl)-amine) ligand has two metal-binding sites that are located in a well-defined geometry determined by the rigid xanthene spacer. The manganese complex was found to have an $[\text{Mn}_2(\mu\text{-O})_2]$ core.

The XT-bterpy ligand also has two metal-binding sites with a well-defined geometry, and has two terpyridine units which provide more rigid and less decomposition-prone organic environment. Three manganese complexes, $[(\text{XT-bterpy})\text{Mn}_2\text{Cl}_4]$, $[(\text{XT-bterpy})\text{Mn}_2(\text{tropolonato})_2](\text{ClO}_4)_2$, and $[(\text{XT-bterpy})\text{Mn}_2(2\text{-picolinato})_2](\text{ClO}_4)_2$, were prepared; the X-ray structure of $[(\text{XT-bterpy})\text{Mn}_2\text{Cl}_4]$ is shown in Figure 2. Either of these three complexes catalyzed disproportionation of H_2O_2 to water and dioxygen, with much higher activity than the related mononuclear complex $[(\text{terpyridine})\text{MnCl}_2]$.

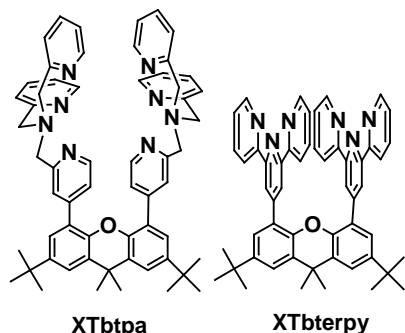


Figure 1. Two xanthene-based binucleating ligands.

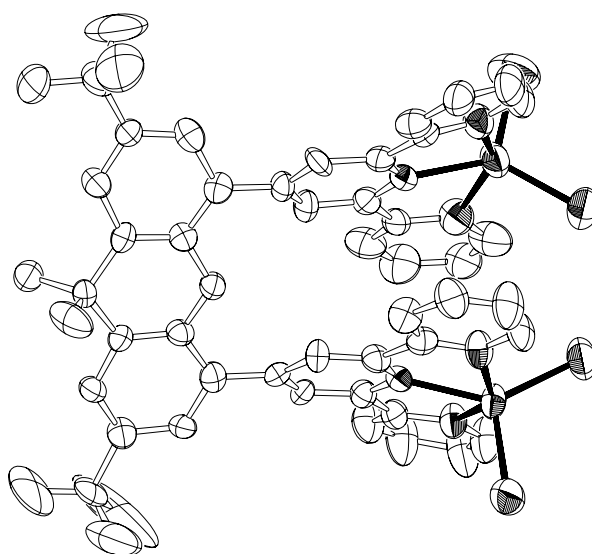


Figure 2. X-ray structure of $[(\text{XT-bterpy})\text{Mn}_2\text{Cl}_4]$.

VIII-H-2 Synthesis and Photochemical Reaction of Porphyrin/Cobalt-complex Dyad Molecules

KIKUZAWA, Yoshihiro¹; NAGATA, Toshi;
OSUKA, Atsuhiko¹
(¹Kyoto Univ.)

One of the essential features in natural photosynthetic reaction centers is ejection of the quinone acceptor from the protein to the "quinone pool," which takes place after photoinduced electron transfer. To mimic this function, we prepared a porphyrin/Co(III)-complex dyad molecule (Figure 1), where the Co(III) moiety is expected to depart from the porphyrin moiety after photoreduction, due to the relative instability of six-coordinate Co(II) complex. The steady-state fluorescence spectrum of this dyad molecule revealed that the excited singlet state of the porphyrin is effectively quenched by the presence of the Co(III) moiety. Electrochemical estimation of the reduction/oxidation potentials suggested photoinduced electron transfer from the excited porphyrin to Co(III) can take place. Irradiation of this dyad molecule in $\text{CD}_3\text{COCD}_3/\text{CD}_3\text{-CN}$ solution led to formation of the Co(III)- CD_3CN complex (80% yield by ^1H NMR) together with the imidazolyl porphyrin without the cobalt moiety. Since this ligand-exchange reaction proceeds only slowly in the absence of light, it is likely that the reaction is

catalyzed by intramolecular photoinduced electron transfer.

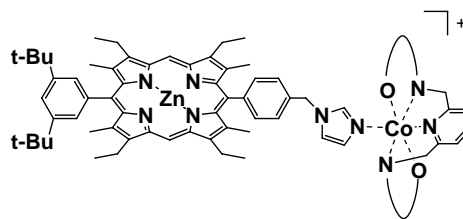


Figure 1. The porphyrin/cobalt(III)-complex dyad molecule.

VIII-I Development of New Metal Complexes as Redox Catalysts

Redox catalysis is an important field of chemistry which translates a flow of electron into chemical transformation. It is also one of the requisites for artificial photosynthesis. This project of ours aims at developing new metal complexes that perform redox catalysis at low overpotential. So far we have succeeded in preparing a series of terpyridine-catechol linked ligands; application of these ligands for development of new redox catalysts is currently in progress.

VIII-I-1 Synthesis of Terpyridine-catechol Linked Ligands and Their Cobalt(III) Complexes

NAGATA, Toshi; TANAKA, Koji

Transition metal catechol complexes are gaining interest because of unique electronic properties of the catechol ligand, specifically the two-electron redox transformation between catechol and quinone forms. Combination with the terpyridine ligand should provide metal complexes with interesting redox properties and well-defined geometry. The chemistry of terpyridine/catechol/metal ternary complexes, however, is often complicated by ligand disproportionation to give stable bis(terpyridine) complexes.

We prepared three terpyridine-catechol linked ligands (Figure 1) and their cobalt(III) complexes. The X-ray structure of two Co(III) complexes are shown in Figure 2. The two complexes have a different number of CH₂ units in the linker between terpyridine and catechol. It was revealed that the C₄ linked complex (part a) has a symmetric structure with the (CH₂)₄ linker running along an approximate mirror plane that contains the catechol ring and bisects the terpyridine ligand, whereas the C₅ linked complex (part b) has no such approximate symmetry. Since the local structures around the Co(III) center are very similar for the two complexes, the structural difference is solely due to the different lengths of the polymethylene linkers; the C₄ linker presents the "just fit" length while the C₅ linker has to go the winding way to accommodate the extra CH₂ unit.

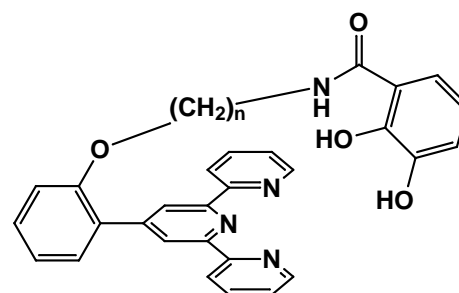


Figure 1. The terpyridine-catechol linked ligands.

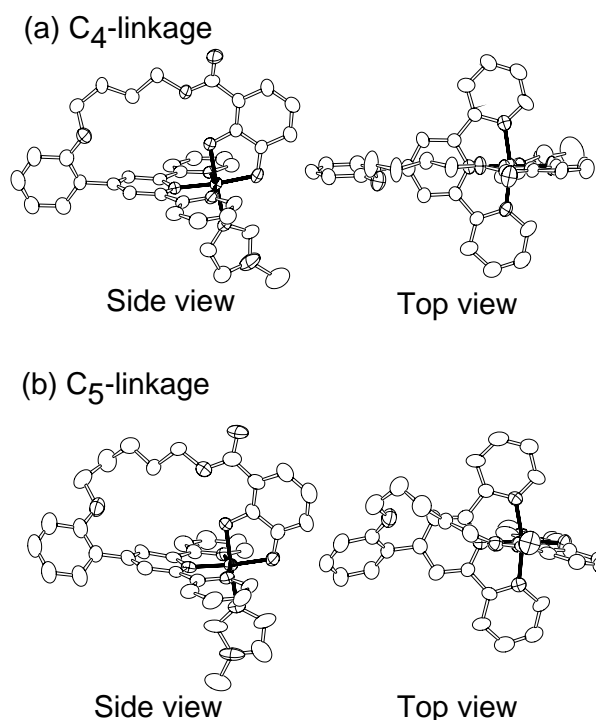


Figure 2. The X-ray structures of cobalt(III) complexes of the C₄- and C₅- linked ligands.

VIII-J Organic Molecular Materials with Novel Electronic Properties

Some aromatic and heterocyclic compounds show intriguing physical properties, such as superconductivity, ferromagnetism, and electroluminescence, in the solid state. The aim of our research is to design and synthesize such molecules. We have been working on three research projects: synthesis of organic conductors, fullerene chemistry, and organic electroluminescent (EL) materials.

VIII-J-1 Synthesis and Electron-Transporting Properties of Perfluorinated Decaphenylenes

**SAKAMOTO, Youichi; HEIDENHAIN, Sophie;
SUZUKI, Toshiyasu; TOKITO, Shizuo¹**
(¹Toyota Central R&D Labs.)

Recently, π -conjugated oligomers such as oligo-phenylenes and oligothiophenes have gained considerable attentions as organic electronic materials. Unlike polymers, these oligomers are monodisperse and can form clean thin films by vacuum deposition. If an electron-deficient oligomer forms a stable amorphous film and transports electrons with high mobility, it will be a good candidate for an electron-transporting material, which is an important component of highly efficient organic electroluminescent (EL) devices. Perfluorinated benzene rings are positively charged due to electronegative fluorine atoms and show intriguing interactions with electron-donating molecules due to quadrupole moments. We have developed the repetitive synthesis method of perfluorinated phenylenes **1-3** containing 10 phenyl rings. All $C_{60}F_{42}$ s are colorless solid and soluble in CH_3Cl , THF, and aromatic solvents such as toluene. The differential scanning calorimetry (DSC) curves indicated that decaphenylenes **1-3** have the glass transitions at $T_g = 123, 128,$ and $131\text{ }^{\circ}C$, respectively. The reduction potential peaks of the cyclic voltammograms (CV) shift more negative in the order **3** (-2.17 V), **2** (-2.24 V), and **1** (-2.49 V vs Fc/Fc^+) in THF. We fabricated organic EL devices with these perfluorinated compounds **1-3** to examine their electron-transporting properties. The luminance-voltage curves (Figure 1) indicated that **3** has the best electron-transporting ability in the three compounds.

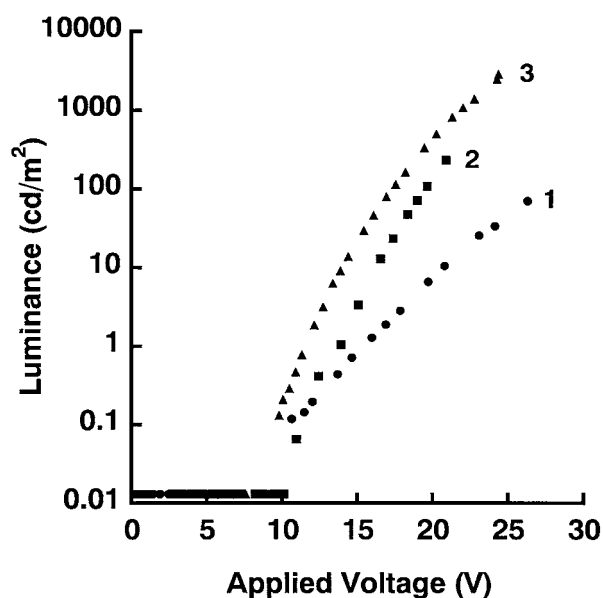
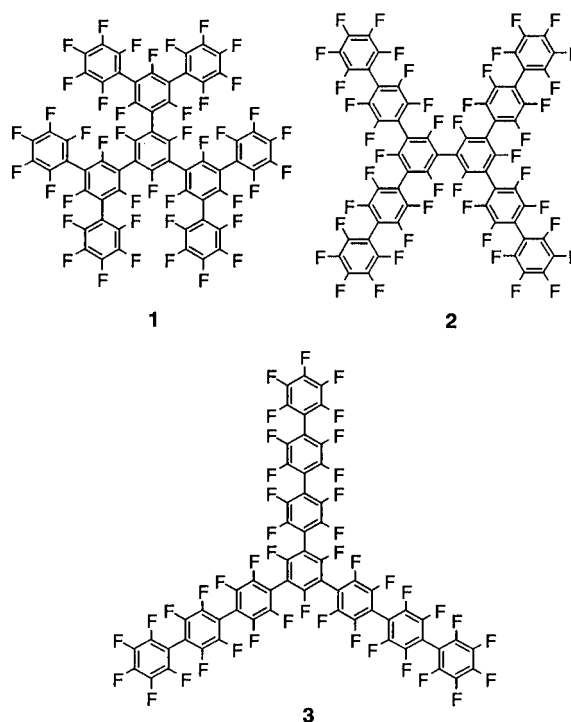


Figure 1. Luminance-voltage characteristics for the EL devices with **1-3** as electron-transporting layers: ITO/TPTE (60 nm)/Alq₃ (40 nm)/**1-3** (20 nm)/LiF (0.5 nm)/Al (160 nm).



VIII-K The Effects of the 2D Spin-Echo NMR Pulse Sequence on Homonuclear Spin Systems

Dipolar interactions for homonuclear spin systems are averaged out by magic-angle sample spinning (MAS). The 2D spin-echo NMR pulse sequence can reintroduce the influence of the homonuclear dipolar interactions into MAS powder signals.

VIII-K-1 Novel Satellites in a Two-Dimensional Spin-Echo NMR Spectrum for a Homonuclear Spin-1/2 Pair in Rotating Solids

KUWAHARA, Daisuke; NAKAI, Toshihito¹; ASHIDA, Jun²; MIYAJIMA Seiichi
(¹Tokyo Univ. Agric. Tech.; ²Kyoto Univ.)

[*Chem. Phys. Lett.* **305**, 244 (1999)]

We found additional resonance lines on both sides of the center line along the F1 axis, when the 2D spin-echo pulse sequence was applied to a solid-state ¹³C-¹³C spin system undergoing MAS. The lines are not attributed to well-known *J*-resolved doublets. To our surprise, the positions of the lines are determined by a quantity κ , which is a function of the sample spinning frequency and the difference of the isotropic chemical shifts. These lines were discovered for the first time as far as we know. The analysis based on a former publication was useful, but could not describe the general experimental scheme which employs an arbitrary value of t_1 increment. An arbitrarily chosen t_1 increment was applied for the experiments in the present study. The analytical representation for the 2D experiment is inevitable to explain the origin of the additional lines. We are now preparing such representation and the optimized simulation spectra.

Equipment Development Center

VIII-L Development of “IMS Machines”

The technical staff of the Equipment Development Center is partly engaged in planning, researching, designing and constructing “IMS machines.” This machine, crowned with the acronym of the Institute for Molecular Science, is a high-tech experimental instrument, with emphasis on new technical idea and co-operative work with members inside and outside the Institute including those in industries. We collect suggestions of new instruments once every year from all of the members of IMS.

In this fiscal year, 1998, three project themes (1 thorough 3) were adopted as IMS machines. IMS machine project 4 (IMS machine 1997) was completed, and project 5 (IMS machine 1997) is under way.

1. **Thin Shaped Cryostat for Opto-magnetic Measurement**
(proposed by Shinji IZUMIDA and Takuhiko KONDOH)
2. **Vibration Method Magnetometer**
(proposed by Yuko HOSOKOSHI, developed by Nobuo MIZUTANI and Yuko HOSOKOSHI)
3. **Preparation and Transfer System for Ice-embedding Sample**
(proposed by Toshio HORIGOME and Shinji HASEGAWA, developed by Mitsukazu SUZUI and Kazuhiro KOBAYASHI)
4. **Surface Profiler of Mirrors for High-Resolution Monochromator**
(proposed by Toyohiko KINOSHITA, developed with Hisashi YOSHIDA, Toshio HORIGOME, and Shuji ASAKA)
5. **Off-Axis Paraboloid Polarizing Mirror for Far-Infrared Light**
(proposed and developed by Hideyuki OHTAKE and Takayuki YANO)

VIII-L-1 Surface Profiler of Mirrors for High-Resolution Monochromator

YOSHIDA, Hisashi; HORIGOME, Toshio; ASAKA, Shuji; KINOSHITA, Toyohiko

We are developing a measurement apparatus for a precise profiling of surfaces of optical elements which are necessary for constructing high-resolution monochromators in UVSOR facility. The outline of the present apparatus is shown in Figure 1. The light beam from the laser (L) incidents upon the sample under measurement (S), and the reflected light on the sample surface is detected by light detectors (D1 or D2). By measuring the direction of the reflected light, we can derive the surface shape of the sample.

We adopted glancing incidence geometry to ease measurement on plane, spherical and non-spherical mirrors with length of 10 cm to 1 m, which are often used in synchrotron radiation facility. In the present setup the position of the reflected light displaces in a relatively wide range during a measurement. To cope with this we used Y-Z translation stages with linear scales and 4-division photodiode detectors.

In order to determine the direction of the reflected light beam, we need to know the positions of arbitrary two points on the beam. One position is measured by detector D2, and the other is measured by detector D1 by detecting the light that is partly reflected by the beam splitter (B).

The present optical system is very sensitive to mechanical vibration, temperature change and air flow. We fixed the whole components on an air-suspended vibration-free table and covered them with a plastic booth in order to stabilize the apparatus.

The outer view of the apparatus is shown in Figures 2 and 3.

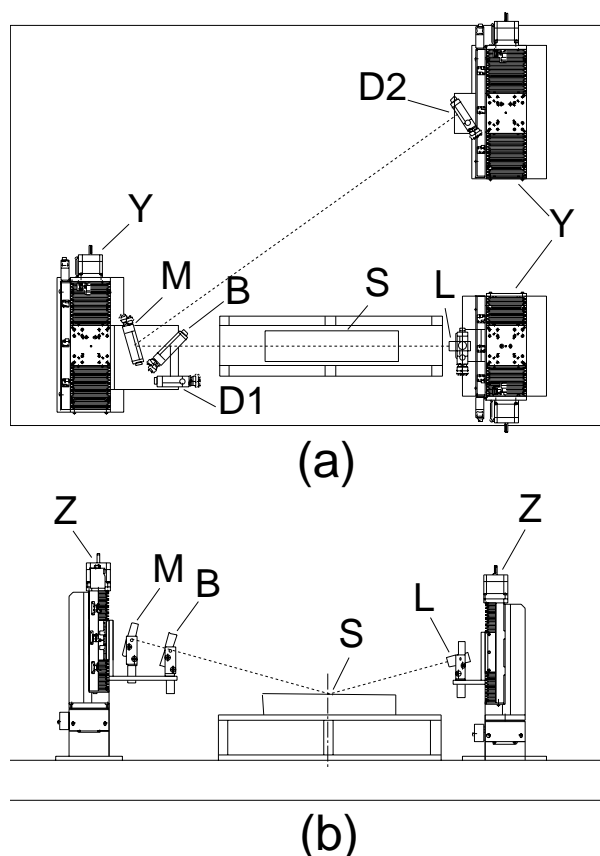


Figure 1. Design of the surface profiler. (a)Top view and (b)front view. L:Laser diode module, S:Sample mirror, B:Beam splitter, M:Mirror, D1 and D2:4-division photo diodes, Y and Z:Linear translation stages driven by stepping motors.

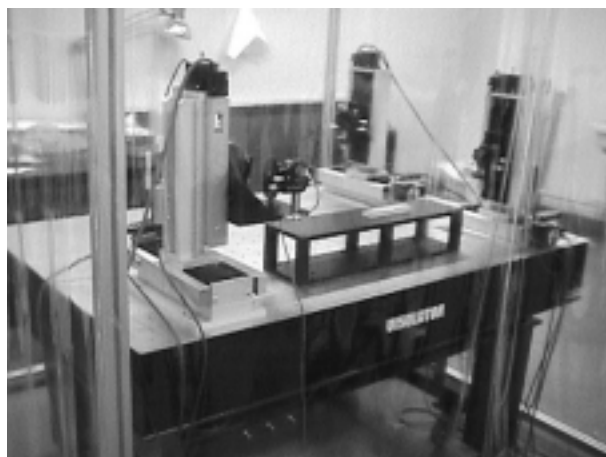


Figure 2. Surface profiler apparatus set up on a vibration-free table.



Figure 3. Driver for linear translation stage and host computer.

VIII-L-2 Preparation and Transfer System for Ice-Embedding Sample

HORIGOME, Toshio; HASEGAWA, Shinji; KOBAYASHI, Kazuhiro; SUZUI, Mitsukazu

Spectral measurement of ice-embedding bio-molecules under ultra high vacuum is promising for detailed understanding of their electronic structure. Few experiments, however, have been succeeded due to technical difficulty, except for electron microscopy. We have a project to develop the preparation and transfer system for ice-embedding sample that is applicable to various spectral techniques.

Figure 1 shows our contrivance to enable the photoemission measurement on ice-embedding bio-molecules. It is made up by three parts for sample preparation with liq. ethane, cryogenic transferring of sample to a measurement chamber, and fast evacuation with the aid of a special inner valve that separates between moderate and ultra high vacuum. Eighty percent of the whole system has been constructed. This system will be situated and work at UVSOR beamline after completion.

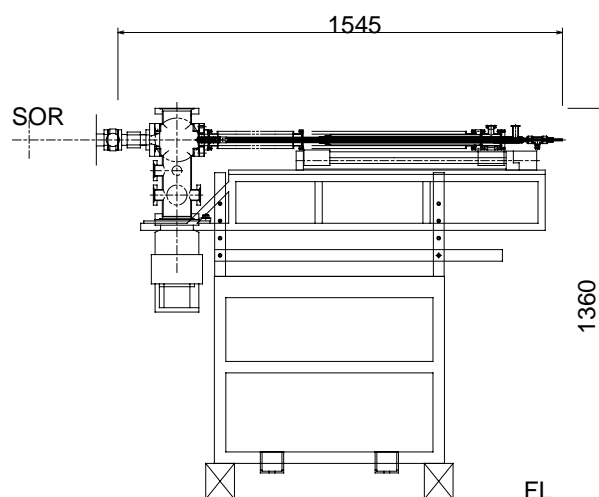


Figure 1. Preparation and transfer system for ice-embedding sample.

VIII-M Development of New Laser Materials

VIII-M-1 Amplification of Impurity-Associated Auger-Free Luminescence in Mixed Rubidium-Caesium Chloride Crystals under Core-Level Excitation with Undulator Radiation

MIKHAILIK, Vitalii B.¹; ITOH, Minoru²; ASAKA, Shuji; BOKUMOTO, Yoshiho²; MURAKAMI, Junichi²; KAMADA, Masao

(¹Lviv Franko State Univ.; ²Shinshu Univ.)

We obtained results of experimental studies aimed at testing the amplification of impurity-associated Auger-free luminescence (275 nm band) in mixed rubidium-caesium chloride crystals under core-level excitation with undulator radiation. The emission features observed under the best collimation of the optical cavity, namely the enhancement of the peak intensity,

the sharpening of the emission spectrum and the shortening of the luminescence decay, suggest a possibility of the light amplification due to inverted population between the valence and 5pCs-impurity core states.

Ultraviolet Synchrotron Orbital Radiation Facility

VIII-N Development of the UVSOR Light Source

VIII-N-1 Influence of Electron Beam Properties on Spontaneous Radiation from an Optical Klystron

HOSAKA, Masahito; YAMAZAKI, Jun-Ichiro; HAMA, Hiroyuki

[*Nucl. Instrum. Methods Phys. Res., Sect. A* **429**, 191 (1999)]

Spectrum of the radiation from an optical klystron is

very sensitive to the beam energy spread which is an important factor for the storage ring free electron laser. In order to make use of the spectrum for a measurement of the relative energy spread, we have investigated influences of the transverse beam property on the spectrum using a helical optical klystron on the UVSOR storage ring. From analysis of the experimental results, it has been found that the most important effect comes from inhomogeneous magnetic fields and a horizontal beam size.

VIII-O Researches by the USE of UVSOR

VIII-O-1 Nano-Second Desorption of Alkali Fluorides Excited by Synchrotron Radiation Pulses

KAMADA, Masao; TAKAHASHI, Naoshi; HIROSE, Sayumi¹

(¹Sumitomo Heavy Industry)

Desorption of the excited-state alkali atoms has been investigated on alkali fluoride crystals in the photon energy region of 20-75 eV, which includes the excitation energy for Li 1s-core excitons, Na 2p-core excitons, and valence excitations. The quantum yield of the excited-state alkali desorption was found to be comparable between valence and core-level excitations. Time response of desorption from LiF and NaF was also observed by using synchrotron radiation pulses. It was found that the time response consists of a nano-second component and slower one, indicating that the fast desorption is due to the lattice instability induced by electronic transition and the slow one is due to the thermal instability of surface defects.

VIII-O-2 Photo-Induced Change in Semiconductor-Vacuum Interface of p-GaAs(100) Studied by Photoelectron Spectroscopy

KAMADA, Masao; MURAKAMI, Junichi¹; TANAKA, Senku²; MORE, Sam Dylan; ITOH, Minoru¹; FUJII, Yasuo²

(¹Shinshu Univ.; ²Osaka City Univ.)

The photo-induced change in the semiconductor-vacuum interface on GaAs (100) and Cs/GaAs(100) has been investigated by using a photoelectron spectroscopic technique with synchrotron radiation and a mode-locked Nd:YAG laser. Both Ga-3d and As-3d photoelectron peaks showed transient energy shifts under the laser irradiation without any spectral change. The amounts of the energy shifts were strongly dependent on the sample temperature and the laser photon flux. It was found that the dependence fits well to the theoretical curve derived from the surface photo-voltage effect based on the band bending scheme in the surface layer of the semi-

conductor.

VIII-O-3 Electronic Structures of Organic Salts DMTSA-BF₄ Using Photoelectron Spectromicroscopy

HARUYAMA, Yuichi¹; KINOSHITA, Toyohiko²; TAKIMIYA, Kazuo³; OTSUBO, Tetsuo³; NAKANO, Chikako; YAKUSHI, Kyuya

(¹Himeji Inst. Tech.; ²Univ. Tokyo; ³Hiroshima Univ.)

The electronic structures of 1:1 charge-transfer organic salts DMTSA-BF₄, where DMTSA is 2,3-dimethyltetraseleno-anthracene, have attracted the interest of many researchers because of the high electrical conductivity and metallic physical property.¹⁾ The photoemission study for DMTSA-BF₄ has not been performed so far since DMTSA-BF₄ is not large enough to carry out the ordinary photoemission experiments. We succeeded to measure the photoemission spectra for DMTSA-BF₄ using the photoelectron spectromicroscopy.

Figure 1 shows the photon energy dependence of the photoemission spectra for DMTSA-BF₄. From the photon energy dependence of the photoionization cross-section, the atomic orbital characters of the observed spectral features are determined. The Se 4p states are located at ~1 eV, ~3 eV, and ~6 eV. The C 2p and F 2p states are located at ~8 eV. In our photoemission measurements, the clear Fermi edge was not observed. This suggests the importance of the electron correlation effect and/or one-dimensional nature for DMTSA-BF₄. The photoemission spectra for DMTSA were also measured in order to compare the electronic structures for DMTSA-BF₄. The Se 3d core level photoemission spectra did not show the chemical shift but the photoemission spectrum for DMTSA-BF₄ showed the tail at the higher binding energy side as compared with that for DMTSA. The difference of the electronic structures between DMTSA and DMTSA-BF₄ is discussed, based on the valence band and Se 3d core level photoemission results.

Reference

- 1) J. Dong, K. Yakushi, K. Takimiya and T. Otsubo, *J. Phys. Soc. Jpn.* **67**, 971 (1998).

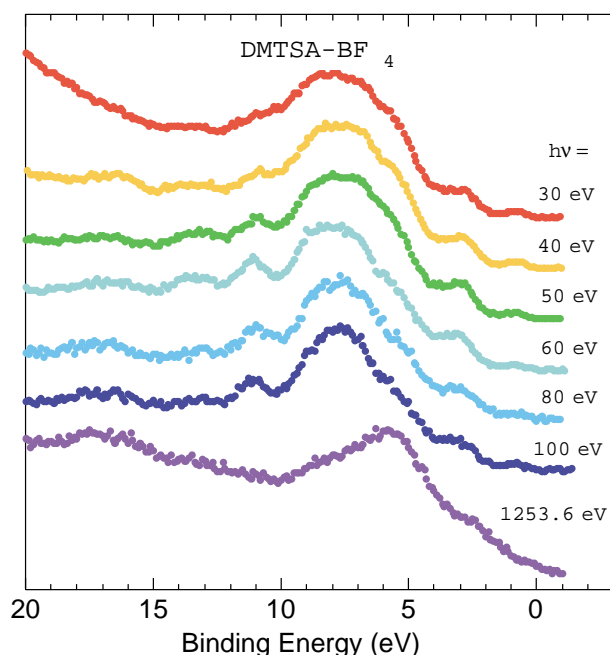


Figure 1. The photon energy dependence of the photoemission spectra for the organic salts DMTSA-BF₄.

VIII-O-4 Photoemission Study of Si(111) Clean Surfaces at High Temperature Using Laser Annealing

HARUYAMA, Yuichi¹; KINOSHITA, Toyohiko²; TANAKA, Shin-ichiro
(¹Himeji Inst. Tech.; ²Univ. Tokyo)

The electronic structures of Si (111) clean surfaces at high temperature have been studied using the photoemission spectroscopy. In the photoemission measurements, it is not easy to observe the electronic structures at high temperature because of the electric field used to anneal the sample to high temperature. By combining the laser annealing and the photoelectron spectromicroscopy, we demonstrate that the photoemission spectra at high temperature are easily obtained.

Figure 1 shows the temperature dependence of the photoemission spectra for Si (111) clean surfaces from room temperature to ~1200 °C. At room temperature, three surface states were observed at ~0.2, ~0.8 and ~1.8 eV. With increasing the annealing temperature, the surface state at ~0.8 eV disappears. The temperature dependence of the spectral features obtained in our measurements is essentially identical to that previously obtained by Yokotsuka *et al.*¹⁾ In addition, we found that the shift of the photoemission spectra was observed at ~0.2 eV higher binding energy side under 0.04~0.89 W laser irradiation. The shift at ~0.2 eV was also observed at the Si 2p core level photoemission spectra. With increasing the annealing temperature, the shift disappears at the laser power of 2.00 W. The observed shift indicates that the surface photovoltage effect²⁾ is caused by the photocarrier, which is induced by the laser irradiation. The disappearance of the surface photovoltage effect may be caused by the metallic nature of the high temperature semiconductor.

References

- 1) T. Yokotsuka, S. Kono, S. Suzuki and T. Sagawa, *Solid State Commun.* **39**, 1001 (1991).
- 2) J. E. Demuth, W. J. Thompson, N. J. DiNardo and R. Imbihl, *Phys. Rev. Lett.* **56**, 1408 (1986).

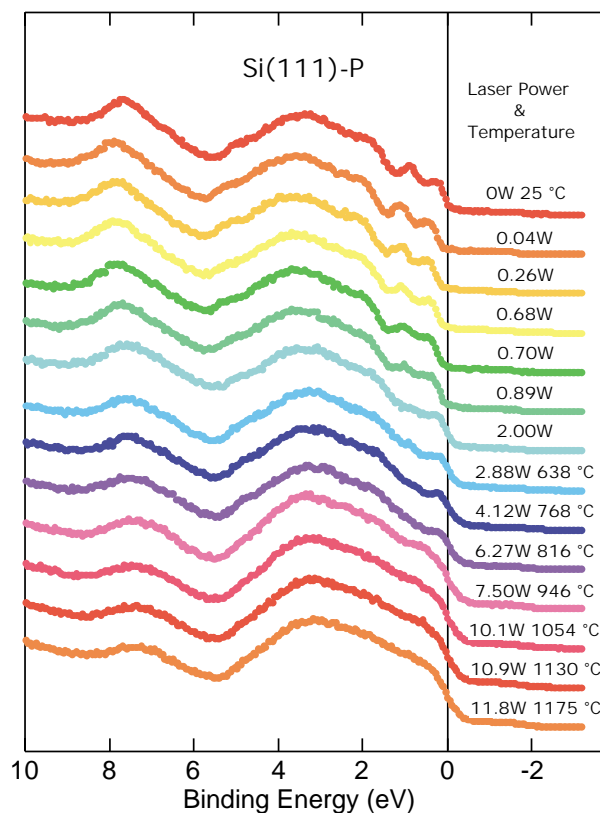


Figure 1. The temperature dependence for the Si (111) clean surface under laser irradiation.

VIII-O-5 Behavior of the “6eV Satellite” in Ni Thin Film Observed by Valence Band Photoemission

NATH, Krishna G.¹; HARUYAMA, Yuichi²; KIMURA, Shin-ichi³; UFUKTEPE, Yüksel⁴; KINOSHITA, Toyohiko⁵
(¹NTT; ²Himeji Inst. Tech.; ³Kobe Univ.; ⁴Univ. Cukurova, Turkey; ⁵Univ. Tokyo)

[*J. Electron Spectrosc. Relat. Phenom.* **101-103**, 257 (1999)]

It is now well established that the electronic structures of thin films are interestingly different from those of bulk. In case of 3d-transition materials, this difference is directly related to the changing of *d*-band width, exchange integral and the magnetic moment with changing of the film thickness.¹⁾ In such situation, any correlation-induced peak in the photoemission, such as Ni-6eV satellite also shows some interesting and varied feature depending on the film thickness. Another important aspect, that has to be considered, is the hybridization effect between the film and substrate. Here, we report the Ni valence band photoemission result for different thickness films on ferromagnetic Co(001) in order to study the 6 eV satellite feature and the resonant effect on magnetic dichroism signal for satellite.

In Figure 1, we show a series of Ni-valence band photoemission spectra taken at $h\nu = 67.2$ eV. The peak around the Fermi level is the main peak assigned by $3d^9$ state. Another peak stayed around 6 eV is the satellite assigned as $3d^8$ state. At $h\nu = 67.2$ eV, the satellite peak shows resonance enhancement.²⁾ The satellite peak positions for all films are indicated by dashed line. It is clear that satellite peak position is shifted to the higher binding energy for thicker films. The origins of this variation are the thickness dependent d -band width and the corresponding d - d correlation effect. For thicker films, the large width of d -band pushes the satellite peak higher binding energy position. In Figure 2, we show the resonance effect on magnetic linear dichroism (MLD) for satellite peak where the sample is 8ML Ni grown on 10ML Co. After comparing with off-resonant result in Figure 2 (b), we found that the in-plane MLD signal for satellite shows resonant behavior.

Reference

- 1) W. Clemens *et al.*, *Solid State Commun.* **81**, 739 (1992).
- 2) C. Guillot *et al.*, *Phys. Rev. Lett.* **39**, 1632 (1977).

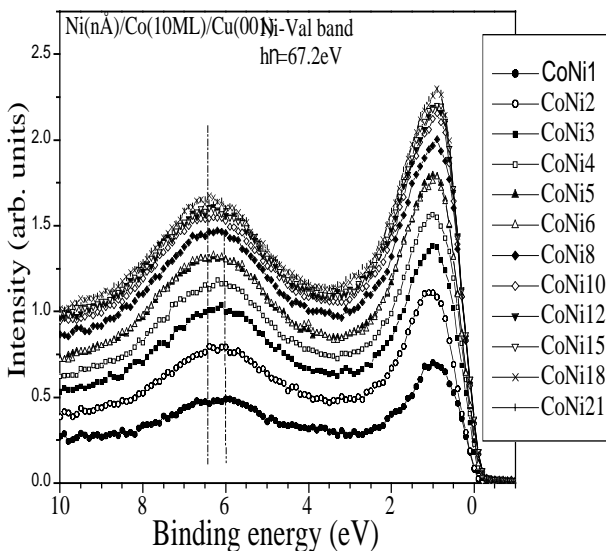


Figure 1. Ni-valence band photoemission spectra for Ni films of different thickness (1–21 Å). The peak around 6.5 eV is the satellite peak, which shows binding energy shift for thicker films as indicated by dashed line.

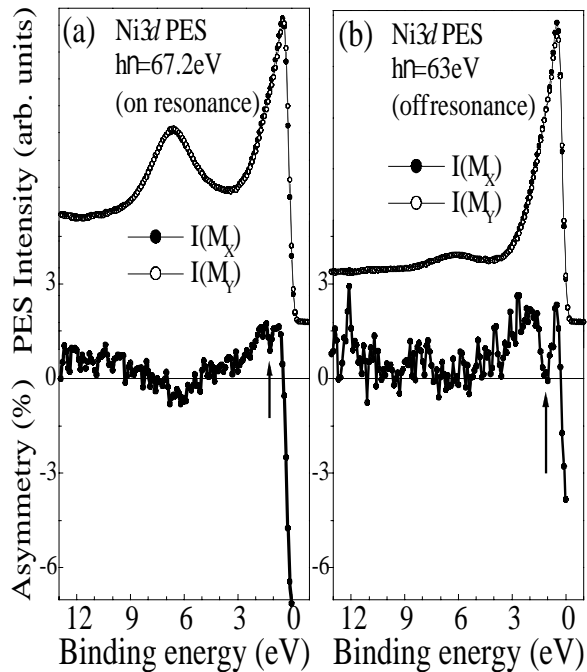


Figure 2. MLD for 8ML Ni on 10 ML ferromagnetic Co. In (a), MLD at on-resonance shows opposite trend for the main peak and the satellite peak. In (b), MLD at off-resonance where satellite shows weak MLD.

VIII-O-6 Magnetic Stability of Co-Film Grown on Oxygen-Rich Cu(001) Surface

NATH, Krishna G.¹; HARUYAMA, Yuichi²; KINOSHITA, Toyohiko³
(¹NTT; ²Himeji Inst. Tech.; ³Univ. Tokyo)

From the points of view of both technological application and fundamental research, it is a common intention to grow metal film on very clean surface (surface without any contamination). Using of clean substrate ensures the perfect crystalline growth, defect-free interface, and in the case of magnetic film, the magnetic stability. Oxygen is considered to be the most defined contamination from which we want to get ride of for getting good epitaxy. But oxygen can be also used as a surfactant¹⁾ (which promotes the layer-by-layer or well-shaped island growth). In the present study, we report the magnetic behavior of Co films grown on oxygen-rich Cu(001) substrate. We also checked the electronic structures, reconstruction phases, surfactant effect *etc.*

Figure 1 shows the magnetic dichroism (a technique to study the magnetism) results for two systems, (a) 5ML Co on clean Cu(001) and (b) 5ML Co on oxygen-rich Cu(001) surface. The oxygen-rich Cu, oxidized by 1200L oxygen, shows $(\sqrt{2} \times \sqrt{2})R45^\circ$ -O reconstructed phase in LEED pattern. The 5ML Co film was then deposited on that oxidized Cu and was characterized by XPS and LEED. It was found that oxygen was segregated to Co surface and promotes to grow the $c(2 \times 2)$ reconstructed phase. The new state of oxygen on Co is the chemisorbed state. The interesting observation is that this reconstructed phase of Co also shows almost similar magnetic behavior to Co on clean Cu. The order

of dichroism signal is nearly same for both cases [as seen in Figure 1(a) and Figure 1(b)]. Therefore, it can be said that the large amount of oxygen on the Cu before Co deposition does not cause any negative effect on the magnetic (ferromagnetic phase) stability of Co film.

Reference

1) C. Tolkes *et al.*, *Phys. Rev. Lett.* **80**, 2877 (1998).

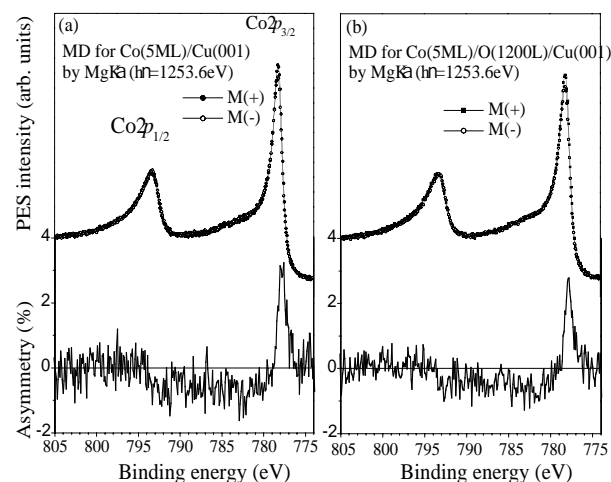


Figure 1. The MUDAD (magnetic dichroism in angular distribution by unpolarized light) for 5ML Co on fresh Cu [in (a)] and on oxidized Cu [in (b)]. The Co 2p peaks were measured for the two-magnetization directions. The almost same order of dichroism signal confirms the magnetic stability of Co films on oxygen-rich Cu.

VIII-O-7 Thickness Dependent Oxidization of Co Films and Observation of Different CoO Phases

NATH, Krishna G.¹; HARUYAMA, Yuichi²; KIMURA, Shin-ichi³; KINOSHITA, Toyohiko⁴
(¹NTT; ²Himeji Inst. Tech.; ³Kobe Univ.; ⁴Univ. Tokyo)

The bulk CoO is a well-known Mott insulator and shows strongly correlated nature. It is known that CoO can be also obtained by oxidization of bulk Co or Co-film. In case of bulk Co, the entire oxidization process is confined to only hcp structure, the only available phase at room temperature. By using artificial Co thin film, we can vary the oxidization process as growth behavior of Co on other metal, *e.g.* Cu(001), differs depending on the thickness. For example, Co films of less than 2ML on Cu show different sizes of island, whereas more than 2ML Co films grow in layer-by-layer mode and show fct (face center tetragonal) structure. We have studied the core level photoemission by growing CoO for different thickness of Co films.

Figure 1 (a), shows the Co2p photoemission spectra for clean and oxidized Co films, where the thickness of the Co is 1.3, 2.3, 3.6, and 5ML, respectively. The films were oxidized by almost same amount of exposure. In (a), spectra with symbols are for oxidized Co and solid lines are for clean ones. Peak at binding energy 778.0 is from elemental Co. Peak at 780.2 eV (dashed line) is assigned to be $d^8\bar{L}$ (L stands for ligand hole state) and the higher binding energy satellite (dotted-dashed line)

is assigned as the final state with a mixture $d^9\bar{L}^2$ and d^7 states on the basis of charge transfer (CT) theory¹⁾ for CoO. The results show that the thinner films are more reactive and show an early formation of CoO. In Figure 1 (b), the difference between the saturated CoO phase for 1ML and 10ML Co films is shown. It is noticed that the features for thinner film seem to be broader. Here we predict that the difference spectrum shown in this figure probably represents the 2D CoO phase, which is different from the bulk CoO phase.

Reference

1) K. Okada *et al.*, *J. Phys. Soc. Jpn.* **61**, 449 (1992)

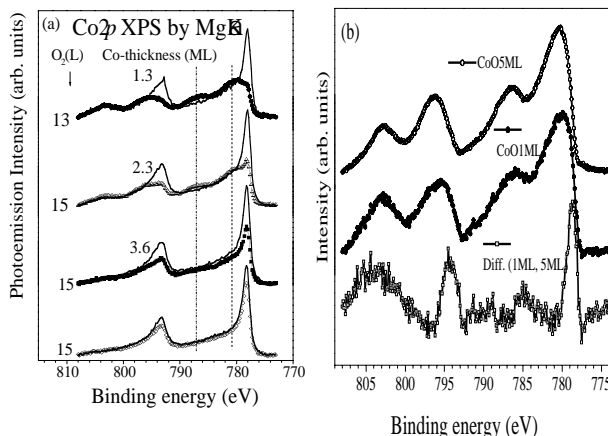


Figure 1. Co2p XPS for different Co films. In (a), the solid spectra for elemental Co and spectra with symbol for oxidized Co films. In (b), the spectra of saturated CoO phase for 1ML and 5 ML Co films and their “difference spectrum.”

VIII-O-8 Satellite Structure Observed in 2p XPS of Co Thin Film

NATH, Krishna G.¹; HARUYAMA, Yuichi²; KINOSHITA, Toyohiko³
(¹NTT; ²Himeji Inst. Tech.; ³Univ. Tokyo)

Satellite structures in the photoemission spectra for 3d-transition metals have been frequently reported for more than twenty years.¹⁾ The well-known example of the satellite structure is the 6eV-satellite in Ni valence band and core level photoemission.²⁾ It is now established that the *d-d* interaction is the origin of the formation of satellite. This interaction might take a strong value at the surfaces and interfaces where the reduction of dimension exists along the surface normal. Therefore, we may expect the variation of satellite intensity if the thickness of the thin film system is considered to be a variable. At the same time, the hybridization between the film and the substrate might play an important role for observing the satellite.

Figure 1 shows the Co2p_{3/2} XPS spectra for different thickness of Co films on the clean Cu(001) substrate. As shown in the figure, we observe a regular change in the four spectra for the both main peak (upper inset) and the satellite region (lower inset). In the case of 1 ML film, the film structure is considered not to be homogeneous, but island type. This situation may make different charge distribution (less *d*-hole) in the valence band at the Co-site. As a result, the chemical environment of the

atom from where the core electron is outgoing is changed. Therefore, the charge transfer process with the Cu and the Coulomb interaction may differ from these in thicker film. The situation causes the binding energy shift for the main peak. In case of satellite region (in lower inset), the intensity difference is also apparent. For 1 ML film, the states around 779.5–783.0 eV binding energy is more intense than those in other films. This is shown clearly in the difference spectra between 1 ML and 10 ML films. The reasons for intense satellite in 1 ML film are the stronger *d-d* correlation and less hybridization with the substrate states.

References

- 1) S. Raaen, *Solid State Commun.* **60**, 991 (1986).
- 2) S. Hüfner *et al.*, *Phys. Lett. A* **51**, 299 (1975).

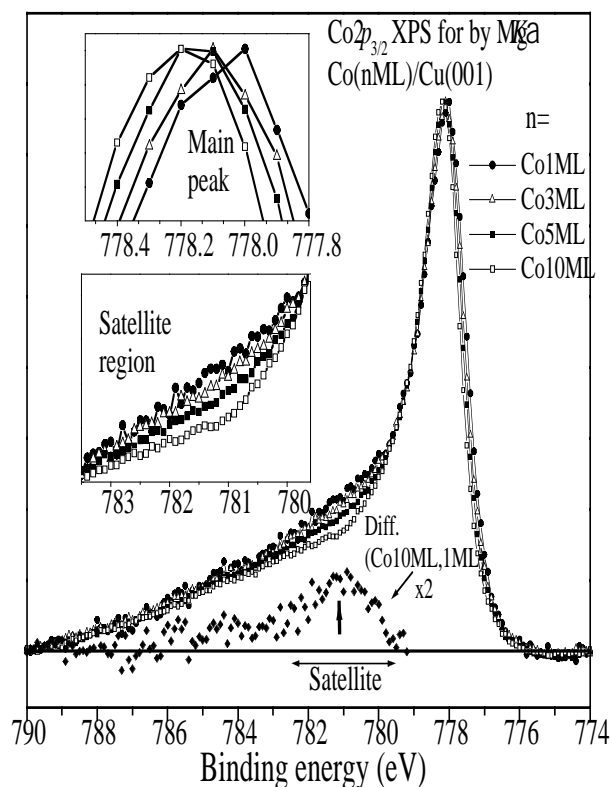


Figure 1. $\text{Co}2p_{3/2}$ photoemission spectra for 1, 3, 5 and 10 ML Co films on Cu(001). **Upper inset.** The binding energy difference in the main peak. **Lower inset.** The intensity difference around the satellite region. This difference is clear in the “difference spectrum” of 1 ML and 10 ML (shown underneath of four spectra).

VIII-O-9 Design Study for a Varied-Line-Spacing Plane Grating Monochromator

SHIGEMASA, Eiji; TAKATA, Yasutaka; GEJO, Tatsuo

Recent conceptual and technological improvements to monochromators have enabled us to realize various studies on vibrational spectroscopy in the soft x-ray range (100–1000 eV), which contains the *K*-shell thresholds of chemically important elements like C, N, and O, even without the use of undulator radiation. At the UVSOR, there is only one monochromator for high

resolution spectroscopy in the photon energy region of interest (250–550 eV). A maximum resolving power of 4000 at 400 eV is achievable with this monochromator, but due to a little complicated scanning mechanism, it has difficulty maintaining such high resolution in the entire photon energy range. Design study for a new monochromator has recently been started in order to improve the situation. A Varied-line-spacing Plane Grating Monochromator (VPGM) has been chosen for this work. Thanks to the availability for high quality gratings and simple scanning mechanism, VPGM seems to be one of the most trustworthy monochromators to realizing high resolution in the soft x-ray range. Figure 1 shows a layout of the optical elements of the present VPGM. The resolution of this monochromator was studied by ray-tracing simulation as well as analytical estimation. This study shows that a resolving power of more than 5000 is achievable over the energy range from 250 to 550 eV with one single grating having the groove density of 1000 l/mm.

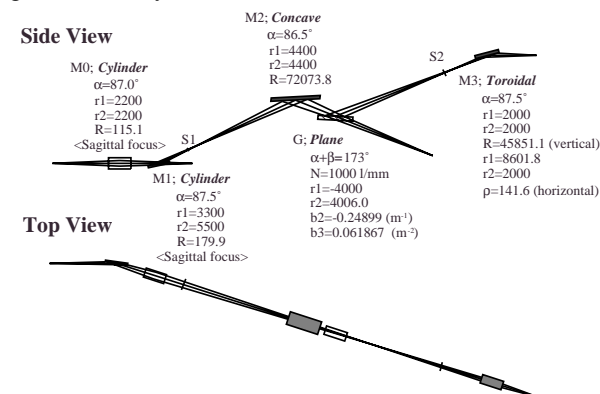


Figure 1. Schematic layout of the designed monochromator.

VIII-O-10 Photodissociation of Ozone in the K-Edge Region

GEJO, Tatsuo; OKADA, Kazumasa¹; IBUKI, Toshio²; SAITO, Norio³

(¹Hiroshima Univ.; ²Kyoto Univ. Edu.; ³ETL)

[*J. Phys. Chem. A* **103**, 4598 (1999)]

Ozone is one of the most important molecules in chemistry since ozone in the stratosphere absorbs UV light emitted from the sun and prohibits humanity from the exposure by the UV light. We have investigated the photochemistry and photodissociation dynamics of Ozone in *K*-edge region with angle-resolved time-of-flight apparatus for the first time. The β values and kinetic energy distributions were calculated from simulation of the TOF spectra obtained. The β value of O^+ at an excitation energy of 529.0 eV is -0.7 , which is consistent our previous assignment that the 529 eV band comes from the $\pi^*(2b_1) \leftarrow 1s(2a_1)$ transition. In contrast to this, the β value at an excitation energy of 535.7 eV is -0.3 . This implies that the transition moment does not lie perpendicular to the molecular plane and that this band should be mixed by more than two transitions. They are consistent with the previous assignments¹⁾ that the 529 eV band is the $\pi^* \leftarrow \text{O}_T(1s)$ resonance excitation and that the 536 eV band is mainly

consisted of two transition, the $\pi^*(2b_1) \leftarrow O_C(1s)$ and the $\sigma^*(7a_1) \leftarrow O_T(1s)$.

Reference

- 1) T. Gejo, K. Okada and T. Ibuki, *Chem. Phys. Lett.* **277**, 497 (1997).

VIII-O-11 Infrared Magnetic Circular Dichroism of Strongly Correlated 4f Electron Systems with Synchrotron Radiation

KIMURA, Shin-ichi

[*Jpn. J. Appl. Phys., Part 1* **38**, 392 (1999).]

Magnetic circular dichroism (MCD) experiment in the infrared region using synchrotron radiation has been done for the first time. Since the off-axis component of the synchrotron radiation is circular polarization in itself, a MCD spectrum in wide energy range can be measured easily by using the infrared synchrotron radiation. The experimental method is suitable for the investigation of strongly correlated electron systems because the electronic structure, which is made by magnetic many-body interactions, is located in the wide energy region near the Fermi level.

VIII-O-12 Optical Conductivity of the Kondo Insulator YbB₁₂: Gap Formation and Low-Energy Excitations

OKAMURA, Hidekazu¹; KIMURA, Shin-ichi; SHINOZAKI, Hidenori¹; NANBA, Takao¹; IGA, Fumitoshi²; SHIMIZU, Naoya²; TAKABATAKE, Toshiro²

(¹Kobe Univ.; ²Hiroshima Univ.)

[*Phys. Rev. B* **58**, R7496 (1998)]

[*Jpn. J. Appl. Phys. Series 11*, 85 (1999)]

[*Physica B* **259-261**, 317 (1999)]

Optical reflectivity experiments have been conducted on single crystals of the kondo insulator YbB₁₂ in order to obtain its optical conductivity, $\sigma(\omega)$. Upon cooling below 70 K, a strong suppression of $\sigma(\omega)$ is seen in the far-infrared region, indicating the opening of an energy gap of ~25 meV. This gap development is coincident with a rapid decrease in the magnetic susceptibility, which shows that the gap opening has significant influence on magnetic properties.

RESEARCH FACILITIES

The Institute for Molecular Science includes five research facilities. This section describes their latest equipment and activities. For further information please refer to older IMS Annual Review issues (1978–1998).

Computer Center

The main computers at the Center are a supercomputer NEC SX-3/34R, NEC SX-5, NEC HPC and IBM SP2. The computers are linked to international networks through Science Information Network (SINET). About 30% of the computer time is used by the research staff at IMS, and the remaining 70% is given out as research grants to scientists outside the institute in molecular science and related field. As of March 1998, the number of project group was 174, consisting of 704 users.

In September, 1998, the SGI Origin 2000 parallel CPU Server was installed.

The library programs of the Center amount to 805. Among them, more than 200 programs can be executed immediately. Information on the library program can be found on our center's home-page (<http://ccinfo.ims.ac.jp/>). The Quantum Chemistry Literature Database (QCLDB) has been developed by the QCLDB group in collaboration with the staff member of computer center, and this database can be accessible through our home page.

Laser Research Center for Molecular Science

This Center was established in 1997 by reorganization of a part of the Instrument Center. The new Center is composed of three research groups which are asked to develop new lasers suitable for pioneering researches in the new field of molecular science. The three groups are

1. Advanced Lasers for Chemical Reaction Studies,
 2. Advanced Lasers for Synchrotron Radiation Applications
- and
3. Advanced UV and IR Tunable Lasers.

The Laser Research Center are newly equipped with profitable all-solid-state light sources in various temporal and spectral regions, including femtosecond and nanosecond Optical Parametric Oscillators (OPO). The synchronously femtosecond OPO (OPAL; SPECTRA PHYSICS) is tunable from 1.1 μm up to 1.6 μm . The nanosecond OPO has extraordinarily wide tuning range from 420 nm down to 2.2 μm . The Laser Center also has a fluorescence analyzer (FLUOROLOG2; SPEX) which is composed of a xenon lamp house, and double and single monochromators for spectroscopy. The detector is changeable by rotating a mirror (CCD and PM). Using these instruments, one can carry out various experiments not only in the ultrafast temporal region but also in the steady-state photon-counting region.

Research Center for Molecular Materials

The center was established by reorganization of Chemical Materials Center, Low-Temperature Center, and a part of Instrument Center in 1997. This center plays an important role in the synthesis and purification of chemical substances. The scientists of this facility carry out their own researches on synthesis of new interesting compounds. Upon request, technicians carry out elemental and mass spectrometric analyses. Laboratory waste matters are also managed here. This center continues the task of Low-Temperature Center which supplies liquid helium and liquid nitrogen to the users in IMS. The total amount of liquid helium and nitrogen supplied from June, 1998 to May, 1999 were 45,097 and 63,064 L, respectively. The center is also equipped with various types of instruments such as NMR, ESR spectrometers and X-ray diffractometers for general use.

Equipment Development Center

A number of research instruments have been designed and constructed at the mechanical, electronic and glass work sections in this Facility. Examples of our works in this fiscal year are listed below.

- Cylindrical hexapole deflector
- Mirror mount for UV laser cavity
- Cylinder for pressure clamp cell made with TiCu alloy
- Mesh filter/photocurrent monitor for a pre-mirror in the beam line
- Lissajous cell holder
- Teflon lens for millimeter wave spectroscopy
- Pulsed supersonic jet nozzle for microwave spectroscopy with a position adjusting system
- Electron impact ionization slit-jet nozzle
- Laser induced fluorescence microwave double resonance spectrometer
- Mount frame for thermal desorption analysis system
- Simple 80 MHz data logger unit with high speed A/D converter
- Precise temperature controller for ^3He refrigerator
- Floating high voltage pulse generator

High speed 14-bit A/D converter
 Quartz cell
 Quartz nozzle for dye laser
 Distiller with safety against bumping

Development of IMS Machines

Equipment Development Center is also engaged in developing IMS Machines. This activity is described in detail in section "RESEARCH ACTIVITIES."

Ultraviolet Synchrotron Orbital Radiation Facility

The UVSOR accelerator complex consists of a 15 MeV injector linac, a 600 MeV booster synchrotron, and a 750 MeV storage ring. The magnet lattice of the storage ring is the so-called double bend achromat. A harmonic cavity was commissioned in Spring 1993 to suppress longitudinal coupled-bunch instability by Landau damping. The double rf system is routinely operated for user beam time, and the lifetime of the beam has been improved to about 5 hours at 200 mA. The storage ring was divided into four sections by gate valves in Spring 1995 in order to make a scheduled shutdown easier. The baking system was also replaced by new one including a controllable indirect heating. The rf power amplifier systems of the booster synchrotron and the storage ring were renewed to solid-state systems in 1996 in order to have more stable operation and easier maintenance. The storage ring is normally operated under multi-bunch mode with partial filling. The single bunch operation is also conducted about three weeks in a year to provide pulsed SR for time-resolved experiments. A resonance transverse kicker was installed in Spring 1997 to keep the bunch purity and to study phase dynamics. Typical beam currents under multi-bunch and single-bunch modes are 200 mA and 50 mA, respectively.

The UVSOR storage ring consists of eight bending magnets and three insertion devices. The bending magnet having 2.2 m in radius provides the synchrotron radiation, the critical energy of which is 425 eV. The superconducting wiggler is a wavelength shifter type. The 4 T magnetic field can provide soft x-rays up to 6 KeV. A planar undulator consists of 24 pairs of permanent magnets, a period of which is 84 mm. The fundamentals from the undulator provide quasi-monochromatic intense radiation in the range from 8 to 52 eV. A helical undulator was installed to one of the four straight sections of the storage ring in 1996. An optional version of the helical undulator is a helical optical klystron, which is powerful for a free electron laser experiment. The helical undulator consists of two sets of permanent magnets producing a vertical magnetic field and four sets of permanent magnets making a horizontal magnetic field. The four sets of magnets can move in the transverse direction to switch the helicity of the circular polarization. The helical undulator can provide the perfectly circular polarization in the range of 2–45 eV, and the elliptic polarization up to 200 eV. Unfortunately, the superconducting wiggler was shutdown at the beginning of June in 1999 due to the serious problem of the cryogenic system. Initially 15 beam lines were constructed giving priority for the study of the four fields; "Spectroscopy," "Photoelectron spectroscopy," "Photochemical reaction," and "Elementary process of chemical reaction." Several years later, 4 beam lines were added to expand the research to the fields, "Solid and surface photochemical reaction" and "Photochemical material processing." In recent years, "Combination of synchrotron radiation with laser beam" was proposed to be added in the important research fields.

The UVSOR have discussed the improvements and upgrades of the beam lines with users. The workshops concerning on VUV beam lines for solid-state research, beam lines for soft x-ray, chemical reaction, and gas phases, beam lines for infrared and far infrared regions, grazing incidence monochromators, and temporal structure of SR and its application were held in 1994, 1995, 1996, 1997, and 1998, respectively. About one third of beam lines have been upgraded in a couple of years. A Seya-Namioka monochromator at beam line 7B has been replaced by a normal-incidence monochromator to improve a resolving power and spectral range for solid state spectroscopy. Another Seya-Namioka monochromator at beam line 2B2 has been also replaced by a Dragon-type monochromator for gaseous experiments in VUV and EUV ranges. A multi-layer monochromator installed to the beam line 4A has provided good spectral distribution for photo-chemical reaction experiments. A 15 m SGM monochromator, which took back of a glancing-incidence monochromator at BL8B1 has been used for solid and gaseous phase experiments with high resolving power in EUV range. A Bruker FT-IR interferometer has been installed to beam line 6A1 besides the old FT-FIR of a Martin-Puplett type, and then the improved system can cover the wide wavelength range from 1 mm to 3 mm. A new monochromator (SGM-TRAIN) constructed at beam line 5A has been used for the experiments on solid and surface with high resolving power. Beam line 2A, which has provided VUV photons for gaseous experiment for a long time, is under renewal for the use of the bio-specimens. The UVSOR has now two soft-x-ray stations equipped with a double-crystal monochromator, eight extreme ultraviolet stations with a glancing incidence or a plane-grating monochromator, four vacuum-ultraviolet stations with a Seya-Namioka-type or a normal incidence-type monochromator, two (far) infrared stations equipped with FT interferometers, a multi-layer monochromator, and three white-light stations without monochromator.

The photoelectron spectroscopy combined with SR is one of the powerful techniques to investigate electronic structures. Several kinds of photoelectron spectrometers are working or ready to work in UVSOR: High-performance electron analyzer at soft x-ray beam line 1A, Two-dimensional spectrometer at VUV beam line 3B, Angle-resolved spectrometer at EUV beam lines 6A2 and 8B2, Photoelectron microscopy system (sometimes this system can be used at another beam line 5B), and Spin- and angle-resolved photoelectron spectrometer at helical undulator beam line 5A besides a high-resolution type. The details are given in the *UVSOR ACTIVITY REPORT*,

which is annually published.

There were lots of troubles, especially electricity-related troubles, in 1998. The capacities for a booster synchrotron were burst in autumn in 1998, resulting in the 3-weeks shutdown. The rotary pumps stopped suddenly due to the breakdown of the conducting coils. Heating cables touched the ground, resulting the electric leakage at BL4A. The monitor system was improved in this spring to watch the electric leakage. Besides these common problems to old facilities in the world, air-leak trouble happened at BL3B. Fortunately, our fast-closing valve system could succeed in protecting the storage-ring from the leakage. We had also several troubles due to careless actions by users in 1998. All these accidents pushed us to confirm the alarm/emergency call system and also the education/safety system for beginner users. New version of the UVSOR guidebook will be published for this purpose. The UVSOR facility strongly asks all users to conduct their experimental procedures according to the beam line manuals and the guidebook.

The persons who want to use the open- and the in-house beam lines are recommended to contact with the station master or supervisor and the representative, respectively. The persons who want to know updated information of the UVSOR facility are requested to open <http://www.uvsor.ims.ac.jp/>.

SPECIAL RESEARCH PROJECTS

IMS has special research projects supported by national funds. Three projects in progress are:

- (1) Development of microscopic environments with functionality and quantum steering for reactions
- (2) Study of molecular solid toward molecular electronics
- (3) Material control in multi-reaction centers

These three projects are being carried out with close collaboration between research divisions and facilities. Collaborations from outside also make important contributions. Research fellows join these projects.

(1) Development of Microscopic Environments with Functionality and Quantum Steering for Reactions

Structures, Reactions and Spectroscopies of Molecules and Clusters

IWATA, Suehiro; TEN-NO, Seiichiro; IKEGAMI, Tsutomu; TSURUSAWA, Takeshi; SATOH, Katsuhiko; CHEN, Feiwu¹; HIRATA, So; OKADA, Kazutoshi²; HASHIMOTO, Tomohiro³

(¹JAT; ²GUAS; ³JST and Keio Univ.)

Ab initio molecular orbital methods were applied to various chemical and physical problems. The density functional theory were also used in some of the studies. Most of works were carried out under close collaboration with several experimental groups. In addition new theoretical techniques in molecular electronic calculations were developed. The followings are the titles the topics we have worked in the last year.

- A. Development of New Theoretical and Numerical Techniques in the Study of Molecular Structure
- B. Water Clusters and Their Complexes with Atomic Ions
- C. Computational Chemistry of Atomic and Molecular Processes in Atmospheric Environment
- D. Application of Ab Initio Molecular Orbital Methods to Experimentally Relevant Systems

Folding Mechanism of Protein Molecules Studied by Generalized-Ensemble Algorithms

OKAMOTO, Yuko; SUGITA, Yuji; NISHIKAWA, Takeshi; MITSUTAKE, Ayori¹; OHTSUKA, Hiroshi¹ (¹GUAS)

Proteins are the most complicated molecules that exist in nature. Since protein Structures are closely related to their biological functions, the understanding of their folding mechanism from the first principles is not only very challenging but also very important a problem in theoretical molecular science. To be more specific, it is widely believed that three-dimensional structure of proteins is determined by their amino-acid sequences. However, nobody has succeeded in predicting it solely from the amino-acid-sequence information (prediction from the first principles.) There are two reasons for the difficulty. One reason is that the inclusion of accurate solvent effects is non-trivial because the number of solvent molecules that have to be considered is very large.

The other reason for the difficulty is that there exist huge number of local minima in the energy function,

and conventional simulation techniques necessarily get trapped in one of the local minima without ever finding the energy global minimum. Generalized-ensemble algorithms are new simulation algorithms that can alleviate this difficulty (for reviews, see References 1 and 2).

The goal of the present project is to further develop and test the effectiveness of generalize-ensemble algorithms in the protein folding problem and to succeed eventually in the prediction of tertiary structures of proteins from the first principles.

References

- 1) Y. Okamoto, *Recent Res. Dev. Pure Appl. Chem.* **2**, 1 (1998).
- 2) U. H. E. Hansmann and Y. Okamoto, *Curr. Opin. Struct. Biol.* **9**, 177 (1999).

Studies of Nonadiabatic Transitions, Chemical Reaction Dynamics, and Their Control

NAKAMURA, Hiroki; ZHU, Chaoyuan; NOBUSADA, Katsuyuki¹; TERANISHI, Yoshiaki²; MISHIMA, Kenji; PICHL, Lukas³; NAGAYA, Kuninobu³; KAMISAKA, Hideyuki³; OSHEROV, Vladimir I.⁴; MIL'NIKOV, Gennady V.⁵

(¹Hokkaido Univ.; ²Inst. Phys. Chem. Res.; ³GUAS; ⁴IMS and Inst. Chem. Phys., Russia; ⁵IMS and Inst. Struct. Macrokinetics, Russia)

Quantum mechanical studies of chemical reactions in heavy-light-heavy systems have been further pursued, and the reaction mechanisms have been clarified in terms of vibrationally adiabatic potential ridge lines and vibrationally nonadiabatic transitions. In addition to these numerical studies, the recently established analytical theory of the Landau-Zener-Stueckelberg type nonadiabatic transitions has been applied to the three-dimensional chemical reaction $O(^3P) + HCl \rightarrow OH + Cl$ and found to reproduce the cumulative reaction probability nicely. The computer code for the quantum reaction dynamics based on the hyperspherical elliptic coordinates has been extended so as to deal with electronically nonadiabatic chemical reactions and a work on the $D + H_2^+$ system is now going on.

The challenging trial is continued to try to formulate a unified theory of nonadiabatic transition which covers the Landau-Zener-Stueckelberg (LZS) and the Rosen-Zener-Demkov type of transitions. Quantum mechanical exact as well as semiclassical solutions have been successfully obtained for certain exponential potential

models.

Controlling molecular processes based on our new idea has been pursued in three ways. One is to control molecular processes by periodically sweeping laser fields (frequency and/or intensity). Depending on the availability of lasers, we can recommend various types of control schemes. The second is to control molecular photodissociation by using the intriguing phenomenon of complete reflection. In this case a static laser field is used and the control is made by appropriately adjusting the laser frequency. The third is a trial to propose a new effective method in NMR by sweeping the magnetic field.

The 5th- and 7th-order 2D Raman Spectroscopy for Intramolecular Vibrational Modes

TANIMURA, Yoshitaka

We calculated the 3rd-, 5th-, and 7th-order Raman signals for an Iodine dimer in the condensed phase, which was modeled by a Morse potential coupled to a heat bath. It is shown that the 5th- and 7th-order signals are very sensitive to the anharmonicity of the potential and useful to study intramolecular vibrational modes. In the case of harmonic vibrational modes, the 5th- and 7th-order signals are the function of both the linear and nonlinear linear coordinate dependence of the polarizability, whereas the present case they are the function of the linear coordinate dependence of the polarizability. Thus, the signals in the present case are expected to be much stronger than in the harmonic case. We also showed that the 7th-order 2D signal for a harmonic system with a nonlinear system-bath interaction, which is a possible model of an inhomogeneously distributed molecular-vibrational system, depends in the lowest order on the nonlinear coordinate dependence of the polarizability and is useful to see the effects of the inhomogeneity, in cases where the 5th-order 2D signals were very weak.

Constructing Molecular Theory of Chemical Process in Solution

HIRATA, Fumio; SATO, Hirofumi; AKIYAMA, Ryo; KOVALENKO, Andriy F.; SETHIA, Ashok; IMAI, Takashi; HARANO, Yuichi; KINOSHITA, Masahiro¹
(¹Kyoto Univ.)

Our current research interests and activities are concentrated upon three important chemical processes in solution, in each of which solvent plays essential role: (A) the electronic structure of a molecule in solution, (B) solvation thermodynamics of protein and related molecules, (C) characterization of spatial and temporal density fluctuation in molecular liquids, and (D) molecular theory of electrode-solution interface.

The RISM theory, an integral equation theory of molecular liquids, is our main machinery to attack the problem, which is coupled with other theoretical methodologies including the ab initio molecular orbital method, molecular simulations, and the generalized Langevin equation. Problems on which we have been

working along the three lines are as follows:

1. Temperature dependence of autoionization of water or pK_w .
2. Self-consistent determination of electronic structure and liquid state properties of water.
3. Solvatochromism of triiodide ion in solutions.
4. Solvent effect on keto-enol tautomers of formamide in aprotic solvents.
5. Type II S_N2 reaction (Menshutkin reaction).
6. Salt effect on solubility of nonpolar solute in water.
7. Solvation dynamics and thermodynamics of ions.
8. Stability of peptide and protein conformations in aqueous solution.
9. Non-equilibrium free energy surface related to electron transfer reactions
10. Dynamical coupling between intra- and inter molecular motions in liquids.
11. Description of collective excitation in liquids by interaction site model.
12. Microscopic characterization of metal-liquid interface.
13. Path integral theory of a hydrated electron.

(1) Studies on Laser Cooling and Trapping of Neutral Atoms

(2) Laser Spectroscopic Studies of Atoms and Ions in Liquid Helium

MORITA, Norio; MORIWAKI, Yoshiki; KUMAKURA, Mitsutaka

In "studies on laser cooling and trapping of neutral atoms," we have carried out precise theoretical calculations to investigate the cause of the isotopic difference in collisional ionization rate coefficients between cold $^4\text{He}(2s^3S_1) + ^4\text{He}(2s^3S_1)$ and $^3\text{He}(2s^3S_1) + ^3\text{He}(2s^3S_1)$ collisions at 0.5 mK, which is observed in our previous magneto-optical trap experiments on He atoms (see II-B-1). The design and construction of a new laser cooling and trapping apparatus, with which we expect to confine a much larger number of He atoms at much lower temperature, are now in progress. On the other hand, in "laser spectroscopic studies of atoms and ions in liquid helium," we have measured some excitation and emission spectra of Mg and Ca in liquid ^3He in order to observe interesting phenomena which arise from quantum features differing between liquid ^3He and ^4He (see II-C-1). For this series of study, we have also been constructing a new spectrometer, which is equipped with an image-intensified CCD camera and will allow us to observe spectra with much higher sensitivity.

Time-Resolved Resonance Raman Study on Mechanisms of Oxygen Reduction by Cytochrome c Oxidase

KITAGAWA, Teizo

Reaction intermediates in the enzymatic reduction of O_2 by bovine cytochrome c oxidase (CcO) were investigated with time-resolved resonance Raman spectroscopy. Six oxygen-associated vibrations were identified in the $\text{O}_2 \rightarrow \text{H}_2\text{O}$ process. The isotopic shift

of the Fe-O₂ stretching frequency for an asymmetrically labeled dioxygen, ¹⁶O¹⁸O, has established that the primary intermediate of cytochrome a₃ is an end-on type O₂ adduct of Fe_{a3} with the Fe-O-O angle of ~120°. The subsequent intermediates appearing around 0.1–3 ms following the start of the reaction yielded Raman bands at 804/764, 785/751, and 356/342 cm⁻¹ for ¹⁸O₂/¹⁶O₂ derivatives, respectively, in H₂O at pH 7.4. While these frequencies were the same between the H₂O and D₂O solutions, the final intermediate appearing around 3 ms gave the Raman bands at 450/425 cm⁻¹ in H₂O and 443/417 cm⁻¹ in D₂O. The last bands are reasonably assigned to the Fe_{a3}-OH(D) stretching mode. The extended measurements at lower temperatures and longer delay times have demonstrated that the 804/764 cm⁻¹ pair appears prior to the 785/751 cm⁻¹ pair and that the conversion from the former to the latter species is significantly delayed in D₂O compared with in H₂O, suggesting that this step of electron transfer is tightly coupled with proton pumping. The experiments using ¹⁶O¹⁸O have established that all the 804/764, 785/751, and 356/342 cm⁻¹ bands arise from the Fe=O heme, but definitely not from the Fe_{a3}-O-O-Cu_B the presence of which has been long postulated. The same three sets of oxygen-isotope sensitive bands have also been observed for the reaction intermediates of oxidized CcO with H₂O₂, indicating the identity of intermediates. IR Study of this enzyme revealed that ligand dissociation from the a₃ heme causes deprotonation of one carboxyl group, that does not perceive outside pH or has pK_a higher than 9.5.

Laser Raman Beat Detection of Magnetic Resonance

KATO, Tatsuhisa; MATSUSHITA, Michio

Laser Raman beat detection is a coherent optical-RF double resonance technique where the optical and RF field induce coherence within a three level system and a resultant Raman beat signal is detected using heterodyne detection. This technique can be applied to the study of electron paramagnetic resonance and nuclear magnetic resonance not only in the ground state of a molecule but also in the electronic excited state.

There are some causes to hide the Raman beat signal, that is, the inhomogeneity of the circumstance of the molecule, the fluctuation of the applied field, and the interference by the crystal phonon. It is the key to success in the Raman beat detection to eliminate these cause of the incoherence. Then it is needed to prepare the sophisticated single crystal sample, the highly stabilized magnetic field, and a cryostat of liquid helium. It has been completed to set up the apparatus, and the Raman beat detection was applied to the study on the quadrupole transitions of ¹³⁹La nuclei around Pr³⁺ doped in LaF₃, and on the delocalized excitation in molecular crystals of 1,4-dibromonaphthalene, in Section II-J-1.

Environment Dependent Association of Acetic Acid in Liquid Phase

NISHI, Nobuyuki; NAKABAYASHI, Takakazu;

KOSUGI, Kentaroh¹; INOKUCHI, Yoshiya (¹GUAS)

Acetic acid is known to form a stable cyclic dimer through two-site hydrogen-bonding in gas phase. Many of literatures describe the presence of such cyclic dimers in pure acetic acid or in aqueous solutions. Through the study of low frequency Raman spectra of various solution of acetic acid as well as the mass spectrometric studies of acetic acid aqueous solutions, we found that the cyclic dimer is not seen in polar solutions. The low frequency Raman spectrum of liquid acetic acid and its temperature dependence on the melting process of the crystalline acid suggest that the structure of the clusters in pure acetic acid is described as the fragments of crystalline acetic acids with chain-type 2-site hydrogen-bonds not only at the O-HO site but also at the O-HC site. Doubly coordination is characteristic of crystalline structure. In water, the situation is quite different. We know that the density of aqueous solution of acetic acid becomes maximum at 1:1 molar mixing ratio ($\chi_A = 0.5$). Apparently, at this concentration we have a closed packed structure of the acetic acid/water mixture. Spectroscopically, we have found that the clusters in this mixture are homogeneous associates of acetic acid. Water clusters are thought to fill the gap among the acetic acid clusters. This is called microphases of acid and water. The acetic acid clusters are thought to be composed of a side-on type dimer unit with a dipole moment of 4.0 Debye (in vacuum). Such a large dipole moment is expected to induce strong dipole-dipole interaction between the dimer units producing fairly large clusters of acetic acids.

Carbon tetrachloride (CCl₄) has a null dipole moment where acetic acids are found to generate aggregates with a structure similar to that of crystalline acetic acid at the concentration $\chi_A \geq 0.1$. The structure of acetic acid associates are thus so sensitive to the environment.

Higher Vibrational States of Molecules and Clusters as Studied by Nonresonant Ionization Detected IR Spectroscopy

FUJII, Masaaki

This special research project, started in April 1997 is planning to study spectroscopy and dynamics of molecules and clusters in higher vibrational state by the nonresonant ionization detected IR spectroscopy. The nonresonant ionization detected IR spectroscopy (shortly NID-IR) is a newly developed IR-UV double resonance spectroscopy which detects IR absorption by the selective ionization of a vibrationally excited molecule. Briefly, a jet-cooled molecule is excited to a vibrational level in the ground state by the IR laser. The vibrationally excited molecule is selectively ionized by the nonresonant two-photon process due to the UV laser. The simplest way of the selective ionization can be achieved by fixing the frequency of the UV laser to energy slightly less than a half of the ionization potential. Under this frequency condition, only the vibrationally excited molecule can be ionized by the two-photon process due to the UV laser. Therefore, the

ion current is detected only when the IR laser is resonant to the vibrational level. This spectroscopy has an advantage in the sensitivity because of the weak background signal and the ionization detection. The experimental setup for the measurement of the nonresonant ionization detected IR spectroscopy has already been described elsewhere (*Annual Review* 1997-1998, *Chem. Phys. Lett.* **252**, 287 (1996) and *Chem. Phys. Lett.* **283**, 243 (1998)).

The nonresonant ionization detected IR spectroscopy has been applied to jet-cooled phenol and various deuterated phenols (C_6H_5OH , C_6H_5OD , C_6D_5OH and C_6D_5OD). Vibrational transitions of jet-cooled phenol have been detected by nonresonant two-photon ionization due to UV laser from 3400 cm^{-1} to 14000 cm^{-1} . The spectra show well-resolved structure due to the first to the fourth quantum of OH (OD) stretching vibrations, CH overtones and various combination vibrations. The vibrational frequency, anharmonicity and the dissociation energy of the OH stretching mode has been measured. The bandwidth of the OH (OD) overtone in C_6H_5OH and C_6D_5OD is found to decrease with increase in the vibrational quantum number. This change in bandwidth suggests that the intramolecular vibrational redistribution (IVR) in C_6H_5OH and C_6D_5OD is not statistical. On the other hand, partially deuterated phenols (C_6H_5OD and C_6D_5OH) show the opposite change that the bandwidth increases in going to the higher overtone, likely to the statistical limit case. The observed results has been explained by the existence of the doorway state in IVR from OH overtones.

Imaging of Chemical Dynamics

SUZUKI, Toshinori; KOHGUCHI, Hiroshi

Femtosecond time-resolved photoelectron imaging method has been developed, for the first time. The scattering distributions of photoelectrons in $[1+1']$ REMPI of NO and $[1+2']$ REMPI of Pyrazine have been observed. In the latter case, ultrafast decay of optically-prepared S_1 character and corresponding build-up of triplet character were visualized. In addition, the results suggested the possibility that intersystem crossing is mediated by $T_2(\pi, \pi^*)$ state. Crossed beam ion imaging method has been applied to inelastic scattering of NO with Ar at the collision energy of 66 meV, and the differential cross sections were compared with scattering calculations by Millard Alexander using the newest *ab initio* surface.

Theoretical Study on the Electronic Structures of Atoms, Molecules, and Clusters

MIYOSHI, Eisaku; GHOSH, Tapas Kumar; SUMI, Tomonari

We have developed various types of model core potentials (MCPs) and applied the MCPs to investigate the electronic structures of atoms, molecules, and clusters. In particular, our research interests are concentrated upon the electronic structures of complexes with coordinate bond between metals,

$(Me_3P)(OC)_4Os-W(CO)_5$, which was recently found in experiments and is interesting because of its potential of application to new materials.

In addition, the electronic structures of weakly bound molecules such as $ArHF$, $Fe(CO)_n$ ($n = 1-3$), C_3O_2 , and $(C_6H_6)_3^+$ were investigated by using sophisticated methods for electron correlation. The methods contain the model core potential (MCP) method, and multi-reference coupled pair approximation. It has been shown that such methods are necessary to compute accurate potential energy surfaces of weakly bound molecules. We have also investigated electronic structures of $TiCl$, $ZrCl$, and MX_4 : $M = Ti, Zr, Hf$ and $X = F, Cl, Br, I$.

Using potential energy surfaces obtained by *ab initio* molecular orbital calculations, molecular dynamics calculations were also performed to investigate physical and chemical properties of liquid mercury and other systems.

Supersonic Jet Submillimeter-Wave Absorption Spectrometer with Backward Wave Oscillator

BELOV, Sergey; HARADA, Kensuke; MIZOGUCHI, Asao; TANAKA, Keiichi¹
(¹IMS and Kyushu Univ.)

Molecular clusters have extremely low-frequency vibrations, so called van der Waals (vdW) Vibrations, which sometimes falls in the submillimeter wave region below 30 cm^{-1} . The backward wave oscillator (BWO) is an ideal light source in the submillimeter wave region for the detection of the vdW vibrations of the molecular cluster, and the oscillator is commercially available up to 1.2 THz. One tube covers about 200 GHz frequency region with output power of 1–50 mW. In the present study, we have set up the submillimeter wave spectrometer with the BWO as a light source for the detection of the vdW vibration of the molecular cluster.

The frequency region from 150 to 800 GHz are covered using three BWO tubes mounted inside of the permanent magnet of 10 kG. The frequency of BWO was phase-locked to the local oscillator with a harmonic mixer, while the frequency of the local oscillator was frequency modulated by applying 36 kHz sinewave. The magnetic enhanced InSb bolometer was used for the detection, and the output of the detector was phase sensitively detected with the second harmonic of the modulation frequency as a reference. The transient absorption of the molecular cluster was phase sensitively detected with the time constant of 100 μs , transferred to the personal computer, and integrated in the computer system.

The sample gas of 1% HCN, 49% Ar, and 50% Ne was used for the detection of Ar-HCN. The sensitivity check was done by detecting the $J = 3-2$ rotational transition of $HC^{15}N$ on the sealed-off condition of the mixed gas. The detection sensitivity of the system was $4.2 \times 10^{-8}\text{ cm}^{-1}$ at the time constant of 180 ms with the path length of 42 cm. Figure 1 shows the $R(5)$ line of the $\Pi_1-\Sigma_0$ vdW bending band of Ar-HCN generated in a supersonic expansion. The signal to noise ratio of 26 was obtained with the effective sampling time of 100 ms for each frequency point.

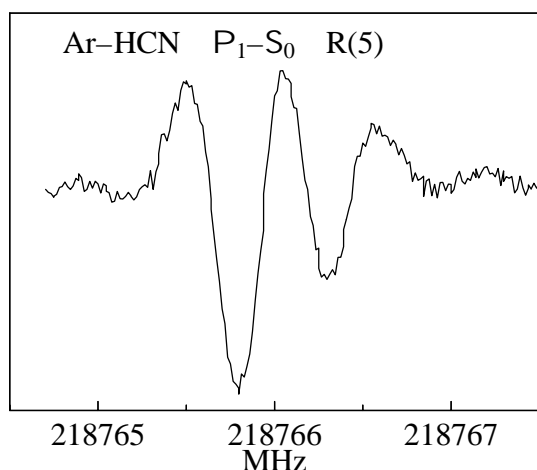


Figure 1. The R(5) line of the $\Pi_1-\Sigma_0$ vdW band of Ar-HCN observed with BWO.

Experimental Study of Ion-Induced Nucleation

NAGATO, Kenkichi

Ultrafine particle formation by ion-induced nucleation has recently gained attention both in atmospheric science and in material processing. However, experimental results of ion-induced nucleation to date show significant deviations from theoretical predictions. One of the reasons is that nucleation theories have not taken account of chemical nature of ions. In order to improve theories, experimental investigations about the influence of ion species on the nucleation process are necessary. For this purpose, we have developed a high-resolution ion mobility/mass spectrometer that is capable of simultaneous measurements of mobility and mass spectra of cluster ions generated by ion-molecule reactions under atmospheric pressure. We have tested the performance of this spectrometer using ions generated in the laboratory air. We are going to investigate the role of ions in ultrafine particle formation in $\text{NH}_3/\text{SO}_2/\text{H}_2\text{O}/\text{Air}$ mixture using this spectrometer. The results will be of importance in developing the model of tropospheric aerosol formation. Experiments will be extended to the study on the nucleation by ion-ion recombination.

Time-Resolved Spectroscopic Study of Photochemical Dynamics in Condensed Phase

TAHARA, Tahei; TAKEUCHI, Satoshi; FUJINO, Tatsuya; ARZHANTSEV, Sergei; MIZUNO, Misao; FUJIYOSHI, Satoru

Time-resolved spectroscopy is one of the most powerful tools for the studies of chemical reactions. It enables us to directly observe the temporal changes occurring in the course of chemical reactions. Recent progress of time-resolved spectroscopy relies on the drastic advance of the laser technology, and we are now able to examine the dynamics of the primary chemical processes with pico/femtosecond time-resolution. The aims of this project are (1) development of new technique and method in time-resolved spectroscopy, and (2) application of pico/femtosecond spectroscopy to the study of dynamics of molecules in condensed phase.

Our research activity of this year consists of the following three. First, we constructed two optical setups to generate ultrashort optical pulses whose duration is in the range from ten to a few tens of femtoseconds. Secondly, with use of time-resolved fluorescence and absorption spectroscopy having a few hundreds femtoseconds time-resolution, we studied ultrafast proton transfer reactions and the relaxation process of the highly excited states of several fundamental molecules in solution. Thirdly, we applied picosecond time-resolved Raman spectroscopy to the study of trans-azobenzene that is a prototypical molecule showing fast cis-trans isomerization. We examined the electronic and vibrational relaxation processes as well as the structure of the S_1 state of this molecule. In addition, while doing time-resolved Raman work, we noticed that amplified picosecond pulses are suitable for the excitation of hyper-Raman scattering.

SR-Pump and Laser-Probe Experiments for the Photofragmentation Dynamics of Atoms and Molecules

MITSUKE, Koichiro; MIZUTANI, Masakazu; IWASAKI, Kota; NIKURA, Hiromichi¹; HIKOSAKA, Yasumasa²
(¹GUAS; ²Inst. Mater. Struct. Sci.)

Synchrotron radiation-laser combination techniques developed at UVSOR have been employed for probing ionic and neutral photofragments produced in the vacuum ultraviolet. First, N_2^+ ($X\ ^2\Sigma_g^+$, $v_X = 0$ and 1) resulting from direct ionization or autoionization of N_2 or N_2O is detected by laser induced fluorescence excitation spectroscopy in the wavelength region of the $B\ ^2\Sigma_u^+ \leftarrow X\ ^2\Sigma_g^+$ transition. The rotational distribution of N_2^+ is considered to be determined by the change in the rotational quantum number in photoionization and by the partitioning of the excess energy impulsively released in dissociation. Second, $\text{S}(3s^23p^4\ ^3P_2)$ produced by predissociation of Rydberg states of OCS is detected by resonance enhanced multiphoton ionization spectroscopy.

The combination technique has been also incorporated into an apparatus for two-dimensional photoelectron spectroscopy of atoms and molecules in order to investigate photoionization dynamics of polarized atoms. Ground state Ar atoms are excited with linearly polarized synchrotron radiation to Rydberg states lying below the first ionization potential. Aligned atoms thus formed are ionized by irradiation of laser which is also linearly polarized. Photoelectrons emitted in the direction of the electric vector of synchrotron radiation are sampled and energy-analyzed. Photoelectron angular distribution is measured with respect to the electric vector of the laser. Derivation is made on the expressions which correlate asymmetric coefficients for the angular distribution with theoretical dynamic parameters involving transition dipole matrix elements. The anisotropy of the present angular distribution can be reasonably explained, assuming that the matrix elements and phase shift differences are essentially independent of the total angular momentum quantum number of the final state and that the spin-orbit interaction in the continuous spectrum is small.

Vibrational Spectroscopy on Cryogenic Surfaces Using Synchrotron Radiation

SAKURAI, Makoto¹; MATSUMOTO, Masuaki²
(¹IMS and Kobe Univ.; ²Univ Tokyo)

Vibrational Spectroscopy makes it possible to analyze dynamical aspects of molecules adsorbed on surfaces. Molecular layers on cryogenic surfaces show specific structures which depend on the interaction between molecules and substrate, and the vibrational spectra reveal the details of the interaction. Infrared reflection absorption spectroscopy (IRAS) and high-resolution electron energy loss spectroscopy (HREELS) are useful tools for vibrational spectroscopy on surfaces, and they have complementary characteristics, that is, IRAS is superior in resolution and stability whereas HREELS has higher sensitivity. Utilization of IRAS with HREELS in an identical vacuum system brings advantageous apparatus for researches of dynamical aspects of adsorbed molecules.

Under this project, we develop an apparatus for vibrational spectroscopy of molecules on cryogenic surfaces. The apparatus comprises both measurement systems (IRAS and HREELS), a cryogenic sample holder and tools for preparation and characterization of surface cleanliness. The IRAS system has optical system for inlet and outlet of synchrotron radiation in far-infrared (FIR) and infrared (IR) regions, since synchrotron radiation is brighter light source than conventional ones in these regions taking into account that the light source necessary for IRAS should have low emittance.

The vacuum system has been constructed and pumped down to UHV region. Spectral distribution of primary light from a conventional light source in an FTIR spectrometer through the whole optical system including the reflection at the clean surface of Ag(111) was measured after the alignment of the optical system.

Similarity Transformed Preconditioners for Green Function Evaluation in Cumulative Reaction Probability Calculations

ITO, Masakatsu; NANBU, Sinkoh; AOYAGI, Mutsumi; WAGNER, Albert F.¹
(¹Argonne Natl. Lab.)

The micro-canonical rate constant of interest for unimolecular reaction is given in terms of the cumulative reaction probability $N(E)$, $k(E) = N(E)/\{h\rho_r(E)\}$, where $\rho_r(E)$ is the density of reactant states per unit energy. The calculation of $N(E)$ is based on a discrete variable representation (DVR) of Hamiltonian and the use of absorbing boundary conditions (ABC). Recently Seidemann, Manthe and Miller showed that $N(E)$ was given as the eigenvalue sum of the probability operator $P(E)$. $P(E)$ is expressed in terms of the ABC Green function $G^{(e)}(E)$,

$$P(E) = 4\varepsilon_r^{1/2} G^{(e)}(E) \varepsilon_p G^{(e)}(E) \varepsilon_r^{1/2}.$$

The use of ABC provides the well-behaved representation of the Green function without having to include information regarding the asymptotic region. Since it is difficult to reproduce a global structures of

the potential energy surface for a many-atom molecule with an analytic function, this feature is efficient for realistic applications.

We employ iterative methods for diagonalizing $P(E)$ and for evaluating $G^{(e)}(E)$. Since the ill-conditioned linear problem of this kind cannot be solved with ordinary iterations, we proposed Kyrlov subspace methods with numerical preconditioning in order to reach a convergence. The resulting iterative expansion with the preconditioner corresponds to the distorted-wave Born expansion of the Green's function.

$$G = G_0 + G_0 \Delta G_0 G_0 + G_0 \Delta G_0 \Delta G_0 + \dots$$

The acceleration with the preconditioning is most effective when the preconditioner is closest to the Green's function. We found that the banded matrix extracted from $E-H-i\varepsilon$ effectively accelerate the convergence, and GMRES and Davidson method can get a convergence even when the bandwidth is only 3% of the matrix size. The LU decomposition of this banded preconditioner, however, needs extremely large amount of memory when the molecule has many degrees of freedom. We overcome this difficulty by employing the similarity transformed preconditioner.

$$M = U \text{Band} (U^+ (E-H-i\varepsilon) U) U^+,$$

where U is prepared for block-diagonalizing the Hamiltonian to reduce the memory requirement. We showed that this kind of preconditioner is as effective as the 'fat' preconditioner.

Developments of Advanced Lasers for Chemical Reaction Controls

SATO, Shin-ichiro; WATANABE, Kazuo

The chemical reaction controls with laser lights are one of the most important subjects of chemistry. The coherence of laser lights has not been considered seriously in the old fashion of the laser controls of chemical reactions. Recent theoretical studies have shown that the more sophisticated controls of chemical reactions. As a first step, we are trying to maximize efficiency of the quantum transition with a chirped ultra short pulsed laser. This technique is based on an adiabatic passage theory of quantum transitions. We are developing a photo waveform shaper of ultra short laser pulses to make an arbitrary shaped pulse, including chirped ones. The spectral components of the incident pulse are spatially dispersed with a grating, modulated or retarded with a liquid crystal array on the Fourier plane and recombined with another grating.

Developments and Researches of New Laser Materials

SARUKURA, Nobuhiko; OHTAKE, Hideyuki; LIU, Zhenlin; KAWAHATA, Eiji; KOZEKI, Toshimasa; ONO, Shingo¹
(¹Sci. Univ. Tokyo)

Although development of lasers is remarkable, there are no lasers which lase in ultraviolet and far infrared regions. However, it is expected that these kinds of lasers break out a great revolution in not only the molecular science but also in the industrial world.

In this project we research characters of new materials for ultraviolet and far infrared lasers, and develop new lasers by using these laser materials.

Development and Research of Advanced Tunable Solid State Lasers

TAIRA, Takunori; KURIMURA, Sunao; SHOJI, Ichiro; PAVEL, Nicolaie; SATO, Yoichi; SAIKAWA, Jiro

The use of diode lasers to pump solid-state lasers opens new horizon in laser science. Diode-pumped solid-state lasers are compact, reliable, and efficient sources of coherent radiation. They can provide excellent spatial mode quality and narrow linewidths. The high spectral power brightness of these lasers has allowed high efficiency frequency extension by nonlinear frequency conversion. Moreover, the availability of new and improved nonlinear optical crystals makes these techniques more practical. Recently attention has been directed to the trivalent ytterbium ion doped YAG. The advantages of Yb:YAG lasers for a high power, high stability and wide tunability laser operation are well recognized due to its small quantum defect, long upper-state life time and wide gain width.

On the other hand, quasi phase matching (QPM) is a new technique instead of conventional birefringent phase matching for compensating phase velocity dispersion in frequency conversion. Inasmuch as the pool of mature nonlinear optical materials is limited and development of new materials takes time and cost, QPM is a useful method for extending the range of available nonlinear optical materials. The ability to pattern a QPM structure allows the nonlinear materials to be engineered for desired interactions, meaning molecular-science-specified lasers are obtainable through these artificial materials.

In this projects we research and develop new diode-pumped-solid-state lasers and new frequency conversion devices. Especially, we will focus on the combination of Yb-doped lasers and QPM devices. These kinds of advanced tunable solid-state light sources which based on microchip lasers will be powerful tools in the research of molecular science.

UHV Tribometer

KONDOH, Takuhiko; ASAKA, Shuji; WATANABE, Michio

For actuators with sliding surfaces to operate smoothly in ultra-vacuum (UHV) it is important to obtain a surface treatment which is excellent in antigalling.

This year we have newly built an UHV tribometer to enable evaluation of sixteen kinds of surface treatment. We have found that among the samples tested MoS₂ coatings formed by sputtering method has had the best performance both in antigalling and in low coefficient of friction. Among the six kinds of coatings formed by electroplating Sn plating showed the best performance. All of the samples coated by five kinds of electroless plating have produced a poor result to show a high

coefficient of friction in early stages of the test.

Investigation of Dynamics on photo-excited Solids and Surfaces by Using Synchrotron Radiation

KAMADA, Masao; TANAKA, Shin-ichiro

Dynamics on solids and surfaces excited by photons has attracted much interest from both of basic and application sides. We have carried out photoelectron spectroscopic studies on semiconductor surfaces using synchrotron radiation and lasers. Core-level shifts observed on GaAs (100) can be interpreted in terms of surface photo-voltage effects induced by laser. Dynamics of the Cs and Oxygen on GaAs surfaces is one of interesting subjects and may be useful to understand the mechanism to produce the negative-electron affinity on GaAs surfaces. We have investigated the formation processes of the negative-electron affinity GaAs surfaces using photoelectron spectroscopy.

It is also important subject to investigate decay dynamics of the core-exciton using resonant photoelectron spectroscopy. The probability of the non-radiative decay of the core-excitons has been estimated on BaF₂ and CsCl, providing idea which explain the missing of the core-exciton peaks in the excitation spectra of the Auger-free luminescence. Moreover, two-photon excited spectroscopy has been applied to investigate the valence-exciton and core-exciton in CaF₂ and BaF₂.

We have been investigating the photon-stimulated desorption (PSD) in recent years, since PSD is interesting and promising field from a point of view from the application to micro-fabrication and the basic surface science. The photoelectron and ion coincidence technique and the laser-induced fluorescence method are powerful to understand the PSD dynamics on semiconductor and insulator surfaces, respectively.

Non-Linear Phenomena and Related Beam Physics in Storage Ring Free Electron Lasers

TANAKA, Hitoshi¹; TAKAO, Masaru¹; SOUTOME, Kouichi¹; HOSAKA, Masahito; HAMA, Hiroyuki (¹SPRING-8)

[*Nucl. Instrum. Methods Phys. Res. A* **431**, 396 (1999)]

We provide a perturbative formulation of nonlinear dispersion for particle motion in storage rings without linearizing the kinematic term and give recursion expressions for higher-order terms up to the fourth order. As an example, the nonlinear dispersion function of the SPRING-8 storage ring is numerically calculated. The numerical calculation shows that the higher-order terms up to third order are not significantly modulated by magnetic error if the dispersion of the linear optics is sufficiently small. An experimental study of the nonlinear dispersion was also carried out and it was found that the agreement between the theory and the measurement was fairly good up to second order.

Photoelectron Spectroscopy Studies of Solids, Surfaces and Interfaces

KINOSHITA, Toyohiko¹; NATH, Krishna G.²; HARUYAMA, Yuichi³

(¹*Univ. Tokyo*; ²*NTT*; ³*Himeji Inst. Tech.*)

The construction of the photoelectron spectro-microscopy equipment (the modified VG ESCALAB 220i-XL) has been completed. Some of the photoelectron spectroscopy and spectromicroscopy studies have been performed as described in this issue; (see, research activities). The combination with the laser annealing system allows us to measure the electronic structures of high temperature phase of solids and surfaces. All the members of the group have been removed from the IMS already. The group of associate professor Dr. K. Fukui may mainly use the system from 1999.

(2) Study of Molecular Solid toward Molecular Electronics

Theory of Electronic Phases in Molecular Conductors and Insulators: Electron Correlations and Dimensional Crossovers

YONEMITSU, Kenji; KISHINE, Jun-ichiro; MORI, Michiyasu; KUWABARA, Makoto; SUN, Xin¹; IMAMURA, Yutaka²
(¹Fudan Univ.; ²GUAS)

Electron correlation in low dimensions brings about variety of electronic phases. i) In quasi-one-dimensional organic conductors (TMTCF)₂X, commensurability of the average electron-electron distance with the lattice spacing causes umklapp processes that are responsible for the Mott insulator phase. When the interchain hopping is small and the charge gap due to the umklapp processes is large, interchain one-particle hopping correlation is suppressed even if the antiferromagnetic long-range order is well developed. Otherwise, the nesting of the Fermi surface leads to instability toward a spin density wave. Such dimensional crossover is studied from high to low temperatures and for the ground states. When random potential exists, the electronic phases compete with the Anderson localization phase, as realized, *e.g.*, in (DCNQI)₂Ag_{1-x}Cu_x. ii) In one-dimensional metal complexes, M₂L₄X, strong electron-lattice coupling and electron-electron interaction bring about variety of charge and lattice ordering states. The electronic phases are reproduced when we consider up to the next-nearest-neighbor repulsion. Overall features are explained from the atomic (*i.e.*, vanishing transfer integrals) limit and the adiabatic/antiadiabatic (*i.e.*, zero/infinite phonon frequencies) limits. Reasonable change of parameters qualitatively reproduces general tendency for the dependence of the electronic state on the interdimer distance and on the presence/absence of counter ions. iii) In two-dimensional metal-assembled complexes Et_nMe_{4-n}Z[Pd(dmit)₂]₂, the presence of two bands with different characters makes the phase diagram richer than that of κ-(BEDT-TTF)₂X. Dimensionality and frustration control the magnetic and transport properties of Et_nMe_{4-n}Z[Pd(dmit)₂]₂, while correlation strength controls the electronic phase of κ-(BEDT-TTF)₂X.

π-d Interaction in Molecular Metals

YAKUSHI, Kyuya; YONEHARA, Yukako; DING, Yuqin; SIMONYAN, Mkhital; NAKANO, Chikako

We have undertaken a systematic study on the solid molecular systems in which transition metals are embedded in a π-conjugated system from the viewpoint of the future design of the superconducting material. The highly conductive phthalocyanine salts such as CoPc(AsF₆)_{0.5} and NiPc(AsF₆)_{0.5} are the prototype of the one-dimensional conductors in which the d- and π-orbitals form a double-chain and two-band system. Subsequently to the high-pressure optical experiment, we performed the high-pressure resistivity measurement in 0.25–0.95 GPa range. The resistivity minimum continuously shifted to higher temperature as we

increased the pressure, reaching up to 283 K at 0.95 GPa. This result is in accord with the prediction of the metal-insulator transition derived from the analysis of the optical spectrum under high pressure. (*See IV-A-2*) This year we expanded our attention to the mixed crystals of Co_xNi_{1-x}Pc(AsF₆)_{0.5} to elucidate the role of the unpaired 3d electron on Co. First the X-ray diffraction and EPMA proved that the mixed crystals were formed in a wide range. Second we found a hyperfine structure in the ESR signal of Ni_{0.99}Co_{0.01}Pc(AsF₆)_{0.5}. The temperature dependence undoubtedly shows the exchange interaction between the localized 3d-electron and itinerant π-electron. (*See IV-A-1*) Third we found new Raman bands only in the mixed crystals Co_xNi_{1-x}Pc(AsF₆)_{0.5}. This observation gives an information of the electronically excited state inherent in mixed crystal. (*See IV-A-3*) From this year we started a new π-d system, DMTSA-FeCl₄, which showed an antiferromagnetic phase transition at 12 K.

Search for Negative-*U* Materials in Molecular Solid

YAKUSHI, Kyuya; URUICHI, Mikio; OUYANG, Jianyong; YAMASHITA, Yoshiro; NAKANO, Chikako

The negative-*U* material comprises the molecule that has a negative on-site Coulomb energy or, in other words, an attractive force between two electrons within the molecule. We are looking for such compounds from the two directions: (1) a strong electron-molecular vibration coupling and (2) a strong nearest neighbor Coulomb repulsion. (1) A strong electron-molecular vibration interaction may overcome the repulsive force within the molecule and stabilize an on-site bipolaron state. The similar state has been found in the insulating compound, Cs₂SbCl₆, superconducting compound, BaPb_{1-x}Bi_xO₃, and conducting polymer, poly-pyrrole, but never been in an organic charge-transfer compound. (2) The molecular distance between the neighboring molecules is about 3.4 Å, whereas recently synthesized long conjugated molecule has more than 15 Å. If we use the long conjugated molecule which is stacked in an eclipsed overlapping mode, the on-site Coulomb repulsion energy happens to be smaller than the nearest neighbor Coulomb repulsion occasionally.

To look for such molecules, multi-step-oxidation properties of electron donors are one of the key parameters. Generally, the difference (Δ*E*) between the first and second oxidation potentials is thought to be a measure of the on-site Coulomb energy in the organic conductor. BEDT-ATD has a small difference (90 meV) in the first and second oxidation potentials. Subsequently to the study of (BEDT-ATD)₂PF₆(THF) that shows a metal-insulator transition, we conducted the low-temperature structural study of (BEDT-ATD)₂X-(solvent) (X = PF₆, AsF₆, BF₄; solvent = THF, DHF, DO). The most interesting point is the ferroelectric order of the solvent molecules in the insulator phase, which might show ferroelectricity near the phase transition. The experiment to examine this possibility is

now in progress. (See IV-B-5)

We examined the band structure of new organic metals based on a long conjugated molecule BDT-TTP. Subsequently to the band structure study of (BDT-TTP)₂-X (X = SbF₆, AsF₆), we expanded our attention to analogous compounds (BDT-TTP)₂X (X = ClO₄, ReO₄), (ST-TTP)₂AsF₆, and (BDS-TTP)₂AsF₆. All of these compounds exhibit very similar reflection spectra, which means similar band structure. The correlation effect seems to be weak along the stacking direction in these compounds. However, we found a weak correlation effect in the spectra polarized along the inter-chain direction according to the analysis of the generalized Drude model. We still have no information on the sign of *U*.

The negative-*U* state is a dynamic state of the charge disproportionation: the paired charge is moving coherently. Contrary to this state, some charge-transfer salts in a mixed-valent state show a static charge disproportionation state. The Raman spectroscopy is an efficient method to detect this kind of charge distribution. From this viewpoint, we examined θ-(BDT-TTP)₂-Cu(NCS)₂ (See I-B-4) and (Et₄N)(DMe-TCNQ)₂ (See IV-B-6), and evaluated the electrostatic energy with counter anion/cation using the Ewald method.

Investigation of Novel Electronic Phases in Molecular-Based Conductors

NAKAMURA, Toshikazu; NAKAZAWA, Yasuhiro; TSUKADA, Hiroshi

The aims of this project are to study the electronic structure and to explore novel electronic phases in molecular-based conductors by microscopic and thermodynamical measurements. Molecular-based conductors are very advantageous because of several features as follows: (1) low-dimensional and simple Fermi surfaces, (2) clean system, (3) various ground states, and (4) molecular internal-freedom. We will perform the investigation with the following procedure: firstly we will understand the fundamental electronic properties by static magnetic susceptibility, EPR and transport measurements. Secondly we study the detailed electronic structure and mechanism of the phase transition by means of (a) EPR, (b) NMR and (c) specific heats measurements. We also try to carry out experiments with new devices under unconventional circumstance.

We start to study on these topics.

- [1] Microscopic Investigation of the charge localized states in a quarter-filled system: (EDT-TTF)₂AuBr₂, is a quarter-filled system with uniform stacked. It undergoes a metal-insulator transition around 20 K. This system has very simple structure but its electronic state is not clarified. We started magnetic investigation of the low-temperature insulating phase.
- [2] Competition between local and itinerant electrons in charge-transfer salts: (CPDT-STF)-TCNQ is a two-band system where the conduction and localized electrons coexist. We investigate possible interaction between them.
- [3] Understanding of the electronic structure of conduct-

ing metal complex from a microscopic point of view: NMR measurements are performed for ¹³C substituted Pd(dmit)₂ families.

Development and Solid State Properties of New Organic Conductors

KOBAYASHI, Hayao; FUJIWARA, Hideki; SATO, Akane; OJIMA, Emiko; ADACHI, Takafumi; NARYMBETOV, Bakhyt; TANAKA, Hisashi¹; KOBAYASHI, Akiko¹

(¹Univ. Tokyo)

We have tried to develop new organic superconductors. The main results obtained in the last one year are as follows: (1) we have found the antiferromagnetic metal phase and superconductivity in λ-BETS₂FeCl₄ at high pressure. To our knowledge, this is the first observation of the coexistence of magnetic order and π metal electrons in organic conducting systems. (2) The first antiferromagnetic organic metal exhibiting superconducting transition, κ-BETS₂FeBr₄ was discovered. From the thermodynamic viewpoint, it will be hardly imagined that the antiferromagnetic ordering of Fe³⁺ (*S* = 5/2) spins developed around 2.5 K is broken by the onset of the superconductivity of the π electron system at 1 K. Therefore, it is highly possible that this system is the first antiferromagnetic organic superconductor, which is one of the final targets in the recent studies on the development of the new organic conductors. (3) A new organic superconductor κ-BETS₂GaBr₄, which is isostructural to the recently discovered magnetic superconductor κ-BETS₂FeBr₄, was found out.

We have studied the low temperature structure of C₆₀ ferromagnets. We have successfully analysed the 7 K structure of unannealed TDAE·C₆₀ crystals. Whereas the annealed crystal exhibiting ferromagnetism below 16 K contains structural disorder even below 10 K. We have recently obtained a reasonable structural model for this disordered ferromagnetic crystal, which will be very important for the studies on the ferromagnetism of this salient system.

In the course of the trials on the establishment of the four-probe high-pressure resistivity technique using diamond anvil cell, we have recently succeeded to measure the resistivity of thin needle organic crystals up to 100 kbar, which will be an important step for the development of the solid state chemistry at high pressure.

NMR Studies of Liquid Crystals

OISHI, Osamu; NAKAI, Toshihito¹; MIYAJIMA, Seiichi

(¹Tokyo Univ. Agric. Tech.)

Extensive high resolution NMR studies were conducted to investigate the dynamics and the microscopic mechanism of antiferroelectric ordering in liquid crystal MHPOBC. (1) Pulsed field gradient spin echo (PGSE) NMR study revealed that MHPOBC molecules are confined in the smectic layers, and therefore the self-diffusion takes place mainly within

the layer. (2) Deuterium NMR for the specifically deuterated samples revealed unusual nature of the chiral chain; the chain is bent from the molecular long axis, and its motion is asymmetrically hindered.

Construction and Characterization of Chiral Molecule-Based Magnets in a Systematic Way

INOUE, Katsuya; KUMAGAI, Hitoshi

The design of molecular materials with interesting magnetic and optical or electrical properties is one of the major challenges in the last few years. We have introduced a strategy of using π -conjugated high-spin oligonitroxide radicals which can be used as bridging ligands for paramagnetic transition metal ions in order to assemble and align the electron spins on a macroscopic scale. The synthesis and study of chiral molecular-based magnetic materials which are transparent for light are of great interest. Novel magneto-optical phenomena have been theoretically predicted and observed in chiral paramagnetic materials in 1997. Although novel properties are expected for such compounds, few examples of chiral molecular-based magnetic materials are still known. To get more insight in their properties it is therefore important to construct such chiral molecule-based magnets in a systematic way. We designed and synthesized a chiral organic radical which can be employed to construct chiral molecular-based magnets. By this strategy, we have made chiral metamagnet of **1**·Mn(hfac)₂ and ferrimagnet of **2**·Mn(hfac)₂ (see V-F). The observation of MChD effect of this complex is now underway.

Studies on Electronic States of Organic Thin Films by Angle-Resolved UPS

UENO, Nobuo¹; HASEGAWA, Shinji; AZUMA, Yasushi^{1,2}; OKUDAIRA, Koji K.¹; ISHII, Hisao³; YOSHIMURA, Daisuke^{2,3}; SEKI, Kazuhiko³
(¹Chiba Univ.; ²IMS; ³Nagoya Univ.)

The archetypal organic semiconductor, perylene-3,4,9,10-tetracarboxylicdianhydride (PTCDA), has recently gained increasing interest as a promising material for organic electroluminescence devices. Furthermore, it was reported that a thin film of PTCDA provides a new state in the PTCDA band gap due to the reaction between the film and the substrate or overlayer materials such as GaAs,¹⁾ In, Al, Ti, and Sn.²⁾ This result is very important because the new band is located very close to the Fermi level, and therefore it is expected that it plays an important role in the organic-device properties. However, there is little information on the origin of the band-gap state.

We performed ARUPS measurements of In/PTCDA interface on a cleaved MoS₂ surface in order to study of the new band-gap state.

Figure 1 shows the take-off-angle (θ) dependencies of the ARUPS of a 3-Å-thick PTCDA [panel (a)] and an In/PTCDA interface [panel (b)] which was prepared by evaporating the In onto the 3-Å-thick PTCDA film. The thickness of the In overlayer was 1 Å. When we compare Figure 2(a) and Figure 2(b), some spectral changes can

be clearly seen. Firstly, a new band X appears at $E_B = 0.8$ eV in the PTCDA band gap after the In deposition. Secondly, at the region of $E_B = 1.5$ –5 eV, some new features arise in the spectra and they are broader than the spectral features of the pristine PTCDA thin film in Figure 2(a). These results are consistent with those obtained by Hirose *et al.*²⁾ Furthermore, the $n_o//$ (oxygen nonbonding orbital with 2px and 2py atomic orbitals) band of PTCDA [band C in Figure 2(a)] was not resolved after the In deposition, while new band X' ($E_B = 3.6$ eV) is observed at $\theta \cong 62^\circ$. These spectral changes originate from a chemical reaction between the PTCDA and the In. The disappearance of the $n_o//$ band in Figure 2(b) suggests that the chemical reaction between the PTCDA and the In atoms takes place at the C=O parts to change the $n_o//$ states. It is expected that the band X' originates from the AO which is distributed parallel to the surface, since the band X' observed at a large value of θ .

On the other hand, we measured high-resolution electron energy loss spectra (HREELS) for the In/PTCDA on the MoS₂ in order to clarify the chemical site of the reaction. The HREELS results showed that the intensities due to the excitation of C=O stretching mode [$\nu(\text{C=O})$] becomes weak relative to that of C-C stretching mode [$\nu(\text{C-C})$] and COC stretching mode [$\nu(\text{COC})$], and only the peak position of the $\nu(\text{C=O})$ shifts to lower wave-number side. These findings indicate that a strong interaction between the PTCDA molecules and the In atoms exists only at the C=O parts. Furthermore, our recent Penning ionization electron spectroscopy (PIES) measurements on the In/PTCDA interface on the MoS₂ surface showed that four In atoms react with the one PTCDA molecule.

In Figure 2, the observed θ dependence of the band X intensity is compared with calculated one, where the calculations were performed using *ab initio* (STO-6G) and SS/MO methods[3-5] for an expected reaction product, In₄PTCDA. The calculated results were obtained by assuming random azimuthal orientation of the molecules for $\beta = 0, 10$ and 20° with the short molecular-axis being parallel to the surface. The calculated θ pattern for $\beta \approx 10^\circ$ agrees better with the observed one in the value of θ max and the width of the angular distribution. This result indicates that the In₄PTCDA are oriented tilt at $\beta \approx 10^\circ$ as shown in Figure 2.

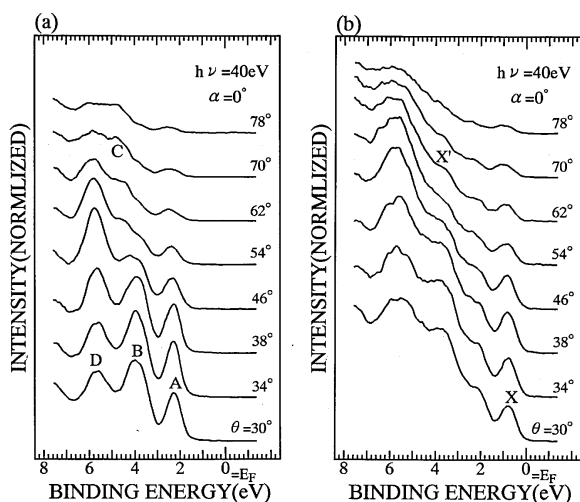


Figure 1. The take-off angle θ dependencies of ARUPS spectra of a 3-Å-thick PTCDA film on MoS₂ before (a) and after 1-Å-thick In overlayer deposition (b). The incidence angle of photon (α) is 0° and $h\nu = 40$ eV. The intensity is normalized to the incidence photon flux.

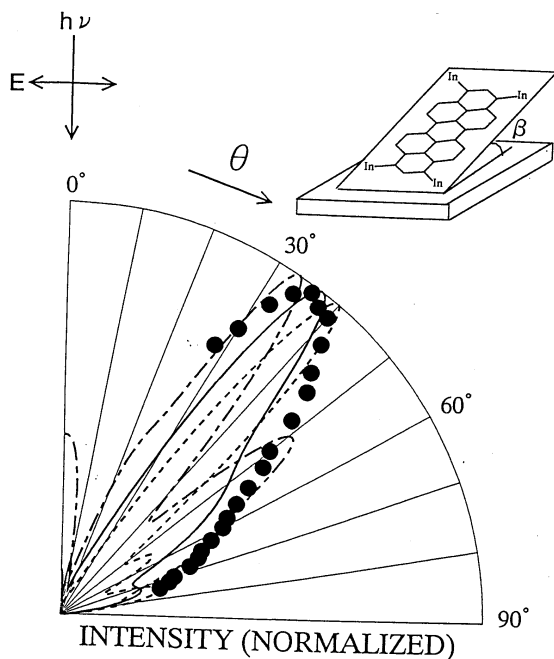


Figure 2. The comparison between the observed and calculated θ dependencies of the photoelectron intensities for the band-gap state. The SS/MO results at $h\nu = 40$ eV and $\alpha = 0^\circ$ are shown for $\beta = 0^\circ$ (-----), 10° (—) and 20° (-·-·-). The calculation was made by assuming azimuthal disorder of the reaction product, In₄PTCDA. The tilt direction of the molecule is also shown.

References

- 1) Y. Hirose, W. Chen, E. I. Haskal and A. Kahn, *Appl. Phys. Lett.* **64**, 3482 (1994).
- 2) Y. Hirose, A. Kahn, V. Aristov, P. Soukiassian, V. Bulovic and S. R. Forrest, *Phys. Rev. B* **54**, 13728 (1996).
- 3) N. Ueno, A. Kitamura, K. K. Okudaira, T. Miyamae, Y. Harada, S. Hasegawa, H. Ishii, H. Inokuchi, T. Fujikawa, T. Miyazaki and K. Seki, *J. Chem. Phys.* **107**, 2079 (1997).
- 4) S. Hasegawa, T. Miyamae, K. Yakushi, H. Inokuchi, K. Seki and N. Ueno, *Phys. Rev. B* **58**, 4927 (1998)

- 5) K. K. Okudaira, S. Hasegawa, H. Ishii, K. Seki, Y. Harada and N. Ueno, *J. Appl. Phys.* **85**, 6453 (1999).

New Advanced Organic Materials Based on Novel Heterocyclic Compounds

YAMASHITA, Yoshiro; TANAKA, Shoji; TOMURA, Masaaki

We have succeeded in preparing new electron donors and acceptors with extended π -conjugation. For example, TTF vinylogues bearing various substituents at the vinyl positions have been prepared using an oxidative dimerization reaction of 1,4-dithiafulvenes. In the derivatives with *o*-substituted phenyl groups the TTF vinylogue skeleton is planar when the aryl part is twisted. We have now found that TTF vinylogues containing one halogen atom at the ortho position afford cation radical salts with Au(CN)₂ anion as single crystals. The unique crystal structures were revealed by the X-ray structure analysis. We have also prepared non-planar BEDT-TTF derivatives fused with tetrahydrofuran (THF) rings. The donor molecule afforded the cation radical salts whose crystal structures are unusual due to the sterically hindered THF rings. On the other hand, bithiophene-TCNQ derivative and a tetracyanodiphenodimethane derivative containing 1,2,5-thiadiazole rings have been newly synthesized as electron acceptors. X-ray analyses revealed the interesting crystal structures where intermolecular networks are formed by short S...N contacts. A new type of hydrogen-bonding system has been developed by using bipyridine and bispyridylethylene as proton acceptor and chloranilic acid as proton donor. The component molecules are combined via three-center hydrogen bonded interactions. Furthermore, we have prepared thiophene oligomers as promising molecular-scale electronic wire which have small energy gaps with a rigid and coplanar main chain. Details of these works are described in VIII-E section.

Design and Synthesis of New Tellurium-Containing Donors

KOBAYASHI, Hayao; SUZUKI, Toshiyasu; FUJIWARA, Hideki; OJIMA, Emiko

In the field of molecular conductors, systems based on tellurium-containing donor molecules have not received as much attention as systems based on sulfur- or selenium-containing donors. By incorporating heavy chalcogen atoms such as tellurium into donor molecules, a new metallic system with a wider bandwidth and a higher dimensionality is expected to appear. We have designed dimeric donor molecules containing two HM-TTeF moiety and been trying to synthesize them. After obtaining these molecules, we are planning to study their crystal structures and physical properties of both neutral and oxidized states.

(3) Material Control in Multi-Reaction Centers

Asymmetric Oxidation Catalyzed by Myoglobin Mutants

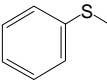
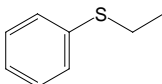
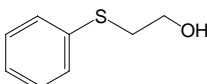
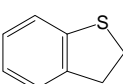
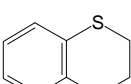
OZAKI, Shin-ichi; YANG, Hui-Jun; MATSUI, Toshitaka; GOTO, Yoshio; WATANABE, Yoshihito

[*Tetrahedron: Asymmetry* **10**, 183 (1999)]

The sperm whale myoglobin active site mutants (L29H/H64L and F43H/H64L Mb) have been shown to catalyze the asymmetric oxidation of sulfides and olefins. Thioanisole, ethyl phenyl sulfide, and *cis*- β -

methylstyrene are oxidized by L29H/H64L Mb with more than 95% enantiomeric excess (% ee). On the other hand, the F43H/H64L mutant transforms *trans*- β -methylstyrene into *trans*-epoxide with 96% ee. The dominant sulfoxide product in the incubation of alkyl phenyl thioethers is the *R* isomer; however, the mutants afford dominantly the *S* isomer of aromatic bicyclic sulfoxides. The results help us for the rationalization of the difference in the preferred stereochemistry of the Mb mutants-catalyzed reactions. Furthermore, the Mb mutants exhibit the improvement of the oxidation rate up to 300-fold with respect to wild type.

Table 1. Enantiospecific Sulfoxidation of Cyclic and Acyclic Thioethers.

		wild type Mb		L29H/H64L Mb		F43H/H64L Mb	
		rate ^a	ee (%)	rate ^a	ee (%)	rate ^a	ee(%)
1 ^b		0.25	25 (R)	5.5	97 (R)	47	85 (R)
2		0.46	7.6 (R)	6.5	95 (R)	26	54 (R)
3		0.65	27 (R) ^c	1.6	71 (R) ^c	3.2	27 (R) ^c
4		2.2	0.2 (R)	24	67 (S)	95	17 (S)
5		0.8	5.4 (R)	3.2	66 (S)	50	34 (S)

(a) The unit for rate is turnover/min.

(b) The results are taken from reference 7f and 8a.

(c) The *R* configuration was assigned by comparison of CD spectra of (*S*)-methyl phenyl sulfoxide and synthetic sulfoxide of 3.

Bio-Inspired Molecular Architecture

SHIONOYA, Mitsuhiro; TANAKA, Kentaro; TASAKA, Motoyuki¹; SHIGEMORI, Kazuki¹; HATANO, Akihiko¹; MORISHITA, Hiromasa¹; CAO, Honghua¹; BU, Xian-He²
(¹GUAS; ²Nankai Univ.)

Nature has produced a limited number of molecular modules such as nucleosides and nucleotides, amino acids, and lipids. However, the chemical diversity of these biomolecules and the different ways they can be polymerized or assembled into precisely-defined three-dimensional shapes provide a wide range of possible forms and functions. Furthermore, owing to advances in chemical synthesis and biotechnology we can combine or chemically modify these molecular building blocks, almost at will, to produce new functional molecules that have not yet been made in Nature. Based on these

concepts, we have been working on the following research projects. Our research programs also consciously focus on structures and functions that have been unknown in living, biological systems.

- (1) Coordination-based artificial DNAs: metal-assisted base pairing.
- (2) Cyclic metalloproteins: efficient cyclization of oligopeptides linked to functional metal complexes.
- (3) Molecular recognition of ss-DNA sequences by self-assembling metal complexes.
- (4) An engineering-up approach to highly controlled hierarchical structures of metal complexes.

Activation of Carbon Dioxide Directed Toward Carbon-Carbon Bond Formation and Energy Conversion from Proton Gradients to Electricity

TANAKA, Koji; TSUGE, Kiyoshi; WADA, Toru; KOBAYASHI, Katsuaki; TOMON, Takashi

A variety of metal complexes have proved to be active as catalysts precursors for the reduction of CO₂, though the reduction products are usually limited to CO and/or HCOOH. The difficulty of multi-electron reduction of CO₂ results from reductive cleavage of metal-CO bond derived from CO₂. We have found that Ru-CO bonds derived from CO₂ are successively activated without the bond-cleavage by utilizing redox reactions of monodentate 1,8-naphthyridine (napy). The ligand localized one- and two-electron reductions greatly enhanced the basicity of the free nitrogen. As a result, intramolecular nucleophilic attack of the free nitrogen to the carbonyl carbon takes place to form metallacyclic rings, where two-electrons are transferred to the carbonyl carbon from the reduced napy without through the central metal. The resultant Ru-CO bonds are activated enough to undergo mild electrophiles such as *tert*-alkyl ammonium salts. We have also achieved the first catalytic formation of ketones, α -keto acids and α -diketones under the electrochemical reduction of CO₂.

ATP synthesis utilized proton gradient is the key reaction for maintenance of biological activity. The proton gradient (Δp) between inside and outside of a cell is depicted as the sum of electric activity ($\Delta\psi$) and chemical activity (ΔpH) components. $\Delta p = \Delta\psi - Z\Delta pH$ ($Z = 2.303RT/F$) Artificial energy conversion from proton gradients to other energy forms except for thermal energy has not been established so far. Biological system creates various valuable energies from the proton gradients, that is the neutralization energy. Basically, neutralization energy is originated from the binding energy of acid and base, namely is one of the chemical energies, which are expected to be converted directly to valuable chemical, electric or mechanical energy in 100% efficiency in principal. Along this line, we tried to convert the neutral energy to electronic energy by using metal complexes. The purpose of the two projects is to develop new methodology for utilization of CO₂ as a C1 resource and to generate reactive species for oxidation of hydrocarbons.

Self-Assembling Molecular Systems

FUJITA, Makoto; KUSUKAWA, Takahiro; HIRAOKA, Shuichi¹; SAKAMOTO, Youichi; TAKEDA, Nobuhiro¹; TAKAHASHI, Masaki²; YU, Shu-Yan²; BIRADHA, Kumar²; HOSSAIN, Delower³; IBUKURO, Fumiaki⁴; AOYAGI, Masaru⁴; ITO, Hirokazu⁴; FUJITA, Norifumi⁴; UMEMOTO, Kazuhiko⁴

(¹CREST; ²JSPS; ³Mie Univ.; ⁴GUAS)

We have been studying the self-assembly of finite and infinite structures based on coordination chemistry, where metal-coordination induces the generation of defined structures. Our studies are focused on the self-assembly of finite structures such as macrocycles, catenanes (interlocked molecules), cages, tubes, and capsules as well as infinite network structures. In the construction of the discrete structure, our strategy may be characterized by the use of palladium's 90 degree

coordination. Based on this concept, we have obtained the following results during 1999.

- Encapsulation of Large, Neutral Molecules in a Self-assembled Nanocage Incorporating Six Palladium(II) Ions: It is shown that self-assembled M₆L₄ type cage can hold as many as four adamantane molecules or *o*-carborane (8 Å in diameter) inside its nanosized cavity.
- "Ship-in-a-bottle" Formation of Stable Hydrophobic Dimers of *cis*-Azobenzene and -Stilbene Derivatives in a Self-assembled Coordination Nanocage: "C-shaped" molecules such as *cis*-azobenzene and -stilbene are enclathrated in the cavity of a nano-sized M₆L₄ type cage complex through "ship-in-a-bottle assembly" into a hydrophobically interacted dimer.
- A Nanometre-Sized Hexahedral Coordination Capsule Assembled from 24 Components: The transition metal-induced assembly of a stable, nanometer sized coordination capsule are achieved from twenty-four small components; eighteen metals and six triangular organic ligands.
- Spontaneous Assembly of Ten Components into a Two Interlocked, Identical Coordination Cages: Two cage complexes efficiently bind each other through giving rise to a ten-component self-assembly into a three-dimensionally interlocked molecule.
- Quantitative Formation of Coordination Nanotubes Templated by Rod-like Guests
- Guest-Selected Formation of Pd(II)-Linked Cages from a Prototypical Dynamic Library
- Quantitative and Spontaneous Formation of a Doubly Interlocking [2]Catenane using Copper(I) and Palladium(II) as Templating and Assembling Centers
- Flexible Coordination Networks with Fluorinated Backbones. Remarkable Ability for Made-to-order Enclathration of Organic Molecules
- Kinetic and Thermodynamic Aspects in the Substrate-Induced Assembly of Optimal Receptors from a Dynamic Library: Pyridine functionalized C_{2v} ligand gives symmetric and asymmetric M₃L₂ receptors and their dimeric M₆L₄ cage; each of them is selected upon the addition of their optimal guests.
- Dynamic Behavior of Rod-like Guest Accommodated in Coordination Nanotubes: Guest molecules are found to shuttle in the coordination nanotube in a one-way direction as revealed by NMR studies.
- Wacker Oxidation in an Aqueous Phase Through the Reversed Phase-transfer Catalysis of a Self-assembled Nanocage: Coordination nanocage shows reversed phase-transfer catalysis toward Wacker oxidation of olefins which is a typical Pd(II)-promoted catalytic reaction.
- Hydrophobic Assembling of a Coordination Nanobowl into a Dimeric Capsule Which can Accommodate upto Six Large Organic Molecules: M₆L₄ coordination nanobowl assembles in aqueous media into a dimeric capsule accommodating as many as six neutral organic molecules.
- Porous Coordination Polytubes: Upon treatment with a transition metal (CuI), a panel-like oligo 3,5-pyridine ligand assembles into polytube structures which accommodate organic guests in the tubular

- cavities with the accessible porosity of *ca.* 30–50%.
- X-Ray And NMR Observation of Encapsulated Molecules in a Self-assembled Coordination Nanocage: Encapsulation of tetrabenzylsilane and di(*p*-methoxybenzoyl) was confirmed by X-ray and NMR studies.

Molecular Mechanism of Oxygen Activation by Metalloenzymes

FUJII, Hiroshi; FUNAHASHI, Yasuhiro; MIZUTANI, Mamoru

Metalloenzymes are a class of biologically important macromolecules which have various functions such as oxygen transport, electron transfer, oxidation, and oxygenation. These diverse functions of metalloenzymes have been thought to depend on the coordination structure of the reaction intermediate formed in the protein matrices, the ligand donors, the geometry, and the coordination mode of reactant and substrate. Furthermore, it has been thought that protein structures in immediate vicinity of active metal ion are related to enzymatic function, regio-selectivity, and stereo-selectivity. In this project, we are studying the molecular mechanism of activation of molecular oxygen mediated by metalloenzymes.

- (1) High valent iron-oxo species have been suggested as the active intermediates for catalytic oxygenation reactions by iron-containing oxygenases. In order to gain insight into the active intermediates, we try to synthesize iron complexes with bulky schiff-base ligands as biomimetic models of mononuclear non-heme iron active sites.
- (2) Copper-dioxygen complexes are suggested as key reaction intermediates in many enzymatic reactions. To investigate the relationship between electronic structure and reactivity of copper-dioxygen complex, we have examined ^{17}O -NMR spectroscopies for several copper-dioxygen complexes.
- (3) Heme oxygenase catalyzes the regiospecific oxidative degradation of iron protoporphyrin IX (heme) to biliverdin, CO and Fe, utilizing molecular oxygen and electrons donated from the NADPH-cytochrome P450 reductase. We have studied the reaction mechanism by using synthetic reaction intermediates and the enzyme obtained from bacterial expression.

Generation of Reactive Species via Electron Transfer on Metal Complexes, as Basis of Chemical Energy Conversion Systems

NAGATA, Toshi; ITO, Hajime; KIKUZAWA, Yoshihiro¹
(¹Kyoto Univ.)

This project aims at developing redox catalysis reactions suitable for chemical energy conversion. Our current interest focuses on modeling photosynthesis, that is, driving endothermic chemical transformation by using light energy via photoinduced electron transfer. Progress has been made in the following topics during the last year:

- A. Development of new binary (terpyridine-catechol) ligands that allow control over the metal coordination environment. This should enable us to design a series of redox catalysts with various electronic demand.
- B. Synthesis and photoreaction of a porphyrin/metal-complex dyad molecule, which exhibits photo-induced electron transfer followed by cleavage of a metal-ligand bond.
- C. Application of photoinduced electron transfer as a synthetic tool, where photoexcited molecules are considered from a synthetic point of view as short-lived reducing/oxidizing reagents.

OKAZAKI CONFERENCES

The Sixty-Second Okazaki Conference

Structural Hierarchy in Molecular Science: From Nano and Meso Structures to Micro Structures (January 10–13, 1999)

Organizers: AIDA, Takuzo (*Univ. Tokyo*)
FUJITA, Makoto (*IMS*)

The precise construction of large structures in the range of 1–1000 nm is of great importance in modern science. For constructing these structures, we need to consider “structural hierarchy” in a molecular world. At the first step, we prepare molecules by conventional syntheses. Then the molecular building blocks are linked together into larger structures by covalent or noncovalent approaches. The covalent approach may involve the use of large molecular units (*e.g.*, porphyrin, C60, carborane *etc.*) or branched polymerization (dendronimer synthesis), whereas noncovalent synthesis requires templating and self-assembly exploiting weak bonds (*e.g.*, donor-acceptor interaction, hydrogen bond, coordination bond). To build up the next structural hierarchy (nano to meso structures), there seem to be little efficient methods. Thus we need to discuss and develop new concepts and methodologies (which could be chemical, physical, or biological). Finally, we also consider micro structures built up from molecules. Crystal engineering is a rapidly developed field which provides a powerful method for obtaining precise micro structures from molecules. However, completely different approaches to micro structures are still awaited. Such view points prompted us to organize a meeting which would bring together scientists active in

a variety of fields: organic chemistry, inorganic chemistry, coordination chemistry, polymer science, material science, biochemistry, theoretical chemistry, *etc.* (that is to say, all fields in chemistry!) The following sessions were run in the conference with fruitful discussions.

- Molecular recognition - the first event for molecule-by-molecule syntheses
- Self-assembled nano structures
- Covalent approaches to nano structures: New class of polymers and dendrimers
- Function of nano structures
- Toward meso structures
- Precise control of micro structures: Crystal engineering
- Bio-related nano structures
- Perspective



The Sixty-Third Okazaki Conference

Laser Spectroscopy of Molecular Clusters — Structure and dynamics— (March 23–25, 1999)

Organizer: EBATA, Takayuki (*Tohoku Univ.*)
FUJII, Masaaki (*IMS*)

Invited Overseas Speakers:

LEUTWYLER, S. (*Univ. Bern*)
NEUSSER, H. J. (*Tech. Univ. München*)
ALBRECHT, A. C. (*Cornell Univ.*)
TOPP, M. (*Univ. Pennsylvania*)
XANTHEAS, S. S. (*Pacific Northwest Lab.*)
KLEINERMANN, K. (*Univ. Düsseldorf*)
LAENEN, R. (*Tech. Univ. München*)
WEINKAUF, R. (*Tech. Univ. München*)
DEDONDER-LARDEUX, C. (*Univ. Paris-sud Orsay*)
PARMENTER, C. (*Indiana Univ.*)

Molecular clusters in which molecules are bound by a weak inter-molecular force such as hydrogen bond or van der Waals force have been extensively studied since they provide us a detailed information of the inter-molecular potential. The information is quite useful to the investigation of the local structure and the vibrational relaxation in condensed phase. Furthermore, it may be possible to find new chemical reactions and them by use of the molecular clusters. However, it is quite recent that the cluster structures are accurately determined experimentally and theoretically. The purpose of the 63rd Okazaki conference was to present recent progress of laser spectroscopy and theory to reveal the structures and the dynamics of not only neutral but also ionic clusters.

We focused our attention on three subjects in this

conference. First is that to what extent the recent laser spectroscopic methods become powerful to determine the structure of the clusters. Second is the recognition how the recent theory, especially ab initio molecular orbital calculation, plays an important role for the determination or the prediction of the cluster structures. Third is that how our knowledge of molecular clusters can be applied to the problem of the condensed phase.

In the conference, 10 invited foreign speakers and 14 Japanese speakers gave excellent talks and 28 posters are presented. In spite of tight schedule, we had stimulated discussions. Many laser spectroscopic methods, that is mass-selected REMPI, MATI, ZEKE, photoelectron, population labeling, and double resonant vibrational spectroscopies were introduced. We saw how the electronic and vibrational spectra of an isolated molecule change upon the cluster formation and discussed how the spectra are compared with the structures predicted by ab initio calculations. The experimental studies on the dynamics of electronically and vibrationally excited clusters were presented. We also understood that in condensed phase the redistribution of the energy to the first shell molecules is the first step of the vibrational relaxation. In that sense, we again realized the importance of the communication between the scientists studied on clusters and on condensed phase.



Okazaki COE Conference

High Resolution Spectroscopy of Molecules and Atoms: Present Status and Future Trends
(March 17–19, 1999)

was very successful. The interdisciplinary discussions were stimulated and the further developments would be promoted.

Organizing Committee:

SAITO Shuji; MORITA Norio; KATO Tatsuhisa
(*Department of Molecular Structure*)

The Institute for Molecular Science (IMS) has been recognized as a Center of Excellence (COE) officially by the Ministry of Education, Science, Culture, and Sports of Japan. By the financial support from the Ministry we have an opportunity to organize an international symposium within this Japanese fiscal year.

Considering the recent remarkable experimental progress in the highly resolved spectroscopy of molecules and atoms not only in gaseous phase but also in condensed phase, we have determined the title of the symposium as "High Resolution Spectroscopy of Molecules and Atoms: Present Status and Future Trends." The symposium was held from March 17 (Wed) through 19 (Fri) in 1999 at the Okazaki Conference Center.

Recent experimental progress in the related various field of the highly resolved spectroscopy is remarkable, and we think that it is really timely and valuable to organize such a symposium to stimulate interdisciplinary information exchange and discussions and to promote further developments. We covered the following subjects: (1) Microwave spectroscopy of transient molecules, (2) Laser spectroscopy of molecules and atoms, (3) high resolution spectroscopy in solid.

Twenty five invited talks and twenty eight posters were presented, and about 100 people attended the conference. Very fruitful discussions were made among the different fields of the spectroscopy. The conference



JOINT STUDIES PROGRAMS

As one of the important functions of an inter-university research institution, IMS undertakes joint studies programs for which funds are available to cover research expenses as well as travel and living expenses of individuals. The proposals from domestic scientists are reviewed and controlled by an inter-university committee. The programs are carried out under one of five categories:

- (1) Joint Studies on Special Projects (a special project of significant relevance to the advancement of molecular science can be carried out by a team of several groups of scientists).
- (2) Research Symposia (a symposium on timely topics organized by collaboration between outside and IMS scientists).
- (3) Cooperative Research (a research program carried out by outside scientists with collaboration from an IMS scientist).
- (4) Use of Facility (a research program carried out by outside scientists at the research facilities of IMS except the UVSOR facility).
- (5) Joint Studies Programs Using beam lines at the UVSOR Facility.

A. Special Projects, B. Cooperative Research Projects, C. Invited Research Projects, D. Use-of-UVSOR Projects.

In the fiscal year 1998, the numbers of joint studies programs accepted for categories (1)–(4) were 1, 10, 107, and 223, respectively, and those accepted for subcategories 5(A)–5(D) were 3, 24, 2, and 157, respectively.

(1) Special Projects

A. Molecular Theory of Chemical Reactions in Solution

HIRATA, Fumio; KINOSHITA, Masahiro¹; SATO, Hirofumi; YOSHIMORI, Akira²; MATUBAYASI, Nobuyuki¹; NISHIYAMA, Katsura³

(¹Kyoto Univ.; ²Kyushu Univ.; ³Osaka Univ)

There are two aspects in chemical reactions: the reactivity or chemical equilibrium and the reaction dynamics. The reactivity of molecules is a synonym of the free energy difference between reactant and product. Two important factors determining the reactivity in solution are the changes in the electronic structure and the solvation free energy. Those quantities can be evaluated by the coupled quantum and the extended RISM equations, or RISM-SCF theory.

The exploration of the reaction dynamics is much more demanding. The reaction dynamics in solutions has two elements to be considered. One of those is the determination of reaction paths, the other the time evolution along the reaction path. The reaction path can be determined most naively by calculating the free energy map of reacting species. The RISM-SCF procedure can be employed for such calculations. If the rate-determining step of the reaction is an equilibrium between the reactant and the transition state, the reaction rate can be determined from the free energy difference of the two states based on the transition state theory. On the other hand, for such a reaction in which dynamics of solvent reorganization determines the reaction rate, the time evolution along the reaction path may be described by a coupled RISM and the generalised Langevin equation (GLE) with the same spirit as the Kramers theory: the time evolution along a reaction path can be viewed as a stochastic barrier crossing driven by thermal fluctuations and damped by friction. Our treatment features microscopic treatment of solvent structure in the level of the density pair

correlation functions, which distinguishes from the earlier attempts using phenomenological solvent models.

In the past year, we have made two important progresses along this line.

A-1 Dynamics of Ions in Water

The first progress we have made in the last year is to describe dynamics of ions in water in terms of interaction-site model of liquids. The friction of ions in water has been naturally decoupled into three contributions, the Stokes, dielectric and their coupling terms: those contributions interplay to give rise to the minimum in the ion-size vs. friction curve. The theory also could have reproduced qualitatively the simulation results for the velocity auto-correlation functions of ions in water. The progress is still very beginning stage toward the description of reaction dynamics, because the latter requires the response of solvent to the structural change of reacting species. However, such development is definitely a prerequisite of microscopic theory of reaction dynamics.

The progress has been reported in the publications listed below along with other related topics.

References

- 1) S. CHONG and F. HIRATA, *Chem. Phys. Lett.* **293**, 119 (1998).
- 2) S. CHONG and F. HIRATA, *Phys. Rev. E* **58** 6188 (1998).
- 3) S. CHONG and F. HIRATA, *Phys. Rev. E* **58** 7296 (1998).
- 4) S. CHONG and F. HIRATA, *J. Chem. Phys.* **111**, 3083 (1999).
- 5) S. CHONG and F. HIRATA, *J. Chem. Phys.* **111**, 3095 (1999).
- 6) S. CHONG and F. HIRATA, *J. Chem. Phys.* **111**, 3654 (1999).
- 7) M. KINOSHITA, Y. OKAMOTO and F. HIRATA, *J. Chem. Phys.* **110**, 4090 (1999).

A-2 Electronic State of a Molecule in Solvent

The other progress we have made in the last year is the excited state dynamics of a molecule in a variety of solvent: the electronic state of a molecule in solvent right after the vertical transition undergoes relaxation

due to solvation dynamics. Such dynamics has been described by means of a time dependent RISM-SCF approach taking benzonitrile as a probe molecule. To our knowledge, this is the first attempt to realize time evolution of electronic charge on atoms in solution after the vertical transition.

The progress has been reported in the publications listed below along with other related topics.

References

- 1) T. ISHIDA, F. HIRATA and S. KATO, *J. Chem. Phys.* **110**, 3938 (1999).
- 2) T. ISHIDA, F. HIRATA and S. KATO, *J. Chem. Phys.* **110**, 11423 (1999).
- 3) K. NAKA, H. SATO, A. MORITA, F. HIRATA and S. KATO, *Theor. Chem. Acc.* **102**, 165 (1999).
- 4) H. SATO and F. HIRATA, *J. Mol. Struct. (THEOCHEM)* **461-462**, 113 (1999).
- 5) H. SATO and F. HIRATA, *J. Am. Chem. Soc.* **121**, 2460 (1999).
- 6) H. SATO and F. HIRATA, *J. Phys. Chem. B* **103**, 6596 (1999).

(2) Research Symposia

(from September '98 to August '99)

1. Photo-Induced Phase Transition and Related Phenomena (October 28-30, 1998)
Chair: **KAMADA, Masao**
2. Recent Developments of Low-Temperature Matrix-Isolation Methods (November 6-7, 1998)
Chair: **NAKATA, Munetaka** (*Tokyo Univ. Agric. Tech.*)
3. Physical Chemistry, Now and Then (December 10, 1998)
Chair: **YOSHIHARA, Keitaro** (*JAIST*)
4. Application of Synchrotron Radiation to the Study of Nano-Structured Materials (March 26-27, 1999)
Chair: **URISU, Tsuneo**
5. Approach to Many-Body Interaction Systems (May 14-15, 1999)
Chair: **AIDA, Misako** (*Hiroshima Univ.*)
6. Symposium on Physical Chemistry for Young Researchers of Molecular Science (June 7, 1999)
Chair: **YAMANOUCHI, Kaoru** (*Univ. Tokyo*)
7. Ultrafast Dynamics of Molecules and Clusters (June 7-8, 1999)
Chair: **SUZUKI, Toshinori**
8. Chemistry of Atmospheric Ion Clusters and its Applications (June 16-17, 1999)
Chair: **NAGATO, Kenkichi**

9. The Role of the Investigation of Molecular Clusters: Present and Perspective (July 22-23, 1999)
Chair: **YAMADA, Kouichi** (*Natl. Inst. Adv. Interdisciplinary Res.*)

10. Photo-Dynamics and Reaction Dynamics of Molecules (July 30-August 2, 1999)
Chair: **UEDA, Kiyoshi** (*Tohoku Univ.*)

(3) Cooperative Research

This is one of the most important categories that IMS undertakes for conducting its own research of the common interest to both outside and IMS scientists by using the facilities at IMS. During the first half of the fiscal year of 1998 ending on September 30, 50 outside scientists joined Cooperative Research programs and during the second half, 57 outside scientists did. The names and affiliations of those collaborators are found in Research Activities.

(4) Use of Facility

The number of projects accepted for the Use-of-Facility Program of the Computer Center during the fiscal year of 1998 amounted 174 (699 users) and computer time spent for these projects is 45,402 hours (converted to the IBM SP2 time), and amounted to 70% of the total annual CPU time used. The numbers of projects accepted for the Use-of-Facility program during the fiscal year of 1998 amounted to 9 for the Laser Research Center for Molecular Science and 40 for the Research Center for Molecular Materials.

(5) UVSOR

In the UVSOR Facility with the 750 MeV electron storage ring, there are twenty beam lines available for synchrotron radiation research (see *UVSOR ACTIVITY REPORT 1998*). The Experimental Facility of each beam line is described also in this report. Under the following programs, a number of SR studies have been carried out by many users outside and inside IMS: A. the UVSOR Special Projects, B. the UVSOR Cooperative Research Projects, C. the UVSOR Invited Research Projects, and D. the Use-of-UVSOR Projects.

A. UVSOR Special Project

In fiscal year of 1998, following UVSOR special projects have been carried out.

1. Title: Upgrade of VUV beam line with installation of new monochromator

Beam Line: 7B

Representative of project: **NAKAGAWA, Hideyuki**
(*Fukui Univ.*)

2. Title: Construction of angle-resolved photoelectron spectrometer for organic thin films

Beam Line: 8B2

Representative of project: **UENO, Nobuo**

3. Title: Construction of high-efficiency beam line for SR-chemical reaction

Beam Line: 4A2

Representative of project: **URISU, Tsuneo**

B. UVSOR Cooperative Research Projects

Under this joint-study program, many synchrotron radiation experiments have been carried out with the beam lines of in-house staff in cooperation with scientists who were invited from other institutions. The total number of the projects in this category was 24 in the fiscal year of 1998.

C. The UVSOR Invited Research Projects

Under this joint-study program, several scientists were invited from other institutions of help for construction of new beam lines and improvement of the UVSOR storage ring and others. The total number of the projects in this category was 2 in the fiscal year of 1998.

D. The Use-of-UVSOR Projects

The out of the total of nineteen UVSOR beam lines are available for general users outside and inside IMS for their synchrotron radiation studies in the field of molecular science. The total number of the projects in this category was 157 in the fiscal year of 1998.

FOREIGN SCHOLARS

Visitors from abroad are always welcome at IMS and they have always played an important role in the research activities of the Institute. The foreign scientists who visited IMS during the past year (September 1998–August 1999) are listed below.

*¹ indicates attendance at an Okazaki Conference; *² a MONBUSHO (the Ministry of Education, Science, Sports and Culture, Japan) or JSPS (the Japan Society for the Promotion of Science) Invited Fellow; *³ an IMS councillor; *⁴ an IMS visiting professor or associate professor from abroad (period of stay from 6 to 12 months); *⁵ a JSPS Post-Doctoral or Ronpaku Fellow; *⁶ an IMS visiting scientist and *⁷ a visitor to IMS.

Scientists who would like to visit IMS under programs *² and *⁴ are invited to make contact with IMS staff in their relevant field.

Dr. Mark P. Roach ^{*5}	University of South Carolina	(Canada)	Nov. '97–
Dr. Maiti C. Nakul ^{*5}	Tata Inst. of Fundamental Research	(India)	Feb. '98–
Dr. Bailleux Stephane ^{*5}	Universite des Sci.s & Technologoede Lille	(France)	Apr. '98–
Prof. Xian-He Bu ^{*2*4}	Nankai University	(China)	Jun. '98–
Prof. Fred Wudl ^{*6}	Univ. of California	(U.S.A.)	Sep. '98
Ms. Ghosh Mahua ^{*7}	Tata Inst. of Fundamental Research	(India)	Sep. '98
Prof. Siva Umapathy ^{*2*4}	Indian Inst. of Science	(India)	Sep. '98–Feb. '99
Dr. Shanta Mukhopadhyay ^{*5}	Ind. Assoc. for the Cultivation of Science	(India)	–Oct. '98
Dr. Mojzsh Peter ^{*7}	Charles Univ.	(Czech)	Oct. '98
Dr. Olga Drozdova ^{*7}	Russian Academy of Sciences	(Russia)	Oct. '98
Prof. Michael Duncan ^{*7}	Univ. of Georgia	(U.S.A.)	Oct. '98
Prof. Maitra Uday ^{*7}	Indian Inst. of Science	(India)	Oct. '98
Prof. Yongfang Li ^{*2}	The Chinese Academy of Sciences	(China)	Oct.–Nov. '98
Prof. Lubomir Pavlov ^{*7}	Inst. of Electronics Bulgarian Academy of Science	(Bulgaria)	Oct.–Nov. '98
Prof. Melvin Okamura ^{*7}	Univ. of California San Diego	(U.S.A.)	Nov. '98
Prof. Gerhard Hirsch ^{*7}	Univ. of Wuppertal	(Germany)	Nov. '98
Prof. Sourav Pal ^{*7}	National Chemistry Lab. Pune	(India)	Nov. '98
Prof. Stang J. Peter ^{*7}	Univ. of Utah	(U.S.A.)	Nov. '98
Dr. Olga Drozdova ^{*7}	Russian Academy of Sciences	(Russia)	Nov.–Dec. '98
Prof. Hans Ågren ^{*2}	Linköping Univ.	(Sweden)	Nov. '98–Jan. '99
Prof. B. L. Tembe ^{*2}	I. I. T. Bombay	(India)	Nov. '98–Mar. '99
Dr. S. Y. Arzhantsev ^{*5}	Moscow State Univ.	(Russia)	Nov. '98–
Dr. Hu Ying ^{*5}	Fudan Univ.	(China)	Nov. '98–
Prof. Marek J. Wojcik ^{*2*4}	Jagiellonian Univ.	(Poland)	–Dec. '98
Prof. T.-C. Chambron ^{*7}	Univ. Louis Pasteur	(France)	Dec. '98
Prof. Dimitra Markovitsi ^{*7}	Laboratoire de Réactiviféet	(France)	Dec. '98
Prof. Keitaro Nakatani ^{*7}	École Normale Supérieure	(France)	Dec. '98
Prof. Denis Rousseau ^{*6}	Albert Einstein College	(U.S.A.)	Dec. '98
Dr. Oleg I. Tolstikhin ^{*6}	Russian Research Center "Kurchatov Inst."	(Russia)	Dec. '98
Dr. Volker Deckert ^{*6}	ETH Zentrum Zuerich	(Switzerland)	Dec. '98
Prof. Vladimir Laukhim ^{*7}	Russian Academy of Sciences	(Russia)	Dec. '98
Prof. Kyoung-Koo Baeck ^{*2}	Kang-Nung National Univ.	(Korea)	Dec. '98–Feb. '99
Prof. Vladimir I. Osherov ^{*6}	Russian Academy of Sciences	(Russia)	Dec. '98–Mar. '99
Prof. Leonard Proniewicz ^{*2}	Jagellonian Univ.	(Poland)	Dec. '98–Mar. '99
Dr. Li Wang ^{*5}	Dalian Institute of Chemical Physics	(China)	–Jan. '99
Dr. Lars Ptersson ^{*2*4}	Stockholm University	(Sweden)	–Jan. '99
Prof. Peter Day ^{*7}	Royal Inst. of the Great Britain	(U.K.)	Jan. '99
Dr. Naimark A. Wendy ^{*7}	California Inst. of Technology	(U.S.A.)	Jan. '99
Dr. Olga Drozdova ^{*7}	Russian Academy of Sciences	(Russia)	Jan. '99
Dr. Mark A. Vander ^{*7}	K. U. Leuven Univ.	(Belgium)	Jan. '99
Prof. Seokmin Shin ^{*2}	Seoul National Univ.	(Korea)	Jan.–Mar. '99
Prof. Younkoo Kim ^{*2*4}	Hankuk University of Foreign Studies	(Korea)	–Feb. '99
Prof. David Parker ^{*7}	Nijmegen Univ.	(Holland)	Feb. '99
Prof. Jamal Musae ^{*7}	Emory Univ.	(U.S.A.)	Feb. '99
Ms. Margarethe Kampling ^{*6}	Fritz Haer Inst.	(Germany)	Feb. '99
Dr. Olga Drozdova ^{*7}	Russian Academy of Sciences	(Russia)	Feb. '99
Prof. Anthony J. Stace ^{*7}	Sussex Univ.	(U.K.)	Feb. '99
Prof. Lubomir Pavlov ^{*6}	Inst. of Electronics Bulgarian Academy of Science	(Bulgaria)	Feb.–Mar. '99
Dr. Petr Toman ^{*6}	Academy of Sciences of the Czech Republic	(Czech)	Feb.–Mar. '99
Prof. Stanislav Nespurek ^{*6}	Academy of Sciences of the Czech Republic	(Czech)	Feb.–Mar. '99
Prof. Yongli Gao ^{*2*4}	Univ. of Rochester	(U.S.A.)	Feb.–Jul. '99
Prof. Jacek Ulanski ^{*2*4}	Technical Univ. of Lodz	(Poland)	Feb.–Aug. '99

Dr. T. C. Whitham ^{*7}	Oxford Univ.	(U.K.)	Mar. '99
Prof. Thomas W. Bell ^{*7}	Univ. of Nevada at Reno	(U.S.A.)	Mar. '99
Dr. Nicoletta N. Kahya ^{*7}	Univ. of Groningen	(Holland)	Mar. '99
Dr. Imtiaz K. Ahmad ^{*7}	Univ. of Cambridge	(U.K.)	Mar. '99
Dr. Thomas Steffen ^{*7}	Philips Reseach Laboratories Eindhoven	(Holland)	Mar. '99
Prof. Peter Bernath ^{*7}	Univ. of Waterloo	(Canada)	Mar. '99
Prof. Michael C. Heaven ^{*7}	Emory Univ.	(U.S.A.)	Mar. '99
Prof. Gregory E. Hall ^{*7}	Brookhaven National Laboratory	(U.S.A.)	Mar. '99
Prof. Michael C. McCarthy ^{*7}	Harvard-Smithsonian Center for Astrophysics	(U.S.A.)	Mar. '99
Prof. C. von Borczyskowski ^{*7}	Univ. of Technology Chemnitz	(Germany)	Mar. '99
Prof. Peter Botschwina ^{*7}	Univ. of Goettingen	(Germany)	Mar. '99
Prof. Andrei F. Vilesov ^{*7}	MPI for Fluid Dynamics	(Germany)	Mar. '99
Prof. K. P. Dinse ^{*7}	TH Darmstadt	(Germany)	Mar. '99
Prof. Timothy C. Steimle ^{*7}	Arizona State Univ.	(U.S.A.)	Mar. '99
Prof. Antoine R. Weis ^{*7}	IAP, Univ. of Bonn	(Germany)	Mar. '99
Prof. Jan Schmidt ^{*7}	Leiden Univ.	(Holland)	Mar. '99
Prof. Takeshi Oka ^{*7}	Univ. of Chicago	(U.S.A.)	Mar. '99
Prof. John M. Brown ^{*7}	Oxford Univ.	(U.K.)	Mar. '99
Prof. John P. Maier ^{*7}	Univ. of Basel	(Switzerland)	Mar. '99
Prof. Karl Kleineremanns ^{*1}	Univ. Munchen	(Germany)	Mar. '99
Dr. Robert Laenen ^{*1}	Univ. Munchen	(Germany)	Mar. '99
Prof. Michael Topp ^{*1}	Univ. of Pennsylvania	(U.S.A.)	Mar. '99
Prof. Samuel Leutwyler ^{*1}	Univ. Bern	(Switzerland)	Mar. '99
Dr. C. Dedonder-Lardeux ^{*1}	Universite de Puris-Sud	(France)	Mar. '99
Prof. Hans Neusser ^{*1}	Univ. Munchen	(Germany)	Mar. '99
Dr. Rainer Weinkauff ^{*1}	Univ. Munchen	(Germany)	Mar. '99
Prof. Andeas Albrecht ^{*1}	Cornell Univ.	(U.S.A.)	Mar. '99
Prof. Soritis Xantheas ^{*1}	Pacific Northwest Laboratory	(U.S.A.)	Mar. '99
Prof. Wendy Flavell ^{*7}	Dept. of Physics UMIST	(U.K.)	Mar. '99
Prof. Bruce Hamilton ^{*7}	Dept. of Physics UMIST	(U.K.)	Mar. '99
Dr. Chris Binns ^{*7}	Univ. of Leicester	(U.K.)	Mar. '99
Dr. Dave Teehan ^{*7}	Synchrotron Radiation Dept. Daresbury Lab.	(U.K.)	Mar. '99
Prof. Ian Munro ^{*7}	Dept. of Physics UMIST	(U.K.)	Mar.-Apr. '99
Dr. Sergei Belov ^{*2}	Inst. of Applied Physics.	(Russia)	Mar.-May '99
Prof. Brian Sutcliffe ^{*2}	Univ. of York	(U.K.)	Mar.-Jun. '99
Dr. Gennady Mil'nikov ^{*5}	Inst. of Chemical Phys	(Russia)	Mar. '99-
Prof. Benjamin Whitaker ^{*6}	Univ. of Leeds	(U.K.)	Apr. '99
Mr. Prasanna Ghulsasi ^{*5}	BhaBha Atomic Research Center	(India)	Apr. '99-
Dr. Puspita Waheeda Jahan ^{*5}	Nagoya Univ.	(Japan)	Apr. '99-
Prof. Ashot Markosyan ^{*2*4}	M. V. Lomonosov Moscow State Univ.	(Russia)	Apr. '99-
Dr. Olga Drozdova ^{*7}	Russian Academy of Sciences	(Russia)	May '99
Dr. Stephen Gray ^{*6}	Argonne National Laboratory	(U.S.A.)	May '99
Dr. Avadh Saxena ^{*7}	Los Alamos National Laboratory	(U.S.A.)	May '99
Prof. Uwe Becker ^{*7}	Fritz Haber Inst. de Max Planck Gesellschaft	(Germany)	May '99
Prof. I. Simandi Laszlo ^{*6}	Hungareian Academy of Science	(Hungary)	May-Jun. '99
Dr. Mkhitary V. Simonyan ^{*2*4}	Inst. for Phys. Res. of Armenian National Acad. of Sci.	(Armenian)	-Jun. '99
Prof. C. A. de Lange ^{*6}	Univ. of Amsterdam	(Holland)	Jun. '99
Prof. Ming Chang Lin ^{*7}	Emory Univ.	(U.S.A.)	Jun. '99
Dr. Olga Drozdova ^{*7}	Russian Academy of Sciences	(Russia)	Jun.-Jul. '99
Prof. Chung Gyusung ^{*2}	Konyang Univ.	(Korea)	Jun.-Aug. '99
Prof. Jong-Ho Choi ^{*2}	Korea Univ.	(Korea)	Jun.-Aug. '99
Prof. Zdenek Herman ^{*6}	J. Heyrovsky Institute of Physical Chemistry	(Czech)	Jul. '99
Prof. Nikolaus Schwentner ^{*7}	Institut Für Experimental physik FU Berlin	(Germany)	Jul. '99
Prof. Sang Yeon Lee ^{*2}	Kyungpook National Univ.	(Korea)	Jul.-Aug. '99
Mr. Alistair David Nelson ^{*2}	Univ. of Edinburgh	(U.K.)	Jul.-Aug. '99
Mr. James Arthur England ^{*2}	Chemistry Department Univ. of Surrey	(U.K.)	Jul.-Aug. '99
Prof. Peter Zimmermann ^{*7}	Technische Universitaet Berlin	(Germany)	Jul.-Aug. '99
Prof. Wim van der Zande ^{*7}	FOM-Inst. for Atomic and Molecular Physics	(Holland)	Jul.-Aug. '99
Prof. Uwe Becker ^{*7}	Fritz Haber Inst. de Max Planck Gesellschaft	(Germany)	Jul.-Aug. '99
Mr. Alberto De Fanis ^{*7}	Univ. of Southampton	(U.K.)	Jul.-Aug. '99
Prof. Nikolay Cherepkov ^{*7}	Photon Factory Inst. of Materials Structure Sci. KEK	(Russia)	Jul.-Aug. '99
Prof. William Miller ^{*7}	Department of Chemistry Univ. of California	(U.S.A.)	Jul.-Aug. '99
Prof. Ulrich Heinzmann ^{*7}	Department of Physics, Univ. of Bielefeld	(Germany)	Jul.-Aug. '99
Prof. John Zhang ^{*7}	New York Univ.	(U.S.A.)	Jul.-Aug. '99

Prof. Mats Larsson ^{*7}	Stockholm Univ.	(Sweden)	Jul.–Aug. '99
Prof. David Manolopoulos ^{*7}	Univ. of Oxford	(U.K.)	Jul.–Aug. '99
Prof. Floyd Davis ^{*7}	Cornell Univ.	(U.S.A.)	Jul.–Aug. '99
Prof. Kopin Liu ^{*7}	Inst. of Atomic and Molecular Sciences	(Taiwan)	Jul.–Aug. '99
Dr. Pascal Lablanquie ^{*7}	LURE Centre, Univ. Paris Sud.	(France)	Jul.–Aug. '99
Dr. Arno Ehresmann ^{*7}	Univ. of Kaiserslautern	(Germany)	Jul.–Aug. '99
Prof. Keith Codling ^{*7}	Univ. of Reading	(U.K.)	Jul.–Aug. '99
Dr. Ottmar Jagutzki ^{*7}	Univ. Frankfurt	(Germany)	Jul.–Aug. '99
Dr. John West ^{*7}	Daresbury Laboratory	(U.K.)	Jul.–Aug. '99
Prof. S. V. K. Kumar ^{*7}	Tata Inst. of Fundamental	(India)	Jul.–Aug. '99
Dr. Shilin Liu ^{*7}	Univ. of Tokyo	(Japan)	Jul.–Aug. '99
Prof. Ronald McCarroll ^{*7}	Universite Pierre et Marie Curie	(France)	Jul.–Aug. '99
Mr. Han-Chul Kwon ^{*7}	Korea Univ.	(Korea)	Jul.–Aug. '99
Mr. Jong-Ho Park ^{*7}	Korea Univ.	(Korea)	Jul.–Aug. '99
Mr. Hee-Kyung Kim ^{*7}	Korea Univ.	(Korea)	Jul.–Aug. '99
Prof. Vijay Kumar ^{*7}	Navrangpura Physical Research Lab.	(India)	Jul.–Aug. '99
Mr. Eun-Sook Kim ^{*7}	Korea Univ.	(Korea)	Jul.–Aug. '99
Prof. H. Schmidt-Boecking ^{*7}	Univ. Frankfurt	(Germany)	Jul.–Aug. '99
Prof. Klaus Müller-Dethlefs ^{*2}	The Univ. of York	(U.K.)	Jul. '99–
Prof. Vladimir I. Osherov ^{*2*4}	Russian Academy of Sciences	(Russia)	Jul. '99–
Prof. Friedlich Siebert ^{*7}	Univ. of Freiburg	(Germany)	Aug. '99
Dr. Samantha Warren ^{*7}	Univ. of Manchester Inst. of Science and Technology	(Germany)	Aug. '99
Prof. Lemee Cailleau ^{*6}	Rennes Univ.	(France)	Aug. '99
Prof. Herve Cailleau ^{*6}	Rennes Univ.	(France)	Aug. '99
Prof. John Dawson ^{*6}	Univ. of South Carolina	(U.S.A.)	Aug. '99
Dr. Franz Xaver Bronold ^{*7}	Otto von Guericke Univ.	(Germany)	Aug. '99–
Prof. Luis Seijo ^{*2}	Universidad Autonoma de Madrid	(Spain)	Aug. '99–

AWARDS

Professor Tanaka's Scientific Achievements

Professor Koji Tanaka of Coordination Chemistry Laboratories received the Divisional Award of the Chemical Society of Japan in Inorganic Chemistry and Analytical Chemistry in 1998 for his contribution to "Studies on Reactivity of Carbon Dioxide Activated on Metal Complexes."

His scientific achievements relevant to the award are summarized as following.

1. Interconversion among $-\text{CO}$, $-\text{COOH}$, $-\text{CO}_2$ on metal complexes. He has proved that the ruthenium carbonyl complex having bipyridine ligands is converted into $-\text{COOH}$ and $-\text{CO}_2$ complex depending on pH. With the isolation and structure analysis, he has clarified the nature of Ru-C bonds in Ru-CO, Ru-COOH and Ru-CO₂.
2. Multi-electron reduction of CO₂ via formyl and acyl complexes. He has proved the carbonyl ligand is converted into formyl and hydroxymethyl ligands in protic condition by the repression of Ru-CO bond cleavage. He has also developed multi-electron reduction catalyst for CO₂ affording acetone via acyl complexes under aprotic conditions.
3. Activation of CO₂ on bridging sulfur atom. He has demonstrated the reduction of CO₂ on bridging sulfur atom produces oxalate and pyruvate without the C-O bond dissociation.

Associate Professor Morita's Scientific Achievements

Associate Professor Norio Morita of Department of Molecular Structure received the Matsuo Science Award in 1998 for his contribution to "Laser Spectroscopy of Antiprotonic Helium Atomcules." He carried out successfully the laser spectroscopy of a new exotic atom, "antiprotonic helium atomcule," in collaboration with an international research group of nuclear physics at CERN, and found out its resonance lines for the first time. The antiprotonic helium atomcule is a helium atom in which one of its two electrons is replaced with an antiproton, and is a completely new compound with both characters of atoms and molecules. However, before his spectroscopic study, the existence of such a strange entity had only been inferred from the extraordinarily long lifetime of antiprotons scattered in liquid helium. His achievement did not only confirm its existence, but also contributed to the establishment of a new interdisciplinary research field.

Associate Professor Kanoda's Scientific Achievements

Associate Professor Kazushi Kanoda of Department of Molecular Assemblies (June '98-: the University of Tokyo) received the IBM Japan Science Prize in 1998 for his contribution to "Investigation on Metal-Insulator Transitions and Mechanism of Superconductivity in Molecular Solids." His scientific achievements are summarized as follows.

1. Clarify the charge and spin states in various electronic phases of κ -type BEDT-TTF compounds with different counter ions by NMR, magnetic susceptibility, electrical conductivity and specific heat measurements.
2. Propose a possible phase diagram of κ -type systems considering bandwidth and electron correlation within the framework of competition between Mott-insulator and highly correlated metal.
3. Observation of the antiferromagnetic spin fluctuation in the paramagnetic states that is one of the characteristic features of highly correlated electron systems.

Associate Professor Taira's Scientific Achievements

Associate professor Takunori Taira of Laser Research Center for Molecular Science received Medal for Review Paper from the Laser Society of Japan in 1999 for his contributions to "Microchip solid-state Lasers."

His scientific achievements related to this award are:

- 1) to have established design rules of microchip solid-state lasers,
- 2) to have first demonstrated a Nd:YVO₄-based microchip laser,
- 3) to have obtained a low-noise, mode-hopping-free, tunable microchip laser,
- 4) to have achieved frequency control of a high power YAG laser injection-seeded by the Nd:YVO₄-based microchip laser.

"Microchip laser," which is coined by the professor, has now become popular even in the commercial world. This is clear evidence that his works have pioneered the field of laser-diode-pumped solid-state compact lasers.

Dr. Takahashi's Scientific Achievements

The 15th Inoue Research Award for Young Scientists in 1998 was given to Dr. Masaki Takahashi, who was a graduate student studying in the Department of Applied Chemistry, Faculty of Engineering, Chiba University. This award is given to young scientists (under 35 years old) who obtained remarkable results during their Ph.D. work in the fields of basic science, engineering, medicine, pharmacy, and agriculture. Dr. Takahashi was awarded this prize for his Ph.D. thesis, "Photochemical Reactions under Chiral Crystalline Environment."

Mr. Nishimoto's Technological Achievements

Mr. Fumio Nishimoto, The chief of the technical section of Computer Center, received the Award of the Technological Development in Chemistry for 1999.

This Award is made every year by the Chemical Society of Japan to a person who has contributed to the development or improvement of the experimental technique in chemistry or chemical engineering. Mr. Fumio Nishimoto is recognized for his contribution to "Development and Popularization of Supercomputer Environments for Molecular Science Computations." Mr. Nishimoto developed the following system and software for the users of Computer Center: (1) Scheduled Power Supply System for general purpose- and super- computer, 1979–1986, (2) Dynamic Job scheduling system for general purpose- and super- computer, 1979–1991, (3) Total environment system for output and printing for user-job, 1979–1991. Since the commercial software for the large scale simulation has not been well established, these system and software has been installed for the use of not only Computer Center but also other universities, *i.e.*, the Univ. of Tokyo, and Hokkaido Univ.

LIST OF PUBLICATIONS

Department of Theoretical Studies

- P. BANDYOPADHYAY, S. TEN-NO and S. IWATA**, "Ab initio Monte Carlo Simulation Using Multicanonical Algorithm: Temperature Dependence of the Average Structure of Water Dimmer," *Mol. Phys.* **96**, 349 (1998).
- S. HIRATA and S. IWATA**, "Analytical Energy Gradients in Second-Order Moller-Plesset Perturbation Theory for Extended Systems," *J. Chem. Phys.* **110**, 121 (1998).
- S. HIRATA and S. IWATA**, "Ab initio Hartree-Fock and Density Functional Studies on the Structures and Vibrations of an Infinite Hydrogen Fluoride Polymer," *J. Phys. Chem.* **102**, 8426 (1998).
- A. WADA, H. KANAMORI and S. IWATA**, "Ab initio MO Studies of van der Waals Molecule (N₂)₂: Potential Energy Surface and Internal Motion," *J. Phys. Chem.* **109**, 9434 (1998).
- T. SUZUKI, T. IKEGAMI, M. FUJII and S. IWATA**, "Theoretical Studies of Internal Methyl Rotations in *m*-Xylene: Comparison of Franck-Condon Factors with the Experimental Spectra," *J. Mol. Struct. (THEOCHEM)* **461-462**, 79 (1999).
- S. TEN-NO, S. IWATA, S. PAL and D. MUKHERJEE**, "Generalization of the Coupled-Cluster Response Theory to Multireference Expansion Spaces: An Application of the Coupled-Cluster Singles and Doubles Effective Hamiltonian," *Theor. Chem. Acc.* **102**, 252 (1999).
- T. IKEGAMI and S. IWATA**, "Photodissociation Dynamics of Argon Cluster Ions," *J. Chem. Phys.* **110**, 8492 (1999).
- P. NACHTIGALL, J. HRUSAK, O. BLUDSKY and S. IWATA**, "Investigation of the Potential Energy Surfaces for the Ground X¹A₁ and Excited C¹B₂ electronic states of SO₂," *Chem. Phys. Lett.* **303**, 441 (1999).
- P. BANDYOPADHYAY, S. TEN-NO and S. IWATA**, "Structures and Photoelectron Spectroscopies of Si₂C₂⁻ Studied with ab initio Multicanonical Monte Carlo Simulation," *J. Phys. Chem. A* **103**, 6442 (1999).
- T. TSURUSAWA and S. IWATA**, "Theoretical Studies of Structures and Ionization Threshold Energies of Water Cluster Complexes with a Group 1 Metal, M(H₂O)_n (M = Li and Na)," *J. Phys. Chem. A* **103**, 6134 (1999).
- S. TEN-NO and S. IWATA**, "On Connection between the Reference Interaction Site Model Integral Equation Theory and the Partial Wave Expansion of the Molecular Orstein-Zernike Equation," *J. Chem. Phys.* **111**, 4865 (1999).
- M. KINOSHITA, Y. OKAMOTO and F. HIRATA**, "Calculation of Solvation Free Energy for a Peptide in Salt Solution Using the RISM Theory," *J. Comput. Chem.* **19**, 1724 (1998).
- U. H. E. HANSMANN, F. EISENMENGER and Y. OKAMOTO**, "Stochastic Dynamics Simulations in a New Generalized Ensemble," *Chem. Phys. Lett.* **297**, 374 (1998).
- M. KINOSHITA, Y. OKAMOTO and F. HIRATA**, "Singular Behavior of the Reference Interaction Site Model Theory Observed for Peptide in Salt Solution," *Chem. Phys. Lett.* **297**, 433 (1998).
- T. NAKAZAWA and Y. OKAMOTO**, "Electrostatic Effects on the α -Helix and β -Strand Folding of BPTI(16-36) as Predicted by Monte Carlo Simulated Annealing," *J. Pept. Res.* **54**, 230 (1999).
- U. H. E. HANSMANN, Y. OKAMOTO and J. N. ONUCHIC**, "The Folding Funnel Landscape for the Peptide Met-Enkephalin," *Proteins: Struct., Funct., Genet.* **34**, 472 (1999).
- U. H. E. HANSMANN and Y. OKAMOTO**, "Finite-Size Scaling of Helix-Coil Transitions in Poly-Alanine Studied by Multicanonical Simulations," *J. Chem. Phys.* **110**, 1267 (1999).
- Y. OKAMOTO, M. MASUYA, M. NABESHIMA and T. NAKAZAWA**, " β -Sheet Formation in BPTI(16-36) by Monte Carlo Simulated Annealing," *Chem. Phys. Lett.* **299**, 17 (1999).
- M. KINOSHITA, Y. OKAMOTO and F. HIRATA**, "Analysis on Conformational Stability of C-Peptide of Ribonuclease A in Water Using the Reference Interaction Site Model Theory and Monte Carlo Simulated Annealing," *J. Chem. Phys.* **110**, 4090 (1999).
- U. H. E. HANSMANN and Y. OKAMOTO**, "Effects of Side-Chain Charges on α -Helix Stability in C-Peptide of Ribonuclease A Studied by Multicanonical Algorithm," *J. Phys. Chem. B* **103**, 1595 (1999).
- A. MITSUTAKE, M. IRISA, Y. OKAMOTO and F. HIRATA**, "Classification of Low-Energy Conformations of Met-Enkephalin in the Gas Phase and in a Model Solvent Based on the Extended Scaled Particle Theory," *Bull. Chem. Soc. Jpn.* **72**, 1717 (1999).
- A. MITSUTAKE and Y. OKAMOTO**, " α -Helix Propensities of Homo-Oligomers in Aqueous Solution Studied by Multicanonical Algorithm," *Chem. Phys. Lett.* **309**, 95 (1999).
- G. V. MIL'NIKOV, C. ZHU, H. NAKAMURA and V. I. OSHEROV**, "Semiclassical Treatment of Resonances in the Collinear O + HO Exchange Reaction," *Chem. Phys. Lett.* **293**, 448 (1998).
- C. ZHU and H. NAKAMURA**, "Improvement of the Adiabatic Phase Integral for the Landau-Zener Type Curve Crossing," *J. Chem. Phys.* **109**, 4689 (1998).
- O. I. TOLSTIKHIN, V. N. OSTROVSKY and H. NAKAMURA**, "Siebert Pseudo-State Formulation of Scattering Theory: One-Channel Case," *Phys. Rev. A* **58**, 2077 (1998).
- V. N. OSTROVSKY and H. NAKAMURA**, "Patterns of Time-Propagation on the Grid of Potential Curves," *Phys. Rev. A* **58**, 4293 (1998).
- Y. TERANISHI and H. NAKAMURA**, "Control of Time-Dependent Nonadiabatic Processes by an External

Field," *Phys. Rev. Lett.* **81**, 2032 (1998).

K. NOBUSADA, O. I. TOLSTIKHIN and H. NAKAMURA, "Quantum Reaction Dynamics of Heavy-Light-Heavy Systems: Reduction of the Number of Potential Curves and Transitions at Avoided Crossings," *J. Phys. Chem. A* **102**, 9445 (1998).

K. NOBUSADA, O. I. TOLSTIKHIN and H. NAKAMURA, "Quantum Reaction Dynamics of $\text{Cl} + \text{HCl} \rightarrow \text{HCl} + \text{Cl}$: Vibrationally Nonadiabatic Reactions," *J. Mol. Struct. (THEOCHEM)* **461-462**, 137 (1999).

V. I. OSHEROV and H. NAKAMURA, "Analytic Solution of Two-State Time-Independent Coupled Schrödinger Equations in an Exponential Model," *Phys. Rev. A* **59**, 2486 (1999).

G. V. MIL'NIKOV, O. I. TOLSTIKHIN, K. NOBUSADA and H. NAKAMURA, "Quantum Reaction Dynamics of Asymmetric Exoergic Heavy-Light-Heavy Systems: $\text{Cl} + \text{HBr} \rightarrow \text{HCl} + \text{Br}$," *Phys. Chem. Chem. Phys.* **1**, 1159 (1999).

H. NAKAMURA, "Molecular Switching in a Two-Dimensional Constriction," *J. Chem. Phys.* **110**, 10253 (1999).

Y. TERANISHI and H. NAKAMURA, "New way of Controlling Molecular Processes by Time-Dependent External Fields," *J. Chem. Phys.* **111**, 1415 (1999).

Y. IMAMURA, S. TEN-NO, K. YONEMITSU and Y. TANIMURA, "Theoretical Study on Correlation of 1-D-(DCNQI)₂M (M = Li, Ag) Salts," *Chem. Phys. Lett.* **298**, 15 (1998).

K. OKUMURA and Y. TANIMURA, "Two-Dimensional THz Spectroscopy of Liquids: Nonlinear Vibrational Response to a Series of THz Laser Pulses," *Chem. Phys. Lett.* **295**, 298 (1998).

K. OKUMURA, A. TOKMAKOFF and Y. TANIMURA, "Structural Information from Two-dimensional Fifth-Order Raman Spectroscopy," *J. Chem. Phys.* **111**, 492 (1999).

G. GANGOPADHYAY, S. GHOSHAL and Y. TANIMURA, "A Thermal Bath Induced New Resonance in Linear and Nonlinear Spectra of Two-Level Systems," *Chem. Phys.* **242**, 367 (1999).

Y. SUZUKI and Y. TANIMURA, "Optimized Perturbation Approach with Legendre Transformation to a Dissipative System: Correlation Functions of a Morse Oscillator," *Phys. Rev. E* **59**, 1475 (1999).

Y. IMAMURA, S. TEN-NO, K. YONEMITSU and Y. TANIMURA, "Ab initio MO Studies on Electronic States of DCNQI Molecules," *J. Phys. Chem. B* **103**, 266 (1999).

H. SUZUKI, N. SHIMAKURA, T. SHIRAI and M. KIMURA, "Molecular-State Treatment of Electron Capture in Collisions of Be^{3+} Ions with He Atoms below 10 keV/u," *J. Phys. B* **31**, 1741 (1998).

J. P. GU, G. HIRSCH, R. J. BUENKER, M. KIMURA, C. M. DUTTA and P. NORDLANDER, "Charge Transfer in Collisions of C^{2+} Ions with H Atoms at Low-keV Energies: A Possible Bound State of CH_2^+ ," *Phys. Rev. A* **57**, 4483 (1998).

O. SUEOKA, H. TAKAGI, A. HAMADA and M. KIMURA, "Total Cross Sections of Electron and Positron Collisions with CHF_3 Molecules: A Comparative Study with CH_4 and CF_4 ," *Chem. Phys. Lett.* **288**, 124 (1998).

J. P. GU, Y. LI, G. HIRSCH, R. J. BUENKER and M. KIMURA, "Ab Initio Calculations of Proton-Hydrocarbon Scattering Cross Sections," *J. Phys. Chem. A* **102**, 7127 (1998).

M. KIMURA, "Electron Capture Processes in Fusion Plasma," *J. Plasma Fusion Res. A* **74**, 542 (1998).

P. STANCIL, J. P. GU, C. C. HAVENER, P. S. KRSTIC, D. R. SCHULTZ, M. KIMURA, B. ZYGELMAN, G. HIRSCH, R. J. BUENKER and M. E. BANNISTER, "Electron Capture in Collisions of C^+ with H and H^+ with C," *J. Phys. B* **31**, 1 (1998).

P. STANCIL, C. C. HAVENER, P. S. KRSTIC, D. R. SCHULTZ, M. KIMURA, J. P. GU, G. HIRSCH, R. J. BUENKER and B. ZYGELMAN, "Charge Transfer in Collisions of C^+ with H and H^+ with C," *Astrophys. J.* **502**, 1006 (1998).

T. KAMBARA, M. KIMURA, Y. AWAYA, T. M. KOJIMA, V. MERGEL, Y. NAKAI and H. SCHMIDT-BOCKING, "State-Selective Differential Cross Sections of Electron Capture in 10 keV Ar^{8+} -He Collisions," *J. Phys. B* **31**, L909 (1998).

A. WATANABE, R. SUZUKI, H. SATO and M. KIMURA, "Calculations of Non-Adiabatic Coupling Matrix Elements in the Molecular Orbital Expansion Method," *Nat. Sci. Rep. Ochanomizu Univ.* **49**, 33 (1998).

M. KIMURA, C. M. DUTTA, P. NORDLANDER, J. P. GU, G. HIRSCH and R. J. BUENKER, "Charge Transfer in Collisions of H^+ Ions with P Atoms below 100 keV," *Phys. Rev. A* **59**, 405 (1998).

H. TANAKA, M. KITAJIMA, O. SUEOKA, A. HAMADA and M. KIMURA, "Total and Differential Cross Sections of C_3H_8 and C_3F_8 by Electron and Positron Impacts," *Phys. Rev. A* **59**, 2006 (1999).

T. KUSAKABE, K. HOSOMI, H. NAKANISHI, H. TAWARA, M. SASAO, Y. NAKAI and M. KIMURA, "Charge Transfer Processes in Collisions of Ground State C^+ Ions with H_2 , D_2 , CO and CO_2 Molecules in the Energy Range from 0.5 keV to 4.5 keV," *Phys. Rev. A* **60**, 345 (1999).

M. KINOSHITA, Y. OKAMOTO and F. HIRATA, "Calculation of Solvation Free Energy for a Peptide in Salt Solution Using the RISM Theory," *J. Comput. Chem.* **19**, 1724 (1998).

M. KINOSHITA, Y. OKAMOTO and F. HIRATA, "Singular Behavior of the Reference Interaction Site Model Theory Observed for Peptide in Salt Solution," *Chem. Phys. Lett.* **297**, 433 (1998).

S. CHONG and F. HIRATA, "Effect of Molecular Symmetry on Electrical Potential Fluctuations of Solvent around Solute in Polar Liquid," *Chem. Phys. Lett.* **293**, 119 (1998).

S. CHONG and F. HIRATA, "Mode-Coupling Theory for Molecular Liquids Based on the Interaction-Site

Model," *Phys. Rev. E* **58**, 6188 (1998).

S. CHONG and F. HIRATA, "Time-Correlation Functions in Molecular Liquids Studied by the Mode-Coupling Theory Based on the Interaction-Site Model," *Phys. Rev. E* **58**, 7296 (1998).

T. ISHIDA, F. HIRATA and S. KATO, "Thermodynamics Analysis of the Solvent Effect on Tautomerization of Acetylacetone: An Ab Initio Approach," *J. Chem. Phys.* **110**, 3938 (1999).

K. NAKA, H. SATO, A. MORITA, F. HIRATA and S. KATO, "RISM-SCF Study for the Free Energy Profile of Menshutkin Type Reaction $\text{NH}_3 + \text{CH}_3\text{Cl} \rightarrow \text{NH}_3\text{CH}_3^+ + \text{Cl}^-$ in Aqueous Solution," *Theor. Chem. Acc.* **102**, 165 (1999).

H. SATO and F. HIRATA, "The Syn-/Anti- Conformational Equilibrium of Acetic Acid in Water Studied by the RISM-SCF/MCSCF Method," *J. Mol. Struct. (THEOCHEM)* **461-462**, 113 (1999).

A. KOVALENKO, S. TEN-NO and F. HIRATA, "Acceleration of Liquid Structure Calculations by Modified Direct Inversion in the Iterative Subspace," *J. Comput. Chem.* **20**, 928 (1999).

M. KINOSHITA, Y. OKAMOTO and F. HIRATA, "Analysis on Conformational Stability of C-Peptide of Ribonuclease A in Water Using the Reference Interaction Site Model Theory and Monte Carlo Simulated Annealing," *J. Chem. Phys.* **110**, 4090 (1999).

H. SATO and F. HIRATA, "Revisiting the Acid-Base Equilibrium in Aqueous Solutions of Hydrogen Halides: Study by the Ab Initio Electronic Structure Theory Combined with the Statistical Mechanics of Molecular Liquids," *J. Am. Chem. Soc.* **121**, 2460 (1999).

A. KOVALENKO and F. HIRATA, "Self-Consistent Description of a Metal-Water Interface by the Khon-Sham Density Functional Theory and Three-Dimensional Reference Interaction Site Model," *J. Chem. Phys.* **110**, 10095 (1999).

A. SETHIA, F. HIRATA and Y. SINGH, "Density Matrix for an Excess Electron in a Classical Fluid. Results for a One Dimensional System," *J. Chem. Phys.* **110**, 10086 (1999).

F. HIRATA and S. CHONG, "Response to Comment on 'Dynamics of Solvated ion in polar liquids: An Interaction-Site-Model Description [*J. Chem. Phys.* **110**, 1833 (1999)]," *J. Chem. Phys.* **110**, 1835 (1999).

S. CHONG and F. HIRATA, "Dynamics of Ions in Liquid Water: An Interaction-Site-Model Description," *J. Chem. Phys.* **111**, 3654 (1999).

S. CHONG and F. HIRATA, "Interaction-Site-Model Description of Collective Excitations in Liquid Water I: Theoretical Study," *J. Chem. Phys.* **111**, 3083 (1999).

S. CHONG and F. HIRATA, "Interaction-Site-Model Description of Collective Excitations in Liquid Water II: Comparison with Simulation Results," *J. Chem. Phys.* **111**, 3095 (1999).

H. SATO and F. HIRATA, "Ab initio Study on Molecular Properties and Thermodynamics of Water: A Theoretical Prediction of pK_w over a Wide Range of Temperature and Density," *J. Phys. Chem. B* **103**, 6596 (1999).

T. ISHIDA, F. HIRATA and S. KATO, "Solvation Dynamics of Benzonitrile Excited State in Polar Solvents: A Time-Dependent Reference Interaction Site Model Self-Consistent Field Approach," *J. Chem. Phys.* **110**, 11423 (1999).

R. AKIYAMA, M. KINOSHITA and F. HIRATA, "Free Energy Profiles of Electron Transfer at Water-Electrode Interface Studied by the Reference Interaction Site Model (RISM) Theory," *Chem. Phys. Lett.* **305**, 251 (1999).

A. MITSUTAKE, M. IRISA, Y. OKAMOTO and F. HIRATA, "Classification of Low-Energy Conformation of Met-Enkephalin in the Gas Phase and in a Model Solvent Based on the Extended Scaled Particle Theory," *Bull. Chem. Soc. Jpn.* **72**, 1717 (1999).

A. SETHIA and B. BAGCHI, "Solvation Dynamics of a Quadrupolar Solute in Dipolar Liquids," *J. Phys. Soc. Jpn.* **68**, 303 (1999).

A. F. KOVALENKO, "Extended States of a Shallow Donor Located Near a Semiconductor-Insulator Interface," *Int. J. Quantum Chem.* **66**, 435 (1998).

R. H. GEE, D. HENDERSON and A. F. KOVALENKO, "Effective Interaction between Hard Sphere Colloidal Particles in a Polymerizing Yukawa Solvent," *J. Chem. Phys.* **110**, 8189 (1999).

J. KISHINE and K. YONEMITSU, "One-Particle vs. Two-Particle Crossover in Weakly Coupled Hubbard Chains and Ladders: Perturbative Renormalization Group Approach," *Recent Prog. Many-Body Theor.* **1**, 408 (1998).

X. H. XU, R. T. FU, K. HU, X. SUN and K. YONEMITSU, "Off-Diagonal Interactions and Spin-Density Waves in Polymers," *Phys. Rev. B* **58**, 9039 (1998).

Y. IMAMURA, S. TEN-NO, K. YONEMITSU and Y. TANIMURA, "Theoretical Study on Electron Correlation of 1-D $(\text{DCNQI})_2\text{M}$ ($\text{M} = \text{Li}, \text{Ag}$) Salts," *Chem. Phys. Lett.* **298**, 15 (1998).

K. YONEMITSU, J. ZHONG and H.-B. SCHÖTTLER, "Berry Phases and Pairing Symmetry in Holstein-Hubbard Polaron Systems," *Phys. Rev. B* **59**, 1444 (1999).

J. KISHINE and K. YONEMITSU, "Effects of Dimerization and Interchain One-Particle Hopping in a Weakly Coupled Dimerized Chain System at Quarter Filling," *Synth. Met.* **103**, 1833 (1999).

M. MORI, K. YONEMITSU and H. KINO, "Possible Magnetic Phases in Two-Band Systems with Different Dimensionality," *Synth. Met.* **103**, 1883 (1999).

T. OGAWA and K. YONEMITSU, "Conductivity and Magnetic Properties of One-Dimensional Heisenberg-Kondo Lattice," *Synth. Met.* **103**, 2149 (1999).

K. YONEMITSU, "Renormalization-Group Study of Competition between Density Waves and Pairing in Quasi-One-Dimensional Electron Systems," *Synth. Met.* **103**, 2216 (1999).

M. OGATA, N. KOBAYASHI and K. YONEMITSU, "Coexistence of SDW and Purely-Electronic CDW in Quarter-Filled Organic Conductors," *Synth. Met.* **103**, 2242 (1999).

X. H. XU, R. T. FU, X. SUN and K. YONEMITSU, "A Correlated-Basis-Function Study of SDW in Polymers," *Synth. Met.* **103**, 2337 (1999).

J. KISHINE and K. YONEMITSU, "Geometry, Universality and Dimensional Crossovers in Weakly-Coupled One-Dimensional Conductors," *Synth. Met.* **103**, 2650 (1999).

J. KISHINE and K. YONEMITSU, "Anisotropic Renormalization-Group Flow of Quasiparticle Weight in a Two-Dimensional Electron System with a Partially Flat Fermi Surface," *Phys. Rev. B* **59**, 14823 (1999).

J. KISHINE and K. YONEMITSU, "Spin-Density-Wave Phase Transitions in Quasi-One-Dimensional Dimerized Quarter-Filled Organic Conductors," *J. Phys. Soc. Jpn.* **68**, 2790 (1999).

Department of Molecular Structure

H. OZEKI and S. SAITO, "Far Infrared Sideband Spectroscopy of the NH_2 Radical," *J. Mol. Spectrosc.* **192**, 183 (1998).

M. ARAKI, H. OZEKI and S. SAITO, "Microwave Spectrum of the SD_3^+ Ion: Molecular Structure," *J. Mol. Spectrosc.* **192**, 228 (1998).

H. FUJIWARA and S. SAITO, "Microwave Spectrum of the AsD_2 (X^2B_1) Radical; Harmonic Force Field and Molecular Structure," *J. Mol. Spectrosc.* **192**, 399 (1998).

I. K. AHMAD, H. OZEKI and S. SAITO, "Microwave Spectroscopic Detection of a Transient Phosphorus-Bearing Molecule, H_3PO ," *J. Chem. Phys.* **110**, 912 (1999).

H. S. P. MUELLER, H. KLEIN, S. P. BELOV, G. WINNEWISSER, I. MORINO, K. M. T. YAMADA and S. SAITO, "Terahertz Spectroscopy of the Amidogen Radical, NH_2 ," *J. Mol. Spectrosc.* **195**, 177 (1999).

C. J. WHITHAM, H. OZEKI and S. SAITO, "Microwave Spectroscopic Detection of Transition Metal Hydroxides: CuOH and AgOH ," *J. Chem. Phys.* **110**, 11109 (1999).

M. ARAKI, H. OZEKI and S. SAITO, "Microwave Spectrum of the Inversion-Rotation Transitions of the D_3O^+ Ion: $\Delta k = \pm 3n$ Interaction and Equilibrium Structure," *Mol. Phys.* **97**, 177 (1999).

F. J. HARTMANN, B. KETZER, C. MAIERL, R. POHL, T. von EGIDY, R.S. HAYANO, M. HORI, T. ISHIKAWA, H. TAMURA, H. A. TORII, M. KUMAKURA, N. MORITA, I. SUGAI, D. HORVATH, J. EADES, E. WIDMANN and T. YAMAZAKI, "Laser Spectroscopy of Metastable States in the $v = 2$ Cascade of Antiprotonic ^3He ," *Phys. Rev. A* **58**, 3604 (1998).

R. POHL, F. J. HARTMANN, B. KETZER, C. MAIERL, T. von EGIDY, J. EADES, E. WIDMANN, T. YAMAZAKI, M. KUMAKURA, N. MORITA, R. S. HAYANO, M. HORI, T. ISHIKAWA, H. A. TORII, I. SUGAI and D. HORVATH, "Influence of Oxygen Admixtures on the Lifetime of Metastable Antiprotonic Helium Atoms," *Phys. Rev. A* **58**, 4406 (1998).

H. A. TORII, R. S. HAYANO, M. HORI, T. ISHIKAWA, N. MORITA, M. KUMAKURA, I. SUGAI, T. YAMAZAKI, B. KETZER, F. J. HARTMANN, T. von EGIDY, R. POHL, C. MAIERL, D. HORVATH, J. EADES and E. WIDMANN, "Laser Measurements of the Density Shifts of Resonance Lines in Antiprotonic Helium Atoms and Stringent Constraint on the Antiproton Charge and Mass," *Phys. Rev. A* **59**, 223 (1999).

Y. MORIWAKI and N. MORITA, "Ultraviolet Spectra of Mg in Liquid Helium," *Eur. Phys. J. D* **5**, 53 (1999).

M. KUMAKURA and N. MORITA, "Laser Trapping of Metastable ^3He Atoms: Isotopic Difference in Cold Penning Collisions," *Phys. Rev. Lett.* **82**, 2848 (1999).

T. AKASAKA, T. SUZUKI, Y. MAEDA, M. ARA, T. WAKAHARA, K. KOBAYASHI, S. NAGASE, M. KAKO, Y. NAKADAIRA, M. FUJITSUKA and O. ITO, "Photochemical Bissilylation of C_{60} with Disilane," *J. Org. Chem.* **64**, 566 (1999).

S. NAGASE, K. KOBAYASHI and T. AKASAKA, "Unconventional Cage Structures of Endohedral Metallofullerenes," *J. Mol. Struct. (THEOCHEM)* **461-462**, 97 (1999).

M. TSUBAKI, M. MOGI and H. HORI, "Fourier-Transform Infrared Studies on Azide Binding to the Binuclear Center of the *Escherichia coli* *bo*-Type Ubiquinol Oxidase," *FEBS Lett.* **449**, 191 (1999).

M. TSUBAKI, M. MOGI and H. HORI, "Fluoride-Binding to the *Escherichia coli* *bd*-Type Ubiquinol Oxidase Studied by Visible Absorption and EPR Spectroscopies," *J. Biochem.* **126**, 98 (1999).

M. TSUBAKI, M. MOGI, and H. HORI, "Azide- and Cyanide-Bindings to the *Escherichia coli* *bd*-Type Ubiquinol Oxidase Studied by Visible Absorption, EPR and FTIR Spectroscopies," *J. Biochem.* **126**, 510 (1999).

X. ZHAO and T. KITAGAWA, "Solvent Effects of 1,4-benzoquinone and its Anion Radicals Probed by Resonance Raman and Absorption Spectra and Their Correlation with Redox Potentials," *J. Raman Spectrosc.* **29**, 773 (1998).

Y. SASAKAWA, K. ONODERA, M. KARASAWA, S-C. IM, E. SUZUKI, F. YOSHIZAKI, Y. SUGIMURA, N. SHIBATA, T. INOUE, Y. KAI, S. NAGATOMO, T. KITAGAWA and T. KOUZUMA, "Spectroscopic Characterization and Kinetic Studies of a Novel Plastocyanin from the Green Alga *Ulva Pertusa*," *Inorg. Chim. Acta* **283**, 184 (1998).

- S. HIROTA, H. MATSUMOTO, H.-W. HUANG, T. SAKURAI, T. KITAGAWA and O. YAMAUCHI**, "Observation of Cu-N_3^- Stretching and N_3 Asymmetric Stretching Bands for Mono-azide Adduct of *Rhus vernicifera* Laccase," *Biochem. Biophys. Res. Commun.* **243**, 435 (1998).
- Y. MIZUTANI**, "Comment on Polarization Effects in Time Resolved Incoherent Anti-Stokes Raman Spectroscopy," *J. Chem. Phys.* **109**, 9197 (1998).
- T. IWASE, C. VAROTSIS, K. SHINZAWA-ITOH, S. YOSHIKAWA and T. KITAGAWA**, "Infrared Evidence for Cu_B Ligation of Photodissociated CO of Cytochrome *c* Oxidase at Ambient Temperatures and Accompanied Deprotonation of a Carboxyl Side Chain of Protein," *J. Am. Chem. Soc.* **121**, 1415 (1999).
- M. NAGAI, H. WAJCMAN, A. LAHARY, T. NAKATSUKASA, S. NAGATOMO and T. KITAGAWA**, "Quaternary Structure Sensitive Tyrosine Residues in Human Hemoglobin: UV Resonance Raman Studies of Mutants at $\alpha 140$, $\beta 35$, and $\beta 145$ Tyrosine," *Biochemistry* **38**, 1243 (1999).
- S. NAGATOMO, M. NAGAI, A. TSUNESHIGE, T. YONETANI and T. KITAGAWA**, "UV Resonance Raman Studies of α -Nitrosyl Hemoglobin Derivatives: Relation between the $\alpha 1$ - $\beta 2$ Subunit Interface Interactions and the Fe-histidine Bonding of α Heme," *Biochemistry* **38**, 9659 (1999).
- S. KAMINAKA, Y. IMAMURA, M. SHINGU, T. KITAGAWA and T. TOYODA**, "Studies of Bovine Enterovirus Structure by Ultraviolet Resonance Raman Spectroscopy," *J. Virol. Methods* **77**, 117 (1999).
- T. KOHZUMA, T. INOUE, F. YOSHIKAWA, Y. SASAKAWA, K. ONODERA, S. NAGATOMO, T. KITAGAWA, S. UZAWA, Y. ISOBE, Y. SUGIMURA, M. GOTOWDA and Y. KAI**, "The Structure and Unusual pH-Dependence of Plastocyanin from the fern *Dryopteris crassirhizoma*: The Protonation of an Active-site Histidine Is Hindered by π - π Interactions," *J. Biol. Chem.* **274**, 11817 (1999).
- T. TOMITA, S. HIROTA, T. OGURA, J. S. OLSON and T. KITAGAWA**, "Resonance Raman Investigation of Fe-N-O Structure of Nitrosylheme in Myoglobin and Its Mutants," *J. Phys. Chem. B* **103**, 7044 (1999).
- S. NEYA, N. FUNASAKI, H. HORI, K. IMAI, S. NAGATOMO, T. IWASE and T. YONETANI**, "Functional Regulation of Myoglobin by Iron Corrophycene," *Chem. Lett.* 989 (1999).

M. MATSUSHITA, A. MUTOH and T. KATO, "Coherent Raman Spectroscopy of Nuclear Quadrupole Resonance of La around Pr^{3+} in LaF_3 ," *Phys. Rev. B* **58**, 14372 (1998).

Department of Electronic Structure

- K. OHASHI and N. NISHI**, "Photodissociation Dynamics of $(\text{C}_6\text{H}_6)_3^+$: Role of the Extra Benzene Molecule Weakly Bound to the Dimer Core," *J. Chem. Phys.* **109**, 3971 (1998).
- T. MATSUOKA, K. KOSUGI, K. HINO, M. NISHIGUCHI, K. OHASHI, N. NISHI and H. SEKIYA**, "Electronic Spectra of Jet-Cooled Anthracene Dimer: Evidence of Two Isomers in the Electronic Ground State," *J. Phys. Chem. A* **102**, 7598 (1998).
- K. OHASHI, Y. NAKANE, Y. INOKUCHI, Y. NAKAI and N. NISHI**, "Photodissociation Spectroscopy of $(\text{Benzene-Toluene})^+$. Charge Delocalization in the Hetero-Dimer Ion," *Chem. Phys.* **239**, 429 (1998).
- N. NISHI**, "Water and Alcohols: Searching the Nature of Mixture States at Molecular Levels," *Bull. Cluster Sci. Tech.* **2**, 3 (1998).
- S. ISHIUCHI and M. FUJII**, "Overtone Spectroscopy of Jet-Cooled Phenol Studied by Nonresonant Ionization Detected IR Spectroscopy," *Resonant Ionization Spectroscopy, 9th International*, American Institute of Physics; NY, 137 (1998).
- R. YOSHINO, K. HASHIMOTO, T. OMI, S. ISHIUCHI and M. FUJII**, "Structure of 1-Naphthol-Water Clusters Studied by IR Dip Spectroscopy and Ab Initio Molecular Orbital Calculation," *J. Phys. Chem. A* **102**, 6227 (1998).
- H. KATAYANAGI, N. YONEKURA and T. SUZUKI**, "C-Br Bond Rupture in 193 nm Photodissociation of Vinyl Bromide," *Chem. Phys.* **231**, 345 (1998).
- Y. MO and T. SUZUKI**, "Quantal and Semiclassical Analysis of Vector Correlation in Molecular Photodissociation," *J. Chem. Phys.* **108**, 6780 (1998).
- Y. MO and T. SUZUKI**, "Geometrical Factors of Two-Photon Absorption for the Determination of Alignment and Orientation," *J. Chem. Phys.* **108**, 4691 (1998).
- T. SUZUKI, H. KATAYANAGI, S. NANBU and M. AOYAGI**, "Non-Adiabatic Bending Dissociation in 16 Valence Electron System OCS," *J. Chem. Phys.* **109**, 5778 (1998).
- Y. SHI and T. SUZUKI**, "Formation of Metastable Triplet Acetylene from the $A(^1A_u)$ State near the Dissociation Threshold," *J. Phys. Chem. A* **102**, 7414 (1998).
- Y. MO, H. KATAYANAGI and T. SUZUKI**, "Probing Alignment of $\text{NO}(X^2\Pi)$ by $[2+1]$ REMPI via $C^2\Pi$ State: A Test of Semiclassical Theory in 355 nm Photodissociation of NO_2 ," *J. Chem. Phys.* **110**, 2029 (1999).
- T. SUZUKI and N. HASHIMOTO**, "Predissociation of Acetylene from the $A(^1A_u)$ State Studied by Absorption, LIF, and H-Atom Action Spectroscopies," *J. Chem. Phys.* **110**, 2042 (1999).
- N. YONEKURA, C. GEBAUER, H. KOHGUCHI and T. SUZUKI**, "A Crossed Molecular Beam Apparatus Using High-Resolution Ion Imaging," *Rev. Sci. Instrum.* **70**, 3265 (1999).

- K. WATANABE, H. KATO and Y. MATSUMOTO**, "Effective Conversion of CO₂ to Carbonate in Surface Oxidation Processes at Si(100)," *J. Phys. Chem. B* **102**, 8042 (1998).
- K. WATANABE, Y. MATSUMOTO, M. KAMPLING, K. AL-SHAMERY and H.-J. FREUND**, "Photochemistry of Methane on Pd/Al₂O₃ Model Catalysts: Control of Photochemistry on Transition Metal Surfaces," *Angew. Chem., Int. Ed. Engl.* **38**, 2192 (1999).
- J. AZUMA, N. TAMAI, A. SHISHIDO and T. IKEDA**, "Time-Resolved Study on Unconventional Fluorescence of an Azobenzene Liquid Crystal and its Phase Transition," *Mol. Cryst. Liq. Cryst.* **314**, 83 (1998).
- Z. ZHANG, A. VERMA, N. TAMAI, K. NAKASHIMA, M. YONEYAMA, K. IRIYAMA and Y. OZAKI**, "Excitation Energy Transfer in Langmuir-Blodgett Films of 5-(4-N-Octadecylpyridyl)-10,15,20-tri-p-tolylporphyrin on Gold-evaporated Glass Substrates Studied by Time-resolved Fluorescence Spectroscopy," *Thin Solid Films* **333**, 1 (1998).
- N. TAMAI, T. NOMOTO, F. TANAKA and N. MATAGA**, "Solvation Dynamics of Excited p-Methoxy-p'-cyanodiphenylacetylene in *n*-Butanol: Simultaneous Analysis of Time-Resolved Fluorescence Anisotropy and Stokes Shift," *Mol. Cryst. Liq. Cryst.* **314**, 131 (1998).
- A. MIURA, K. MATSUMURA, X. SU and N. TAMAI**, "Time-Resolved and Near-Field Scanning Optical Microscopy Study on Porphyrin J-aggregate," *Acta Phys. Pol.* **94**, 835 (1998).
- S. MITRA and N. TAMAI**, "A Combined Experimental and Theoretical Study on the Photochromism of Aromatic Anils," *Chem. Phys.* **246**, 463 (1999).

Department of Molecular Assemblies

- S. HASEGAWA, T. MIYAMAE, K. YAKUSHI, H. INOKUCHI, K. SEKI and N. UENO**, "Origin of the Photoemission Intensity Oscillation of C₆₀," *Phys. Rev. B* **58**, 4927 (1998).
- M. URUICHI, K. YAKUSHI, and Y. YAMASHITA**, "Spectroscopic Study of Narrow-Band Metal (BEDT-ATD)₂PF₆(THF) without Dimerized Structure," *J. Phys. Soc. Jpn.* **68**, 531 (1999).
- J. OUYANG, K. YAKUSHI, K. TAKIMIYA, T. OTSUBO and H. TAJIMA**, "Low-Energy Electronic Transition in Organic Metal, DMTSA-BF₄," *Solid State Commun.* **110**, 63 (1999).
- K. GOTO, T. KUBO, K. YAMAMOTO, K. NAKASUJI, K. SATO, D. SHIOMI, T. TAKUI, M. KUBOTA, T. KOBAYASHI, K. YAKUSHI and J. OUYANG**, "A Stable Neutral Hydrocarbon Radical: Synthesis, Crystal Structure, and Physical Properties of 2,5,8-Tri-tert-butyl-phenalenyl," *J. Am. Chem. Soc.* **121**, 1619 (1999).
- K. YAKUSHI, J. DONG, J. OUYANG, K. TAKIMIYA, T. OTSUBO and H. TAJIMA**, "Metallic Properties of 1:1 Charge-Transfer Salt DMTSA-BF₄," *Synth. Met.* **103**, 2208 (1999).
- J. OUYANG, K. YAKUSHI, Y. MISAKI and K. TAKIMIYA**, "Band Structure of (BDT-TTP)₂X (X = SbF₆, AsF₆, ClO₄) Studied by Reflection Spectroscopy," *Synth. Met.* **103**, 2207 (1999).
- M. URUICHI, K. YAKUSHI and Y. YAMASHITA**, "Temperature-dependent Reflection Spectra of Metallic (BEDT-ATD)₂X(THF) (X = PF₆, AsF₆)," *Synth. Met.* **103**, 2206 (1999).
- Y. YONEHARA and K. YAKUSHI**, "Optical Spectra of Phthalocyanine Salts," *Synth. Met.* **103**, 2214 (1999).
- M. INOKUCHI, K. YAKUSHI, M. KINOSHITA and G. SAITO**, "Optical Properties of α'-(BEDT-TTF)₂IBr₂," *Synth. Met.* **103**, 2101 (1999).
- C. YANG, J. QIN, K. YAKUSHI, Y. NAKAZAWA and K. ICHIMURA**, "BEDT-TTF Being Inserted into a Layered MnPS₃," *Synth. Met.* **102**, 1482 (1999).
- T. NAKAMURA, W. MINAGAWA, R. KINAMI, Y. KONISHI and T. TAKAHASHI**, "Low-Temperature Electronic States in θ-(BEDT-TTF)₂RbZn(SCN)₄: Competition of Different Ground States," *Synth. Met.* **103**, 1898 (1999).
- T. NAKAMURA, T. TAKAHASHI, M. TANIGUCHI, Y. MISAKI and K. TANAKA**, "Magnetic Properties of a New Two-Chain Organic Conductor: (CPDT-STF)-TCNQ," *Synth. Met.* **103**, 1900 (1999).
- T. NAKAMURA, H. YAMANE, T. TAKAHASHI, S. AONUMA and R. KATO**, "ESR and NMR Investigation of β'-R₄Z[Pd(dmit)₂]₂," *Synth. Met.* **103**, 2142 (1999).
- K. KODAMA, T. NAKAMURA, T. TAKAHASHI, E. OJIMA and H. KOBAYASHI**, "Metal-Insulator Transition in α-(BEDT-TSeF)₂I₃ and α-(BEDT-TTF)₂I₃," *Synth. Met.* **103**, 1963 (1999).
- M. HISANO, T. NAKAMURA, T. TAKAHASHI and G. SAITO**, "SDW Wave Number and Charge Localization in (TMTTF)₂Br: ¹H-NMR investigation," *Synth. Met.* **103**, 2195 (1999).
- M. YAMANE, T. NAKAMURA, T. TAKAHASHI, S. AONUMA, R. KATO and H. SAWA**, "Impurity Effect on the Spin-Peierls State of (DMe-DCNQI)₂Cu_xLi_{1-x}," *Synth. Met.* **103**, 2196 (1999).
- Y. NAKAZAWA and K. KANODA**, "Thermodynamic Investigation of the Electronic States of Deuterated κ-(BEDT-TTF)₂Cu[N(CN)₂]Br," *Phys. Rev. B* **60**, 4263 (1999).
- Y. NAKAZAWA and K. KANODA**, "Thermodynamics of BEDT-TTF Based Dimeric Salts," *Synth. Met.* **103**, 1903 (1999).
- H. TANIGUCHI, A. KAWAMOTO, Y. NAKAZAWA and K. KANODA**, "Metal-Insulator Transition in Partially Deuterated κ-(BEDT-TTF)₂Cu[N(CN)₂]Br," *Synth. Met.* **103**, 2250 (1999).
- K. IMAEDA, F. TIAN, H. INOKUCHI and K. ICHIMURA**, "Three Component Organic Superconductors: Intercalation of KH into C₆₀," *J. Solid State Chem.* **145**, 421 (1999).

- K. K. OKUDAIRA, S. HASEGAWA, H. ISHII K. SEKI, Y. HARADA and N. UENO**, "Structure of Copper- and H₂-Phthalocyanine Thin Films on MoS₂ by means of Angle-Resolved UPS and LEED," *J. Appl. Phys.* **85**, 6453 (1999).
- T. MIYAMAE, N. UENO, S. HASEGAWA, Y. SAITO, T. YAMAMOTO and K. SEKI**, "Electronic structure of Poly(1,10-phenanthroline-3,8-diyl) and Its K-Doped State Studied by Photoelectron Spectroscopy," *J. Chem. Phys.* **110**, 2552 (1999).
- D. YOSHIMURA, T. YOKOYAMA, E. ITO, H. ISHII, Y. OUCHI, S. HASEGAWA and K. SEKI**, "Electronic Structures of Alq₃/LiF/Al Interfaces Studied by UV Photoemission," *Synth. Met.* **102**, 1145 (1999).
- K. SUGIYAMA, D. YOSHIMURA, T. MIYAZAKI, T. MIYAMAE, H. ISHII, Y. OUCHI and K. SEKI**, "Electronic Structures of Organic Molecular Materials for Organic Electroluminescent Devices Studied by Ultraviolet Photoemission," *Spectrosc. J. Appl. Phys.* **83**, 4928 (1998).
- H. AKUTSU, K. KATO, E. OJIMA, H. KOBAYASHI, H. TANAKA, A. KBAYASHI and P. CASSOUX**, "Coupling of Metal-Insulator and Antiferromagnetic Transitions in the Highly Correlated Organic Conductor Incorporating Magnetic Anions, λ -(BETS)₂FeBr_xCl_{4-x}," *Phys. Rev. B* **58**, 9 (1998).
- B. Z. NARYMBETOV, N. D. KUSHCH, L. V. ZORINA, S. S. KHASANOV, R. P. SHIBAEVA, T. G. TOGONIDZE, A. E. KOVALEV, M. V. KARTSOVNIK, L. I. BURAVOV, E. B. YAGUBSKII, E. CANADELL, A. KOBAYASHI and H. KOBAYASHI**, "New Stable Organic Metal: κ -(BETS)₂C(CN)₃. The First κ -Type Radical Cation Salt with a Planar-Triangular Discrete Organic Anion," *Eur. Phys. J. B* **1**, 179 (1998).
- N. D. KUSHCH, L. I. BURAVOV, S. I. PESOTSKII, R. B. LYUBOVSKII, E. B. YAGUBSKII, M. G. KAPLUNOV, E. V. GOLUBEV, B. Zh. NARYMBETOV, S. S. KHASANOV, L. V. ZORINA, L. ROZENBERG, R. SHIBAEVA, A. KOBAYASHI and H. KOBAYASHI**, "A New Stable Organic Metal in the Well-known Family of Radical Cation α -Salts: α -(BETS)₂TlHg(SeCN)₄. Synthesis, Structure and Properties," *J. Mater. Chem.* **8**, 897 (1998).
- H. TANAKA, A. KOBAYASHI and H. KOBAYASHI**, "Electrical and Magnetic Properties of BETS Conductor with Modified λ -type Structure, λ' -(BETS)₂GaBr₄," *Chem. Lett.* 133 (1999).
- H. TANAKA, A. KOBAYASHI, A. SATO, H. AKUTSU and H. KOBAYASHI**, "Chemical Control of Electrical Properties and Phase Diagram of a Series of λ -Type BETS Superconductors, λ -(BETS)₂GaBr_xCl_{4-x}," *J. Am. Chem. Soc.* **121**, 760 (1999).
- M. A. TANATAR, T. ISHIGURO, H. TANAKA, A. KOBAYASHI and H. KOBAYASHI**, "Anisotropy of Upper Critical Field of the Organic Superconductor λ -(BETS)₂GaCl₄," *J. Supercond.* **12**, 511 (1999).
- H. KOBAYASHI, H. AKUTSU, H. TANAKA, A. KOBAYASHI, M. TOKUMOTO, L. BROSSARD and P. CASSOUX**, "On the Low-temperature State of Highly Correlated BETS Conductors," *Synth. Met.* **102**, 1654 (1999).
- H. KOBAYASHI, H. AKUTSU, E. OJIMA, A. SATO, H. TANAKA, A. KOBAYASHI and P. CASSOUX**, "Superconductor-to-Insulator Transition of λ -(BETS)₂GaBr_xCl_{4-x}," *Synth. Met.* **103**, 1837 (1999).
- N. D. KUSHCH, O. A. DYACHENKO, V. V. GRITSENKO, L. I. BURAVOV, V. A. TKACHEVA, E. B. YAGUBSKII, M. G. KAPLUNOV, E. N. GOLUBRV, T. G. TOGONIDE, A. KOBAYASHI and H. KOBAYASHI**, "Novel Organic Metal of α -(BETTS)₂Cu₅I₆ with a Two-Dimensional Polymeric Anion Network; Synthesis, Structure and Properties," *J. Mater. Chem.* **9**, 687 (1999).
- K. KODAMA, T. NAKAMURA, T. TAKAHASHI, E. OJIMA and H. KOBAYASHI**, "Metal-Insulator Transition in α -(BEDT-TSeF)₂I₃ and (BEDT-TTF)₂I₃," *Synth. Met.* **103**, 1963 (1999).
- B. NARYMBETOV, H. KOBAYASHI, M. TOKUMOTO, A. OMERZU and G. MIHAJLOVIC**, "Low Temperature Structure Analysis of Unannealed TDAE·C₆₀ Single Crystal," *Chem. Commun.* 1511 (1999).
- A. KOBAYASHI, A. SATO and H. KOBAYASHI**, "Stable Two-Dimensional Metallic State with Stacking Motif of 'Spanning Overlap' in γ -[(CH₃)₂(C₂H₅)₂N][Ni(dmit)₂]₂," *J. Solid State Chem.* **145**, 564 (1999).
- S. I. PESOTSKII, R. B. LYUBOVSKII, N. D. KUSH, M. V. KARTSOVNIK, W. BIBERACHER, K. ANDRES, H. KOBAYASHI and A. KOBAYASHI**, "de Haars-van Alphen Oscillations and Angular Magnetoresistance Oscillations in the Organic Metal κ -(BETS)₂GaCl₄," *J. Exp. Theor. Phys.* **88**, 114 (1999).
- E. OJIMA, H. FUJIWARA, K. KATO, H. KOBAYASHI, H. TANAKA, A. KOBAYASHI, M. TOKUMOTO and P. CASSOUX**, "Antiferromagnetic Organic Metal Exhibiting Superconducting Transition, κ -(BETS)₂FeBr₄ [BETS = Bis(ethylenedithio)tetraselenafulvalene]," *J. Am. Chem. Soc.* **121**, 5581 (1999).
- H. FUJIWARA, T. NISHIKAWA, Y. MISAKI and T. YAMABE**, "Synthesis and Properties of Tris-Fused Donor Containing Thiopyran Ring," *Synth. Met.* **102**, 1737 (1999).
- H. FUJIWARA and H. KOBAYASHI**, "Synthesis and Properties of New Organic Donor Containing Organic Radical Part," *Synth. Met.* **102**, 1740 (1999).
- H. FUJIWARA, E. OJIMA, H. KOBAYASHI, T. COURCET, I. Malfant and P. CASSOUX**, "Synthesis, Structure and Physical Properties of Tetraalkylammonium Bis(5,6-dihydro-1,4-dithiin-2,3-diselenolato)-nickelate, (R₄N)[Ni(ddd)₂] (R = Me, Et and *n*-Bu) and Neutral Complex [Ni(ddd)₂]₂," *Eur. J. Inorg. Chem.* 631 (1998).
- H. FUJIWARA, E. ARAI and H. KOBAYASHI**, "Synthesis, Structure and Properties of Novel TTF Dimers Bridged by Two Trisulfide Chains," *Synth. Met.* **102**, 1739 (1999).
- E. OJIMA, H. FUJIWARA and H. KOBAYASHI**, "Synthesis, Structures and Properties of an Unsymmetrical Tetraselenafulvalene Donor Fused with a Pyrazino-Ring (PEDTTSeF) and its Cation Radical Salts," *Adv. Mater.* **11**, 459 (1999).

- E. OJIMA, H. FUJIWARA and H. KOBAYASHI**, "Synthesis, Structures and Physical Properties of 4,5-Ethylenedithio-4,5-Pentathiotetrathiafulvalene and Its Perchlorate Salt," *Adv. Mater.* **11**, 758 (1999).
- E. OJIMA, B. Zh. NARYMBETOV, H. FUJIWARA, H. KOBAYASHI, A. KOBAYASHI, K. TAKIMIYA, T. OTSUBO and F. OGURA**, "New Stable Metallic Salt Based on a Donor Molecule Containing *peri*-Ditellurium Bridges, $\text{TMTTeN}(\text{SCN})_{0.88}$," *Chem. Lett.* 845 (1999).
- A. KOBAYASHI, M. NAKATA, E. ARAI, H. FUJIWARA, H. KOBAYASHI, K. TAKIMIYA, T. OTSUBO and F. OGURA**, "Three Dimensional Metals Based on a Tellurium-Containing Donors, TMTTeN and Related Conductors," *Synth. Met.* **103**, 1865 (1999).
- T. NAKAI, S. MIYAJIMA, Y. TAKANISHI, S. YOSHIDA and A. FUKUDA**, "High Resolution 13 NMR Study of an Antiferroelectric Liquid Crystal: Verification of the Bent Chain Structure," *J. Phys. Chem. B* **103**, 406 (1999).
- T. NAKAI, H. FUJIMORI, D. KUWAHARA and S. MIYAJIMA**, "Complete Assignment of 13C NMR Spectra and Determination of Orientational Order Parameter for Antiferroelectric Liquid-Crystalline MHPOBC," *J. Phys. Chem. B* **103**, 417 (1999).
- S. YOSHIDA, B. JIN, Y. TAKANISHI, K. TOKUMARU, K. ISHIKAWA, H. TAKEZOE, A. FUKUDA, T. KUSUMOTO, T. NAKAI and S. MIYAJIMA**, "A Bent and Asymmetrically Hindered Chiral Alkyl Chain of an Antiferroelectric Liquid Crystal as Observed by 2H NMR" *J. Phys. Soc. Jpn.* **68**, 46 (1999).
- K. TOKUMARU, B. JIN, S. YOSHIDA, Y. TAKANISHI, K. ISHIKAWA, H. TAKEZOE, A. FUKUDA, T. NAKAI and S. MIYAJIMA**, "Molecular Rotation in an Antiferroelectric Liquid Crystal by 13C Nuclear Magnetic Resonance Spin-Lattice Relaxation Time Measurement," *Jpn. J. Appl. Phys.* **38**, 255 (1999).
- D. KUWAHARA, T. NAKAI and S. MIYAJIMA**, "Two-Dimensional NMR Measurements of Heteronuclear Dipolar Powder Spectra Using the Chemical-Shift-Anisotropy Recovery Technique," *Chem. Phys. Lett.* **291**, 244 (1998).
- D. KUWAHARA, T. NAKAI, J. ASHIDA and S. MIYAJIMA**, "Novel Satellites in a Two-Dimensional Spin-Echo NMR Experiment for Homonuclear Dipole-Coupled Spins in Rotating Solids," *Chem. Phys. Lett.* **305**, 35 (1999).
- P. BERDAGUE, J. P. BAYLE, H. FUJIMORI, and S. MIYAJIMA**, "Influence of Large Lateral Substituents on the Nematic Liquid Crystalline Properties Studied by 13C NMR," *New J. Chem.* 1005 (1998).
- V. RAYSSAC, P. JUDEINSTEIN, J. P. BAYLE, D. KUWAHARA, H. OGATA and S. MIYAJIMA**, "NMR Investigation of the Oxyethylene Unit Ordering in Some Related Dialkoxy Laterally Substituted Nematogens," *Liq. Cryst.* **25**, 427 (1998).
- C. BENEDICT, U. LANGER, H. H. LIMBACH, H. OGATA and S. TAKEDA**, "Observation of Thermal Tautomerism in Thermochromic Salicylideneaniline Derivatives in the Solid State by N-15 CPMAS NMR Down to Cryogenic Temperatures," *Ber. Bunsen-Ges.* **102**, 335 (1998).
- H. OGATA and S. MIYAJIMA**, "Structural and Electronic Properties of Hydrogen-Absorbed Alkali-C₆₀ Compounds," *Synth. Met.* **103**, 2378 (1999).
- K. SUGIURA, K. IWASAKI, K. UMISHITA, S. HINO, H. OGATA, S. MIYAJIMA and Y. SAKATA**, "X-Ray Photoelectron Spectroscopy of Metallo Porphyrins Having Bulky Substituents: Standard Values of Core Ionization Potentials," *Chem. Lett.* 841 (1999).
- K. SATO, S. TAKEDA, S. FUKUDA, T. MINAMISONO, M. TANIGAKI, T. MIYAKE, Y. MARUYAMA, K. MATSUTA, M. FUKUDA and Y. NOJIRI**, "FT-NMR Detection of ⁴⁵Sc, ⁴⁹Ti and ⁹³Nb in TiO₂ Single Crystal," *Z. Naturforsch., A* **53**, 549 (1998).
- T. MINAMISONO, K. SATO, H. AKAI, S. TAKEDA, Y. MARUYAMA, K. MATSUTA, M. FUKUDA, T. MIYAKE, A. MORISHITA, T. IZUMIKAWA and Y. NOJIRI**, "Electric Quadrupole Interactions of the Short-Lived β -Emitter ¹²N in Insulator Crystals (¹²N Implanted in Single Crystal TiO₂)," *Z. Naturforsch., A* **53**, 293 (1998).
- S. TAKEDA, T. INABE, C. BENEDICT, U. LANGER and H. H. LIMBACH**, "Proton Dynamics in Interacting Hydrogen Bonds in the Solid State: Proton Tunneling in the NHO Hydrogen Bonds of N,N'-Di(2-hydroxy-1-Naphthylmethylene)-p-Phenylenediamine," *Ber. Bunsen-Ges.* **102**, 1358 (1998).
- M. TANIGAKI, S. TAKEDA, K. MATSUTA, Y. MATSUMOTO, T. MINAMISONO, H. AKAI, K. SATO, T. MIYAKE, Y. MARUYAMA, A. MORISHITA, M. FUKUDA and Y. NORJIRI**, "NMR Detection of Oxygen Isotopes in TiO₂ Single Crystal," *Z. Naturforsch., A* **53**, 305 (1998).
- S. TAKAMIZAWA, W. MORI, M. FURIHATA, S. TAKEDA and K. YAMAGUCHI**, "Synthesis and Gas-Occlusion Properties of Dinuclear Molybdenum(II) Dicarboxylates (Fumarate, Terephthalate, *trans-trans*-Muconate, Pyridine-2,5-Dicarboxylate, and *trans*-1,4-Cyclohexanedicarboxylate)," *Inorg. Chim. Acta* **283**, 268 (1998).
- G. MARUTA, S. TAKEDA, R. IMACHI, T. ISHIDA, T. NOGAMI and K. YAMAGUCHI**, "Solid State High Resolution ¹H and ²D NMR Study of the Electron Spin Density Distribution of Hydrogen-Bonded Organic Ferromagnetic Compound 4-Hydroxyimino-TEMPO," *J. Am. Chem. Soc.* **121**, 424 (1999).
- R. IMAMURA, K. MATSUI, S. TAKEDA, J. OZAKI and A. OYA**, "A New Role for Phosphorous in Graphitization of Phenolic Resin," *Carbon* **37**, 261 (1999).
- S. TAKEDA, G. MARUTA, K. TERASAWA, N. FUKUDA and K. YAMAGUCHI**, "Local Magnetic Structure of Layered Compounds Cu₂(OD)₃X with Exchangeable Acid Anion X Studied by Solid State High Resolution

Deuterium NMR," *Mol. Cryst. Liq. Cryst.* **335**, 723 (1999).

G. MARUTA, S. TAKEDA, A. YAMAGUCHI, T. OKUNO, K. AWAGA and K. YAMAGUCHI, "Magic Angle Spinning ^1H -NMR Study of the Spin Density Distribution of Pyridyl Nitronyl Nitroxides in the Crystalline Phase," *Mol. Cryst. Liq. Cryst.* **334**, 295 (1999).

A. ODA, T. KAWAKAMI, G. MARUTA, S. TAKEDA, W. MORI, K. YAMAGUCHI, M. M. MATSUSHITA and T. SUGAWARA, "Theoretical Studies of Magnetic Interactions in 3',5'-Dihydroxyphenyl Nitronyl Nitroxide Crystal," *Mol. Cryst. Liq. Cryst.* **335**, 1355 (1999).

T. KAWAKAMI, A. ODA, S. TAKEDA, W. MORI and K. YAMAGUCHI, "Theoretical Studies on Magnetic Interaction in TMAO," *Mol. Cryst. Liq. Cryst.* **335**, 1409 (1999).

T. MORI, "Structural Genealogy of BEDT-TTF-Based Organic Conductors I. Parallel Molecules: β and β' Phases," *Bull. Chem. Soc. Jpn.* **71**, 2509 (1998).

T. MORI, H. MORI and S. TANAKA, "Structural Genealogy of BEDT-TTF-Based Organic Conductors II. Inclined Molecules: θ , α , and κ Phases," *Bull. Chem. Soc. Jpn.* **72**, 179 (1999).

G. K. Rohan SENADEERA, T. KAWAMOTO, T. MORI, J. YAMAURA and T. ENOKI, " $2k_F$ CDW Transition in β -(BEDT-TTF) $_2$ PF $_6$ Family Salts," *J. Phys. Soc. Jpn.* **67**, 4193 (1998).

S. HANAZATO, T. MORI, H. MORI and S. TANAKA, "Transport Properties of α' -Phase Organic Conductors, (BEDT-TTF) $_2$ CsHg(SCN) $_4$ and (BEDT-TTF) $_2$ K $_{1.4}$ Co(SCN) $_4$," *Physica C* **316**, 243 (1999).

Department of Applied Molecular Science

Y. GOTO, Y. WATANABE, S. FUKUZUMI, J. P. JONES, and J. P. DINNOCENZO, "The Mechanisms of *N*-Demethylation Catalyzed by Heme Enzymes: Direct Observation of *N*-Demethylation by Compound I of Horseradish Peroxidase and Its Model Complex," *J. Am. Chem. Soc.* **120**, 10762 (1998).

S. OGO, S. NAKAMURA, H. CHEN, K. ISOBE, Y. WATANABE and R. H. FISH, "A New, Aqueous ^1H NMR Shift Reagent Based on Host-Guest Molecular Recognition Principles for organic Compound Structural Analysis: Non-Covalent π - π and Hydrophobic Interactions Using a Supramolecular Host, [Cp* Rh (2'-deoxyadenosine)] $_3$ (OTf) $_3$," *J. Org. Chem.* **63**, 7151 (1998).

T. MATSUI, S. OZAKI, E. LIONG, G. N. PHILLIPS and Y. WATANABE, "Effects of the Location of Distal Histidine in the Reaction of Myoglobin with Hydrogen Peroxide," *J. Biol. Chem.* **273**, 2838 (1999).

T. MURAKAMI, I. MORISHIMA, T. MATSUI, S. OZAKI, I. HARA, H.-J. YANG and Y. WATANABE, "Effects of the Arrangement of Distal Catalytic Residue on Regioselectivity and Reactivity in the Coupled oxidation of Sperm Whale Myoglobin Mutants," *J. Am. Chem. Soc.* **121**, 2007 (1999).

S. OZAKI, H.-J. YANG, T. MATSUI, Y. GOTO and Y. WATANABE, "Asymmetric Oxidation Catalyzed by Myoglobin Mutants," *Tetrahedron: Asymmetry* **10**, 183 (1999).

A. WADA, S. OGO, Y. WATANABE, M. MUKAI, T. KITAGAWA, K. JITSUKAWA, H. MASUDA and H. EINAGA, "Synthesis and Characterization of Novel Alkylperoxo Mononuclear Iron(III) Complexes with a Tripodal Pyridylamine Ligands: A Model for Peroxo Intermediates in Reactions Catalyzed by Non-Heme Iron Enzymes," *Inorg. Chem.* **38**, 3592 (1999).

T. MANABE, M. YAMASHITA, T. KAWASHIMA, H. OKAMOTO, H. KITAGAWA, T. MITANI, K. TORIUMI, H. MIYAMAE, K. INOUE and K. YAKUSHI, "Competition Between Electron-Correlation in Ni^{III} States and Electron-Phonon Interaction in Pd^{II} - Pd^{IV} Mixed-Valence States in Quasi-One-Dimensional Halogen-Bridged Mixed-Metal Complexes, $\text{Ni}_{1-x}\text{Pd}_x(\text{chxn})_2\text{Br}_3$," *Proc. SPIE-Int. Soc. Opt. Eng.* **3145**, 106 (1998).

S. HAYAMI, K. INOUE, S. OSAKI and Y. MAEDA, "Synthesis and Magnetic Properties of Binuclear Iron(III) Complex Containing Photoisomerization Ligand," *Chem. Lett.* 987 (1998).

H. KUMAGAI and K. INOUE, "A Chiral Molecule-based Metamagnet Made by Chiral Organic Radical and Manganese Ion," *Angew. Chem., Int. Ed. Engl.* **38**, 1601 (1999).

I. S. DUBENKO, I. Yu. GAIDUKOVA, Y. HOSOKOSHI, K. INOUE and A. S. MARKOSYAN, "The Magnetic Phase Diagram and the Effect of Pressure on the Magnetic Properties of the $\text{Y}_{1-x}\text{Gd}_x\text{Mn}_2$ Intermetallic Compounds," *J. Phys.: Condens. Matter* **11**, 62937 (1999).

Y. HOSOKOSHI and K. INOUE, "Pressure Effects on Organic Radicals with Ferromagnetic and Antiferromagnetic Interactions," *Synth. Met.* **103**, 2323 (1999).

F. IWAHORI, K. INOUE and H. IWAMURA, "Mn(II)-Induced Formation and Structural Elucidation of a [3+3] Benzene Dimer Derivative from *m*-Phenylenebis(*N*-tert-butylaminoxyl)," *J. Am. Chem. Soc.* **121**, 7264 (1999).

S. HAYAMI and K. INOUE, "Structure and Magnetic Property of the Organic Triradical with Triazine Skeleton; 2,4,6-Tris[*p*-(*N*-oxy-*N*-tert-butylamino)phenyl]triazine," *Chem. Lett.* 545 (1999).

M. MITO, T. KAWAE, Y. HOSOKOSHI, K. INOUE, M. KINOSHITA and K. TAKEDA, "Pressure-Induced Crossover from Alternating to Uniform Interaction in a $S = 1/2$ One-Dimensional Heisenberg Antiferromagnet," *Solid State Commun.* **111**, 607 (1999).

I. S. DUBENKO, I. Yu. GAIDUKOVA, Y. HOSOKOSHI, K. INOUE and A. S. MARKOSYAN, "Concentration and Pressure Dependence of Magnetic Ordering in $\text{Y}(\text{Mn}_{1-x}\text{Me}_x)_2$ Compounds with $\text{Me} = \text{Al, Fe and Ni}$," *J. Magn. Magn. Mater.* **195**, 687 (1999).

N. V. BARANOV, A. A. YERMAKOV, A. N. PIROGOV, A. E. TEPLYKH, K. INOUE and Y.

HOSOKOSHI, "The Magnetic State of the Co-sublattice in $\text{Tb}_{1-x}\text{Y}_x\text{Co}_2$," *Physica B* **269**, 284 (1999).

Y. MISAKI, K. TANAKA, M. TANIGUCHI, T. YAMABE and T. MORI, "Structures and Properties of a New κ -Type Organic Metal: $(\text{CPEO-TTP})(\text{SbF}_6)_{0.4}$," *Adv. Mater.* **11**, 25 (1999).

T. KAIBUKI, Y. MISAKI, K. TANAKA, K. TAKIMIYA, A. MORIKAMI and T. OTSUBO, "Synthesis and Properties of New PDT- and TPDT-TTP Analogues," *Synth. Met.* **102**, 1621 (1999).

Y. MISAKI, T. KOCHI and T. YAMABE, "Synthesis and Properties of TTF Vinylogues Fused with 1,3-Dithiol-2-ylidene Moiety," *Synth. Met.* **102**, 1673 (1999).

Y. MISAKI, T. KOCHI, M. TANIGUCHI, T. YAMABE, K. TANAKA, K. TAKIMIYA, A. MORIKAMI, T. OTSUBO and T. MORI, "Structural Feature of Radical Cation Salts Based on TTP and Its Selenium Analogues," *Synth. Met.* **102**, 1675 (1999).

K. TANAKA, M. TANIGUCHI, Y. MISAKI, T. YAMABE, T. KAWAMOTO and T. MORI, "Structure and Properties of TTP Conductors Substituted with Ethylenedioxy Group," *Synth. Met.* **102**, 1720 (1999).

M. TANIGUCHI, Y. MISAKI, K. TANAKA, T. YAMABE and T. MORI, "Structures and Properties of Organic Metals Based on Dimethyl Substituted TTP Analogue," *Synth. Met.* **102**, 1721 (1999).

Y. MISAKI, T. KAIBUKI, T. MONOBE, K. TANAKA, M. TANIGUCHI, K. TANAKA, T. YAMABE, K. TAKIMIYA, A. MORIKAMI, T. OTSUBO and T. MORI, "Synthesis and Properties of Methylthio Substituted ST-TTP Derivatives," *Synth. Met.* **102**, 1781 (1999).

M. TANIGUCHI, Y. MISAKI, T. YAMABE, K. TANAKA, K. MURATA and T. MORI, "(CPDT-STF)-(TCNQ): A New Charge-Transfer Complex Metallic down to Low Temperature," *Solid State Commun.* **111**, 559 (1999).

T. SUMI, E. MIYOSHI, Y. SAKAI and O. MATSUOKA, "Molecular Orbital and Molecular Dynamics Study of Mercury," *Phys. Rev. B* **57**, 914 (1998).

E. MIYOSHI, Y. MIYAKE, Y. SAKAI and S. KATSUKI, "Theoretical Study on the Electronic Structures of Various F Centers in MgO Crystals," *J. Mol. Struct. (THEOCHEM)* **451**, 81 (1998).

E. MIYOSHI, Y. SAKAI, K. TANAKA and M. MASAMURA, "Relativistic dsp-Model Core Potentials for Main Group Elements in the Fourth, Fifth, and Sixth-Row and their Applications," *J. Mol. Struct. (THEOCHEM)* **451**, 73 (1998).

N. HONJOU and E. MIYOSHI, "Ab Initio Study on the Electronic Structure of the 3^2S_u^+ , 3^2S_g^+ and 4^2S_g^+ States of N_2^+ ," *J. Mol. Struct. (THEOCHEM)* **451**, 41 (1998).

Y. SAKAI, E. MIYOSHI and H. TATEWAKI, "Model Core Potentials for the Lanthanides," *J. Mol. Struct. (THEOCHEM)* **451**, 143 (1998).

S. A. DECKER, M. KLOBUKOWSKI, Y. SAKAI and E. MIYOSHI, "Calibration and Benchmarking of Model Core Potentials: Applications to Systems containing Main-Group Elements," *J. Mol. Struct. (THEOCHEM)* **451**, 215 (1998).

E. MIYOSHI, J. MAKI, T. NORO and K. TANAKA, "Multi-Reference Coupled Pair Approximation (MRCPA) Calculations for the Ground State of the ArI_2 Complex," *J. Mol. Struct. (THEOCHEM)* **461-462**, 547 (1999).

T. SUMI, E. MIYOSHI and K. TANAKA, "Molecular-Dynamics Study of Liquid Mercury in the Density Region between Metal and Nonmetal," *Phys. Rev. B* **59**, 914 (1999).

E. MIYOSHI and N. SHIDA, "Ab initio Study on the Structure of the Ground State of the C_3O_2 Molecule," *Chem. Phys. Lett.* **303**, 50 (1999).

Y. SAKAI, K. MOGI and E. MIYOSHI, "Theoretical Study of Low-Lying Electronic States of TiCl and ZrCl ," *J. Chem. Phys.* **111**, 3989 (1999).

M. ISHIGURO, K. HARADA, K. TANAKA and T. TANAKA, "Color Center Laser Infrared Absorption Spectroscopy of the ν_{12} Band of Benzene Cooled in a Pulsed Jet," *J. Mol. Spectrosc.* **192**, 235 (1998).

O. DOPFER, S. A. NIZKORODOV, R. V. OLKHOV, J. P. MAIER and K. HARADA, "Infrared Spectrum of the Ar-NH_2^+ Ionic Complex," *J. Phys. Chem. A* **102**, 10017 (1999).

K. TANAKA, H. HONJO, T. TANAKA, H. KOHGUCHI, Y. OHSHIMA and Y. ENDO, "Determination of the Proton Tunneling Splitting of Tropolone in the Ground State by Microwave Spectroscopy," *J. Chem. Phys.* **110**, 1969 (1999).

T. BABA, T. TANAKA, I. MORINO, K. M. T. YAMADA and K. TANAKA, "Detection of the Tunneling-rotation Transitions of Malonaldehyde in the Submillimeter-Wave Region," *J. Chem. Phys.* **110**, 4131 (1999).

T. OKABAYASHI, K. TANAKA and T. TANAKA, "Analysis of Intervibrational Resonances of FCCCN Observed in the Microwave Spectrum," *J. Mol. Spectrosc.* **195**, 22 (1999).

Department of Vacuum UV Photoscience

J. J. NEVILLE, A. JÖRGENSEN, R. G. CAVELL, N. KOSUGI and A. P. HITCHCOCK, "Inner-shell Excitation of PF_3 , PCl_3 , PCl_2CF_3 , OPF_3 and SPF_3 ," *Chem. Phys.* **238**, 201 (1998).

J. ADACHI, Y. TAKATA, N. KOSUGI, E. SHIGEMASA, A. YAGISHITA and Y. KITAJIMA, "Kinetic Energy Dependence of Anisotropic Yields of Ionic Fragmentations Following S 1s Excitations of SO_2 ," *Chem. Phys. Lett.* **294**, 559 (1998).

- T. HATSUI, Y. TAKATA and N. KOSUGI**, "Metal-to-Ligand Charge Transfer Bands Observed in Polarized Ni 2p Photoabsorption Spectra of $[\text{Ni}(\text{mnt})_2]^{2-}$," *J. Electron Spectrosc. Relat. Phenom.* **101-103**, 827 (1999).
- T. HATSUI, Y. TAKATA and N. KOSUGI**, "Strong Metal-to-Ligand Charge Transfer Bands Observed in Ni K- and L-edge XANES of Planar Ni Complexes," *J. Synchrotron Radiat.* **6**, 376 (1999).
- T. HATSUI, Y. TAKATA and N. KOSUGI**, "Polarized Ni K- and L-edge and S K-edge XANES Study of $[\text{Ni}(\text{III})(\text{mnt})_2]^{1-}$," *J. Synchrotron Radiat.* **6**, 379 (1999).
- Y. TAKATA, T. HATSUI and N. KOSUGI**, "A Unified View of Resonant Photoemission of Metallic, Molecular and Correlated Solid Systems," *J. Electron Spectrosc. Relat. Phenom.* **101-103**, 443 (1999).
- S. TAKEUCHI and T. TAHARA**, "Femtosecond Ultraviolet-Visible Fluorescence Study of the Excited-State Proton Transfer Reaction of 7-Azaindole Dimer," *J. Phys. Chem. A* **102**, 7740 (1998).
- N. SARKAR, S. TAKEUCHI and T. TAHARA**, "Vibronic Relaxation of Polyatomic Molecule in Non-polar Solvent: Femtosecond Anisotropy/Intensity Measurements of the S_n and S_1 Fluorescence of Tetracene," *J. Phys. Chem. A* **103**, 4808 (1999).
- S. C. JEOUNG, S. TAKEUCHI, T. TAHARA and D. KIM**, "Ultrafast Decay Dynamics of Photoexcited $\text{Cu}(\text{II})(\text{TMpy-P4})$ in Water Solvent," *Chem. Phys. Lett.* **309**, 369 (1999).
- S. I. GHEYAS, T. URISU, S. HIRANO, H. WATANABE, S. IWATA, M. AOYAGI, M. NISHIO and H. OGAWA**, "Chemisorption of Deuterium on an Ultrathin Ge film deposited over $\text{Si}(100)\text{-}2\times 1$: Existence of a Dideuteride Phase," *Phys. Rev. B* **58**, 9949 (1998).
- Y. IMAIZUMI, H. MEKARU and T. URISU**, "Quantum Yield and Carbon Contamination in Thin Film Deposition Reaction by Core Electron Excitations," *Appl. Organometallic Chem.* **13**, 195 (1999).
- T. URISU**, "Synchrotron Radiation Process and in-situ Observation Technique; Infrared Reflection Absorption Spectroscopy," *Proc. SPIE-Int. Soc. Opt. Eng.* **3331**, 342 (1998).
- S. HIRANO, T. YOSHIGOE, M. NAGASONO, J. OOHARA, Y. NONOGAKI, Y. TAKEDA and T. URISU**, "Ultra High Vacuum Reaction Apparatus for Synchrotron Radiation Stimulated Process," *J. Synchrotron Radiat.* **5**, 1363 (1998).
- M. NAGASONO, K. MASE, S. TANAKA and T. URISU**, "State-Selected Ion Desorption from Condensed H_2O at 80 K Studied by Auger Electron-Photoion Coincidence Spectroscopy," *Chem. Phys. Lett.* **298**, 141 (1998).
- T. MIYAMAE, H. UCHIDA, I. H. MUNRO and T. URCISU**, "Synchrotron Radiation Stimulated Desorption of SiO_2 Thin Films on $\text{Si}(111)$ Surfaces Observed by Scanning Tunneling Microscopy," *J. Vac. Sci. Technol., A* **17**, 1733 (1999).
- H. MEKARU, Y. TSUSAKA, T. MIYAMAE, T. KINOSHITA, T. URISU, S. MASUI, E. TOYOTA and H. TAKENAKA**, "Construction of the Multilayered-Mirror Monochromator Beam Line for the Study of Synchrotron Radiation Stimulated Process," *Rev. Sci. Instrum.* **70**, 2601 (1999).
- T. MIYAMAE, T. URISU, H. UCHIDA and I. H. MUNRO**, "Scanning Tunneling Microscopy for the Study of the Synchrotron-Radiation Stimulated Process; Synchrotron-Radiation Stimulated Desorption of SiO_2 Films on $\text{Si}(111)$ Surface," *Jpn. J. Appl. Phys., Part 1* **38**, 249 (1999).
- T. URISU**, "Infrared Reflection Absorption Spectroscopy of Selective Etching and Decomposition Stimulated by Synchrotron Radiation," *MRS Bulletin* **24**, 46 (1999).
- M. NAGASONO, K. MASE and S. TANAKA**, "Study of Ion Desorption Induced by Resonant Core-Electron Excitation of Isolated NH_3 Monolayer Adsorbed on a Xe Film Using Auger Electron Photoion Coincidence Spectroscopy," *Jpn. J. Appl. Phys., Part 1* **38**, 325 (1999).
- H. NODA, H. NAGAI, M. SHIMAKURA, M. HIRAMATSU and M. NAWATA**, "Synthesis of Diamond Using a Low Pressure, Radio Frequency, Inductively Coupled Plasma," *J. Vac. Sci. Technol., A* **16**, 3170 (1998).
- M. HIRAMATSU, H. NODA, H. NAGAI, M. SHIMAKURA and M. NAWATA**, "Diamond Deposition from Methanol-Hydrogen-Water Mixed Gas Using a Low Pressure, Radio Frequency, Inductively-Coupled Plasma," *Thin Solid Films* **332**, 136 (1998).
- S. HIRANO, H. NODA, A. YOSHIGOE, S. I. GHEYAS and T. URISU**, "Annealing and Synchrotron Irradiation Effects on Hydrogen Terminated $\text{Si}(100)$ Surfaces Investigated by Infrared Reflection Absorption Spectroscopy," *Jpn. J. Appl. Phys.* **37**, 6991 (1998).
- K. MASE and S. TANAKA**, "An Electron Ion Coincidence Spectroscopy Study of Ion Desorption Induced by Core-Electron Transitions of Surfaces," *Jpn. J. Appl. Phys., Part 1* **38**, 233 (1999).
- K. MASE, M. NAGASONO and S. TANAKA**, "Mechanism of Ion Desorption Induced by Core-Electron Transitions of Condensed Molecules and Adsorbates Studied by Electron-Ion Coincidence Spectroscopy," *J. Electron Spectrosc. Relat. Phenom.* **101-103**, 13 (1999).
- T. SEKITANI, E. IKENAGA, K. FUJII, K. MASE, N. UENO and K. TANAKA**, "Control of Chemical Bond Scission by Using Site-Specific Photochemical Surface Reactions," *J. Electron Spectrosc. Relat. Phenom.* **101-103**, 135 (1999).
- Y. HIKOSAKA, H. HATTORI and K. MITSUKE**, "Spectator- and Participant-Like Behavior of a Rydberg Electron on Predissociation of Superexcited States of OCS ," *J. Chem. Phys.* **110**, 335 (1999).
- G. K. JARVIS, M. EVANS, C. Y. NG and K. MITSUKE**, "Rotational-Resolved Pulsed Field Ionization Photoelectron Study of NO^+ ($X^1\Sigma^+$, $v^+ = 0\text{-}32$) in the Energy Range of 9.24-16.80 eV," *J. Chem. Phys.* **111**, 3058

(1999).

T. MATSUO, T. KOHNO, S. MAKINO, M. MIZUTANI, T. TONUMA, A. KITAGAWA, T. MURAKAMI and H. TAWARA, "Gross Ionization Cross Sections for Rare-Gas Atoms and Simple Molecules in 6-MeV/amu Fully-Stripped Ion Impact," *Phys. Rev. A* **60**, 3000 (1999).

S. HASEGAWA, T. MIYAMAE, K. YAKUSHI, H. INOKUCHI, K. SEKI and N. UENO, "Origin of Photoemission Intensity Oscillation of C_{60} ," *Phys. Rev. B* **58**, 4927 (1998).

A. ABDUREYIM, S. KERA, H. SETOYAMA, R. SUZUKI, M. AOKI, S. MASUDA, K. K. OKUDAIRA, M. YAMAMOTO, N. UENO and Y. HARADA, "Penning Ionization Electron Spectroscopy on Self-Assembled Monolayers of 1-mercapt-8-bromooctane on Au(111)," *Mol. Cryst. Liq. Cryst.* **322**, 203 (1998).

N. UENO, Y. AZUMA, M. TSUTSUI, K. K. OKUDAIRA and Y. HARADA, "Thickness Dependent Orientation of Pendant Phenyl Group at the Surface of Polystyrene Thin Films," *Jpn. J. Appl. Phys.* **37**, 4979 (1998).

K. K. OKUDAIRA, S. HASEGAWA, H. ISHII, K. SEKI, Y. HARADA and N. UENO, "Structure of Copper- and H₂-phthalocyanine Thin Films on MoS₂ by means of Angle Resolved UPS and LEED," *J. Appl. Phys.* **85**, 6453 (1999).

T. MIYAMAE, N. UENO, S. HASEGAWA, Y. SAITO, T. YAMAMOTO and K. SEKI, "Electronic Structure of Poly(1,10-phenanthroline-3,8-diyl) and Its K-Doped State Studied by Photoelectron Spectroscopy," *J. Chem. Phys.* **110**, 2552 (1999).

Y. YAMAMOTO, H. OHARA, K. KAJIWARA, H. ISHII, N. UENO, K. SEKI and Y. OUCHI, "A Differential Thermal Analysis and Ultraviolet Photoemission Study on Surface Freezing of *n*-Alkanes," *Chem. Phys. Lett.* **304**, 231 (1999).

N. UENO, "Angle-Resolved UPS Studies of Organic Thin Films," *Jpn. J. Appl. Phys., Part I* **38**, 226 (1999).

K. KUROSAWA, P. R. HERMAN and W. SASAKI, "Radiation Effects of Vacuum Ultraviolet Lasers on Silica Glasses," *J. Photopolymer Sci. Tech.* **11**, 367 (1998).

N. TAKEZOE, A. YOKOTANI, K. KUROSAWA, W. SASAKI, T. IGARASHI and H. MATSUNO, "SiO₂ Thin Film Preparation Using Dielectric Barrier Discharge-Driven Excimer Lamps," *Appl. Surf. Sci.* **138-139**, 340 (1999).

Y. TAKIGAWA, T. IMOTO, T. SAKAKIBARA and K. KUROSAWA, "Thermoelectric Properties of AgBiTe₂-Ag₂Te Composite," *Mater. Res. Soc. Symp. Proc.* **545**, 105 (1999).

K. KUROSAWA, N. TAKEZOE, H. NAYAGIDA, R. NOMURA and A. YOKOTANI, "SiO₂ Film Coatings with VUV Excimer Lamp CVD," *Mater. Res. Soc. Symp. Proc.* **555**, 167 (1999).

K. KUROSAWA, P. R. HERMAN, E. Z. KURMAEV, S. N. SHAMIN, V. R. GALAKHOV, Y. TAKIGAWA, A. YOKOTANI, A. KAMEYAMA and W. SASAKI, "X-Ray Emission Spectroscopic Studies of Silicon Precipitation in Surface Layer of SiO₂ Induced by Argon Excimer Laser Irradiation," *Appl. Surf. Sci.* **126**, 83 (1998).

M. OHMUKAI, Y. TAKIGAWA and K. KUROSAWA, "Polycrystalline Silicon Precipitates on SiO₂ Using an Argon Excimer Laser," *Appl. Surf. Sci.* **137**, 78 (1999).

H. YAMASHITA, M. KATTO, S. OHNISHI, Y. KURIOKA, Y. TAKIGAWA, K. KUROSAWA, T. YAMANAKA and J. MIYAHARA, "Response Characteristics of Imaging Plate in UV Region," *Rev. Laser Eng.* **26**, 812 (1998).

N. NAKAMURA, J. ASADA, F. J. CURRELL, T. FUKAMI, T. HIRAYAMA, D. KATO, K. MOTOHASHI, E. NOJIKAWA, S. OHTANI, K. OKAZAKI, M. SAKURAI, H. SHIMIZU, N. TADA, S. TSURUBUCHI and H. WATANABE, "The Present Status of the Tokyo Electron Beam Ion Trap," *Rev. Sci. Instrum.* **69**, 694 (1998).

M. SAKURAI, H. OKAMURA, M. WATANABE, T. NANBA, S. KIMURA and M. KAMADA, "Upgraded Infrared Beamline at UVSOR," *J. Synchrotron Radiat.* **5**, 578 (1998).

H. S. MARGOLIS, J. ASADA, T. V. BACK, D. J. BIEBER, F. J. CURRELL, E. G. MYERS, N. NAKAMURA, S. OHTANI, P. K. OXLEY, M. SAKURAI, J. D. SILVER and H. WATANABE, "Recent Research Using the Oxford Electron Beam Ion Trap," *Hyperfine Interact.* **115**, 139 (1998).

M. MATSUMOTO, N. TATSUMI, K. FUKUTANI, T. OKANO, T. YAMADA, K. MIYAKE, K. HATA and H. SHIGEKAWA, "Adsorption Structures of NO/Pt(111) Investigated by Scanning Tunneling Microscopy," *J. Vac. Sci. Technol., A* **17**, 1577 (1999).

N. TATSUMI, M. MATSUMOTO, H. AIZAWA, S. TSUNEYUKI, K. FUKUTANI and T. OKANO, "Adsorption Structures of NO Molecules on a Pt(111) Surface," *J. Vac. Soc. Jpn.* **42**, 572 (1999).

K. FUKUI, H. NAKAGAWA, I. SHIMOYAMA, K. NAKAGAWA, H. OKAMURA, T. NANBA, M. HASUMOTO and T. KINOSHITA, "Reconstruction of BL7B for UV, VIS and IR Spectroscopy with a 3 m Normal Incidence Monochromator," *J. Synchrotron Radiat.* **5**, 836 (1998).

K. FUKUI, K. ASAKURA, K. NIMI, I. ISHIZUE and H. NAKAGAWA, "Absorption and Luminescence Spectra of Amorphous CdI₂ Thin Films," *J. Electron Spectrosc. Relat. Phenom.* **101-103**, 299 (1999).

H. OKAMURA, J. NAITOH, T. NANBA, M. MATOBA, M. NISHIOKA, S. ANZAI, I. SHIMOYAMA, K. FUKUI, H. MIURA, H. NAKAGAWA, K. NAKAGAWA and T. KINOSHITA, "Optical Study of the Metal-Nonmetal Transition in Ni_{1-δ}S," *Solid State Commun.* **112**, 91 (1999).

K. FUKUI, R. HIRAI, A. YAMAMOTO, S. NAOE and S. TANAKA, "Soft X-ray Absorption Study of III-V Nitrides," *Jpn. J. Appl. Phys., Part 1* **38**, 538 (1999).

S. NAGAOKA, K. MUKAI and U. NAGASHIMA, "Ab Initio Study on Magnetic Properties of 1,1',5,5'-Tetramethyl-6,6'-Dithioxo-3,3'-Biverdazyl Homo-Biradical and 3-(2',6'-di-*t*-Butyl-4'-Phenoxy)-1,5-Dimethyl-6-Thioxoverdazyl Hetero-Biradical," *J. Mol. Struct. (THEOCHEM)* **455**, 199 (1998).

K. SAWADA, S. ONODERA, H. ENOMOTO, S. NAGAOKA and K. MUKAI, "Spin-Probe Investigation of the Dynamic Behavior of Low Molecule Additive in Polyvinylchloride," *J. Chem. Soc. Jpn.* 169 (1999).

S. NAGAOKA, J. KUSUNOKI, T. FUJIBUCHI, S. HATAKENAKA, K. MUKAI and U. NAGASHIMA, "Nodal-Plane Model of the Excited-State Intramolecular Proton Transfer of 2-(*o*-Hydroxyaryl)benzazoles," *J. Photochem. Photobiol., A* **122**, 151 (1999).

K. SAWADA, S. ONODERA, H. ENOMOTO, S. NAGAOKA and K. MUKAI, "Spin-Label Investigation of the Dynamic Behavior of Stearic Acid Additives in Poly(vinyl chloride)," *Polymer Rep.* **56**, 298 (1999).

H. TOMODA, K. KITAJIMA, M. NAKAI, S. YAMAMOTO and S. NAGAOKA, "Development of Polishing Fluids for Titanium Alloy Using Lapping Tape (2nd Report) —Influence of Sulfuric Molecules for Titanium Alloy on Polishing Characteristics—," *J. Precision Eng. Jpn.* **65**, 851 (1999).

Coordination Chemistry Laboratories

Y. NISHIDA, "Important Role of Substrate in Activation of Dioxygen in Biological Oxygenases," *Trends Inorg. Chem.* **5**, 89 (1998).

S. NISHINO, T. KOBAYASHI, M. KUNITA, S. ITO and Y. NISHIDA, "Structural Variety of Copper(II)-Peroxide Adducts and Its Relevance to DNA Cleavage," *J. Bioscience* **54C**, 94 (1999).

Y. NISHIDA, M. KUNITA and S. NISHINO, "Mechanism of DNA Cleavage due to Green Cobalt(III)-Bleomycin Hydroperoxide irradiated by Visible Light," *Inorg. Chem. Commun.* **2**, 15 6(1999).

S. NISHINO, H. HOSOMI, S. OHBA, H. MATSUSHIMA, T. TOKII and Y. NISHIDA, "Selective Dioxygenation of Cyclohexane Catalyzed by Hydrogen Peroxide and Dinuclear Iron(III) Complexes with μ -Alkoxo Bridge," *J. Chem. Soc., Dalton Trans.* 1509 (1999).

Y. SASAKI, T. KOBAYASHI, H. MASUDA, H. EINAGA, S. OHBA and Y. NISHIDA, "Interaction between the Peroxide Ion and Acetate Moiety of the Ligand System in a Cobalt(II) Complex with a Binucleating Ligand," *Inorg. Chem. Commun.* **2**, 244 (1999).

W. OKUTSU, S. ITO and Y. NISHIDA, "Electrospray Mass Spectrometry of Peroxide Adduct of Monomeric Fe(III) Complex Containing Phenol Group," *Inorg. Chem. Commun.* **2**, 308 (1999).

T. KOBAYASHI, Y. SASAKI, T. AKAMATSU, T. ISHII, H. MASUDA, H. EINAGA and Y. NISHIDA, "High Activity of Binuclear Cobalt(II) Complex for Ethylene Evolution from 1-Aminocyclopropane-1-carboxylic Acid in the presence of Hydrogen Peroxide," *Z. Naturforsch., C* **54**, 534 (1999).

S. ITO, Y. SASAKI, Y. TAKAHASHI, S. OHBA and Y. NISHIDA, "Oxygenation of Nucleosides by Peroxide Adduct of Binuclear Iron(III) Complex with a μ -Oxo Bridge," *Z. Naturforsch., C* **54**, 554 (1999).

A. HATANO, H. MORISHITA, K. TANAKA and M. SHIONOYA, "Metal-Assisted Formation of Artificial Nucleic Acids," *Nucleic Acids, Symp. Ser.* **39**, 93 (1998).

K. TANAKA, H. CAO and M. SHIONOYA, "Double Strands Formation of Artificial DNAs Induced by Metal Complexation," *Nucleic Acids, Symp. Ser.* **39**, 171 (1998).

H. KUROSAKI, K. HAYASHI, Y. ISHIKAWA, M. GOTO, K. INADA, I. TANIGUCHI, M. SHIONOYA and E. KIMURA, "New Robust Bleomycin Analogues: Synthesis, Spectroscopy, and Crystal Structures of the Copper(II) Complexes," *Inorg. Chem.* **38**, 2824 (1999).

K. TANAKA and M. SHIONOYA, "Synthesis of a Novel Nucleoside for Alternative DNA Base Pairing through Metal Complexation," *J. Org. Chem.* **64**, 5002 (1999).

C. ARITA, H. SEINO, Y. MIZOBE and M. HIDAI, "Formation of Linear Tetradentate Phosphine Ligand o -C₆H₄(PPhCH₂CH₂PPh₂)₂ by Coupling of Two Diphosphine Ligands Bound to Low-Valent Mo or W Center. Synthesis and Structure of [M{*o*-C₆H₄(PPhCH₂CH₂PPh₂)₂}(Ph₂PCH₂CH₂PPh₂)] (M = Mo, W)," *Chem. Lett.* 611 (1999).

H. NAKAJIMA, K. TSUGE, K. TOYOHARA and K. TANAKA, "Stabilization of [Ru(bpy)₂(CO)(η^1 -CO₂)] and Unprecedented Reversible Oxide Transfer Reactions from CO₃²⁻ to [Ru(bpy)₂(CO)₂]²⁺ and from [Ru(bpy)₂(CO)(η^1 -CO₂)] to CO₂," *J. Organomet. Chem.* **569**, 61 (1998).

M. KURIHARA, S. DANIELE, K. TSUGE, H. SUGIMOTO and K. TANAKA, "Synthesis and Characterization of Ruthenium Terpyridine Dioxolene Complexes: Resonance Equilibrium between Ru^{III}-Catechol and Ru^{II}-Semiquinone Forms," *Bull. Chem. Soc. Jpn.* **71**, 867 (1998).

H. SUGIMOTO, K. TSUGE and K. TANAKA, "Novel Intramolecular Rearrangement of Hepta-Coordiante Rhenium(V) Complex with Catecholato and Terpyridine Ligands," *Chem. Lett.* 719 (1998).

M. M. ALI, H. SATO, K. TANAKA, M. HAGA, A. YOSHIMURA and T. OHNO, "Two-Electron Reduction of [(bpy)₂Ru(dmabbbpy)]₃Ru⁸⁺ from (BNA)₂ via Photoinduced Electron Transfer [dmabbbpy = 2,2'-Bis(N-methyl-

benzimidazole-2-yl)-4,4'-bipyridine],” *Inorg. Chem.* **37**, 6176 (1998).

T. MIZUKAWA, K. TSUGE, H. NAKAJIMA and K. TANAKA, “Selective Production of Acetone in Electrochemical Reduction of CO₂ Catalyzed by Ru-naphthyridine Complex,” *Angew. Chem., Int. Ed. Engl.* **38**, 362 (1999).

K. TSUGE and K. TANAKA, “First Artificial Energy Conversion from Proton Gradient to Electricity,” *Chem. Lett.* 1069 (1998).

T. KUSUKAWA and M. FUJITA, “Encapsulation of Large, Neutral Molecules in a Self-assembled Nanocage Incorporating Six Palladium(II) Ions,” *Angew. Chem., Int. Ed. Engl.* **37**, 3142 (1998).

T. KUSUKAWA and M. FUJITA, “‘Ship-in-a-Bottle’ Formation of Stable Hydrophobic Dimers of *cis*-Azobenzene and -Stilbene Derivatives in a Self-Assembled Coordination Nanocage,” *J. Am. Chem. Soc.* **121**, 1397 (1998).

N. TAKEDA, K. UMEMOTO, K. YAMAGUCHI and M. FUJITA, “A Nanometre-Sized Hexahedral Coordination Capsule Assembled from 24 Components,” *Nature* **398**, 794 (1999).

M. FUJITA, N. FUJITA, K. OGURA and K. YAMAGUCHI, “Spontaneous Assembling of Ten Small Components into a Three-Dimensionally Interlocked Compound Consisting of the Same Two Cage Frameworks,” *Nature* **400**, 52 (1999).

M. AOYAGI, K. BIRADHA and M. FUJITA, “Quantitative Formation of Coordination Nanotubes Templated by Rod-like Guests,” *J. Am. Chem. Soc.* **121**, 7457 (1999).

H. TOBITA, K. HASEGAWA, J. J. G. MINGLANA, L.-S. LUH, M. OKAZAKI and H. OGINO, “Extremely Facile Arene Exchange on a Ruthenium(II) Complex Having a Novel Bis(silyl) Chelate Ligand (9,9-Dimethyl-xanthene-4,5-diyl)bis(dimethylsilyl) (Xantsil),” *Organometallics* **18**, 2058 (1999).

Computer Center

T. NISHIKAWA, T. KINOSHITA, S. NANBU and M. AOYAGI, “A Theoretical Study on Structures and Vibrational Spectra of C₈₄ Fullerene Isomers,” *J. Mol. Struct. (THEOCHEM)* **461-462**, 453 (1999).

S. I. GHEYAS, T. URIS, S. HIRANO, H. WATANABE, S. IWATA, M. AOYAGI, M. NISHINO and H. OGAWA, “Chemisorption of Deuterium on an Ultrathin Ge Film Deposited over Si(100)-2×1: Existence of a Dideuteride Phase,” *Phys. Rev. B* **58**, 9949 (1998).

S. KONDO, K. TOKUHASHI, H. NAGAI, A. TAKAHASHI, M. SUGIE and M. AOYAGI, “Ab Initio Molecular Orbital Studies of Isomerization Reaction from *c*-OSiH₂O to *t*-OSiHOH,” *J. Mol. Struct. (THEOCHEM)* **469**, 25 (1999).

Laser Research Center for Molecular Science

S. SATO, K. OMIYA and K. KIMURA, “Cation Vibrational Spectra of Pyrimidine and Its van der Waals Complexes with Ar and N₂ by ZEKE Photoelectron Spectroscopy,” *J. Electron Spectrosc.* **97**, 121 (1998).

D. TANAKA, S. SATO and K. KIMURA, “ZEKE Electron Spectroscopy of Azulene-Argon,” *Chem. Phys.* **239**, 437 (1998).

Z. LIU, H. OHTAKE, N. SARUKURA, M. A. DUBINSKII, R. Yu. ABDULSABIROV and S. L. KORABLEVA, “All-Solid-State Tunable Ultraviolet Picosecond Ce³⁺:LiLuF₄ Laser with Direct Pumping by the Fifth Harmonic of a Nd:YAG Laser,” *OSA TOPS Vol. 19 Advanced Solid State Lasers* 13 (1998).

H. OHTAKE, Z. LIU, S. IZUMIDA, S. ONO, N. SARUKURA, T. ITATANI, T. SUGAYA, T. NAKAGAWA and Y. SUGIYAMA, “All-Solid-State, THz-Radiation Source Using a Femtosecond Mode-locked Laser with a Saturable Bragg Reflector in a Magnetic Field,” *OSA TOPS Vol. 19 Advanced Solid State Lasers* 367 (1998).

Z. LIU, H. OHTAKE, S. IZUMIDA, S. ONO and N. SARUKURA, “Sub-mW, Short-Pulse THz-Radiation from Femtosecond-Laser Irradiated InAs and Its Polarization and Spatial Properties,” *OSA TOPS Vol. 19 Advanced Solid State Lasers* 370 (1998).

H. OHTAKE and N. SARUKURA, “Enhanced Terahertz-Radiation from Semiconductors under Magnetic Field,” *Rev. Laser Eng. (in Japanese)* **26**, 527 (1998).

S. IZUMIDA, S. ONO, H. OHTAKE, Z. LIU and N. SARUKURA, “Visualization of the Beam Waist and Focusability of Intense Short-Pulse Terahertz Radiation,” *Rev. Laser Eng. (in Japanese)* **26**, 551 (1998).

N. SARUKURA, H. OHTAKE, S. IZUMIDA and Z. LIU, “High Average-Power THz Radiation from Femtosecond Laser-Irradiated InAs in a Magnetic Field and Its Elliptical Polarization Characteristics,” *J. Appl. Phys.* **84**, 654 (1998).

N. SARUKURA, Z. LIU, S. IZUMIDA, M. A. DUBINSKII, R. Yu. ABDULSABIROV and S. L. KORABLEVA, “All-Solid-State Tunable Ultraviolet Subnanosecond Laser with Direct Pumping by the Fifth Harmonic of a Nd:YAG Laser,” *Appl. Opt.* **37**, 6446 (1998).

Z. LIU, S. IZUMIDA, H. OHTAKE, N. SARUKURA, K. SHIMAMURA, N. MUJILATU, S. L. BALDOCHI and T. FUKUDA, “High-Pulse-Energy, All-Solid-State, Ultraviolet Laser Oscillator Using Large Czochralski-grown Ce:LiCAF Crystal,” *Jpn. J. Appl. Phys.* **37**, L1318 (1998).

K. SHIMAMURA, N. MUJILATU, K. NAKANO, S. L. BALDOCHI, Z. LIU, H. OHTAKE, N. SARUKURA and T. FUKUDA, "Growth and Characterization of Ce-doped LiCaAlF₆ Single Crystals," *J. Cryst. Growth* **197**, 896 (1999).

Z. LIU, N. SARUKURA, M. A. DUBINSKII, R. Yu. ABDULSABIROV and S. L. KORABLEVA, "All-Solid-State Subnanosecond Tunable Ultraviolet Laser Sources Based on Ce³⁺-activated Fluoride Crystals," *J. Nonlinear Opt. Phys. Mater.* **8**, 41 (1999).

S. IZUMIDA, S. ONO, Z. LIU, H. OHTAKE and N. SARUKURA, "Intense THz-Radiation Sources Using Semiconductors Irradiated with Femtosecond Laser Pulses in a Magnetic Field," *J. Nonlinear Opt. Phys. Mater.* **8**, 71 (1999).

Z. LIU, S. IZUMIDA, S. ONO, H. OHTAKE and N. SARUKURA, "High-Repetition-Rate, High-Average-Power, Mode-Locked Ti:sapphire Laser with an Intracavity Continuous-Wave Amplification Scheme," *Appl. Phys. Lett.* **74**, 3622 (1999).

S. IZUMIDA, S. ONO, Z. LIU, H. OHTAKE and N. SARUKURA, "Spectrum Control of THz Radiation from InAs in a Magnetic Field by Duration and Frequency Chirp of the Excitation Pulses," *Appl. Phys. Lett.* **75**, 451 (1999).

N. PAVEL, M. FURUHATA and T. TAIRA, "High-Efficiency Longitudinally-Pumped Miniature Nd:YVO₄ Laser," *Opt. Laser Tech.* **30**, 275 (1998).

S. KURIMURA, R. BATCHKO, J. MANSELL, R. ROUTE, M. FEJER and R. BYER, "Twinned Quartz for Quasi-Phase-Matched Ultraviolet Generation," *Center for Nonlinear Optical Materials Annual Report 97-98 A4* (1998).

N. PAVEL, S. KURIMURA and T. TAIRA, "Design Criteria for Optimization of Fiber-Coupled Diode Longitudinally-Pumped Lasers using Pump-Beam M² Factor," *OSA TOPS on Advanced Solid-State Lasers* **26**, 253 (1999).

I. SHOJI, H. NAKAMURA, K. OHDAIRA, T. KONDO, R. ITO, T. OKAMOTO, K. TATSUKI and S. KUBOTA, "Absolute Measurement of Second-Order Nonlinear-Optical Coefficients of β -BaB₂O₄ for Visible to Ultraviolet Second-Harmonic Wavelengths," *J. Opt. Soc. Am. B* **16**, 620 (1999).

S. KOH, T. KONDO, M. EBIHARA, T. ISHIWADA, H. SAWADA, H. ICHINOSE, I. SHOJI and R. ITO, "GaAs/Ge/GaAs Sublattice Reversal Epitaxy on GaAs (100) and (111) Substrates for Nonlinear Optical Devices," *Jpn. J. Appl. Phys.* **38**, L508 (1999).

T. TAIRA, S. KURIMURA, J. SAIKAWA, A. IKESUE and K. YOSHIDA, "Highly Trivalent Neodymium Ion Doped YAG Ceramic for Microchip Lasers," *OSA TOPS on Advanced Solid-State Lasers* **26**, 212 (1999).

Research Center for Molecular Materials

Y. YAMASHITA, M. TOMURA, M. B. ZAMAN and K. IMAEDA, "Synthesis and Properties of Novel Tetrathiafulvalene Vinylogues," *Chem. Commun.* 1657 (1998).

T. FUKUSHIMA, N. OKAZERI, T. MIYASHI, K. SUZUKI, Y. YAMASHITA and T. SUZUKI, "First Stable Tetracyanodiphenodimethane with a Completely Planar Geometry: Preparation, X-ray Structure, and Highly Conductive Complexes of Bis[1,2,5]thiadiazolo-TCNDQ," *Tetrahedron Lett.* **40**, 1175 (1999).

S. IRIE, S. ISODA, K. KUWAMOTO, M. J. MILES, T. KOBAYASHI and Y. YAMASHITA, "Monolayer Epitaxy of a Triangular Molecule on Graphite," *J. Cryst. Growth* **198/199**, 939 (1999).

M. B. ZAMAN, M. TOMURA and Y. YAMASHITA, "Novel Supramolecular Synthon in Crystal Engineering: Ionic Complexes of 4,4'-bipyridine and 1,2-bis(2-pyridyl)ethylene with 2,5-dichloro-3,6-dihydroxy-1,4-benzoquinone," *Chem. Commun.* 999 (1999).

S. TANAKA and Y. YAMASHITA, "New Building Unit for Rigid and Coplanar Oligo-Aromatic Molecular Wires with Insulating Mantel," *Synth. Met.* **101**, 532 (1999).

K. SUZUKI, M. TOMURA and Y. YAMASHITA, "TCNQ Analogues Composed of Heterocyclic Rings," *Synth. Met.* **102**, 1480 (1999).

H. YAMOCHI, S. NAKAMURA, G. SAITO, M. B. ZAMAN, J. TOYODA, Y. MORITA, K. NAKASUJI and Y. YAMASHITA, "Cyananilate Anion as Hydrogen Bonded Counter Ion in Conducting CT Complexes," *Synth. Met.* **102**, 1729 (1999).

Y. YAMASHITA, M. TOMURA, S. TANAKA and K. IMAEDA, "Novel TTF Vinylogues Affording Stable Cation Radicals," *Synth. Met.* **102**, 1730 (1999).

T. IKEUE, Y. OHGO, A. UCHIDA, M. NAKAMURA, H. FUJII and M. YOKOYAMA, "High-Spin (meso-Tetraalkylporphyrinato)iron(III) Complexes As Studied by X-ray Crystallography, EPR, and Dynamic NMR Spectroscopies," *Inorg. Chem.* **38**, 1276 (1999).

K. CZARNECKI, L. M. PRONIEWICZ, H. FUJII, D. JI, R. S. CZERNUSZEWICZ and J. R. KINCAID, "Insensitivity of Vanadyl-Oxygen Bond Strengths to Radical Type (²A_{1u} vs. ²A_{2u}) in Vanadyl Porphyrin Cation Radicals," *Inorg. Chem.* **38**, 1543 (1999).

M. NAKAMURA, T. IKEUE, A. IKEZAKI, Y. OHGO and H. FUJII, "Electron Configuration of Ferric Ions in Low-Spin (Dicyano)(meso-tetraarylporphyrinato)iron(III) Complexes," *Inorg. Chem.* **38**, 3857 (1999).

C. T. MIGITA, H. FUJII, K. M. MATERA, S. TAKAHASHI, H. ZHOU, T. YOSHIDA and M. IKEDA-

SAITO, "Molecular Oxygen Oxidizes the Porphyrin Ring of the Ferric α -Hydroxyheme in Heme Oxygenase in the Absence of Reducing Equivalent," *Biochim. Biophys. Acta* **1432**, 203 (1999).

H. IIKURA and T. NAGATA, "Structural Variation in Manganese Complexes: Synthesis and Characterization of Manganese Complexes from Carboxylate-Containing Chelating Ligands," *Inorg. Chem.* **37**, 4702 (1998).

T. AKASAKA, T. SUZUKI, Y. MAEDA, M. ARA, T. WAKAHARA, K. KOBAYASHI, S. NAGASE, M. KAKO, Y. NAKADAIRA, M. FUJITSUKA and O. ITO, "Photochemical Bissilylation of C_{60} with Disilane," *J. Org. Chem.* **64**, 566 (1999).

D. KUWAHARA, T. NAKAI, J. ASHIDA and S. MIYAJIMA, "Novel Satellites in a Two-Dimensional Spin-Echo NMR Experiment for Homonuclear Dipole-Coupled Spins in Rotating Solids," *Chem. Phys. Lett.* **305**, 35 (1999).

Equipment Development Center

M. KAMADA, S. ASAKA, T. TSUJIBAYASHI, O. ARIMOTO, M. WATANABE, S. NAKANISHI, H. ITOH, S. HIROSE and M. ITOH, "Combination of Synchrotron Radiation and Lasers for Solid- and Surface-Researches," *J. Jpn. Soc. Synchrotron Radiat. Res.* **12**, 48 (1999).

Ultraviolet Synchrotron Orbital Radiation Facility

N. SANADA, S. MOCHIZUKI, S. ICHIKAWA, N. UTSUMI, M. SHIMOMURA, G. KANEDA, A. TAKEUCHI, Y. SUZUKI, Y. FUKUDA, S. TANAKA and M. KAMADA, "The (2×4) and (2×1) Structures of the Clean GaP(001) Surface," *Surf. Sci.* **419**, 120 (1999).

M. KOBAYASHI, T. NAMBA, M. KAMADA and S. ENDO, "Proton Order-Disorder Transition of Ice Investigated by Far-Infrared Spectroscopy under High Pressure," *J. Phys.: Condens. Matter* **10**, 11551 (1998).

K. OHTANI, H. DOSHITA, M. KOHAMA, Y. TAKAMINE, K. ASAO, S. TANAKA, M. KAMADA and A. NAMIKI, "Physisorption Lifetimes of Cl_2 on the Si(100) Surfaces Adsorbed with Cs and Cl," *Surf. Sci.* **414**, 85 (1998).

T. NODA, T. NAKANAE, K. OZAWA, K. EDAMOTO, S. TANAKA and S. OTANI, "Photoemission Study of the Oxidation of ZrC(111)," *Solid State Commun.* **107**, 145 (1998).

M. NAGASONO, K. MASE, S. TANAKA and T. URISU, "State-Selected Desorption from Condensed H_2O at 80 K Studied by Auger Electron-Photoion Coincidence Spectroscopy," *Chem. Phys. Lett.* **298**, 141 (1998).

M. SANO, Y. SEIMIYA, Y. OHNO, T. MATSUSHIMA, S. TANAKA and M. KAMADA, "Orientation of Oxygen Admolecules on a Stepped Platinum(133) Surface," *Surf. Sci.* **421**, 386 (1999).

M. NAGASONO, K. MASE, S. TANAKA and T. URISU, "Study of Ion Desorption Induced by Resonant Core-Electron Excitation of Isolated NH_3 Monolayer Adsorbed on a Xe Film Using Auger Electron Photoion Coincidence Spectroscopy," *Jpn. J. Appl. Phys.* **38**, 325 (1999).

K. MASE and S. TANAKA, "An Electron Ion Coincidence Spectroscopy Study of Ion Desorption Induced by Core-Electron Transitions of Surfaces," *Jpn. J. Appl. Phys.* **38**, 233 (1999).

I. OUCHI, I. NAKAI, M. KAMADA, S. TANAKA, T. GEJO and T. HAGIWARA, "Structure and Core Electron Absorption Spectra of Polyester Films," *Jpn. J. Appl. Phys.* **38**, 183 (1999).

K. MASE, M. NAGASONO, and S. TANAKA, "Mechanism of Ion Desorption Induced by Core-Electron Transitions of Condensed Molecules and Adsorbates Studied by Electron Ion Coincidence Spectroscopy," *J. Electron Spectrosc. Relat. Phenom.* **101-103**, 13 (1999).

M. NAGASONO, K. MASE, S. TANAKA and T. URISU, "Ultrafast H^+ Desorption from an Isolated NH_3 Monolayer Adsorbed on a Xe Film Induced by a Resonant Core Electron-Photoion Coincidence Spectroscopy," *J. Jpn. Appl. Phys.* **38**, 325 (1999).

H. HAMA and M. HOSAKA, "Longitudinal Beam Dynamics and FEL Interaction on a Negative Momentum Compaction Storage Ring," *Nucl. Instrum. Methods Phys. Res., Sect. A* **429**, 172 (1999).

M. HOSAKA, J. YAMAZAKI and H. HAMA, "Influence of Electron Beam Properties on Spontaneous Radiation from an Optical Klystron," *Nucl. Instrum. Methods Phys. Res., Sect. A* **429**, 191 (1999).

H. TANAKA, M. TAKAO, K. SOUTOME, H. HAMA and M. HOSAKA, "A Perturbative Formulation of Nonlinear Dispersion for Particle Motion in Storage Rings," *Nucl. Instrum. Methods Phys. Res., Sect. A* **431**, 396 (1999).

S. KIMURA, K. G. NATH, Y. HARUYAMA, T. KINOSHITA, S. YOSHII and M. KASAYA, "Anisotropic Optical Conductivity of RPtAs ($R = La, Ce$)," *Physica B* **259-261**, 1163 (1999).

H. MEKARU, Y. TSUSAKA, T. IYAMAE, T. KINOSHITA, T. URISU, S. MASUI, E. TOYOTA and H. TAKENAKA, "Construction of the Multilayered-Mirror Monochromator Beam Line for the Study of Synchrotron Radiation Stimulated Process," *Rev. Sci. Instrum.* **70**, 2601 (1999).

Y. HARUYAMA, K. G. NATH, S. KIMURA, Y. UFUKTEPE, T. KINOSHITA, K. HIRAKI and K.

KANODA, "Electronic Structures of Organic Salts (DI-DCNQI)₂M (M = Cu and Ag) Using Photoelectron Spectromicroscopy," *Solid State Commun.* **110**, 17 (1999).

K. G. NATH, Y. HARUYAMA, S. KIMURA, Y. UFUKTEPE and T. KINOSHITA, "Study of Magnetic Linear Dichroism (MLD) for Different Thickness of Ni Thin Film Grown on Ferromagnetic Co(001) in Element Specific Photoemission," *J. Electron Spectrosc. Relat. Phenom.* **101-103**, 257 (1999).

T. GEJO, K. OKADA, T. IBUKI and N. SAITO, "Photodissociation of Ozone in the K-Edge Region," *J. Phys. Chem. A* **103**, 4598 (1999).

J. ADACHI, Y. TAKATA, N. KOSUGI, E. SHIGEMASA, A. YAGISHITA and Y. KITAJIMA, "Kinetic Energy Dependence of Anisotropic Yields of Ionic Fragmentations Following S 1s Excitations of SO₂," *Chem. Phys. Lett.* **294**, 559 (1998).

A. A. PAVLYCHEV, N. G. FOMINYKH, N. WATANABE, K. SOEJIMA, E. SHIGEMASA and A. YAGISHITA, "Dynamic Properties of N and O 1s⁻¹ σ_u^* Shape Resonances in N₂ and CO₂ Molecules," *Phys. Rev. Lett.* **81**, 3623 (1998).

T. HAYAISHI, T. TANAKA, H. YOSHII, E. MURAKAMI, E. SHIGEMASA, A. YAGISHITA, F. KOIKE and Y. MORIOKA, "Post-Collision Interaction Effects of Threshold Photoelectrons in Kr L₃-shell Photoionization," *J. Phys. B* **32**, 1507 (1999).

S. KIMURA, "Infrared Magnetic Circular Dichroism of Strongly Correlated 4f Electron Systems with Synchrotron Radiation," *Jpn. J. Appl. Phys., Part 1* **38**, 392 (1999).

S. KIMURA, H. OKAMURA, T. NANBA, M. IKEZAWA, S. KUNII, F. IGA, N. SHIMIZU and T. TAKABATAKE, "Optical Spectra of RB_x (R = rare-earth, x = 4, 6, 12)," *J. Electron Spectrosc. Relat. Phenom.* **101-103**, 761 (1999).

H. OKAMURA, S. KIMURA, H. SHINOZAKI, T. NANBA, F. IGA, N. SHIMIZU and T. TAKABATAKE, "Optical Study of Gap Opening and Low Energy Excitation in YbB₁₂," *Physica B* **259-261**, 317 (1999).

S. KIMURA, K. G. NATH, Y. HARUYAMA, T. KINOSHITA, S. YOSHII and M. KASAYA, "Anisotropic Optical Conductivity of RPtAs (R = La, Ce)," *Physica B* **259-261**, 1163 (1999).

H. OKAMURA, S. KIMURA, H. SHINOZAKI, T. NANBA, F. IGA, N. SHIMIZU and T. TAKABATAKE, "Optical Spectra of the Kondo Semiconductor YbB₁₂," *Jpn. J. Appl. Phys. Series 11*, 85-87 (1999).

S. KIMURA, D. X. LI, Y. HAGA and T. SUZUKI, "Magneto-Optical Study on GdAs in the Infrared Region," *Jpn. J. Appl. Phys. Series 11*, 126-128 (1999).

H. OKAMURA, S. KIMURA, H. SHINOZAKI, T. NANBA, F. IGA, N. SHIMIZU and T. TAKABATAKE, "Optical Conductivity of the Kondo Insulator YbB₁₂: Gap Formation and Low-Energy Excitations," *Phys. Rev. B* **58**, R7496 (1998).

S. KIMURA, D. X. LI, Y. HAGA and T. SUZUKI, "Magnetic Field Dependence of Low Energy Excitation of GdAs," *J. Magn. Magn. Mater.* **177-181**, 351 (1998).

REVIEW ARTICLES AND TEXTBOOKS

Department of Theoretical Studies

T. IKEGAMI and S. IWATA, "Intracuster Reaction Dynamics of Ar_4^+ ," in *The Transition State, Theoretical Approach*, Fueno, Ed., Kodansha; Tokyo, p. 115, (1999).

Y. OKAMOTO, "Protein Folding Mechanism as Studied by Monte Carlo Simulations" (in Japanese), *Bussei Kenkyu* **70**, September, pp.719-742 (1998).

Y. OKAMOTO, "New Sampling Method That Solves Complex Systems:Multicanonical Molecular Dynamics Algorithm" (in Japanese), *Chemistry* **53**, September, pp. 66-67 (1998).

Y. OKAMOTO, "Protein Tertiary Structure Predictions by Monte Carlo Simulations" (in Japanese), *Biophysics* **38**, October, pp. 203-207 (1998).

Y. OKAMOTO, "Protein Folding Simulations by Generalized-Ensemble Algorithms" (in Japanese), *Bussei Kenkyu* **71**, December, pp. 335-347 (1998).

U. H. E. HANSMANN and Y. OKAMOTO, "The Generalized-Ensemble Approach for Protein Folding Simulations" in *Annual Reviews of Computational Physics VI*, D. Stauffer, Ed., World Scientific; Singapore, pp. 129-157 (1999).

U. H. E. HANSMANN and Y. OKAMOTO, "Tackling the Protein Folding Problem by a Generalized-Ensemble Approach with Tsallis Statistics," in Special Issue, 'Nonextensive statistical mechanics and thermodynamics,' *Braz. J. Phys.* **29**, pp. 187-198 (1999).

U. H. E. HANSMANN and Y. OKAMOTO, "New Monte Carlo Algorithms for Protein Folding," *Curr. Opin. Struct. Biol.* **9**, pp. 177-183 (1999).

H. NAKAMURA, "Chemical Reaction Dynamics and Potential Ridge—Beyond the Transition State" in *The Transition State—A Theoretical Approach*, T. Fueno, Ed., Kohdansha and John Wiley & Sons; pp. 193-215 (1999).

M. HIYAMA and H. NAKAMURA, "Characteristics and Dynamics of Superexcited States of Diatomic Molecules" in *Strucutre and Dynamics of Electronic Excited States*, J. Laane, H. Takahashi and A. Bandrauk, Eds., Springer-Verlag, pp. 296-315 (1999).

Y. TANIMURA, K. YAMASHITA and P. A. ANFINRUD, "Femtochemistry," *Proc. Natl. Acad. Sci. U. S. A.* **96**, pp. 8823-8824 (1999).

K. OKUMURA, "Liquid Dynamics Probed by Two-Dimensional Raman Spectroscopy—An Approach by the Brownian Oscillator Model," *Kagaku to Kogyo (Chemistry and Chemical Industry)* (in Japanese) **52-2**, pp. 115-118 (1999).

F. HIRATA, H. SATO, S. TEN-NO and S. KATO, "RISM-SCF Study of Solvent Effect on Electronic Structure and Chemical Reaction in Solution: Temperature Dependence of pK_w " in *Combined Quantum Mechanical and Molecular Mechanical Methods*, J. Gao and M. A. Thompson Eds., ACS symposium series 712, American Chemical Society; Washington DC, pp. 188-200 (1998).

Department of Molecular Structure

S. SAITO, "Sulfur-Bearing Carbon-Chain Molecules in Space and in the Laboratory," *Sulfur Reports* **21**, 401 (1999).

T. AKASAKA, T. WAKAHARA, S. NAGASE and K. KOBAYASHI, "Are Encapsulated Metals inside a Fullerene Cage Still?" *Kagaku* (in Japanese) **53**, 72 (1998).

T. AKASAKA, S. OKUBO, T. WAKAHARA, K. KOBAYASHI, S. NAGASE, M. KAKO, Y. NAKADAIRA, T. KATO, K. YAMAMOTO, H. FUNASAKA and K. MATSUURA, "Endohedrally Metal-Doped Hetero-fullerenes," in *Recent Advances in the Chemistry and Physics of Fullerenes*, K. Kadish and R. Ruoff, Eds., The Electrochemical Society; Pennington, NJ (1998).

S. NAGASE, K. KOBAYASHI and T. AKASAKA, "Recent Advances in the Structural Determination of Endohedral Metallofullerenes," *J. Comput. Chem.* **19**, 232 (1998).

Y. MIZUTANI, "Vibrational Energy Relaxation of Hemeproteins: A Physicochemical Process in Proteins" (in Japanese), *Seibutsu Butsuri* **38**, 256 (1998).

T. KATO, "Spectroscopic Studies on Radicals of Fullerenes" in *Recent Research and Development in Physical Chemistry*, Transworld Research Network, vol. 2, 981 (1998).

T. KATO, K. SATO, T. TAKUI, D. HURUM, R. W. KREILICK, S. OKUBO and T. AKASAKA, "Determination of the Cage Structure of La@C_{82} " in *Proceedings of the Symposium on Recent Advances in the Chemistry and Physics of Fullerenes and Related Materials*, K. M. Kadish, Ed., The Electrochemical Society, Inc.; Pennington, **6**, 967 (1998).

Department of Electronic Structure

N. NISHI, "Cluster Structures in Hydrogen-bonding Solutions" in *Development in Microcluster Science*, Kikan Kagaku Sosetsu No. 38, Japan Scientific Societies Press, 173 (1998).

Y. ENDO and M. FUJII, "Double Resonance (MODR, OODR) Spectroscopy," in *Nonlinear Spectroscopy for Molecular Structure Determination*, R. W. Field, E. Hirota, J. P. Maier and S. Tsuchiya, Eds., Blackwell Science, pp. 29-54 (1998).

M. FUJII, "Jahn-Teller Effect," *Chemistry* **53**, pp. 48-49 (1998).

M. FUJII, "Observation of Highly Vibrationally Excited Molecules and Possibility of Application to Reaction Control," *The Review of Laser Engineering* **27**, 404 (1999).

Y. MO and T. SUZUKI, "Optical Detection of Angular Momentum Polarization and Its Application to Photodissociation Dynamics" in *Advances in Multi-Photon Processes and Spectroscopy* **12**, S. H. Lin, A. A. Villaeys and Y. Fujimura, Eds., World Scientific; Singapore (1999).

N. TAMAI, "Spectroscopy with the Best Temporal Resolution" in *World Record Collection in Chemistry* (in Japanese), Kagakudojin, 10 (1999).

X. YANG, A. MIURA and N. TAMAI, "Electron Transfer and Carrier Dynamics of Titanium Dioxide Electrodes," *Photochemistry* (in Japanese) **30**, 128 (1999).

Department of Molecular Assemblies

S. MIYAJIMA and O. OISHI, "Measurement of Anisotropic Self-Diffusion Coefficient Tensors by PGSE-NMR," *DIM Newsletter* **12**, pp. 16-20 (1998).

S. MIYAJIMA and T. NAKAI, "Experimental Spectroscopy of Liquid Crystals, No. 4, NMR Spectroscopy -1-," *EKISHO* (in Japanese) **3**, 43-51 (1999).

S. MIYAJIMA and T. NAKAI, "Experimental Spectroscopy of Liquid Crystals, No. 5, NMR Spectroscopy -2-," *EKISHO* (in Japanese) **3**, 124-132 (1999).

S. MIYAJIMA and T. NAKAI, "Experimental Spectroscopy of Liquid Crystals, No. 6, NMR Spectroscopy -3-," *EKISHO* (in Japanese) **3**, 205-212 (1999).

S. MIYAJIMA, *Essential Dictionary of Chemistry* (in Japanese) Tokyo Kagaku Dojin (1999).

Department of Applied Molecular Science

Y. MISAKI and T. MORI, "TTP Type Conductors —Development of p-Electron Framework Toward Increase of Dimensionality—," *Solid State Physics* (in Japanese) **33**, pp. 1014-1024 (1999).

K. NAGATO, "Chemical Composition of Atmospheric Ions," *Proceedings of the Institute of Electrostatics of Japan* (in Japanese) **23**, 37 (1999).

Department of Vacuum UV Photoscience

Y. TAKATA and N. KOSUGI, "A Unified View of Inner-Shell Resonant Photoemission at the Ni 2p Absorption Edge of Nickel Oxide, Metal and Complexes," *J. Jpn. Soc. Synchrotron Radiat. Res.* (in Japanese) **12**, 117 (1999).

W. SASAKI, K. KUROSAWA, S. KUBODERA and J. KAWANAKA, "The State of the Art of Rare Gas Excimer Lasers and Lamps as a Light Source For Giga-Bit Lithography," *J. Photopolymer Sci. Tech.* **11**, 361 (1998).

N. TAKEZOE, A. YOKOTANI and K. KUROSAWA, "Thin Film Preparation Using Vacuum Ultraviolet Rare Gas Excimer Lamps," *Hyomen Kagaku* (in Japanese) **20**, 402 (1999).

K. KUROSAWA, "Understanding Lasers," *OPTRONICS* (in Japanese) (1999).

Coordination Chemistry Laboratories

M. FUJITA, "Metal-Directed Self-Assembly of Two- and Three-Dimensional Synthetic Receptors," *Chem. Soc. Rev.* **27**, pp. 417-425 (1998).

M. FUJITA, "Self-Assembly of [2]Catenanes Containing Metals in Their Backbones," *Acc. Chem. Soc.* **32**, pp. 53-61 (1999).

M. FUJITA, "Transition Metal-Incorporating Catenanes" in *Molecular Catenanes, Rotaxanes, and Knots*, Sauvage, J.-P. and Dietrich-Buchecker, C. O., Eds., Wiley-VCH; Weinheim, USA, Chapter 4 (1999).

Laser Research Center for Molecular Science

N. SARUKURA, "Special Issues on New Materials in Ultraviolet Region," *Rev. Laser Eng.* (in Japanese) **27**, 518 (1999).

T. TAIRA, "Concept for Measuring Laser Beam-Quality Parameters," *Rev. Laser Eng.* **26**, 723 (1998).

S. KURIMURA *et al.*, "Handbook of Optical Science," *Optronics* (1998).

S. KURIMURA *et al.*, "Handbook of Optical-Device Fabrication," *Optronics* (1998).

T. TAIRA, "Microchip Solid-State Lasers," *Rev. Laser Eng.* **26**, 847 (1998).

T. TAIRA, "Yb³⁺-Doped Solid-State Lasers," *Kougaku* **28**, 435 (1999).

ANNUAL REVIEW, 1999

AUTHOR INDEX TO RESEARCH ACTIVITIES AND SPECIAL RESEARCH PROJECTS

A

ABDUREYIM, Abduaini 156
 ADACHI, Jun-ichi 135-136
 ADACHI, Takafumi 88, 92, 95, 230
 ADACHI, Takashi 123, 162
 AGUI, Akane 137
 AIKAWA, Katsuji 204
 AIZAWA, Hideaki 163
 AKAMATSU, Tetsuya 172
 AKASAKA, Takeshi 49, 58
 AKIYAMA, Ryo 38, 222
 AKUTSU, Hiroki 87
 ALI, Md. Meser 180
 ANAZAWA, Toshihisa 69
 ANTOINE, Laurence 98
 ANZAI, Shunichiro 164
 AOKI, Masaru 156
 AONUMA, Shuji 82
 AOYAGI, Masaru 183-185, 234
 AOYAGI, Mutsumi 189-190, 226
 ARAI, Masahiro 106
 ARAKAWA, Ichiro 123, 162
 ARAKAWA, Ryuichi 54
 ARAKI, Mitsunori 46
 ARITA, Chirima 178
 ARZHANTSEV, Sergei 142-143, 225
 ASAKA, Shuji 208-209, 227
 ASAKURA, Kenji 164
 ASANO-SOMEDA, Motoko 143
 ASATO, Masaki 63
 AWAGA, Kunio 105
 AZUMA, Jun 71
 AZUMA, Yasushi 156, 231

B

BABA, Takeshi 131
 BAECK, Kyoung K. 21
 BAGCHI, Biman 28, 37
 BAILLEUX, Stephane 131
 BALDOCHI, Sonia L. 193
 BANDO, Hideki 53
 BANDO, Syunji 100
 BELOV, Sergey 224
 BENEDICT, Claudia 107
 BIRADHA, Kumar 176, 183-185, 234
 BLUDSKÝ, Ota 20

BOKUMOTO, Yoshiho 209
 BRADSHAW, Alexander M. 135
 BROWN, John M. 45
 BU, Xian-He 176, 233
 BUENKER, Robert J. 30-31

C

CAO, Honghua 175, 233
 CASSOUX, Patrick 88-89
 CAVELL, Ronald G. 135
 CHEN, Feiwu 21, 221
 CHOI, Heechol 21
 CHONG, Song-Ho 35-36
 CZARNECKI, Kazimierz 202

D

DECKER, Stephan A. 127
 DING, Yuqin 75-76, 229
 DONG, Jian 76
 DROZDOVA, Olga 79
 DUBENKO, Igor S. 121-122

E

EBIHARA, Masahiro 173
 EINAGA, Hisahiko 112-113, 171-172
 EMURA, Shuichi 104
 ENGLAND, James 20
 ENOKI, Toshiaki 98, 101, 109

F

FAN, Kang-Nian 22
 FU, Rouli 42
 FUJII, Hiroshi 201-203, 235
 FUJII, Masaaki 64, 67, 223
 FUJII, Yasuo 210
 FUJIKI, Satoshi 104
 FUJIMOTO, Seiki 177
 FUJINAMI, Shuhei 55, 112
 FUJINO, Tatsuya 145-146, 225
 FUJISAWA, Yae 177
 FUJITA, Makoto 182-186, 234
 FUJITA, Norifumi 182, 234
 FUJIWARA, Akihiko 104
 FUJIWARA, Hideki 88-90, 93-94, 230, 232
 FUJIWARA, Yasufumi 150

FUJIYOSHI, Satoru 139, 225
 FUKAISHI, Kenji 180
 FUKUDA, Atsuo 97
 FUKUDA, Nobuya 106
 FUKUDA, Tsuguo 193
 FUKUI, Kazutoshi 164
 FUKUSHIMA, Takanori 199
 FUKUTANI, Katsuyuki 163
 FUKUZUMI, Shunichi 53-54, 111
 FUNABIKI, Takuzo 113
 FUNAHASHI, Yasuhiro 202, 235
 FURUKAWA, Nobuo 44
 FURUTA, Fumio 167

G

GAIDUKOVA, Irina Yu 121-122
 GALAKHOV, V. 159
 GANGOPADHAYAY, Gautam 28
 GAO, Yongli 149
 GEE, Richard H. 39
 GEJO, Tatsuo 214
 GHOSH, Tapas Kumar 128, 224
 GHOSHAL, Sharmistha 28
 GOTO, Tsuneaki 119
 GOTO, Yoshio 111, 233
 GOTOWDA, Masaharu 54
 GRAY, Stephen K. 189
 GU, Jian-ping 30-31
 GUERARD, Daniel 98

H

HAGA, Masa-aki 180
 HAMA, Hiroyuki 210, 227
 HAMAGUCHI, Hiro-o 146
 HANAZATO, Shiogo 109
 HANSMANN, Ulrich H. E. 23
 HARA, Isao 112
 HARADA, Kensuke 131-133, 224
 HARADA, Yoshiya 85, 156
 HARANO, Yuichi 222
 HARUYAMA, Yuichi 210-213, 228
 HASEGAWA, Kenji 188
 HASEGAWA, Shinji 85-86, 156-157, 209, 231
 HASHIMOTO, Kenro 67
 HASHIMOTO, Tomohiro 20, 221
 HASUMOTO, Masami 164
 HATA, Kenji 163

- HATANO, Akihiko 233
 HATATE, Hitoshi 150
 HATSUI, Takaki 137-138
 HATTORI, Hideo 155
 HAYAMA, Akira 123, 162
 HAYAMI, Shinya 115
 HAYASHI, Hideki 55, 112
 HAYASHI, Naoki 59
 HEIDENHAIN, Sophie 206
 HENDERSON, Douglas 39
 HERMAN, Peter 159
 HERMAN, Zdenek 21
 HIDAI, Masanobu 178
 HIKOSAKA, Yasumasa 152-153, 225
 HIRAI, Ryouzuke 164
 HIRAMATSU, Mineo 148
 HIRAOKA, Shuichi 183-184, 234
 HIRATA, Fumio 23, 32-39, 62, 222
 HIRATA, So 221
 HIRAYAMA, Takato 123, 162
 HIROSE, Sayumi 210
 HIROTA, Shun 53
 HIRSCH, Gerhard 30
 HIRSCH, Gerhart 31
 HITCHCOCK, Adam P. 135
 HONDA, Hiroaki 128
 HORACEK, Jiri 26
 HORI, Hiroshi 50
 Horigome, Toshio 208-209
 HORIUCHI, Sachio 79
 HOSAKA, Masahito 210, 227
 HOSOKOSHI, Yuko 88, 116, 119-122
 HOSOMI, Hiroyuki 170
 HOSSAIN, Delower 234
 HRUŠÁK, Jan 20-21
 HUANG, Hong-Wei 53
- I**
- IBUKI, Toshio 214
 IBUKURO, Fumiaki 184, 234
 ICHIMURA, Kenji 86
 ICHISE, Tomoko 51
 IGA, Fumitoshi 215
 IGARASHI, Tatsushi 158
 IIBA, Masami 173
 IKADA, Tomotake 178
 IKEDA, Tomiki 71
 IKEDA-SAITO, Masao 203
 IKEGAMI, Tsutomu 17, 221
 IKENAGA, Eiji 151
 IKESUE, Akio 196
 IKEUE, Takahisa 201
 IKEZAKI, Akira 201
 IM, Sang-Choul 53
 IMACHI, Ron 105
 IMAEDA, Kenichi 86, 197
 IMAI, Takashi 222
 IMAMURA, Yoshihiro 53
 IMAMURA, Yutaka 28-29, 44, 229
- IMOU, Kazumichi 30
 INABE, Tamotsu 107
 INADA, Takanori 177
 INO, Daisuke 70
 INOKUCHI, Hiroo 85-86, 156
 INOKUCHI, Yoshiya 64-66, 223
 INOUE, Katsuya 88, 115-122, 231
 INOUE, Shin-ichi 86
 INOUE, Tsuyoshi 53-54
 IRISA, Masayuki 23
 IRIYAMA, Keiji 72
 ISHIDA, Takayuki 105
 ISHIDA, Tateki 33
 ISHIGURO, Masazumi 133
 ISHII, Hisao 85-86, 156-157, 231
 ISHII, Kenji 104
 ISHII, Toshihiro 172
 ISHII, Youichi 178
 ISHIKAWA, Ken 97
 ISHIUCHI, Shun-ichi 67
 ISHIZUE, Ikuto 164
 ISOBE, Kiyoshi 114
 ISOBE, Yoshiaki 54
 ITIKAWA, Yukikazu 30
 ITO, Eisuke 86
 ITO, Hajime 235
 ITO, Hirokazu 185, 234
 ITO, Hirotugu 71
 ITO, Masakatsu 189, 226
 ITO, Sayo 170-172
 ITOH, Minoru 209-210
 ITOH, Shinobu 53-54
 IWAHORI, Fumiyasu 115, 117
 IWAMURA, Hiizu 115, 117, 120
 IWASA, Yoshihiro 104
 IWASAKI, Kota 153, 225
 IWATA, Koichi 143
 IWATA, Suehiro 17-22, 221
 IWAZUMI, Toshiaki 138
- J**
- JEOUNG, Sae Chae 144
 JIN, Bo 97
 JITSUKAWA, Koichiro 112-113
 JÜRGENSEN, Astrid 135
- K**
- KAI, Yasushi 53-54
 KAIBUKI, Tadahiyo 125
 KAJIWARA, Kotaro 157
 KAKO, Masahiro 49
 KAMADA, Masao 162, 209-210, 227
 KAMBAYASHI, Hide 180
 KAMEYAMA, Akihiro 159
 KAMINAKA, Shouji 53
 KAMISAKA, Hideyuki 221
 KANAMORI, Kan 177
 KANDA, Kazuhiro 160
 KANODA, Kazushi 79, 83-84
 KARASAWA, Machiko 53
 KASAI, Kayoko 184
- KASHINO, Setsuo 104
 KATO, Kiyonori 89
 KATO, Reizo 82
 KATO, Shigeaki 32-33
 KATO, Tatsuhisa 49, 58-59, 223
 KATOH, Keiichi 119
 KATTO, Masahoto 160
 KAWABE, Kenji 177
 KAWAE, Tatsuya 120
 KAWAHATA, Eiji 192-193, 226
 KAWAMOTO, Atsushi 79, 84
 KAWAMOTO, Tadashi 109
 KAWAMURA, Takashi 173
 KAWASAKI, Yasuhiro 158
 KERA, Satoshi 156
 KIKUZAWA, Yoshihiro 204, 235
 KIM, Dongho 144
 KIMURA, Katsumi 191
 KIMURA, Kenichi 167
 KIMURA, Mineo 30-31
 KIMURA, Shin-ichi 162, 211, 213, 215
 KINAMI, Ryoji 81, 82
 KINCAID, James R. 202
 KINO, Hiori 43
 KINOSHITA, Ikuo 70
 KINOSHITA, Isamu 114
 KINOSHITA, Masahiro 34-35, 38, 222
 KINOSHITA, Minoru 120
 KINOSHITA, Tomoko 189-190
 KINOSHITA, Toyohiko 149, 164, 208, 210-213, 228
 KISHINE, Jun-ichiro 40-41, 44, 229
 KITAGAWA, Teizo 52-57, 112, 222
 KITAJIMA, Masashi 30
 KITAYAMA, Yoshie 49
 KLOBUKOWSKI, Mariusz 127
 KOBAYAKAWA, Hisashi 167
 KOBAYASHI, Akiko 87-93, 95, 230
 KOBAYASHI, Hayao 87-95, 102, 230, 232
 KOBAYASHI, Kaoru 49
 KOBAYASHI, Katsuaki 233
 KOBAYASHI, Kazuhiro 209
 KOBAYASHI, Kazuo 51
 KOBAYASHI, Teruyuki 170-172
 KOCHI, Takuya 178
 KOHGUCHI, Hiroshi 68, 224
 KOHZUMA, Takamitsu 53-54
 KOJIMA, Yoshitane 177
 KONDO, Shigeo 189-190
 KONDO, Tetsuo 79
 KONDOH, Takuhiko 227
 KONISHI, Yukihiko 81
 KOSUGI, Kentaroh 61-62, 65, 223
 KOSUGI, Nobuhiro 135-138
 KOVALENKO, Andriy F. 38-39, 222
 KOZEKI, Toshimasa 192-193, 226
 KRUGLIK, Sergei G. 56

- KUBODERA, Shoichi 159
 KUBOTA, Yasuo 184
 KUBOZONO, Yoshihiro 104
 KUGE, Katsuaki 188
 KUMAGAI, Hitoshi 117-118, 231
 KUMAKURA, Mitsutaka 47, 222
 KUMAR, Biradha 185
 KUMASAKI, Mieko 95
 KUMEI, Hideyuki 54
 KUNITA, Mami 170
 KUNO, Syougo 100
 KURIMURA, Sunao 195-196, 227
 KURIOKA, Yutaka 160
 KURMAEV, E. 159
 KUROSAWA, Kou 158-160
 KUSAKABE, Toshio 30
 KUSUKAWA, Takahiro 182, 185-186, 234
 KUSUMOTO, Tetsuo 97
 KUWABARA, Makoto 42, 229
 KUWATA, Shigeki 178
- L**
- LANGER, Uwe 107
 LEE, Sang Yeon 20
 LI, Lei 42
 LIMBACH, Hans-Heinrich 107
 LIU, Zhenlin 192-193, 226
 LUH, Lung-Shiang 187-188
- M**
- MACCARLEY, L. Robin 85
 MAESONO, Yoshihiro 158
 MAGNUSON, Martin 137
 MAKIHARA, Nobuyuki 114
 MAKSIMUK, Mikhail 79
 MARKOSYAN, Ashot S. 115-116, 121-122
 MARUTA, Goro 105-106
 MARUYAMA, Yusei 103
 MASE, Kazuhiko 151, 162, 166
 MASUDA, Hideki 112-113, 171-172
 MASUDA, Shigeru 156
 MASUI, Shin 149
 MATAGA, Noboru 71
 MATERA, Kathryn M. 203
 MATOBA, Masanori 164
 MATSUI, Shinji 160
 MATSUI, Toshitaka 111-112, 233
 MATSUMOTO, Hiroki 53
 MATSUMOTO, Hiroshi 167
 MATSUMOTO, Masaki 63
 MATSUMOTO, Masuaki 163, 226
 MATSUMOTO, Yoshiyasu 69-70
 MATSUMURA, Kazuo 72
 MATSUNO, Hiromitsu 158
 MATSUOKA, Hiroaki 173
 MATSUSHIMA, Hideaki 170
 MATSUSHITA, Michio 58, 223
 MATSUSHITA, Rokuji 177
 MATSUURA, Kenji 49
- MEKARU, Harutaka 149-150, 160
 MIGITA, Catharina T. 203
 MIHAILOVIC, Gragan 90-91
 MIKHAILIK, Vitalii B. 209
 MIL'NIKOV, Gennady V. 24, 221
 MINAGAWA, Waka 81-82
 MINGLANA, Jim Josephus Gabrillo 188
 MISAKE, Yohji 77, 81, 124-125
 MISHIMA, Kenji 221
 MITANI, Masaki 22
 MITANI, Tadaoki 104
 MITO, Masaki 120
 MITRA, Sivaprasad 71
 MITSUKE, Koichiro 152-155, 225
 MITSUTAKE, Ayori 23, 221
 MIURA, Atsushi 72
 MIURA, Hiroshi 164
 MIYAJIMA, Seiichi 96-98, 101, 230
 MIYAKE, Koji 163
 MIYAMAE, Takayuki 86, 148-149, 156-157
 MIYASHI, Tsutomu 199
 MIYAZAKI, Takafumi 92
 MIYOSHI, Eisaku 127-129, 224
 MIZOBE, Yasushi 178
 MIZOGUCHI, Asao 131-132, 224
 MIZUKAWA, Tetsunori 180
 MIZUNO, Misao 146, 225
 MIZUTANI, Mamoru 202, 235
 MIZUTANI, Masakazu 154, 225
 MIZUTANI, Yasuhisa 55-57
 MO, Yuxiang 68
 MOGI, Kouichi 127
 MOGI, Tatsushi 50
 MONOBE, Tae 125
 MORE, Sam Dylan 210
 MORI, Hatsumi 108-109
 MORI, Michiyasu 43, 229
 MORI, Takehiko 108-109, 124-125
 MORIKAMI, Atsushi 125
 MORIKAWA, Eizi 85
 MORISHIMA, Isao 112
 MORISHITA, Hiromasa 176, 233
 MORITA, Akihiro 32
 MORITA, Norio 47, 222
 MORIWAKI, Yoshiki 47, 222
 MORIYAMA, Hiroshi 91, 102
 MORO-OKA, Yoshihiko 112
 MOTOHASHI, Satoru 103
 MUJILATU, Na 193
 MUKAI, Masahiro 52, 112
 MUKHERJEE, Debashis 17
 MUNRO, Ian H. 148-149
 MURAKAMI, Junichi 209-210
 MURAKAMI, Tatsuya 112
 MURAKAMI, Youichi 104
 MURATA, Kyoji 124
- N**
- NACHTIGAL, Petr 20
 NAGAI, Hidekazu 189
 NAGAI, Masako 52
 NAGAOKA, Shin-ichi 166
 NAGAOKA, Takashi 177
 NAGASE, Shigeru 49
 NAGASHIMA, Umpei 166
 NAGASONO, Mitsuru 151, 162, 166
 NAGATA, Takashi 21
 NAGATA, Toshi 204-205, 235
 NAGATO, Kenkichi 225
 NAGATOMO, Shigenori 52-55
 NAGAYA, Kuninobu 26, 221
 NAITOH, Jun 164
 NAKA, Kazunari 32
 NAKABAYASHI, Takakazu 61-62, 64, 223
 NAKADAIRA, Yasuhiro 49
 NAKAGAWA, Hideyuki 164
 NAKAGAWA, Kazumichi 164
 NAKAI, Toshihito 97-98, 230
 NAKAI, Yohta 30
 NAKAJIMA, Hiroshi 179-180
 NAKAKITA, Satoshi 86
 NAKAMOTO, Masami 180
 NAKAMURA, Hiroki 24-26, 221
 NAKAMURA, Mikio 201
 NAKAMURA, Shinsuke 167
 NAKAMURA, Toshikazu 81-82, 230
 NAKANISHI, Akio 192
 NAKANISHI, Hiroshi 30
 NAKANISHI, Tsutomu 167
 NAKANO, Chikako 78, 210, 229
 NAKANO, Hiroki 119
 NAKANO, Kenji 193
 NAKASHIMA, Kenichi 72
 NAKASHIMA, Satoru 52, 56-57
 NAKATO, Yoshihiro 72
 NAKAZAWA, Yasuhiro 83-84, 90, 119, 230
 NANBA, Takao 162, 164, 215
 NANBU, Shinkoh 189-190
 NANBU, Sinkoh 226
 NAOE, Syun-ichi 164
 NARYMBETOV, Bakhyt 90-93, 95, 230
 NATH, Krishna G. 211-213, 228
 NEEB, Matthias 135
 NELSON, Alistair 20
 NEVILLE, John J. 135
 NIKURA, Hiromichi 154, 225
 NIIMI, Ken-ichi 164
 NISHI, Nobuyuki 61-66, 223
 NISHIDA, Yuzo 169-172
 NISHIKAWA, Koji 114
 NISHIKAWA, Takeshi 190, 221
 NISHINO, Satoshi 170
 NISHIOKA, Masaya 164
 NISHITANI, Tomohiro 167
 NISHIZAWA, Seizi 192
 NOBUSADA, Katsuyuki 24-25, 221
 NODA, Hideyuki 148, 150, 160

- NOGAMI, Takashi 105
 NOMOTO, Takeo 71
 NOMURA, Ryo 158
 NOMURA, Yasuo 178
 NONOGAKI, Youichi 150
 NORDGREN, Joseph 137
 NORO, Takeshi 127-128
- O**
- OBA, Tomoru 193
 OGA, Ryo 150
 OGATA, Hironori 91, 98-104
 OGINO, Hiroshi 187-188
 OGO, Seiji 55, 112-114
 OGURA, Fumio 93
 OGURA, Katsuyuki 182
 OHARA, Hideaki 157
 OHBA, Shigeru 170-172
 OHGO, Yoshiki 201
 OHMUKAI, Masato 160
 OHNISI, Shunshiro 160
 OHNO, Takeshi 180
 OHSHITA, Joji 166
 OHTAKE, Hideyuki 192-193, 226
 OHTSUKA, Hiroshi 221
 OISHI, Osamu 96-97, 230
 OJIMA, Emiko 88-91, 93, 230, 232
 OKADA, Kazumasa 214
 OKADA, Kazutoshi 19-21, 221
 OKADA, Tadashi 57
 OKAMOTO, Hiroshi 86
 OKAMOTO, Yuko 23, 34-35, 221
 OKAMURA, Hidekazu 162-164, 215
 OKANO, Tatsuo 163
 OKAZAKI, Masaaki 188
 OKAZERI, Nobuharu 199
 OKUBO, Shingo 49, 58
 OKUDAIRA, Koji K. 85, 156, 231
 OKUMI, Shoji 167
 OKUMURA, Ko 27-28
 OKUNO, Tsunehisa 105
 OKUTSU, Wataru 171
 OLSON, John S. 52, 56
 OMERZU, Ales 90-91
 OMI, Takuichiro 67
 ONO, Masaki 155
 ONO, Shingo 192-193, 226
 ONODERA, Kazuhiko 53-54
 OOKUBO, Kenji 79
 ORLOVICH, Valentin A. 56
 OSANAI, You 127
 OSHEROV, Vladimir I. 25, 221
 OSTROVSKY, Valentin N. 25
 OSUKA, Atsuhiko 57, 204
 OTSUBO, Tetsuo 76-77, 93, 125, 210
 OUAHAB, Lahcène 79
 OUCHI, Yukio 86, 157
 OUYANG, Jianyong 76-77, 229
 OZAKI, Shin-ichi 111-112, 233
 OZAKI, Yukihiko 72
- OZEKI, Hiroyuki 45-46
- P**
- PAL, Sourav 17
 PAVEL, Nicolaie 195, 227
 PETTERSSON, Lars G. M. 137
 PICHL, Lukas 25-26, 221
- R**
- RUBENSSON, Jan-Erik 137
- S**
- SAEKI, Morihisa 21
 SAIKAWA, Jiro 195-196, 227
 SAILE, Volker 85
 SAITO, Gunzi 79-80
 SAITO, Ko 22
 SAITO, Norio 214
 SAITO, Shuji 45-46
 SAITO, Yahachi 100
 SAITO, Yutaka 86, 157
 SAKAI, Makoto 64
 SAKAI, Masahiro 193
 SAKAI, Yoshiko 127
 SAKAMOTO, Youichi 206, 234
 SAKURADA, Norio 54
 SAKURAI, Hiromu 177
 SAKURAI, Makoto 123, 162-163, 226
 SAKURAI, Takeshi 53
 SARKAR, Nilmoni 140
 SARUKURA, Nobuhiko 192-193, 226
 SASAKAWA, Yuki 53-54
 SASAKI, Wataru 158-159
 SASAKI, Yumiko 171-172
 SATHE, Conny 137
 SATO, Akane 87-88, 95, 230
 SATO, Hirofumi 32-33, 62, 222
 SATO, Hirohiko 101
 SATO, Hiroyasu 180
 SATO, Shin-ichiro 64, 191, 226
 SATO, Yoichi 227
 SATOH, Katsuhiko 19, 221
 SATOH, Shinichi 30
 SAUVAGE, Jean-Pierre 184
 SEGAWA, Yusaburo 193
 SEINO, Hidetake 178
 SEKI, Kazuhiko 85-86, 156-157, 231
 SEKITANI, Tetsuji 151
 SENADEERA, G. K. Rohan 109
 SETHIA, Ashok 37, 222
 SETOYAMA, Hiroyuki 156
 SHAMIN, S. 159
 SHANG, Zhi-Liang 176
 SHIBATA, Naoki 53
 SHIDA, Norihiro 128
 SHIGEKAWA, Hidemi 163
 SHIGEMASA, Eiji 135-136, 214
 SHIGEMORI, Kazuki 176, 233
- SHIMAKURA, Noriyuki 31
 SHIMAMURA, Kiyoshi 193
 SHIMIZU, Naoya 215
 SHIMOYAMA, Iwao 164
 SHINGU, Masahisa 53
 SHINOZAKI, Hidenori 215
 SHIONOYA, Mitsuhiko 175-176, 233
 SHIRASAKA, Mitsuaki 131
 SHIREN, Kazushi 112
 SHISHIDO, Atsushi 71
 SHOJI, Hironobu 138
 SHOJI, Ichiro 227
 SHVEDKO, Alexander G. 56
 SIMONYAN, Mkhital 229
 SIMONYAN, Mkhitar 75-77
 SINGH, Yashwant 37
 SOUTOME, Kouichi 227
 SPRUNGER, T. Phillip 85
 STANCIL, P. C. 30-31
 STEFFEN, Thomas 27
 SU, Xingguang 72
 SUEKUNI, Tomonari 177
 SUEMATSU, Hiroyoshi 104
 SUEOKA, Osamu 30
 SUGIE, Masaaki 189-190
 SUGIMOTO, Hideki 181
 SUGIMOTO, Toyonari 106
 SUGIMOTO, Toyoshige 78
 SUGIMURA, Yasutomo 53-54
 SUGITA, Yuji 23, 221
 SUGIYAMA, Harue 167
 SUMI, Tomonari 129
 SUN, Xin 42, 229
 SUZUI, Mitsukazu 209
 SUZUKI, Chihiro 167
 SUZUKI, Eiji 53
 SUZUKI, Kazuharu 198-199
 SUZUKI, Kenji 103
 SUZUKI, Kentaro 120
 SUZUKI, Masatatsu 55, 112
 SUZUKI, Ryouichi 156
 SUZUKI, Satoshi 31
 SUZUKI, Takanori 199
 SUZUKI, Toshinori 68, 224
 SUZUKI, Toshiyasu 49, 206, 232
 SUZUKI, Yoko 28
- T**
- TABATA, Masaaki 63
 TADOKORO, Makoto 177
 TAGATA, Tsuyoshi 180
 TAGAWA, Seiichi 51
 TAHARA, Tahei 139-140, 142-146, 225
 TAIRA, Takunori 195-196, 227
 TAKABATAKE, Toshiro 215
 TAKABAYASHI, Yasuhiro 104
 TAKADA, Jitsuya 177
 TAKAGI, Sigenori 103
 TAKAHASHI, Akifumi 189-190
 TAKAHASHI, Masaki 234
 TAKAHASHI, Minoru 119

- TAKAHASHI, Naoshi 210
 TAKAHASHI, Osamu 22
 TAKAHASHI, Satoshi 203
 TAKAHASHI, Toshihiro 81-82
 TAKAHASHI, Yasuyuki 172
 TAKAMI, Toshiya 190
 TAKAMUKU, Toshiyuki 63
 TAKANISHI, Yoichi 97
 TAKAO, Masaru 227
 TAKARA, Satoshi 114
 TAKASHIMA, Yoshifumi 167
 TAKATA, Yasutaka 135-138, 214
 TAKAYAMA, Shigehisa 54
 TAKEDA, Kazuyoshi 120
 TAKEDA, Nobuhiro 182, 234
 TAKEDA, Sadamu 105-107
 TAKEDA, Yoshikazu 150
 TAKEKAWA, Michiya 30
 TAKENAKA, Hisataka 150
 TAKEUCHI, Fusako 51
 TAKEUCHI, Satoshi 139-140, 142-144, 225
 TAKEZOE, Hideo 97
 TAKEZOE, Noritaka 158, 160
 TAKI, Masayasu 54
 TAKIGAWA, Yasuo 159-160
 TAKIMIYA, Kazuo 76-77, 93, 125, 210
 TAKIZAWA, Kohichi 119
 TAMAI, Naoto 71-72
 TAMASSIA, Filippo 45
 TAMURA, Hideyuki 177
 TANAKA, Daisaku 191
 TANAKA, Fumio 71
 TANAKA, Hiroshi 30
 TANAKA, Hisashi 87-90, 95, 230
 TANAKA, Hitoshi 227
 TANAKA, Kazuyoshi 77, 81, 124-125
 TANAKA, Keiichi 131-133, 224
 TANAKA, Kenichiro 151
 TANAKA, Kentaro 175-176, 233
 TANAKA, Kiyoshi 128-129
 TANAKA, Koji 125, 179-181, 205, 233
 TANAKA, Satoru 164
 TANAKA, Senku 210
 TANAKA, Shin-ichiro 151, 162, 166, 211, 227
 TANAKA, Shoji 108-109, 200, 232
 TANAKA, Takehiko 133
 TANG, Hai-Rong 22
 TANG, Zhen 178
 TANIGUCHI, Hiromi 79, 84
 TANIGUCHI, Masateru 81, 124-125
 TANIGUCHI, Seiji 57
 TANIMURA, Yoshitaka 27-29, 37, 44, 222
 TANIYAMA, Junko 177
 TASAKA, Motoyuki 175, 233
 TATSUMI, Natsuo 163
 TAWA, Riichi 177
 TAWARA, Hiroyuki 30
 TEN-NO, Seiichiro 17, 28-29, 38, 44, 221
 TERANISHI, Yoshiaki 25-26, 221
 TERASAWA, Katsumasa 106
 TIAN, Fuli 86
 TOBITA, Hiromi 187-188
 TOGAWA, Kazuaki 167
 TOKII, Tadashi 170
 TOKITO, Shizuo 206
 TOKMAKOFF, Andrei 27
 TOKUHASHI, Kazuaki 189-190
 TOKUMARU, Koh 97
 TOKUMOTO, Madoka 89-92
 TOLSTIKHIN, Oleg I. 24
 TOMITA, Noriaki 30
 TOMON, Takashi 233
 TOMURA, Masaaki 197-199, 232
 TORII, Hajime 95
 TOYODA, Tetsuya 53
 TOYOHARA, Kiyotsuna 179
 TOYOTA, Eijiro 149
 TSUBAKI, Motonari 50-51
 TSUGE, Kiyoshi 179-181, 233
 TSUKADA, Hiroshi 230
 TSUKAMOTO, Takeyo 192
 TSUKUDA, Tatsuya 21
 TSUNESHIGE, Antonio 52
 TSUNEYUKI, Shinji 163
 TSURUSAWA, Takeshi 18, 221
 TSUSAKA, Yoshiyuki 149
U
 UCHIDA, Akira 201
 UCHIDA, Hironaga 148-149
 UCHIDA, Hiroyuki 160
 UCHIDA, Keiko 177
 UDAGAWA, Yasuo 17
 UEDA, Kazumasa 106
 UEDA, Kazushi 78
 UEHARA, Akira 55, 112
 UENO, Nobuo 85-86, 156-157, 231
 UESU, Yoshiaki 196
 UESUGI, Yuki 55-56
 UFUKTEPE, Yüksel 211
 ULANSKI, Jacek 79-80
 UMEMOTO, Kazuhiko 182, 234
 URISU, Tsuneo 148-151, 160, 166
 URUICHI, Mikio 78-79, 229
 UZAWA, Sachiko 54
V
 VERMA, Atul 72
W
 WADA, Akira 112
 WADA, Hiroaki 187
 WADA, Kouji 167
 WADA, Toru 233
 WAGNER, Albert F. 226
 WAKAHARA, Takatsugu 49
 WAKITA, Hisanobu 63
 WANG, Li 68
 WANG, Wen-Ning 22
 WATANABE, Hiromi 177
 WATANABE, Katsumi 162
 WATANABE, Kazuo 64, 69, 191, 226
 WATANABE, Kazuya 69-70
 WATANABE, Michio 227
 WATANABE, Noboru 17
 WATANABE, Yoshihito 55, 111-114, 233
 WEN, Yuh-Sheng 187
 WHITHAM, Christopher J. 45
 WILLICUT, J. Robert 85
X
 XU, Qiang 176
Y
 YAGISHITA, Akira 135, 136
 YAKUSHI, Kyuya 75-80, 85, 102, 156, 210, 229
 YAMABE, Tokio 124-125
 YAMADA, Toshiyuki 163
 YAMAGUCHI, Akira 105
 YAMAGUCHI, Atsushi 63
 YAMAGUCHI, Kentaro 182, 184
 YAMAGUCHI, Kizashi 105-106
 YAMAGUCHI, Toshio 63
 YAMAHARA, Ryo 113
 YAMAMOTO, Akio 164
 YAMAMOTO, Kazunori 49
 YAMAMOTO, Kohji 56
 YAMAMOTO, Makoto 156
 YAMAMOTO, Masahiro 167
 YAMAMOTO, Shunsuke 150
 YAMAMOTO, Takakazu 86, 157
 YAMAMOTO, Yasushi 157
 YAMANAKA, Tatsuhiko 160
 YAMASHITA, Hiroshi 160
 YAMASHITA, Yoshiro 78, 197-200, 229, 232
 YAMATO, Kazuhiro 177
 YAMAUCHI, Osamu 53
 YAMAURA, Junichi 109
 YAMAZAKI, Jun-Ichiro 210
 YAMOCCHI, Hideki 79-80
 YANAGIDA, Hideaki 158, 160
 YANG, Hui-Jun 112, 233
 YANG, Xiujuan 72
 YASUI, Hiroyuki 177
 YOKOTANI, Atsushi 158-159
 YOKOYAMA, Masataka 201
 YOKOYAMA, Takahiro 86
 YONEHARA, Yukako 75-76, 229
 YONEMITSU, Kenji 28-29, 40-44, 229
 YONETANI, Takashi 52
 YONEYAMA, Michio 72
 YOSHIDA, Hiroaki 155

YOSHIDA, Hisashi	208
YOSHIDA, Koji	63
YOSHIDA, Kunio	196
YOSHIDA, Makoto	192
YOSHIDA, Shohei	97
YOSHIDA, Tadashi	203
YOSHIKAWA, Yuuhi	101
YOSHIMURA, Akio	180
YOSHIMURA, Daisuke	86, 231
YOSHINO, Ruriko	67
YOSHIOKA, Masakazu	167
YOSHIZAKI, Fuminori	53-54
YU, Shu-Yan	185, 234

Z

ZAMAN, Md. Badruz	199
ZHANG, Ruo-Hua	176
ZHANG, Zhijun	72
ZHAO, Qi-Hua	176
ZHOU, Hong	203
ZHU, Chaoyuan	25, 221